This Page is Inserted by IFW Indexing and Scanning Operations and is not part of the Official Record

BEST AVAILABLE IMAGES

Defective images within this document are accurate representations of the original documents submitted by the applicant.

Defects in the images include but are not limited to the items checked:

- ☐ BLACK BORDERS
- ☐ IMAGE CUT OFF AT TOP, BOTTOM OR SIDES
- ☐ FADED TEXT OR DRAWING
- ☐ BLURRED OR ILLEGIBLE TEXT OR DRAWING
- ☐ SKEWED/SLANTED IMAGES
- ☐ COLOR OR BLACK AND WHITE PHOTOGRAPHS
- ☐ GRAY SCALE DOCUMENTS
- ☐ LINES OR MARKS ON ORIGINAL DOCUMENT
- ☐ REFERENCE(S) OR EXHIBIT(S) SUBMITTED ARE POOR QUALITY
- ☐ OTHER: _____

IMAGES ARE BEST AVAILABLE COPY.
As rescanning these documents will not correct the image problems checked, please do not report these problems to the IFW Image Problem Mailbox.

DALY, J. J. (1964). *J. Chem. Soc.* pp. 3799–3810.
MAZHAR-UL-HAQUE, TAYIM, H. A., AHMED, J. & HORNE, W. (1985). *J. Crystallogr. Spectrosc. Res.* **15**, 561–571.
SHELDRICK, G. M. (1986). *SHELXTL-Plus. An Integrated System for Solving, Refining and Displaying Crystal Structures from Diffraction Data.* For Nicolet *R3m/V*. Univ. of Göttingen, Federal Republic of Germany.
SOBOLEV, A. N., BELSKY, V. K., CHERNIKOVA, N. YU. & AKHMADULINA, F. YU. (1983). *J. Organomet. Chem.* **244**, 129–136.
SOBOLEV, A. N., ROMM., I. P., BELSKY, V. K. & GURYANOVA, E. N. (1979). *J. Organomet. Chem.* **179**, 153–156.
SOBOLEV, A. N., ROMM, I. P., BELSKY, V. K., SYUTKINA, O. P. & GURYANOVA, E. N. (1981). *J. Organomet. Chem.* **209**, 49–54.

Acta Cryst. (1990). C**46**, 919–922

Structures of Three Related Biphenyl Compounds: 4,4′-Biphenyldiol, 3,3′,5,5′-Tetra-*tert*-butyl-4,4′-biphenyldiol, and 3,3′,5,5′-Tetra-*tert*-butyl-1,1′-bicyclohexa-2,5-dienylidene-4,4′-dione

BY MARGO A. JACKISCH, FRANK R. FRONCZEK, C. CECIL GEIGER, PAUL S. HALE, WILLIAM H. DALY AND LESLIE G. BUTLER*

Department of Chemistry, Louisiana State University, Baton Rouge, LA 70803, USA

(*Received* 11 *May* 1989; *accepted* 30 *October* 1989)

Abstract. 4,4′-Biphenyldiol (I), $C_{12}H_{10}O_2$, M_r = 186·2, monoclinic, $P2_1/c$, a = 10·5512 (9), b = 5·359 (2), c = 7·9939 (8) Å, β = 95·736 (8)°, V = 449·7 (6) Å^3, Z = 2, D_x = 1·375 g cm^{-3}, λ(Cu $K\alpha$) = 1·54184 Å, μ = 7·13 cm^{-1}, $F(000)$ = 196, T = 299 (1) K, R = 0·037 for 738 reflections with $I > 3\sigma(I)$ (919 unique observations). This is a redetermination; the original study was based on visually estimated film data, with R = 0·20 for 240 observations [Akhmed, Farag & Amin (1971). *J. Struct. Chem.* (*USSR*), **12**, 676–677; *Zh. Strukt. Khim.* **12**, 738–739]. The molecule is centrosymmetric, and the biphenyl ring system is planar, with average deviation 0·002 (1) Å. The O atom lies 0·013 (1) Å out of this plane, and the hydroxy H atom lies 0·26 (2) Å out of the plane. The central C—C bond has length 1·4954 (11) Å, and the C—O bond 1·3845 (12) Å. Chains of hydrogen bonds along the b direction exist, with O···O 2·8940 (8) Å and a 167 (2)° angle at H. 3,3′,5,5′-Tetra-*tert*-butyl-4,4′-biphenyldiol (II), $C_{28}H_{42}O_2$, M_r = 410·6, orthorhombic, $Fdd2$, a = 20·719 (3), b = 19·905 (3), c = 12·836 (2) Å, V = 5293·7 (14) Å^3, Z = 8, D_x = 1·030 g cm^{-3}, λ(Cu $K\alpha$) = 1·54184 Å, μ = 4·49 cm^{-1}, $F(000)$ = 1808, T = 298 (1) K, R = 0·032 for 1031 reflections with $I > 3\sigma(I)$ (1457 unique observations). The long axis of the molecule lies along a twofold axis. The two phenyl rings are twisted slightly with respect to each other, forming a dihedral angle of 159·4 (2)°. One of the rings exhibits out-of-plane deviations of 0·010 (2) Å for its off-axis atoms, while these deviations are 0·001 (2) Å for the other ring. The central C—C bond of the molecule has length 1·486 (4) Å, with C—O bond lengths 1·385 (4) and 1·391 (3) Å. The C—C bonds of the *tert*-butyl groups are 1·527 (3)–1·545 (4) Å in length. Each of the hydroxy H atoms is disordered into two equally populated positions. 3,3′,5,5′-Tetra-*tert*-butyl-1,1′-bicyclohexa-2,5-dienylidene-4,4′-dione (III), $C_{28}H_{40}O_2$, M_r = 408·6, triclinic, $P\bar{1}$, a = 6·1004 (10), b = 10·4197 (11), c = 10·5260 (14) Å, α = 81·490 (8), β = 75·991 (11), γ = 81·582 (14)°, V = 637·8 (2) Å^3, Z = 1, D_x = 1·064 g cm^{-3}, λ(Cu $K\alpha$) = 1·54184 Å, μ = 4·65 cm^{-1}, $F(000)$ = 224, T = 295 (1) K, R = 0·045 for 2199 reflections with $I > 3\sigma(I)$ (2628 unique observations). This determination confirms the recent determination of Khan, Osman & Tuck [*Acta Cryst.* (1986), C**42**, 1399–1402], which was based on 1131 observed data with Mo $K\alpha$ radiation. Although the present results represent a doubling of the precision, the agreement between the two determinations is excellent, with the largest single difference in a bond distance being only 0·008 Å (2σ).

Experimental. Intensity data for all three structures were obtained on a Enraf–Nonius CAD-4 diffractometer with a graphite incident-beam monochromator using Cu $K\alpha$ radiation. The ω–2θ scans were made at variable scan rates. Absorption corrections were based on ψ scans. All structures were solved by direct methods using *MULTAN* (Main, Fiske, Hull, Lessinger, Germain, Declercq & Woolfson, 1980). The structures were refined by full-matrix least squares with Enraf–Nonius *SDP*

* To whom correspondence should be addressed.

0108-2701/90/050919-04$03.00

© 1990 International Union of Crystallography

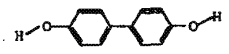
UM00011527
NOVARTIS EXHIBIT 1517
Novartis v. Regents, IPR2023-01347
Page 273 of 4460

Table 1. *Experimental details* (I), (II), (III)

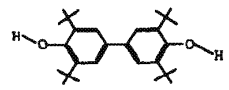
	(I)	(II)	(III)
Crystal	Colorless	Yellow	Yellowish-red transmitted; metallic purple reflected
Dimensions	0·05 × 0·24 × 0·53 mm	0·13 × 0·23 × 0·33 mm	0·10 × 0·30 × 0·55 mm
Unit cell	25 reflections $25 < \theta < 30°$	25 reflections $22 < \theta < 27°$	25 reflections $20 < \theta < 30°$
Standards	500, 040, 002	800, 220, 004	200, 020, 004
R_{int}	0·014	0·018	0·011
Corrections	Background, Lorentz–polarization Empirical absorption [0·8616–0·9963 on (*I*)]	Background, Lorentz–polarization Empirical absorption [0·9346–0·9941 on (*I*)]	Background, Lorentz–polarization Empirical absorption [0·8861–0·9978 on (*I*)] Linear decay [0·9825–1·0968 on (*I*)]
Scan rates (° min^{-1})	0·75–3·30	0·46–3·30	0·37–3·30
2θ range (°)	4–150 (full sphere)	4–150 (2 octants)	4–150 (full sphere)
hkl	$h = -13$ to 13	$h = 0$ to 24	$h = -7$ to 7
	$k = -6$ to 6	$k = 0$ to 24	$k = -13$ to 13
	$l = -10$ to 10	$l = -16$ to 16	$l = -13$ to 13
Reflections	3684 total	2912 total	5266 total
	919 unique	1457 unique	2628 unique
	738 with $I > 3\sigma(I)$	1031 with $I > 3\sigma(I)$	2199 with $I > 3\sigma(I)$
Parameters refined	85	139	217
R, wR, R (all)	0·037, 0·052, 0·044	0·035, 0·037, 0·055	0·045, 0·070, 0·051
Goodness of fit, S	2·373	1·531	3·641
Maximum shift/e.s.d.	0·03	0·01	0·02
$\Delta\rho$ (e Å^{-3})	0·16, −0·14	0·13, −0·10	0·24, −0·26
H atoms	Refined, iso.	Fixed contributions	Refined, iso.
Extinction	1·88 (9) × 10^{-5}	5·2 (2) × 10^{-5}	1·36 (4) × 10^{-5}

(Frenz, 1985), where the function minimized was $\sum w(|F_o| - |F_c|)^2$ and the weight, w, was defined as $4F_o^2\mathrm{Lp}^2/[S^2(C + R^2B) + (0{\cdot}020F_o^2)^2]$, S = scan rate, C = integrated count, R = scan time/background time, and B = background count. Atomic scattering factors, including those for anomalous dispersion, were taken from *International Tables for X-ray Crystallography* (1974). C and O atoms were refined anisotropically. H atoms were located in difference maps and were refined isotropically for (I) and (III). They were placed in calculated positions for (II), with C—H distance 0·95 Å and $B = 1{\cdot}3\ B_{eq}$ for the bonded C atom. Each of the OH H atoms in (II) is disordered into two 50% occupied sites; these atoms were included as fixed contributions.

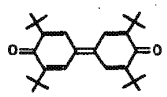
Compound (I) was purchased from Aldrich and recrystallized from ethanol/water (1/5). Details of the data collection and structural refinement are given in Table 1. Final positional and equivalent isotropic



(I)



(II)



(III)

Table 2. *Positional parameters and their e.s.d.'s* (I)

	x	y	z	B_{eq}(Å^2)*
O	0·44802 (7)	−0·0077 (2)	0·2479 (1)	4·00 (2)
C1	0·06798 (8)	−0·0001 (2)	0·0369 (1)	2·27 (2)
C2	0·11630 (9)	−0·1876 (2)	0·1461 (2)	2·90 (2)
C3	0·2425 (1)	−0·1878 (3)	0·2151 (2)	3·18 (2)
C4	0·32330 (9)	0·0001 (2)	0·1754 (1)	2·76 (2)
C5	0·2792 (1)	0·1881 (2)	0·0667 (2)	3·15 (2)
C6	0·1524 (1)	0·1865 (2)	−0·0009 (1)	2·99 (2)

* $B_{eq} = (8\pi^2/3)\sum_i\sum_j U_{ij}a_i^*a_j^*\mathbf{a}_i.\mathbf{a}_j$.

Table 3. *Selected bond lengths* (Å), *bond angles* (°) (I)

O—C4	1·3845 (12)	C2—C3	1·389 (2)
O—H1OH	0·96 (2)	C3—C4	1·377 (2)
C1—C1′	1·4954 (11)	C4—C5	1·380 (2)
C1—C2	1·393 (2)	C5—C6	1·393 (2)
C1—C6	1·392 (2)		

C4—O—H1OH	105·3 (9)	O—C4—C3	117·78 (10)
C1′—C1—C2	121·60 (9)	O—C4—C5	122·12 (10)
C1′—C1—C6	121·53 (9)	C3—C4—C5	120·10 (9)
C2—C1—C6	116·87 (8)	C4—C5—C6	119·35 (11)
C1—C2—C3	121·71 (10)	C1—C6—C5	122·07 (10)
C2—C3—C4	119·91 (11)		

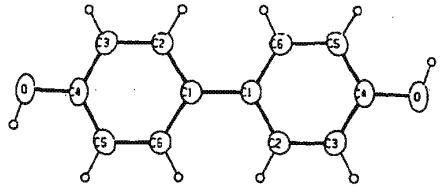


Fig. 1. 40% Ellipsoids of (I) (Johnson, 1965).

UM00011528
NOVARTIS EXHIBIT 1517
Novartis v. Regents, IPR2023-01347
Page 274 of 4460

Table 4. *Positional parameters and their e.s.d.'s* (II)

	x	y	z	B_{eq}(Å²)*
O1	0	0	0	6·08 (6)
O2	0	0	0·7661 (2)	6·82 (6)
C1	0	0	0·1084 (2)	3·96 (6)
C2	0·0353 (1)	−0·0496 (1)	0·1604 (2)	3·75 (4)
C3	0·0347 (1)	−0·0471 (1)	0·2685 (2)	3·78 (4)
C4	0	0	0·3253 (2)	3·37 (5)
C5	0	0	0·4411 (2)	3·55 (6)
C6	0·0162 (1)	−0·0572 (1)	0·4974 (2)	3·98 (4)
C7	0·0168 (1)	−0·0592 (1)	0·6059 (2)	4·12 (4)
C8	0	0	0·6582 (2)	4·55 (7)
C9	0·0739 (1)	−0·1048 (1)	0·1033 (2)	4·49 (5)
C10	0·1017 (2)	−0·1564 (1)	0·1795 (2)	7·23 (7)
C11	0·0299 (2)	−0·1453 (1)	0·0309 (2)	6·50 (7)
C12	0·1296 (2)	−0·0738 (2)	0·0423 (3)	7·75 (7)
C13	0·0357 (1)	−0·1242 (1)	0·6630 (2)	5·02 (5)
C14	0·0520 (2)	−0·1812 (1)	0·5873 (3)	6·82 (7)
C15	−0·0211 (1)	−0·1489 (1)	0·7310 (3)	7·26 (7)
C16	0·0964 (1)	−0·1125 (2)	0·7298 (2)	6·59 (7)

$B_{eq} = (8\pi^2/3)\Sigma_i\Sigma_j U_{ij} a_i^* a_j^* \mathbf{a}_i.\mathbf{a}_j.$

Table 5. *Selected bond lengths* (Å), *bond angles* (°) *and torsion angles* (°) (II)

O1—C1	1·391 (3)	C7—C8	1·400 (3)
O2—C8	1·385 (4)	C7—C13	1·539 (3)
C1—C2	1·399 (2)	C9—C10	1·531 (4)
C2—C3	1·389 (3)	C9—C11	1·531 (4)
C2—C9	1·543 (3)	C9—C12	1·527 (4)
C3—C4	1·389 (3)	C13—C14	1·531 (4)
C4—C5	1·486 (4)	C13—C15	1·545 (4)
C5—C6	1·389 (3)	C13—C16	1·541 (4)
C6—C7	1·394 (3)		
C2—C1—C2'	123·0 (2)	C7—C8—C7'	122·7 (2)
O1—C1—C2	118·5 (1)	C2—C9—C10	111·6 (2)
C1—C2—C3	116·5 (2)	C2—C9—C11	110·8 (2)
C1—C2—C9	123·2 (2)	C2—C9—C12	110·3 (2)
C3—C2—C9	120·3 (2)	C10—C9—C11	105·1 (2)
C2—C3—C4	123·6 (2)	C10—C9—C12	108·3 (2)
C3—C4—C5	121·7 (1)	C11—C9—C12	110·6 (2)
C4—C5—C6	121·3 (1)	C7—C13—C14	112·2 (2)
C5—C6—C7	123·0 (2)	C7—C13—C15	110·1 (2)
C6—C7—C8	117·0 (2)	C7—C13—C16	110·2 (2)
C6—C7—C13	120·1 (2)	C14—C13—C15	106·9 (2)
C8—C7—C13	122·9 (2)	C14—C13—C16	106·6 (2)
O2—C8—C7	118·7 (1)	C15—C13—C16	110·8 (2)
C3—C4—C3'	116·6 (2)	C6—C5—C6'	117·4 (2)
C1—C2—C9—C10	−174·0 (2)	C13—C7—C8—O2	−0·3 (2)
C1—C2—C9—C11	−57·2 (3)	C6—C7—C13—C14	−0·1 (3)
C1—C2—C9—C12	65·6 (3)	C6—C7—C13—C15	−119·0 (2)
C3—C2—C9—C10	6·4 (3)	C6—C7—C13—C16	118·5 (2)
C3—C2—C9—C11	123·1 (2)	C8—C7—C13—C14	−179·8 (2)
C3—C2—C9—C12	−114·0 (2)	C8—C7—C13—C15	61·2 (3)
C3—C4—C5—C6	−21·1 (1)	C8—C7—C13—C16	−61·3 (3)

thermal parameters are given in Table 2, and bond lengths and bond angles are listed in Table 3.* Fig. 1 shows the molecule and the atomic numbering scheme.

Compound (II) was prepared by reducing (III) with sodium hydrosulfite (Kharasch & Johi, 1957).

* Lists of structure factors, anisotropic thermal parameters and H-atom parameters have been deposited with the British Library Document Supply Centre as Supplementary Publication No. SUP 52381 (37 pp.). Copies may be obtained through The Technical Editor, International Union of Crystallography, 5 Abbey Square, Chester CH1 2HU, England.

Table 6. *Positional parameters and their e.s.d.'s* (III)

	x	y	z	B_{eq}(Å²)*
O1	0·5470 (2)	−0·35497 (9)	0·0812 (1)	6·40 (2)
C1	0·9319 (2)	−0·0508 (1)	0·0113 (1)	2·94 (2)
C2	0·9266 (2)	−0·1273 (1)	−0·0918 (1)	3·08 (2)
C3	0·7987 (2)	−0·2264 (1)	−0·0744 (1)	3·00 (2)
C4	0·6579 (2)	−0·2620 (1)	0·0593 (1)	3·61 (2)
C5	0·6560 (2)	−0·1834 (1)	0·1663 (1)	2·98 (2)
C6	0·7872 (2)	−0·0847 (1)	0·1394 (1)	3·10 (2)
C7	0·7923 (2)	−0·3035 (1)	−0·1862 (1)	3·31 (2)
C8	0·9429 (3)	−0·2510 (1)	−0·3171 (1)	4·75 (3)
C9	0·8802 (3)	−0·4479 (1)	−0·1551 (2)	4·72 (3)
C10	0·5487 (2)	−0·2923 (2)	−0·2056 (2)	4·82 (3)
C11	0·5049 (2)	−0·2173 (1)	0·3034 (1)	3·30 (2)
C12	0·5240 (3)	−0·1258 (1)	0·4003 (1)	4·78 (3)
C13	0·5774 (3)	−0·3566 (2)	0·3605 (2)	5·48 (4)
C14	0·2552 (3)	−0·2028 (2)	0·2937 (2)	5·24 (4)

* $B_{eq} = (8\pi^2/3)\Sigma_i\Sigma_j U_{ij} a_i^* a_j^* \mathbf{a}_i.\mathbf{a}_j.$

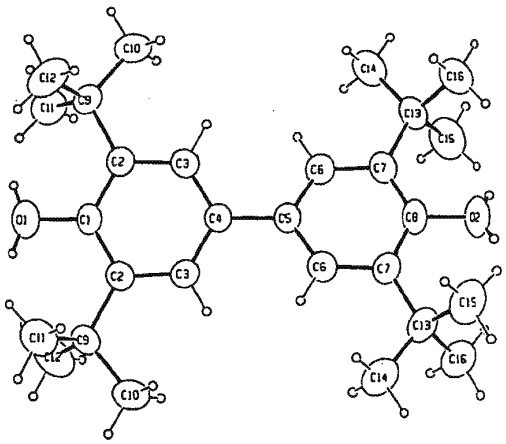


Fig. 2. 40% Ellipsoids of (II) (Johnson, 1965). The hydroxyl H-atom positions are half populated.

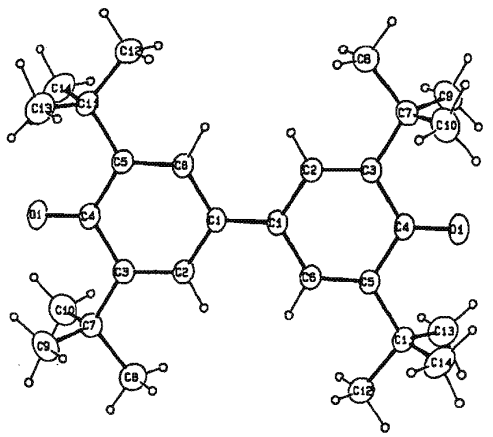


Fig. 3. 40% Ellipsoids of (III) (Johnson, 1965).

UM00011529
NOVARTIS EXHIBIT 1517
Novartis v. Regents, IPR2023-01347
Page 275 of 4460

Crystals were grown for X-ray analysis in diethyl ether. Details of the data collection and structural refinement are given in Table 1. Final positional and equivalent isotropic thermal parameters are given in Table 4, and both lengths, bond angles, and torsion angles, are listed in Table 5.* Fig. 2 shows the molecule and the atomic numbering scheme.

Compound (III) was prepared by passing oxygen through a vigorously stirred solution of 2,6-di-*tert*-butylphenol, CuCl and *N,N,N',N'*-tetramethylethylenediamine in 95% ethanol (Hay, 1969). Crystals were grown for X-ray analysis in ethyl acetate. Details of the data collection and structural refinement are given in Table 1. Final positional and equivalent isotropic thermal parameters are given in Table 6.* Fig. 3 shows the molecule and the atomic numbering scheme.

Related literature. Original crystal structure of (I): Akhmed, Farag & Amin (1971). The structure of hydroquinone: Maartmann–Moe (1966); structure of 2,6-di-*tert*-butyl-4-phenylphenol: Bekkouch, Perrin & Thozet (1988) related to our compounds (I) and (II); structure of *p*-benzoquinone: Trotter (1960). Original crystal structure of (III): Khan, Osman & Tuck (1986).

* See deposition footnote

The support of the donors of the Petroleum Research Fund, administered by the American Chemical Society and the Louisiana Educational Quality Support Fund is gratefully acknowledged.

References

AKHMED, N. A., FARAG, M. S. & AMIN, A. (1971). *J. Struct. Chem. (USSR)*, **12**, 676–677; (1971). *Zh. Strukt. Khim.* **12**, 738–739.

BEKKOUCH, K., PERRIN, M. & THOZET, A. (1988). *Acta Cryst.* C**44**, 2161–2163.

FRENZ, B. A. (1985). *Enraf–Nonius Structure Determination Package SDP/VAX V*3.0. Enraf–Nonius, Delft, The Netherlands.

HAY, A. S. (1969). *J. Org. Chem.* **34**, 1160–1161.

International Tables for X-ray Crystallography (1974). Vol. IV. Birmingham: Kynoch Press. (Present distributor Kluwer Academic Publishers, Dordrecht.)

JOHNSON, C. K. (1965). *ORTEP*. Report ORNL-3794. Oak Ridge National Laboratory, Tennessee, USA.

KHAN, M. A., OSMAN, A. J. & TUCK, D. G. (1986). *Acta Cryst.* C**42**, 1399–1402.

KHARASCH, M. S. & JOHI, B. S. (1957). *J. Org. Chem.* **22**, 1439–1442.

MAARTMANN-MOE, K. (1966). *Acta Cryst.* **21**, 979–982.

MAIN, P., FISKE, S. J., HULL, S. E., LESSINGER, L., GERMAIN, G., DECLERCQ, J.-P. & WOOLFSON, M. M. (1980). *MULTAN80. A System of Computer Programs for the Automatic Solution of Crystal Structures from X-ray Diffraction Data*. Univs. of York, England, and Louvain, Belgium.

TROTTER, J. (1960). *Acta Cryst.* **13**, 86–95.

Acta Cryst. (1990). C**46**, 922–924

A Bichromophoric Difulvene from 1,5-Cyclooctadione

BY FRANK R. FRONCZEK, JOHN M. CRONAN JR AND MARK L. MCLAUGHLIN*

Department of Chemistry, Louisiana State University, Baton Rouge, Louisiana 70803-1804, *USA*

(*Received* 23 *August* 1989; *accepted* 27 *November* 1989)

Abstract. 1,5-Bis(2,4-cyclopentadien-1-ylidene)cyclooctane, $C_{18}H_{20}$, $M_r = 236{\cdot}4$, monoclinic, $P2_1/n$, $a = 7{\cdot}498\ (2)$, $b = 11{\cdot}415\ (3)$, $c = 16{\cdot}555\ (3)$ Å, $\beta = 97{\cdot}80\ (2)°$, $V = 1403{\cdot}7\ (10)$ Å^3, $Z = 4$, $D_x = 1{\cdot}118$ g cm^{-3}, λ(Mo $K\alpha$) = 0·71073 Å, $\mu = 0{\cdot}58$ cm^{-1}, $F(000) = 512$, $T = 296$ K, $R = 0{\cdot}050$ for 1550 observations with $I > 1\sigma(I)$ (of 2471 unique data). The eight-membered ring of the title molecule adopts a boat–chair conformation with considerable bond angle distortions observed for all the methylenes forming the eight-membered ring. These six bond angles range from 113·3 (2)–116·1 (2)°. The bond angles exocyclic to the cyclopentadienylidene ring are 116·7 (2) and 116·6 (2)°. The intramolecular distance, 2·957 (2) Å, between the carbons that are exocyclic to the cyclopentadienylidene ring is well within the sum of van der Waals radii. The title compound exhibits a molar absorptivity which is less than half that of a single fulvene chromophore. The cyclopentadienylidene rings are nearly planar, with maximum deviations of 0·008 (2) and 0·013 (2) Å, and they form a dihedral angle of 32·2 (1)°.

Experimental. The title compound was prepared by condensing 1,5-cyclooctadione and 1,3-cyclopentadiene with pyrrolidine as a catalyst in methanol (Stone & Little, 1985). Crystals grown by slow cooling of refluxing hexane, m.p. 396–397 K, were suitable; a yellow crystal 0·10 × 0·48 × 0·75 mm was mounted in a capillary on an Enraf–Nonius CAD-4 diffractometer with Mo $K\alpha$ radiation and a graphite monochromator. Cell dimensions were determined

* Author to whom correspondence should be addressed.

0108-2701/90/050922-03$03.00 © 1990 International Union of Crystallography

UM00011530

NOVARTIS EXHIBIT 1517
Novartis v. Regents, IPR2023-01347
Page 276 of 4460

THE STRUCTURE OF A CRYSTALLINE COMPLEX CONTAINING ONE PHENOBARBITAL MOLECULE AND TWO ADENINE DERIVATIVES*

By Sung-Hou Kim and Alexander Rich

DEPARTMENT OF BIOLOGY, MASSACHUSETTS INSTITUTE OF TECHNOLOGY, CAMBRIDGE, MASSACHUSETTS

Communicated by Linus Pauling, April 4, 1968

The barbiturates are derivatives of uracil, a component of the nucleic acids. They have been used extensively in medical and biological studies for many years, but the molecular basis of their mode of action is unknown. Recent infrared studies have shown that the barbiturates have a high selective affinity for forming hydrogen-bonded complexes with molecules containing adenine.[1] This phenomenon may be related to the way in which the barbiturates act in living systems. Selectivity in hydrogen-bond formation is an important component of biological organization, especially in the nucleic acids. The purine and pyrimidine components of these molecules have an affinity for each other. Derivatives of adenine form hydrogen bonds selectively with thymine or uracil derivatives, whereas guanine derivatives bond selectively with cytosine derivatives.[2-4] These effects, called electronic complementarity,[5] reinforce the geometrical complementarity which is found as a structural component of the double-helical form of the nucleic acids. In the infrared study,[1] it was found that association constants for hydrogen bonding between the barbiturates and adenine derivatives are an order of magnitude greater than those found between uracil and adenine derivatives. In the course of that investigation, intermolecular crystalline complexes were observed to form between a variety of barbiturates and several different adenine derivatives. Here we report the structure of the intermolecular complex containing one phenobarbital and two 8-bromo-9-ethyladenine molecules. It is found that one adenine derivative is hydrogen-bonded to the barbiturate ring using the same bonds found between the adenine and thymine pair in the double-helical form of DNA.[6] The other adenine derivative is hydrogen-bonded to a second site on the same barbiturate ring. In addition, the adenine derivatives are hydrogen-bonded to each other using the same system of hydrogen bonds found in the helical form of polyadenylic acid.[7]

Materials and Methods.—Commercial phenobarbital tablets were dissolved in chloroform and the phenobarbital was purified by solvent extraction. 8-Bromo-9-ethyladenine was purchased from Cyclo Chemical Company, Los Angeles, California. Phenobarbital and 8-bromo-9-ethyladenine were initially dissolved separately in chloroform solutions. When the two solutions were mixed together in an equimolar ratio, a white precipitate formed which was collected on filter paper and dissolved in hot water. The aqueous solution was allowed to cool and then evaporate at room temperature until well-formed, clear prismatic crystals appeared. The crystals had edges over a millimeter in length. Individual crystals were isolated and dissolved in water. The ultraviolet absorption spectrum revealed the presence of the two components in the solution. However, due to the character of the phenobarbital absorption spectrum, it was not possible to determine the mole ratio of the constituents.

The unit-cell and space-group determinations were carried out with Weissenberg and precession cameras, and the density of the crystals was measured by the flotation tech-

UM00011531
NOVARTIS EXHIBIT 1517
Novartis v. Regents, IPR2023-01347
Page 277 of 4460

TABLE 1. *Unit-cell and space-group data for phenobarbital: 8-bromo-9-ethyladenine complex.*

Space group	Unit Cell		Density	
			Calc	Obs
$P\bar{1}$	$a = 9.703$ Å	$\alpha = 114.72°$	1.56 gm/cm³	1.57 gm/cm³
$Z = 2$	$b = 12.295$ Å	$\beta = 83.65°$		
	$c = 14.712$ Å	$\gamma = 74.75°$		

nique. The density measurements were compatible with either a 1:2 or 2:1 complex. Three dimensional X-ray diffraction data were collected on a Picker FACS-1 diffractometer system which was computer-controlled. The data were collected out to a 2θ value of 100°. Slightly over 3000 independent reflections were registered with copper Kα radiation, which was monochromatized by a highly oriented graphite monochrometer. Intensities were measured by the 2θ scan technique. The intensity data were reduced to structure factors (F) by correcting for the Lorentz-polarization factor. The crystal measured approximately 0.2 by 0.3 by 0.7 mm, and no corrections were made for X-ray absorption.

Results.—The molecules crystallized in a triclinic lattice. The normalized structure factors (E) were calculated from the structure factors and were used to calculate a three-dimensional sharpened (E^2) Patterson function. The Patterson map revealed two very heavy peaks and two peaks of half their height. This would be anticipated if there were two bromine atoms in the asymmetric unit and a center of symmetry. From this and the statistics of the normalized structure factors[8] it could be concluded that the space group was $P\bar{1}$ rather than P1. The existence of two bromine atoms in the asymmetric unit implied that the unit cell contained two phenobarbital molecules and four molecules of 8-bromo-9-ethyladenine; thus the crystal is a 1:2 complex. The unit-cell and space-group data for the complex of phenobarbital and 8-bromo-9-ethyladenine are listed in Table 1 together with the observed and calculated densities.

These intense peaks were used to assign trial coordinates to the two bromine atoms in an asymmetric unit. A trial electron density map was calculated in which the phases were strongly determined by the bromine atoms. Only those structure factors were used in which $|F\text{ (obs)}|$ was large and $F\text{ (calc)}/F\text{ (obs)} > kN_{\text{bromine}}/N_{\text{total}}$, where k is a constant (0.6) and N is number of electrons. The initial electron density map revealed unambiguously 32 out of the total of 43 nonhydrogen atoms in the asymmetric unit. The atoms not located included those in the phenyl and ethyl groups of phenobarbital and the ethyl group of one adenine and the terminal carbon atom of the ethyl group in the other adenine derivative. Another electron density map was calculated using all the atoms which had been located and a criterion similar to that used in choosing the phases. This map showed all of the remaining atoms except ethyl carbons of phenobarbital. These emerged in the difference Fourier map calculated after two cycles of least-squares refinement of isotropic temperature factors and coordinates. At this stage the residual factor was 21 per cent. Three cycles of least-squares refinement were carried out, two of which utilized isotropic temperature factors and one anisotropic temperature factors.[9] The final residual was 8.4 per cent. At this stage, 13 of the 28 hydrogens in the structure could be seen in a difference Fourier map. The coordinates of all the atoms other than hydrogen are listed in Table 2, together with the numbering system.

Description of the Structure.—The molecules crystallize into elongated lath-

UM00011532
NOVARTIS EXHIBIT 1517
Novartis v. Regents, IPR2023-01347
Page 278 of 4460

TABLE 2. *Fractional coordinates of the crystal structure phenobarbital: 2(8-bromo-9-ethyladenine).**

Phenobarbital				8-Bromo-9-ethyladenine(II)				8-Bromo-9-ethyladenine(I)			
Atom	x/a	y/b	z/c	Atom	x/a	y/b	z/c	Atom	x/a	y/b	z/c
N1	.3302	.2862	.2485	Br	−.0323	.8779	.0511	Br	.6860	.6703	.2471
C2	.3228	.1753	.1744	N1	.2381	.4970	.2123	N1	.5978	.1529	−.0010
N3	.4002	.0628	.1716	C2	.2759	.5971	.2712	C2	.6589	.1305	.0685
C4	.4810	.0555	.2401	N3	.2473	.7081	.2707	N3	.6950	.2091	.1467
C5	.4572	.1762	.3395	C4	.1722	.7127	.2016	C4	.6696	.3231	.1477
C6	.4045	.2939	.3228	C5	.1277	.6194	.1365	C5	.6108	.3579	.0802
C7	.6050	.1631	.3708	C6	.1641	.5033	.1422	C6	.5686	.2694	.0033
C8	.5944	.2597	.4825	N7	.0500	.6586	.0754	N7	.6066	.4817	.1033
C9	3340	.1835	.4181	C8	.0542	.7736	.1060	C8	.6595	.5136	.1816
C10	.3525	.0800	.4389	N9	.1230	.8141	.1806	N9	.6991	.4249	.2159
C11	.2437	.0821	.5111	C10	.1451	.9374	.2328	C10	.7461	.4358	.3111
C12	.1146	.1875	.5612	C11	.0120	1.0365	.3192	C11	.9082	.3688	.2828
C13	.0941	.2907	.5418	N6	.1296	.4035	.0822	N6	.5035	.2923	−.0657
C14	.2056	.2874	.4693								
O2	.2530	.1762	.1115								
O4	.5617	−.0490	.2222								
O6	.4224	.3922	.3753								

*The numbering system used is the same as that shown in Fig. 2*a*. Carbonyl oxygen or amino group nitrogen atoms have the same numbers as the carbon atoms to which they are attached. The alpha carbon atom of the ethyl group in the adenine derivative is C10; beta is C11. In phenobarbital, the alpha carbon atom in the ethyl group is C7; beta is C8. The six phenyl carbon atoms are C9–C14, where C9 is attached to C5 of the pyrimidine ring.

shaped hydrogen-bonded chains. The pyrimidine ring of phenobarbital and the purine rings of the adenine derivative lie approximately in the same plane and form the hydrogen-bonded array illustrated in Figure 1. This extended array of molecules runs in the direction [1 2 0]. The average molecular plane is approximately parallel to $(\bar{2}\ \bar{1}\ 2)$ and the planes are stacked with a mean spacing of 3.8 Å. The crystal is built out of an assembly of stacked laths held together by van der Waals interactions. The phenyl and ethyl groups of phenobarbital and the ethyl groups of the adenine derivatives are clustered together on the outside of the stacked laths, where they fill the interface between the stacks. The phenyl group of phenobarbital is stabilized on one side by a van der Waals contact with the bromine atom from an adenine molecule in the adjoining lath and on the other side by an interaction with an ethyl group of adenine from the layer above. Thus the molecules are held together by hydrogen bonding in one direction, a stacking of planar purines and pyrimidines in a second direction, and by several contacts involving the ethyl and phenyl groups in the third direction.

The most interesting feature in this crystal structure is the variety of hydrogen-bonded interactions between the various components of the molecular complex. There are four different sets of hydrogen bonds containing three different types of interactions between the molecules in the structure. Barbituric acid is 6-oxyuracil, and the barbiturates are characteristically substituted on C5 of the ring. They may be regarded as analogues of thymine, which has a methyl group on C5. One of the types of hydrogen bonding in the crystal may be regarded as analogous to the binding of adenine to thymine. This is shown schematically in Figure 2. Figure 2*a* shows the normal hydrogen bonding found between adenine and thymine in double-stranded DNA.[6] In that base pair the carbonyl O4 and

UM00011533
NOVARTIS EXHIBIT 1517
Novartis v. Regents, IPR2023-01347
Page 279 of 4460

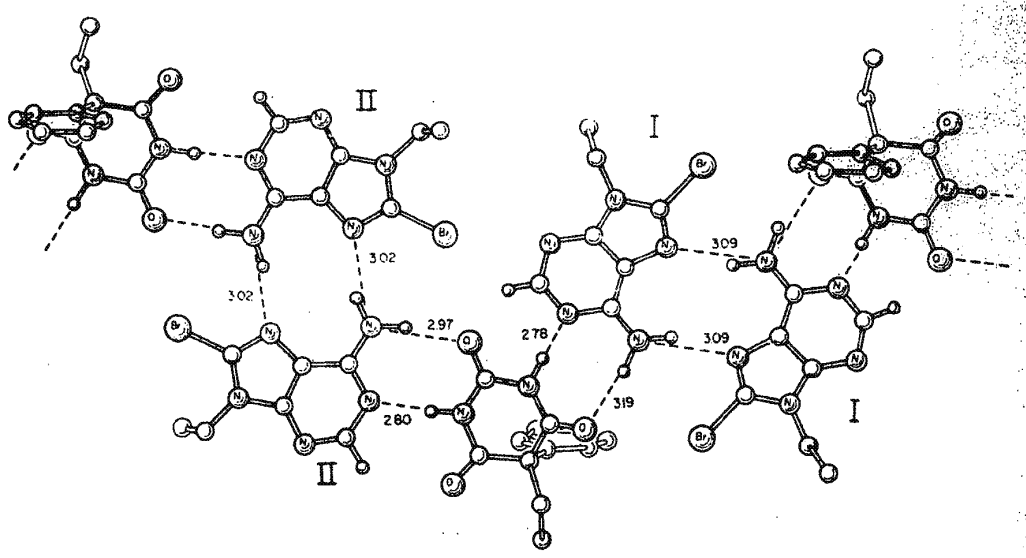


FIG. 1.—View of one level in the intermolecular complex of phenobarbital:2(8-bromo-9-ethyladenine). The hydrogen bond lengths are given in angstrom units. The two different adenine derivatives in the complex are labeled I and II. The molecules are approximately coplanar.

N3 of the thymine ring are connected by hydrogen bonds to the amino group and to N1 of the adenine ring. This pairing is analogous to the hydrogen bonding between phenobarbital and 8-bromo-9-ethyladenine (1) shown in Figure 2*a*.

The barbiturates may be also looked upon as analogues of pseudouridine, a common constituent of transfer RNA which has ribose attached to C5 rather than N1. Because of this, N1 of the pyrimidine ring has a proton bonded to it and this, together with the carbonyl O2, provides a second site which can be used for hydrogen-bond formation (Fig. 2*b*). A second type of hydrogen bonding in the crystal is analogous to the binding of adenine to pseudouracil. In this manner, adenine (II) in Figure 1 is attached to phenobarbital through two hydrogen bonds between the amino group and N1 of adenine and the carbonyl O2 and N1 of phenobarbital.

The third type of hydrogen bonding seen in the structure is the association between the adenine derivatives. In the crystal this involves a pairing between the amino group and N7 around a center of symmetry (Fig 2*c*). There are two different pairings of this type in the crystal. One of these pairs (I-I) is held together with two hydrogen bonds of length 3.09 Å each, the other (II-II) has bonds of 3.02 Å. This hydrogen-bonding arrangement is the same as that found in crystals of adenine hydrochloride[10] or in the helical form of polyadenylic acid in which the adenine is protonated on the N1 position.[7] This is shown in Figure 2*c*.

The extended hydrogen-bonded array deviates slightly from planarity. If the array shown in Figure 1 were completely planar, the bromine atom of 8-bromo-9-ethyladenine (II) would be 2.4 Å from the hydrogen atom attached to C2 of the adjoining adenine (I) residue. The sum of the van der Waals radii of these atoms is close to 2.95 Å. Adjacent adenine rings are therefore staggered so that they lie on either side of the mean plane of the extended lath shown in Figure

UM00011534
NOVARTIS EXHIBIT 1517
Novartis v. Regents, IPR2023-01347
Page 280 of 4460

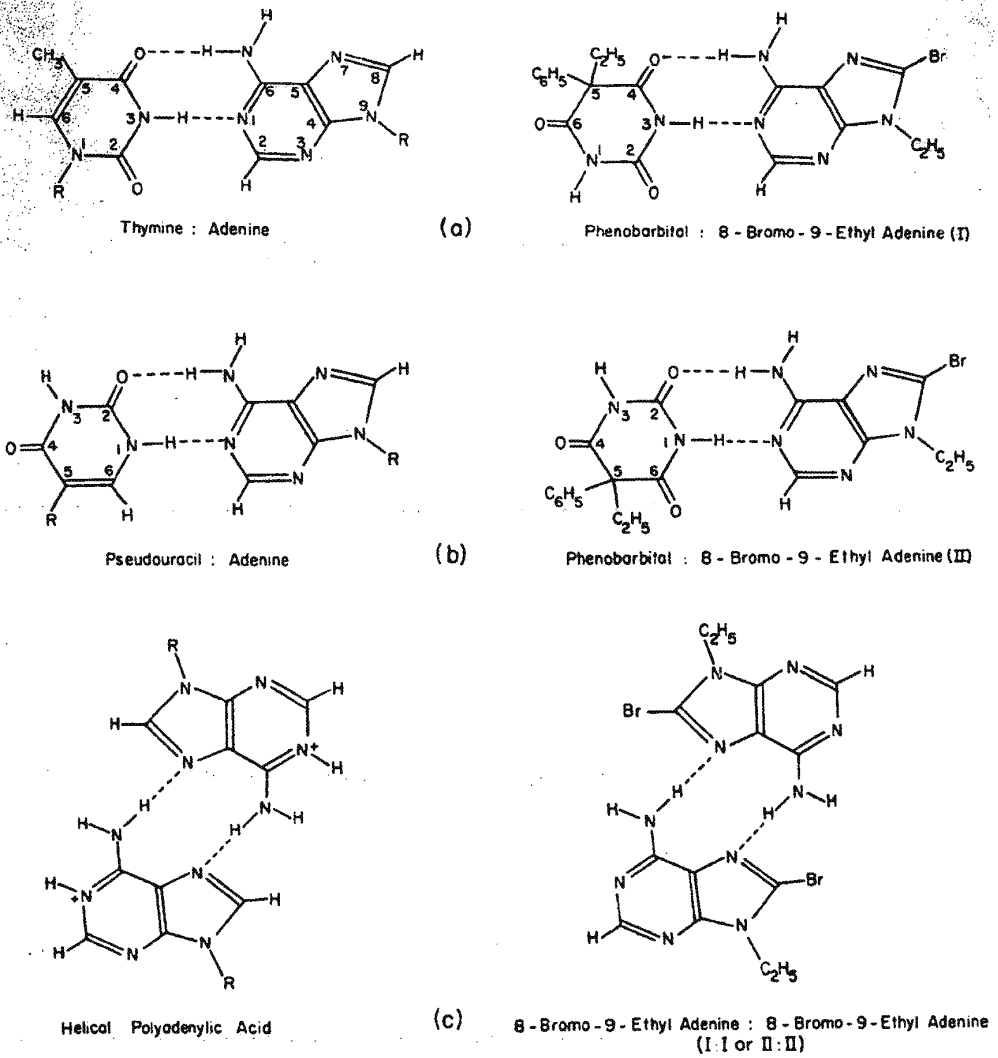


FIG. 2.—Different types of hydrogen-bonding interactions and their analogues in the intermolecular complex. (*a*) The hydrogen-bonding system between adenine and thymine in double-helical DNA (*left*) and the analogous pairing between phenobarbital and adenine derivative (I). R = deoxyribose. (*b*) A possible hydrogen-bonding system between pseudouracil and adenine (*left*) and the analogous pairing between phenobarbital and adenine derivative (II). R = ribose. (*c*) Hydrogen bonding between adenine derivatives in helical polyadenylic acid (*left*) and the analogous pairs of adenine derivatives, either I-I or II-II. R = ribose.

1. This displacement from the mean plane is partially reflected in the dihedral angles between the hydrogen-bonded bases.

All of the atoms in the adenine derivative, with the exception of the terminal carbon atoms of the ethyl side chain, are coplanar within 0.12 Å in adenine (I) and within 0.02 Å in adenine (II). In phenobarbital, C5 is 0.35 Å out of the least-squares plane of the pyrimidine ring. A similar displacement has been observed in alloxan[11] (5,5-dihydroxyl barbituric acid), but not in other barbiturates such as barbital or amobarbital.[12] The dihedral angle between phenobarbital and adenine (I) is 17.5°, whereas that between phenobarbital and adenine

UM00011535
NOVARTIS EXHIBIT 1517
Novartis v. Regents, IPR2023-01347
Page 281 of 4460

(II) is 16.3°. Crystals of hydrogen-bonded purines and pyrimidines often have small dihedral angles between them,[13] although they are usually somewhat smaller than those observed in the present structure.

The hydrogen bond between carbonyl O4 of phenobarbital and the amino group of adenine (I) has a length of 3.19 Å, which is longer than normal. The two N H . . . N hydrogen bonds between phenobarbital and adenine have lengths of 2.78 and 2.80 Å, which is slightly shorter than normal. The remaining hydrogen bond lengths are in the range of values normally seen.

Discussion.—To date, seven cocrystals have been found, involving four different adenine derivatives and three different barbiturates. Thus the phenomenon of cocrystallization appears to be a general one and is clearly related to the very high association constants for hydrogen bonding which have been determined from solution studies.[1] This is the first determination of the structure of an intermolecular complex between a barbiturate and an adenine derivative. The structure has some unusual features. It is the first case in which a pyrimidine derivative has cocrystallized with two purine derivatives. The adenine molecule has two sites capable of forming pairs of hydrogen bonds with thymine or uracil derivatives. These involve the amino group and either N1 or N7. The structures of several intermolecular complexes of adenine and uracil derivatives have been determined; most of them have 1:1 stoichiometry,[13] and they usually involve the N7 rather than N1 site. However, intermolecular complexes containing derivatives of 2,6-diamino purine have cocrystallized with two uracil derivatives on both N1 and N7 sites.[14] Uracil or thymine derivatives normally have only one site available for hydrogen-bond formation when there is a substituent on the glycosidic N1 atom. However, the barbiturates have side chains attached to the C5 position and a proton is found on N1. This allows the barbiturate to form the double set of hydrogen-bonded structures seen in the present crystal. It is interesting to note, however, that some of the other barbiturate-adenine complexes form 1:1 crystals. Their structure will be reported elsewhere.[15]

Both of the adenine derivatives are hydrogen-bonded to the barbiturate ring through N1 of adenine rather than N7. This is not surprising because the bromine atom blocks the formation of a hydrogen bond between N7 of adenine and N3 of uracil due to steric hindrance. When the uracil carbonyl O2 is in van der Waals contact with the bromine atom on C8, the uracil N3 is approximately 3.5 Å from the adenine N7. Thus a hydrogen bond cannot form. However, the bromine does not block the formation of the hydrogen-bonded adenine pair that is a component of helical polyadenylic acid.[7] It is interesting in the present context that there are two different sets of adenine-adenine hydrogen bonds involving molecules in the pairs I-I and II-II with slightly different hydrogen-bonding distances.

The barbiturates are highly active molecules in biological systems. In addition to their central nervous system activity, they also modify a wide variety of biological systems. Indeed, one of the puzzling features concerning their pharmacological action is the large number of different systems affected by them. The strong interaction observed between barbiturates and several adenine derivatives

UM00011536
NOVARTIS EXHIBIT 1517
Novartis v. Regents, IPR2023-01347
Page 282 of 4460

has led to a theory regarding the molecular mechanism underlying the mode of action of the barbiturates.[1, 16] The suggestion put forward is that the barbiturates specifically bind and inactivate a variety of molecules containing adenine, including coenzymes and adenosine 5'-triphosphate. An important component of this interaction is a lipophilic environment which aids in the binding of the barbiturate side chains. Thus, many of the affected systems are imbedded in membranes. The postulated inactivation mechanism involves the formation of specific hydrogen bonds between various adenine-containing compounds and the barbiturates. The present crystal structure analysis may be regarded as a prototype of this postulated interaction in that it illustrates the two potential kinds of binding of a barbiturate to molecules containing adenine. These interactions may not be too different from the kind of hydrogen bonding to adenine-containing coenzymes or nucleotides which is believed to take place in biological membranes or on the surface of selected enzymes.

Summary.—An intermolecular crystalline complex forms between 8-bromo-9-ethyladenine and phenobarbital. The structure of this complex has been solved by X-ray diffraction analysis. The phenobarbital forms two different sets of hydrogen bonds with the two adenine derivatives. These hydrogen-bonded triplets are joined together by means of adenine-adenine pairs of hydrogen bonds. Some of these sets of hydrogen bonds are analogous to those which occur in helical polynucleotides. The hydrogen bonding between barbiturates and adenine derivatives is a general phenomenon which may be related to the mode of action of barbiturates in biological systems.

We thank the Picker X-Ray Corporation for allowing us to use their FACS-1 system to collect the data. We acknowledge technical assistance of Misses D. Fisher and B. Yasney.

* This work was supported by research grants from the National Institutes of Health, the National Science Foundation, and the Office of Naval Research.

[1] Kyogoku, Y., R. C. Lord, and A. Rich, *Nature*, **218**, 69 (1968).

[2] Hamlin, R. M., R. C. Lord, and A. Rich, *Science*, **148**, 1734 (1965); Kyogoku, Y., R. C. Lord, and A. Rich, *J. Am. Chem. Soc.*, **89**, 496 (1967).

[3] Kyogoku, Y., R. C. Lord, and A. Rich, *Science*, **154**, 518 (1966).

[4] Katz, L., and S. Penman, *J. Mol. Biol.*, **15**, 220 (1966); Shoup, R. R., H. T. Miles, and E. D. Becker, *Biochem. Biophys. Res. Commun.*, **23**, 194 (1966).

[5] Kyogoku, Y., R. C. Lord, and A. Rich, these PROCEEDINGS, **57**, 250 (1967).

[6] Watson, J. D., and F. H. C. Crick, *Nature*, **171**, 964 (1953).

[7] Rich, A., D. R. Davies, F. H. C. Crick, and J. D. Watson, *J. Mol. Biol.*, **3**, 71 (1961).

[8] Karle, J., and H. Hauptman, *Acta Cryst.*, **9**, 635 (1956).

[9] Busing, W. R., K. O. Martin, and H. A. Levy, ORNL-TM-305, Oak Ridge National Laboratory, Oak Ridge, Tenn. (1963).

[10] Cochran, W., *Acta Cryst.*, **4**, 81 (1951).

[11] Singh, C., *Acta Cryst.*, **19**, 759 (1965).

[12] Personal communication from B. Craven, reported at American Crystallography Association meetings, 1967 and 1968.

[13] Hoogsteen, K., *Acta Cryst.*, **16**, 907 (1963); Mathews, F. S., and A. Rich, *J. Mol. Biol.*, **8**, 89 (1964); Haschemeyer, A. E. V., and H. M. Sobell, these PROCEEDINGS, **50**, 872 (1963); Katz, L., K. Tomita, and A. Rich, *J. Mol. Biol.*, **13**, 340 (1965).

[14] Labana, L. L., and H. M. Sobell, these PROCEEDINGS, **57**, 459 (1967); Chandross, R., and A. Rich, to be published.

[15] Kim, S. H., D. Voet, and A. Rich, to be published.

[16] Rich, A., to be published.

UM00011537
NOVARTIS EXHIBIT 1517
Novartis v. Regents, IPR2023-01347
Page 283 of 4460

This Page is Inserted by IFW Indexing and Scanning Operations and is not part of the Official Record

BEST AVAILABLE IMAGES

Defective images within this document are accurate representations of the original documents submitted by the applicant.

Defects in the images include but are not limited to the items checked:

- ❑ BLACK BORDERS
- ❑ IMAGE CUT OFF AT TOP, BOTTOM OR SIDES
- ❑ FADED TEXT OR DRAWING
- ❑ BLURRED OR ILLEGIBLE TEXT OR DRAWING
- ❑ SKEWED/SLANTED IMAGES
- ❑ COLOR OR BLACK AND WHITE PHOTOGRAPHS
- ❑ GRAY SCALE DOCUMENTS
- ❑ LINES OR MARKS ON ORIGINAL DOCUMENT
- ❑ REFERENCE(S) OR EXHIBIT(S) SUBMITTED ARE POOR QUALITY
- ❑ OTHER: _____

IMAGES ARE BEST AVAILABLE COPY.
As rescanning these documents will not correct the image problems checked, please do not report these problems to the IFW Image Problem Mailbox.

Acta Cryst. (1974). B30, 1010

Sinusoidal Structure of the 1:1 Complex of Phenothiazine and 7,7,8,8-Tetracyanoquinodimethane, PTZ–TCNQ

BY H. KOBAYASHI

Department of Chemistry, Faculty of Science, Toho University, Narashino, Chiba 275, Japan

(*Received* 9 *June* 1973; *accepted* 25 *December* 1973)

The X-ray diffraction patterns of the crystals of the 1:1 complex of phenothiazine (PTZ) and 7,7,8,8-tetracyanoquinodimethane (TCNQ) show satellite reflexions, which can be explained on the basis of a sinusoidally modulated structure. The cell constants of the fundamental lattice are $a=7{\cdot}04$ (2), $b=25{\cdot}38$ (2), $c=10{\cdot}51$ (8) Å, $\beta=92{\cdot}1$ (7)° and the space group is $C2/c$. The fundamental structure was determined from three-dimensional X-ray data recorded on equi-inclination Weissenberg photographs and refined by the block-diagonal least-squares method ($R=0{\cdot}120$). PTZ and TCNQ are stacked alternately in infinite columns along the a axis. The sequence of columns along **b** is sinusoidally modulated. This was deduced from satellite reflexions. The components of the transverse sinusoidal modulation wave are 0·85 and 0·75 Å along the $-$**a** and **c** directions, respectively. The period is $(4{\cdot}35\pm0{\cdot}37)b$. The most plausible structure is constructed from the paired columns, which are held together by hydrogen bonds of the N–H···N type.

Introduction

Crystal structures of some charge-transfer complexes containing TCNQ molecules as acceptors have been determined (Hanson, 1965; Williams & Wallwork, 1968; Colton & Henn, 1970; Goldberg & Shmueli, 1973). Most of the complexes have mixed stacking columns of alternating donor and acceptor (TCNQ) molecules. Crystals of carbazole–TCNQ are particularly interesting because they have domain structures consisting of mixed-stacks of TCNQ and carbazole (Kobayashi, 1973*a*). Another modified columnar structure will be reported in this paper. Crystals of the 1:1 complex of TCNQ and phenothiazine (PTZ) were subjected to X-ray crystal analysis in order to elucidate the sinusoidal structure of this complex.

Experimental

The complex of PTZ–TCNQ crystallizes in the form of needles elongated along the a axis. As reported briefly (Kobayashi & Saito, 1971), the crystal data of the fundamental structure are: $(C_{12}H_9NS)(C_{12}H_4N_4)$, F.W. 403·5; monoclinic, $a=7{\cdot}04$ (2), $b=25{\cdot}38$ (2), $c=10{\cdot}51$ (8) Å, $\beta=92{\cdot}1$ (7)°; space group, $C2/c$ or Cc from systematic absences; $U=1877{\cdot}7$ Å^3; $Z=4$, $D_x=1{\cdot}428$ g cm^{-3}.

Intensity data were recorded on equi-inclination Weissenberg photographs with Cu $K\alpha$ radiation. The multiple-film technique was employed. The relative intensities were estimated visually with a set of standard scales. The usual Lorentz-polarization and shape corrections were applied. No correction was made, however, for absorption in view of the small size of the crystal, which had a maximum dimension of about 0·25 mm. Some of the oscillation and Weissenberg photographs are shown in Fig. 1; satellite reflexions appear along the b^* axis. These diffraction patterns indicate that PTZ–TCNQ has a sinusoidally modulated lattice.

For the convenience of discussions, it may be worth while to quote the intensity formula of X-ray diffraction by the crystal with transverse phase modulation (Korekawa, 1964). Further details are shown in the Appendix. Consider the simple sinusoidal structure where the position of the jth atom of nth cell $[n=(n_1, n_2, n_3)]$ is given by†

$$\mathbf{r}_{nj}=n_1\mathbf{a}+n_2\mathbf{b}+n_3\mathbf{c}+\mathbf{d}_j+(p\mathbf{a}/a+q\mathbf{c}/c)\times\sin 2\pi\sigma n_2 \quad (1)$$

where $\mathbf{d}_j$ is the positional vector of the jth atom in the fundamental lattice, p and q are components of the amplitude of the transverse modulation wave and b/σ is the period of modulation. The direction of propagation of the modulation wave is parallel to the b axis. Then the intensity formula can be written as:

$$\begin{aligned}I(\xi\eta\zeta)&=|F(\xi\eta\zeta)|^2\\&=N_1^2N_2^2N_3^2|F^0(\xi\eta\zeta)|^2\sum_n J_n^2[2\pi(p\xi/a+q\zeta/c)]\\&\times\delta(\xi-h)\delta(\eta-k-n\sigma)\delta(\zeta-l)\\&=\begin{cases}N_1^2N_2^2N_3^2|F^0(hkl)|^2J_0^2[2\pi(ph/a+ql/c)]\ldots\\\qquad\qquad(hkl) \quad (2)\\N_1^2N_2^2N_3^2|F^0(h,k\pm n\sigma,l)|^2J_n^2[2\pi(ph/a+ql/c)]\\\qquad\qquad\ldots(hk\pm n\sigma l) \quad (3)\end{cases}\end{aligned}$$

† The phase factor of the wave is not important for the intensity formula in most cases (Korekawa, 1964).

UM00011539
NOVARTIS EXHIBIT 1517
Novartis v. Regents, IPR2023-01347
Page 285 of 4460

where J_n is the nth order Bessel function and h, k and l are integers. The diffraction maxima corresponding to equations (2) and (3) represent main and satellite reflexions respectively. Schematic drawings of the sinusoidally modulated lattice and its diffraction patterns are shown in Fig. 2. Characteristic features of the oscillation and Weissenberg photographs (Fig. 1) are as follows:

(1) Satellite reflexions appear along the b^* axis at a constant interval.

(2) As shown in Fig. 1(*c*) and (*e*), almost all Bragg reflexions are accompanied by some satellite reflexions except the Bragg reflexions that lie on the b^* axis ($0k0$).

(3) The number of the observed satellites becomes larger with increase in Bragg indices h or l.

(4) Relative intensities of satellites increase as the intensity of the main reflexion decreases.

(5) In higher layer lines [Figs. 1(*d*) and (*f*)], the reflexions lying on the [$2k0$] (or [$0k2$]) axis have some satellites and those without satellites appear elsewhere in reciprocal space.

The above features of the diffraction patterns obtained agree excellently with the X-ray diffraction patterns by the model of the sinusoidal structure shown in Fig. 2.

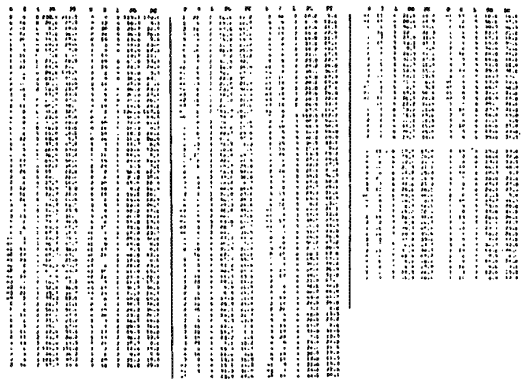
Determination of the fundamental structure

Considering the properties of Bessel functions $[\sum_{n=-\infty}^{\infty} J_n^2(x)=1]$, the structure amplitudes of the fundamental structure are given by

$$|F(hkl)|^2 \doteqdot \sum_n |F(hk \pm n\sigma l)|^2 ,$$

where $F(hk \pm n\sigma l)$ is given in equations (2) and (3) (see also Appendix). $F(hkl)$ is approximately equal to $F^0(hkl)$ $\{=\sum_j f_j \exp[2\pi i(hx_j+ky_j+lz_j)]\}$. The intensity distribution of X-ray diffraction patterns of the fundamental structure of PTZ–TCNQ resembles that of *N*-methylphenothiazine–TCNQ (Kobayashi, 1973*b*). So the trial structure was easily deduced. The space group $C2/c$ was assumed and this seemed to be verified by the reasonable convergence of the structure at a

Table 1. *Observed and calculated structure factors of the fundamental structure*



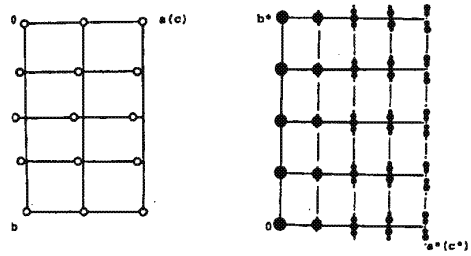


Fig. 2. Schematic drawing of a sinusoidally modulated lattice and its diffraction patterns.

Table 2. *Atomic parameters of the fundamental structure*

Positional and thermal parameters of the non-hydrogen atoms, with their estimated standard deviations in parentheses. The B_{ij}'s are defined by $\exp[-(h^2B_{11}+k^2B_{22}+l^2B_{33}+2hkB_{12}+2hlB_{13}+2klB_{23})]$.

	x ($\times 10^3$)	y ($\times 10^4$)	z ($\times 10^3$)	B_{11} ($\times 10^3$)	B_{22} ($\times 10^4$)	B_{33} ($\times 10^3$)	B_{12} ($\times 10^3$)	B_{13} ($\times 10^3$)	B_{23} ($\times 10^3$)
S	0	538 (3)	250	52 (5)	11 (1)	24 (2)	0	−22 (2)	0
N(1)	0	1736 (8)	250	24 (11)	14 (5)	8 (4)	0	13 (5)	0
C(1)	55 (4)	956 (9)	375 (2)	28 (10)	35 (6)	3 (3)	4 (2)	3 (4)	−1 (1)
C(2)	110 (4)	742 (9)	488 (2)	3 (7)	32 (6)	2 (3)	2 (2)	12 (4)	−1 (1)
C(3)	171 (4)	1014 (11)	588 (2)	16 (8)	50 (8)	4 (3)	0 (2)	10 (5)	−2 (1)
C(4)	135 (4)	1568 (12)	582 (2)	29 (10)	72 (10)	3 (3)	5 (2)	−6 (5)	0 (1)
C(5)	98 (5)	1801 (9)	468 (2)	84 (15)	22 (6)	13 (4)	−4 (2)	−15 (6)	3 (1)
C(6)	53 (3)	1527 (8)	365 (2)	21 (9)	20 (4)	7 (3)	−2 (2)	−2 (4)	−1 (1)
N(2)	664 (3)	428 (7)	624 (2)	54 (9)	15 (4)	27 (4)	−2 (2)	−16 (5)	−1 (1)
N(3)	655 (3)	2110 (7)	633 (2)	72 (10)	22 (4)	17 (3)	0 (2)	−17 (5)	0 (1)
C(7)	517 (4)	806 (7)	309 (2)	39 (9)	14 (4)	7 (4)	−2 (2)	−2 (6)	−1 (1)
C(8)	555 (4)	1299 (7)	377 (2)	12 (6)	17 (4)	3 (2)	2 (2)	1 (3)	1 (1)
C(9)	532 (2)	1786 (6)	308 (2)	4 (8)	10 (3)	13 (4)	0 (1)	−3 (4)	0 (1)
C(10)	605 (3)	1281 (6)	500 (2)	17 (7)	6 (3)	10 (3)	1 (1)	4 (4)	−1 (1)
C(11)	649 (3)	803 (9)	561 (2)	21 (9)	25 (5)	9 (4)	−1 (2)	14 (5)	0 (1)
C(12)	634 (4)	1754 (9)	574 (3)	56 (13)	23 (5)	19 (5)	−2 (2)	−22 (7)	0 (1)

UM00011540
NOVARTIS EXHIBIT 1517
Novartis v. Regents, IPR2023-01347
Page 286 of 4460

BEST AVAILABLE COPY

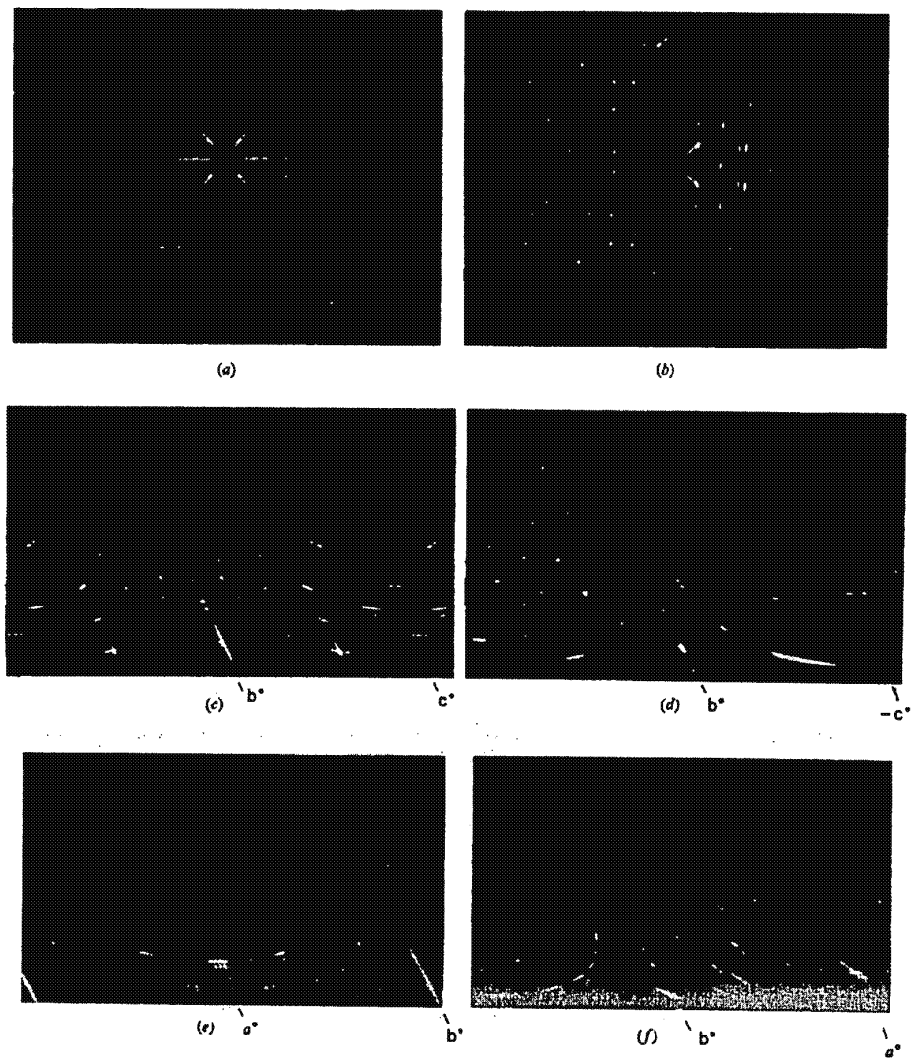


Fig. 1. Oscillation and Weissenberg photographs. (*a*) [100], (*b*) [010], (*c*) ($0\eta\zeta$), (*d*) ($2\eta\zeta$), (*e*) ($\xi\eta 0$), (*f*) ($\xi\eta 2$).

[*To face p.* 1011]

UM00011541
NOVARTIS EXHIBIT 1517
Novartis v. Regents, IPR2023-01347
Page 287 of 4460

Table 2 (*cont.*)

Atomic parameters of the hydrogen atoms

	x ($\times 10^2$)	y ($\times 10^3$)	z ($\times 10^3$)	B (Å^2)
H(1)	0	212	250	4·0
H(2)	10	33	487	3·5
H(3)	10	217	467	5·0
H(4)	20	72	666	5·0
H(5)	15	180	660	5·0
H(6)	55	50	387	3·0
H(7)	55	210	367	3·0

later stage of the refinement. The atomic parameters were refined anisotropically. Isotropic thermal parameters were used for the hydrogen atoms, which were located from the difference Fourier syntheses and were included in the later calculations. The refinement was performed by the block-diagonal least-squares method. The R value converged at 0·120. The weight of the reflexion is 1·0 for all the observed reflexions. The atomic scattering factors were taken from *International Tables for X-ray Crystallography* (1962). Observed and calculated structure factors were compared in Table 1. The final atomic parameters are listed in Table 2.

Description of the fundamental structure

The structure viewed along the a axis is shown in Fig. 3. PTZ and TCNQ are stacked alternately in infinite columns along the a axis. The intermolecular distance is 3·44 Å. The mode of overlapping is the ring–external bond type observed in other charge-transfer complexes containing TCNQ molecules and is shown in Fig. 4. It closely resembles the mode of overlapping found in *N*-methylphenothiazine–TCNQ (Kobayashi, 1973*b*). The short intermolecular contacts are listed in Table 3. TCNQ and PTZ are both planar and their molecular symmetries are C_2. The least-squares planes are

$$\text{PZT}: -0{\cdot}9640X + 0{\cdot}0236Y + 0{\cdot}2649Z + 0{\cdot}8540 = 0{\cdot}0$$
$$\text{TCNQ}: -0{\cdot}9696X + 0{\cdot}0160Y + 0{\cdot}2444Z + 4{\cdot}2018 = 0{\cdot}0,$$

where X, Y and Z are coordinates (in Å) referred to the crystal axes a, b and c^* respectively.

Table 3. *Interatomic distances for non-hydrogen atoms*

(i)	$1+x$,	y,	z	(iii)	$\frac{1}{2}-x$,	$\frac{1}{2}-y$,	$1-z$
(ii)	$1-x$,	y,	$\frac{1}{2}-z$	(iv)	$1-x$,	$-y$,	$-z$

C(1)···C(7)	3·37 (4) Å
C(3)···C(10)	3·30 (3)
S·····C(7)	3·73 (3)
C(11)···C(2^{i})	3·36 (4)
C(9) N(1^{i})	3·38 (2)
C(7)···S^{i}	3·55 (3)
N(3)···N(3^{ii})	3·35 (3)
N(3)···N(1^{iii})	3·37 (3)
S·····N(2^{iv})	3·63 (2)

The neutral molecules of PTZ (Bell, Blount, Briscoe & Freeman, 1968) and *N*-methylphenothiazine (Wakayama, 1971) are not planar but have a folded configuration, so the approximation used in the structure analysis is probably responsible for the planar structure of PTZ. Bond lengths and angles are shown in Fig. 5. The bonds of PTZ parallel to the twofold axis are normal but others are about 0·04 Å shorter than the usual values. A similar situation was found in the crystals of *N*-methylphenothiazine–TCNQ, where *N*-methylphenothiazine is planar owing to the disorder of the molecule. C–N(PTZ) is 1·36 Å and C–S is 1·73 Å. The values for a neutral PTZ are 1·41 and 1·77 Å, respectively (Bell, Blount, Briscoe & Freeman, 1968). The shortening of the bonds vertical to twofold axis is also observed in TCNQ. Nevertheless, the bond lengths seem to show a strong quinonoid character for TCNQ.

Determination of the parameters of the modulation wave

Equations (2) and (3) indicate that the main and satellite reflexions appear at intervals of σ along $\mathbf{b}^*$. The distances between these spots were measured on about 20 reflexions. The result gives σ of $0{\cdot}232 \pm 0{\cdot}020$. The period of the modulation wave, b/σ, is $109{\cdot}4 \pm 9{\cdot}4$ Å.

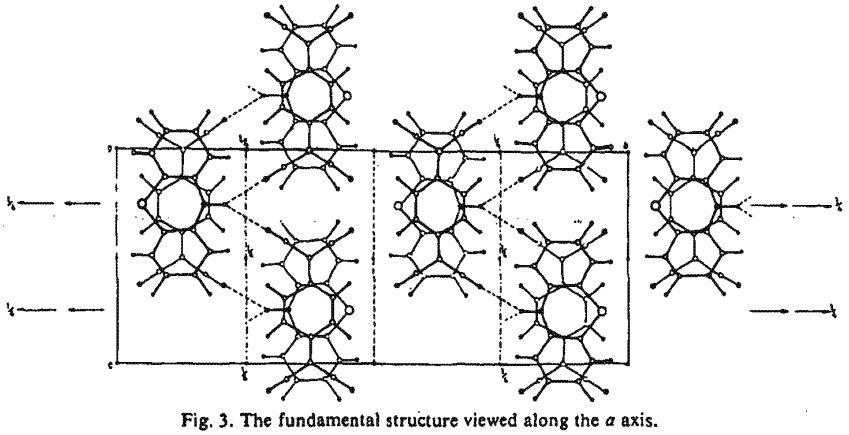


Fig. 3. The fundamental structure viewed along the a axis.

UM00011542
NOVARTIS EXHIBIT 1517
Novartis v. Regents, IPR2023-01347
Page 288 of 4460

The amplitude of the transverse modulation wave was also determined from equations (2) and (3). Since $J_0(x)$ is zero when $x=2{\cdot}405$, the intensity of the main reflexion becomes zero when

$$2\pi(ph/a+ql/c)=2{\cdot}405\,, \qquad (4)$$

where p and q are two independent components of amplitude of the transverse wave. $J_n(x)$ $(n=1,2,3,\ldots)$ is zero when $x=0{\cdot}0$. Then no satellite reflexion appears if

$$ph/a+ql/c=0{\cdot}0\,. \qquad (5)$$

The components of the reciprocal vectors (ξa^*, ηb^*, ζc^*) which satisfy equations (4) or (5) are easily determined by looking for the positions where all satellites or main spots disappear on Weissenberg photographs. Then the following equations (4′) and (5′) hold.

$$2\pi(p\xi_i/a+q\zeta_i/c)=2{\cdot}405 \qquad (4')$$

$$p\xi_j/a+q\zeta_j/c=0{\cdot}0 \qquad (5')$$

These equations are easily solved using the observed values of $(\xi_i\eta_i\zeta_i)$. The mean values of p and q thus obtained are:

$$p=-0{\cdot}85\pm0{\cdot}10\,,\quad q=0{\cdot}75\pm0{\cdot}10\ \text{Å}\,.$$

The amplitudes of the modulation wave are 0·85 and 0·75 Å in the $-\mathbf{a}$ and $\mathbf{c}$ directions respectively.

By inserting the observed values of p and q into equations (2) and (3), the relative intensities of the main and satellite reflexions were calculated. In the calculation the following equation is assumed:

$$\sum_k |F^0(hkl)|^2 \doteqdot \tfrac{1}{2}[\sum_k (|F^0(hk+n\sigma l)|^2 + |F^0(hk-n\sigma l)|^2)],\ (n=1,2,3,\ldots). \qquad (6)$$

From equations (2), (3) and (6) and the properties of Bessel functions $[\sum_{n=-\infty}^{\infty} J_n^2(x)=1]$, we have

$$J_0^2[2\pi(ph/a+ql/c)] = \sum_k |F(hkl0)|^2 / \sum_{n=-\infty}^{\infty}\sum_k |F(hkln)|^2 \qquad (7)$$

$$J_n^2[2\pi(ph/a+ql/c)] = \sum_k [|F(hkln)|^2+|F(hkl-n)|^2]/2 \sum_{n=+\infty}^{\infty}\sum_k |F(hkln)|^2 \qquad (7')$$

where $F(hkln)\equiv F(h,k+n\sigma,l)$. k runs through all the observed reflexions with the same indices of h and l. $\sum_{n=-\infty}^{\infty} |F(hkln)|^2$ stands for the sum of the intensities of the main reflexion and satellite reflexions associated with it. The satellites could be observed up to the 4th order ($|n|\leq 4$). In addition, the values of J_0^2 and J_n^2 were obtained from the tables of Bessel functions and compared with those calculated from observed intensities using equations (7) and (7′). The result is given in Fig. 6. The agreement is excellent.

The analysis of the sinusoidal structure

The fundamental structure is modulated by the transverse wave. Its period is b/σ. In order to analyse by use of the program of normal structure analysis, an approximate value of σ was introduced, which satisfies the following equation,

$$N/M=1/\sigma\,,$$

where N and M are integers and have no common divisor. Then the period along the b axis is Nb, that is, the lattice constant b of the sinusoidal structure is N times of that of the fundamental structure. The value of $1/\sigma=\frac{4}{17}$ $(\sigma=0{\cdot}2308)$ is a good approximation to σ_{obs} $(=0{\cdot}232\pm0{\cdot}020)$. In this case, the lattice spacing is about 329·9 Å (13b). $1/\sigma=4$ $(\sigma=0{\cdot}250)$ is a relatively poor approximation which gives a shorter spacing of 101·5 Å (4b). Schematic pictures of these structures are

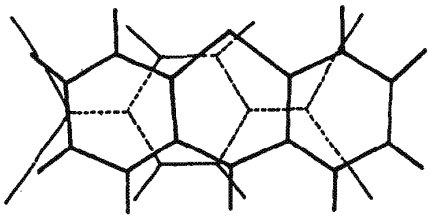


Fig. 4. Molecular overlap.

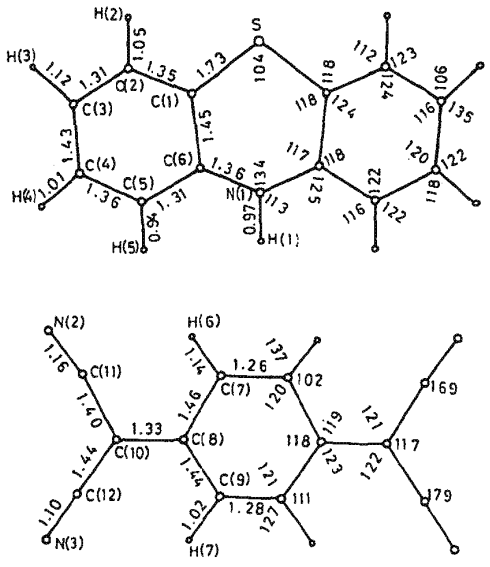


Fig. 5. Bond lengths (Å) and angles (°). Estimated standard deviations of bond lengths and angles are about 0·03 Å and 2·0°, respectively.

UM00011543
NOVARTIS EXHIBIT 1517
Novartis v. Regents, IPR2023-01347
Page 289 of 4460

illustrated in Fig. 7. The space group the of the 'thirteenfold structure' (13*b*) is $P2_1/n$ and that of the 'fourfold structure' (4*b*) is $P2_1/c$.

Using these models, the observed and calculated structure factors were compared. The observed structures were obtained by visual estimation of the intensities of the individual main and satellite reflexions.

Owing to the limitation on the number of the observed reflexions, it is very difficult to make an analysis without any assumption, even if an approximate value of σ is used. The object of this section is mainly to obtain the simplest structural model which has the essential features of the true structure.

(i) *A model of the 'thirteenfold simple sinusoidal structure'*

The atomic positions are assumed to be

$$\mathbf{r}_j = \mathbf{d}_j + (-0{\cdot}85\mathbf{a}/a + 0{\cdot}75\mathbf{c}/c) \sin 2\pi(0{\cdot}2308P)$$

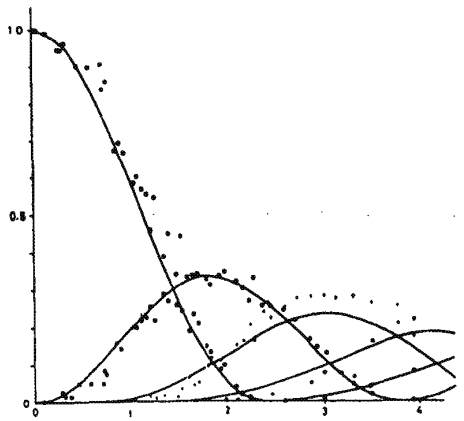


Fig. 6. Relative intensities of the main and satellite reflexions and comparisons with the values of the Bessel functions [see equations (7) and (7')]. ●, main reflexions; ○, 1st satellites; +, 2nd satellites; •, 3rd satellites. Ordinate and abscissa represent relative intensities [or $J_n^2(x)$] and $2\pi(ph/a + ql/c)$ (or x), respectively.

where $\mathbf{d}_j$ [$= (x_j y_j z_j)$] is the positional vector of jth atom in the fundamental structure and P is the y coordinate of the centre of gravity of the column to which the jth atom belongs. The phase factor was neglected. Strictly speaking, the molecules related by the n-glide in the fundamental structure must be treated as crystallographically independent in the sinusoidal structure. But in this calculation these molecules were assumed to be related to each other by translational symmetry expressed by the transverse modulation wave. The number of independent atoms is 43 ($C_{12}H_9NS.C_{12}H_4N_4$) and the number of the symmetry operations is $13M$, where 13 is the number of translational symmetry and M is the number of independent symmetry operations of the space group $P2_1/n$. Comparison of the observed and calculated structure factors gave an R value of 0·195. The temperature factors used are the same as those of the fundamental structure.

(ii) *A model of the 'fourfold simple sinusoidal structure'*

The atomic position is given as,

$$\mathbf{r}_j = \mathbf{d}_j + (-0{\cdot}85\mathbf{a}/a + 0{\cdot}75\mathbf{c}/c) \sin 2\pi(0{\cdot}250P).$$

The 43 atoms are independent and the number of the symmetry operation is $4M$, where 4 is the number of the translational symmetry expressed by the transverse sinusoidal wave and M is the number of symmetry operations of space group $P2_1/c$. The comparison of the observed and calculated structure factors gave an R value of 0·20.

The thirteenfold structure is better than the fourfold structure but the difference is small. Therefore the fourfold structure is more suitable for the calculation and was refined by the block-diagonal least-squares method in order to examine the validity of this model. Assumed symmetry operations are listed in Table 4. The final R value was 0·178. The B_{33} of four atoms were negative, which is probably due to the fact that approximate symmetry operations were used for convenience in the calculation.

(iii) *A model of the 'paired column structure'*

Another model was also examined, which elucidates more clearly the origin of the sinusoidal modulation.

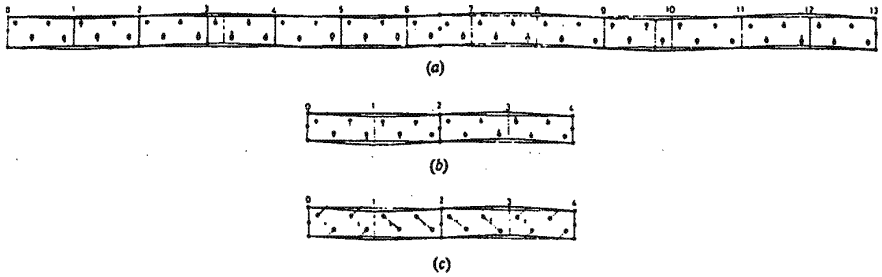


Fig. 7. Models of the sinusoidal structure. (*a*) The thirteenfold simple sinusoidal structure. (*b*) The fourfold simple sinusoidal structure. (*c*) The paired column structure.

UM00011544
NOVARTIS EXHIBIT 1517
Novartis v. Regents, IPR2023-01347
Page 290 of 4460

Table 4. *The approximate symmetry operations assumed to simplify the calculations*

An atomic position is given as

$$x = R_1 x_0 + T_x, \quad y = R_2 y_0 + T_y, \quad z = R_3 z_0 + T_z$$

where (x_0, y_0, z_0) are the atomic coordinates of the fundamental structure [see equation (1) and Fig. 7].

(i) Fourfold simple sinusoidal structure

	R_1	R_2	R_3	T_x	T_y	T_z
(1)	1	1	1	−0·02361	0·0	0·01389
(2)	1	1	1	0·39939	0·125	0·05920
(3)	−1	−1	−1	0·43278	0·125	0·03956
(4)	−1	−1	−1	0·88133	0·250	0·06983

(ii) Paired column structure

	R_1	R_2	R_3	T_x	T_y	T_z
(1)	1	1	1	−0·02361	0·0	0·01390
(2)	−1	−1	−1	0·43091	0·125	0·04054
(3)	1	1	1	0·41089	0·125	0·05245
(4)	−1	−1	−1	−0·13459	0·250	0·07909

In the fourfold structure, all the molecules move according to the coordinate of the mixed stacking column to which they belong, whereas in the 'paired column structure' two neighbouring columns (Fig. 7), which are interrelated by the *n*-glide in the fundamental structure, move in pairs; that is, the crystal is assumed to be constructed from the paired columns. The position of the centre of gravity of the pair moves sinusoidally. The structure was refined by the block-diagonal least-squares method with the starting parameters deduced from those of the fundamental structure. The approximate symmetry operations used are listed in Table 4. Some reflexions were not included in the calculation because a few higher-order satellite reflexions appeared in the middle of two neighbouring main reflexions and could not be indexed. After six cycles, the refinement converged with $R = 0{\cdot}165$. The B_{33} of three atoms and B_{11} of one atom became negative. Thus the refinement is not complete. Nevertheless, considering the many assumptions made in this analysis, this result seems to be fairly satisfactory. The atomic coordinates obtained are essentially the same as those of the fundamental structure. Structure amplitudes of satellite reflexions are listed in Table 5 together with calculated structure amplitudes.

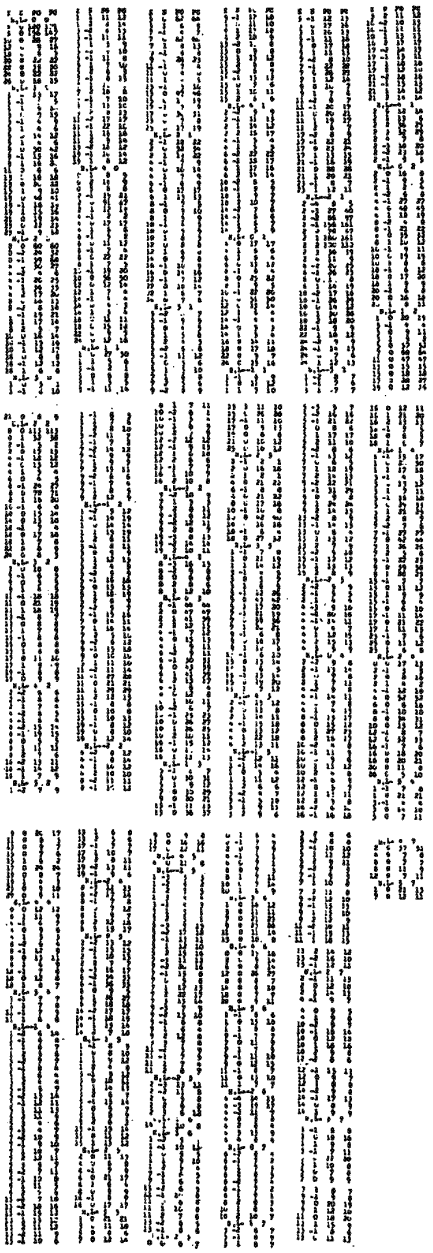
Discussion of the sinusoidal structure

The model of the 'paired column structure' seems to be a little better than the fourfold simple sinusoidal structure in view of the R value. Moreover, the paired column structure seems to indicate some clear physical implications on the origin of the sinusoidal structure. The paired column structure viewed along the a axis is shown in Fig. 8.

The interatomic distance between the nitrogen atoms of PTZ and TCNQ in neighbouring columns is 3·37 Å in the fundamental structure and the angle of N–H···N is about 140°. In the sinusoidal structure, the N···N distance is changed by the transverse modulation wave, which indicates that it can be reduced to about 3·24 Å. Considering that this contact

Table 5. *Calculated and observed structure amplitudes*

N indicates *n*th-order satellite.



UM00011545
NOVARTIS EXHIBIT 1517
Novartis v. Regents, IPR2023-01347
Page 291 of 4460

(3·37 Å) is the shortest between these two adjacent columns in the fundamental structure, the decrease in the distance of N···N seems to increase the atomic repulsion. Therefore it may be reasonable to conclude that the two atoms are linked by hydrogen bonds of the N–H···N type. The N···N distance in hydrogen bonds of the N–H···N type ranges from 2·8 to 3·4 Å (Pimentel & McClellan, 1960). The distance of 3·37 Å (fundamental structure) indicates that the hydrogen bond is very weak even if it exists, whereas the value of 3·24 Å (sinusoidal structure), calculated from the amplitude of the modulation wave, indicates weak hydrogen bonds in the sinusoidal structure.

Considering the existence of the charge-transfer interaction within a column and the hydrogen bonds formed between adjacent columns, a stable conformation of paired columns may be constructed (Fig. 9). As can be easily seen from the fundamental structure, hydrogen bonds can be formed between two equivalent pairs. Fig. 10 illustrates the two types of hydrogen bonds, which may distort to some extent the crystal lattice according to the strength of the hydrogen bond. Many types of modulated structures will appear by various combinations of these two structures. If two types of the hydrogen bonds are repeated alternately at every four cells, an approximately sinusoidal structure may result. There must be some origin for the force that prevents the infinite sequence of one type of hydrogen bond or the random sequence of two types of hydrogen bonds in order to explain the appearance of the sinusoidal structure. It may be a long-range force. Considering the polar structure of PTZ, it seems to be dipole–dipole interaction, which probably gives the largest stabilization energy in the regular arrangement of molecules and may act as a restoring force against the lattice distortion produced by the formation of hydrogen bonds. Thus the appearance of the sinusoidal structure may be due to the delicate balance of the short-range forces (hydrogen bonding, charge-transfer interaction, van der Waals force, ...) and the long-range forces (dipole–dipole interaction between PTZ molecules, ...). The interatomic distances for N···N obtained by the refinement of the simple sinusoidal structure and the paired column structure are 3·27 and 3·30 Å (with e.s.d.'s of about 0·05 Å), respectively. The value estimated using the parameters of the modulation wave is 3·24 Å as described previously. All these values indicate weak hydrogen bonding and may support the above picture of the origin of the sinusoidal structure.

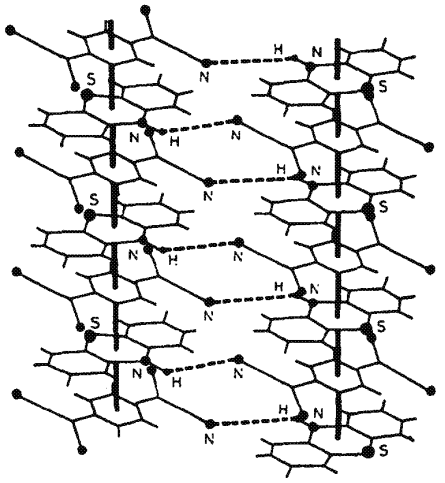


Fig. 9. The paired column of PTZ and TCNQ.

Recently, Bhat & Kinoshita (private communication) have examined infrared spectra of PTZ–TCNQ and found a small band shift of ν_{N-H}. The frequency ν_{N-H} of PTZ in the complex and of the neutral PTZ are 3362 and 3440 cm^{-1}, respectively. They have concluded that the small shift of 78 cm^{-1} indicates the existence of a weak hydrogen bond with an N···N distance of about 3·30 Å, which was calculated from the empirical formula of $\Delta\nu_{N-H}=1{\cdot}05\times10^3$ (3·38′$-R$). Their conclusion is in fairly good agreement with the result of the present X-ray analysis.

The author would like to express his sincere thanks to Professor Yoshihiko Saito for his keen interest and encouragements. He also thanks to Professor Minoru Kinoshita and Dr N. S. Bhat for many valuable discussions and information.

APPENDIX

Consider a modulated lattice in which an atomic position of the nth cell $[n=(n_1,n_2,n_3)]$ is displaced from its original position through a distance $(pa/a+qc/c)$ sin $2\pi\sigma n_2$. The structure amplitude of the crystal is given by

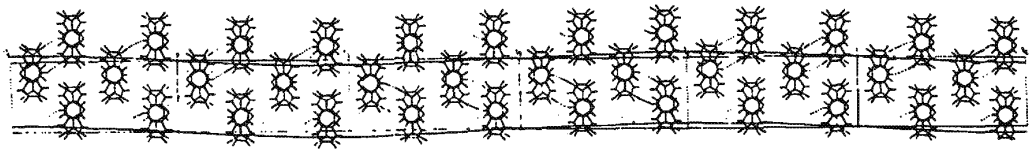


Fig. 8. The paired column structure viewed along the a axis.

UM00011546
NOVARTIS EXHIBIT 1517
Novartis v. Regents, IPR2023-01347
Page 292 of 4460

$$F(\xi\eta\zeta)=\sum_{n_1=1}^{N_1}\sum_{n_2=1}^{N_2}\sum_{n_3=1}^{N_3}\{\sum_j f_j \times\exp[2\pi i(\xi x_j+\eta y_j+\zeta z_j)] \times\exp\{2\pi i[\eta_1\xi+n_2\eta+n_3\zeta+(p\xi/a+q\zeta/c) \times\sin 2\pi\sigma n_2]\}$$

where the scattering vector s is represented by

$$\mathbf{s}=\xi\mathbf{a}^*+\eta\mathbf{b}^*+\zeta\mathbf{c}^*$$

and

$$\mathbf{d}_j=x_j\mathbf{a}+y_j\mathbf{b}+z_j\mathbf{c}\,.$$

The first term in the triple summation, $\sum_j f_j \exp[2\pi i(\xi x_j+\eta y_j+\zeta y_j)]$ is the structure factor of the crystal without modulation. The intensity formula of the X-ray diffraction is given as follows:

$$I(\xi\eta\zeta)=|F(\xi\eta\zeta)|^2 =|F^0(\xi\eta\zeta)|^2|G(\xi)|^2|G(\zeta)|^2\sum_m\sum_n G^*(\eta+\sigma m) \times G(\eta+\sigma n)J_m[2\pi(p\xi/a+q\zeta/c)]J_n[2\pi(p\xi/a+q\zeta/c)]$$

where

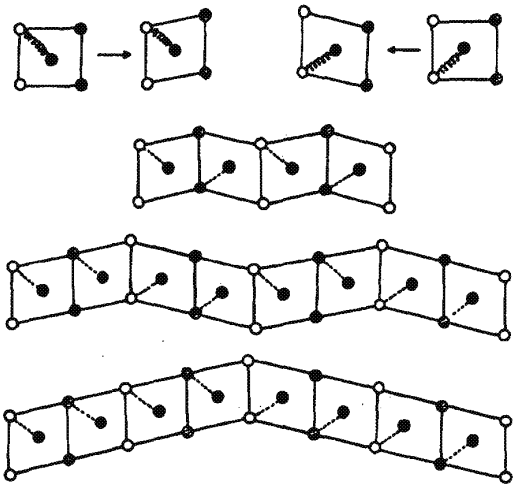


Fig. 10. Two models of the cells distorted by formation of hydrogen bonds and some possible superlattice structures constructed of these two cells.

$$F^0(\xi\eta\zeta)=\sum_j f_j \exp[2\pi i(\xi x_j+\eta y_i+\zeta z_j)]\,,$$

$$G(\xi)=\exp[\pi i(N_1-1)\xi]\sin N_1\pi\xi/\sin\pi\xi\,,$$

$$G(\eta+\sigma m)=\exp[\pi i(N_2-1)\eta]\sin N_2\pi(\eta+\sigma m)/\sin\pi(\eta+\sigma m)$$

and J_n is an nth order Bessel function. From the well-known properties of the Laue function $G(x)$, maxima occur at

$$\eta+\sigma m=k'$$
$$\eta+\sigma n=k''$$

where k' and k'' are integers. Higher-order Bessel functions are very small for the values of p, q and σ used in this paper. Therefore, $\sum_m\sum_n G^*(\eta+\sigma m)G(\eta+\sigma n)$ is approximately equal to $\sum_n|G|(\eta+\sigma n)|^2$. Then the intensity formula becomes

$$I(\xi\eta\zeta)=|F(\xi\eta\zeta)|^2 =N_1^2N_2^2N_3^2|F^0(\xi\eta\zeta)|^2\sum_n J_n^2[2\pi(p\xi/a+q\zeta/c)] \times\delta(\xi-h)\delta(\eta-k-n\sigma)\delta(\zeta-l) =\begin{cases}N_1^2N_2^2N_3^2|F^0(hkl)|^2J_0^2[2\pi(ph/a+ql/c)]\ \ldots \\ (hkl)\\ N_1^2N_2^2N_3^2|F^0(hk\pm n\sigma l)|^2J_n^2[2\pi(ph/a \\ +ql/c)]\ \ldots\ (hk\pm n\sigma l)\end{cases}$$

where h, k and l are integers and $n=1,2,3,\ldots$.

References

Bell, J. D., Blount, J. F., Briscoe, O. V. & Freeman, H. C. (1968). *Chem. Commun.* pp. 1656–1657.

Colton, R. H. & Henn, D. H. (1970). *J. Chem. Soc.* (*B*), pp. 1532–1535.

Goldberg, I. & Shmueli, U. (1973). *Acta Cryst.* B**29**, 421–448.

Hanson, A. W. (1965). *Acta Cryst.* **19**, 610–613.

International Tables for X-ray Crystallography (1962). Vol. III. Birmingham: Kynoch Press.

Kobayashi, H. (1973*a*). *Bull. Chem. Soc. Japan*, **46**, 2675–2683.

Kobayashi, H. (1973*b*). *Bull. Chem. Soc. Japan.* **46**, 2945–2949.

Kobayashi, H. & Saito, Y. (1971). *Bull. Chem. Soc. Japan*, **44**, 1444.

Korekawa, M. (1964). *J. Cryst. Soc. Japan*, **6**, 2–16.

Pimentel, G. C. & McClellan, A. L. (1960). *The Hydrogen Bond.* New York: Freeman.

Wakayama, N. (1971). *Bull. Chem. Soc. Japan*, **44**, 2847–2848.

Williams, R. M. & Wallwork, S. C. (1968). *Acta Cryst.* B**24**, 168–174.

UM00011547

NOVARTIS EXHIBIT 1517
Novartis v. Regents, IPR2023-01347
Page 293 of 4460

KEYNOTE ARTICLE

Molecular Recognition among Alcohols and Amines: Super-tetrahedral Crystal Architectures of Linear Diphenol–Diamine Complexes and Aminophenols

Otto Ermer* and Andreas Eling
Institut für Organische Chemie der Universität, Greinstrasse 4, D-50939 Köln, Germany

Hydroxy and amino groups are complementary as regards hydrogen-bond donors and acceptors. This is expected to lead to molecular recognition among alcohols and primary amines, *i.e.*, to a propensity towards formation of 1:1 alcohol–amine complexes, driven by a 50% increase of the number of hydrogen bonds as compared with the uncomplexed constituents. Possible hydrogen-bonded architectures of such complexes are suggested, and the concept is successfully exploited for crystal engineering purposes by drawing upon linear diphenols, aromatic diamines, and amino-phenols as supramolecular partners. Specifically, the crystal-structural chemistry is reported of the 1:1 molecular complexes between hydroquinone and *p*-phenylenediamine, hydroquinone and benzidine, 4,4′-dihydroxybiphenyl and *p*-phenylenediamine, 4,4′-dihydroxybiphenyl and benzidine, as well as of *p*-aminophenol, and of 4,4′-hydroxyaminobiphenyl. The diphenol–diamine complexes form hydrogen-bonded super-diamond lattices with 1.5 O(H)N bonds per oxygen and nitrogen atoms, respectively. Again exclusively *via* O(H)N bonds, the aminophenol structures are also super-tetrahedral but after the manner of the polar wurtzite variant. Some similar reported structures are analysed in the light of the present concepts and results, and implications are discussed of the finding that molecular recognition is possible among molecules as standard as simple alcohols and amines.

Introduction

Alcohols and primary amines molecules do not completely satisfy, by themselves, their valencies for hydrogen bonding. This follows simply from the fact that the number of the respective donors and acceptors is different. While the hydroxy function can donate one H atom to a hydrogen bond and possesses two oxygen lone pairs as acceptors, the amino group involves two donor H atoms but only one acceptor lone pair (Fig. 1). Therefore, crystalline alcohols and primary amines can form only one hydrogen bond per hydroxy and amino group, respectively, and necessarily have to dispense with a potentially possible, additional half hydrogen bond per OH and NH_2 group, respectively. Usually, crystalline alcohols and amines build up hydrogen-bonded (zig-zag or helical) chains with one 'silent' hydroxy lone pair and amino hydrogen atom, respectively (Fig. 2). However, cyclic patterns are also known, especially among polyfunctional alcohols, well-known examples being pentaerythritol[1] with hydrogen-bonded $(OH)_4$ rings and hydroquinone[2] with $(OH)_6$ rings. Thus, two hydrogen bonds emanate from each oxygen and nitrogen atom, respectively, in the chain, *i.e.*, one counts one hydrogen bond per oxygen and nitrogen atom, respectively.

With regard to hydrogen bonding, alcohols and amines are obviously complementary both stoichiometrically and geometrically. Interchange of H-bond donors and acceptors transforms the bonding pattern of the hydroxy group into that of the amino group, and *vice versa*, and in both cases the geometrical disposition of valencies is tetrahedral (Fig. 1). Therefore, molecular recognition[3] may be expected between alcohols and primary amines since complementarity represents the crucial prerequisite supporting favourable interactions between the molecular partners. In a 1:1 alcohol–amine complex the number of H-bond donors and acceptors is balanced and the possibility opens up for complete saturation of all potential H-bond valencies. Within fourfold tetrahedral



Fig. 1 H-Bond donor–acceptor complementarity of alcohols and amines

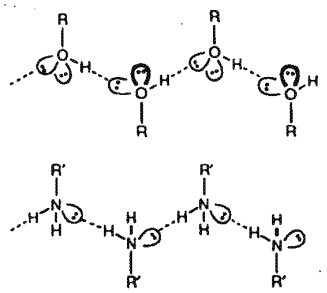


Fig. 2 Usual chain-like pattern of H-bonding in alcohols (top) and amines (bottom) with one H-bond per O and N atoms, respectively

coordination, from every oxygen and nitrogen atom three hydrogen bonds would then emanate, as compared with only two in the free alcohol and amine, respectively. Per O and N atom one would then count 1.5 hydrogen bonds in the 'super-tetrahedral' 1:1 alcohol–amine complex, the formation of which is thus seen to be accompanied by a 50% increase in the number of H bonds.

It is worth noting in the present context that the water molecule is self-complementary as regards optimal hydrogen bonding since, of course, it involves two donors (H atoms) and two acceptors (lone pairs) with tetrahedral directionality (Fig. 3). In crystalline water, therefore, the two maximally possible hydrogen bonds per oxygen atom may be made by building up

UM00011548
NOVARTIS EXHIBIT 1517
Novartis v. Regents, IPR2023-01347
Page 294 of 4460

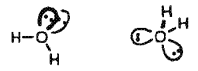


Fig. 3 Donor–acceptor self-complementarity of water

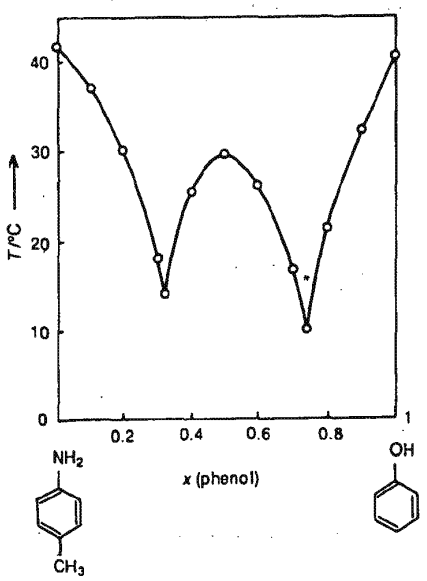


Fig. 4 Melting-point diagram of the binary system phenol–*p*-toluidine (adapted from ref. 6)

a super-tetrahedral three-dimensional framework with four hydrogen bonds emanating from each oxygen atom. The normal hexagonal polymorph of ice (ice-I_h) has a super-wurtzite (hexagonal diamond, tridymite) architecture, the slightly less stable cubic form (ice-I_c) a super-diamond (cristobalite) structure, and a cubic high-pressure form (ice-VII, VIII) is double-diamondoid with two interpenetrating super-diamond networks; other high-pressure polymorphs of ice also have super-tetrahedral structures, albeit distorted.[4a] However, despite the complete saturation of H-bond valencies, water is not fully satisfied either, since the O(H)O hydrogen bonds cannot attain lengths short enough to prevent porous super-tetrahedral frameworks of ice-I_h and I_c.[4b] The energetic disadvantage of this hollowness of the normal ice structure contributes to give rise to a variety of most important characteristic and unique water properties, such as the density anomaly of ice-water, propensity of hydrate and clathrate formation, extremely versatile hydration, solvation, and catalytic properties.

The possible 50% increase of the number of hydrogen bonds stated above should clearly provide a significant driving force towards formation of 1:1 complexes between alcohols and primary amines. Support in favour of this conjecture may for instance be gleaned from a survey of melting-point diagrams[5] of binary alcohol–amine mixtures, which quite frequently show pronounced dystectic maxima (congruent melting points) at 1:1 hydroxy–amino stoichiometry indicating the expected 1:1 complex formation; as a typical example the melting point diagram of the system phenol–*p*-toluidine[6] is reproduced in Fig. 4. It is noted parenthetically that from simple melting-point diagrams quite generally valuable information may be derived as regards molecular recognition phenomena, *i.e.*, supramolecular complex formation. Unfortunately, comprehensive and up-to-date respective thermochemical tabulations of phase equilibria and melting diagrams are not readily available.

Various reasonable structural possibilities with maximum H-bonding may be foreseen for 1:1 complexes between alcohols, R–OH, and primary amines, R′–NH_2 (Figs. 5 and 6). The usual hydrogen-bonded alcohol and amine zig-zag chains of Fig. 2 may simply be joined together alternately by N(H)O hydrogen bonds [Fig. 5(*a*)] generating puckered sheets of *trans*-fused 'super-cyclohexane' rings with chair-like 'super-conformations'. These sheets are held together exclusively by hydrogen bonds, one third each of the type O(H)O, N(H)N and N(H)O. Topologically, they may be related to the sheet structure of the stable allotrope of (grey) arsenic and be referred to as 'super-arsenic' sheets, which in turn may be cut out of both the cubic diamond (zincblende, cristobalite) lattice and the hexagonal diamond (wurtzite, tridymite) lattice. From generation of the H-bonded super-arsenic sheets of Fig. 5(*a*) from the H-bonded alcohol and amine chains (Fig. 2) by means of N(H)O bonds, the 50% increase in the number of H bonds, *i.e.*, the new N(H)O bonds, becomes particularly obvious on complex formation. In the sheets we have 1.5 H bonds per O and N atom, respectively, as compared with only 1.0 in the chains of the constituent free alcohols and amines, respectively.

It appears reasonable to expect, in our complexes, a general tendency to avoid N(H)N hydrogen bonds, which, according to known structural evidence and electronegativity considerations are particularly weak, *i.e.*, comparatively long and of low polarity. N(H)N bonds may indeed be completely avoided if the hydrogen-bonded super-arsenic sheets are entirely made up of (stronger) N(H)O bonds, *i.e.*, if the alcohol and amine molecules are rearranged in such a way that each oxygen atom has exclusively nitrogen atoms as hydrogen-bonded neighbours, and each nitrogen atom exclusively oxygen neighbours [Fig. 5(*b*)]. Less regular or irregular (disordered) distributions of O(H)O, N(H)N and N(H)O bonds in the super-arsenic sheets are, in principle, also conceivable. Whatever the distribution, however, it is clear that the numbers of N(H)N and O(H)O bonds must always be equal, *i.e.*, transforming an N(H)O bond in Fig. 5(*b*) into an N(H)N bond is necessarily to be accompanied by transformation of another N(H)O bond into an O(H)O bond. It must be conceded, however, that this stoichiometric necessity appears to weaken the expected propensity of N(H)N avoidance since it is coupled to O(H)O avoidance of equal extent, and the latter type of hydrogen bond is of course relatively strong. The experimental results of our work reported further on nevertheless indicate complete N(H)O preference in the alcohol–amine complexes studied.

If two thirds of the *trans*-fusions between the super-cyclohexane chairs of Figs. 5(*a*), (*b*) are replaced by *cis*-fusions such as shown in Fig. 5(*c*), one arrives at H-bonded sheets analogous to those of black phosphorus, which again may be cut out of the cubic, yet not the hexagonal diamond lattice. Only the variant with N(H)O bonds throughout is drawn in Fig. 5(*c*). It would appear that the super-black phosphorus sheets of Fig. 5(*c*) are more restricted with regard to the size of the residues R and R′, respectively, than are the super-arsenic sheets of Fig. 5(*b*).

An intriguing structural possibility for 1:1 alcohol–amine complexes are polyhedral H-bonded architectures as depicted in Fig. 6. In principle, any polyhedron may be considered with three edges emanating from each vertex. (Polyhedra of this kind necessarily have the required even number of vertices since their number of edges is of course equal to 1.5 times the number of vertices.) In the following, we discuss a number of highly symmetric possibilities. Thus, polyhedral H-bond clusters taking the shape of a tetrahedron [Fig. 6(*a*)], a cube [Fig. 6(*b*)], or a pentagonal dodecahedron [Fig. 6(*c*)] may be envisaged. While the small tetrahedral cluster is angularly unfavourable with H-bonds heavily bent outward, and the large, angularly almost ideal dodecahedral cage is hollow requiring suitable

UM00011549
NOVARTIS EXHIBIT 1517
Novartis v. Regents, IPR2023-01347
Page 295 of 4460

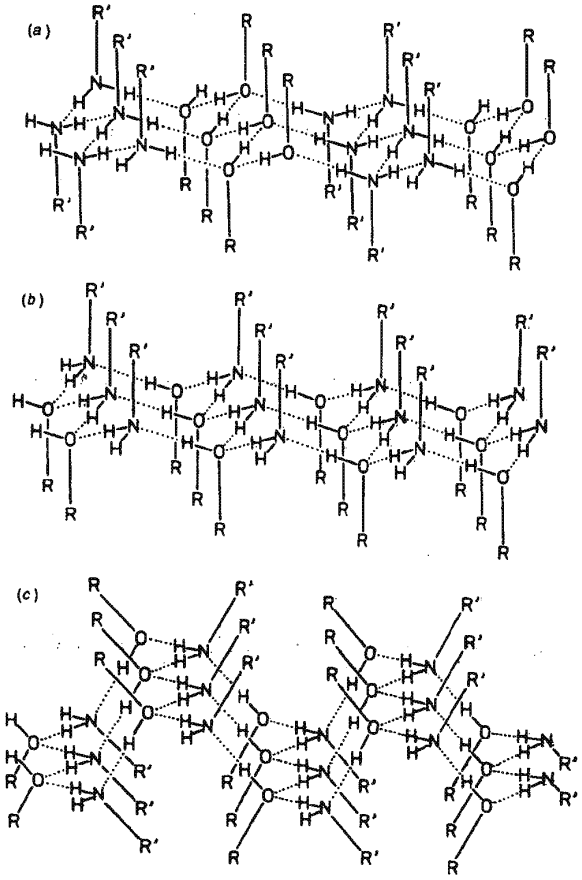


Fig. 5 H-Bonded sheets of a 1:1 alcohol–amine complex: (*a*) super-arsenic type with $\frac{1}{3}$ O(H)O, N(H)N and O(H)N bonds each; (*b*) super-arsenic type with O(H)N bonds exclusively; (*c*) super-black phosphorus type with O(H)N bonds exclusively

guest species for stabilization, the cube-shaped complex appears acceptable in both these respects. Interestingly, a cube-shaped octameric $(H_2O)_8$ cluster H-bonded analogously to Fig. 6(*b*) (four H-atoms not involved in cluster bonding) has recently been invoked in modelling the heat capacity of water.[7] Dodecahedral $(H_2O)_{20}$ clusters (10 H-atoms not involved in cluster bonding) play a prominent role as hosts in water clathrates.[8] Apart from the above Platonian polyhedra, for instance trigonal-prismatic, truncated-octahedral, or even extremely hollow truncated-icosahedral H-bonded clusters within 1:1 alcohol–amine complexes may be conceived [Figs. 6(*d*)–(*f*)]; inspiration for still other polyhedral possibilities may be gleaned from water clathrate studies.[8a] The huge truncated icosahedral cluster with 60 vertices (angularly somewhat unfavourable with H-bonds bent inward) has of course the topology of a modern soccer ball; its central cavity would indeed have about the right size to house an analogously shaped C_{60} (covalent) cluster! Similarly, a truncated-icosahedral H-bonded $(H_2O)_{60}$ cluster would provide a rather intriguing model for hydration of C_{60}; some of the 30 O–H bonds not involved in the cluster bonding could in fact point inward to form H bonds with the enclathrated C_{60} molecule similar to those in the water–benzene system.[9]

It is clear that in the envisaged polyhedral alcohol–amine complexes N(H)N [and O(H)O] bonds can only be completely avoided if all polygons (faces) of the underlying polyhedra have even numbers of vertices [Figs. 6(*b*), (*e*)], in which cases the H-bonding may be accomplished entirely by N(H)O bonds. Finally, it is noted that for simple topological reasons (see above) in the polyhedral complexes of Fig. 6 one of course again counts 1.5 hydrogen bonds per oxygen and nitrogen atom, respectively, as in the sheet-like architectures of Fig. 5. Thus polyhedral alcohol–amine complex formation again benefits from a 50% increase of the number of H-bonds, as compared with the uncomplexed educts.

In order to create genuinely favourable conditions for 1:1 alcohol–amine complex formation, *i.e.*, to improve the constituents' mutual molecular recognition, the sizes and shapes of the residues R and R', and possibly also their specific intermolecular interactions have to be properly adjusted (tuned). Model considerations and density estimates, as well as the melting-point diagram of the binary system phenol–*p*-toluidine (see above, Fig. 4), and the crystal structure of *p*-aminophenol (see below) indicate that the phenyl group offers favourable prerequisites in support of H-bonded super-arsenic sheets as shown in Figs. 5(*a*), (*b*). Linear aliphatic side chains R, R' also appear to fit reasonably well into an H-bond architecture of this kind. Bulkier substituents R, R' than phenyl or ethyl are expected to favour the formation of small polyhedral alcohol–amine complexes [*e.g.*, the cases of Figs. 6(*a*), (*b*), (*d*)] with severely curved convex outer cluster surfaces, whereas smaller residues could provide a steric incentive to

UM00011550
NOVARTIS EXHIBIT 1517
Novartis v. Regents, IPR2023-01347
Page 296 of 4460

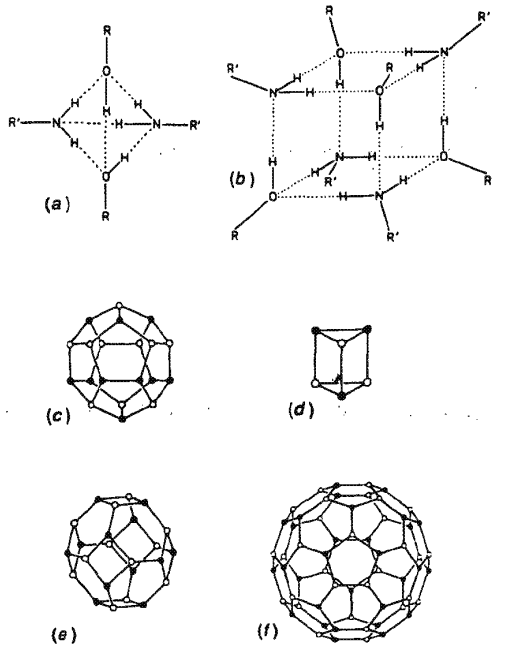


Fig. 6 Hypothetical polyhedral 1:1 alcohol–amine complexes. The H-bonded clusters take the shapes of a tetrahedron (*a*), cube (*b*), pentagonal dodecahedron (*c*), trigonal prism (*d*), truncated octahedron (*e*), truncated icosahedron (*f*). The possibilities (*a*) and (*b*) are shown in full, otherwise only oxygen and nitrogen atoms are drawn (empty and filled circles, respectively) and interconnected by straight lines representing the H-bonds.

build up larger polyhedral clusters [*e.g.*, as in Figs. 6(*c*), (*e*), (*f*)] with their smaller curvatures offering lesser convex space. For example, a tetrahedral 1:1 complex as sketched in Fig. 6(*a*) appears feasible between the bulky molecules of triphenylmethanol (trityl alcohol) and triphenylmethylamine (tritylamine); the crystal structure of trityl alcohol[10] is suggestive in this sense since it consists of tetrahedral tetramers similar to the envisaged complex structure.

Conceptually, the two-dimensional super-arsenic sheets of Figs. 5(*a*), (*b*) may be joined to build up three-dimensional super-tetrahedral, *i.e.*, in particular super-diamond or super-wurtzite, networks through replacing the monofunctional alcohol and amine components R–OH and R′–NH_2 by linear dialcohols HO–R_{di}–OH and diamines H_2N–R'_{di}–NH_2, respectively [Figs. 7(*a*), (*b*)]. We have recently been interested in H-bonded (multiple) super-diamond architectures of tetrahedral tetracarboxylic acids with intriguing properties, for example remarkable solid-state inclusion behaviour.[11] Suitable choices for R_{di} and R'_{di} appeared to be 1,4-phenylene and 4,4′-biphenylylene, and we report here the crystal structures of the possible 1:1 complexes between hydroquinone **1**, 4,4′-dihydroxybiphenyl **2**, *p*-phenylenediamine **3**, and benzidine **4**, *i.e.*, the molecular compounds **1·3**, **1·4**, **2·3** and **2·4**. The 'supramolecular synthesis'[12] of these adducts turned out to be straightforward as expected from our structural design outlined above, and likewise their crystal architectures comply with the anticipated super-tetrahedral properties, as shown in the following. Obviously, the selection of dialcohols and diamines for our complexation experiments also has crystallographic virtues since the 3-dimensional H-bonded networks represent relatively rigid molecular assemblies as compared with the sheet-like patterns expected in 1:1 complexes of monoalcohols and monoamines. Furthermore, the complexes involving hydroquinone **1** could be expected to form with particular ease since **1** is well known to possess a pronounced propensity to engage in inclusion compounds and molecular complexes.[2,13]

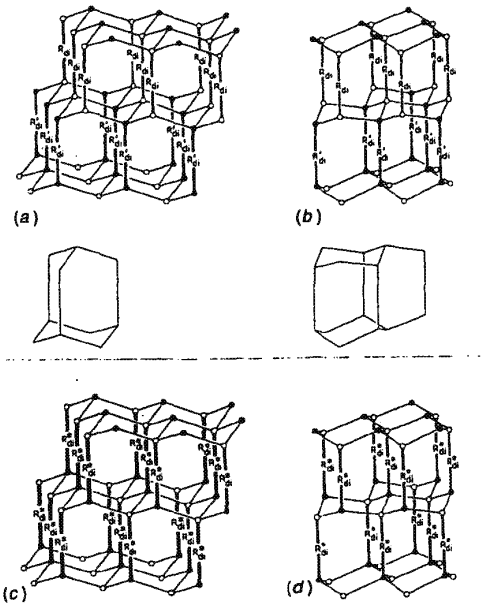
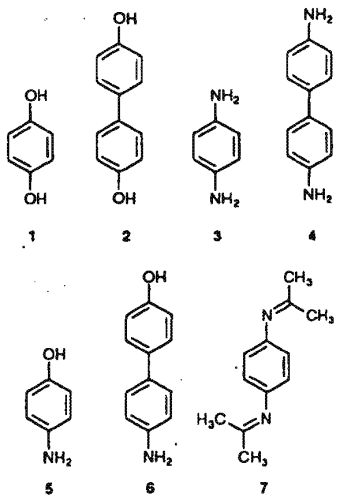


Fig. 7 3D super-tetrahedral H-bonded architectures of 1:1 complexes between linear dialcohols, HO–R_{di}–OH, and linear diamines, H_2N–R'_{di}–NH_2, and of linear amino alcohols, HO–R^*_{di}–NH_2. Oxygen atoms are represented as empty, nitrogen atoms as filled circles. The covalent linear linkers R_{di}, R'_{di} and R^*_{di} are drawn as thick rods, the H-bonds as thin lines omitting the bridging H atoms. The aggregation of the molecules is such that exclusively O(H)N hydrogen bonds are formed: (*a*) super-diamond network of dialcohol–diamine complex; super-adamantane building block diagrammatically shown below; (*b*) super-wurtzite network of dialcohol–diamine complex; combined super-iceane and super-bicyclo[2.2.2]octane building block below; (*c*) super-diamond, (*d*) super-wurtzite network of amino alcohol. The complexes **1·3**, **1·4**, **2·3** and **2·4** described in this paper aggregate diamond-like (*a*) in the crystal, the aminophenols **5** and **6** wurtzite-like (*d*).



UM00011551
NOVARTIS EXHIBIT 1517
Novartis v. Regents, IPR2023-01347
Page 297 of 4460

Table 1 Crystallographic details of the X-ray measurements[a]

Molecular system	1·3	1·4	2·3	2·4	5	6
Crystal system	Monoclinic	Monoclinic	Monoclinic	Monoclinic	Orthorhombic	Orthorhombic
Space group	$P2_1/c$	$P2_1/c$	$P2_1/c$	$P2_1/c$	$Pna2_1$	$Pna2_1$
Z	2	2	2	2	4	4
a/Å	13.0889(12)	17.094(3)	17.397(3)	21.321(3)	8.184(1)	8.096(1)
b/Å	5.2291(8)	5.351(1)	5.345(1)	5.403(1)	5.262(1)	5.396(1)
c/Å	8.2427(8)	8.130(3)	8.111(2)	8.076(1)	12.951(2)	21.217(2)
β/°	98.714(8)	92.68(2)	101.05(2)	95.61(1)		
V/Å^3	557.6(1)	742.8(3)	740.2(3)	925.9(2)	557.7(2)	926.9(2)
d_x/g cm^{-3}	1.300	1.316	1.320	1.329	1.300	1.327
d_m/g cm^{-3}	—	—	1.31	1.34	1.30	1.32
θ_{max}/°	30	27	27	27	30	27
N_{tot}	2163	2213	2174	2724	1196	1293
N_{indep}	1627	1617	1610	2015	912	1037
$[F_o/\sigma(F_o)]_{min}$	4	4	4	4	4	3
N_{ref}	1386	927	1007	1476	728	668
N_{var}	101	136	136	171	101	171
ρ_{res}/e Å^{-3}	0.23	0.42	0.17	0.15	0.18	0.20
p	0.0001	0.04	0.0005	0.0001	0.04	0.0006
R	0.043	0.065	0.049	0.043	0.043	0.055
R_w	0.045	0.072	0.049	0.041	0.047	0.049

[a] Collection of intensities on a CAD4 4-circle diffractometer at room temperature; Mo Kα radiation with λ = 0.710 69 Å; reflection weights in the refinements $w(F_o) = [\sigma^2(F_o) + pF_o^2]^{-1}$; reflections with $F_o/\sigma(F_o) < [F_o/\sigma(F_o)]_{min}$ excluded from refinement; N_{tot}, total number of reflections recorded; N_{indep}, number of independent reflections; N_{ref}, number of reflections included in refinement; N_{var}, number of refined variables; ρ_{res}, maximum residual electron density after refinement. The crystallographic calculations were performed with the program systems SDP (B. A. Frenz, Enraf-Nonius, Delft, Holland, 1978) and SHELX76 (G. M. Sheldrick, University of Cambridge, England, 1976).

This probably has to do with the fact that hydroquinone apparently has no possibility of establishing entirely satisfactory crystal packing as evidenced by its marked polymorphism (α, β, γ forms).[2] It is clear that the super-tetrahedral networks of Figs. 7(*a*), (*b*) created by the inter-(supra-) molecular combination of linear dialcohols and diamines should also be a favourable crystal-structural choice for linear amino alcohols H_2N–R^*_{di}–OH, such as *p*-aminophenol **5** and 4′-aminobiphenyl-4-ol **6**, which have their hydroxy and amino groups combined intramolecularly [Figs. 7(*c*), (*d*)]. X-Ray analyses of crystalline **5** and **6** have therefore also been undertaken; the resulting structures are described subsequently and their characteristics again turned out to be in line with our supramolecular design. It is noteworthy that a crude X-ray study of **5** was reported more than 40 years ago (photographic intensity estimates, incomplete refinements without consideration of H atoms, R = 0.19);[14] it is largely, yet not entirely, confirmed by our remeasurement as pointed out in the following section.

Experimental

Crystallizations

Commercial samples were used for the crystallizations, except 4′-aminobiphenyl-4-ol **6**, which was prepared from benzidine **4** by partial diazotization and subsequent hydrolysis. The 1:1 dialcohol–diamine molecular complexes **1·3**, **1·4**, **2·3** and **2·4** were grown from acetone at room temperature by dissolving equimolar amounts of the components and subsequent slow evaporation of the solvent. *p*-Aminophenol **5** was also crystallized from acetone at room temperature, **6** from ether. It is emphasized that the complex components and **5** were *dissolved* in acetone at room temperature, too, since heating easily leads to the formation of the Schiff bases between the amines and the solvent. This condensation reaction occurs to some extent even at room temperature and sometimes crystal mixtures were obtained. Obviously, the Schiff condensation is subject to acid catalysis, and the presence of the relatively acidic phenolic hydroxy groups may accelerate the reaction. It was found that addition of a small amount of triethylamine to the acetone solutions effectively quenches this acid catalysis leading to the desired crystals of the alcohol–amine molecular complexes and aminophenols, respectively, without complications. The double Schiff bases from the diamines and acetone are themselves capable of forming molecular complexes with hydroquinone **1** and 4,4′-dihydroxybiphenyl **2**. One example, *i.e.*, the 1:1 molecular complex (**1·7**) of hydroquinone **1** and the double Schiff base from *p*-phenylenediamine **3** and acetone, 1,4-bis-(isopropylideneamino)benzene **7**, was studied crystallographically in detail, and the results of the respective X-ray analysis are given in the Appendix. Samples of the complex crystals were redissolved and NMR spectra recorded in order to verify their composition and 1:1 stoichiometry.

X-Ray Analysis and Structure Refinement

The X-ray measurements were performed at room temperature on a four-circle diffractometer. Crystal data and details of the intensity measurements are collected in Table 1. All structures could be solved by conventional direct phasing methods without difficulties. The subsequent least-squares refinements likewise proceeded routinely and related data are included in Table 1. However, some comment is in order concerning one not entirely trivial point, that is the discrimination between oxygen and nitrogen atoms in the present crystal structures. This required some extra analytical efforts since the X-ray scattering power of oxygen and nitrogen is rather similar as the electron numbers of both atoms differ by one only, of course. The problem is thus in particular the distinction between hydroquinone **1** and *p*-phenylenediamine **3** in the crystals of their 1:1 complex **1·3**, and the identification of the analogous biphenyl systems **2** and **4** in **2·4**. Similarly, in the aminophenols **5** and **6**, the distinction between O and N establishes the orientation of the ON vector of these polar molecules in the crystal, *i.e.*, the direction of the molecular dipoles. Obviously, the problem of O,N distinction does not arise for the 'mixed' phenylene–biphenylene complexes **1·4** and **2·3**, for simple chemical reasons. Furthermore, it is clear that the assignment of O and N atoms is intrinsically related to the question of whether the crystal structures concerned are ordered or not. Now, in

UM00011552
NOVARTIS EXHIBIT 1517
Novartis v. Regents, IPR2023-01347
Page 298 of 4460

Table 2 Comparison of some characteristic bond lengths, bond angles, torsion angles, hydrogen-bond lengths, and 'super-torsion angles' of the described super-tetrahedral molecular complexes and aminophenols[a]

Molecular system	1·3	1·4	2·3	2·4	5	6
d CO/Å	1.376	1.373	1.379	1.378	1.379	1.390
d CN/Å	1.431	1.422	1.433	1.432	1.440	1.432
∠CCO/°	122.9	122.9	122.3	122.4	122.4	121.9
	117.8	118.3	118.1	118.4	118.0	118.5
∠CCN/°	121.4	121.6	121.0	121.3	120.7	121.1
	120.0	120.9	120.2	120.3	120.0	120.2
∠HOCC/°	10	3	12	12	11	6
∠HNCC/°	−43	−48	−46	−46	−48	−51
	18	6	16	15	14	10
d ON(O–H ··· N)/Å	2.773	2.780	2.786	2.796	2.776	2.811
d ON(O ··· H–N)/Å	3.127	3.131	3.152	3.155	3.142	3.137
	3.254	3.225	3.282	3.220	3.259	3.314
∠O(H)N(H)O(H)N/°	62.2	63.7	63.5	64.2	62.5	63.5
	−58.6	−61.6	−62.8	−64.1	−64.2	−64.4
	56.5	56.2	54.8	54.9	55.4	55.3
	−64.0	−65.3	−64.8	−65.4	−62.8	−64.4
	57.7	60.7	61.9	63.1	62.5	63.3
	−47.0	−45.9	−45.6	−45.3	−47.5	−45.9

[a] The top CCO and CCN angles are defined within the more synplanar HOCC and HNCC torsion angles (Fig. 8). Of the latter, those with magnitudes > 90° are not given. The super-torsion angles are defined within the H-bonded super-cyclohexane rings and are given in cyclic order (see the text). Standard deviations are in the range of the last significant digits and may roughly be estimated with the help of Fig. 8.

short, all the six crystal structures discussed here turned out to be completely ordered within the experimental crystallographic data available, both as regards the N,O distribution and the location of the bridging H atoms in the hydrogen bonds. Given this, the discrimination between O and N in these X-ray analyses was based on the following five criteria. (1) Interchange of O and N leads to *R*-factor increases typically of about 0.03 in suitable test refinements. (2) The temperature motion of O and N is similar if correctly assigned; if not, the atom mistakenly chosen as O assumes an isotropic B_{iso} value typically 2 Å^2 larger than that of the atom wrongly assigned as N, with their sum amounting roughly to twice the correct value. (3) Difference Fourier electron density maxima around O and N corresponding to hydrogen atoms unambiguously support the assignment chosen, in line with the other criteria throughout. (4) The C–O bond length is consistently shorter than the C–N length, on average by 0.055 Å (Table 2, Fig. 8; average C–O and C–N lengths measured for the six crystal structures, 1.378 and 1.433 Å, respectively), in agreement with other structural evidence on phenols and aromatic amines. (5) The two phenolic CCO angles differ by 4–5°, the angle *syn* to the HOC angle being the larger one throughout, in accord with earlier observations;[15] on the other hand, the two amine CCN angles deviate by only 0.6–1.4° (Table 8, Fig. 8). Altogether, these criteria provide compelling evidence for the O,N assignments adopted in the present crystal structure analyses; a still more rigorous discrimination than is possible with X-ray methods would require neutron diffraction measurements. Based on these same criteria, no disorder was perceptible in the six crystal structures under discussion (see above), and this conclusion is further corroborated by a general crystal chemical, *i.e.*, supramolecular comparison of the two 'mixed' phenylene–biphenylene complexes **1·4** and **2·3** with the other structures (see below). Finally, it should be noted that the above N,O discrimination and disorder tests, when applied to *p*-aminophenol **5**, consistently indicated that the choice of oxygen and nitrogen in the old X-ray study of Brown[14] was the wrong one and is to be reversed.

Details of the present X-ray analyses and selected structural data are collected in Table 1 and Fig. 8; atomic coordinates and temperature factors have been deposited at the Cambridge Crystallographic Data Centre*. In Table 2, some characteristic geometrical data of the six crystal structures are grouped together for comparison. The atomic numbering, bond lengths, and bond angles, as well as certain temperature motion properties may be found in Fig. 8. Figs. 9 and 10 present packing diagrams and characteristic supramolecular architectures of the individual structures.

Results and Discussion

Space Group and Molecular Symmetries

The four diphenol–diamine complexes **1·3**, **1·4**, **2·3** and **2·4** all crystallize in the centrosymmetric space group $P2_1/c$ with two formula units of complex in the unit cell (Table 1). Therefore, the molecular components of these complexes are all centrosymmetric in the crystal. This might have been expected for hydroquinone **1** and *p*-phenylenediamine **3**, since molecules centrosymmetric in the gas phase have a general propensity to retain this symmetry in the crystal.[16] The (average) crystallographic centrosymmetry of the biphenyl systems **2** and **4** is less trivial and implies effective planarity of these molecules, whereas, in the gas phase, non-centrosymmetric, non-planar structures twisted around the central C–C bond have to be reckoned with (see the section on Molecular Structure).

The two non-centrosymmetric, polar aminophenols **5** and **6** both crystallize in the likewise non-centrosymmetric, polar space group $Pna2_1$, with four molecules in the unit cell. Therefore, **5** and **6** have no crystallographic molecular symmetry, and no further structural conclusions may be drawn. Nonetheless, from the X-ray analysis the biphenyl compound **6** also turned out to have an essentially planar structure in the crystal. It is briefly anticipated at this point that a comparison of the cell constants of the six crystal structures under discussion (Table 1) would reveal striking similarities and regularities among the shapes of their unit cells. Clearly, this reflects close structural relationships between the six crystal architectures, and we shall come back to this more relevant point of our comparative supramolecular analysis in the section on Supramolecular Structure.

* For details of the CCDC deposition scheme, see 'Instructions for Authors (1994),' *J. Chem. Soc., Perkin Trans. 2*, 1994, issue 1.

UM00011553
NOVARTIS EXHIBIT 1517
Novartis v. Regents, IPR2023-01347
Page 299 of 4460

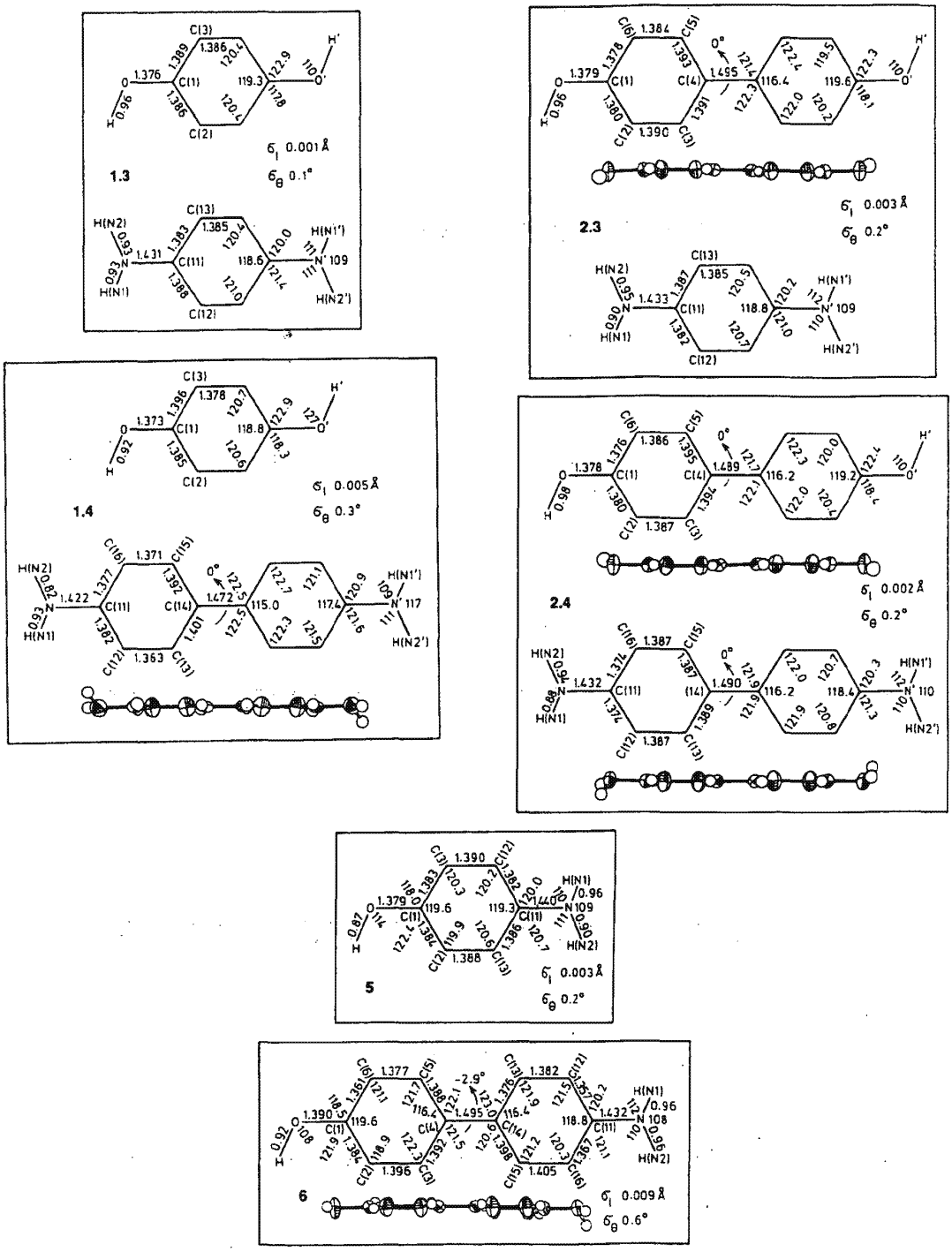


Fig. 8 Molecular structural data and atomic numbering of the diphenol–diamine complexes **1·3**, **1·4**, **2·3** and **2·4**, and the aminophenols **5** and **6**: bond lengths (Å), bond angles (deg), twist angle around central C–C bond of biphenyl systems; average estimated standard deviations of heavy-atom bond lengths (σ_l) and angles (σ_θ). For the biphenyl systems **2**, **4** and **6**, side views with heavy-atom anisotropic vibrational ellipsoids of 50% probability are shown (isotropic temperature factors of H-atoms divided by 3).

UM00011554
NOVARTIS EXHIBIT 1517
Novartis v. Regents, IPR2023-01347
Page 300 of 4460

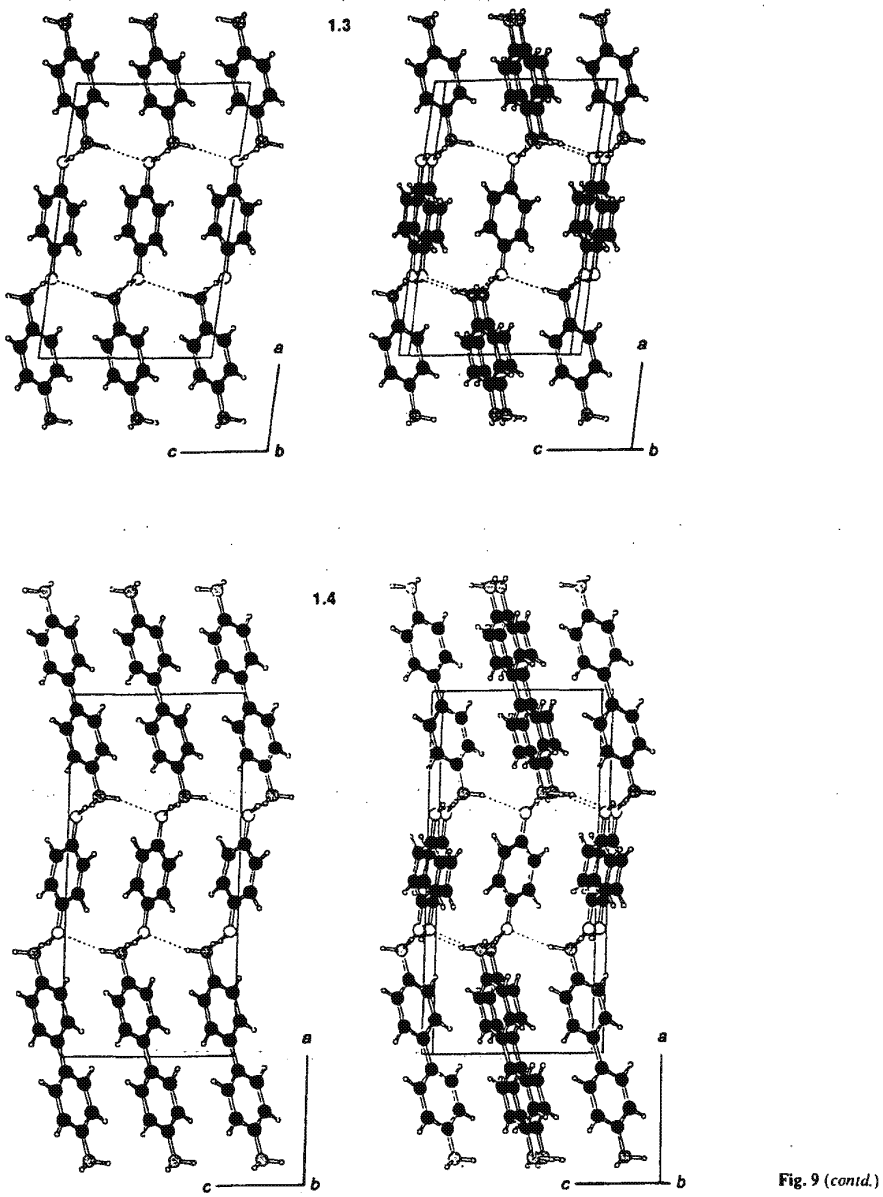


Fig. 9 (*contd.*)

Molecular Structure

The intramolecular geometrics of the molecules **1–6** making up the six crystal structures compared in this work are rather unexceptional and only a few points merit explicit comment. Numerical data substantiating the following discussion may be found in Table 2 and Fig. 8. Since both the intra- and intermolecular geometrical details of the various structures are strikingly similar, it is not necessary to analyse them individually but rather in summary.

The C–O bond lengths in the six crystal structures are normal (average 1.378 Å) and compare well with those of hydroquinone[2,15] and phenol (gas-phase value 1.374 Å[17]). However, the C–N bonds in the present structures (average length 1.433 Å) are somewhat longer than in crystalline and gaseous *p*-phenylenediamine (averages 1.409,[18a] 1.416,[18b] and 1.424 Å,[18b] respectively), or in gaseous aniline (1.402 Å[19]). Hydrogen bonding may be influential inasmuch as in the present structures the nitrogen lone pairs are involved in a relatively short O–H · · · N bond (average ON distance 2.787 Å) and are thus not fully available for π overlap with the aromatic ring. In crystalline *p*-phenylenediamine the weaker N(H)N bonds are all longer than 3.2 Å.[18] Furthermore, for the same reason the bonding geometry at the nitrogen atoms is more pyramidal in the present cases than in *p*-phenylenediamine and aniline. The crystal structural study of a complex, say, between hydroquinone and aniline (1:2) would be helpful to check this reasoning. The central C–C bond linking the two benzene rings of the present biphenyl systems is about 0.02 Å longer (average

UM00011555
NOVARTIS EXHIBIT 1517
Novartis v. Regents, IPR2023-01347
Page 301 of 4460

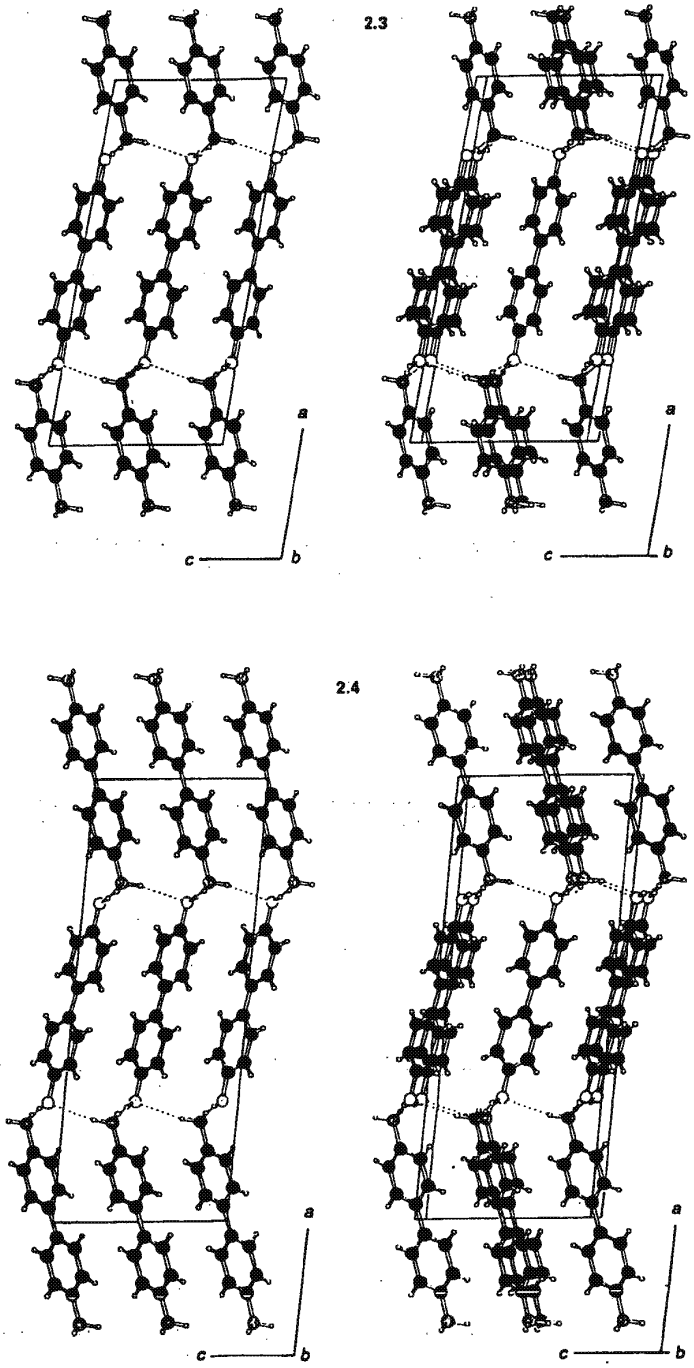


Fig. 9 (*contd.*)

1.488 Å) than a normal $C(sp^2)$–$C(sp^2)$ single bond owing to the inner non-bonded H···H repulsions (see below).

The CCO and CCN bond angles in the present structures merit a short comment. Their differences were used as a criterion to discriminate between O and N in the structure refinements as detailed in the Experimental section. The CCO angles a in *syn* disposition with respect to the COH angles are, on average, 4.4° larger than their *anti* partners. The effect has been noted earlier;[15] in the planar gaseous phenol molecule this angular difference amounts to 5.1°.[17] For obvious symmetry reasons, the corresponding CCN angular difference is much smaller (average 0.9°) but consistently the CCN angle involved

UM00011556
NOVARTIS EXHIBIT 1517
Novartis v. Regents, IPR2023-01347
Page 302 of 4460

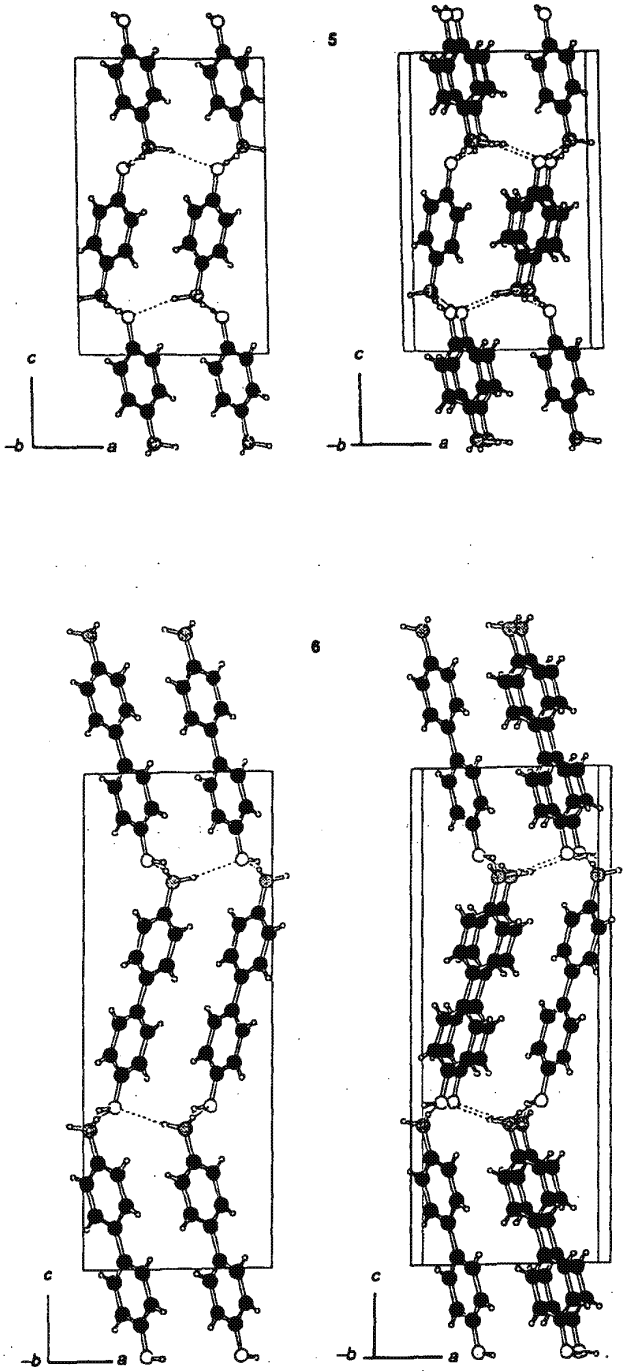


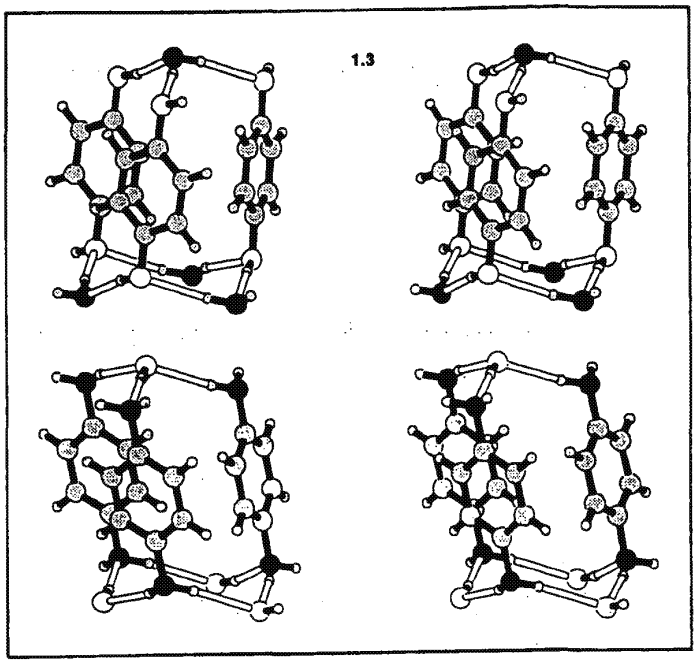
Fig. 9 Stereo packing diagrams of diphenol–diamine complexes and aminophenols with cell edges outlined: O, white; N, grey; C, black; H-bonds dotted. For all left-handed members of the stereo pairs, the view is along the short cell edge *b* (*ca.* 5.3 Å) defined by a 1,3 distance of the puckered H-bonded super-arsenic sheets,

in the smaller (roughly synplanar) CCCN torsion angle is again the larger one.

As regards the torsional structure of the present phenols and amines, two topics are highlighted, that is the planarity of the biphenyl systems and the conformations of the hydroxy and amino groups. The torsional structure of biphenyl has been the

UM00011557

NOVARTIS EXHIBIT 1517
Novartis v. Regents, IPR2023-01347
Page 303 of 4460



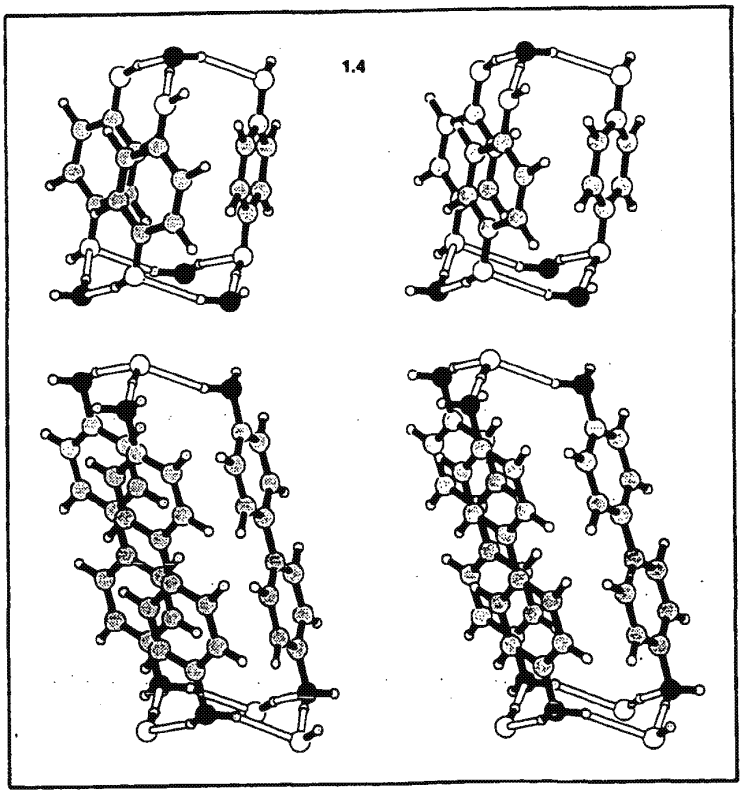


Fig. 10 (*contd.*)

UM00011558
NOVARTIS EXHIBIT 1517
Novartis v. Regents, IPR2023-01347
Page 304 of 4460

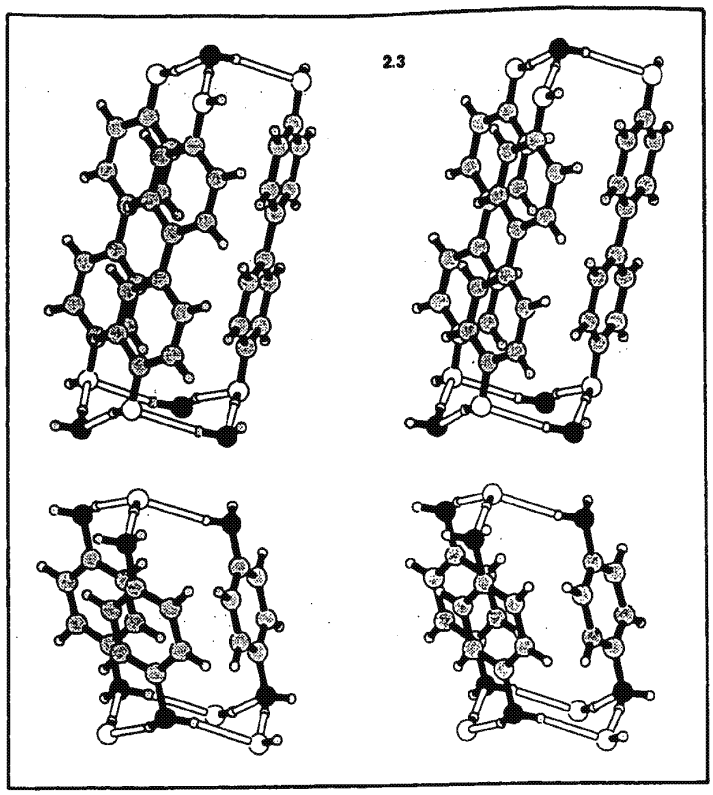


Fig. 10 (*contd.*)

subject of numerous experimental and theoretical studies[20a] since it depends on a subtle balance between π overlap of the benzene rings (favouring planarity) and the inner non-bonded H···H repulsions (favouring a non-planar structure twisted about the central C–C bond). The two opposing effects almost cancel each other. In the gas phase, biphenyl has a non-planar structure of D_2 symmetry with the two benzene rings twisted about the central C–C bond by *ca.* 45°[20a] whereas in the crystal at room temperature the molecule is (on average) centrosymmetric (space group $P2_1/c$ with two molecules in the unit cell) indicating effective planarity. Temperature motion analysis yields relatively large librational motion about the central C–C bond, however, which may, in fact, correspond to a double-minimum twisting potential such that the crystal structure would be disordered and consist of a statistical mixture of twisted molecules executing low-energy high-amplitude twisting vibrations across a shallow barrier, *i.e.*, a planar transition state.[21] At 40 K, biphenyl undergoes a phase transition leading to a non-centrosymmetric crystal structure, and at 22 K a twist angle of about 10° was measured by neutron diffraction.[20b] A number of substituted biphenyls (excluding *ortho* substitution) were found to behave largely alike.[20c]

In the four present crystal structures involving biphenyl systems, *i.e.*, **1**·**4**, **2**·**3**, **2**·**4** and **6**, the heavy-atom skeletons of these molecules are effectively planar. In the three molecular complexes, crystallographic centrosymmetry is imposed (see the above section on Space Group and Molecular Symmetries), which implies untwisted structures and, together with the observed trigonal planar bonding at the sp^2 carbon atoms, planarity. Inspection of the anisotropic temperature motion, *i.e.*, the atomic vibrational ellipsoids shown in Fig. 8, suggests some enhanced, but not excessive, torsional motion around the central C–C bonds of **2** and **4**, such that, all in all, it appears appropriate to refer to them as virtually planar. Clearly, this reasoning strictly applies only to *average* structures and symmetries, and subtle disorder effects in terms of torsionally interconverting, slightly twisted structures cannot be rigorously ruled out. No crystallographic symmetry is imposed on 4'-aminobiphenyl-4-ol **6**, which is nevertheless also observed to be essentially planar in the crystal (twist angle around the central C–C bond 2.9°). There is room for the belief that biphenyl planarity is stabilized in the present cases by crystal packing forces, *i.e.*, by the stacking of the aromatic rings and hydrogen bonding constraints, but quantitative evidence supporting this assumption is hard to produce from our data. As noted above, planarity of crystalline biphenylene itself is also supported by packing forces, and the stacking of the molecules is similar to that of the biphenylylene units in our present cases (see below). Finally, the direct intramolecular influence of the substituents in our biphenyl derivatives is difficult to assess without quantitative calculations.

The phenolic OH groups in the present crystal structures lie approximately in the plane of the benzene rings and the maximum deviations of the HOCC torsion angles from planarity amount to 12° (average 9°, Table 8). This may be compared with the phenol molecule, which, in the gas phase, is completely planar.[17] Likewise, the conformation of the amino groups in the present structures is roughly similar to that in aniline, which in the gas phase involves a mirror plane running perpendicular to the benzene ring and bisecting the NH_2 group.[19] On average, the amino groups of the present molecules are rotated out of this symmetric arrangement by a maximum

UM00011559
NOVARTIS EXHIBIT 1517
Novartis v. Regents, IPR2023-01347
Page 305 of 4460

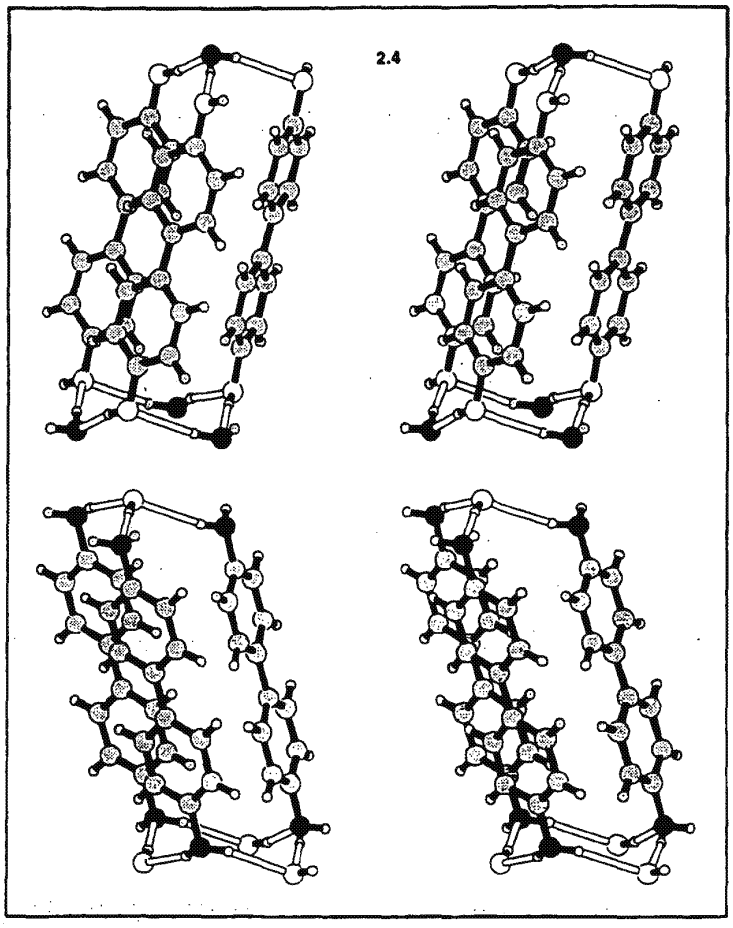


Fig. 10 (*contd.*)

of 21° (averaged 17°, Table 8). Obviously, these conformational deviations from ideal mirror symmetries are dictated by packing requirements such as favourable hydrogen bonding and efficient stacking of the aromatic residues.

Supramolecular Structure

The four linear dialcohol–diamine molecular complexes **1**·**3**, **1**·**4**, **2**·**3**, **2**·**4**, and the two linear aminophenols **5** and **6** build up the expected (see the Introduction) super-tetrahedral H-bonded architectures in the crystal. In the perfectly ordered crystal structures, every O and N atom is engaged in 3 H bonds with approximately tetrahedral coordination. In all six cases, exclusively O(H)N bonds are observed. *i.e.*, each oxygen atom is H-bonded to three nitrogen atoms, and each nitrogen atom to three oxygen atoms. The hydrogen bonds are arranged in all-*trans* fused 'super-cyclohexane' chairs, which form infinite H-bonded 'super-arsenic' sheets [Fig. 5(*b*)] held together by the covalent *p*-phenylene and *p*,*p*'-biphenylylene bridges (spacers). The puckered H-bonded sheets are, in all respects, very similar structurally (Table 2, Figs. 9–11). In all cases, we have three crystallographically independent O(H)N bonds, one O–H···N and two O···H–N bonds, as stoichiometrically required. The H-bonds of the former type are relatively short (average ON distance 2.787 Å), those of the latter type rather long (average ON distances 3.141 and 3.292 Å; Table 2). The degree of puckering of the H-bonded super-arsenic sheets may be quantified by the O(H)N(H)O(H)N 'super-torsion angles' of the super-cyclohexane chairs, whose values averaged over the six crystal structures are in cyclic order 63.3, −62.6, 55.5, −64.5, 61.5, −46.2° (Table 2; note the strikingly close similarity of the individual values). It is readily seen that these super-torsion angles satisfy fairly well D_{3d} and closely C_2 chair ring symmetry. Furthermore, their roughly synclinal magnitudes imply approximately tetrahedral N(H)O(H)N and O(H)N(H)O angles on average, and thus the super-cyclohexane chair ring pucker of the H-bonded super-arsenic sheets happens to be similar to that of cyclohexane itself.

The extensive supramolecular similarities and regularities among the present six super-tetrahedral crystal architectures are already expressed rather conspicuously through the dimensions of their crystallographic unit cells (Table 1). It may be seen that all these cells have a similar small edge of about 5.3 Å length and a similar medium edge about 8.1 Å long. These lengths are determined by the dimensions of the H-bonded super-arsenic sheets, and correspond to 1,3 and 1,5 distances within the fused super-cyclohexane architectures as illustrated in Fig. 11. The large cell edges may be grouped into three pairs of about 13.0, 17.2 and 21.3 Å length. They are essentially brought about by the width of the H-bonded super-arsenic

UM00011560
NOVARTIS EXHIBIT 1517
Novartis v. Regents, IPR2023-01347
Page 306 of 4460

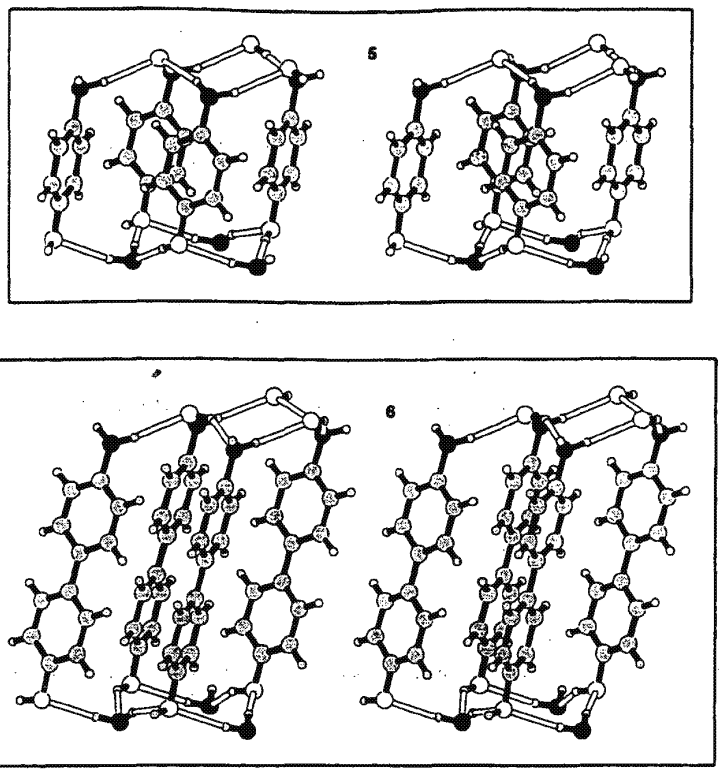


Fig. 10 Stereo views of the super-adamantane building blocks of the complexes **1·3**, **1·4**, **2·3** and **2·4**, and the fused super iceane/super-bicyclo-[2.2.2]octane units of **5** and **6** as cut out of the H-bonded super-diamond and super-wurtzite networks, respectively: O, white, N, black, C, grey; H-bonds represented as open rods. In the complexes, two different super-adamantane units occur, depending on whether the *p*-phenylene and *p*,*p*′-biphenylylene spacers involved belong to the diphenol (top) or the diamine partner. Note that the long axes of the aromatic spacers do not run exactly orthogonal to the mean planes of the H-bonded sheets, but are tilted away from orthogonality at the O and N atoms in opposite directions (see the text for details concerning these distortions).

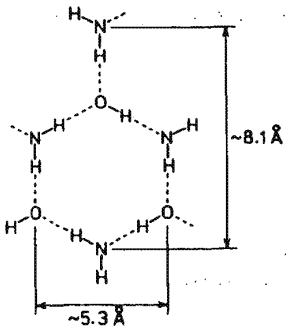


Fig. 11 Interpretation of the small and medium unit cell edges of the complexes **1·3**, **1·4**, **2·3** and **2·4**, as well as **5** and **6**, in terms of the dimensions of the puckered H-bonded sheets. The larger cell edges are determined by the length of the aromatic spacer bridges protruding roughly (but not exactly) at right angles from the H-bonded sheets, and by the latter's thickness.

sheets (*ca.* 1.00 Å) and the length of the *p*-phenylene and *p*,*p*′-biphenylylene spacers linking them. These spacer lengths may be approximated as multiples of an average bond length of *ca.* 1.38 Å, and, with the help of Fig. 9, it may be seen that the lengths (in Å) of the large cell edges are reproduced rather well by the expression $2 \times 1.00 + 8 \times 1.38 + 3n \times 1.38 = 2.00 + (8 + 3n) \times 1.38$, where n equals 0,1,2 depending on whether the spacers are exclusively *p*-phenylene as in **1·3** and **5**, alternately *p*-phenylene and *p*,*p*′-biphenylylene as in **1·4** and **2·3**, or exclusively *p*,*p*′-biphenylylene as in **2·4** and **6**. Note that this geometric analysis does not account for the fact that the long axes of the spacers are not exactly orthogonal to the mean plane of the H-bonded super-arsenic sheets (see below) and that the cell edges of the monoclinic complexes are of course not all exactly orthogonal; ensuing corrections are small, however. As detailed further below, it so happens that the steric requirements for satisfactory hydrogen bonding in the puckered super-arsenic sheets and favourable lateral stacking of the aromatic spacers comply well with each other, as is required, of course, for an energetically favourable overall crystal packing.

The very similar super-tetrahedral H-bonded crystal architectures of the four linear diphenol–diamine complexes **1·3**, **1·4**, **2·3** and **2·4** are distorted cubic-diamond-like or zinc-blende-like, those of the linear aminophenols **5** and **6** distorted hexagonal-diamond-like or wurtzite-like (Figs. 7, 9, 10). The wurtzite analogy of the latter is closer than the zincblende relationship of the former, since, in the crystals of **5** and **6**, every oxygen atom is indeed tetrahedrally coordinated to four nitrogen atoms and every nitrogen atom to four oxygen atoms [three times *via* O(H)N hydrogen bonds, once *via* the covalent aromatic bridge]; in the diamondoid complexes every oxygen atom is coordinated to three nitrogen atoms and one oxygen atom, and every nitrogen atom to three oxygen atoms and one

UM00011561
NOVARTIS EXHIBIT 1517
Novartis v. Regents, IPR2023-01347
Page 307 of 4460

nitrogen atom. Fig. 10 provides views of characteristic building blocks cut out of the super-tetrahedral networks, *i.e.*, super-adamantane units to represent the super-diamond architectures, and fused super-iceane/super-bicyclo [2.2.2]octane units to represent the super-wurtzite networks. (As regards the trivial name 'iceane' attached to tetracyclo[5.3.1.$1^{2,6}$.$0^{4,9}$]dodecane, note that normal hexagonal ice builds up a super-wurtzite network; *cf.* the Introduction.)

The diamondoid nature of the crystal architectures of the diphenol–diamine complexes and, in particular, the wurtzite-like crystal structures of the aminophenols are also expressed by comparing the associated space-group symmetries. The space group of the former, $P2_1/c$, is a (remote) subgroup of that of cubic diamond, $Fd\bar{3}m$, while the space group of the latter, $Pna2_1$, is a maximal non-isomorphous subgroup of that of wurtzite, $P6_3mc$.[22] (Note that the wurtzite space group is in turn a subgroup of $P6_3/mmc$ applying to hexagonal diamond.) On the other hand, $P2_1/c$ is not a subgroup of the non-centrosymmetric zincblende space group $F\bar{4}3m$. ($F\bar{4}3m$ is of course a subgroup of the diamond space group $Fd\bar{3}m$.) Thus the crystallographic molecular centres of symmetry of the diphenol–diamine complexes are the only remaining point-group symmetries of the diamond lattice, *i.e.*, a quarter of diamond's symmetry centres located on the midpoints of the C–C bonds. On reducing the crystal symmetry of wurtzite to that of the aminophenols no point group symmetry is conserved.

It is of some interest to reflect briefly on the abovementioned distortions of the H-bonded super-diamond and super-wurtzite networks in the diphenol–diamine complexes and aminophenols, respectively, relative to the ideal geometries of diamond and wurtzite themselves. Clearly, the present supramolecular lattices are elongated along former threefold axes of diamond and wurtzite since the covalent aromatic spacer bridges are longer than the O(H)N distances of the hydrogen bonds. A second, more interesting mode of distortion refers to the fact that the long axes of the aromatic spacers, *i.e.*, the vectors interconnecting the two hetero atoms, do not run exactly orthogonal to the mean planes of the puckered H-bonded super-arsenic sheets, but in all cases are tilted away from orthogonality by typically 10–15° (Figs. 9, 10). The tilt essentially corresponds to a rotation about the short crystallographic *b* axis by this amount. Inspection of the Figures reveals that the tilts at oxygen and nitrogen are always opposite in the sense that in all cases at the oxygen atoms the aromatic bridges are tilted outward away from the interior of an H-bonded super-cyclohexane ring, while at the nitrogen atoms, a corresponding inward tilt toward an $(OHNH)_3$ ring interior is always observed. Probably, the tilt phenomenon has to do with how the aromatic spacers pack together in their layers between the H-bonded super-arsenic sheets. This aromatic stacking follows a herring-bone pattern with edge-to-face (ETF) contacts among neighbouring aromatic systems. The observed tilting distortion ensures that aromatic H-atoms roughly assume a (favourable) position above the interior of a benzene ring of an ETF disposed neighbouring molecule (Figs. 9, 10). It is interesting to note that the corresponding packing characteristics of the parent hydrocarbons benzene[23] and biphenyl[24] are exactly alike.[25] However, we have no convincing explanation to offer as regards the *opposite* direction of tilting at the oxygen and nitrogen atoms, respectively.

The question arises as to why the four diphenol–diamine complexes **1**·**3**, **1**·**4**, **2**·**3** and **2**·**4** choose to build up super-diamond architectures in the crystal, whereas the two aminophenols **5** and **6** prefer the super-wurtzite alternative. An explanation of this different supramolecular behaviour is not obvious, since both packing modes are expected to be energetically very similar. (Note that hexagonal diamond is only about 1.5 kcal mol^{-1} less stable than cubic diamond.) That the four molecular complexes aggregate in diamondoid fashion appears empirically plausible since they are made up of centrosymmetric molecules, which generally tend to preserve this symmetry in the crystal (see the section on Space Group and Molecular Symmetries). Obviously, centrosymmetry may only be kept in a diamondoid network, not in a polar wurtzite-like architecture. But why are the H-bonded super-arsenic sheets in the two aminophenol crystals connected wurtzite-like and not zincblende (diamond)-like by the aromatic spacer bridges? A partial answer may possibly be provided by the following line of arguments. It was noted above that the aromatic spacer bridges experience a tilt with respect to the normal of the planes of the H-bonded sheets in order to improve the edge-to-face stacking within the aromatic layers, and that this tilt is always opposite at oxygen and nitrogen. Whatever the deeper reasons for these opposing orientational preferences at oxygen and nitrogen may be, it is immediately clear that in case of the aminophenols they may only be satisfied within a wurtzite-type lattice, since here the tilting distortion is anti-symmetric with respect to the mean plane through the aromatic layers. In the diphenol–diamine complexes, on the other hand, the tilting direction at both ends of the spacer bridges is the same, which is only ensured in a diamond-type lattice, since here the tilting distortion is symmetric with respect to the aromatic symmetry centres. Thus it appears possible that the opposite tilting preferences at oxygen and nitrogen determine whether a super-zincblende or a super-wurtzite network is built up. Another possibility could be that the super-wurtzite and super-zincblende supramolecular alternatives, respectively, of our systems exist as energetically similar polymorphs; variable temperature studies would be required to settle this question.

The supramolecular H-bonded crystal architectures of the aminophenols **5** and **6** are the first organic examples of super-wurtzite structures, counting, for example, the stable form (I_h) of ice or the SiO_2 polymorph tridymite as inorganic representatives. A partly organic case of a large H-bonded super-wurtzite network is discussed in the following section on Related Structures. It may generally be stated that large super-wurtzite architectures are rare, whereas many examples of the super-diamond alternative are, by now, known. This holds in particular for multiple, interpenetrating super-tetrahedral networks,[11] which are diamondoid in all cases studied so far. Why is this so? In the case of single networks there is little to argue in favour of either one of the two alternatives, which should occur with about equal abundance. The small energetic differences between the diamondoid and wurtzite-like structures of ice (ice-I_c, ice-I_h), SiO_2 (crystobalite, tridymite), and also of carbon (cubic diamond, hexagonal diamond; see above) and ZnS (zincblende, wurtzite) themselves may serve to support this expectation. Solid-state inclusion compounds with single super-tetrahedral host lattices based on $Cd(CN)_2$,[26,27] metal complexes of tetrahedral tetranitriles,[27] and tetrahedral tetralactams[28] have recently been described, which are all diamondoid. This might also be due to the guest species inasmuch as it seems conceivable that a super-wurtzite framework is more shape-demanding towards molecular guests since it involves two types of cage (50% larger super-iceane, 50% smaller super-bicyclo[2.2.2]octane cavities), whereas a super-diamond host has exclusively (medium-sized) super-adamantane cages. (But note, however, that a super-zincblende network with two different types of tetrahedral centre has, likewise, two different kinds of super-adamantane cage!) On the other hand, the fact that multiple, (self-) interpenetrating super-wurtzite networks have never been observed, may readily be rationalized in terms of simple but stringent symmetry requirements: the iceane and bicyclo[2.2.2]octane cages of the wurtzite lattice have only trigonal symmetry (ideally D_{3h}), whereas the local symmetry of the tetravalent lattice points is

UM00011562
NOVARTIS EXHIBIT 1517
Novartis v. Regents, IPR2023-01347
Page 308 of 4460

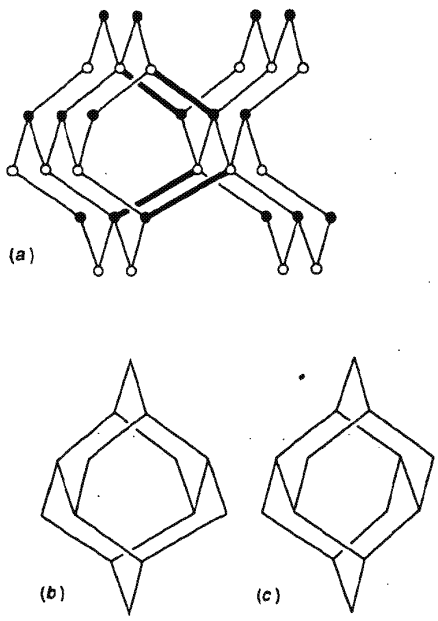


Fig. 12 (*a*) Super-tetrahedral H-bonded 3D network of crystalline ethanolamine, $HOCH_2CH_2NH_2$ (diagrammatic, based on X-ray data of ref. 31). O, white, N, black spheres; O(H)N hydrogen bonds drawn as thin lines, covalent ethylene linkers, $-CH_2CH_2-$, as thick black rods. The H bonds span 'super-black phosphorus' sheets with *cis*-decalin-like structural elements, which are covalently bridged by the ethylene linkers in non-diamondoid fashion (non-equivalent ON distances of the H-bonds, 2.785, 3.138, 3.282 Å[31]). (*b*) Skeleton of hypothetical D_2 symmetric 'isodiamantane' (pentacyclo-[8.4.0.0^{3,8}.0^{5,14}.0^{7,12}]tetradecane), which may be cut out of the H-bonded ethanolamine network and represents its characteristic building block. (*c*) Skeleton of D_{3d} symmetric diamantane (pentacyclo-[7.3.1.1^{4,12}.0^{2,7}.0^{6,11}]tetradecane).

tetrahedral (ideally T_d), such that self-interpenetration is hardly possible; for extremely large networks this might perhaps not hold, but even then the degree of interpenetration should be limited. In contrast, the lattice points and adamantane cages of the diamond lattice have the same symmetry (T_d) and self-interpenetration of super-diamond networks is readily possible. A similar case in point is the octahedral cubic primitive polonium (or ReO_3) lattice whose hexavalent lattice points and cube-shaped cages have the same symmetry (O_h) thus permitting supramolecular self-interpenetration. Multiple, interpenetrating super-octahedral networks are present in β-hydroquinone and related inclusion compounds,[2] Nb_6F_{15},[29] and $Ag_3Co(CN)_6$[30] with double, double and triple (distorted) super-polonium networks, respectively.

Related Structures

The crystal structure of ethanolamine, $HOCH_2CH_2NH_2$, has recently been reported[31] but no description of the type of hydrogen-bonded network adopted in the crystal was given. Not unexpectedly, a closer look at this architecture reveals it to be (distorted) super-tetrahedral, but in a novel fashion. As in our present cases, exclusively O(H)N hydrogen bonds are formed, 1.5 each per oxygen and nitrogen atom, which, however, do not span super-arsenic but super-black phosphorus sheets [Fig. 5(*c*)]. These sheets with partially *cis*-fused super-cyclohexane chairs are bridged covalently by the ethylene units, $-CH_2CH_2-$, to form a single three-dimensional super-tetrahedral network, yet not in diamondoid fashion. The characteristic building block of this network corresponds to the twisted carbon skeleton of hypothetical pentacyclo-[8.4.0.0^{3,8}.0^{5,14}.0^{7,12}]tetradecane ('isodiamantane', symmetry D_2), which might be related to that of diamantane (D_{3d}) as shown in Fig. 12. As in the aminophenols **5** and **6** with wurtzite-like H-bonded networks, every oxygen atom of ethanolamine is coordinated to four nitrogen atoms and *vice versa*, such that we might refer to the H-bonding pattern of $HOCH_2CH_2NH_2$ as 'isozincblende'-like. We are not aware of another example of this new variant of a 3D 4-connected network.

Given the super-tetrahedral 3D network of ethanolamine brought about by forming the maximum possible number of hydrogen bonds, 1:1 complex formation between ethyleneglycol, $HOCH_2CH_2OH$, and ethylenediamine, $H_2NCH_2CH_2NH_2$, may be expected and again a supertetrahedral, probably also 3D 4-connected network foreseen in the crystal. We have not studied this system as yet, which would require low-temperature crystallizations and X-ray intensity measurements. Support in favour of complex formation between ethyleneglycol and ethylenediamine may be derived from the simple observation that mixing of the two liquids is accompanied by very substantial heat evolution.

As a lower homologue of ethanolamine, hydroxylamine, $HONH_2$, the simplest possible amino alcohol, is, of course, also a potential candidate as regards the creation of a H-bonded super-tetrahedral network. X-Ray crystallographic evidence on hydroxylamine[32] indeed bears out this conjecture. Hydroxylamine forms a single 3D 4-connected network in the crystal consisting of undulating H-bonded sheets linked by covalent O–N bonds (Fig. 13). Every oxygen atom is H-bonded to three nitrogen atoms and *vice versa*, in a rather distorted tetrahedral fashion. Thus again exclusively O(H)N hydrogen bonds occur. The H-bonded sheets consist of fused distorted super-cyclohexane boats, and are connected by the covalent O–N bonds, in a mode which is neither diamond- nor wurtzite-like. Again we are not aware of any other example with this type of network.

We conclude this section with a brief discussion of the only other chiefly organic super-wurtzite architecture known (to us). It occurs in a formal 1:1 complex between ammonium tetrafluoroborate and urotropin, $NH_4BF_4\cdot(CH_2)_6N_4$, the crystal structure of which was determined some time ago[33] yet not analysed as regards packing and supramolecular structure. The super-wurtzite network is undistorted in this case and brought about by super-tetrahedral N(H)N hydrogen bonding between the tetrahedral ammonium cations and the tetrahedral urotropin molecules, which are readily seen to enjoy a relationship of perfect H-bond donor–acceptor complementarity. The symmetry characteristics of this super-wurtzite network are exactly the same as those of wurtzite itself, *i.e.*, the crystallographic space group is, in both cases, $P6_3mc$ with two formula units in the unit cells. Transforming both crystal architectures into one another simply requires replacement of Zn^{2+} by NH_4^+ and of S^{2-} by $(CH_2)_6N_4$, or *vice versa*. Each super-iceane cage of the cationic H-bonded $NH_4^+\cdot(CH_2)_6N_4$ super-wurtzite network houses a BF_4^- anion, while the super-bicyclo[2.2.2]octane cages are essentially filled up by their own constituents without leaving empty spaces (Fig. 14). $NH_4BF_4\cdot(CH_2)_6N_4$ therefore has the characteristics of a solid-state host–guest inclusion compound and should be more appropriately formulated as $[NH_4\cdot(CH_2)_6N_4]BF_4$. The shape complementarity of the BF_4^- guest anions and the cavities of a super-diamond (super-zincblende) host architecture of H-bonded NH_4^+ and urotropin is apparently less good than in the super-wurtzite alternative, and various qualitative speculations may be advanced to explain this; a more rigorous molecular modelling study should provide quantitative insight. The ammonium-

UM00011563
NOVARTIS EXHIBIT 1517
Novartis v. Regents, IPR2023-01347
Page 309 of 4460

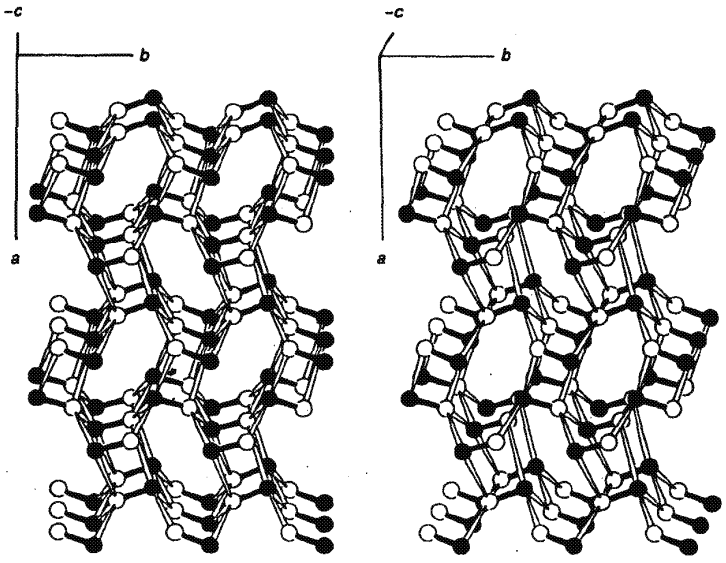


Fig. 13 Stereoview of the super-tetrahedral H-bonded 3D network of crystalline hydroxylamine, $HONH_2$ (based on O, N X-ray coordinates of ref. 32, H atoms not localized in this analysis): O, white, N, black spheres; O(H)N hydrogen bonds drawn as open white, covalent O–N bonds as filled black sticks. The H-bonds span undulating sheets consisting of fused distorted 'super-cyclohexane' boats connected covalently by the O–N bonds neither diamond- nor wurtzite-like (non-equivalent ON distances of the H-bonds, 2.74, 3.07, 3.18 Å [32]).

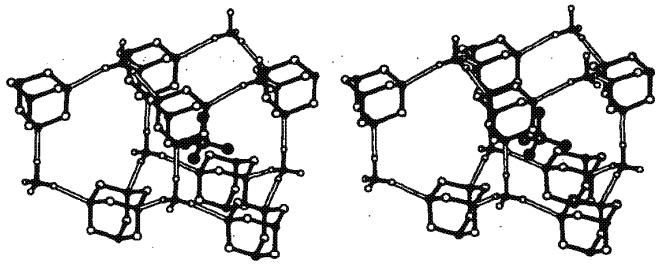


Fig. 14 Stereoview of the combined super-iceane and super-bicyclo[2.2.2]octane building block cut out of the cationic H-bonded, undistorted super-wurtzite network of $[NH_4{\cdot}(CH_2)_6N_4]BF_4$ (based on the X-ray coordinates of ref. 33; non-equivalent NN distances of H bonds, 2.999 and 3.025 Å): N, black, C, white large spheres, methylene H atoms omitted; H bonds drawn as open white sticks. The 3D network is made up of H-bonded ammonium cations and urotropin; each of its super-iceane cages enclathrates a tetrafluoroborate anion, which is also illustrated.

urotropin super-wurtzite network involves two symmetry-independent H_3N^+–H···N hydrogen bonds with NN distances of 2.999 and 3.025 Å. For an N(H)N hydrogen bond, these values are comparatively short, most likely chiefly due to the positive ammonium charge. The negative charge on the BF_4^- anions might also help to contract the host lattice and thus the hydrogen bonds. It is amusing to note that the original authors of this interesting super-tetrahedral structure confined their published discussion to essentially the single statement: 'Indications supporting hydrogen bonds are not observed' [33]!

Conclusions

The present study shows that even with standard organic chemicals interesting new supramolecular chemistry can be engineered on the basis of simple but effective complementarity criteria. Specifically, it could be shown that due to the complementarity of the hydroxy and amino groups, molecular recognition occurs among alcohols and primary amines. The respective molecular complex formation is accompanied by a 50% increase of the number of hydrogen bonds, and in the case of the present dialcohols and diamines, as well as amino alcohols, leads to H-bonded three-dimensional, super-tetrahedral networks, in particular super-diamond and super-wurtzite architectures (3D 4-connected nets). However, other network types should also be possible, including sheet-like 2D 4-connected nets. Indeed, the study of H-bonded supramolecular structures may lead to the creation or perception of entirely new network connectivities.

The present concept of H-bond maximization through complex formation between systems with complementary H-bond donors and acceptors may be extended from the three-dimensional tetrahedral to the two-dimensional trigonal-planar case. An example is the pair cyanuric acid–melamine forming a very stable 1 : 1 molecular complex, which probably takes up a planar trigonal 'super-graphite' sheet structure (the analogy with trigonal boron nitride, BN, being even closer) with triply hydrogen-bonded molecular neighbours [Fig. 15(*a*)].[34] It is easily seen that the in-plane H-bond donors and acceptors (lone pairs) of cyanuric acid and melamine are perfectly complementary both as regards their number and directionality: cyanuric acid has three in-plane donors and six acceptors,

UM00011564
NOVARTIS EXHIBIT 1517
Novartis v. Regents, IPR2023-01347
Page 310 of 4460

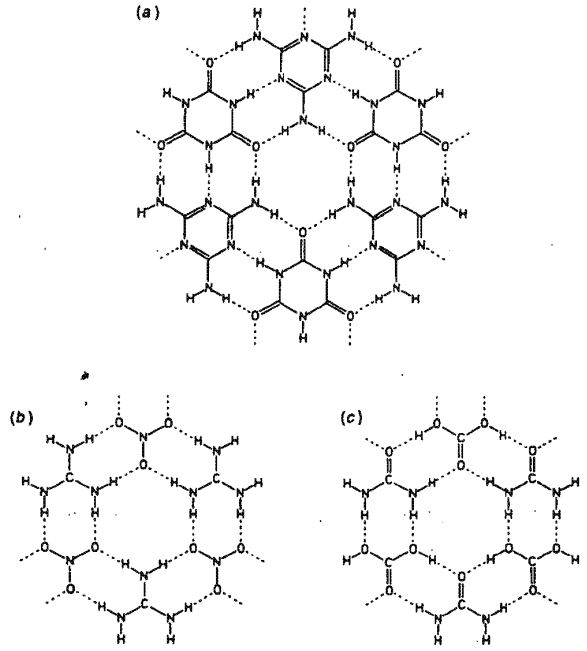


Fig. 15 (*a*) Probable triply H-bonded 2D sheet architecture of the 1 : 1 complex between melamine and cyanuric acid; (*b*) probable doubly H-bonded sheet structure of guanidinium nitrate; (*c*) suggested doubly H-bonded sheet structure of the hypothetical 1 : 1 complex between urea and carbonic acid

melamine six donors and three acceptors. Thus in the 1 : 1 complex the number of donors and acceptors is balanced, which, together with the directional complementarity, allows maximum H-bonding.[35] Another lucid example is provided by guanidinium nitrate, $C(NH_2)_3NO_3$, which is likely to form analogous, yet only doubly H-bonded planar sheets [Fig. 15(*b*)]. In line with this conjecture, we obtained large trigonal-pyramidal crystals of this salt from aqueous solution, which are rather hard along the trigonal axis, yet very soft perpendicular to it (graphite-like behaviour). X-Ray photographs show reflections of poor sharpness probably owing to disturbed, partially disordered sheet stacking. Crude unit-cell dimensions could nevertheless be obtained, which support the suggested sheet structure (rhombohedral crystal symmetry, hexagonal cell edges approximately $a = 7.3$, $c = 18.6$ Å, indicating an O(H)N distance of 2.90 Å and an average stacking separation of $c/6 =$ 3.1 Å; the large c constant implies a rather complex stacking pattern with six sheets per repeating unit). This architecture is very similar to that of orthoboric acid, $B(OH)_3$, which displays graphitic cleavage properties, too (potential lubricants). With its trigonally oriented three OH groups and three in-plane lone pairs, boric acid is of course perfectly self-complementary as regards optimal in-plane hydrogen bonding. The structure of guanidinium perchlorate is also of this sheet-type with one oxygen atom not involved in H-bonding.[36] A third hypothetical example worth speculating about in this context concerns a conceivable 1 : 1 complex between urea, $CO(NH_2)_2$, and carbonic acid, $CO(OH)_2$ [Fig. 15(*c*)]. Strictly speaking, only stoichiometric complementarity of in-plane H-bond donors and acceptors is present in this molecular pair without, however, precluding the possibility of creating doubly H-bonded super-graphite trigonal sheets similar to those of guanidinium nitrate or $B(OH)_3$. 'Expanding' carbonic acid in this hypothetical aggregate to 5-nitroisophthalic acid may also be envisaged, but the doubly H-bonded honeycomb sheets of such a complex would suffer from appreciable hexagonal holes.

Two potential applications exploiting the affinity between alcohols and primary amines as established in the present work, might be the following. (1) Alcohol–amine complexes could be useful as crystalline supramolecular derivatives of alcohols and amines with poor crystallization propensity, in particular of polyols, notoriously troublesome in this respect. (2) Bio-ethanol from fermentation processes is obtained in dilute aqueous solution and has to be concentrated for fuel use by energetically costly means. An extractive procedure appears conceivable using cheap liquid (*e.g.*, aromatic) amines immiscible with water. Although interesting, ethanol-complexing molecular agents so far discussed in this context[37] appear too sophisticated and expensive to be of practical use on a technologically large scale. On the other hand, an obvious drawback of amines for ethanol extraction would be their toxicity.

Acknowledgements

Financial support of the *Fonds der Chemischen Industrie* is gratefully acknowledged.

Appendix

Crystal Structure of the 1:1 *Molecular Complex Between Hydroquinone and the Double Schiff Base* 1,4-*Bis(isopropylideneamino)benzene* **1·7**.—This complex was inadvertently obtained when attempting to crystallize the hydroquinone–*p*-phenylenediamine complex **1·3** from *hot* acetone solution. Similarly, Schiff-base formation had previously been encountered in the course of early crystallographic work on *p*-aminophenol, and the ensuing confusion was at last resolved by a crystal structure analysis of 4-isopropylideneamino-

UM00011565
NOVARTIS EXHIBIT 1517
Novartis v. Regents, IPR2023-01347
Page 311 of 4460

phenol[38] showing the molecules to be aggregated in chains through O(H)N hydrogen bonds between the hydroxy oxygen and imino nitrogen atoms (ON distance 2.66 Å). We deemed it worthwhile to look at the crystal structure of **1**·**7** in detail by X-ray methods and briefly report the results in order to add yet another facet to the notoriously rich supramolecular chemistry of hydroquinone.

Crystals of **1**·**7** are monoclinic, a = 5.680(1), b = 11.830(2), c = 12.569(4) Å, β = 99.31(3)°, space group $P2_1/n$ with Z = 2 formula units in the cell, *i.e.*, crystallographic centrosymmetry of both complex components, d_x = 1.189, d_m = 1.20 g cm^{-3}; structure solution and refinement (C, N, O anisotropic, H isotropic) based on 873 reflections with $F_o > 4\sigma(F_o)$, R = 0.069, R_w = 0.061, maximum residual electron density 0.23 e Å^{-3}. Atomic coordinates and temperature factors, and a stereo view of the crystal structure have been deposited at the Cambridge Crystallographic Data Centre. The molecular geometries of **1** and **7** in their complex **1**·**7** are unexceptional besides a slight out-of-plane bending deformation at C(11) and some bond angle widenings in **7**, such that more room is provided for the congested methyl group C(16)H_3.

The crystal structure of the molecular complex **1**·**7** is characterized by zig-zag chains of alternating hydroquinone and double-Schiff-base molecules held together by single O(H)N hydrogen bonds (ON distance 2.758 Å). The aromatic rings in the chains are not co-planar as in quinhydrone[39] (with chains of H-bonded quinone and hydroquinone molecules) due to the non-planarity of the double-Schiff base **7**. For steric reasons, the isopropylidene groups are twisted out of the aromatic plane around the C–N single bonds by 73°. The ensuing loss of π-overlap is partially compensated by overlap of the nitrogen lone pairs with the aromatic π-system, which in turn is weakened, however, by the H-bonding. The respective conformational behaviour of 4-isopropylideneaminophenol as well as its H-bond characteristics[38] are similar. On the whole, it may be stated that the crystal structure and H-bonding relationship between **1**·**7** and 4-isopropylideneaminophenol is a one-dimensional analogue of that between **1**·**3** and **5** (intermolecular *vs.* intramolecular combination of hydroxy and imino, and of hydroxy and amino groups, respectively).

References

1 D. Eilerman and R. Rudman, *Acta Crystallogr., Sect. B*, 1979, **35**, 2458; F. J. Llewellyn, E. G. Cox and T. H. Goodwin, *J. Chem. Soc.*, 1937, 883.

2 H. M. Powell, *J. Chem. Soc.*, 1948, 61; S. V. Lindeman, V. E. Shklover and Yu. T. Struchkov, *Cryst. Struct. Commun.*, 1981, **10**, 1173; D. D. MacNicol, in *Inclusion Compounds*, eds. J. L. Atwood, J. E. D. Davies and D. D. MacNicol, Academic Press, New York, 1984, Vol. 2, p. 1.

3 J.-M. Lehn, *Angew. Chem., Int. Ed. Engl.*, 1988, **27**, 89; 1990, **29**, 1304; D. J. Cram. *Angew. Chem., Int. Ed. Engl.* 1988, **27**, 1009.

4 (*a*) W. C. Hamilton, B. Kamb, S. J. LaPlaca and A. Prakash, *Physics of Ice*, Plenum, New York, 1969, p. 44*ff*; T. C. W. Mak and G.-D. Zhou, *Crystallography in Modern Chemistry*, Wiley, New York, 1992, p. 185*ff*; (*b*) Note that the OH · · · O distance in ice is shorter than in the gas-phase water dimer and in liquid water (1.72, 2.02 and 1.85 Å, respectively); see: G. A Jeffrey and W. Saenger, *Hydrogen Bonding in Biological Structures*, Springer, Berlin, 1991, p. 27. This helps to reduce the size of the holes in ice.

5 A. Kofler, in *Landolt-Börnstein, Zahlenwerte und Funktionen aus Physik, Chemie, Astronomie, Geophysik und Technik*, 6th edn., eds. K. Schäfer and E. Lax, Springer, Berlin, 1956, Vol. II, Part 3, p. 350*ff*.

6 E. A. Moelwyn-Hughes, *Physical Chemistry*, 2nd edn., Pergamon, Oxford, 1961, 1964, p. 1060.

7 S. W. Benson and E. D. Siebert, *J. Am. Chem. Soc.*, 1992, **114**, 4269.

8 (*a*) G. A. Jeffrey, in *Inclusion Compounds*, eds. J. L. Atwood, J. E. D. Davies and D. D. MacNicol, Academic Press, New York, 1984, Vol. 1, p. 135; (*b*) S. Wei, Z. Shi and A. W. Castleman, *J. Chem. Phys.*, 1991, **94**, 3268; X. Yang and A. W. Castleman, *J. Am. Chem. Soc.*, 1989, **111**, 6845.

9 S. Suzuki, P. G. Green, R. E. Bumgarner, S. Dasgupta, W. A. Goddard III and G. A. Blake, *Science*, 1992, **257**, 942.

10 G. Ferguson, J. F. Gallagher, C. Glidewell, J. N. Low and S. N. Scrimgeour, *Acta Crystallogr., Sect. C*, 1992, **48**, 1272.

11 O. Ermer and L. Lindenberg, *Helv. Chim. Acta*, 1991, **74**, 825; O. Ermer, *J. Am. Chem. Soc.*, 1988, **110**, 3747.

12 Relevant work on supramolecular engineering by means of hydrogen bonds: (*a*) K. S. Jeong, T. Tjivikua, A. Muehldorf, G. Deslongchamps, M. Famulok and J. Rebek, *J. Am. Chem. Soc.*, 1991, **113**, 201; J. Rebek, *Angew. Chem., Int. Ed. Engl.*, 1990, **29**, 245; R. Wyler, J. de Mendoza and J. Rebek, *Angew. Chem.*, 1993, **105**, 1820; (*b*) R. P. Dixon, S. J. Geib and A. D. Hamilton, *J. Am. Chem. Soc.*, 1992, **114**, 365; S. J. Geib, C. Vicent, E. Fau and A. D. Hamilton, *Angew. Chem., Int. Ed. Engl.*, 1993, **32**, 119; (*c*) G. M. Whitesides, J. P. Mathias and C. T. Seto, *Science*, 1992, **254**, 1312; J. P. Mathias, E. E. Simanek, C. T. Seto and G. M. Whitesides, *Angew. Chem.*, 1993, **105**, 1848; (*d*) M. C. Etter and S. M. Rentzel, *J. Am. Chem. Soc.*, 1991, **113**, 2586; M. C. Etter, *Acc. Chem. Res.*, 1990, **23**, 120; (*e*) Z. Berkovitch-Yellin, S. Ariel and L. Leiserowitz, *J. Am. Chem. Soc.*, 1983, **105**, 765; L. Leiserowitz and A. T. Hagler, *Proc. R. Soc. London*, 1983, **388**, 133; (*f*) G. R. Desiraju, *Crystal Engineering. The Design of Organic Solids*, Elsevier, Amsterdam, 1989.

13 O. Ermer, *Helv. Chim. Acta*, 1991, **74**, 1339; O. Ermer and C. Röbke, *J. Am. Chem. Soc.*, 1993, **115**, 10077.

14 C. J. Brown, *Acta Crystallogr.*, 1951, **4**, 100.

15 K. Maartmann-Moe, *Acta Crystallogr.*, 1966, **21**, 979; S. C. Wallwork and H. M. Powell, *J. Chem. Soc.*, 1980, 641; F. L. Hirshfeld, *Isr. J. Chem.*, 1964, **2**, 87.

16 A. I. Kitaigorodsky, *Molecular Crystals and Molecules*, Academic Press, New York, 1973; Chap. IA.6.

17 N. W. Larsen, *J. Mol. Struct.*, 1979, **51**, 175.

18 (*a*) Z. P. Poveteva and Z. V. Zvonkova, *Kristallografija*, 1975, **20**, 69; (*b*) M. Colapietro, A. Domenicano, G. Portalone, G. Schultz and I. Hargittai, *J. Phys. Chem.*, 1987, **91**, 1728.

19 D. G. Lister, J. K. Tyler, J. H. Hög and N. W. Larsen, *J. Mol. Struct.*, 1974, **23**, 253.

20 For summaries and relevant references, see: (*a*) A. Almenningen, O. Bastiansen, L. Fernholt, B. N. Cyvin, S. J. Cyvin and S. Samdal, *J. Mol. Struct.*, 1985, **128**, 59; (*b*) H. Calleau, J. L. Bandour and C. M. E. Zeyen, *Acta Crystallogr., Sect. B*, 1979, **35**, 426; (*c*) O. Bastiansen and S. Samdal, *J. Mol. Struct.*, 1985, **128**, 115; (*d*) C. P. Brock and K. L. Haller, *J. Phys. Chem.*, 1984, **88**, 3570; C. P. Brock, M.-S. Kuo and H. A. Levy, *Acta Crystallogr., Sect. B*, 1978, **34**, 981.

21 G. P. Charbonneau and Y. Delugeard, *Acta Crystallogr., Sect. B*, 1977, **33**, 1586; 1976, **32**, 1420.

22 *International Tables for Crystallography*, 2nd edn., ed. T. Hahn, Reidel, Dordrecht, 1987, Vol. A, *Space Group Symmetry*.

23 E. G. Cox, D. W. J. Cruickshank and J. A. S. Smith, *Proc. R. Soc. London, Ser. A*, 1958, **247**, 1; G. E. Bacon, N. A. Curry and S. A. Wilson, *Proc. R. Soc. London, Ser. A*, 1964, **279**, 98; G. A. Jeffrey, J. R. Ruble, R. K. McMullan and J. A. Pople, *Proc. R. Soc. London, Ser. A*, 1987, **414**, 47.

24 J. Trotter, *Acta Crystallogr.*, 1961, **14**, 1135; A. Hargreaves and J. H. Rizvi, *Acta Crystallogr.*, 1962, **15**, 365.

25 For a discussion of edge-to-face and face-to-face interactions among aromatic systems, see: W. L. Jorgensen and D. L. Severance, *J. Am. Chem. Soc.*, 1990, **112**, 4768.

26 T. Kitazawa, S. Nishikiori, R. Kuroda and T. Iwamoto, *Chem. Lett.*, 1988, 1729.

27 B. F. Hoskins and R. Robson, *J. Am. Chem. Soc.*, 1990, **112**, 1546.

28 M. Simard, D. Su and J. D. Wuest, *J. Am. Chem. Soc.*, 1991, **113**, 4696.

29 H. Schäfer, H. G. von Schnering, K.-J. Niehues and H. G. Nieder-Vahrenholz, *J. Less-Common Met.*, 1965, **9**, 95.

30 L. Pauling and P. Pauling, *Proc. Natl. Acad. Sci. USA*, 1968, **60**, 362.

31 D. Mootz, D. Brodalla and M. Wiebcke, *Acta Crystallogr., Sect. C*, 1989, **45**, 754.

32 E. A. Meyers and W. N. Lipscomb, *Acta Crystallogr.*, 1955, **8**, 583; B. Jerslev, *Acta Crystallogr.*, 1958, **11**, 511; J. Donohue, *Acta Crystallogr.*, 1958, **11**, 512.

33 E. Fluck and W. Schwarz, *Z. Anorg. Allg. Chem.*, 1978, **444**, 121.

34 C. T. Seto and G. M. Whitesides, *J. Am. Chem. Soc.*, 1990, **112**, 6409.

35 Similarly, complementary derivatives of 2,4,6-triaminopyrimidine

UM00011566
NOVARTIS EXHIBIT 1517
Novartis v. Regents, IPR2023-01347
Page 312 of 4460

and barbituric acid have been shown to form 1 : 1 aggregates with triply H-bonded chain structures: J.-M. Lehn, M. Mascal, A. DeCian and J. Fischer, *J. Chem. Soc., Chem. Commun.*, 1990, 479.
36 Z. Pajak, M. Grottel and A. E. Koziol, *J. Chem. Soc., Perkin Trans. 2*, 1982, **78**, 1529. Interesting crystal engineering of guanidinium sulfonates has been reported recently: V. A. Russell, M. C. Etter and M. D. Ward, *J. Am. Chem. Soc.*, 1994, **116**, 1941.
37 F. Toda, *Top. Curr. Chem.*, 1987, **140**, 43; F. Toda, in *Inclusion Compounds*, eds. J. L. Atwood, J. E. D. Davies and D. D. MacNicol, Oxford University Press, Oxford, 1991; Vol. 4, p. 126*ff*; S. A. Bourne, L. R. Nassimbeni, K. Skobridis and E. Weber, *J. Chem. Soc., Chem. Commun.*, 1991, 282.
38 D. R. Holmes and H. M. Powell, *Acta Crystallogr.*, 1953, **6**, 256.
39 T. Sakurai, *Acta Crystallogr.*, 1965, **19**, 320; *Sect. B*, 1968, **24**, 403.

Paper 3/05750J
Received 23*rd September* 1993
Accepted 1*st February* 1994

UM00011567
NOVARTIS EXHIBIT 1517
Novartis v. Regents, IPR2023-01347
Page 313 of 4460

Polyphenol–Caffeine Complexation

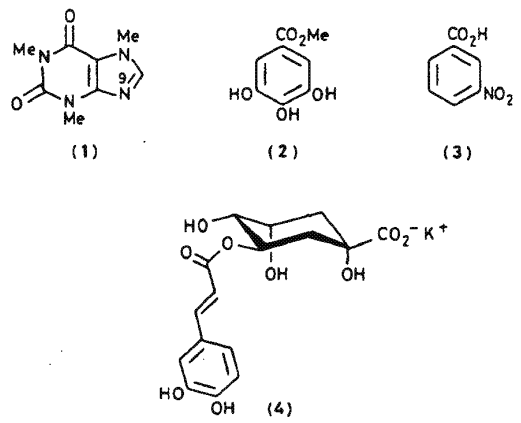
Russell Martin,[a] Terence H. Lilley,[a]* Neil A. Bailey,[a] Christopher P. Falshaw,[a] Edwin Haslam,[a]* Daniele Magnolato,[b] and Michael J. Begley[c]

[a] *Department of Chemistry, University of Sheffield, Sheffield S3 7HF, U.K.*
[b] *Nestlé Research Department, Nestec Co. Ltd., CH-1800 Vevey, Switzerland*
[c] *Department of Chemistry, University of Nottingham, Nottingham NG7 2RD, U.K.*

Crystal structures of complexes of caffeine (**1**) with methyl gallate (**2**), *m*-nitrobenzoic acid (**3**), and potassium chlorogenate (**4**) are described; the results are used to comment on possible modes of association of natural polyphenols with substrates such as proteins.

Polyphenols (proanthocyanidins[1] and esters of gallic and hexahydroxydiphenic acid[2]) constitute a distinctive and unique group of higher plant secondary metabolites.[3] Their uniqueness lies not only in their polyphenolic character but also in their relatively large molecular size (M_r up to 20 000). Together these features permit facile reversible association with various alkaloids and natural macromolecules such as proteins, carbohydrates, and nucleic acids. Studies of such intermolecular associations are not only of intrinsic scientific interest but they are also of considerable practical significance since the characteristics (nutritional, antimicrobial, antiviral, pharmacological, and astringent) of many plant products are determined by the polyphenols they contain.[4,5] Circumstantial evidence suggests[6,7] that complexation is mediated principally by hydrogen bonding and hydrophobic effects.

Caffeine (**1**) has been crystallised as 1:1 adducts with methyl gallate (**2**),†‡ *m*-nitrobenzoic acid (**3**),‡§ and potassium chlorogenate (**4**) and the complexes subjected to *X*-ray crystallographic analysis. Complexes formed with (**2**) and (**3**) show layer lattice structures with layers perpendicular to c^* consisting alternately of caffeine and the substrate. Adjacent layers are broadly parallel at mean separations of 3.37 and 3.36 Å [$1/(2c^*)$] respectively. In the methyl gallate (**2**) complex phenolic molecules above and below the caffeine are both related to the in-plane reference molecule by 2_1 symmetry. The two six-membered rings of caffeine and methyl gallate approximately eclipse each other in this stacking arrangement (Figure 1). In the caffeine–*m*-nitrobenzoic acid complex, however, the *m*-nitrobenzoic acid molecules above and below, which most nearly overlay the caffeine, are related to their reference molecule by inversion symmetry (through ½,0,½) and 2_1 symmetry through (¼,*y*,0) respectively. They are not parallel and are inclined at 1.9 and 4.6° to the caffeine and 5.4° to each other. In-plane cohesion in both complexes is achieved by hydrogen bonding. In the caffeine–*m*-nitrobenzoic acid complex, association occurs *via* a single hydrogen bond between the basic nitrogen (N-9) and the carboxy hydrogen. In the corresponding methyl gallate complex the association is



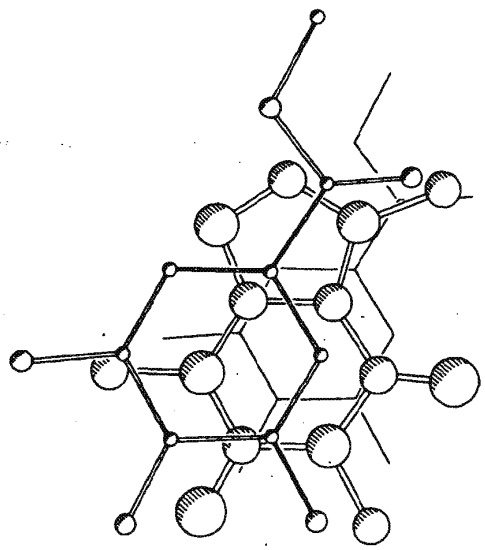


Figure 1. Layer lattice structure: caffeine–methyl gallate.

† $C_8H_{10}N_4O_2 \cdot C_8H_8O_5$; M = 378.34, crystallises from H_2O as colourless needles; crystal dimensions 0.41 × 0.07 × 0.04 mm. Monoclinic, a = 24.14(5), b = 10.057(20), c = 7.005(4) Å, β = 106.55(11)°, U = 1630(4) Å^3, Z = 4, D_c = 1.542 g cm^{-3}, space group $P2_1/a$ (a non-standard setting of $P2_1/c$, C_{2h}^5, No. 14), Mo-K_α radiation ($\bar{\lambda}$ = 0.71069 Å), μ(Mo-K_α) = 1.150 cm^{-1}, F(000) = 792, R = 0.0551, 758 reflections with $I > 3.0\sigma(I)$, $6.5 < 2\theta < 50°$.

‡ The atomic co-ordinates for this work are available on request from the Director of the Cambridge Crystallographic Data Centre, University Chemical Laboratory, Lensfield Rd., Cambridge CB2 1EW. Any request should be accompanied by the full literature citation for this communication.

§ $C_8H_{10}N_4O_2 \cdot C_7H_5NO_4$; M = 361.31, crystallises as colourless elongated plates from H_2O; crystal dimensions 0.35 × 0.10 × 0.04 mm. Monoclinic, a = 17.76(5), b = 14.09(5), c = 8.607(38) Å, β = 130.45(16)°, U = 1639(10) Å^3, Z = 4, D_c = 1.464 g cm^{-3}, space group $P2_1/a$ (a non-standard setting of $P2_1/c$, C_{2h}^5, No. 14), Mo-K_α radiation ($\bar{\lambda}$ = 0.71069 Å), μ(Mo-K_α) = 1.084 cm^{-1}, F(000) = 752, R = 0.0635, 1271 reflections with $I > 3.0\sigma(I)$, $6.5 < 2\theta < 50°$.

UM00011568
NOVARTIS EXHIBIT 1517
Novartis v. Regents, IPR2023-01347
Page 314 of 4460

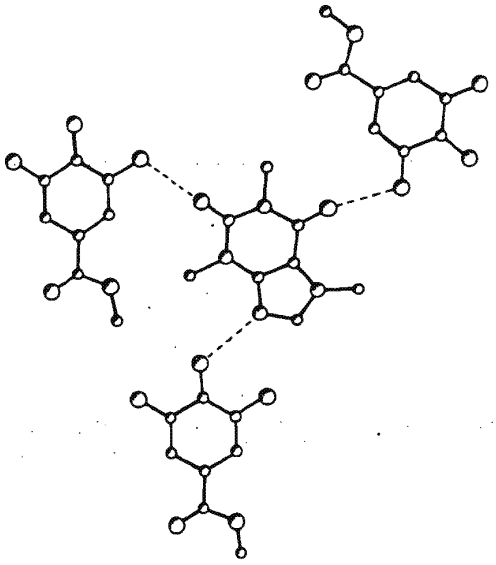


Figure 2. Caffeine–methyl gallate: in-plane hydrogen bonds.

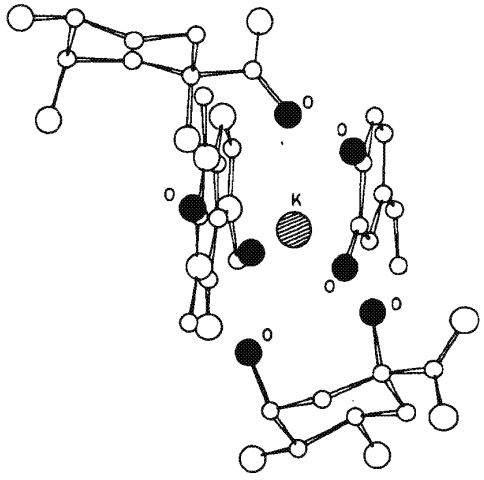


Figure 3. Potassium–caffeine–chlorogenate: co-ordination around the potassium ion.

much more extensive and gives rise (Figure 2) to an extended two-dimensional array. Each of the three phenolic groups is hydrogen bonded to a different caffeine molecule *via* either of the two keto-amide groups or the basic nitrogen (N-9). The crystal data for these two complexes show analogies to data obtained previously for the 5-chlorosalicyclic acid complex[8] and preliminary data for a pyrogallol complex.[9]

Potassium chlorogenate (**4**) was isolated from green coffee beans by Gorter[10] in 1907 as a crystalline complex with caffeine which could be crystallised from ethanol–water.‡¶ *X*-Ray analysis reveals several of the features noted in the complexes with (**2**) and (**3**). The aryl ring of (**4**) is located in a similar layer lattice structure with caffeine and the minimum separations between adjacent rings are 3.39 and 3.44 Å. The phenolic nuclei are parallel to one another but inclined (3.6°) to the plane of the caffeine ring. Hydrogen bonding again stabilises this arrangement between different molecules. However an additional critical stabilising factor is the co-ordination of seven oxygen atoms in an irregular polyhedral arrangement around the central potassium cation ($K^+ \cdots O$ distances lie between 2.67 and 2.85 Å, Figure 3). Two of the oxygen atoms originate respectively from the aliphatic hydroxy groups at C-1 and C-3 of the chlorogenate ion and one from the keto-amide (C-2) of caffeine. The remaining four oxygen atoms are related by symmetry operations. These are both phenolic oxygen atoms of a caffeoyl group $(-x,\frac{1}{2}+y,\frac{1}{2}-z)$, an oxygen of the carboxylate group of the chlorogenate ion $(\frac{1}{2}+x,\frac{1}{2}-y,-z)$, and finally a water molecule $(x-\frac{1}{2},\frac{1}{2}-y,-z)$. The pattern resembles in some respects that found in the co-ordination of metal ions by polyether antibiotics, *e.g.* monensin.[11]

¶ $C_{16}H_{17}O_9K \cdot C_8H_{10}N_4O_2 \cdot 2H_2O$, M = 622.63. Orthorhombic, a = 7.0521(3), b = 11.5848(9), c = 33.8621(27) Å, U = 2766.4 Å^3, D_c = 1.49 g cm^{-3}, Z = 4, space group $P2_12_12_1$. Cu-K_α radiation (λ = 1.5418 Å), μ = 23.35 cm^{-1}, $F(000)$ = 1304, R = 0.0551, R_w = 0.0621 for 1682 reflections, $\theta \leq 66°$, $I \geq 2\sigma(I)$.

The evidence presented demonstrates that the primary intermolecular forces in the solid-state complexes formed between caffeine and phenolic substrates are (i) hydrogen bonding, (ii) apolar interactions which manifest themselves in solution as hydrophobic effects, and, where this is appropriate, (iii) co-ordination around a metal ion. The u.v. absorption spectra of the caffeine complexes with (**2**), (**3**), and (**4**) showed no evidence of charge-transfer complex formation. Whilst it is not possible to extrapolate directly to behaviour in solution this evidence nevertheless confirms the important roles which (i) and (ii), *vide supra*, play in complexation of caffeine and polyphenols. In so far as caffeine resembles a peptide-like structure it also substantiates the importance of these same non-covalent interactions in protein association with polyphenols.[12]

The authors thank the directors of Nestec Co. Ltd., Switzerland, for a grant and permission to publish this work.

Received, 15th July 1985; Com. 1005

References

1 E. Haslam, *Phytochemistry*, 1977, **16**, 1625.
2 E. Haslam, *Fortschr. Chem. Org. Naturst.*, 1982, **41**, 1.
3 E. Haslam, in 'The Biochemistry of Plants,' vol. 7, ed. E. E. Conn, Academic Press, London and New York, 1981, p. 527.
4 E. C. Bate-Smith, *Food*, 1954, **23**, 124.
5 T. White, *J. Sci. Food Agric.*, 1957, **8**, 377.
6 E. Haslam, *Biochem. J.*, 1974, **139**, 285.
7 W. D. Loomis, *Methods Enzymol.*, 1974, **31**, 528.
8 E. Shefter, *J. Pharm. Sci.*, 1969, **58**, 710.
9 A. Arnone and R. H. Marchessault, 'Molecular Association in Biological and Related Systems,' Am. Chem. Soc. Publication, 1968, no. 84, p. 235.
10 K. Gorter, *Liebigs Ann. Chem.*, 1907, **358**, 327; 1908, **359**, 217.
11 W. K. Lutz, F. W. Winkler, and J. D. Dunitz, *Helv. Chim. Acta*, 1971, **54**, 103; M. Pinkerton and L. K. Steinrauf, *J. Mol. Biol.*, 1970, **49**, 533.
12 J. P. McManus, K. G. Davis, S. H. Gaffney, J. E. Beart, T. H. Lilley, and E. Haslam, *J. Chem. Soc., Perkin Trans. 2*, 1985, 1429.

UM00011569
NOVARTIS EXHIBIT 1517
Novartis v. Regents, IPR2023-01347
Page 315 of 4460

the long axis of Fc is approximately normal to the axis of β-CDx (Figure 1).

Received, 28th November 1989; Com. 9/05090F

References

1 K. Harata and H. Uedaira, *Bull. Chem. Soc. Jpn.*, 1975, **48**, 375; K. Harata, *ibid.*, 1979, **52**, 1807; H. Shimizu, A. Kaito, and M. Hatano, *ibid.*, 1979, **52**, 2678; 1981, **54**, 513; *J. Am. Chem. Soc.*, 1983, **102**, 7059; N. Kobayashi, *J. Chem. Soc., Chem. Commun.*, 1988, 918.

2 Some representative reports are: (a) R. Breslow, M. F. Czarniecki, J. Emert, and H. Hamaguchi, *J. Am. Chem. Soc.*, 1980, **102**, 762; (b) R. Breslow, G. L. Trainor, and A. Ueno, *ibid.*, 1983, **105**, 2739; (c) A. Harada and S. Takahashi, *J. Chem. Soc., Chem. Commun.*, 1984, 645; *J. Incl. Phenom.*, 1984, **2**, 791; (d) T. Matsue, D. H. Evans, T. Osa, and N. Kobayashi, *J. Am. Chem. Soc.*, 1985, **107**, 2745; (e) A. Ueno, F. Moriwaki, T. Osa, F. Hamada, and K. Murai, *Tetrahedron Lett.*, 1985, **26**, 899; (f) Y. Maeda, N. Ogawa, and Y. Tahashima, *J. Chem. Soc., Dalton Trans.*, 1987, 627; (g) N. Kobayashi and T. Osa, *Chem. Lett.*, 1986, 421; (h) F. M. Menger and M. J. Sherrod, *J. Am. Chem. Soc.*, 1988, **110**, 8606.

3 S. Akabori, Y. Habata, Y. Sakamoto, M. Sato, and S. Ebine, *Bull. Chem. Soc. Jpn.*, 1983, **56**, 537; A. N. Nesmeyanov, B. A. Sazonova, and V. N. Drozd, *Chem. Ber.*, 1960, **93**, 2117.

4 (a) D. R. Scott and R. S. Becker, *J. Chem. Phys.*, 1961, **35**, 516, and refs. 1—17 therein; (b) A. T. Armstrong, D. G. Carroll, and S. P. McGlynn, *ibid.*, 1967, **47**, 1104; (c) Y. S. Sohn, D. N. Hendrickson, and H. B. Glay, *J. Am. Chem. Soc.*, 1971, **93**, 3603; (d) D. Nielson, D. Boone, and H. Eyring, *J. Phys. Chem.*, 1972, **76**, 511.

Molecular Recognition directed Self-assembly of Ordered Supramolecular Strands by Cocrystallization of Complementary Molecular Components

Jean-Marie Lehn,*[a] Mark Mascal,[a] André DeCian,[b] and Jean Fischer[b]

[a] *Laboratoire de Chimie Supramoléculaire, URA 422 of the CNRS* and [b] *Laboratoire de Cristallochimie, URA 424 of the CNRS, Institut Le Bel, Université Louis Pasteur, 4, rue Blaise Pascal, 6700 Strasbourg, France*

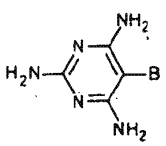
The interaction of two suitably designed complementary ditopic molecular components (**1**, **2**) and (**3**, **4**) generates spontaneously an organized supramolecular architecture displaying molecular sorting and orientation.

The spontaneous generation of organized structures requires the design of molecular components capable of self-assembling into supramolecular species presenting the desired architectural and functional features. The nature of the species obtained will depend on the information stored in the components. In particular, the self-assembling process may be directed by molecular recognition between two or more complementary subunits so as to form a given supramolecular architecture. If these molecular units incorporate specific optical, electrical, magnetic, binding, *etc.* properties their ordering may induce a range of novel features. Among the means to realize molecular organization are the use of molecular backbones (such as polymers, the natural double helix of DNA, or the self-assembled inorganic double helix of helicates[1]), liquid crystalline phases, molecular films and layers, or solid state lattices. Thus, the formation of mesophases may be induced by molecular recognition between suitable components.[2]

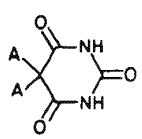
We present here a simple and general concept for generating molecular order. It is based on the recognition directed spontaneous assembling of a supramolecular strand from complementary molecular components each of which presents two identical recognition sites (Figure 1). The interaction of two such units may generate organized polymolecular strands in solution, in a mesomorphic phase, or in the solid state by cocrystallization. In the latter case, recognition based crystal engineering may allow the design of the structure of organic solids. It is seen (Figure 1) that all residues of the same type are located on the same side of the strand, thus providing spontaneous like/unlike *sorting* (into two substrands) and *orientation* of the molecular components in the supramolecular arrangement.

Molecular interactions in the solid state or at surfaces play a basic role in controlling the growth and dissolution of organic crystals,[3,4] the generation of solid state structures,[3,7] and the formation of crystalline inclusion complexes.[5,7]

The formation of a triply hydrogen bonded molecular complex between units of the 2,6-diaminopyridine and uracil type is well documented.[8] Therefore, one may expect 2,4,6-triaminopyrimidine and barbituric acid derivatives, each of



(**1**) B = Bu
(**2**) B = C_8H_{17}



(**3**) A = Et
(**4**) A = Bu

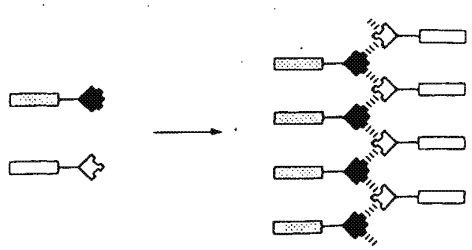


Figure 1. Schematic representation of the formation of an ordered supramolecular strand by the molecular recognition induced association of two different molecular units. Each unit contains a group that possesses two identical binding sites complementary to those of the other unit.

UM00011570
NOVARTIS EXHIBIT 1517
Novartis v. Regents, IPR2023-01347
Page 316 of 4460

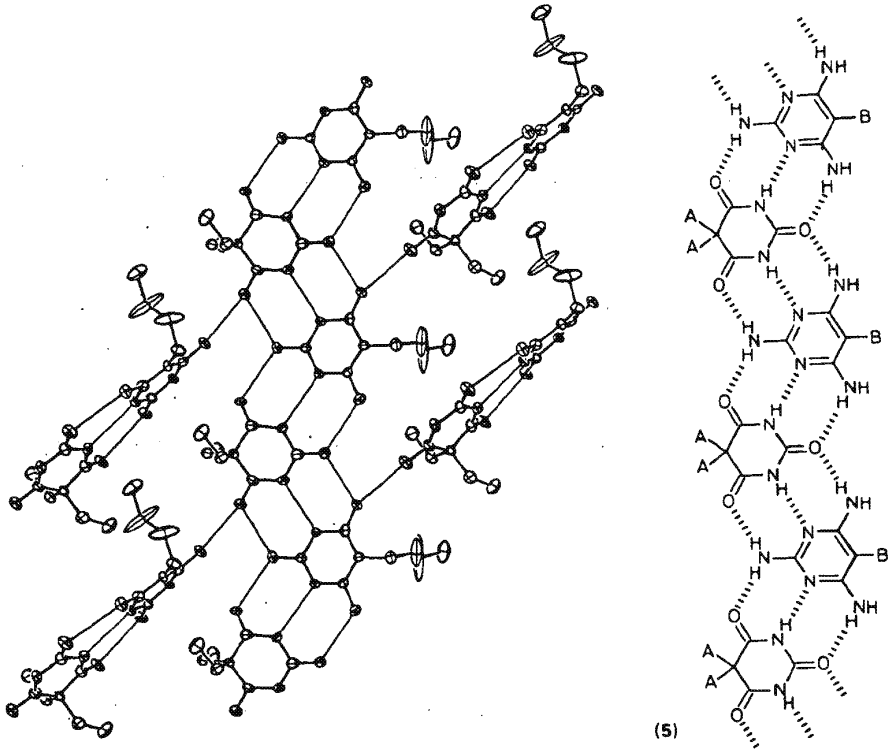


Figure 2. *X*-Ray structure of the cocrystal of the 1/1 species (**5**) formed by the components (**1**) and (**3**).

which contain two identical subunits of these types, to be able to form extended arrays of three hydrogen bonds. This should lead to the self-assembling of either a cyclic hexamer or a linear oligomeric strand depending on the relative orientation of the components.[6] Each of these supramolecular species has characteristic features and it was therefore of interest to study the interaction between such components both in solution and in the solid state.

The substituted triaminopyrimidines (**1**) and (**2**) were obtained by alkylation of malononitrile [NaH, RBr, dimethylsulphoxide (DMSO)] followed by condensation with guanidine.[9] The barbituric acid derivatives (**3**) and (**4**) were prepared in the usual way, by condensing the corresponding disubstituted diethylmalonate with urea.[10]

Whereas all four materials (**1**)—(**4**) are soluble in chloroform, mixing (**1**) with one equivalent of (**3**) or (**4**) led to the rapid precipitation of a solid that contained equimolar amounts of each component. The same species was formed by mixing non-equimolar quantities of the starting compounds. Solids were also obtained by concentration of 1/1 solutions of (**2** + **3**) and (**2** + **4**). All of these cocrystalline solids had significantly higher melting points [215—216 °C for (**1** + **3**); 268—269 °C for (**1** + **4**); 207—208 °C for (**2** + **3**); 215—216 °C for (**2** + **4**)] than the individual components (**1**) (200—201 °C), (**2**) (132—133 °C), (**3**) (191—192 °C), and (**4**) (159—160 °C). The 1/1 mixtures of (**2** + **3**) and (**2** + **4**) were soluble in $CDCl_3$ and showed appreciable downfield shifts for the NH ^{1}H NMR signals with respect to the pure compounds. The IR spectrum (KBr) of the (**1** + **3**) compound contained a very broad N–H stretching band shifted to lower frequencies around 2600 cm^{-1}, which was absent in the components. Both spectral features correspond to what is expected if association by hydrogen bonding occurs.[8,11] The ^{13}C NMR relaxation times of the ring carbons C-4 and C-6 are much shorther for the (**2** + **3**) mixtures [1.8 s in (**2**), 3.2 s in (**3**)] than in the components [14.6 s, for (**2**), 22.2 s for (**3**)] indicating a marked increase in molecular size (conc. 6 mM in $CDCl_3$).

Tonometry determinations showed that the apparent molecular weight of the species formed averaged 544 in the 6—24 mM range (in CH_2Cl_2) indicating molecular association. Measurements at higher concentrations require more soluble materials (work in progress).

The crystal structure of the mixed compound (**1** + **3**) was determined and is shown in Figure 2.† It can be seen that the components (**1**) and (**3**) are arranged in mixed supramolecular strands in which each unit forms six hydrogen bonds with its

† *Crystal data* for (**5**): $C_{16}H_{27}N_7O_3$, M = 365.44, monoclinic, space group Cc, a = 16.230(5), b = 10.088(3), c = 13.554(4) Å, β = 124.08(2)°, U = 1838 Å^3, D_c = 1.321 gcm^{-3}, Z = 4, μ(Cu-K_α) = 7.12 cm^{-1} (graphite monochromated). A total of 1105 reflections were collected using a Philips PW1100/16 automatic diffractometer. Quantitative data were obtained at −100 °C using a local-build gas flow device. The resulting data set was analysed using an Enraf-Nonius SDP/VAX package.[15] Three standard reflections measured every hour during the data collection period showed no significant trend. The raw step-scan data were converted to intensities using the Lehmann–Larsen method[16] and corrected for Lorentz and polarization factors. The structure was then solved using MULTAN[17] and refined to $R(F)$ = 0.064. Atomic co-ordinates, bond lengths and angles, and thermal parameters have been deposited at the Cambridge Crystallographic Data Centre. See Notice to Authors, Issue No. 1.

UM00011571
NOVARTIS EXHIBIT 1517
Novartis v. Regents, IPR2023-01347
Page 317 of 4460

two complementary neighbours, as represented schematically by structure (5).[12] Each ribbon-like flat strand is flanked by (1, 3) pairs (belonging to perpendicularly oriented ribbons) that are connected to the strand by a single hydrogen bond and are all oriented in the same direction. Thus, as a consequence of molecular recognition, expressed by the hydrogen bonding pattern between (1) and (3), *all like residues* A and B are respectively located on the same side of the strand, as represented in Figure 1 and in structure (5). This therefore amounts to a spontaneous separation and a parallel orientation of the A and B groups. For a given strand, this arrangement corresponds in one dimension to the two-dimensional organization induced by the formation of oriented molecular layers. One may also consider that the species formed represents a kind of self-assembled 'ladder' polymer[13] of supramolecular nature. Of special significance is the fact that these features should hold not only in the solid state but also in (concentrated) *solution* or in a *mesophase*. The crystal packing consists of sheets of polar molecular strands related to each other by translation. As a result the entire three-dimensional structure becomes polar.

Thus, the recognition interaction between the present complementary components spontaneously induces molecular sorting of like/unlike species and generates long range order, orientation, and left/right differentiation at the molecular level. The process may be considered as the operation of a programmed molecular system that contains the information required for the self-assembling of an organized supramolecular architecture (see also ref. 1).

The arrangement produced may confer specific properties on the material at the macroscopic level. Considering the barbituric unit as the 'assembler' component, mixing it with a triaminopyrimidine derivative should automatically lead to the generation of an *oriented series* of B groups along a strand,‡ thus offering the opportunity of inducing novel properties (optical, electronic, ionic, magnetic, *etc.*). For instance, such a process may allow the designed engineering of (non-centrosymmetric) cocrystals of organic molecules possessing non-linear optical,[14] electron transfer, or energy transfer properties.

Received, 5th December 1989; Com. 9/05171F

‡ This, of course, only holds if the recognition interactions directing the process are stronger than other interactions in the various species that may be formed.

References

1 J.-M. Lehn, A. Rigault, J. Siegel, J. Harrowfield, B. Chevrier, and D. Moras, *Proc. Natl. Acad. Sci. USA*, 1987, **84**, 2565; J.-M. Lehn and A. Rigault, *Angew. Chem., Int. Ed. Engl.*, 1988, **27**, 1095.

2 M.-J. Brienne, J. Gabard, J.-M. Lehn, and I. Stibor, *J. Chem. Soc., Chem. Commun.*, 1989, 1868; C. Fouquey, J.-M. Lehn, and A.-M. Levelut, *Adv. Mater.*, 1990, **2**, in the press.

3 L. Addadi, Z. Berkovich-Yellin, I. Weissbuh, J. van Mil, L. J. W. Shimon, M. Lahav, and L. Leiserowitz, *Angew. Chem., Int. Ed. Engl.*, 1985, **24**, 466.

4 'Molecular Engineering and Structural Design,' *Isr. J. Chem.*, 1985, 25.

5 'Molecular Inclusion and Molecular Recognition,' *Top. Curr. Chem.*, 1987, 140; 1988, 149; ed. F. Vögtle, Springer-Verlag, Berlin.

6 For related cases, see Y. Ducharme and J. D. Wuest, *J. Org. Chem.*, 1988, **53**, 5788; M. C. Etter and G. M. Vojta, *J. Mol. Graphics*, 1989, **7**, 3.

7 E. Weber, *J. Mol. Graphics*, 1989, **7**, 12.

8 See, for instance, G. Simundza, T. D. Sakore, and H. M. Sobell, *J. Mol. Biol.*, 1970, **48**, 263; F. E. Scarbrough, H.-S. Shieh, and D. Voet, *Proc. Natl. Acad. Sci. USA*, 1976, **73**, 3807; B. Feibush, A. Figueroa, R. Charles, K. D. Onan, P. Feibush, and B. L. Karger, *J. Am. Chem. Soc.*, 1986, **108**, 3310; A. D. Hamilton, *J. Incl. Phen. Molec. Reco. Chem.*, 1989, **7**, 27, and references cited therein.

9 P. B. Russell and G. H. Hitchings, *J. Am. Chem. Soc.*, 1952, **74**, 3443.

10 E. Fischer and A. Dilthey, *Annalen*, 1904, **335**, 334.

11 S. N. Vinogradov and R. H. Linnell, 'Hydrogen Bonding,' Van Nostrand Reinhold, New York, 1971, ch. 3.

12 For examples of related hydrogen bonded sequences, see D. Voet, *J. Am. Chem. Soc.*, 1972, **94**, 8213; N. Shimizu, S. Nishigaki, and K. Osaki, *Acta Crystallogr., Sect. B*, 1982, **38**, 2309.

13 W. J. Bailey, in 'Encyclopaedia of Polymer Science and Technology,' eds. H. F. Mark and N. G. Gaylord, Wiley-Interscience, New York, 1968, vol. 8, pp. 97—120.

14 For recent approaches, see M. C. Etter and G. M. Frankenbach, *Chem. of Materials*, 1989, **1**, 10; I. Weissbuch, M. Lahav, L. Leiserowitz, G. R. Meredith, and H. Vanherzeele, *ibid.*, 1989, **1**, 114; S. R. Marder, J. W. Perry, and W. P. Schaefer, *Science*, 1989, **245**, 626.

15 B. A. Frenz, 'The Enraf-Nonius CAD4-SDP,' in 'Computing in Crystallography,' eds. H. Schenk, R. Olthof-Hazekamp, H. Van Koningveld, and G. C. Bassi, pp. 64—71, Delft University Press, 1978.

16 M. S. Lehmann and F. K. Larsen, *Acta Crystallogr., Sect. A*, 974, **30**, 580.

17 G. Germain, P. Main, and M. M. Woolfson, *Acta Crystallogr., Sect. B*, 1970, **26**, 274; *ibid., Sect. A*, 1971, **27**, 368.

Intermolecular Carbon–Carbon Bond forming Reactions involving Allylic Sulphones

Iain W. Harvey, Eifion D. Phillips, and Gordon H. Whitham*

Dyson Perrins Laboratory, South Parks Road, Oxford OX1 3QY, U.K.

Adducts (3) are formed in satisfactory yield from allylic sulphones (2) and monosubstituted alkenes (1) under free radical conditions provided that the X substituent in the sulphone is electron withdrawing.

The potential in organic synthesis of free radical reactions, particularly those leading to the formation of carbon–carbon bonds, has attracted much attention in recent years.[1] Our investigations have been concerned with free radical addition–elimination reactions of allylic sulphones, and we have previously described 1,3-rearrangement reactions of allylic sulphones[2] and cyclisations of suitably constituted unsaturated allylic sulphones[3] occurring *via* this type of process. The cyclisation reactions involve intramolecular interaction between a double bond and an allylic sulphone. We report

UM00011572
NOVARTIS EXHIBIT 1517
Novartis v. Regents, IPR2023-01347
Page 318 of 4460

Aust. J. Chem., 1994, **47**, 1097–1115

Molecular Cocrystals of Carboxylic Acids. XV* Preparation and Characterization of Heterocyclic Base Adducts with a Series of Carboxylic Acids, and the Crystal Structures of the Adducts of 2-Aminopyrimidine with 2,6-Dihydroxybenzoic Acid, 4-Aminobenzoic Acid, Phenoxyacetic Acid, (2,4-Dichlorophenoxy)acetic Acid, (3,4-Dichlorophenoxy)-acetic Acid and Salicylic Acid, and 2-Aminopyridine with 2,6-Dihydroxybenzoic Acid

Daniel E. Lynch,[A] *Graham Smith,*[A,B] *Dell Freney,*[A] *Karl A. Byriel*[C] *and Colin H. L. Kennard*[C]

[A] School of Chemistry, Queensland University of Technology, P.O. Box 2434, Brisbane, Qld. 4001.
[B] Author to whom correspondence should be addressed.
[C] Department of Chemistry, The University of Queensland, St. Lucia, Qld. 4072.

Abstract

The molecular adducts of the heterocyclic base 2-aminopyrimidine with the aromatic and aromatic aliphatic carboxylic acids salicylic acid, 2,6-dihydroxybenzoic acid and 4-aminobenzoic acid, phenoxyacetic acid, (2,4-dichlorophenoxy)acetic acid, and (3,4-dichlorophenoxy)acetic acid have been prepared, and their interactive modes characterized by single-crystal X-ray diffraction methods. In addition, the complexes with (4-chlorophenoxy)acetic acid, (2,3-dichlorophenoxy)acetic acid, (4-chloro-2-methylphenoxy)acetic acid and (2,4,5-trichlorophenoxy)acetic acid have been characterized by analytical methods, including infrared spectroscopy. Except for the phenoxyacetic acid adduct (2:1), all form 1:1 molecular associations in which the carboxylic acid shows a variable tendency to protonate the hetero nitrogen of the base. The 1:1 complex of 2-aminopyridine with 2,6-dihydroxybenzoic acid has also been characterized by single-crystal X-ray diffraction.

Introduction

Recent studies by Etter *et al.*[1,2] have shown the hydrogen-bonding preferences of 2-aminopyrimidine (2-ap) with carboxylic acids to associate through an eight-membered hydrogen-bonded dimer [graph set $R_2^2(8)$],[3] as seen in (I). Furthermore if 1:1 molar ratios of 2-ap and monocarboxylic acids are complexed, the resultant heterodimer (I) will give secondary 'dimer' formation through the second proton acceptor nitrogen, as seen in (II). This occurs for acids with no other attached

* Part XIV, *Aust. J. Chem.*, 1994, **47**, 309.

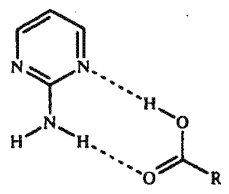
[1] Etter, M. C., and Adsmond, D. A., *J. Chem. Soc., Chem. Commun.*, 1990, 589.
[2] Etter, M. C., Adsmond, D. A., and Britton, D., *Acta Crystallogr., Sect. C*, 1990, **46**, 933.
[3] Etter, M. C., *Acc. Chem. Res.*, 1990, **23**, 120.

Manuscript received 4 October 1993 0004-9425/94/061097$05.00

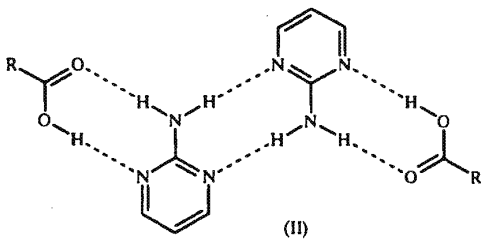
UM00011573
NOVARTIS EXHIBIT 1517
Novartis v. Regents, IPR2023-01347
Page 319 of 4460

groups having hydrogen-bonding potential. Examples of monocarboxylic acids with groups of this type are hydroxy- and amino-substituted benzoic acids and substituted phenoxyacetic acids.

Salicylic acid (sa) has already proved to be useful for adduct formation, eight adducts with various biologically active organic compounds being known,[4–10] five of which associate in a type (I) heterodimer. 2,6-Dihydroxybenzoic acid (dhba) forms a complex adduct with cytosine[11] while chloro-substituted phenoxyacetic acids have more recently been used in adduct formation.[12–18] One feature of the phenoxyacetic acid series is the ability of the ether oxygen to involve itself in hydrogen bonding, as in the 2:4 complex of phenoxyacetic acid (pa) with 3,5-dinitrobenzoic acid (dnba) $[(pa)_2(dnba)_4.2H_2O]$.[12] It might be expected that if 1:1 molar ratios of 2-ap and the chosen acids are combined, all the acids will associate predictably to give type (I) adducts. However, additional questions arise about the mode of packing resulting from the use of 2-aminopyridine (2-apy) which is analogous to 2-aminopyrimidine but is devoid of the second hetero nitrogen. The 1:1 adduct of 2-aminopyridine with salicylic acid is already known[7] but no structural information is available.



(I)



(II)

[4] Kim, H. S., and Jeffrey, G. A., *Acta Crystallogr., Sect. B*, 1971, **27**, 1123.
[5] Tamura, C., Yoshikawa, M., Sato, S., and Hata, T., *Chem. Lett.*, 1973, 1221.
[6] Kartha, G., and Varughese, K. I., *Acta Crystallogr., Sect. A*, 1978, **34**, S90.
[7] Gellert, R. W., and Hsu, I.-N., *Acta Crystallogr., Sect. A*, 1981, **37**, C93.
[8] Shimizu, N., Nishigaki, S., Nakai, Y., and Osaki, K., *Acta Crystallogr., Sect. C*, 1983, **39**, 891.
[9] Bryant, P. K., Colby, J., Jenks, R. G., Lowe, P. R., and Schwalbe, C. H., *Acta Crystallogr., Sect. A*, 1984, **40**, C79.
[10] Patel, U., Haridas, M., and Singh, T. P., *Acta Crystallogr., Sect. C*, 1988, **44**, 1264.
[11] Tamura, C., Sato, S., and Hata, T., *Bull. Chem. Soc. Jpn*, 1973, **46**, 2388.
[12] Lynch, D. E., Smith, G., Byriel, K. A., and Kennard, C. H. L., *Aust. J. Chem.*, 1991, **44**, 1017.
[13] Lynch, D. E., Smith, G., Byriel, K. A., and Kennard, C. H. L., *Z. Kristallogr.*, 1992, **200**, 73.
[14] Byriel, K. A., Lynch, D. E., Smith, G., and Kennard, C. H. L., *Aust. J. Chem.*, 1991, **44**, 1459.
[15] Lynch, D. E., Smith, G., Byriel, K. A., and Kennard, C. H. L., *Aust. J. Chem.*, 1992, **45**, 835.
[16] Byriel, K. A., Kennard, C. H. L., Lynch, D. E., Smith, G., and Thompson, J. G., *Aust. J. Chem.*, 1992, **45**, 969.
[17] Lynch, D. E., Smith, G., Byriel, K. A., and Kennard, C. H. L., *Acta Crystallogr., Sect. C*, 1993, in press.
[18] Lynch, D. E., Smith, G., Byriel, K. A., and Kennard, C. H. L., *Acta Crystallogr., Sect. C*, 1993, in press.

UM00011574
NOVARTIS EXHIBIT 1517
Novartis v. Regents, IPR2023-01347
Page 320 of 4460

In this present study the following adducts (usually 1 : 1) have been prepared and characterized of 2-aminopyrimidine (2-ap) with 2,6-dihydroxybenzoic acid (dhba), [(2-ap)(dhba)] (1); 4-aminobenzoic acid (4-aba), [(2-ap)(4-aba)] (2); phenoxyacetic acid (pa), [(2-ap)(pa)$_2$] (1 : 2 complex) (3); (4-chlorophenoxy)acetic acid (4-clpa), [(2-ap)(4-clpa)] (4); (2,3-dichlorophenoxy)acetic acid (2,3-d), [(2-ap)(2,3-d)] (5); (2,4-dichlorophenoxy)acetic acid (2,4-d), [(2-ap)(2,4-d)] (6); (3,4-dichlorophenoxy)acetic acid (3,4-d), [(2-ap)(3,4-d)] (7); (4-chloro-2-methylphenoxy)acetic acid (mcpa), [(2-ap)(mcpa)] (8); (2,4,5-trichlorophenoxy)acetic acid (2,4,5-t), [(2-ap)(2,4,5-t)] (9); and salicylic acid (sa), [(2-ap)(sa)] [two polymorphs (10a) and (10b)]. In addition, the 1 : 1 adduct of 2-aminopyridine (2-apy) with 2,6-dihydroxybenzoic acid (dhba), [(2-apy)(dhba)] (11), has been prepared and its hydrogen-bonding interactions have been characterized by using infrared spectroscopy. The crystal structures of complexes (1)–(3), (6), (7), (10b) and (11) have been determined, and are presented in this report.

Experimental

Complexes (1)–(10a) were prepared by refluxing equimolar amounts of 2-aminopyrimidine (2-ap) and 2,6-dihydroxybenzoic acid (dhba) (1), 4-aminobenzoic acid (4-aba) (2), phenoxyacetic acid (pa) (3), (4-chlorophenoxy)acetic acid (4-clpa) (4), (2,3-dichlorophenoxy)acetic acid (2,3-d) (5), (2,4-dichlorophenoxy)acetic acid (2,4-d) (6), (3,4-dichlorophenoxy)acetic acid (3,4-d) (7), (4-chloro-2-methylphenoxy)acetic acid (mcpa) (8), (2,4,5-trichlorophenoxy)acetic acid (2,4,5-t) (9) and salicylic acid (sa) (10a), in ethanol for 20 min at *c.* 110°C. The following products were obtained by total evaporation of the solvent at room temperature: for (1) light brown *prisms* (m.p. 248–250°C); for (2) brown *prisms* (m.p. 169–170·5°C); for (3) large colourless *plates* (m.p. 102–104°C); for (4) pale yellow *needles* (m.p. 137–140°C); for (5) a white *powder* (m.p. 125–126·5°C); for (6) colourless *prisms* (m.p. 130–132°C); for (7) thin colourless *plates* (m.p. 153–155°C); for (8) a pale yellow *powder* (m.p. 109–111°C); for (9) a pale brown *powder* (m.p. 175–176·5°C); for (10a) a white *powder* (m.p. 89–91°C) [Found for (1): C, 52·9; H, 4·6; N, 16·9. $C_{11}H_{11}N_3O_4$ requires C, 53·0; H, 4·4; N, 16·9%. Found for (2): C, 56·9; H, 5·3; N, 24·2%. $C_{11}H_{12}N_4O_2$ requires C, 56·8; H, 5·2; N, 24·1%. Found for (3): C, 60·4; H, 5·4; N, 10·6. $C_{20}H_{21}N_3O_6$ requires C, 60·7; H, 5·3; N, 10·6%. Found for (4): C, 51·1; H, 4·3; N, 14·8. $C_{12}H_{12}ClN_3O_3$ requires C, 51·1; H, 4·3; N, 14·9%. Found for (5): C, 44·8; H, 3·3; N, 13·1. $C_{12}H_{11}Cl_2N_3O_3$ requires C, 45·6; H, 3·5; N, 13·3%. Found for (6): C, 45·3; H, 3·4; N, 13·2. $C_{12}H_{11}Cl_2N_3O_3$ requires C, 45·6; H, 3·5; N, 13·3%. Found for (7): C, 45·5; H, 3·5; N, 13·4. $C_{12}H_{11}Cl_2N_3O_3$ requires C, 45·6; H, 3·5; N, 13·3%. Found for (8): C, 52·7; H, 4·7; N, 14·2. $C_{13}H_{14}ClN_3O_3$ requires C, 52·8; H, 4·7; N, 14·2%. Found for (9): C, 47·4; H, 3·2; N, 14·0. $C_{12}H_{10}Cl_3N_3O_3$ requires C, 47·6; H, 3·3; N, 13·9%. Found for (10a): C, 56·5; H, 4·7; N, 18·0. $C_{11}H_{11}N_3O_3$ requires C, 56·6; H, 4·8; N, 18·0%]. X-Ray powder diffraction data: *d* (*I*/*I*$_0$) 3·39 (100%), 6·82 (70), 3·26 Å (57) for (1); *d* (*I*/*I*$_0$) 5·02 (100%), 3·29 (46), 5·69 Å (43) for (2); *d* (*I*/*I*$_0$) 3·46 (100%), 3·31 (83), 4·99 Å (55) for (3); *d* (*I*/*I*$_0$) 3·28 (100%), 4·56 (80), 3·75 Å (70) for (4); *d* (*I*/*I*$_0$) 3·34 (100%), 7·01 (60), 9·40 Å (50) for (5); *d* (*I*/*I*$_0$) 4·55 (100%), 3·49 (92), 3·53 Å (78) for (6); *d* (*I*/*I*$_0$) 3·31 (100%), 5·64 (92), 3·37 Å (65) for (7); *d* (*I*/*I*$_0$) 5·31 (100%), 3·32 (100), 17·70 Å (20) for (8); *d* (*I*/*I*$_0$) 3·27 (100%), 4·82 (45), 4·64 Å (30) for (9); *d* (*I*/*I*$_0$) 5·79 (100%), 5·69 (100), 3·20 Å (80) for (10a).

Complex (10b) was prepared in a similar manner to complexes (1)–(10a) by refluxing 1 : 1 molar ratios of 2-aminopyrimidine (2-ap) and the product of the attempted preparation of (2-carboxyphenoxy)acetic acid from sodium salicylate and ethyl bromoacetate (by the general procedure of Synerholm and Zimmerman[19]), in ethanol for 20 min at *c.* 110°C. However, formation of (2-carboxyphenoxy)acetic acid by this reaction was subsequently achieved only by extending the reflux period to 5 h (cf. 1 h for the general procedure). Large colourless *prisms* (m.p. 104–106°C) formed upon total evaporation of the solvent at room temperature

[19] Synerholm, M. E., and Zimmerman, P. W., *Contrib. Boyce Thompson Inst.*, 1945, 14, 91.

UM00011575
NOVARTIS EXHIBIT 1517
Novartis v. Regents, IPR2023-01347
Page 321 of 4460

[Found for (10b): C, 56·4; H, 4·7; N, 18·0. $C_{11}H_{11}N_3O_3$ requires C, 56·6; H, 4·8; N, 18·0%]. *d* (I/I_0) 3·41 (100%), 5·98 (76), 4·95 Å (61). The difference in the formation of (10a) cf. (10b) is attributed to the presence of the unreacted starting materials in the crystallization step. This effect has been observed previously.

Complex (11) was prepared by refluxing equimolar amounts of 2-aminopyridine (2-apy) and 2,6-dihydroxybenzoic acid (dhba) in ethanol for 20 min at *c.* 110°C. Colourless *plates* (m.p. 180–182°C) formed upon total evaporation of the solvent at room temperature [Found for (11): C, 58·1; H, 4·8; N, 11·4. $C_{12}H_{12}N_2O_4$ requires C, 58·0; H, 4·8; N, 11·3%]. *d* (I/I_0) 11·04 (100%), 8·85 (41), 6·80 Å (39).

Complex formation was identified in each case by X-ray powder diffraction techniques by using an Enraf–Nonius Guinier camera (Cu Kα X-radiation). For 2-ap, *d* (I/I_0) are 3·57 (100%), 3·03 (100), 7·53 Å (80). Infrared spectra were recorded for all samples as KBr disks on a Perkin–Elmer 1600 Fourier-transform infrared spectrometer.

Crystallography

Crystal Data

(1) [$(C_7H_5O_4)^-.(C_4H_6N_3)^+$], mol. wt 249·2, monoclinic, space group $P2_1/n$, *a* 8·307(2), *b* 13·018(3), *c* 10·772(3) Å, β 90·63(1)°, *V* 1164·9(5) Å^3, *F*(000) 520, $D_c(Z=4)$ 1·421 g cm^{-3}, μ(Mo Kα) 1·0 cm^{-1}, temperature 297 K.

(2) [$(C_7H_7NO_2).(C_4H_5N_3)$], mol. wt 232·2, monoclinic, space group $P2_1/n$, *a* 5·282(1), *b* 18·230(3), *c* 11·972(3) Å, β 92·21(1)°, *V* 1151·9(5) Å^3, *F*(000) 488, $D_c(Z=4)$ 1·339 g cm^{-3}, μ(Mo Kα) 0·9 cm^{-1}, temperature 297 K.

(3) [$(C_8H_8O_3)_2.(C_4H_5N_3)$], mol. wt 399·4, monoclinic, space group *Cc*, *a* 10·897(4), *b* 10·556(4), *c* 34·91(2) Å, β 97·56(2)°, *V* 3980(3) Å^3, *F*(000) 1680, $D_c(Z=8)$ 1·333 g cm^{-3}, μ(Mo Kα) 0·9 cm^{-1}, temperature 297 K.

(6) [$(C_8H_6Cl_2O_3).(C_4H_5N_3)$], mol. wt 316·1, monoclinic, space group $P2_1/n$, *a* 14·545(6), *b* 4·1921(6), *c* 23·042(7) Å, β 98·82(1)°, *V* 1388·3(7) Å^3, *F*(000) 648, $D_c(Z=4)$ 1·512 g cm^{-3}, μ(Mo Kα) 4·8 cm^{-1}, temperature 297 K.

(7) [$(C_8H_6Cl_2O_3).(C_4H_5N_3)$], mol. wt 316·1, triclinic, space group $P\bar{1}$, *a* 6·395(4), *b* 7·084(5), *c* 15·34(1) Å, α 92·97(4), β 92·44(4), γ 103·83(4)°, *V* 672·6(8) Å^3, *F*(000) 324, $D_c(Z=2)$ 1·561 g cm^{-3}, μ(Mo Kα) 4·9 cm^{-1}, temperature 297 K.

(10b) [$(C_7H_5O_3)^-.(C_4H_6N_3)^+$], mol. wt 233·2, orthorhombic, space group *Pbca*, *a* 7·0782(7), *b* 12·354(3), *c* 25·198(6) Å, *V* 2203·4(8) Å^3, *F*(000) 976, $D_c(Z=8)$ 1·406 g cm^{-3}, μ(Mo Kα) 1·0 cm^{-1}, temperature 297 K.

(11) [$(C_7H_5O_4)^-.(C_5H_7N_2)^+$], mol. wt 248·2, monoclinic, space group $P2_1/n$, *a* 9·594(5), *b* 10·389(1), *c* 12·029(6) Å, β 106·06(2)°, *V* 1152·1(9) Å^3, *F*(000) 520, $D_c(Z=4)$ 1·431 g cm^{-3}, μ(Mo Kα) 1·0 cm^{-1}, temperature 297 K.

Data Collection, Structure Solution and Refinement

X-Ray diffraction data were collected from crystals of dimensions 0·26 by 0·30 by 0·30 mm (1), 0·24 by 0·36 by 0·28 mm (2), 0·24 by 0·24 by 0·26 mm (3), 0·24 by 0·34 by 0·30 mm (6), 0·05 by 0·38 by 0·18 mm (7), 0·26 by 0·36 by 0·28 mm (10b), and 0·18 by 0·44 by 0·24 mm (11) on an Enraf–Nonius CAD-4 diffractometer by using crystal-monochromatized Mo Kα X-radiation (λ 0·71073 Å). Negligible change in the intensities of three standards monitored throughout the data collection period for each adduct indicated no significant crystal decomposition. Of 4391 (1), 2343 (2), 3039 (3), 2411 (6), 4730 (7), 2045 (10b) and 2030 (11) unique reflections collected up to $2\theta_{max}$ 50°, 2674 (1), 1404 (2), 1828 (6), 2594 (7), 951 (10b) and 1135 (11) with $I > 2{\cdot}5\sigma(I_o)$, and 1954 with $F > 4\sigma(F_o)$ (3), were considered observed and were used in the structure analysis. Data were corrected for Lorentz and polarization effects with empirical absorption correction being applied in each case. All structures were solved by direct methods (SHELXS-86[20]). Full-matrix least-squares refinement [SHELX-76;[21]

[20] Sheldrick, G. M., SHELXS-86, Structure Solution Package, University of Göttingen, Federal Republic of Germany, 1986.

[21] Sheldrick, G. M., SHELX-76, Program for Crystal Structure Determination, University of Cambridge, England, 1976.

UM00011576
NOVARTIS EXHIBIT 1517
Novartis v. Regents, IPR2023-01347
Page 322 of 4460

SHELXL-93[22] for (3) only] with anisotropic thermal parameters for all non-hydrogen atoms gave residuals* R 0·063 (1), 0·032 (2), 0·029 (6), 0·035 (7), 0·038 (10a), 0·037 (11) and R_w 0·069 (1), 0·039 (2), 0·033 (6), 0·036 (7), 0·043 (10b), 0·037 (11), while for (3) R_1 was 0·163 and wR_2 0·396. The values of B in the weighting scheme $w = (\sigma^2 F_o + BF_o^2)^{-1}$ were $1·97\times10^{-4}$ (1), $1·93\times10^{-3}$ (2), $1·91\times10^{-4}$ (6), $3·40\times10^{-4}$ (7), $2·13\times10^{-3}$ (10b) and $1·23\times10^{-3}$ (11), while for (3) $w = [\sigma^2 F_o^2 + (0·2895P)^2]^{-1}$ where $P = [\max(F_o^2,0)+2F_c^2]/3$. Hydrogens were located by difference methods, and both positional and thermal parameters were refined [except for (1) and (3)]. For complex (1) hydrogen thermal parameters were set invariant at 0·05 Å^2. Hydrogen positions for complex (3) were included at generated positions. The high residual for (3) was the result of poor crystal quality. However, the results reported are adequate to allow a meaningful interpretation of the intermolecular interactions involved. For (3), no higher symmetry could be detected by using standard cell reduction programs.

Results

Final atomic coordinates are given in Table 1, while bond distances and angles are listed in Tables 2 and 3. Table 4 lists the comparative hydrogen-bonding distances within the dimer units. Lists of anisotropic thermal parameters, observed and calculated structure factors, and hydrogen atom coordinates for compounds (1)–(3), (6), (7), (10b) and (11), as well as atomic coordinates for (3), have been deposited as an Accessory Publication.† Molecular arrangements and atom numbering schemes for these compounds are shown in Figs 1–7 while unit cell packing diagrams are shown in Figs 8–13.

Discussion

[(2-ap)(dhba)] (1)

The 1:1 complex of 2-aminopyrimidine with 2,6-dihydroxybenzoic acid [(2-ap)(dhba)] (1) conforms to the type (I) interactive mode already described. Oxygens of the carboxylic group form an eight-membered hydrogen-bonded dimer (or adduct) [graph set $R_2^2(8)$] with two nitrogens of 2-ap, one hetero, one amino (for distances, see Table 4). The carboxylic acid proton is located on the adjacent pyrimidine nitrogen (Fig. 1). Two intramolecular hydrogen bonds involving the dhba molecule are found [O(10B)···O(21B), 2·534(4) Å: graph set S(6); O(11B)···O(61B), 2·547(4) Å: graph set S(6); combined graph set $S_2^2(10)$]. As expected with (1:1) 2-aminopyrimidine/carboxylic acid complexes, each adduct interacts with another adduct across the other 2-ap nitrogens. However, in this case a single hydrogen bond exists between the amine group and one of the hydroxy groups [N(21A)···O(21B), 2·957(4) Å: $\frac{1}{2}-x$, $-\frac{1}{2}+y$, $\frac{1}{2}-z$] completing a zigzag hydrogen-bonded polymer along the b cell direction [graph set C(6)] (Fig. 8).

* Residuals R, R_1 and wR_2: $R = R_1 = \Sigma||F_o|-|F_c||/\Sigma|F_o|$; $R_w = [\Sigma w||F_o|-|F_c||^2/\Sigma w|F_o|^2]^{1/2}$; $wR_2 = [\Sigma w(F_o^2-F_c^2)^2/\Sigma w(F_o^2)^2]^{1/2}$.

† Copies are available from the Australian Journal of Chemistry, P.O. Box 89, East Melbourne, Vic. 3002.

[22] Sheldrick, G. M., SHELXL-93, Program for Crystal Structure Determination, University of Göttingen, Germany, 1993.

UM00011577
NOVARTIS EXHIBIT 1517
Novartis v. Regents, IPR2023-01347
Page 323 of 4460

Table 1. Atomic coordinates, and equivalent isotropic thermal parameters U_{eq} (defined as one-third of the orthogonalized U_{ij} tensor)

Compound	Atom	*X/a*	*Y/b*	*Z/c*	$10^3 U_{eq}$ (Å^2)
(1)	N(1A)	−0·2034(3)	0·2621(2)	0·0594(3)	44·1(9)
	C(2A)	−0·0854(4)	0·1996(2)	0·1040(3)	42·6(11)
	N(21A)	0·0358(4)	0·2380(2)	0·1652(3)	54·3(10)
	N(3A)	−0·0904(3)	0·0974(2)	0·0807(3)	52·4(10)
	C(4A)	−0·2147(5)	0·0642(3)	0·0170(4)	57·3(15)
	C(5A)	−0·3394(5)	0·1238(3)	−0·0286(4)	56·8(14)
	C(6A)	−0·3312(4)	0·2260(3)	−0·0024(3)	49·0(11)
	C(1B)	−0·0819(4)	0·6212(2)	0·1654(3)	41·2(11)
	C(11B)	−0·0800(4)	0·5077(2)	0·1493(3)	45·5(11)
	O(10B)	0·0336(3)	0·4569(2)	0·1973(2)	67·3(10)
	O(11B)	−0·1948(3)	0·4656(2)	0·0913(2)	61·1(9)
	C(2B)	0·0437(4)	0·6716(2)	0·2267(3)	46·6(11)
	O(21B)	0·1701(3)	0·6184(2)	0·2771(3)	76·7(13)
	C(3B)	0·0425(4)	0·7772(3)	0·2442(3)	54·1(14)
	C(4B)	−0·0831(5)	0·8319(3)	0·1939(4)	56·2(13)
	C(5B)	−0·2070(5)	0·7868(2)	0·1327(4)	58·1(14)
	C(6B)	−0·2079(4)	0·6808(2)	0·1158(3)	48·7(11)
	O(61B)	−0·3325(3)	0·6378(2)	0·0540(3)	72·1(10)
(2)	N(1A)	0·3233(3)	0·50605(8)	0·7060(1)	54·6(5)
	C(2A)	0·3929(3)	0·50743(9)	0·8157(1)	49·5(5)
	N(21A)	0·2537(3)	0·4686(1)	0·8855(1)	65·6(6)
	N(3A)	0·5919(3)	0·54485(8)	0·8602(1)	56·7(5)
	C(4A)	0·7273(4)	0·5824(1)	0·7887(2)	67·3(7)
	C(5A)	0·6688(4)	0·5857(1)	0·6759(2)	73·5(8)
	C(6A)	0·4625(4)	0·5462(1)	0·6390(2)	64·3(7)
	C(1B)	−0·3257(3)	0·32123(9)	0·6188(1)	48·5(5)
	C(11B)	−0·1599(3)	0·37806(9)	0·6683(1)	49·5(5)
	O(10B)	−0·1588(2)	0·39383(7)	0·76751(9)	64·4(5)
	O(11B)	−0·0115(3)	0·41210(7)	0·59891(9)	64·1(5)
	C(2B)	−0·2949(4)	0·2943(1)	0·5110(1)	55·7(6)
	C(3B)	−0·4508(4)	0·2401(1)	0·4681(2)	56·9(6)
	C(4B)	−0·6446(3)	0·21073(9)	0·5301(1)	50·4(5)
	N(41B)	−0·7972(4)	0·1574(1)	0·4870(2)	71·4(7)
	C(5B)	−0·6743(4)	0·2380(1)	0·6382(1)	57·3(6)
	C(6B)	−0·5170(4)	0·2915(1)	0·6810(2)	55·8(6)
(6)	N(1A)	0·8268(1)	0·4333(4)	0·9066(1)	53·5(5)
	C(2A)	0·8940(1)	0·2701(5)	0·9407(1)	52·0(7)
	N(21A)	0·9648(1)	0·1560(6)	0·9165(1)	72·2(8)
	N(3A)	0·8950(1)	0·2128(4)	0·9984(1)	61·4(6)
	C(4A)	0·8232(2)	0·3224(6)	1·0210(1)	66·9(8)
	C(5A)	0·7507(2)	0·4860(7)	0·9900(1)	70·9(9)
	C(6A)	0·7555(2)	0·5385(6)	0·9316(1)	62·9(8)
	C(1B)	1·0072(1)	0·5549(5)	0·6669(1)	43·4(6)
	C(2B)	1·0481(1)	0·4421(5)	0·6199(1)	46·3(6)
	Cl(2B)	0·98318(4)	0·2206(1)	0·56503(2)	64·9(2)
	C(3B)	1·1395(1)	0·5072(5)	0·6160(1)	52·8(7)
	C(4B)	1·1909(1)	0·6871(5)	0·6588(1)	54·1(7)
	Cl(4B)	1·30791(4)	0·7665(2)	0·65513(3)	76·7(2)
	C(5B)	1·1518(2)	0·8063(5)	0·7049(1)	56·4(7)
	C(6B)	1·0601(2)	0·7389(5)	0·7089(1)	51·3(7)
	O(7B)	0·9165(1)	0·4698(3)	0·6673(1)	50·0(5)
	C(8B)	0·8655(1)	0·6358(5)	0·7063(1)	48·1(7)
	C(9B)	0·8815(1)	0·5074(5)	0·7682(1)	45·6(6)
	O(10B)	0·9399(1)	0·3100(4)	0·7860(1)	59·9(5)
	O(11B)	0·8238(1)	0·6378(4)	0·7994(1)	57·5(5)

UM00011578
NOVARTIS EXHIBIT 1517
Novartis v. Regents, IPR2023-01347
Page 324 of 4460

Table 1 *(Continued)*

Compound	Atom	*X/a*	*Y/b*	*Z/c*	$10^3 U_{eq}$ (Å^2)
(7)	N(1A)	−0·2348(3)	0·8207(3)	1·2606(1)	47·9(7)
	C(2A)	−0·0205(4)	0·8986(3)	1·2737(2)	49·2(9)
	N(21A)	0·0570(4)	0·9424(4)	1·3554(2)	64·6(9)
	N(3A)	0·1148(3)	0·9325(3)	1·2085(1)	64·1(9)
	C(4A)	0·0270(5)	0·8867(4)	1·1283(2)	64·2(11)
	C(5A)	−0·1890(5)	0·8077(4)	1·1092(2)	65·4(11)
	C(6A)	−0·3139(5)	0·7778(4)	1·1778(2)	61·0(10)
	C(1B)	0·3099(4)	0·6972(3)	0·6674(1)	49·1(9)
	C(2B)	0·3954(4)	0·7393(4)	0·7527(2)	49·7(9)
	C(3B)	0·2642(4)	0·7010(3)	0·8214(1)	46·9(9)
	Cl(3B)	0·3764(1)	0·7567(1)	0·92752(4)	69·8(3)
	C(4B)	0·0443(4)	0·6193(3)	0·8063(2)	49·1(9)
	Cl(4B)	−0·1238(1)	0·5755(1)	0·89225(4)	70·8(3)
	C(5B)	−0·0388(4)	0·5761(4)	0·7217(2)	59·4(1)
	C(6B)	0·0914(4)	0·6130(4)	0·6522(2)	58·0(10)
	O(7B)	0·4537(2)	0·7436(3)	0·6039(1)	60·9(6)
	C(8B)	0·3716(4)	0·7056(5)	0·5158(2)	51·4(10)
	C(9B)	0·5523(4)	0·7702(3)	0·4560(2)	50·0(9)
	O(10B)	0·7365(3)	0·8425(3)	0·4837(1)	73·6(7)
	O(11B)	0·4892(3)	0·7368(3)	0·3756(1)	73·4(8)
(10b)	N(1A)	0·2086(3)	0·4609(2)	−0·0397(1)	47·9(9)
	C(2A)	0·2004(4)	0·3511(2)	−0·0374(1)	51·3(10)
	N(21A)	0·2382(6)	0·3041(2)	0·0082(1)	77·5(13)
	N(3A)	0·1552(4)	0·2909(2)	−0·0802(1)	58·0(9)
	C(4A)	0·1196(5)	0·3442(3)	−0·1240(1)	60·7(12)
	C(5A)	0·1236(5)	0·4559(3)	−0·1286(1)	59·7(12)
	C(6A)	0·1711(4)	0·5129(3)	−0·0853(1)	53·4(11)
	C(1B)	0·1094(4)	0·0943(2)	0·1368(1)	45·8(10)
	C(11B)	0·1628(4)	0·0330(2)	0·0883(1)	48·2(10)
	O(10B)	0·1477(4)	−0·0684(2)	0·0907(1)	73·9(9)
	O(11B)	0·2170(3)	0·0815(1)	0·0473(1)	55·7(8)
	C(2B)	0·0312(5)	0·0428(3)	0·1806(1)	57·5(11)
	O(21B)	0·0074(4)	−0·0659(2)	0·1822(1)	84·9(11)
	C(3B)	−0·0299(5)	0·1043(4)	0·2242(1)	73·0(16)
	C(4B)	−0·0087(5)	0·2145(4)	0·2246(2)	75·7(14)
	C(5B)	0·0734(5)	0·2653(3)	0·1822(1)	70·0(14)
	C(6B)	0·1301(5)	0·2064(3)	0·1389(1)	55·7(11)
(11)	N(1A)	0·5614(2)	1·2194(2)	1·5551(2)	43·6(8)
	C(2A)	0·5512(3)	1·1859(3)	1·4449(2)	42·4(9)
	N(21A)	0·4589(3)	1·2506(3)	1·3607(2)	55·0(10)
	C(3A)	0·6380(3)	1·0851(3)	1·4254(3)	51·6(11)
	C(4A)	0·7293(3)	1·0244(3)	1·5158(3)	62·3(11)
	C(5A)	0·7368(3)	1·0603(3)	1·6300(3)	60·6(11)
	C(6A)	0·6529(3)	1·1568(3)	1·6466(2)	51·9(10)
	C(1B)	0·2905(3)	1·0702(2)	0·9464(2)	39·4(8)
	C(11B)	0·1993(3)	0·9698(3)	0·9774(2)	44·1(9)
	O(10B)	0·2187(2)	0·9434(2)	1·0834(2)	61·5(8)
	O(11B)	0·1041(2)	0·9141(2)	0·8978(2)	57·2(7)
	C(2B)	0·3990(3)	1·1346(3)	1·0315(2)	45·0(9)
	O(21B)	0·4195(2)	1·1043(2)	1·1452(2)	60·1(8)
	C(3B)	0·4836(4)	1·2279(3)	1·0025(3)	56·9(11)
	C(4B)	0·4627(4)	1·2596(3)	0·8881(3)	61·5(11)
	C(5B)	0·3577(3)	1·2007(3)	0·8021(3)	53·6(11)
	C(6B)	0·2726(3)	1·1063(2)	0·8301(2)	42·4(9)
	O(61B)	0·1702(2)	1·0499(2)	0·7428(2)	58·1(8)

UM00011579
NOVARTIS EXHIBIT 1517
Novartis v. Regents, IPR2023-01347
Page 325 of 4460

Table 2. Bond distances (Å)

Compound (1)	C(2A)–N(1A)	1·357(4)	C(6A)–N(1A)	1·333(4)
	N(21A)–C(2A)	1·298(4)	N(3A)–C(2A)	1·354(4)
	C(4A)–N(3A)	1·307(4)	C(5A)–C(4A)	1·380(5)
	C(6A)–C(5A)	1·361(4)	C(11B)–C(1B)	1·488(4)
	C(2B)–C(1B)	1·393(4)	C(6B)–C(1B)	1·403(4)
	O(10B)–C(11B)	1·258(3)	O(11B)–C(11B)	1·260(3)
	O(21B)–C(2B)	1·366(4)	C(3B)–C(2B)	1·387(4)
	C(4B)–C(3B)	1·371(5)	C(5B)–C(4B)	1·350(5)
	C(6B)–C(5B)	1·393(4)	O(61B)–C(6B)	1·347(4)
Compound (2)	C(2A)–N(1A)	1·350(2)	C(6A)–N(1A)	1·328(2)
	N(21A)–C(2A)	1·337(2)	C(3A)–C(2A)	1·346(2)
	C(4A)–N(3A)	1·327(2)	C(5A)–C(4A)	1·374(3)
	C(6A)–C(5A)	1·366(3)	C(11B)–C(1B)	1·467(2)
	C(2B)–C(1B)	1·395(2)	C(6B)–C(1B)	1·389(2)
	O(10B)–C(11B)	1·222(2)	O(11B)–C(11B)	1·319(2)
	C(3B)–C(2B)	1·374(3)	C(4B)–C(3B)	1·395(2)
	N(41B)–C(4B)	1·352(2)	C(5B)–C(4B)	1·401(2)
	C(6B)–C(5B)	1·368(3)		
Compound (6)	C(2A)–N(1A)	1·344(2)	C(6A)–N(1A)	1·335(3)
	N(21A)–C(2A)	1·332(3)	C(2A)–N(3A)	1·351(2)
	C(4A)–N(3A)	1·320(3)	C(4A)–C(5A)	1·365(3)
	C(5A)–C(6A)	1·374(3)	C(2B)–C(1B)	1·396(2)
	C(6B)–C(1B)	1·375(3)	O(7B)–C(1B)	1·367(2)
	Cl(2B)–C(2B)	1·729(2)	C(3B)–C(2B)	1·373(3)
	C(4B)–C(3B)	1·368(3)	Cl(4B)–C(4B)	1·749(2)
	C(5B)–C(4B)	1·373(3)	C(6B)–C(5B)	1·381(3)
	C(8B)–O(7B)	1·430(2)	C(9B)–C(8B)	1·508(3)
	O(10B)–C(9B)	1·211(2)	O(11B)–C(9B)	1·307(2)
Compound (7)	C(2A)–N(1A)	1·351(3)	C(6A)–N(1A)	1·338(3)
	N(21A)–C(2A)	1·320(3)	N(3A)–C(2A)	1·344(3)
	C(4A)–N(3A)	1·321(3)	C(5A)–C(4A)	1·373(4)
	C(6A)–C(5A)	1·342(4)	C(2B)–C(1B)	1·385(3)
	C(6B)–C(1B)	1·386(3)	C(7B)–C(1B)	1·366(2)
	C(3B)–C(2B)	1·373(3)	Cl(3B)–C(3B)	1·737(2)
	C(4B)–C(3B)	1·391(3)	Cl(4B)–C(4B)	1·731(2)
	C(5B)–C(4B)	1·371(3)	C(6B)–C(5B)	1·377(3)
	C(8B)–O(7B)	1·416(3)	C(9B)–C(8B)	1·506(3)
	O(10B)–C(9B)	1·215(2)	O(11B)–C(9B)	1·273(3)
Compound (10b)	C(2A)–N(1A)	1·358(3)	C(6A)–N(1A)	1·344(3)
	N(21A)–C(2A)	1·315(3)	C(3A)–C(2A)	1·349(3)
	C(4A)–N(3A)	1·309(3)	C(5A)–C(4A)	1·385(4)
	C(6A)–C(5A)	1·342(4)	C(11B)–C(1B)	1·486(4)
	C(2B)–C(1B)	1·390(3)	C(6B)–C(1B)	1·394(4)
	O(10B)–C(11B)	1·259(3)	O(11B)–C(11B)	1·253(3)
	O(21B)–C(2B)	1·354(3)	C(3B)–C(2B)	1·403(4)
	C(4B)–C(3B)	1·370(5)	C(5B)–C(4B)	1·369(5)
	C(6B)–C(5B)	1·371(4)		
Compound (11)	C(2A)–N(1A)	1·348(3)	C(6A)–N(1A)	1·367(3)
	N(21A)–C(2A)	1·329(3)	C(3A)–C(2A)	1·398(4)
	C(4A)–C(3A)	1·349(4)	C(5A)–C(4A)	1·406(4)
	C(6A)–C(5A)	1·335(4)	C(11B)–C(1B)	1·474(3)
	C(2B)–C(1B)	1·410(3)	C(6B)–C(1B)	1·412(3)
	O(10B)–C(11B)	1·266(3)	O(11B)–C(11B)	1·266(3)
	O(21B)–C(2B)	1·363(3)	C(3B)–C(2B)	1·370(4)
	C(4B)–C(3B)	1·375(4)	C(5B)–C(4B)	1·371(4)
	C(6B)–C(5B)	1·376(4)	O(61B)–C(6B)	1·356(3)

UM00011580
NOVARTIS EXHIBIT 1517
Novartis v. Regents, IPR2023-01347
Page 326 of 4460

Table 3. Bond angles (degrees)

Compound (1)	C(6A)–N(1A)–C(2A)	116·2(2)	N(21A)–C(2A)–N(1A)	117·6(2)
	N(3A)–C(2A)–N(1A)	125·0(2)	N(3A)–C(2A)–N(21A)	117·5(2)
	C(4A)–N(3A)–C(2A)	116·0(2)	C(5A)–C(4A)–N(3A)	123·4(2)
	C(6A)–C(5A)–C(4A)	116·2(2)	C(5A)–C(6A)–N(1A)	123·3(2)
	C(2B)–C(1B)–C(11B)	122·2(2)	C(6B)–C(1B)–C(11B)	119·6(1)
	C(6B)–C(1B)–C(2B)	118·2(2)	O(10B)–C(11B)–C(1B)	122·6(2)
	O(11B)–C(11B)–C(1B)	115·9(1)	O(11B)–C(11B)–O(10B)	121·4(2)
	C(3B)–C(2B)–C(1B)	120·6(2)	C(4B)–C(3B)–C(2B)	121·3(2)
	C(41B)–C(4B)–C(3B)	120·8(2)	C(5B)–C(4B)–C(3B)	117·8(2)
	C(5B)–C(4B)–N(41B)	121·4(2)	C(6B)–C(5B)–C(4B)	120·8(2)
	C(5B)–C(6B)–C(1B)	121·4(2)		
Compound (2)	C(6A)–N(1A)–C(2A)	122·3(3)	N(21A)–C(2A)–N(1A)	120·1(3)
	N(3A)–C(2A)–N(1A)	120·2(3)	N(3A)–C(2A)–N(21A)	119·6(3)
	C(4A)–N(3A)–C(2A)	116·4(3)	C(5A)–C(4A)–N(3A)	125·9(3)
	C(6A)–C(5A)–C(4A)	116·1(3)	C(5A)–C(6A)–N(1A)	119·1(3)
	C(2B)–C(1B)–C(11B)	121·0(3)	C(6B)–C(1B)–C(11B)	120·9(3)
	C(6B)–C(1B)–C(2B)	118·1(3)	O(10B)–C(11B)–C(1B)	118·9(3)
	O(11B)–C(11B)–C(1B)	118·7(3)	O(11B)–C(11B)–O(10B)	122·4(3)
	O(21B)–C(2B)–C(1B)	121·2(3)	C(3B)–C(2B)–C(1B)	121·7(3)
	C(3B)–C(2B)–O(21B)	117·0(3)	C(4B)–C(3B)–C(2B)	117·9(3)
	C(5B)–C(4B)–C(3B)	122·7(3)	C(6B)–C(5B)–C(4B)	119·8(3)
	C(5B)–C(6B)–C(1B)	119·7(3)	O(61B)–C(6B)–C(1B)	121·7(3)
	O(61B)–C(6B)–C(5B)	118·6(3)		
Compound (6)	N(1A)–C(2A)–N(21A)	118·6(2)	C(6A)–N(1A)–C(2A)	117·4(2)
	N(21A)–C(2A)–N(3A)	117·2(2)	N(1A)–C(2A)–N(3A)	124·2(2)
	C(4A)–N(3A)–C(2A)	115·9(2)	C(4A)–C(5A)–C(6A)	116·2(2)
	C(5A)–C(6A)–N(1A)	121·9(2)	C(5A)–C(4A)–N(3A)	124·3(2)
	C(6B)–C(1B)–C(2B)	118·4(2)	O(7B)–C(1B)–C(2B)	116·3(2)
	O(7B)–C(1B)–C(6B)	125·3(2)	Cl(2B)–C(2B)–C(1B)	120·0(1)
	C(3B)–C(2B)–C(1B)	121·0(2)	C(3B)–C(2B)–Cl(2B)	119·0(1)
	C(4B)–C(3B)–C(2B)	119·3(2)	Cl(4B)–C(4B)–C(3B)	119·9(2)
	C(5B)–C(4B)–C(3B)	120·8(2)	C(5B)–C(4B)–Cl(4B)	119·3(2)
	C(6B)–C(5B)–C(4B)	119·8(2)	C(5B)–C(6B)–C(1B)	120·6(2)
	C(8B)–O(7B)–C(1B)	118·1(1)	C(9B)–C(8B)–O(7B)	113·6(2)
	O(10B)–C(9B)–C(8B)	124·2(2)	O(11B)–C(9B)–C(8B)	110·7(2)
	O(11B)–C(9B)–O(10B)	125·1(2)		
Compound (7)	C(6A)–N(1A)–C(2A)	117·4(2)	N(21A)–C(2A)–N(1A)	117·4(2)
	N(3A)–C(2A)–N(1A)	123·4(2)	N(3A)–C(2A)–N(21A)	119·2(2)
	C(4A)–N(3A)–C(2A)	116·3(2)	C(5A)–C(4A)–N(3A)	124·0(3)
	C(6A)–C(5A)–C(4A)	116·3(3)	C(5A)–C(6A)–N(1A)	122·6(3)
	C(6B)–C(1B)–C(2B)	119·4(2)	O(7B)–C(1B)–C(2B)	115·6(2)
	O(7B)–C(1B)–C(6B)	125·1(2)	C(3B)–C(2B)–C(1B)	120·3(2)
	Cl(3B)–C(3B)–C(2B)	119·1(2)	C(4B)–C(3B)–C(2B)	120·5(2)
	C(4B)–C(3B)–Cl(3B)	120·5(2)	Cl(4B)–C(4B)–C(3B)	120·9(2)
	C(5B)–C(4B)–C(3B)	118·9(2)	C(5B)–C(4B)–Cl(4B)	120·1(2)
	C(6B)–C(5B)–C(4B)	121·1(2)	C(5B)–C(6B)–C(1B)	119·9(2)
	C(8B)–O(7B)–C(1B)	117·2(2)	C(9B)–C(8B)–O(7B)	109·4(2)
	O(10B)–C(9B)–C(8B)	122·2(2)	O(11B)–C(9B)–C(8B)	112·4(2)
	O(11B)–C(9B)–O(10B)	125·4(2)		
Compound (10b)	C(6A)–N(1A)–C(2A)	120·4(3)	N(21A)–C(2A)–N(1A)	118·1(3)
	N(3A)–C(2A)–N(1A)	121·7(3)	N(3A)–C(2A)–N(21A)	120·2(3)
	C(4A)–N(3A)–C(2A)	116·3(3)	C(5A)–C(4A)–N(3A)	124·6(3)
	C(6A)–C(5A)–C(4A)	117·4(3)	C(5A)–C(6A)–N(1A)	119·6(3)
	C(2B)–C(1B)–C(11B)	121·5(2)	C(6B)–C(1B)–C(11B)	120·7(2)
	C(6B)–C(1B)–C(2B)	117·8(3)	O(10B)–C(11B)–C(1B)	116·5(3)
	O(11B)–C(11B)–C(1B)	120·7(2)	O(11B)–C(11B)–O(10B)	122·8(3)
	O(21B)–C(2B)–C(1B)	121·8(3)	C(3B)–C(2B)–C(1B)	119·8(3)
	C(3B)–C(2B)–O(21B)	118·4(3)	C(4B)–C(3B)–C(2B)	120·6(4)
	C(5B)–C(4B)–C(3B)	119·8(4)	C(6B)–C(5B)–C(4B)	120·1(4)
	C(5B)–C(6B)–C(1B)	121·8(3)		
Compound (11)	C(6A)–N(1A)–C(2A)	121·6(3)	N(21A)–C(2A)–N(1A)	118·1(3)
	C(3A)–C(2A)–N(1A)	118·3(2)	C(3A)–C(2A)–N(21A)	123·6(2)
	C(4A)–C(3A)–C(2A)	119·9(3)	C(5A)–C(4A)–C(3A)	120·7(3)
	C(6A)–C(5A)–C(4A)	118·4(3)	C(5A)–C(6A)–N(1A)	121·1(3)
	C(2B)–C(1B)–C(11B)	121·5(2)	C(6B)–C(1B)–C(11B)	121·3(2)
	C(6B)–C(1B)–C(2B)	117·1(2)	O(10B)–C(11B)–C(1B)	118·4(2)
	O(11B)–C(11B)–C(1B)	119·1(2)	O(11B)–C(11B)–O(10B)	122·5(3)
	O(21B)–C(2B)–C(1B)	119·4(3)	C(3B)–C(2B)–C(1B)	121·4(2)
	C(3B)–C(2B)–O(21B)	119·2(2)	C(4B)–C(3B)–C(2B)	119·4(3)
	C(5B)–C(4B)–C(3B)	121·4(3)	C(6B)–C(5B)–C(4B)	119·7(3)
	C(5B)–C(6B)–C(1B)	120·9(2)	O(61B)–C(6B)–C(1B)	121·1(2)
	O(61B)–C(6B)–C(5B)	118·0(2)		

UM00011581
NOVARTIS EXHIBIT 1517
Novartis v. Regents, IPR2023-01347
Page 327 of 4460

Table 4. Relevant distances (Å) within the eight-membered hydrogen-bonded heteromolecular rings for complexes (1)–(3), (6), (7), (10b) and (11)

Complex	Designation	N(1A)···O(11B)	N(21A)···O(10B)
[(2-ap)(dhba)]	(1)	2·672(4)	2·870(4)
[(2-ap)(4-aba)]	(2)	2·744(3)	2·892(3)
[(2-ap)(pa)$_2$]	(3)	2·67(2)	2·93(2)
		2·60(2)[A]	2·93(2)[D]
		2·70(2)[B]	2·94(2)[E]
		2·66(2)[C]	2·97(2)[F]
[(2-ap)(2,4-d)]	(6)	2·608(3)	3·043(3)
[(2-ap)(3,4-d)]	(7)	2·541(3)	2·893(3)
[(2-ap)(sa)]	(10b)	2·704(4)	2·730(4)
[(2-apy)(dhba)]	(11)	2·726(4)	2·829(4)

[A] N(3)···O(11) between molecules A and C. [B] N(1)···O(11) between molecules D and E. [C] N(3)···O(11) between molecules D and F. [D] N(21)···O(10) between molecules A and C. [E] N(21)···O(10) between molecules D and E. [F] N(21)···O(10) between molecules D and F.

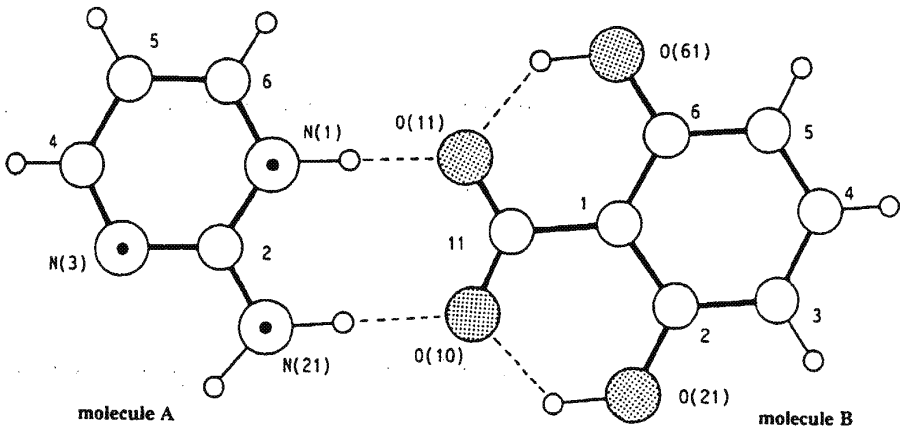


Fig. 1. Molecular configuration and atom naming scheme for (1). Unless otherwise indicated, atoms are carbon. Hydrogen-bonding interactions are indicated by dashed lines.

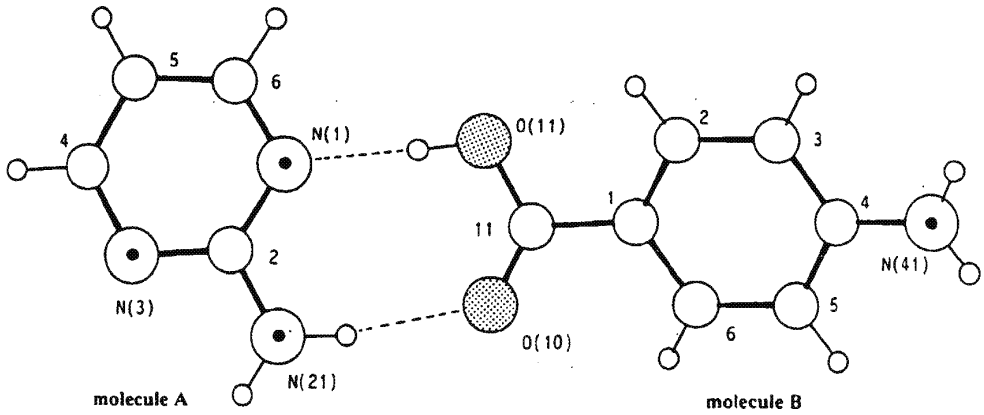


Fig. 2. Molecular configuration and atom naming scheme for (2).

UM00011582
NOVARTIS EXHIBIT 1517
Novartis v. Regents, IPR2023-01347
Page 328 of 4460

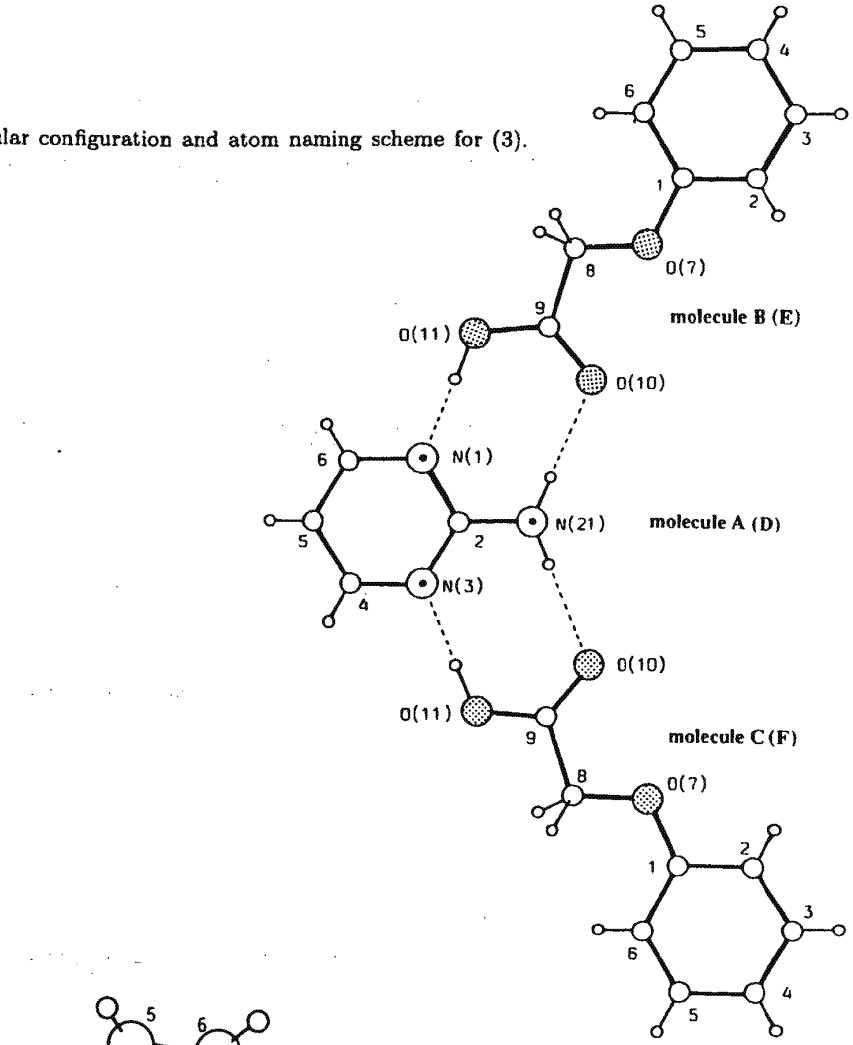


Fig. 3. Molecular configuration and atom naming scheme for (3).

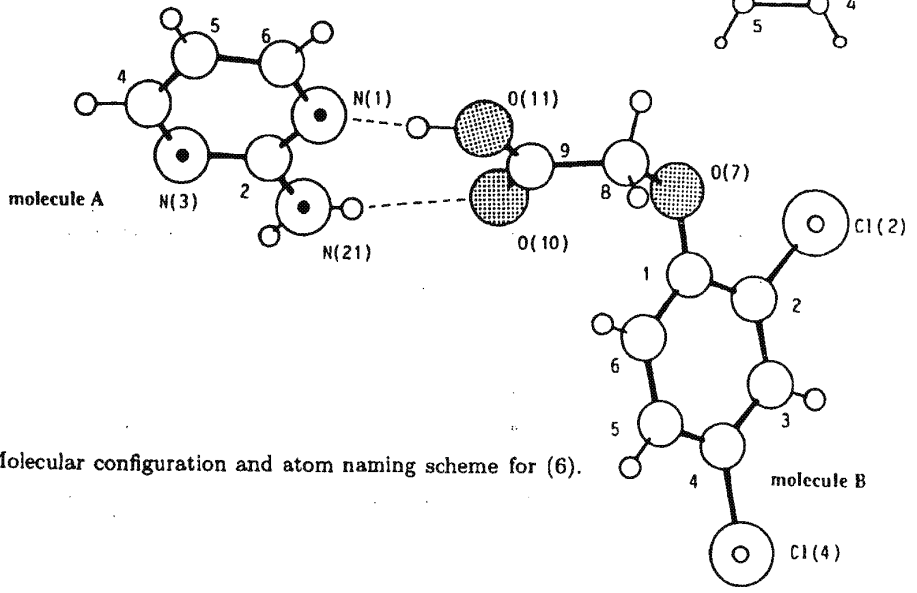


Fig. 4. Molecular configuration and atom naming scheme for (6).

UM00011583
NOVARTIS EXHIBIT 1517
Novartis v. Regents, IPR2023-01347
Page 329 of 4460

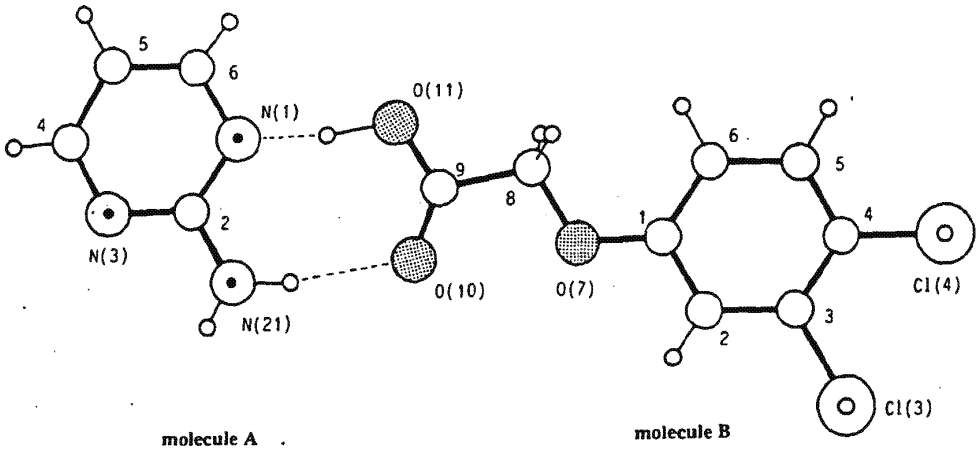


Fig. 5. Molecular configuration and atom naming scheme for (7).

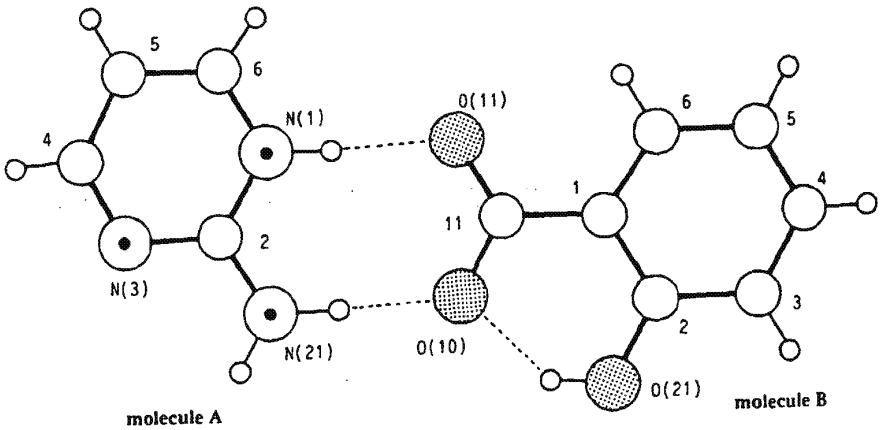


Fig. 6. Molecular configuration and atom naming scheme for (10b).

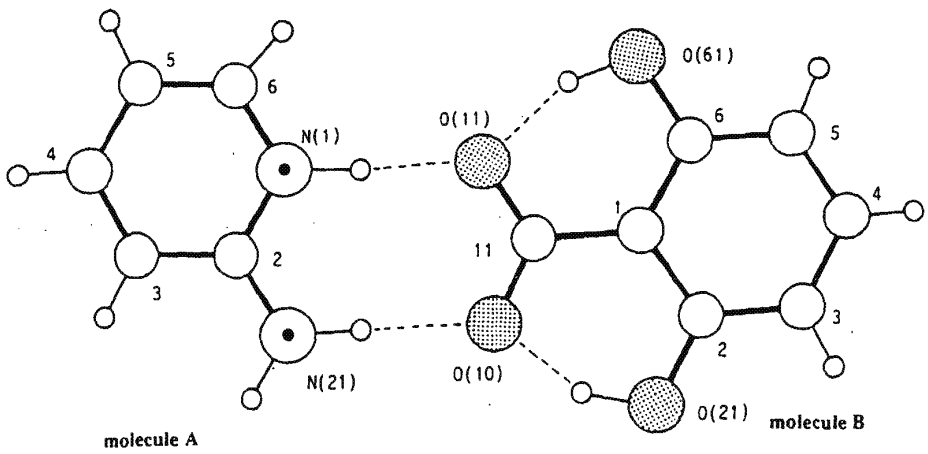


Fig. 7. Molecular configuration and atom naming scheme for (11).

UM00011584

NOVARTIS EXHIBIT 1517
Novartis v. Regents, IPR2023-01347
Page 330 of 4460

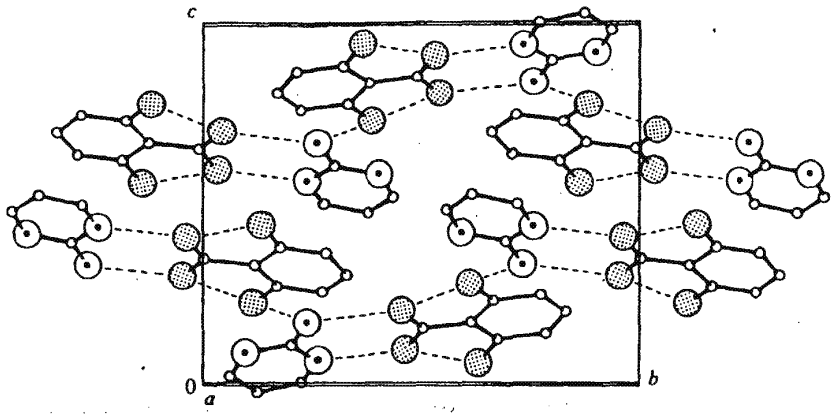


Fig. 8. Packing of (1) in the unit cell viewed down *a*.

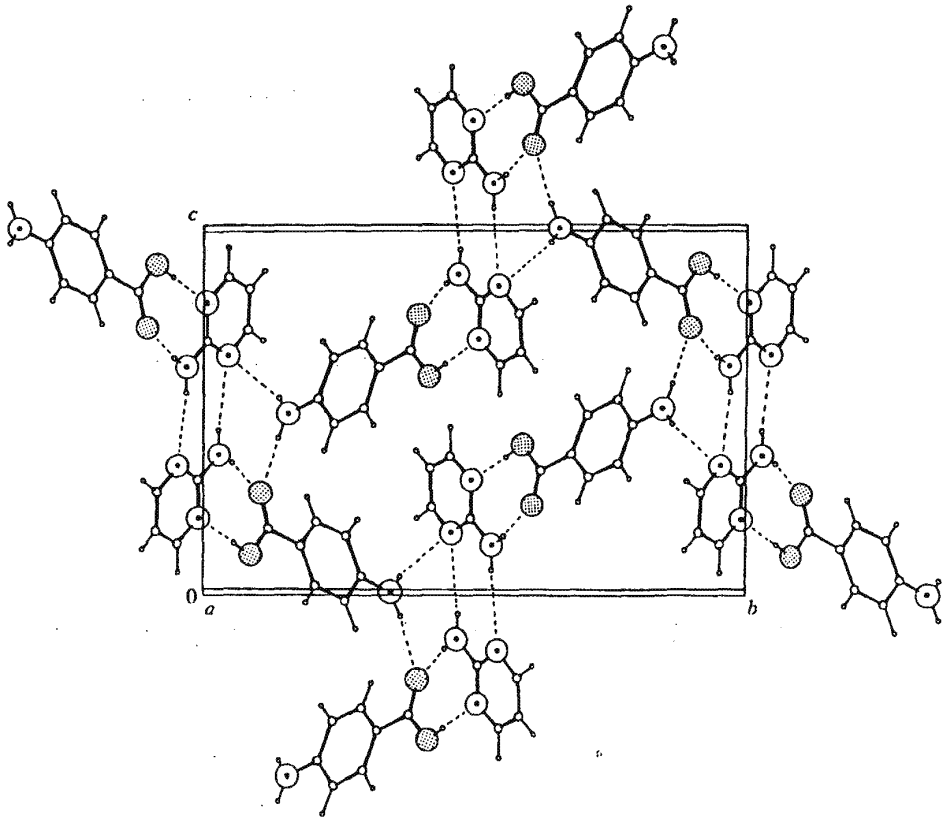


Fig. 9. Packing of (2) in the unit cell viewed down *a*.

UM00011585
NOVARTIS EXHIBIT 1517
Novartis v. Regents, IPR2023-01347
Page 331 of 4460

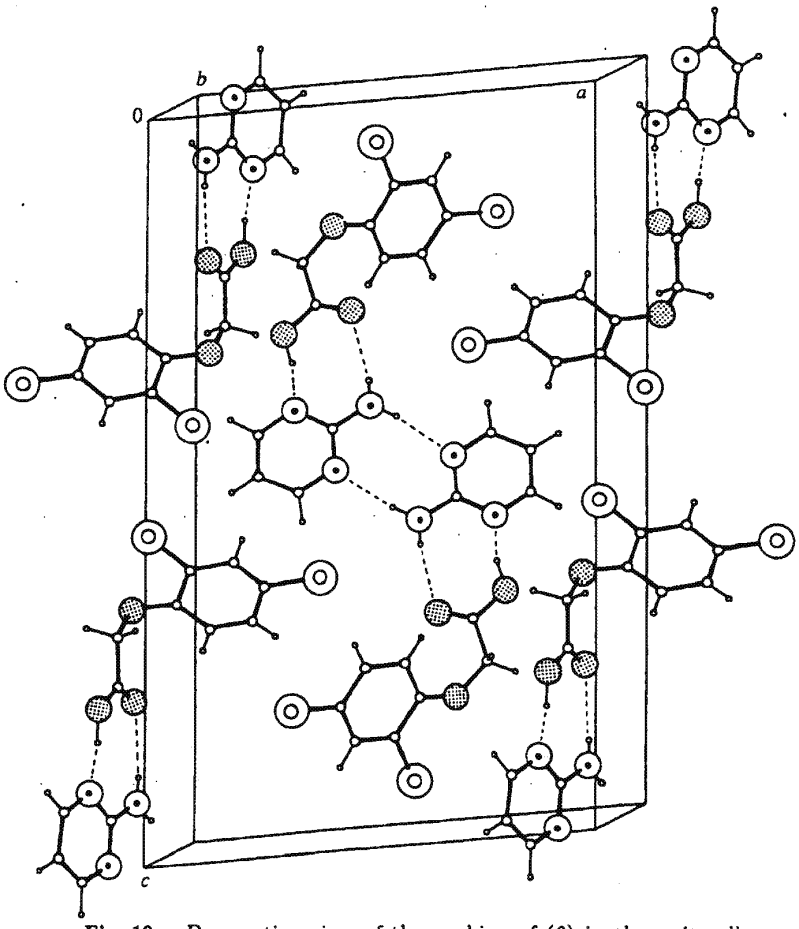


Fig. 10. Perspective view of the packing of (6) in the unit cell.

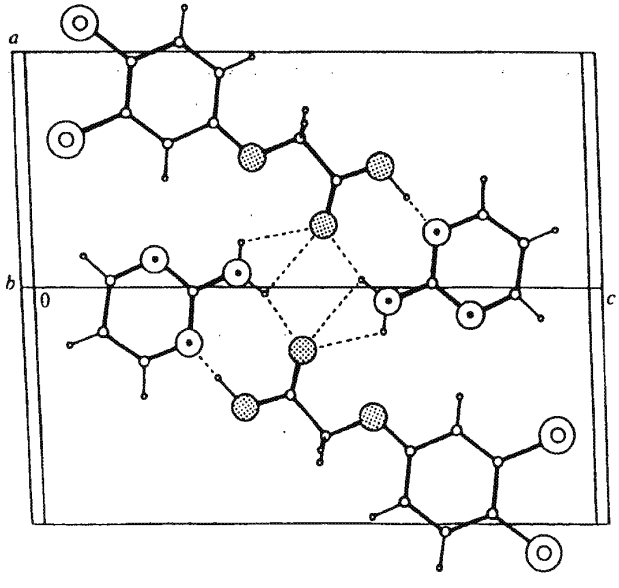


Fig. 11. Packing of (7) in the unit cell viewed down *b*.

UM00011586
NOVARTIS EXHIBIT 1517
Novartis v. Regents, IPR2023-01347
Page 332 of 4460

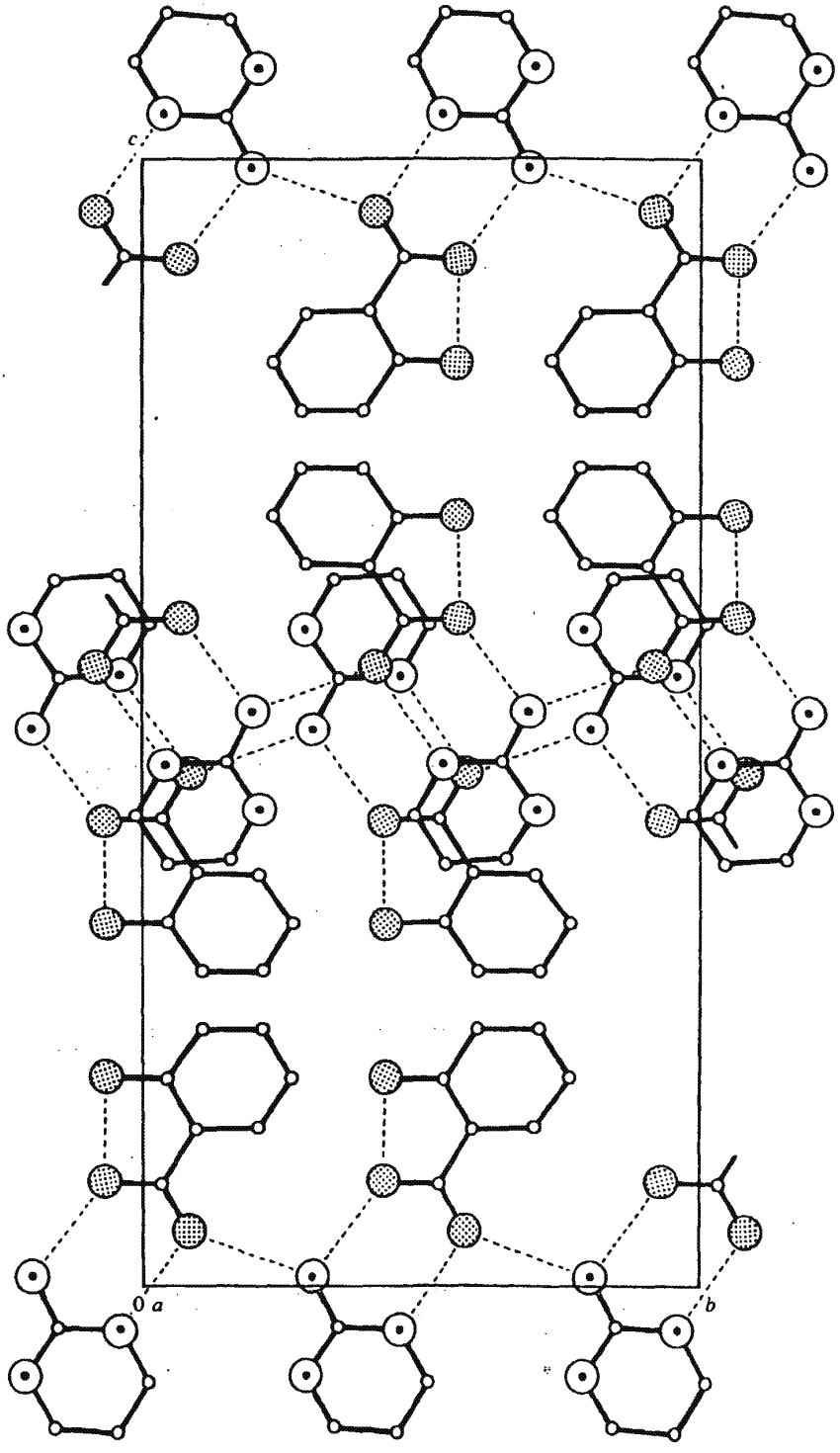


Fig. 12. Packing of (10b) in the unit cell viewed down *a*.

UM00011587
NOVARTIS EXHIBIT 1517
Novartis v. Regents, IPR2023-01347
Page 333 of 4460

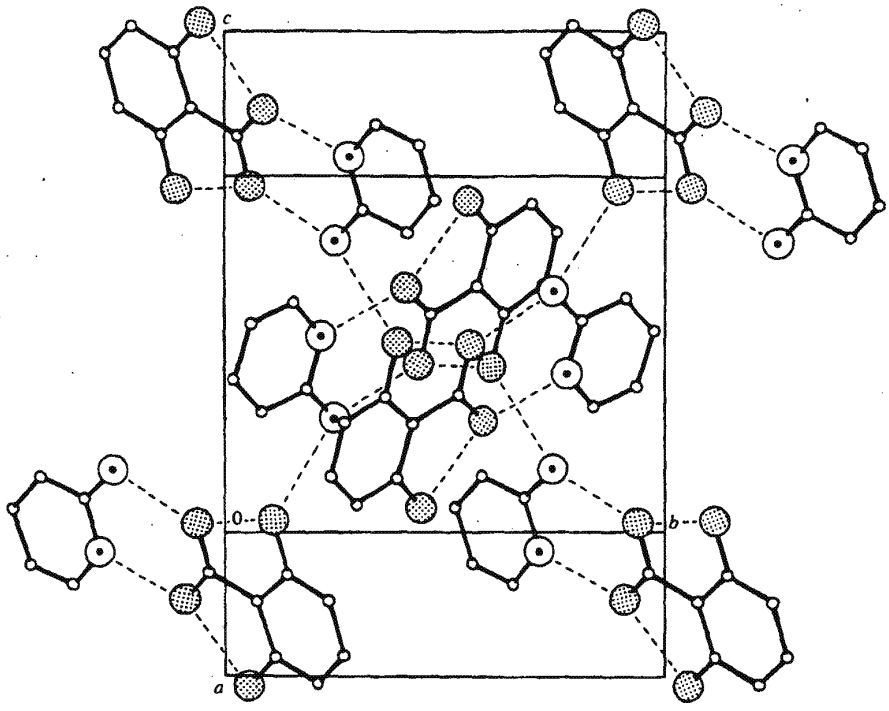


Fig. 13. Perspective view of the packing of (11) in the unit cell.

[(2-ap)(4-aba)] (2)

The 1 : 1 complex of 2-aminopyrimidine with 4-aminobenzoic acid [(2-ap)(4-aba)] (2) not only forms an eight-membered dimer (or adduct) through the carboxylic acid group to 2-ap (distances: Table 4) (Fig. 2), but two adducts also associate through the pyrimidine nitrogens [N(21A)···N(3A), 3·131(3) Å: $\frac{3}{2}-x$, $\frac{3}{2}+y$, $\frac{5}{2}-z$]. The acid group of 4-aba remains protonated. The amino group of 4-aba is hydrogen-bonded through one hydrogen to the carbonyl oxygen of another 4-aba molecule [N(41B)···O(10B), 2·909(3) Å: $\frac{1}{2}-x$, $\frac{1}{2}-y$, $\frac{1}{2}+z$], and through the other hydrogen to a heterocyclic nitrogen of 2-ap [N(41B)···N(3A), 3·193(3) Å: $-1-x$, $-1-y$, $1-z$] creating another eight-membered hydrogen-bonded ring [graph set $R_4^2(8)$] (Fig. 9).

[(2-ap)(pa)$_2$] (3)

The 1 : 2 2-aminopyrimidine/phenoxyacetic acid complex [(2-ap)(pa)$_2$] (3) packs as expected for a 1 : 2 2-aminopyrimidine/monocarboxylic acid complex with the two interactive sites on the 2-ap molecule forming cyclic dimer rings with the carboxylic acid groups (Fig. 3). However, what is very surprising is the preference for formation of the 1 : 2 complex over the 1 : 1 complex. The interaction of 1 : 1 stoichiometric amounts of 2-ap and pa invariably resulted in formation of the 1 : 2 complex (3). Similar to the parent structure[23] the phenoxyacetic acid molecule is essentially planar.

[23] Kennard, C. H. L., Smith, G., and White, A. H., *Acta Crystallogr., Sect. B.*, 1982, **38**, 868.

UM00011588
NOVARTIS EXHIBIT 1517
Novartis v. Regents, IPR2023-01347
Page 334 of 4460

[(2-ap)(2,4-d)] (6)

The 1:1 2-aminopyrimidine/(2,4-dichlorophenoxy)acetic acid complex [(2-ap)(2,4-d)] (6) consists of the two eight-membered hydrogen-bonded rings similar to complex (2) [N(21A)···N(1A), 3·027(3) Å: $2-x$, $-y$, $2-z$] (Fig. 4). The acid group of 2,4-d remains protonated. No other hydrogen-bonding interactions exist (Fig. 10). Typically the 2,4-d molecule in (6) is non-planar [torsion angles: C(2)–C(1)–O(7)–C(8), −166·0°; C(1)–O(7)–C(8)–C(9), −84·0°; O(7)–C(8)–C(9)–O(11), −171·2°], similar to the parent acid[24] [comparative torsion angles: −179·1, −80·4 and +173·1° respectively]. The distance between ether and carbonyl oxygens [O(7B)···O(10B)] in the adduct is 2·785(3) Å, while the dihedral angle between the plane of the ring and the plane of the carboxylic acid group is 108·6°. These compare with 2·717 Å and 85·2° respectively for the parent acid.[25]

[(2-ap)(3,4-d)] (7)

The 1:1 complex of 2-aminopyrimidine with (3,4-dichlorophenoxy)acetic acid [(2-ap)(3,4-d)] (7) forms as expected across an eight-membered hydrogen-bonded cyclic dimer (or adduct) (distances: Table 4) (Fig. 5). However, the dimeric associations involving the amino group of 2-ap through a reverse three-centre hydrogen bond to the carbonyl oxygen of 3,4-d are different [N(21A)···O(10B), 2·920(3) Å: $-x$, $2-y$, $3-z$] [graph set $R_2^2(4)$]. The two adducts in this further 'dimer' are not coplanar (Fig. 11). The 3,4-d molecule in (7) is essentially planar [torsion angles: C(2)–C(1)–O(7)–C(8), −179·0(2)°; C(1)–O(7)–C(8)–C(9), 178·7(2)°; O(7)–C(8)–C(9)–O(11), 178·9(2)°] similar to the parent acid[25] [torsion angles: 178·2(6), 174·5(6) and 178·6(6)°, respectively]. The distance between ether and carbonyl oxygens [O(7B)···O(10B)] is 2·640(3) Å, and the dihedral angle between the plane of the ring and the plane of the carboxylic acid group is 0·9(2)°.

[(2-ap)(sa)] (10b)

The 1:1 2-aminopyrimidine/salicylic acid complex [(2-ap)(sa)] (10b) (Fig. 6) has a similar associative mode to complex (1). As in complex (1), the carboxylic acid proton of salicylic acid is located on the adjacent heterocyclic nitrogen. An intramolecular hydrogen bond is found between the hydroxy oxygen and one carboxylate oxygen of salicylic acid [O(21B)···O(10B), 2·512(4) Å: $\frac{1}{2}-x$, $-\frac{1}{2}+y$, z]. This compares with 2·62 Å for a similar bond in the parent acid.[26] Unlike in complex (1), the amine group of 2-ap is also hydrogen-bonded to another carboxylate oxygen [N(21A)···O(11B), 2·925(4) Å], forming a hydrogen-bonded zigzag polymer along the b cell direction [graph set C(6)] (Fig. 12).

[24] Smith, G., Kennard, C. H. L., and White, A. H., *J. Chem. Soc., Perkin Trans. 2*, 1976, 791.
[25] Smith, G., Kennard, C. H. L., and White, A. H., *Acta Crystallogr., Sect. B*, 1981, **37**, 1454.
[26] Sundaralingam, M., and Jenson, L. H., *Acta Crystallogr.*, 1965, **18**, 1053.

UM00011589

NOVARTIS EXHIBIT 1517
Novartis v. Regents, IPR2023-01347
Page 335 of 4460

[(2-apy)(dhba)] (11)

The structure of the 1 : 1 adduct of 2-aminopyridine with 2,6-dihydroxybenzoic acid [(2-apy)(dhba)] (11) consists of an eight-membered heteromolecular hydrogen-bonded ring (Fig. 7), similar to the interactive mode found for 2-ap. The acid group protonates the adjacent heterocyclic nitrogen. Two intramolecular hydrogen bonds exist in the dhba molecule [O(21B)···O(10B), 2·502(4) Å; O(61B)···O(11B), 2·554(4) Å], again giving graph sets similar to those found in complex (1). The packing is also similar to (1) with the amino group of 2-ap hydrogen-bonded to a hydroxy group [N(21A)···O(21B), 2·938(4) Å: $\frac{1}{2}-x$, $-\frac{1}{2}+y$, $\frac{5}{2}-z$] completing a hydrogen-bonded zigzag polymer along the b cell direction [graph set C(6)] (Fig. 13).

Hydrogen Bonding

Although the hydrogen-bonding patterns of 2-aminopyrimidines are well known, two new patterns have been found when 2-aminopyrimidine forms adducts with salicylic and phenoxyacetic acids. Characteristically both acid types form heterodimers with 2-ap. However, in the first new pattern the second amino hydrogen on 2-ap interacts with either a carboxylate oxygen {salicylic acid, [(2-ap)(sa)] (10b)} or a hydroxy oxygen {2,6-dihydroxybenzoic acid [(2-ap)(dhba)] (1)} leaving the second ring nitrogen on 2-ap free of any interactions. Commonly in (1:1) 2-ap adducts the complexed pairs form 'dimers' through the second amine hydrogens and ring nitrogens of 2-ap. The new pattern for (1) is identical to the hydrogen-bonding network found in the complex of 2-aminopyridine with 2,6-dihydroxybenzoic acid [(2-apy)(dhba)] (11), which does not have a second ring nitrogen on the hetrocyclic base. The 1:1 complex of 2-ap with (3,4-dichlorophenoxy)acetic acid, [(2-ap)(3,4-d)] (7), consists of the constituent pairs in the adducts which in turn form a non-coplanar 'dimer' through the amine hydrogens of 2-ap and carbonyl oxygens of the carboxylic acid group, once again leaving the second ring nitrogen free of any interactions. With compounds (1)–(11), no generalizations may be made about the predictability of protonation of the heterocyclic nitrogen by the acid to give an N^+–H···O association. With pyridine, it has been determined that, for proton transfer to take place, the pK_a difference (ΔpK_a) between the pair must be at least 3.[27] However, with other heterocyclic bases, including 2-aminopyrimidine (pK_a 2·8), this ΔpK_a value may be considerably less, possibly due to stabilization through secondary hydrogen bonding.[28]

Infrared Spectroscopy

For each compound, complexation with 2-ap can be recognized in the infrared spectrum by the presence of a number of medium broad peaks between 2500 and 1800 cm^{-1}. According to the literature[29] these peaks should indicate N^+–H

[27] Johnson, S. L., and Rumon, K. A., *J. Phys. Chem.*, 1965, **69**, 74.
[28] Etter, M. C., personal communication, 1991.
[29] Williams, D. H., and Fleming, I., 'Spectroscopic Methods in Organic Chemistry' 2nd Edn, pp. 35–73 (McGraw Hill: London 1973).

UM00011590
NOVARTIS EXHIBIT 1517
Novartis v. Regents, IPR2023-01347
Page 336 of 4460

stretching (as previously discussed for this series[16]) but are also present in the non-zwitterionic complexes of 2-ap. Complexes (2)–(9) all show a strong carbonyl (C=O) peak ($\geq$1700 cm^{-1}); this indicates that the acid group for each compound remains protonated. However, for complexes (1), (10a,b) and (11), characteristic carboxylate ion (CO_2^-) peaks are present, indicating interzwitterionic associations. Carboxylate ion antisymmetric and symmetric stretching frequencies range from 1567 to 1585 cm^{-1} and from 1331 to 1388 cm^{-1} (lit. 1610–1550 and 1420–1300 cm^{-1} respectively).[29] Each of these spectra also has a medium-to-weak peak between 1614 and 1634 cm^{-1} due to the amine salt. For N^+–H$\cdots$O associations in these dimers, a characteristic peak appears at 1694 cm^{-1}.[16] Only complex (10b) shows this peak (1694 cm^{-1}), while complexes (1), (10a) and (11) all have a strong peak at higher frequency (*c.* 1980 cm^{-1}).

Acknowledgments

The authors acknowledge financial support from the Centre for Instrumental and Developmental Chemistry of the Queensland University of Technology, the Australian Research Council, and the University of Queensland.

UM00011591

NOVARTIS EXHIBIT 1517
Novartis v. Regents, IPR2023-01347
Page 337 of 4460

This Page is Inserted by IFW Indexing and Scanning Operations and is not part of the Official Record

BEST AVAILABLE IMAGES

Defective images within this document are accurate representations of the original documents submitted by the applicant.

Defects in the images include but are not limited to the items checked:

- ☐ BLACK BORDERS
- ☐ IMAGE CUT OFF AT TOP, BOTTOM OR SIDES
- ☐ FADED TEXT OR DRAWING
- ☐ BLURRED OR ILLEGIBLE TEXT OR DRAWING
- ☐ SKEWED/SLANTED IMAGES
- ☐ COLOR OR BLACK AND WHITE PHOTOGRAPHS
- ☐ GRAY SCALE DOCUMENTS
- ☐ LINES OR MARKS ON ORIGINAL DOCUMENT
- ☐ REFERENCE(S) OR EXHIBIT(S) SUBMITTED ARE POOR QUALITY
- ☐ OTHER: _____

IMAGES ARE BEST AVAILABLE COPY.
As rescanning these documents will not correct the image problems checked, please do not report these problems to the IFW Image Problem Mailbox.

Aust. J. Chem., 2000, 53, 383–387

1 : 1 Molecular Complexes of 4-Amino-*N*-(4,6-dimethylpyrimidin-2-yl)benzenesulfonamide (Sulfamethazine) with Indole-2-carboxylic Acid and 2,4-Dinitrobenzoic Acid

Daniel E. Lynch,[A,B] *Pardeep Sandhu*[A] *and Simon Parsons*[C]

[A] School of Natural and Environmental Sciences, Coventry University, Coventry CV1 5FB, U.K.
[B] Author to whom correspondence should be addressed.
[C] Department of Chemistry, The University of Edinburgh, West Mains Road, Edinburgh EH9 3JJ, U.K.

The 1 : 1 molecular adducts of 4-amino-*N*-(4,6-dimethylpyrimidin-2-yl)benzenesulfonamide (Sulfamethazine) with respectively indole-2-carboxylic acid (1) and 2,4-dinitrobenzoic acid (2) have been prepared and their X-ray crystal structures determined. The acid groups in both structures form associative $R_2^2(8)$ graph set hydrogen-bonding interactions across the N(11)–H/N(17) site of Sulfamethazine. A comparison of the two distances between relevant non-hydrogen atoms in this configuration reveals that this association is not symmetrical. An average difference of 0.144 Å is observed for seven listed complexes of Sulfamethazine, five having been previously reported. This average difference compares with a value of 0.265 Å for the same interaction seen in carboxylic acid adducts of 2-aminopyrimidine.

Keywords. Sulfamethazine; carboxylic acid adducts; X-ray crystal structure.

Introduction

Complexation of a carboxylic acid with a 2-amino substituted heterocyclic, containing an sp^2 nitrogen atom adjacent to the amino group, predictably yields a hydrogen-bonded $R_2^2(8)$ graph set[1] interaction (Fig. 1*a*). This particular hydrogen bonding synthon (interestingly not listed by Desiraju in ref. 2) has been studied using, as the Lewis base, 2-aminopyridine,[3] 2-aminopyrimidine,[4,5] 2-aminotriazole,[6] 2-aminothiazole[7,8] and 2-aminooxazole[9] derivatives. Depending on the complexing agents, the association of a carboxylic acid with these bases may result in proton-transfer from the carboxylic O–H to the heterocyclic nitrogen resulting in an organic salt structure (Fig. 1*b*). Investigations into the two distances between associated non-hydrogen atoms reveals that this configuration is acentric and differences of 0.1–0.27 Å are observed.[4–9] There are to date over 20 examples for the structures of 2-aminopyridine type adducts with carboxylic acids, which display the large distance difference.[4,5] The authors' attention has now been directed at carboxylic acid adducts of molecules containing a 2-aminopyridine moiety but substituted on the amino nitrogen so that only one amino proton is available for intermolecular interaction. The number of commercially available organic bases that fit this criterion is large so we constrained our choice to molecules which have already had similar adduct structures reported. This also helps to increase the available data corresponding to the target $R_2^2(8)$ interaction. Our search led to Sulfamethazine* (or Sulfadimidine) (Fig. 2), which is a member of the sulfonamide class of drugs; other members include Sulfapyridine, Sulfadiazine, Sulfamethoxazole and Sulfathiazole. First synthesized in 1941[10] it has, since the early 1950s, been used as an antibacterial drug in animal feed.[11] However, studies by both academic[12,13] and government agencies[11,14] in the U.S.A. in the late 1980s to early 1990s showed Sulfamethazine (smz) to be carcenogenic in

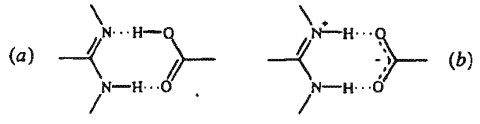


Fig. 1. The $R_2^2(8)$ graph set configuration seen for (*a*) the adduct and (*b*) the organic salt of a carboxylic acid/2-amino 1-aza heterocyclic base complex.

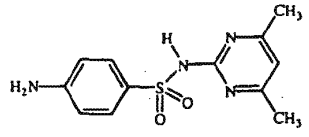


Fig. 2. Sulfamethazine.

* 4-Amino-*N*-(4,6-dimethylpyrimidin-2-yl)benzenesulfonamide.

Manuscript received 2 February 2000 © CSIRO 2000

10.1071/CH00021 0004-9425/00/050383

UM00011593
NOVARTIS EXHIBIT 1517
Novartis v. Regents, IPR2023-01347
Page 339 of 4460

laboratory animals. In recent years, its presence, particularly in the muscle tissue of swine,[15] in milk[11,16,17] and in chicken eggs,[18] has been monitored and thus current studies have concentrated on its detection[19] and the determination of safe levels.[12,16-18] From a crystal engineering point of view, smz not only contains a site suitable for carboxylic acid complexation, but it also contains two hydrogen-bond accepting sulfur bound oxygens, an additional hydrogen-bond accepting heterocyclic nitrogen and a hydrogen-bond donating amino group. The presence of these groups does not guarantee successful complexation and crystallization but they are helpful, particularly if a carboxylic acid containing other hydrogen-bond active groups is used. The structure of smz has been reported,[20] as has the methanol solvate structure,[21] but of more importance to this work are the adduct structures with trimethoprim (1 : 1 methanol solvate[22] and 2 : 1 water solvate[23]), salicylic acid,[24] 2-aminobenzoic acid,[25] 4-aminobenzoic acid,[25] acetylsalicylic acid[26] and 4-aminosalicylic acid,[26] all of which are not organic salts.

In this paper we report the 1 : 1 adduct structures of Sulfamethazine with respectively indole-2-carboxylic acid [(smz)(ica)] (1) and 2,4-dinitrobenzoic acid [(smz)(dnba)] (2) and summarize the two non-hydrogen distances involved in the $R_2^2(8)$ association observed in all of the carboxylic acid adducts of smz.

Experimental

Preparations

Complexes (1) and (2) were prepared using equimolar amounts (2.2 mmol) of Sulfamethazine with respectively indole-2-carboxylic acid and 2,4-dinitrobenzoic acid and involved refluxing for 20 min at *c.* 80°C in 40 ml of 95% ethanol. Products were subsequently obtained by the total evaporation of the solvent at room temperature. Crystals suitable for data collection were obtained in each case by vapour diffusion methods using water into ethanol: for (1), colourless needles (m.p. 210–212.5°C); for (2), yellow prisms (m.p. 180–182.5°C).

Crystallography

Crystal Data

Compound (1). $C_{21}H_{21}N_5O_4S$, mol. wt 439.5, monoclinic, space group $P2_1/n$, a 8.6764(15), b 18.072(3), c 13.712(4) Å, β 100.38(2)°, V 2114.9(9) Å^3, F(000) 920, D_c(Z = 4) 1.380 g cm^{-3}, μ(Mo Kα) 1.92 cm^{-1}, temperature 220(2) K.

Compound (2). $C_{10}H_{18}N_6O_8S$, mol. wt 490.5, triclinic, space group $P\bar{1}$, a 8.110(3), b 9.108(4), c 16.521(9) Å, α 77.68(3), β 87.60(4), γ 64.619(16)°, V 1075.5(8) Å^3, F(000) 508, D_c(Z = 2) 1.515 g cm^{-3}, μ(Mo Kα) 2.12 cm^{-1}, temperature 220(2) K.

Data Collection, Structure Solution and Refinement

X-ray diffraction data for compounds (1) and (2) were collected from crystals of dimensions 0.70 by 0.19 by 0.16 mm (1) and 0.54 by 0.46 by 0.27 mm (2) on an Stoe Stadi-4 diffractometer equipped with an Oxford Cryosystems low-temperature device operating at −53°C using monochromatized Mo Kα X-radiation (λ 0.71073 Å). Negligible change in the intensities of three standards monitored throughout the respective data collection periods indicated no significant crystal decomposition. Of 3693 (1) and 3772 (2) unique reflections collected up to $2\theta_{max}$ 50°, 1668 (1) and 2162 (2) with $F_o > 4.0\sigma(F_o)$ were considered observed and were used in the expression of the conventional refinement value. Data were corrected for Lorentz and polarization effects, but no absorption corrections were applied. The structures were solved by direct methods and refined using full matrix least squares (SHELX-97[27]) with anisotropic thermal parameters for all non-hydrogen atoms, which gave residuals* R_1, wR_2 and S of 0.057, 0.131 and 0.83 (1), and 0.055, 0.127 and 0.88 (2). The values for A and B in the weighting scheme $w = [\sigma^2(F_o^2) + (AP)^2 + BP]^{-1}$ {where $P = [(\text{max. } F_o^2, 0) + 2(F_c^2)]/3$} were 0.1000, 0.00 (1) and 0.1000, 0.00 (2). Hydrogen atoms were located by difference methods and both positional and thermal parameters were refined, although the methyl hydrogens in compound (1) were included in the refinement, at calculated positions, as riding models.

Results

Final atomic coordinates for compounds (1) and (2) are given in Table 1. Bond distances and angles, anisotropic thermal parameters, hydrogen atom coordinates and observed and calculated structure factors for both compounds have been deposited as an Accessory Publication.†

Discussion

Crystal Structures of [(smz)(ica)] (1) and [(smz)(dnba)] (2)

The structures of complexes (1) and (2) are shown in Figs 3 and 4 respectively and are presented in essentially

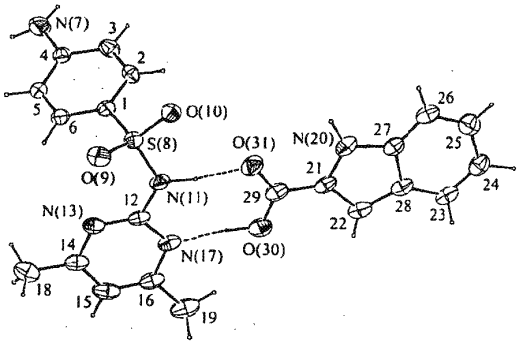


Fig. 3. Atom numbering scheme for (1). Unless otherwise indicated, atoms are carbon. Displacement ellipsoids are drawn at the 30% probability level. Hydrogen-bonding interactions are shown as dotted lines.

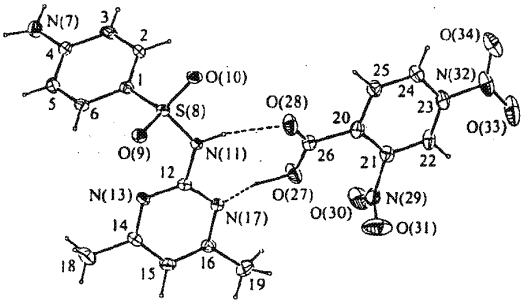


Fig. 4. Atom numbering scheme for (2). Unless otherwise indicated, atoms are carbon. Displacement ellipsoids are drawn at the 30% probability level. Hydrogen-bonding interactions are shown as dotted lines.

* $R_1 = \Sigma||F_o|-|F_c||/\Sigma|F_o|$ and $wR_2 = [\Sigma w(F_o^2-F_c^2)^2/\Sigma w(F_o)^2]^{1/2}$.

† Copies are available (until 31 December 2005) from the Australian Journal of Chemistry, P.O. Box 1139, Collingwood, Vic. 3066.

UM00011594
NOVARTIS EXHIBIT 1517
Novartis v. Regents, IPR2023-01347
Page 340 of 4460

the same conformation as for the five previously reported carboxylic acid adducts of smz; similar naming schemes have also been employed. The conformation of smz itself is defined by four geometric factors, the three torsion angles C(6)–C(1)–S(8)–N(11) (τ_1), C(1)–S(8)–N(11)–C(12) (τ_2), S(8)–N(11)–C(12)–N(13) (τ_3) and the dihedral angle between the two aromatic rings (ϕ), listed in Table 2. The first torsion angle τ_1 is obtuse (*c.* 93–165°) with only five [including both (1) and (2)] of the thirteen angles being negative. Interestingly, these five negative angles all fall between *c.* 93° and 101° with four of them being between *c.* 98° and 101°. The second torsion angle τ_2 for the examples given, the main angle influencing ϕ, is high acute with values ranging from *c.* 48° to 84° with approximately half being in the 60–70° range and eight of the thirteen being negative. The third torsion angle τ_3, for all samples, is low acute (*c.* 0–38°) with half being *c.* ≤13°. Thus, a combination of these three geometrical factors gives rise to ϕ, which for all examples (except one unpublished smz structure)[21] ranges from *c.* 42° to 109° with eight falling between *c.* 70° and 92°.

Table 1. Atomic coordinates and equivalent isotropic displacement parameters (Å²) for compounds (1) and (2)

U_{eq} is defined as one-third of the trace of the orthogonalized U_{ij} tensor

Compound	Atom	10^4x	10^4y	10^4z	10^3U_{eq}
(smz)(ica) (1)	C(1)	2065(5)	2413(2)	5809(3)	40(1)
	C(2)	1901(6)	2468(3)	4778(3)	51(1)
	C(3)	3182(6)	2548(3)	4346(4)	53(1)
	C(4)	4688(5)	2582(2)	4913(3)	47(1)
	C(5)	4845(6)	2493(3)	5937(4)	51(1)
	C(6)	3569(6)	2407(3)	6376(3)	49(1)
	N(7)	5952(6)	2730(3)	4489(4)	72(2)
	S(8)	408(1)	2354(1)	6354(1)	49(1)
	O(9)	762(4)	2655(2)	7334(2)	60(1)
	O(10)	-883(3)	2671(2)	5674(2)	56(1)
	N(11)	-90(5)	1487(2)	6387(3)	52(1)
	C(12)	751(6)	947(3)	6963(4)	48(1)
	N(13)	1914(5)	1132(2)	7692(3)	49(1)
	C(14)	2604(6)	578(3)	8249(4)	54(1)
	C(15)	2122(7)	-145(3)	8061(5)	65(2)
	C(16)	945(7)	-302(3)	7291(4)	58(1)
	N(17)	232(5)	253(2)	6721(3)	52(1)
	C(18)	3894(6)	778(3)	9075(4)	71(2)
	C(19)	372(7)	-1063(3)	7004(4)	81(2)
	N(20)	4827(5)	755(3)	6716(3)	58(1)
	C(21)	4111(6)	-228(3)	6071(4)	50(1)
	C(29)	2816(6)	-431(3)	5287(4)	58(1)
	O(30)	2138(5)	117(2)	4767(3)	63(1)
	O(31)	2426(4)	-1083(2)	5144(3)	67(1)
	C(22)	4785(7)	437(3)	6310(4)	51(1)
	C(23)	7065(7)	800(3)	7733(5)	63(2)
	C(24)	8076(7)	513(3)	8515(5)	66(2)
	C(25)	8036(7)	-238(4)	8749(5)	70(2)
	C(26)	7005(7)	-714(4)	8203(5)	64(2)
	C(27)	5981(6)	-423(3)	7393(4)	52(1)
	C(28)	5972(6)	330(3)	7141(4)	52(1)
(smz)(dnba) (2)	C(1)	4892(5)	-74(5)	3640(2)	26(1)
	C(2)	3078(6)	574(5)	3341(3)	29(1)
	C(3)	1941(6)	-83(6)	3725(3)	33(1)
	C(4)	2554(6)	-1394(5)	4417(3)	29(1)
	C(5)	4389(6)	-2046(6)	4705(3)	34(1)
	C(6)	5527(6)	-1403(6)	4323(3)	31(1)
	N(7)	1412(6)	-2044(6)	4798(3)	40(1)
	S(8)	6274(1)	833(1)	3172(1)	27(1)
	O(9)	7764(4)	426(4)	3737(2)	34(1)
	O(10)	5170(4)	2533(3)	2799(2)	34(1)
	N(11)	7079(5)	26(4)	2356(2)	31(1)
	C(12)	8385(5)	-1567(5)	2370(3)	27(1)
	N(13)	9086(5)	-2582(4)	3094(2)	32(1)
	C(14)	10460(6)	-4067(5)	3068(3)	35(1)
	C(15)	11073(6)	-4510(6)	2324(3)	39(1)
	C(16)	10192(6)	-3448(5)	1605(3)	33(1)
	N(17)	8803(4)	-1942(4)	1624(2)	29(1)
	C(18)	11271(10)	-5217(7)	3885(4)	52(2)
	C(19)	10641(9)	-3839(8)	771(4)	54(2)
	C(20)	4444(6)	-2368(6)	680(3)	34(1)
	C(21)	3923(6)	-1732(5)	1389(3)	35(1)
	C(22)	4675(7)	-2669(6)	2168(3)	42(1)
	C(23)	5996(7)	-4254(6)	2230(3)	41(1)
	C(24)	6585(7)	-4938(6)	1549(3)	43(1)
	C(25)	5795(7)	-4000(6)	787(3)	41(1)
	C(26)	3671(6)	-1403(6)	-182(3)	38(1)
	O(27)	2828(5)	169(4)	-248(2)	59(1)
	O(28)	3872(5)	-2114(4)	-743(2)	54(1)
	N(29)	2503(6)	-28(5)	1355(2)	46(1)
	O(30)	3019(6)	1045(4)	1357(2)	66(1)
	O(31)	967(6)	189(6)	1347(4)	98(2)
	N(32)	6853(8)	-5248(6)	3059(3)	59(1)
	O(33)	5967(8)	-4865(5)	3650(3)	91(2)
	O(34)	8371(6)	-6387(6)	3089(3)	76(1)

An abundance of hydrogen-bonding groups in both complexes has led to additional interactions, other than the associative $R_2^2(8)$ configuration, which create intricate hydrogen-bonding networks. For (1), the two smz amino protons associate respectively to the sulfonyl oxygens, attached to different molecules [N(7)–H(71)···O(9) 3.011(6) Å, ∠N–H···O 160(3)°; N(7)–H(72)···O(10) 2.930(6) Å, ∠N–H···O 160(3)°], while the indole N–H also associates to O(9), the same molecule as for N(7)–N(71) [N(20)–H(20)···O(9) 3.235(6) Å, ∠N–H···O 154(3)°]. For (2), the presence of the nitro groups as hydrogen-bond acceptors rivals the sulfonyl oxygens because one smz amino proton binds to O(9) [N(7)–H(71)···O(9) 3.152(4) Å, ∠N–H···O 158(3)°], while the other forms a three-centre interaction with the two nitro oxygens O(33) and O(34) [N(7)–H(72)···O(33) 3.356(4) Å, ∠N–H···O 150(3)°; N(7)–H(72)···O(34) 3.459(4) Å, ∠N–H···O 160(3)°]. The sulfonyl oxygen O(9) is also bound by a C–H···O association [C(3)–H(3)···O(9) 3.217(4) Å, ∠N–H···O 148(3)°], so too is O(10) [C(15)–H(15)···O(10) 3.249(4) Å, ∠N–H···O 150(3)°] and O(30) [C(2)–H(2)···O(30) 3.214(4) Å, ∠N–H···O 126(3)°].

Comments on the $R_2^2(8)$ *Graph Set Interaction*

Interesting comparisons can be made with the differing non-hydrogen distances (listed in Table 2) in the $R_2^2(8)$ association, characteristically observed in all the carboxylic acid adducts with smz. The distances for compound (1) are the most similar with a distance difference of only 0.035 Å whereas, for compound (2), the largest difference between the N–(H)···O and O–(H)···N atoms is observed, 0.314 Å. Compound (2) also has the shortest O–(H)···N distance, being well below 2.6 Å; the average distance for the other six complexes is 2.673(4) Å. The O–(H)···N distance observed in (2) can potentially be explained by the pK_a strength of the dnba molecule (pK_a = 1.42)[28] but this argument does not hold for the remainder because the next strongest acid, 4-aminosalicylic acid (pK_a = 1.99),[28] has the longest O–(H)···N distance of the seven compounds listed in Table 2. For comparison, the order of increasing acid strength after these first two substituted benzoic acids proceeds via 2-aminobenzoic acid (pK_a = 2.05), 4-aminobenzoic acid (pK_a = 2.38), salicylic acid (pK_a = 2.75),

UM00011595
NOVARTIS EXHIBIT 1517
Novartis v. Regents, IPR2023-01347
Page 341 of 4460

Table 2. Conformational data and hydrogen-bonding interactions for Sulfamethazine and its adduct structures; e.s.d. values are included where possible

τ_1, C(6)–C(1)–S(8)–N(11); τ_2, C(1)–S(8)–N(11)–C(12); τ_3, S(8)–N(11)–C(12)–N(13); ϕ, dihedral angle.
tmp, trimethoprim; sa, salicylic acid; 2-aba, 2-aminobenzoic acid; 4-aba, 4-aminobenzoic acid; acsa, acetylsalicylic acid; 4-asa, 4-aminosalicylic acid

Compound	τ_1 (deg)	τ_2 (deg)	τ_3 (deg)	ϕ (deg)	N–H···O (Å)	O–H···N (Å)	Ref.
smz	130.6	84.2(6)	37.9	102			18
smz	129	–82	34				19
[(smz)(MeOH)]	95(1)	–68(1)	4(1)	42.2			19
[(smz)(tmp)(MeOH)]	131.2(2)	–65.2(2)	10.5(2)	92.2(1)			20
$[(smz)_2(tmp)(H_2O)]$	–101.2[A]	68.5(3)	–8.0(4)	107.8(1)			21
	–97.7(2)	48.1(3)	35.0(4)	72.3(1)			
[(smz)(sa)]	–97.5	–66.4(3)	–7.7	109.0(4)	2.719(4)	2.603(3)	22
[(smz)(2-aba)]	112.4(3)	–59.6(3)	–0.7(4)	89.2	2.838(2)	2.663(2)	23
[(smz)(4-aba)]	164.6(2)	–83.2(2)	22.6(3)	83.2	2.811(2)	2.676(2)	23
[(smz)(4-asa)]	104.2(2)	–64.7(2)	–5.9(4)	84.1	2.779(3)	2.724(4)	24
[(smz)(acsa)]	159.8(3)	–82.8(4)	23.0(5)	84.6	2.842(4)	2.664(4)	24
[(smz)(ica)] (1)	–92.8(5)	68.1(5)	13.3(5)	77.8(5)	2.742(6)[B]	2.707(6)[C]	this work
[(smz)(dnba)] (2)	–98.3(4)	72.4(4)	–0.2(4)	70.3(4)	2.840(4)[B]	2.526(4)[C]	this work
					2.796(4)[D]	2.652(4)[D]	

[A] Converted to the obtuse angle.
[B] ∠N–H···O 172(3)° (1) and 164(3)° (2).
[C] ∠O–H···N 171(3)° (1) and 168(3)° (2).
[D] Average value.

indole-2-carboxylic acid (pK_a = 3.64) and acetylsalicylic acid (pK_a = 4.57).[28]

The average distances for the non-hydrogen atoms in the $R_2^2(8)$ association are stated in Table 2 and expectedly a difference of 0.144 Å is observed in favour of the O–H···N(pyrimidine) interaction. The same difference between the average distances for associated non-hydrogen atoms in carboxylic acid adducts of 2-aminopyrimidine is 0.265 Å.[4]* It is also interesting to note that in a series of nineteen,[5] plus three,[4] plus three[29–31] listed carboxylic acid adducts with 2-aminopyrimidine, seven are definitely proton-transfer complexes, five are unknown, while the remaining thirteen are neutral adducts where the carboxylic acids have retained their O–H protons. With the additional two structures reported in this paper, all seven known acid adducts with smz are not organic salts. A mechanism for the occurrence of proton transfer in acid/2-aminopyridine type complexes remains unclear but it will now be interesting to adduct smz with a very strong benzoic acid such as 2,4,6-trinitrobenzoic acid to possibly incur a salt structure.

Acknowledgment

The authors acknowledge financial support from the School of Natural and Environmental Sciences of Coventry University.

References

[1] Etter, M. C., *Acc. Chem. Res.*, 1990, **23**, 120.
[2] Desiraju, G. M., *Angew. Chem., Int. Ed. Engl.*, 1995, **34**, 2311.
[3] Lynch, D. E., Smith, G., Freney, D., Byriel, K. A., and Kennard, C. H. L., *Aust. J. Chem.*, 1994, **47**, 1097.
[4] Lynch, D. E., Latif, T., Smith, G., Byriel, K. A., Kennard, C. H. L., and Parsons, S., *Aust. J. Chem.*, 1998, **51**, 403.
[5] Lynch, D. E., Latif, T., Smith, G., Byriel, K. A., and Kennard, C. H. L., *J. Chem. Crystallogr.*, 1997, **27**, 567.
[6] Lynch, D. E., Dougall, T., Smith, G., Byriel, K. A., and Kennard, C. H. L., *J. Chem. Crystallogr.*, 1999, **29**, 67.
[7] Lynch, D. E., Nicholls, L. J., Smith, G., Byriel, K. A., and Kennard, C. H. L., *Acta Crystallogr., Sect. B*, 1999, **55**, 758.
[8] Lynch, D. E., Cooper, C. J., Chauhan, V., Smith, G., Healy, P., and Parsons, S., *Aust. J. Chem.*, 1999, **52**, 695.
[9] Lynch, D. E., Singh, M., and Parsons, S., *Crystal Eng.*, 2000, in press.
[10] Caldwell, W. T., Kornfield, E. C., and Donnell, C. K., *J. Am. Chem. Soc.*, 1941, **63**, 2188.
[11] http://www.trufax.org/research/f43.htm
[12] Littlefield, N. A., Sheldon, W. G., Allen, R., and Gaylor, D. W., *Food Chem. Toxicol.*, 1990, **28**, 157.
[13] Peters, J. H., Gordon, G. R., Lin, E., Green, C. E., and Tyson C. A., *Anticancer Res.*, 1990, **10**, 225.
[14] Mitchell, G. A., *Can. Vet. J.*, 1988, **29**, 327.
[15] http://muextension.missouri.edu/xlpor/agguides/ansci/g02358.htm
[16] Sternesjö, Å., Mellgren, C., and Björck, L., *Anal. Biochem.*, 1995, **226**, 175.
[17] http://www.fda.gov/bbs/topics/NEWS/NEW00061.htm
[18] http://www.nal.usda.gov/ttic/tektran/data/000008/11/0000081156.html
[19] Diaz, T. G., Cabanillas, G., Valenzuela, M. I. A., and Salinas, F., *Analyst.*, 1996, **121**, 547, and references therein.
[20] Tiwari, R. K., Haridas, M., and Singh, T. P., *Acta Crystallogr., Sect. C*, 1984, **40**, 655.
[21] Rambaud, J., Maury, L., Pauvert, B., Audran, M., Lasserre, Y., and Berge, G., *Acta Crystallogr., Sect. C*, 1985, **41**, 133.
[22] Bettinetti, G., and Sardone, N., *Acta Crystallogr., Sect. C*, 1997, **53**, 594.
[23] Sardone, N., Bettinetti, G., and Sorrenti, M., *Acta Crystallogr., Sect. C*, 1997, **53**, 1295.
[24] Patel, 1988,
[25] Caira.
[26] Caira.
[27] Sheld Repul
[28] Rapp Identi

* This value does not include the three structures contained in refs 29–31.

UM00011596
NOVARTIS EXHIBIT 1517
Novartis v. Regents, IPR2023-01347
Page 342 of 4460

[24] Patel, U., Haridas, M., and Singh, T. P., *Acta Crystallogr., Sect. C*, 1988, **44**, 655.
[25] Caira, M. R., *J. Cryst. Spec. Res.*, 1991, **21**, 641.
[26] Caira, M. R., *J. Cryst. Spec. Res.*, 1992, **22**, 193.
[27] Sheldrick, G. M., SHELX-97, University of Göttingen, Federal Republic of Germany, 1997.
[28] Rappoport, Z., (Ed.) 'Handbook of Tables for Organic Compound Identification' 3rd Edn, pp. 429–433 (CRC: Ohio 1967).
[29] Goswami, S., Mahapatra, A. K., Ghosh, K., Nigam, G. D., Chinnakali, K., and Fun, H, -K, *Acta Crystallogr., Sect. C*, 1999, **55**, 87.
[30] Chinnakall, K., Fun, H, -K, Goswami, S., Mahapatra, A. K., and Nigam, G. D., *Acta Crystallogr., Sect. C*, 1999, **55**, 399.
[31] Goswami, S., Mahapatra, A. K., Nigam, G. D., Chinnakali, K., Fun, H, -K, and Razak, I. A., *Acta Crystallogr., Sect. C*, 1999, **55**, 583.

UM00011597
NOVARTIS EXHIBIT 1517
Novartis v. Regents, IPR2023-01347
Page 343 of 4460

This Page is Inserted by IFW Indexing and Scanning Operations and is not part of the Official Record

BEST AVAILABLE IMAGES

Defective images within this document are accurate representations of the original documents submitted by the applicant.

Defects in the images include but are not limited to the items checked:

- ☐ BLACK BORDERS
- ☐ IMAGE CUT OFF AT TOP, BOTTOM OR SIDES
- ☐ FADED TEXT OR DRAWING
- ☐ BLURRED OR ILLEGIBLE TEXT OR DRAWING
- ☐ SKEWED/SLANTED IMAGES
- ☐ COLOR OR BLACK AND WHITE PHOTOGRAPHS
- ☐ GRAY SCALE DOCUMENTS
- ☐ LINES OR MARKS ON ORIGINAL DOCUMENT
- ☐ REFERENCE(S) OR EXHIBIT(S) SUBMITTED ARE POOR QUALITY
- ☐ OTHER: _____

IMAGES ARE BEST AVAILABLE COPY.
As rescanning these documents will not correct the image problems checked, please do not report these problems to the IFW Image Problem Mailbox.

CHEMOTHERAPEUTIC DRUGS IN ANAEROBIC INFECTIONS OF WOUNDS *

JAMES MCINTOSH, M D, LL D ABERD
PROFESSOR OF PATHOLOGY IN THE UNIVERSITY OF LONDON; DIRECTOR, BLAND-SUTTON INSTITUTE

F. R. SELBIE
M D ABERD
ASSISTANT PATHOLOGIST, BLAND-SUTTON INSTITUTE

(From the Bland-Sutton Institute of Pathology, Middlesex Hospital, and the Central Laboratory, EMS, Stoke Mandeville Hospital)

NUMEROUS investigations have been carried out on the chemotherapy of gas gangrene, both from the experimental aspect and in its practical application, but there is still diversity of opinion as to its real value. An analysis of recent returns on cases of gas gangrene from casualties among the fighting forces and civilians failed to show any appreciable reduction in its incidence in spite of both prophylactic and therapeutic chemotherapy.

We reviewed some of the published work in a previous paper in which we pointed out that the experimental findings did not give such good results as had been hoped for when applied to war wounds and air-raid casualties (McIntosh and Selbie 1942). In this paper are given the results of some further experimental investigations carried out with the idea of explaining the discrepancy and finding more efficient remedies. A large number of chemotherapeutic substances have been tested, but here we have restricted the details to those found most effective, in particular the sulphonamides, the acridines and penicillin.

Much of the discrepancy appears to arise from the fact that the testing of chemotherapeutic substances on anaerobes is a complex procedure. This is due to two factors. The first is the inherent difficulty of anaerobic cultivation, intensified as it is by the use of the poor media necessary for bacteriostatic testing—it often needs careful balancing between nutritional value and anti-bacteriostatic effects of the medium to get a reading at all, particularly with recently isolated strains. The second difficulty is the therapeutic test in animals, in which many different procedures are used to produce the experimental infections. In some procedures little or no account is taken of the actual number of bacteria injected, and again divers methods are employed to produce the muscle injury, either mechanical or chemical; sometimes open wounds are preferred and sometimes closed. In estimating the chemotherapeutic value of a drug it is also necessary to take into consideration both its bacteriostatic action and toxicity.

Earlier experiments showed that mice are relatively susceptible to anaerobic infections, and therefore to facilitate the testing (an important consideration in wartime) only mice have been used in our recent experiments. The method adopted for the therapeutic testing was to inject the known dose of bacteria into the muscle of the right thigh and an hour later to inject in the same site the chemotherapeutic substance. This interval allows the microbes to penetrate into the muscle and so establish a spreading gas-gangrene infection. If the remedy is injected immediately after the injected dose its effects are of course much enhanced, but the action is apparently that of an antiseptic, since substances with no chemotherapeutic action may be effective.

BACTERIOSTATIC ACTION

The medium found satisfactory for the bacteriostatic tests was ½ strength meat broth plus 0·2% glucose, but where difficulty has been found in obtaining satisfactory growth with this medium full strength broth has been substituted.

The medium is inoculated with 0·5 c.cm. of an 18-hour culture of the anaerobe containing approximately a million viable bacteria, though in the case of some anaerobes, particularly *Clostridium œdematiens* when freshly isolated, at least double this amount is required. Before use the medium, to which sterile glucose has just been added, is boiled for 10–15 minutes and then cooled rapidly; the required amount of drug is added to the first tube and then serial dilutions are made quickly in the remaining tubes. The tubes are then inoculated with a young growing culture (18 hours), placed in a McIntosh and Fildes jar and incubated for 24–48 hours; the tube in which bacteriostatic action is complete is then noted. The bacteriostatic effects of the remedies are given in table I; the dilutions are expressed as direct dilutions.

Bacteriostatic action as a rule bears some relation to chemotherapeutic action, but this is not necessarily so because at times a substance with high bacteriostatic action, such as notatin, apparently has little or no chemotherapeutic power.

TABLE I—BACTERIOSTATIC ACTION

—	Dilution giving complete bacteriostasis		
	Cl. welchii	*Cl. œdematiens*	*Cl. septicum*
Sulphanilamide	1/400	1/500	1/2900
Sulphathiazole	1/800	1/1000	1/102,000
5-aminoacridine hydrochloride	1/160,000	1/640,000	1/640,000
2 : 7-diamino-acridine hydrochloride	1/80,000	1/640,000	1/640,000
2 : 8-diamino-acridine sulphate	1/160,000	1/640,000	1/640,000
Penicillin	1/250,000	1/500,000	1/500,000
Notatin	1/1,000,000,000	1/1,000,000,000	1/1,000,000,000
Propamidine	1/320,000	1/40,000,000	1/320,000

TOXICITY

The toxicity tests are carried out on mice by the ordinary procedure. A certain quantity of the drug in milligrammes is weighed out, dissolved or suspended in saline, and increasing doses of it injected into the thigh, the local and general toxic effects being noted. Comparisons are then made with the therapeutic dose.

General toxic effect.—Our experience of the general toxicity in mice of the therapeutic acridines is in general agreement with the findings of Albert and others (1938) and of Rubbo, Albert and Maxwell (1942). The therapeutic dose we have employed in mice (0·5 mg.) is about ¼ of the maximum tolerated dose of proflavine or about ½ of the L 50% dose. The margin was slightly greater with 2 : 7-diaminoacridine and rather less with 5-aminoacridine. With the sulphonamides (40 mg.) the margin was about the same, and with penicillin very much greater.

Local effect.—Proflavine and 2 : 7-diaminoacridine in therapeutic doses produced little or no local effect, whereas 5-aminoacridine caused some local inflammatory reaction. The sulphonamides caused little or no reaction and penicillin had no local effect.†

THERAPEUTIC ACTION

Method of testing.—In table II the layout of an experiment and the method of estimating the relative value of drugs is demonstrated. The mice are injected intramuscularly in the right thigh with 0·2 c.cm. of washed organisms suspended in a solution of 2·5% calcium chloride. Washing is necessary to remove any toxin. The dose of micro-organisms is standardised so that it contains 100 lethal doses; that is usually about 400 million in the case of *Cl. welchii* and *Cl. œdematiens* and 100,000 for *Cl. septicum*, as measured by standard opacity tubes for *Bacterium coli* which give comparable figures. The drug to be tested is injected an hour later in solution or suspension in quantities of 0·1 or 0·2 c.cm. at the same site as the infecting injection. The strains of clostridia employed were: *Cl. welchii* BSI No. 186 and S 107 supplied by Miss Robertson; *Cl. septicum* BSI strain 84; and *Cl. œdematiens* Jolly and HI. *Cl. welchii* BSI No. 186 and *Cl. œdematiens* HI are recently isolated strains from cases of gas gangrene.

We chose the interval of an hour because by that time the infection has developed, as shown by the presence of considerable œdema. Histological examination has

* This work was done on behalf of the War Wounds Committee of the Medical Research Council.

† There has lately been some criticism of the use of the acridine series of drugs in the treatment of wounds, on account of their tendency to produce local necrotic action and delay in healing. Our observations however have clearly shown that in the doses recommended such untoward effects are at a minimum and certainly no more severe than that of some other compounds now in use. We hope to publish shortly a detailed account of our observations on the toxicity of these drugs.

UM00011599
NOVARTIS EXHIBIT 1517
Novartis v. Regents, IPR2023-01347
Page 345 of 4460

confirmed this and has shown that the bacteria have invaded the muscle. At this time the infection is still relatively local since organisms cannot be recovered from the blood-stream till after 3 hours.

In the estimation of the chemotherapeutic value the average survival-rate of the mice in a 3-day period was used. The figure is obtained by dividing the total number of whole days survived in each group of mice by the number of mice in the group (Whitby 1937). The mortality for only 3 days is considered because mice living beyond this period usually survive indefinitely. Thus the maximum or complete survival figure would be 3·0, and this figure is occasionally reached. A typical result of a test is given in table II.

TABLE II—LOCAL TREATMENT OF *Cl. welchii* (s107) INFECTION IN MICE

Infecting dose : 0·1 c.cm. washed suspension of *Cl. welchii* + 0·1 c.cm. 5% CaCl, intramuscularly in right thigh.
Treatment : 0·1 or 0·2 c.cm. of solution or suspension of drug injected at same site 1 hour after infection.

TREATED MICE (400 million *Cl. welchii*)	No. of mice	Deaths on day 1	Deaths on day 2	Deaths on day 3	Survivors at 3 days	Survivors at 7 days	Av. no. of days survived* at 3 days
Penicillin, 34 units ..	6	1	1	0	4	3	2·2
2 : 8-diaminoacridine (proflavine), 0·5 mg.	6	2	3	1	0	0	0·8
2 : 7-diaminoacridine, 0·5 mg. ..	6	4	0	0	2	2	1·0
5-aminoacridine 0·5 mg..	6	2	1	0	3	2	1·7
Sulphathiazole 40 mg.	6	6	..	..	0	0	0
CONTROL MICE							
400 million *Cl. welchii*	6	6	..	..	0	0	0
40 ,, ,,	4	4	..	..	0	0	0
4 ,, ,,	4	2	1	1	0	0	0·75

* The average number of days survived is obtained by dividing the total number of whole days survived by the number of mice in the group.

Results.—The results of our tests on the three chief causative agents in gas gangrene are summarised in tables III and IV. These tables show that as good an estimate was obtained at the end of 3 days as at the end of 7, since the majority of mice surviving for 3 days survived indefinitely.

TABLE III—EFFECT OF LOCAL TREATMENT 1 HOUR AFTER INFECTION IN MICE

Treatment	No. of expts.	No. of mice	Per cent. survivors at 3 days	Per cent. survivors at 7 days	Av. no. of days survived at 3 days
Cl. welchii INFECTION					
Sulphanilamide 40 mg. ..	3	30	23	17	0·8
Sulphathiazole 40 mg. ..	5	30	3	3	0·3
Sulphadiazine 40 mg.	1	6	0	0	0·3
2 : 8-diaminoacridine (proflavine) 0·5 mg..	10	78	44	38	1·6
2 : 7-diaminoacridine 0·5 mg...	4	24	58	50	1·9
5-aminoacridine 0·5 mg. ..	4	24	50	46	1·7
Penicillin 34 units	5	36	86	78	2·7
Propamidine 0·5 mg.	4	22	14	14	0·8
Notatin 0·02 mg.	2	12	0	0	0
Nil	14	104	0	0	0
Cl. septicum INFECTION					
Sulphathiazole 40 mg. ..	3	18	78	72	2·7
Sulphathiazole 10 mg. ..	2	12	50	33	2·2
Sulphadiazine 10 mg. ..	1	6	17	17	0·8
2 : 8-diaminoacridine 0·5 mg.	2	12	0	0	0·9
2 : 7-diaminoacridine 0·3 mg.	1	6	17	0	1·3
5-aminoacridine 0·5 mg. ..	2	12	25	0	1·8
Penicillin 34 units	2	12	17	0	1·4
Propamidine 0·5 mg. ..	3	18	0	0	0·3
Notatin 0·02 mg.	2	12	0	0	0
Nil	5	30	0	0	0
Cl. œdematiens INFECTION					
Sulphathiazole 40 mg. ..	4	24	0	0	0·25
Sulphadiazine 40 mg. ..	2	12	0	0	0·3
2 : 8-diaminoacridine 0·5 mg.	2	12	0	0	1·1
5-aminoacridine 0·5 mg. ..	4	24	0	0	1·2
Penicillin 34 units	4	24	0	0	1·3
Propamidine 0·5 mg. ..	2	12	0	0	0·8
Nil	4	24	0	0	0

TABLE IV—SUMMARY OF CHEMOTHERAPEUTIC EFFECTS OF THE THREE MOST ACTIVE SUBSTANCES

Treatment 1 hr. after infection	Av. no. of days survived at 3 days		
	Cl. welchii	*Cl. septicum*	*Cl. œdematiens*
Sulphathiazole ..	0·3	2·7	0·2
Acridines	1·7	1·4	1·1
Penicillin	2·7	1·4	1·3

EFFECTS OF MIXTURES OF SULPHATHIAZOLE AND 5-AMINOACRIDINE ON *Cl. welchii* AND *Cl. septicum* INFECTIONS

Tests were then made with various mixtures of the more active chemotherapeutic remedies, to determine whether there was any interference with their individual therapeutic action. In the first experiment (table v), 5-aminoacridine and sulphathiazole were used because 5-aminoacridine was more active than proflavine on *Cl. welchii* and sulphathiazole most active on *Cl. septicum*. The doses of drug used here were a quarter of those usually employed, so that evidence of synergism might be obtained, and each group consisted of 6 mice. In the second experiment (table v), a dry mixture of 99 parts of sulphathiazole and 1 part of 5-aminoacridine prepared by Mr. F. A. Robinson was used, of which the dose injected corresponded to sulphathiazole 40 mg. and

TABLE V—EFFECTS OF MIXTURES OF SULPHATHIAZOLE AND 5-AMINOACRIDINE ON *Cl. welchii* AND *Cl. septicum* INFECTIONS IN MICE

Treatment at 1 hr.	Av. no. of days survived at 3 days			
	Expt. 1		Expt. 2	
	Cl. welchii	*Cl. septicum*	*Cl. welchii*	*Cl. septicum*
5-aminoacridine and sulphathiazole ..	0·8	2·5	1·2	3·0
5-aminoacridine ..	0·8	0·7	1·7	1·7
Sulphathiazole ..	0·2	1·8	0·2	2·3
Nil	0	0	0	0

Each group consisted of 6 mice.
Doses of drugs { Expt. 1 : 5-aminoacridine 0·1 mg., sulphathiazole 10 mg. / Expt. 2 : 5-aminoacridine 0·4 mg., sulphathiazole 40 mg.

5-aminoacridine 0·4 mg. The two experiments show that there was no interference with the individual therapeutic action of the two drugs. A synergic action was shown against *Cl. septicum*, in which infection both drugs are highly effective ; against *Cl. welchii* there was no evidence of synergism, probably because sulphathiazole, in the doses used, has little effect.

DISCUSSION

The discrepancy between the experimental and field results in the chemotherapy of gas gangrene seems largely due to the fact that most of the experimental anaerobic infections used as tests are not severe enough to be comparable with the disease in man ; thus the chemotherapeutic remedies are made to appear much more effective than they really are. In the present tests we have tried to overcome this by devising a standard severe infection in mice. The disease is produced by the intramuscular injection of 100 minimal doses of the bacteria with calcium chloride as a stimulant, followed an hour later in the same site by an injection of the chemotherapeutic drug under test. This interval of an hour does give consistent results with repeated tests.

The results show that good effects may be hoped for by the local application of a chemotherapeutic drug while the disease is in an early stage. The test we have used might be more aptly described as a prophylactic one. Owing to the rapidity with which gas gangrene spreads the value of local treatment becomes restricted, and general treatment, including antitoxins, is then essential.

Since no one drug appears to be equally active against the three common pathogenic anaerobes found in gas

UM00011600
NOVARTIS EXHIBIT 1517
Novartis v. Regents, IPR2023-01347
Page 346 of 4460

gangrene the best results are likely to be achieved with a mixture of drugs. Our experience suggests that the most effective mixture would be penicillin and sulphathiazole, but while penicillin is not available in quantity we would suggest a mixture of sulphathiazole and an acridine. The acridine we would suggest is proflavine, since it is of low toxicity and very slightly inferior in its action to the other two acridines; it is easily prepared and can be obtained in large amounts. For the early treatment of war wounds in general we suggest the local application of a mixed powder of these two drugs in the proportion of 100 parts sulphathiazole to 1 part of proflavine, using the dosage recommended for sulphathiazole. In actual cases of gas gangrene this local treatment should be supplemented by antitoxin therapy and other general measures..

These drugs of course may be applied suspended in a vehicle, but our experience with vehicles so far recommended is that those which are likely to remain in situ for any length of time are toxic, producing various degrees of local necrosis or considerable foreign-body reaction. There is therefore a danger that the use of vehicles may give rise to unsatisfactory conditions for wound healing. These objections however do not apply to the use of drug-containing vehicles in the field as emergency dressings for superficial injuries or burns. A vehicle which we have found generally satisfactory for this purpose is composed of gum acacia 20%, glycerin 10%, gelatin 1·75% and castor oil 5% in water. In no instance however should the mixture be applied to the brain or nerve tissue.

We have also attempted to evaluate the relationship of the more active chemotherapeutic drugs to serum therapy on the lines of Henderson and Gorer (1940). The effect of antitoxin on this type of infection is irregular but we have found that during the early stages of infection greater therapeutic effect could be got by combining the drug and antitoxin than by either alone. Experiments are now in hand to determine the effects of combined treatment in the more advanced stages of the disease.

SUMMARY

A reliable technique for testing the comparative value of chemotherapeutic remedies on anaerobic infections in mice has been described.

In the doses used the most effective chemotherapeutic substances against the individual infections were penicillin against *Cl. welchii* and *Cl. œdematiens*, and sulphathiazole against *Cl. septicum*. The acridines possess a fairly powerful action against all three anaerobes, though in a lower degree. Propamidine had a lower activity against all three organisms, though its individual action in the case of *Cl. welchii* and *Cl. œdematiens* compared favourably with the sulphonamides.

The tests show that the anaerobes of gas gangrene are variable in their individual susceptibility to chemotherapeutic agents, in that as a rule no one drug is equally active against the three common anaerobes responsible for gas gangrene (*Cl. welchii*, *Cl. septicum* and *Cl. œdematiens*). The best prophylactic results are therefore most likely to be achieved by the use of a mixture of drugs and our experience suggests the local application of a mixture of sulphathiazole and proflavine. We further recommend that the use of vehicles should be confined to superficial application.

Treatment in the more advanced stages of the disease is difficult and requires additional measures and the use of antitoxins.

REFERENCES

Albert, A., Francis, A. E., Garrod, L. P. and Linnell, W. H. (1938) *Brit. J. exp. Path.* 19, 41.
Henderson, D. W. and Gorer, P. A. (1940) *J. Hyg., Camb.* 40, 345.
McIntosh, J. and Selbie, F. R. (1942) *Lancet*, ii, 750.
Rubbo, S. D., Albert, A., Maxwell, M. (1942) *Brit. J. exp. Path.* 23, 69.
Whitby, L. E. H. (1937) *Lancet*, i, 1517.

ULSTER DOCTORS IN THE SERVICES.—Three out of every four men who have qualified for the medical profession in Northern Ireland since 1938 have volunteered for the medical branches of the Fighting Services. Almost all of them enlisted immediately on completing their statutory six months residence in a hospital. So many members of the medical staffs of the Ulster voluntary hospitals have joined up that it has been possible to carry on the work only by bringing back from retirement senior members of the staffs.

HYDATID DISEASE IN WALES

H. R. I. WOLFE, MB LOND, FRCS

SURGEON LIEUT.-COMMANDER RNVR; ASSISTANT SURGEON, SURGICAL UNIT, WELSH NATIONAL SCHOOL OF MEDICINE, ROYAL INFIRMARY, CARDIFF

IN England hydatid disease is generally accepted as rare, but I assisted in the treatment of 10 new and 1 recurrent case in the Royal Infirmary, Cardiff, between 1936 and 1938. This experience suggested that the disease is more prevalent in Wales than elsewhere in the British Isles. I was unable to find support in published work for this view, but in the records of the hospital I found that 34 patients had been treated from 1926 to 1938. Reports of only 4 of these have been previously published. Tables I and II give evidence of the comparatively high incidence of the condition in Wales.

The figures are of course small in comparison with those of countries where sheep-rearing is a prominent industry, but they show that diagnosis is difficult and manifestations protean in a disease previously supposed so rare, and probably often overlooked. The prevalence of the disease in Wales demands measures to stamp it out.

TABLE I—INCIDENCE OF HYDATID DISEASE IN ENGLAND, SCOTLAND AND WALES FROM 1931 TO 1935 INCLUSIVE

Country	Population	Deaths from hydatid disease	Deaths per head of population
England ..	38,322,120	103	1 : 372,000
Scotland ..	4,966,300	2	1 : 2,483,000
Wales ..	2,526,880	35	1 : 72,000

Compiled from the Registrar-General's statistical review for England and Wales and from Scottish figures supplied by Dr P. L. McKinlay.

TABLE II—CASES OF HYDATID DISEASE TREATED IN SOUTH WALES (90 CASES) AND IN THE LONDON TEACHING HOSPITALS (28 CASES)

Hospital	Beds	Period reviewed (yr)	Cases of hydatid disease admitted
SOUTH WALES			
Cardiff Royal Infirmary ..	380	14	34
Swansea General	336	13	17
Hospitals of Welsh National Memorial Assoc. ..	..	13	25
Royal Gwent, Newport ..	210	8	10
Merthyr General	123	13	4
LONDON			
St. Thomas's	682	12	9*
London Hospital	849	9	10**
Guy's	692	10	9

* 2 cases were from New Zealand. ** Diagnosis doubtful in 1 case. Between 1926 and 1936 only one case of hydatid disease was admitted to a local hospital in a county adjacent to Wales.

That it is preventable is clear, for hydatid disease is now very rare in Iceland (Sambon 1925), and there is also evidence to show that it is diminishing in Australia (Kneebone 1938). Control of the number of dogs, stringent regulations concerning the disposal of offal, and education of the public have led to a decrease in the incidence in Shetland where it was once fairly common (Lawson Dick 1938). There is no reason to doubt that a similar satisfactory result can be achieved in Wales by adopting appropriate measures.

EPIDEMIOLOGY

Source of infection.—Dogs are undoubtedly the chief source of human infection. They become infested by feeding on the offal of infected sheep. In some districts in South Wales offal from ineffectively supervised abattoirs is either thrown on refuse heaps or sold for manure, and no provision is made to prevent dogs

UM00011601
NOVARTIS EXHIBIT 1517
Novartis v. Regents, IPR2023-01347
Page 347 of 4460

patient had douched that morning and there were no clinical findings except for palpable glands in the groin. All pathological tests were negative for gonorrhœa and syphilis and the patient returned in 5 days to hear these results and for further examination. She was then found to have a thin frothy discharge due to *Trichomonas vaginalis*; smears, cultures, Wassermann and Kahn were again negative. Antiseptics were withheld and only palliative treatment for the trichomonas infection advised. Further examinations and blood tests were carried out Aug. 20 and Sept. 10; no clinical evidence of syphilis was found and Wassermann and Kahn tests were again negative.

The patient returned on Oct. 15. Externally there was no sign of infection, and a speculum was passed to examine vagina and cervix. After swabbing the cervix was clear and uninflamed but a minute cream-coloured spot at one edge of the speculum was seen. The first thought was that a wisp of cotton-wool had been left behind after swabbing, but on slightly withdrawing the Ferguson speculum the "wisp" became one corner of a somewhat triangular ulcer high on the lateral wall of the left fornix. The speculum was removed but digital examination only with difficulty detected the ulcer and a satisfactory view was only obtained by using a bivalve speculum. Clinically the ulcer was syphilitic: a scraping showed *Spirochæta pallida* and blood tests were returned positive.

These two cases illustrate the ease with which early syphilis can go undetected even when being searched for. In the first the difficulty arose from the long incubation period coupled with the minor fact of a sheath having been used during intercourse; in the second from the unusual position of the primary sore in the lateral fornix.

ZINC PEROXIDE, PROFLAVINE AND PENICILLIN IN EXPERIMENTAL CL. WELCHII INFECTIONS

JAMES MCINTOSH
M D, LLD ABERD
PROFESSOR OF PATHOLOGY IN THE UNIVERSITY OF LONDON

F. R. SELBIE
M D ABERD
ASSISTANT PATHOLOGIST AT THE BLAND-SUTTON INSTITUTE

(From the laboratory at the Bland-Sutton Institute of Pathology, Middlesex Hospital, and the Central Pathology Laboratory, EMS, Sector V)

EVEN with the most up-to-date treatment (surgery, serum therapy and chemotherapy) gas gangrene remains a serious complication of battle and air-raid wounds on account of its high fatality (30%–50%). The rapidity with which the disease can develop in torn and lacerated muscles makes preventive treatment difficult, and this is particularly the case with *Clostridium welchii*, the commonest cause of gas gangrene in Western Europe. We are now trying to find out the most suitable chemotherapeutic and specific treatment immediately after wounding. We have already shown that the sulphonamides are of value in preventing the development of gas gangrene in mice when administered locally in large quantities and soon after infection (McIntosh and Selbie 1941). Several publications, notably those of Hawking (1941) and Reed and Orr (1941) have supported our findings. Other further studies include investigations on the action of zinc peroxide, proflavine, penicillin and gramicidin on *Cl. welchii* infection.

MATERIAL AND METHODS

The strain of *Cl. welchii* and the methods used were the same as in our previous experiments except that bacterial suspensions for infection were prepared from 18-hour anaerobic cultures in 4% Difco proteose-peptone in distilled water. With this medium it was possible to obtain highly virulent cultures with much greater regularity than with Robinson's meat broth. Throughout the experiments we found that the intramuscular injection in the right thigh of 0·1 c.cm. of a washed suspension containing 2000 or 4000 million *Cl. welchii* and 0·1 c.cm. of 5% calcium chloride was sufficient to kill all untreated mice within 24 hours. This dose has usually been equivalent to at least 100 lethal doses and is therefore a severe test of preventive and therapeutic measures. It will become evident, however, that there were considerable variations in the severity of the infection, in that there was a variable response to treatment with the same drug. The substances to be tested for their prophylactic or therapeutic effect were injected into the right thigh at the site of infection immediately after or at varying intervals after infection.

EXPERIMENTAL RESULTS

The results are presented in a series of tables in which the mortality for only 3 days is considered since mice surviving that time usually survive indefinitely. The average number of days survived, shown in each table, is obtained by dividing the total number of whole days survived in each group of mice by the number of mice in the group. The sum of a number of experiments with sulphanilamide, done during the same period, is included in table I for comparison.

TABLE I—EFFECT ON *Cl. welchii* INFECTION IN MICE OF SULPHANILAMIDE, ZINC PEROXIDE, PROFLAVINE, AND PENICILLIN, ADMINISTERED LOCALLY AT TIME OF INFECTION

Drug	No. of expts.	Mice	Mice dying on day			Survived 3 days and %	Av. no. of days survived
			1	2	3		
Sulphanilamide 40 mg.	7	60	11	13	5	31 (52)	1·9
Zinc peroxide 20 mg.	4	36	7	7	4	18 (50)	1·9
Proflavine 0·5 mg. ..	6	48	7	3	1	37 (77)	2·4
Penicillin 34 units ..	3	24	0	0	0	24 (100)	3·0

A control group of untreated mice in each experiment all died within 24 hours.

Zinc peroxide.—The preparation used in these experiments contains about 20% zinc peroxide. It will be seen from table I that 20 mg. of zinc peroxide is as effective as 40 mg. of sulphanilamide when administered locally at the time of infection. This result is confirmed by expt. 1, table II, where the two drugs are compared directly. In expts. 2 and 3, table II, the prophylactic action of zinc peroxide is compared with 'Hyperol' (Richter), a solid preparation of hydrogen peroxide and urea yielding 35% hydrogen peroxide by weight, and with zinc oxide. These experiments show that 10 mg. of zinc peroxide is of more value than 100 mg. of hyperol and that zinc oxide is as effective as zinc peroxide. It seems therefore that, although the oxygenating chemicals may be of some value in preventing the development of *Cl. welchii* infection, the zinc ion probably plays a large part in the bacteriostatic action of zinc peroxide. Tests for the effect of delay on the local application of zinc peroxide and hyperol show that an hour's delay in administration totally annuls their preventive effect, as is shown for zinc peroxide in expt. 3, table III. It can be concluded that although zinc peroxide has a powerful bacteriostatic action on *Cl. welchii* it is unable to exert this action once the organisms have invaded the tissues.

Proflavine.—The usual dose of proflavine used was 0·1 c.cm. of a 0·5% solution in distilled water, equivalent to 0·5 mg. of the drug. This dose is ¼ of the LD 50 dose as determined by Rubbo, Albert and Maxwell (1942) and is probably less than half the maximum tolerated dose. It will be seen from table I, which summarises a number of experiments, that 0·5 mg. of proflavine is of greater value than 40 mg. of sulphanilamide in preventing the development of *Cl. welchii* infection when it is applied locally at the time of infection. The superiority of proflavine to sulphanilamide in this respect is borne out by expt. 4 in table II, where their prophylactic action is compared directly. A further test is required to determine whether proflavine, like the sulphonamides, can exert its bacteriostatic action on *Cl. welchii* which have invaded the tissues. Such a test is shown in expt. 1, table III; when the local administration of proflavine is delayed for an hour its preventive value is only slightly diminished, but after 3 or more hours, when the organisms have invaded the blood-stream, treatment with proflavine is apparently of little or no value. These results are similar to those previously obtained with sulphanilamide (McIntosh and Selbie 1941), except that in delayed treatment the preventive action of proflavine is greater than that of sulphanilamide. When the effect of 0·5 mg. of proflavine

UM00011602
NOVARTIS EXHIBIT 1517
Novartis v. Regents, IPR2023-01347
Page 348 of 4460

is compared directly with that of 40 mg. of sulphanilamide applied locally an hour after infection, as in expt. 3, table III, it will be seen that proflavine is much more active than sulphanilamide in preventing the development of *Cl. welchii* infection. Expt. 4, table III, compares the action of proflavine and sulphathiazole at 1½ hours after infection and again shows the superiority of proflavine. In the latter experiment combined treatment with full doses of proflavine and sulphathiazole appears to be of less value than treatment with either drug alone.

Penicillin.—A sample of penicillin was kindly supplied by Dr. C. G. Pope of the Wellcome Physiological Research Laboratories. This preparation, PN183, consists of a solution of the barium salt and contains 170 Oxford units per c.cm. The dose employed in mice was 0·2 c.cm., equivalent to 34 Oxford units. This dose was sufficient to save all the mice in three experiments (table I). Expt. 2, table III, shows that penicillin is also of great value in preventing death from *Cl. welchii* when it is administered after a delay of an hour, and is also of some value in delaying death when it is administered 3 and 6 hours after infection. The superiority of penicillin to proflavine in local treatment is shown in expt. 5, table III, where the effect of immediate and delayed administration of the two drugs is directly compared. From these results it appears that penicillin is of greater value than proflavine or the sulphonamides in preventing the development of *Cl. welchii* infection.

Gramicidin.—A sample of tyrothricin, the preparation used in these experiments, was supplied to us by the Medical Research Council through the courtesy of Sir Henry Dale. It is a water insoluble, alcohol soluble, fraction of the bactericidal substance originally prepared by Dubos (1939) from a soil bacterium. It contains both gramicidin, active against gram-positive bacteria, and tyrocidine, which is also active against gram-negative organisms (Hotchkiss and Dubos 1940). In our hands this preparation inhibits the growth cultures of *Cl. welchii*, *Cl. septique* and *Cl. œdematiens* in a concentration of 1·0 μg. per c.cm. and has occasionally prevented the growth of *Cl. welchii* in a concentration of 0·1 μg. per c.cm.

The action of tyrothricin on the development of *Cl. welchii* in mice was tested by injecting a suspension in saline, immediately after infection. The results were discouraging in that most of the treated mice died within 24 hours and none survived to the third day even with doses of 2 μg. It appears therefore that although tyrothricin has a powerful bacteriostatic action on *Cl.*

TABLE II—COMPARATIVE EFFECTS ON *Cl. welchii* INFECTION IN MICE OF ZINC PEROXIDE AND SULPHANILAMIDE, HYPEROL AND ZINC OXIDE, AND OF PROFLAVINE AND SULPHANILAMIDE, ADMINISTERED LOCALLY AT THE TIME OF INFECTION

Expt.	Drug	Mice	Mice dying on day			Survived 3 days	Av. no. of days survived
			1	2	3		
1	Zinc peroxide 20 mg.	12	1	3	0	8	2·3
	Sulphanilamide 40 mg.	12	0	2	2	8	2·5
2	Zinc peroxide 10 mg.	12	2	2	0	8	2·2
	Hyperol 100 mg. ..	12	6	1	0	5	1·3
3	Zinc peroxide 20 mg.	6	3	3	..	0	0·5
	Zinc oxide 20 mg. ..	6	3	3	..	0	0·5
4	Proflavine 0·5 mg. ..	12	0	1	0	11	2·8
	Sulphanilamide 40 mg.	12	3	0	1	8	2·2

In each experiment a control group of untreated mice, equal in number to the treated groups, all died within 24 hours.

welchii in vitro it is not likely to give commensurate results clinically in its present form.

DISCUSSION

In trying to assess the true preventive and therapeutic values of the remedies reported on here an endeavour has been made to produce an experimental infection comparable to the natural infection. Human gas gangrene develops when limb muscles have been severely

TABLE III—EFFECT ON *Cl. welchii* INFECTION IN MICE OF DELAYED LOCAL ADMINISTRATION OF PROFLAVINE AND PENICILLIN AND COMPARATIVE EFFECTS OF DELAY ON PREVENTIVE ACTION OF PROFLAVINE, SULPHANILAMIDE, SULPHATHIAZOLE AND ZINC PEROXIDE, AND OF PROFLAVINE AND PENICILLIN

Expt.	Drug	Treatment given after hours	Mice	Mice dying on day			Survived 3 days	Av. no. of days survived
				1	2	3		
1	Proflavine, 1·0 mg.	0	6	2	0	0	4	2·0
		1	6	2	0	1	3	1·8
		3	6	4	2	..	0	0·3
		6	6	6	..	..	0	0
2	Penicillin, 34 units	0	6	0	0	0	6	3·0
		1	6	1	0	0	5	2·5
		3	6	2	2	2	0	1·0
		6	6	3	3	..	0	0·5
3	Proflavine, 0·5 mg.	1	12	6	0	0	6	1·5
	Sulphanilamide 40 mg.	1	12	8	1	0	3	0·8
	Zinc peroxide 20 mg.	1	12	12	..	..	0	0
4	Proflavine 0·5 mg. ..	1½	6	3	1	0	2	1·2
	Sulphathiazole 40 mg.	1½	6	3	2	0	1	0·8
	Proflavine 0·5 mg. and sulphathiazole 40 mg.	1½	6	3	3	..	0	0·5
5	Proflavine 0·5 mg.	0	12	3	0	0	9	2·3
		2	12	6	3	0	3	1·0
	Penicillin 34 units	0	12	0	0	0	12	3·0
		2	12	1	0	0	11	2·8

In each experiment a control group of untreated mice, equal in number to the treated groups, all died within 24 hours.

lacerated and simultaneously contaminated with soil bacteria. In the natural disease the clostridia are in the resting (sporing) stage and thus when the wound is infected there can be none of their own bacterial aggressin (toxin) present. The inciting agent was shown by Bullock (Gye) and Cramer (1919) in the last war to be in all probability the calcium ion. They showed that pathogenic clostridia washed free of all toxin were no longer capable of inciting an infection but could do so if a small amount of calcium chloride was injected along with them.

We have therefore induced our experimental infection in mice with toxin-free clostridia, using calcium chloride as the aggressin, the infective dose being so standardised that about 100 lethal (infecting) doses were used as the test inoculum. This dose produces at first a purely local infection which in the course of 3 or 4 hours becomes generalised as shown by the presence of clostridia in the blood. Thus we have a local and general infection on which the remedies can be tested, and these present different problems.

Experimental work on the action of zinc peroxide on *Cl. welchii* infection has given somewhat conflicting results. Reed and Orr (1942) found that in *Cl. welchii* infection in guineapigs the local application of zinc peroxide was a powerful prophylactic and that it was only slightly less effective than sulphathiazole in an established infection. On the other hand, Bliss, Long and Smith (1941) found that zinc peroxide administered locally had no effect on *Cl. welchii* infection in mice but was effective against infections with *Cl. septique*, *Cl. œdematiens* and *Cl. tetani*. Our results show that zinc peroxide is an effective prophylactic against *Cl. welchii* infection, but is without action once the organisms get into the tissues. This result would be expected if zinc peroxide acted through its oxygenating action, which can have a considerable effect as has been shown in our experiments with hyperol, because this would be more effective on unprotected bacteria than on bacteria protected from oxidative changes by the tissue fluids. The tissues may also act as a deterrent if, as Garrod (1940) has suggested and we have shown here, the zinc ion plays a large part in its antibacterial action.

Hawking (1941) has shown that proflavine will prevent infection of wounds in guineapigs by anaerobes subsequently inserted. On reopening such wounds on the third day he found fairly healthy tissues and only small numbers of bacilli. He however decided that the usefulness of proflavine was limited in view of the mediocre results obtained with acridine compounds in

UM00011603
NOVARTIS EXHIBIT 1517
Novartis v. Regents, IPR2023-01347
Page 349 of 4460

the last war, presumably through their inability to reach bacteria situated inside the tissues. But we have shown that proflavine is not only more active than sulphanilamide in preventing the development of *Cl. welchii* infection in mice but that it is at least as active as sulphanilamide and sulphathiazole in an infection that has already developed. Proflavine has also the advantages of being bacteriostatic to a wide range of organisms and of having a low toxicity to tissue, as Garrod (1940) has emphasised. Although Jacoby, Medawar and Willmer (1941) found that proflavine is toxic to fibroblasts in tissue culture, Russell and Falconer (1941) and Manifold (1941) have shown that neutral solutions of proflavine are less toxic than sulphonamides to brain tissue. The recent experience of Mitchell and Buttle (1942) has also shown that large quantities of proflavine can be inserted in wounds with good results. In the doses we have used we have seen no injurious effects in mice. In clinical practice, however, large doses of proflavine should be neutralised immediately before application because much of the irritant effects of this drug are due to its high acidity. Much of the criticism that has been directed against the use of the acridine drugs in wound infections has been based on previous experience with acriflavine which is much more toxic than proflavine and should not therefore discourage further trials of proflavine in wound therapy. As Garrod (1940) has pointed out, proflavine is also much more easily prepared and of more regular composition than acriflavine, which is a mixture of compounds, so that proflavine is the drug of choice at the moment. We have experiments in hand on the effects of the new acridines described by Albert and others (1938) and Rubbo, Albert and Maxwell (1942) in clostridial infections.

The therapeutic action of penicillin on *Cl. septique* infection in mice was investigated by Chain and others (1940). In an infection which killed all untreated mice within 24 hours they were able to save all mice receiving repeated injections of penicillin. In our experiments the injection in the infected site of a single dose within 2 hours of infection was sufficient to save a high proportion of mice subjected to a severe infection. Compared with proflavine and the sulphonamides it appears to be the most powerful of the therapeutic substances that we have yet tested experimentally against this type of infection. It is also noteworthy that, judging by the statement of Florey and Jennings (1942) that 20 mg. of therapeutic penicillin containing 40–50 units per mg. caused serious embarrassment but not death in a mouse, the effective dose in our experiments is only about a 20th to a 30th of the toxic dose. The great therapeutic power and the low toxicity of penicillin seem to warrant extensive clinical trial when enough of this substance becomes available.

Gramicidin, another naturally occurring antibacterial substance, provides a striking contrast to penicillin. In spite of its great activity in vitro against *Cl. welchii* it has proved in our hands to be of little value against *Cl. welchii* infection in mice. It has also the great disadvantage of being highly toxic.

The various substances that we have tested fall into two distinct groups. In the first are the oxidising chemicals, zinc peroxide and hyperol, which appear to possess only an antiseptic action, because when their application to the infected site is delayed they fail to exercise preventive action. In the second group are the sulphonamides, proflavine and penicillin, which can be given after an hour's delay and still prevent infection to a large extent. The latter may be said to have selective chemotherapeutic action in that they can reach and exert their bacteriostatic effects on organisms that have invaded the tissues. When the infection becomes generalised the curative action of the local application of these substances is much reduced and with the exception of proflavine and penicillin is ineffective.

SUMMARY

The local application of zinc peroxide is apparently of no value in preventing the development of *Cl. welchii* infection in mice when the organisms have invaded the tissues.

Proflavine is of greater value than sulphanilamide and is at least as good as sulphathiazole in the local prophylaxis and treatment of *Cl. welchii* infection in mice and its use therefore as a wound dressing should be further explored.

Penicillin, injected at the site of infection within 3 hours of infection, is a powerful prophylactic against *Cl. welchii* infection in mice and is superior to proflavine and the sulphonamides in this respect.

REFERENCES

Albert, A., Francis, A. E., Garrod, L. P. and Linnell, W. H. (1938) *Brit. J. exp. Path.* 19, 41.
Bliss, E. A., Long, P. H. and Smith, D. G. (1941) *War Med.* 1, 799.
Bullock, W. E. and Cramer, W. (1919) *Proc. Roy. Soc.* B, 90, 513.
Chain, E., Florey, H. W., Gardner, A. D., Heatley, N. G., Jennings M. A., Orr-Ewing, J. and Sanders, A. G. (1940) *Lancet*, ii, 226.
Dubos, R. J. (1939) *J. exp. Med.* 70, 1.
Florey, H. W. and Jennings, M. A. (1942) *Brit. J. exp. Path.* 23, 120.
Garrod, L. P. (1940) *Lancet*, i, 798.
Hawking, F. (1941) *Brit. med. J.* i, 263.
Hotchkiss, R. D. and Dubos, R. J. (1940) *J. biol. Chem.* 136, 803.
Jacoby, F., Medawar, P. B. and Willmer, E. N. (1941) *Brit. med. J.* ii, 149.
McIntosh, J. and Selbie, F. R. (1941) *Lancet*, i, 240.
Manifold, M. C. (1941) *Brit. J. exp. Path.* 22, 111.
Mitchell, G. A. G. and Buttle, G. A. H. (1942) *Lancet*, ii, 416.
Reed, G. B. and Orr, J. H. (1941) *Ibid*, i, 376. (1942) *War Med.* 2, 79.
Rubbo, S. D., Albert, A. and Maxwell, M. (1942) *Brit. J. exp. Path.* 23, 69.
Russell, D. S. and Falconer, M. A. (1941) *Brit. J. Surg.* 28, 472.

CONTROL OF PULMONARY TUBERCULOSIS IN MENTAL HOSPITALS

W. P. BERRINGTON
M D BELF, D P M
FIRST ASSISTANT MO

C. E. GREENWOOD
B M OXFD, D P M
SECOND ASSISTANT MO

WEST PARK HOSPITAL, EPSOM

THE report of the Medical Research Council's committee on tuberculosis in war-time [1] and Trail's comprehensive study [2] have dealt adequately with tuberculosis in the general population. The committee have also investigated the present situation in mental hospitals, but as far as we are aware no figures based on research in these hospitals exist. We present here the results of such research on a small community of male psychotics, and suggest a method for the control of tuberculosis in this type of community—a method owing its inception entirely to the economic exigencies of the moment.

In May, 1941, it became obvious that the mortality-rate from pulmonary tubercle, particularly in the male population of this hospital, was rapidly increasing. Looking up our records, we find that deaths from this disease from 1932 to 1941 were as follows:

1932	1933	1934	1935	1936	1937	1938	1939	1940	1941
7	7	9	5	6	8	10	11	15	27

During these years the male population of the hospital remained stationary at about 1100.

In the MRC report we find that mental hospitals have had, at least since 1910, the reputation of eclipsing the mortality-rate in the general population. Thus in peacetime the rate was 9 or 10 times that of the general population and rose to more than twice its peace-time rate in 1918. Now, the rate has again risen steeply, to a greater extent in the males than in females. Measures advocated for early diagnosis—chiefly mass miniature radiography—are now well known and have already, to some extent, been put into practice among the general public. This method, to some extent and in due course, will doubtless be put into operation in mental hospitals. The questions we must ask are to what extent, and in what period of time?

It now seems certain that X-ray facilities will be made available to all mental hospitals, but not apparently in the form of mass miniature radiography. To quote from the report—" the Committee therefore recommends that . . . efforts should be made, so far as possible, to take periodical chest radiographs of all residents, whether they have symptoms or not, in order to discover and treat early cases. Many hospitals already have X-ray apparatus suitable to this purpose." In other words some hospitals will still be committed to taking full sized X-ray photographs. In our own case we viewed the expense of this programme in 1100 patients (or, including females, over 2000) with dismay, and we think that this

1. *Spec. Rep. Ser. med. Res. Coun., Lond.* No. 246, 1942.
2. Trail, R. R. *Lancet*, 1942, ii, 413.

UM00011604
NOVARTIS EXHIBIT 1517
Novartis v. Regents, IPR2023-01347
Page 350 of 4460

Aust. J. Chem., 1995, **48**, 1151–1166

Molecular Cocrystals of Carboxylic Acids. XXI* The Role of Secondary Group Interactions in Adduct Formation between 2-Aminopyrimidine and Substituted Benzoic Acids: the Crystal Structures of the Adducts with *o*-Phthalic Acid, *o*-Nitrobenzoic Acid, *o*-Aminobenzoic Acid and *m*-Aminobenzoic Acid

Graham Smith,[A,B] *Janene M. Gentner,*[A] *Daniel E. Lynch,*[A] *Karl A. Byriel*[C] *and Colin H. L. Kennard*[C]

[A] School of Chemistry, Queensland University of Technology, P.O. Box 2434, Brisbane, Qld. 4001.
[B] Author to whom correspondence should be addressed.
[C] Department of Chemistry, The University of Queensland, St. Lucia, Qld. 4072.

Abstract

The crystalline adducts of 2-aminopyrimidine (2-ap) with a series of mainly *ortho*-substituted benzoic acids, *o*-phthalic acid (opht) [(2-ap)(opht)] (1), 2-nitrobenzoic acid (2-nba) [(2-ap)(2-bna)$_2$] (2), 2-aminobenzoic acid (2-aba) [(2-aba) [(2-ap)(2-aba)$_2$] (3) and 3-aminobenzoic acid (3-aba) [(2-ap)(3-aba)] (4) have been prepared and their hydrogen-bonding motifs characterized by using single-crystal X-ray diffraction. The role of substituent groups in secondary associations with cocrystal formation is considered for the 2-aminopyrimidine system.

Introduction

The utility of 2-aminopyrimidine (2-ap) as an acid for crystallization of associated hetero-organic molecules is well known.[1–3] The molecule is unique in its duality in possessing both proton-donating and proton-accepting properties through its amino group and its two *meta*-related ring nitrogens, providing sites for the formation of stable cyclic eight-membered hydrogen bonded rings. These are analogous to those found in both solid state and low temperature solution-state structures of the majority of carboxylic acids,[4] which associate via centrosymmetric cyclic dimers. In the crystal structure of 2-ap,[5] this (P-P) dimeric association is found, while for a 1 : 1 interaction of 2-ap with a carboxylic acid (A), either a basic (P-A) interaction or variations on a (P-P) or (P-A) building unit result.[2] Most known 1 : 1 examples involving monocarboxylic acids fall into these categories, e.g. (P-A) (discretely monomeric) [with (2,4-dichlorophenoxy)acetic acid[6]]; (P-A)$_n$

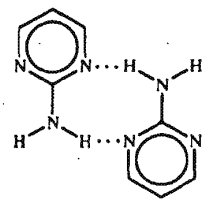
* Part XX, *Aust. J. Chem.*, 1995, **48**, 1133.

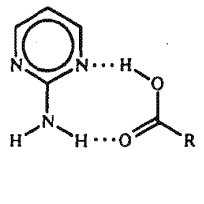
[1] Adsmond, D. A., Ph.D. Thesis, University of Minnesota, 1991.
[2] Etter, M. C., and Adsmond, D. A., *J. Chem. Soc., Chem. Commun.*, 1990, 589.
[3] Bernstein, J., Etter, M. C., and Leiserowitz, L., in 'Structure Correlation' (Eds H.-B. Bürgi and J. D. Dunitz) Vol. 2, pp. 490–507 (VCH: Weinheim, FRG, 1994).
[4] Leiserowitz, L., *Acta Crystallogr., Sect. B*, 1976, **32**, 775.
[5] Scheinbein, J., and Schempp, E., *Acta Crystallogr., Sect. B*, 1976, **32**, 607.
[6] Lynch, D. E., Smith, G., Freney, D., Byriel, K. A., and Kennard, C. H. L., *Aust. J. Chem.*, 1994, **47**, 1097.

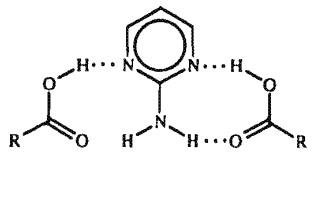
Manuscript received 30 September 1994 0004-9425/95/061151$05.00

UM00011605
NOVARTIS EXHIBIT 1517
Novartis v. Regents, IPR2023-01347
Page 351 of 4460

chain polymeric (with salicylic acid and 2,6-dihydroxybenzoic acid[6]); (A-P-P-A) (monomeric) [with (3,5-dichlorophenoxy)acetic acid[6]], $(A\text{-}P\text{-}P\text{-}A)_n$ (chain polymeric) (with 4-aminobenzoic acid[6]). One 1:2 adduct is known [(2-ap)(phenoxyacetic acid)$_2$[6]], which has the monomeric (A-P-A) structure. A variation which does not exactly fit these categories is $(A\text{-}P)_2$, a centrosymmetric face-to-tail tetramer based on an (A-P) dimer [with (3,4-dichlorophenoxy)acetic acid[6]].







As a further consideration in the formation process which assumes a primary (P-A) interaction followed by a secondary structure-making procedure until all interactive sites on both donor and acceptor molecules are utilized, the role of these interactive sites on the acid molecule (i.e. type and position) has not been investigated, in relation to prediction of the structural motif. With examples reported to date, consideration has been given mainly to *m*- and *p*-substituted aromatic acids with the view to promoting asymmetry in the packing, a necessary criterion for the enhancement of non-linear optical properties.[7-8] Little has been done with *o*-substituted acids. To this end, a series of 2-aminopyrimidine adducts was prepared with *o*-phthalic acid (opht), 2-nitrobenzoic acid (2-nba), 2-aminobenzoic acid (2-aba) and 3-aminobenzoic acid (3-aba) and their crystal structures are reported here. These are [(2-ap)(opht)] (1), [(2-ap)(2-nba)$_2$] (2), [(2-ap)(2-aba)$_2$] (3) and [(2-ap)(3-aba)] (4). The structure of the 1:1 adduct of 2-ap with 4-aminobenzoic acid is already known.[6] The role of secondary group association is also considered with respect to the nature of the complex formed and the constituent stoichiometry. With the latter point, occurrence of 1:1 stoichiometries is predominant among 2-aminopyrimidine/carboxylic acid adducts, including those with dicarboxylic acids, e.g. *m*-phthalic acid and oxalic acid. However, with others both 1:1 and 2:1 stoichiometries result from solid state reaction, e.g. succinic acid although only 1:1 $[(A\text{-}P)_n]$ cocrystals are formed from solution reaction.[2]

Experimental

Complexes (1)–(4) were prepared by using equimolar amounts of 2-aminopyrimidine (2-ap) and the appropriate acids, *o*-phthalic acid (opht) for (1), 2-nitrobenzoic acid (2-nba) for (2), 2-aminobenzoic acid (anthranilic acid) (2-aba) for (3), and 3-aminobenzoic acid (3-aba) for (4). Preparations involved refluxing reactants for 15 min at *c.* 110°C in 95% aqueous ethanol. For (1) pale yellow *plates* (m.p. 126–128°C); for (2) yellow *prisms* (m.p. 152–153°C); for (3) brown *prisms* (m.p. 108–110°C); and for (4) pale brown *plates* (m.p. 137–138°C) were obtained by

[7] Etter, M. C., Frankenbach, G. M., and Adsmond, D. A., *Mol. Cryst. Liq. Cryst.*, 1990, **187**, 25.
[8] Etter, M. C., *Chem. Mater.*, 1989, **1**, 10.

UM00011606
NOVARTIS EXHIBIT 1517
Novartis v. Regents, IPR2023-01347
Page 352 of 4460

partial or total evaporation of the solvent at room temperature [Found for (1): C, 45·7; H, 4·4; N, 12·4. $C_{13}H_{15}N_3O_8$ requires C, 45·8; H, 4·4; N, 12·3%. Found for (2): C, 50·3; H, 3·5; N, 16·5. $C_{18}H_{15}N_5O_8$ requires C, 50·4; H, 3·5; N, 16·3%. Found for (3): C, 58·5; H, 5·2; N, 18·7. $C_{18}H_{19}N_5O_4$ requires C, 58·5; H, 5·2; N, 19·0%. Found for (4): C, 56·8; H, 5·3; N, 24·3. $C_{11}H_{12}N_4O_2$ requires C, 56·9; H, 5·2; N, 24·1%]. Infrared spectra were also recorded for all samples as pressed disks in KBr on a Perkin–Elmer 1600 Fourier-transform infrared spectrometer. Qualitative second harmonic generation (SHG) measurements on a powdered sample of compound (3) were carried out by using methods and apparatus previously

Table 1. Atomic coordinates and equivalent isotropic thermal parameters (Å^2)

U_{eq} is defined as one-third of the orthogonalized U_{ij} tensor

Compound	Atom	$10^4 X/a$	$10^4 Y/b$	$10^4 Z/c$	$10^3 U_{eq}$
(1)	C(11)	8372(1)	2955(2)	6031(1)	43(1)
	C(21)	7998(1)	2544(2)	6523(1)	41(1)
	C(31)	7965(1)	3778(2)	6957(1)	50(1)
	C(41)	8293(1)	5408(2)	6907(1)	57(1)
	C(51)	8661(2)	5824(3)	6423(1)	61(1)
	C(61)	8706(1)	4606(2)	5991(1)	54(1)
	C(101)	8420(1)	1655(2)	5558(1)	43(1)
	O(111)	8078(1)	232(2)	5543(1)	57(1)
	O(121)	8874(1)	2194(2)	5169(1)	62(1)
	C(201)	7641(1)	794(2)	6612(1)	45(1)
	O(211)	6708(1)	626(2)	6360(1)	62(1)
	O(221)	8144(1)	−286(2)	6915(1)	62(1)
	C(22)	8820(1)	−1540(2)	4206(1)	47(1)
	N(22)	8449(1)	−2319(3)	4619(1)	63(1)
	N(12)	9080(1)	101(2)	4311(1)	47(1)
	C(62)	9476(1)	853(3)	3911(1)	52(1)
	C(52)	9621(1)	18(3)	3409(1)	57(1)
	C(42)	9324(1)	−1634(3)	3333(1)	56(1)
	N(32)	8925(1)	−2442(2)	3720(1)	53(1)
(2)	N(11)	4519(2)	−2926(2)	−4164(1)	42(1)
	C(21)	2818(3)	−3762(2)	−4484(2)	40(1)
	N(21)	2748(3)	−4879(2)	−4317(2)	54(1)
	N(31)	1212(2)	−3445(2)	−4963(1)	45(1)
	C(41)	1367(3)	−2320(2)	−5126(2)	48(1)
	C(51)	3086(3)	−1441(2)	−4843(2)	52(1)
	C(61)	4652(3)	−1785(2)	−4350(2)	48(1)
	C(12)	820(3)	4336(2)	1833(2)	37(1)
	C(112)	2478(3)	4259(2)	2674(2)	44(1)
	O(122)	2476(2)	3234(2)	2893(2)	65(1)
	O(132)	3713(2)	5244(1)	3129(1)	51(1)
	C(22)	307(3)	3492(2)	813(2)	37(1)
	N(22)	1544(3)	2596(2)	451(2)	53(1)
	O(212)	762(4)	1522(2)	−16(2)	88(1)
	O(222)	3291(3)	2968(2)	636(2)	86(1)
	C(32)	−1313(3)	3497(2)	85(2)	44(1)
	C(42)	−2476(3)	4354(2)	377(2)	49(1)
	C(52)	−2005(3)	5207(2)	1376(2)	55(1)
	C(62)	−361(3)	5209(2)	2094(2)	50(1)
	C(13)	3907(3)	941(2)	−2332(2)	38(1)
	C(113)	4180(3)	2031(2)	−2824(2)	38(1)
	O(123)	3139(2)	2097(2)	−3623(1)	58(1)
	O(133)	5710(2)	2878(1)	−2309(1)	50(1)

UM00011607
NOVARTIS EXHIBIT 1517
Novartis v. Regents, IPR2023-01347
Page 353 of 4460

Table 1 ***(Continued)***

Compound	Atom	$10^4 X/a$	$10^4 Y/b$	$10^4 Z/c$	$10^3 U_{eq}$
(2)	C(23)	2093(3)	189(2)	−2439(2)	42(1)
	N(23)	333(3)	573(2)	−2881(2)	54(1)
	O(213)	49(3)	1616(2)	−2487(2)	71(1)
	O(223)	−796(3)	−200(2)	−3619(2)	90(1)
	C(33)	1859(4)	−900(2)	−2102(2)	56(1)
	C(43)	3467(4)	−1249(2)	−1623(2)	63(1)
	C(53)	5284(4)	−519(2)	−1479(2)	60(1)
	C(63)	5492(3)	557(2)	−1841(2)	48(1)
(3)	N(11)	11457(4)	10528(12)	12635(4)	52(1)
	C(21)	10489(5)	11074(15)	11968(4)	52(2)
	N(21)	9599(5)	9631(15)	11953(4)	67(2)
	N(31)	10377(4)	12977(13)	11322(4)	57(2)
	C(41)	11288(7)	14459(22)	11364(6)	64(2)
	C(51)	12295(6)	14056(16)	12003(6)	58(2)
	C(61)	12348(6)	12033(17)	12648(5)	56(2)
	C(12)	6690(6)	13304(17)	9015(5)	55(2)
	C(22)	5642(6)	12099(17)	8865(5)	59(2)
	N(22)	5455(8)	10281(22)	9442(6)	85(3)
	C(32)	4765(7)	12861(21)	8083(5)	74(2)
	C(42)	4903(9)	14700(22)	7492(6)	83(3)
	C(52)	5920(9)	15950(22)	7633(6)	91(3)
	C(62)	6807(8)	15207(22)	8397(6)	75(2)
	C(112)	7652(6)	12662(17)	9829(5)	58(2)
	O(122)	7619(4)	11061(13)	10421(3)	74(2)
	O(132)	8581(4)	13880(13)	9851(3)	82(2)
	C(13)	6241(5)	6892(15)	4712(4)	45(2)
	N(23)	4288(5)	7829(18)	4487(5)	69(2)
	C(23)	5405(5)	8315(15)	4919(4)	48(2)
	C(33)	5721(7)	10346(19)	5600(5)	59(2)
	C(43)	6823(6)	10863(17)	6068(5)	60(2)
	C(53)	7652(6)	9443(17)	5877(5)	60(2)
	C(63)	7359(5)	7505(16)	5207(5)	50(2)
	C(113)	5966(5)	4752(16)	3990(4)	52(2)
	O(123)	5008(4)	4219(11)	3493(3)	64(1)
	O(133)	6835(3)	3467(10)	3910(3)	55(1)
(4)	N(11)	2747(3)	−3639(7)	921(2)	56(1)
	C(21)	1727(4)	−4125(8)	561(2)	50(1)
	N(211)	824(4)	−2669(9)	670(3)	70(1)
	N(31)	1561(3)	−5989(7)	84(2)	60(1)
	C(41)	2482(5)	−7370(10)	−28(3)	69(1)
	C(51)	3558(5)	−7007(10)	302(3)	72(1)
	C(61)	3640(4)	−5104(10)	780(3)	67(1)
	C(12)	2581(3)	3147(8)	2643(2)	47(1)
	C(22)	1688(3)	4608(8)	2880(2)	50(1)
	C(112)	2302(3)	1192(8)	2101(2)	49(1)
	O(122)	1340(2)	955(7)	1815(2)	73(1)
	O(132)	3187(2)	−195(6)	1940(2)	60(1)
	C(32)	1903(3)	6513(8)	3370(2)	52(1)
	N(312)	1007(4)	7932(11)	3603(3)	91(2)
	C(42)	3059(4)	6911(9)	3610(2)	56(1)
	C(52)	3942(4)	5473(9)	3372(2)	59(1)
	C(62)	3732(4)	3562(9)	2891(2)	56(1)

UM00011608
NOVARTIS EXHIBIT 1517
Novartis v. Regents, IPR2023-01347
Page 354 of 4460

Table 2. Bond distances (Å)

Compound	Atoms	Distance	Atoms	Distance
(1)	C(11)–C(61)	1·391(3)	C(201)–O(221)	1·199(2)
	C(11)–C(21)	1·398(2)	C(201)–O(211)	1·320(2)
	C(11)–C(101)	1·490(2)	C(22)–N(12)	1·341(2)
	C(21)–C(31)	1·386(2)	C(22)–N(22)	1·342(2)
	C(21)–C(201)	1·497(2)	C(22)–N(32)	1·346(2)
	C(31)–C(41)	1·377(3)	N(12)–C(62)	1·330(2)
	C(41)–C(51)	1·379(3)	C(62)–C(52)	1·373(3)
	C(51)–C(61)	1·377(3)	C(52)–C(42)	1·359(3)
	C(101)–O(111)	1·216(2)	C(42)–N(32)	1·332(2)
	C(101)–O(121)	1·301(2)		
(2)	N(11)–C(61)	1·342(3)	C(32)–C(42)	1·369(3)
	N(11)–C(21)	1·357(3)	C(42)–C(52)	1·371(3)
	C(21)–N(21)	1·309(3)	C(52)–C(62)	1·383(3)
	C(21)–N(31)	1·350(3)	C(13)–C(63)	1·384(3)
	N(31)–C(41)	1·312(3)	C(13)–C(23)	1·395(3)
	C(41)–C(51)	1·391(3)	C(13)–C(113)	1·495(3)
	C(51)–C(61)	1·350(3)	C(113)–O(123)	1·204(2)
	C(12)–C(62)	1·383(3)	C(113)–O(133)	1·311(2)
	C(12)–C(22)	1·388(3)	C(23)–C(33)	1·376(3)
	C(12)–C(112)	1·511(3)	C(23)–N(23)	1·461(3)
	C(112)–O(122)	1·239(3)	N(23)–O(213)	1·212(3)
	C(112)–O(132)	1·263(2)	N(23)–O(223)	1·222(3)
	C(22)–C(32)	1·380(3)	C(33)–C(43)	1·370(4)
	C(22)–N(22)	1·457(3)	C(43)–C(53)	1·379(4)
	N(22)–O(222)	1·214(3)	C(53)–C(63)	1·380(3)
	N(22)–O(212)	1·219(3)		
(3)	N(11)–C(61)	1·338(9)	C(52)–C(62)	1·387(12)
	N(11)–C(21)	1·345(8)	C(112)–O(122)	1·221(9)
	C(21)–N(21)	1·321(9)	C(112)–O(132)	1·310(9)
	C(21)–N(31)	1·336(9)	C(13)–C(23)	1·395(8)
	N(31)–C(41)	1·342(10)	C(13)–C(63)	1·402(9)
	C(41)–C(51)	1·347(11)	C(13)–C(113)	1·479(10)
	C(51)–C(61)	1·388(11)	N(23)–C(23)	1·372(9)
	C(12)–C(62)	1·378(12)	C(23)–C(33)	1·399(11)
	C(12)–C(22)	1·399(10)	C(33)–C(43)	1·368(11)
	C(12)–C(112)	1·473(10)	C(43)–C(53)	1·374(10)
	C(22)–N(22)	1·338(11)	C(53)–C(63)	1·357(10)
	C(22)–C(32)	1·401(10)	C(113)–O(123)	1·231(7)
	C(32)–C(42)	1·337(13)	C(113)–O(133)	1·310(8)
	C(42)–C(52)	1·374(14)		
(4)	N(11)–C(61)	1·330(6)	C(12)–C(112)	1·487(6)
	N(11)–C(21)	1·349(5)	C(22)–C(32)	1·392(6)
	C(21)–N(211)	1·324(6)	C(112)–O(122)	1·211(4)
	C(21)–N(31)	1·352(5)	C(112)–O(132)	1·306(5)
	N(31)–C(41)	1·318(6)	C(32)–N(312)	1·365(6)
	C(41)–C(51)	1·368(7)	C(32)–C(42)	1·396(5)
	C(51)–C(61)	1·361(7)	C(42)–C(52)	1·363(6)
	C(12)–C(22)	1·377(6)	C(52)–C(62)	1·383(6)
	C(12)–C(62)	1·397(5)		

UM00011609
NOVARTIS EXHIBIT 1517
Novartis v. Regents, IPR2023-01347
Page 355 of 4460

Table 3. Bond angles (degrees)

Compound	Atoms	Angle	Atoms	Angle
(1)	C(61)–C(11)–C(21)	118·8(2)	O(121)–C(101)–C(11)	113·1(2)
	C(61)–C(11)–C(101)	120·2(2)	O(221)–C(201)–O(211)	124·3(2)
	C(21)–C(11)–C(101)	121·0(2)	O(221)–C(201)–C(21)	123·0(2)
	C(31)–C(21)–C(11)	119·7(2)	O(211)–C(201)–C(21)	112·5(2)
	C(31)–C(21)–C(201)	117·5(2)	N(12)–C(22)–N(22)	117·3(2)
	C(11)–C(21)–C(201)	122·7(1)	N(12)–C(22)–N(32)	123·9(2)
	C(41)–C(31)–C(21)	120·6(2)	N(22)–C(22)–N(32)	118·8(2)
	C(31)–C(41)–C(51)	120·0(2)	C(62)–N(12)–C(22)	117·2(2)
	C(61)–C(51)–C(41)	120·0(2)	N(12)–C(62)–C(52)	122·6(2)
	C(51)–C(61)–C(11)	120·8(2)	C(42)–C(52)–C(62)	116·3(2)
	O(111)–C(101)–O(121)	123·7(2)	N(32)–C(42)–C(52)	123·2(2)
	O(111)–C(101)–C(11)	123·2(2)	C(42)–N(32)–C(22)	116·8(2)
(2)	C(61)–N(11)–C(21)	120·6(2)	C(42)–C(32)–C(22)	119·2(2)
	N(21)–C(21)–N(31)	120·2(2)	C(32)–C(42)–C(52)	119·9(2)
	N(21)–C(21)–N(11)	119·2(2)	C(42)–C(52)–C(62)	120·6(2)
	N(31)–C(21)–N(11)	120·6(2)	C(52)–C(62)–C(12)	120·9(2)
	C(41)–N(31)–C(21)	117·8(2)	C(63)–C(13)–C(23)	116·7(2)
	N(31)–C(41)–C(51)	123·9(2)	C(63)–C(13)–C(113)	120·7(2)
	C(61)–C(51)–C(41)	116·5(2)	C(23)–C(13)–C(113)	122·3(2)
	N(11)–C(61)–C(51)	120·5(2)	O(123)–C(113)–O(133)	124·2(2)
	C(62)–C(12)–C(22)	117·0(2)	O(123)–C(113)–C(13)	123·4(2)
	C(62)–C(12)–C(112)	120·1(2)	O(133)–C(113)–C(13)	112·4(2)
	C(22)–C(12)–C(112)	122·6(2)	C(33)–C(23)–C(13)	122·7(2)
	O(122)–C(112)–O(132)	125·0(2)	C(33)–C(23)–N(23)	117·2(2)
	O(122)–C(112)–C(12)	116·9(2)	C(13)–C(23)–N(23)	120·1(2)
	O(132)–C(112)–C(12)	118·1(2)	O(213)–N(23)–O(223)	123·8(2)
	C(32)–C(22)–C(12)	122·4(2)	O(213)–N(23)–C(23)	119·0(2)
	C(32)–C(22)–N(22)	117·2(2)	O(223)–N(23)–C(23)	117·2(2)
	C(12)–C(22)–N(22)	120·3(2)	C(43)–C(33)–C(23)	118·8(2)
	O(222)–N(22)–O(212)	124·2(2)	C(33)–C(43)–C(53)	120·4(2)
	O(222)–N(22)–C(22)	117·8(2)	C(63)–C(53)–C(43)	119·9(2)
	O(212)–N(22)–C(22)	118·0(2)	C(53)–C(63)–C(13)	121·5(2)
(3)	C(61)–N(11)–C(21)	117·1(6)	C(12)–C(62)–C(52)	122·1(9)
	N(21)–C(21)–N(31)	118·3(6)	O(122)–C(112)–O(132)	121·8(7)
	N(21)–C(21)–N(11)	117·8(6)	O(122)–C(112)–C(12)	124·2(7)
	N(31)–C(21)–N(11)	124·0(6)	O(132)–C(112)–C(12)	113·9(7)
	C(21)–N(31)–C(41)	117·1(7)	C(23)–C(13)–C(63)	118·8(6)
	N(31)–C(41)–C(51)	123·3(9)	C(23)–C(13)–C(113)	121·3(5)
	C(41)–C(51)–C(61)	116·3(8)	C(63)–C(13)–C(113)	119·9(6)
	N(11)–C(61)–C(51)	122·3(7)	N(23)–C(23)–C(13)	123·3(6)
	C(62)–C(12)–C(22)	118·7(6)	N(23)–C(23)–C(33)	118·3(7)
	C(62)–C(12)–C(112)	119·7(7)	C(13)–C(23)–C(33)	118·4(6)
	C(22)–C(12)–C(112)	121·5(6)	C(43)–C(33)–C(23)	120·7(8)
	N(22)–C(22)–C(12)	122·3(7)	C(33)–C(43)–C(53)	121·3(8)
	N(22)–C(22)–C(32)	119·7(8)	C(63)–C(53)–C(43)	118·7(7)
	C(12)–C(22)–C(32)	118·0(7)	C(53)–C(63)–C(13)	122·0(7)
	C(42)–C(32)–C(22)	122·0(9)	O(123)–C(113)–O(133)	122·0(7)
	C(32)–C(42)–C(52)	121·1(9)	O(123)–C(113)–C(13)	123·6(6)
	C(42)–C(52)–C(62)	118·1(9)	O(133)–C(113)–C(13)	114·4(5)
(4)	C(61)–N(11)–C(21)	116·3(4)	C(12)–C(22)–C(32)	121·4(4)
	N(211)–C(21)–N(11)	118·3(4)	O(122)–C(112)–O(132)	122·7(4)
	N(211)–C(21)–N(31)	117·2(4)	O(122)–C(112)–C(12)	122·6(4)
	N(11)–C(21)–N(31)	124·5(4)	O(132)–C(112)–C(12)	114·7(3)
	C(41)–N(31)–C(21)	115·9(4)	N(312)–C(32)–C(22)	120·6(4)
	N(31)–C(41)–C(51)	124·1(5)	N(312)–C(32)–C(42)	121·7(4)
	C(61)–C(51)–C(41)	115·9(5)	C(22)–C(32)–C(42)	117·7(4)
	N(11)–C(61)–C(51)	123·3(5)	C(52)–C(42)–C(32)	120·9(4)
	C(22)–C(12)–C(62)	120·2(4)	C(42)–C(52)–C(62)	121·6(4)
	C(22)–C(12)–C(112)	118·9(3)	C(52)–C(62)–C(12)	118·2(4)
	C(62)–C(12)–C(112)	120·8(4)		

UM00011610
NOVARTIS EXHIBIT 1517
Novartis v. Regents, IPR2023-01347
Page 356 of 4460

Table 4. Types of interactions in crystallographically characterized adducts of 2-ap (P) with carboxylic acids (A)

4-aba, 4-aminobenzoic acid; tnba, 2,4,6-trinitrobenzoic acid; dhba, 2,6-dihydroxybenzoic acid; sa, salicylic acid; 2,4-d, (2,4-dichlorophenoxy)acetic acid; 3,4-d, (3,4-dichlorophenoxy)acetic acid; pa, phenoxyacetic acid; succ, succinic acid

Acid	Stoichiometry (P : A)	Proton transfer	Mode	Reference
2-aba	1 : 2	no	$[(A)P\text{-}A]_n$	this work (3)
3-aba	1 : 1	no	$[P\text{-}A]_n$	this work (4)
4-aba	1 : 1	no	$[A(A)\text{-}P\text{-}P\text{-}(A)A]_n$	6
2-nba	1 : 2	yes	$[(A)A\text{-}P\text{-}P\text{-}A(A)]$	this work (2)
opht	1 : 1	no	$[P\text{-}A]_2$	this work (1)
sa	1 : 1	yes	$[P\text{-}A]_n$	6
3,4-d	1 : 1	no	$[P\text{-}A]_2$	6
pa	1 : 2	no	[A-P-A]	6
2,4-d	1 : 1	no	[P-A]	6
succ	1 : 1	no	$[P\text{-}A]_n$	2
tnba	1 : 1	yes	[A-P-P-A]	18

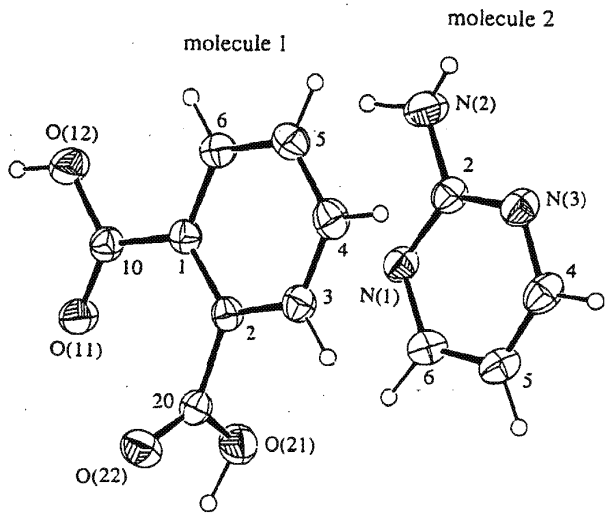


Fig. 1. Molecular configuration and atom naming scheme for the individual molecules comprising the adduct (1). Unless otherwise indicated, atoms are carbon.

described.[9] Attempted preparation of adducts with different stoichiometry, using 1 : 2 rather than 1 : 1 ratios of 2-ap and the acid, invariably gave the same products (1)–(4), confirmed by melting points, elemental analysis and single-crystal X-ray examination.

Crystallography

Crystal Data

(1) $[(C_4H_5N_3)(C_8H_6O_4)]$, mol. wt 261·2, monoclinic, space group $C2/c$, a 14·462(6), b 7·8298(8), c 22·55(1) Å, β 105·91(2)°, V 2456(2) Å^3, $F(000)$ 1088, $D_c(Z = 8)$ 1·413 g cm^{-3}, μ(Mo Kα) 1·1 cm^{-1}, temperature 298(2) K.

[9] Ashwell, G. J., Dawnay, E. J. C., Kuczynski, A. P., and Martin, P. J., *SPIE-Int. Soc. Opt. Eng.*, 1991, **1361**, 589.

UM00011611
NOVARTIS EXHIBIT 1517
Novartis v. Regents, IPR2023-01347
Page 357 of 4460

(2) $[(C_4H_6N_3)^+(C_7H_4NO_4)^-(C_7H_5NO_4)]$, mol. wt 429·4, triclinic, space group $P\bar{1}$, a 7·054(3), b 11·163(7), c 12·804(3) Å, α 103·51(2), β 97·45(3), γ 98·45(3)°, V 955·5(8) Å^3, $F(000)$ 444, $D_c(Z = 2)$ 1·492 g cm^{-3}, μ(Mo Kα) 1·2 cm^{-1}, temperature 298(2) K.

(3) $[(C_4H_5N_3)(C_7H_7NO_2)_2]$, mol. wt 369·4, monoclinic, space group Pa, a 12·773(6), b 14·7492(5), c 15·855(7) Å, β 110·25(2)°, V 902·3(6) Å^3, $F(000)$ 388 $D_c(Z = 2)$ 1·360 g cm^{-3}, μ(Mo Kα) 0·99 cm^{-1}, temperature 298(2) K.

(4) $[(C_4H_5N_3)(C_7H_7NO_2)]$, mol. wt 232·3, monoclinic, space group $P2_1/c$, a 11·437(4), b 5·4692(7), c 18·320(5) Å, β 91·90(1)°, V 1145·3(5) Å^3, $F(000)$ 488, $D_c(Z = 4)$ 1·347 g cm^{-3}, μ(Mo Kα) 0·97 cm^{-1}, temperature 298(2) K.

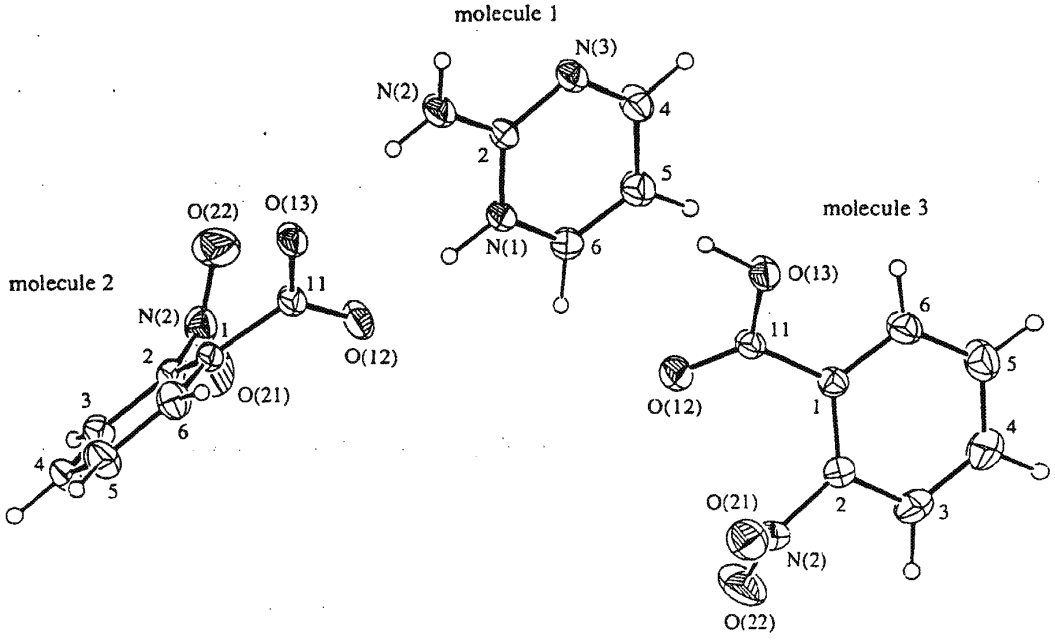


Fig. 2. Molecular configuration and atom naming scheme for (2).

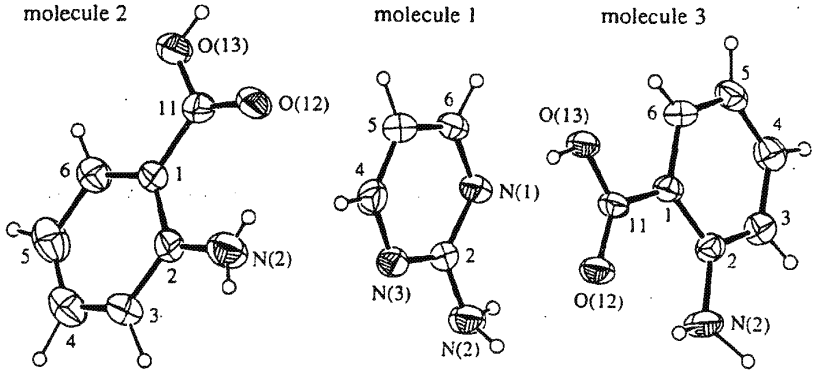


Fig. 3. Molecular configuration and atom naming scheme for (3).

UM00011612
NOVARTIS EXHIBIT 1517
Novartis v. Regents, IPR2023-01347
Page 358 of 4460

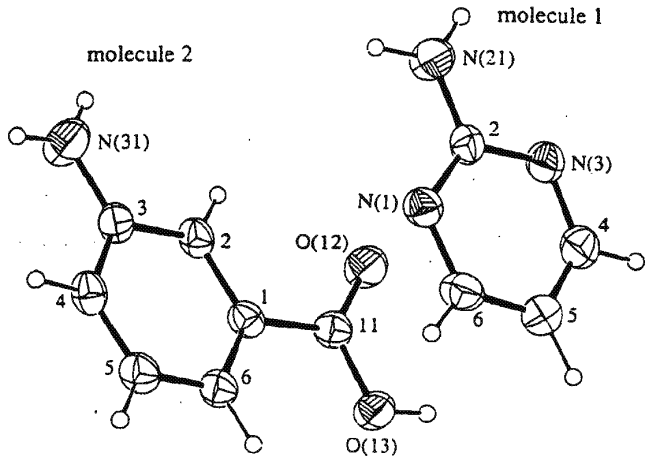


Fig. 4. Molecular configuration and atom naming scheme for (4).

Data Collection, Structure Solution and Refinement

X-Ray diffraction data were collected from crystals of dimensions 0·50 by 0·38 by 0·35 mm (1), 0·50 by 0·25 by 0·16 mm (2), 0·20 by 0·35 by 0·12 mm (3) and 0·30 by 0·25 by 0·12 mm (4) on an Enraf–Nonius CAD-4 diffractometer by using crystal monochromatized Mo Kα X-radiation (λ 0·71073 Å). Negligible change in the intensities of three standards monitored throughout the data collection periods for compounds (1)–(3) indicated no significant crystal decomposition. However, for (4), a loss in intensity of *c.* 12% indicated crystal decay, which was allowed for by scaling of data. Of 2171 (1), 3361 (2), 1674 (3) and 2012 (4) unique reflections collected up to $2\theta_{max}$ 50°, 1716 for (1), 2479 for (2), 974 for (3) and 980 for (4) with $I > 2{\cdot}0\sigma(I)$ were considered observed and were used in the structure analysis. Data were corrected for Lorentz and polarization effects with empirical absorption correction being applied.[10] The structures were solved by direct methods (SHELXS-86).[11] Full-matrix least-squares refinement (on F^2) (SHELXL-93),[12] with anisotropic thermal parameters for all non-hydrogen atoms, gave conventional residuals* R_1 0·036 for (1), 0·039 for (2), 0·038 for (3) and 0·041 for (4), and wR_2 0·101 for (1), 0·108 for (2), 0·124 (3) and 0·121 for (4). The values for A and B in the weighting scheme $w = [(\sigma^2(F_o^2) + (AP)^2 + BP]^{-1}$ were (0·094, 2·36) (1), (0·118, 0·53) (2), (0·111, 0) (3) and (0·150, 2·25) (4) respectively (where $P = [(\text{max. } F_o^2, 0) + 2(F_c^2)]/3$). Hydrogens were located by difference methods and both positional and thermal parameters were refined.

Results

Final atomic coordinates for adducts (1)–(4) are given in Table 1 while bond distances and angles are listed in Tables 2 and 3. Lists of anisotropic thermal parameters observed and calculated structure factors and hydrogen

* $R_1 = \sum ||F_o| - |F_c|| / \sum |F_o||$ and $wR_2 = [\sum w(||F_o| - |F_c||)^2 / \sum w(|F_o|)^2]^{\frac{1}{2}}$.

[10] Fair, C. K., 'MolEN, An Interactive Intelligent System for Crystal Structure Analysis' (Enraf–Nonius: Delft, the Netherlands, 1990).

[11] Sheldrick, G. M., SHELXS-86, Structure Solution Package, University of Göttingen, Federal Republic of Germany, 1986.

[12] Sheldrick, G. M., SHELXL-93, Program for Crystal Determination, University of Göttingen, Federal Republic of Germany, 1993.

UM00011613
NOVARTIS EXHIBIT 1517
Novartis v. Regents, IPR2023-01347
Page 359 of 4460

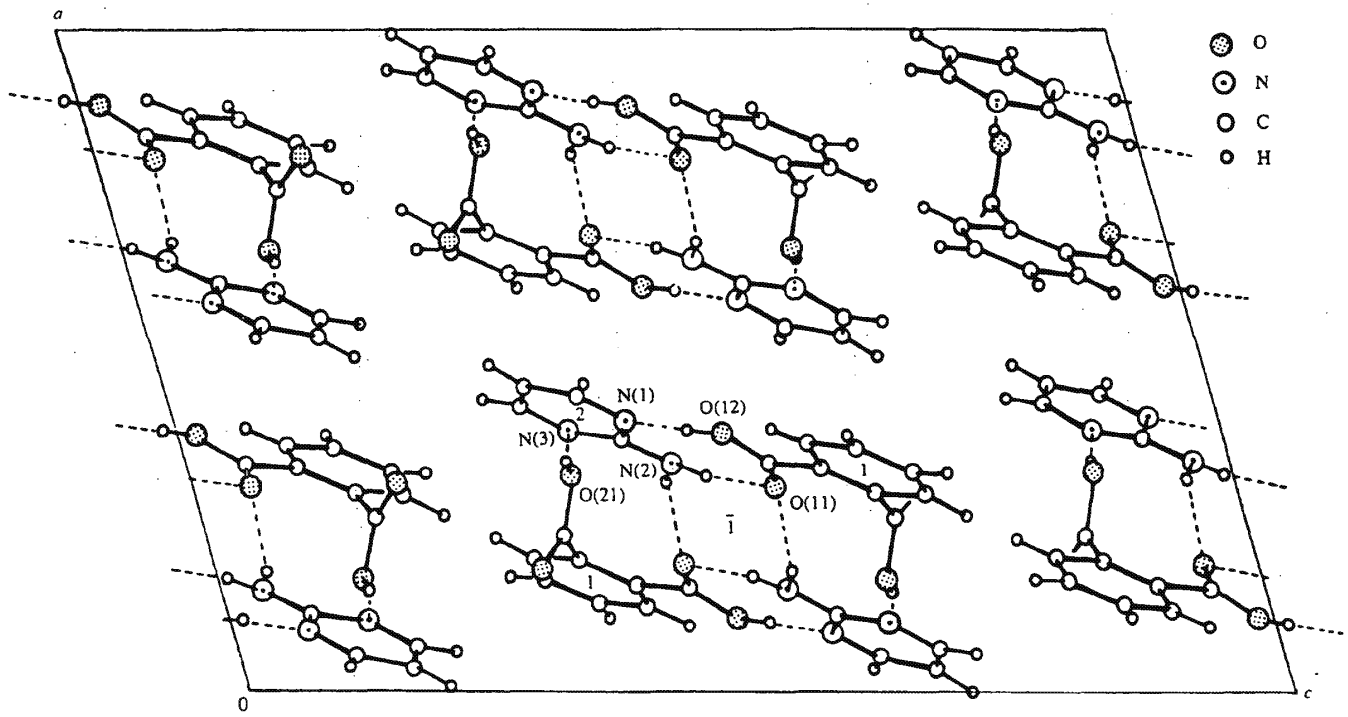


Fig. 5. Packing of (1) in the unit cell viewed down *b*.

UM00011614

NOVARTIS EXHIBIT 1517
Novartis v. Regents, IPR2023-01347
Page 360 of 4460

atom coordinates for compounds (1)–(4) have been deposited as an Accessory Publication.* The atom numbering schemes for the individual molecular types comprising the formula units in complexes (1)–(4) are shown in Figs 1–4.

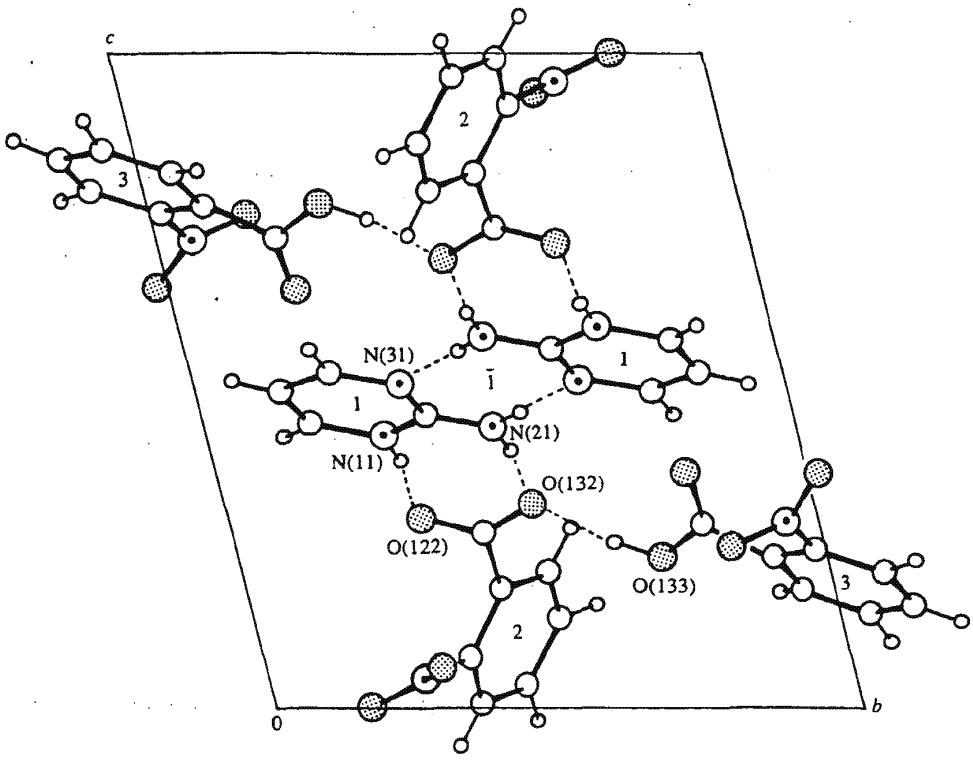


Fig. 6. Packing of (2) in the unit cell viewed down *a*.

Discussion

[(2-ap)(opht)] (1)

The structure of the 1 : 1 complex between 2-aminopyrimidine (molecule 2) and phthalic acid (molecule 1) [(2-ap)(opht)] (1) is unique and is based on an unusual discrete centrosymmetric tetramer unit (Fig. 5), involving two planar hydrogen-bonded heterodimers linked together by secondary hydrogen bonds. No proton transfer occurs. The hydrogen bonds forming the primary (2-ap)–carboxylic acid association are of the normal (P-A) type expected for heterodimers between 2-ap and neutral carboxylic acid species, with both links between the carboxylic oxygen and a nitrogen of the pyrimidine ring [O(12)–H···N(1), 2·615(3) Å; O–H···N, 174°] and between the second (carboxyl) oxygen and the amino nitrogen [O(11)···H–N(2), 3·038(3) Å; O···H–N, 170°]. This is similar to the primary (P-A) association between 2-ap and salicylic acid, 2,6-dihydroxybenzoic acid,[6] and succinic acid.[2] However, between the planar dimers are found secondary

* Copies are available from the Australian Journal of Chemistry, P.O. Box 89, East Melbourne, Vic. 3002.

UM00011615
NOVARTIS EXHIBIT 1517
Novartis v. Regents, IPR2023-01347
Page 361 of 4460

associations forming the tetramer, involving a carboxyl oxygen [O(11)] and the second amino hydrogen in a three-centre bond [O(11)···H(22)–N(2), 3·125(3) Å; (O···H–N, 151°] [graph set $R_4^2(8)$]. The 'outer' links are between the second carboxyl oxygen [O(21)] and the second pyrimidine nitrogen [N(3)] [O–H(21)···N, 2·644(3) Å; O–H···N, 168°] [graph set $R_2^2(11)$] giving an interplanar separation of *c.* 3·4 Å [e.g. 3·407(3) Å for C(42)–C(11)]. This is close to the van der Waals interactive distance for aromatic ring separation and is suggestive of some π–π interaction between the ring systems, which are offset. The stacking of alternate electron-donating functional groups with their parent ring systems near parallel but offset can be indicative of basic electron donor–acceptor system.[13] This, together with no significant intertetramer associations, is consistent with the perfect three-dimensional rhombic cleavage observed for crystals of this compound.

The conformation of *o*-phthalic acid in this adduct is considerably different from that of the parent acid.[14] One carboxylic acid group (involved in the primary dimer association) is almost coplanar with the benzene ring [torsion angle C(21)–C(11)–C(101)–O(121), 173·5(2)°] while the other (involved in interdimer association) is close to perpendicular [torsion angle C(11)–C(21)–C(201)–O(211) 93·4(2)°]. These values compare with 141° for the corresponding angle in the parent acid,[14] where the molecules are constrained to twofold symmetry axes.

[(2-ap)(2-nba)$_2$] (2)

The primary association in the (1 : 2) 2-aminopyrimidine/2-nitrobenzoic acid completely [(2-ap)(2-nba)$_2$] has a centrosymmetric (A-P-P-A) motif, with proton transfer from the carboxylic acid group of one of the 2-nba molecules (molecule 2) to the heterocyclic nitrogen [N(1)] of the pyrimidine ring (molecule 1). The characteristic eight-membered cyclic dimeric association results [N–H···O(12), 2·617(3) Å; N–H···O, 168°; N(21)–H···O(13), 2·880(3) Å; N–H···O, 172°] (Fig. 6). The separation between the two pyrimidine rings across the inversion centre in this (P-P) interaction [N(21)–H···N(6), 3·026(3) Å] compares with a distance of 3·073(2) Å for the parent 2-ap dimer.[5] The secondary association involves a single 'linear' hydrogen bond between the carboxylic acid oxygen of molecule 2 [O(13)] and the protonated carboxylic oxygen of molecule 3 [O(13), O···O, 2·563(3) Å; O–H···O, 160°]. In this respect the association differs from that observed for the 1 : 2 2-aminopyrimidine/2-aminobenzoic acid complex [compound (3)], in which the hydrogen-bonding linkage is from the second acid to the heterocyclic nitrogen of 2-ap. In the present example, no significant intermolecular hydrogen-bonding linkages involving the nitro group exist. This is in contrast to the situation with the cocrystalline complexes of other nitrobenzoic acids, e.g. with 3,5-dinitrosalicylic acid and 5-nitrosalicylic acid,[15] although these do not involve 2-ap.

[(2-ap)(2-aba)$_2$] (3)

The (1 : 2) complex of 2-aminopyrimidine (molecule 1) and 2-aminobenzoic acid (molecules 2 and 3) involves no proton transfer and comprises a relatively simple

[13] Sheppod, T. J., Petti, M. A., and Dougherty, D. A., *J. Am. Chem. Soc.*, 1988, **110**, 1983.
[14] Nowacki, T. J., and Jaggi, H., *Z. Kristallogr.*, 1957, **109**, 272.
[15] Smith, G., Lynch, D. E., Byriel, K. A., and Kennard, C. H. L., unpublished data.

UM00011616
NOVARTIS EXHIBIT 1517
Novartis v. Regents, IPR2023-01347
Page 362 of 4460

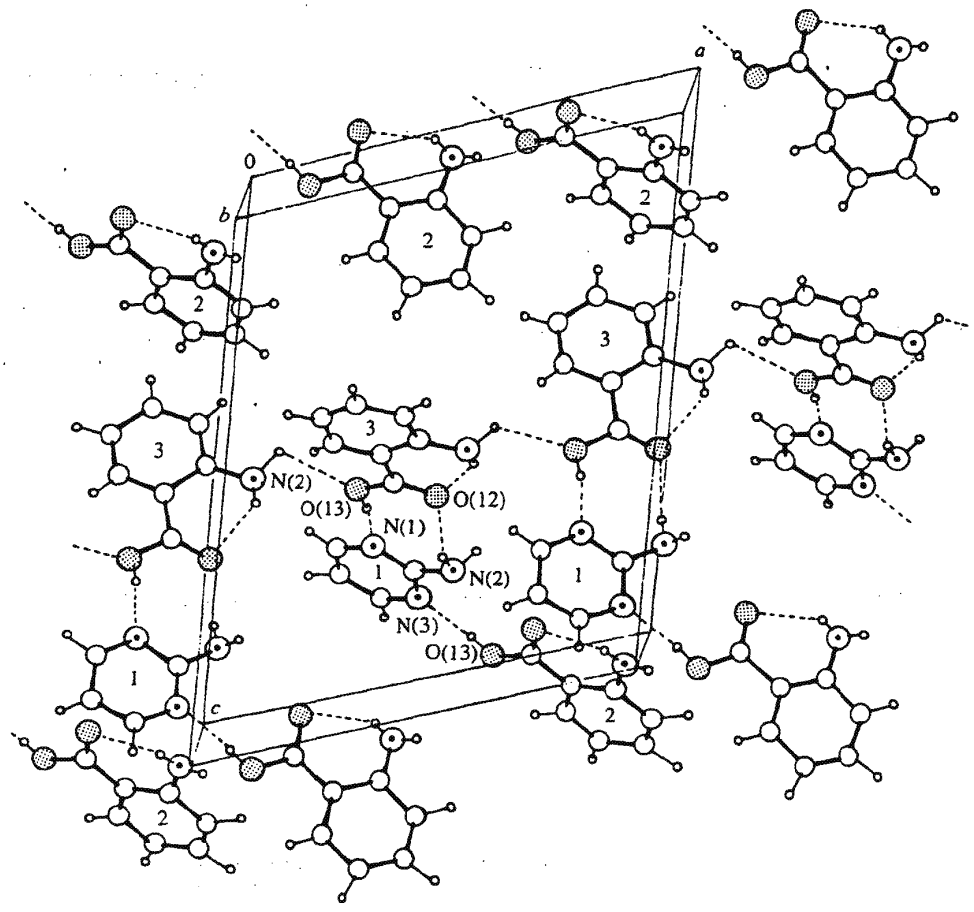


Fig. 7. Perspective view of the packing of (3) in the unit cell viewed down *b*.

hydrogen-bonding network (Fig. 7), made up of a primary, interacting (1:1) (P-A) heteropair which is hydrogen bonded through the acid group of one of the 2-aba molecules (molecule 3) and both the amino and ring nitrogens of the 2-ap molecule [O(13)–H···N(1), 2·692(2) Å; O–H···N, 168°; O(12)···H–N(2), 2·950(3) Å; O···H–N, 156°]. This gives a conventional cyclic dimer [graph set $R_2^2(8)$] similar to that found in the primary (P-A) interaction for 2-ap complexes with the majority of aromatic carboxylic acids. However, the important difference between this example and the others in this series lies in the secondary interdimer interactions. The first involves one of the carboxyl oxygens of the primary 2-aba molecule and the amine proton of an adjacent 2-ap molecule (molecule 2) [O(13)···H–N(2), 3·008(2) Å; O···H–N, 110°]. The second is a single linear hydrogen bond between the carboxyl group of the second 2-aba molecule (molecule 2) and the second pyrimidine nitrogen [O(13)–H···N(3), 2·679(2) Å; O–H···N, 170°]. The net effect is to produce alternating ribbons comprising molecules of 2-ap, 2-aba (type 1) and 2-aba (type 2) extending along the *a* cell direction, completing a

UM00011617
NOVARTIS EXHIBIT 1517
Novartis v. Regents, IPR2023-01347
Page 363 of 4460

$[(A)P\text{-}A]_n$ polymer motif. Only the primary 2-aba molecules are linked in this direction, the secondary 2-aba molecules and the 2-ap molecules giving transverse crosslinks. Because of this molecular packing asymmetry, reflected in the space group for the crystals, preliminary second harmonic generation tests were made on a powdered sample of the compound. No quantitative SHG measurements were possible for the compound but a strong SHG signal was evident as a visible green glow (532 nm) from the Nd:YAG laser source (1064 nm), observed through narrow band filters on the oscilloscope.

The individual molecules of 2-aba are planar [torsion angles for C(2)–C(1)–C(11)–O(13) −177·7(6)° and 176·0(6)° for the molecules 2 and 3 respectively] while the substituent amine groups are intramolecularly bonded to the *ortho*-related carboxyl oxygens [N···O, 2·680, 2·697(8) Å; N–H···O, 130, 132° respectively]. These features are similar to those found for all crystal polymorphs of the parent

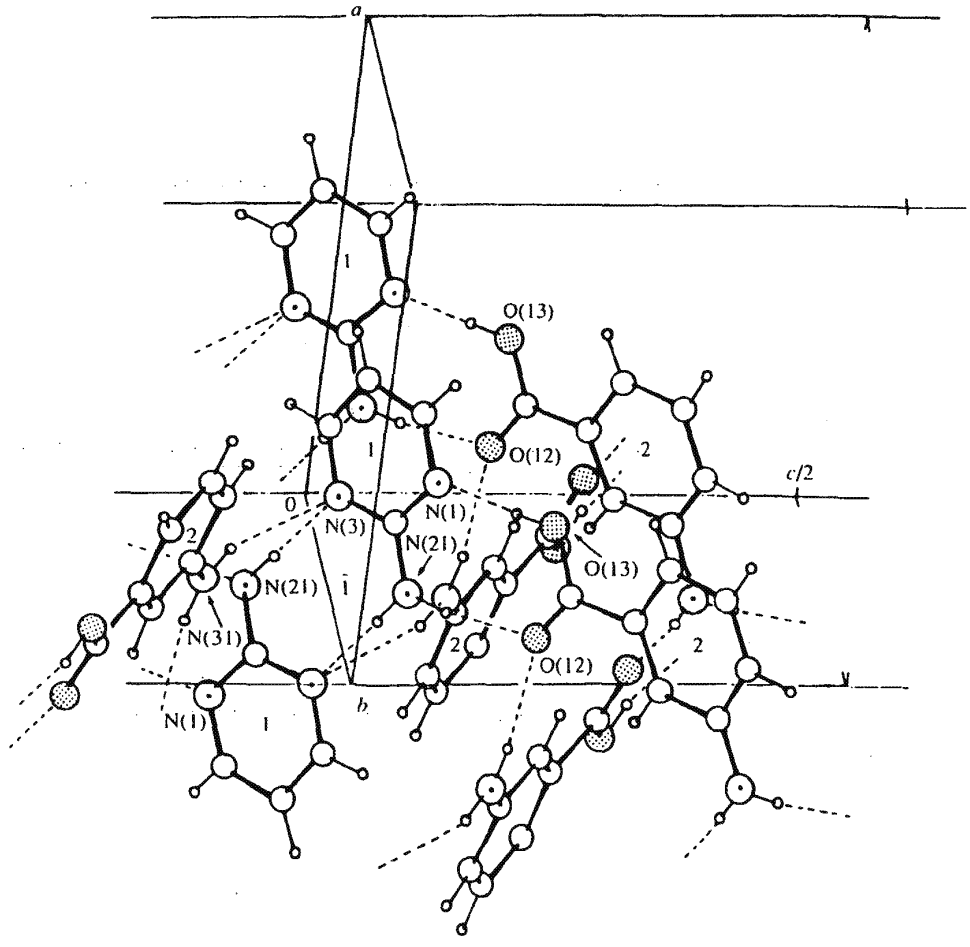


Fig. 8. Packing of (4) in the unit cell viewed down *b*.

UM00011618
NOVARTIS EXHIBIT 1517
Novartis v. Regents, IPR2023-01347
Page 364 of 4460

acid.[16] The reason for this unusual secondary interaction, together with the 1:2 molecular interaction, irrespective of reactant stoichiometry in the preparation, is considered to be the formation of this intramolecular association, which restricts the interactive effectiveness of the second amine proton in giving the more symmetrical packing motif found in the (1:1) (2-ap)/3-aba complex (4) or in the (1:1) (2-ap)/4-aba complex.[6]

[(2-ap)(3-aba)] (4)

The structure of the 1:1 molecular complex of 2-aminopyrimidine with 3-aminobenzoic acid [(2-ap)(3-aba)] (3) involves 2-ap (molecule 1) and (3-aba) (molecule 2) in a primary (A-P) cyclic hydrogen-bonded carboxyl–pyrimidine association [graph set $R_2^2(8)$], with secondary interdimer associations. With the primary interaction between the carboxyl and pyrimidine centres, the geometry is [O(13)–H···N(1), 2·688(6) Å; O–H···N, 168°; and O(12)···H(21)–N(2), 2·931(6) Å; O···H–N, 170°]. The geometry for the centrosymmetric (P-P) association between the two 2-ap molecules [N(3)···H(22)–N(21), 3·104(5) Å; N···H–O, 170°] is similar to the parent dimer.[5] Secondary interactions involve both protons of the *meta*-related amine group of 3-aba, the first with a carboxyl oxygen [O(12)] [N(31)–H(31)···O, 2·970(5) Å; N–H···O, 165°], the second with a *c*-glide related pyrimidine ring nitrogen in a three-centre bond [N(31)–H(32)···N(3), 3·231(5) Å; N–H···N, 158°]. In this respect it is very similar to the $(\text{A-P-P-A})_n$, structure of 2-ap with 4-aminobenzoic acid [(2-ap)(4-aba],[6] except that the *meta*-related amino groups of 3-aba in (4) give an angular offset (chain polymer association), in contrast to the almost linear associations provided by the 4-aba molecules which link via the *para*-related amino group (cyclic association).

General Consideration

While no new types of primary association are described among the adducts (1)–(4), considerable information about secondary interactive effects becomes available. It is assumed that the primary interaction with 2-ap proceeds according to the general hierarchial rules of Etter and Adsmond[2] [OH > NH > N(ring)] with secondary interactions following to the consumption of the available donor–acceptor sites, giving the crystal lattices. Formation of all known complexes of 2-ap, including those reported here (see Table 4), appears to proceed according to these basic rules, but the importance of the secondary group interactions in explaining the anomalous and somewhat unpredictable behaviour with respect to both proton transfer and adduct stoichiometry, has not been fully appreciated. With pyridine, which is devoid of secondary proton acceptor sites, it has been recognized that proton transfer from an acid donor will occur only if the pK_a difference between donor and acceptor is greater than 3·75.[17] However, with 2-ap adducts, prediction cannot be made on the basis of pK_a difference,[2,6] as shown in the adducts with salicylic acid,[6] 2,6-dihydroxybenzoic acid,[6] 2,4,6-trinitrobenzoic

[16] Brown, C. J., *Proc. R. Soc. London, Ser. A*, 1968, **302**, 185; Boone, D. G., Derissen, J. L., and Schoone, J. C., *Acta Crystallogr., Sect. B*, 1977, **33**, 3205; Khan, Y., and Srivastava, P., *Indian J. Pure Appl. Phys.*, 1968, **6**, 166; Hardy, G. E., Kaska, W. C., Chandra, B. P., and Zink, J. I., *J. Am. Chem. Soc.*, 1981, **103**, 1074.
[17] Johnson, S. L., and Roumon, K. A., *J. Phys. Chem.*, 1965, **69**, 74.

UM00011619
NOVARTIS EXHIBIT 1517
Novartis v. Regents, IPR2023-01347
Page 365 of 4460

acid[18] and *o*-phthalic acid [compound (1)]. Salicylic acid ($pK_a = 2{\cdot}97$), 2,6-dihydroxybenzoic acid ($pK_a = 1{\cdot}08$) and 2,4,6-trinitrobenzoic acid ($pK_a = 2{\cdot}82$) give transfer in their complexes, but with phthalic acid ($pK_{a_1} = 2{\cdot}95$) no transfer takes place. This anomalous effect may only be explained on the basis of the position and type of the secondary group in a role previously seen as being responsible in (1) for the formation of the unusual dimeric $(P\text{-}A)_2$ association. This is primarily because of the ambivalence of the second carboxyl group, allowing inversion linkage between the (P-A) pairs. While the salicylic acid types have an associative OH substituent in an *ortho* position, it is considered inert with respect to secondary association because of the intramolecular hydrogen bonding. The *o*-nitro-substituted examples [including compound (2)] may also be considerd non-associative and show no important secondary effects. With the amino-substituted benzoic acids, their weak acidity precludes proton transfer. However, this associative group influences the stoichiometry and may, as in the case of (3) introduce crystal asymmetry. Considering the basic symmetry of the fundamental units inherent in the 2-ap/carboxylic acid association, it is not surprising that (3) represents only the second non-centrosymmetric 2-ap adduct (the first was with phenoxyacetic acid $[(2\text{-ap})(pa)_2]$[6]) and is the only one which also shows SHG properties. In addition, the 1 : 2 (2-ap to acid) stoichiometry, in the case of (3) formed irrespective of reactant ratios, appears to be favoured over (1 : 1) because of the stereochemical and interactive influence of the *ortho*-related amine substituent on the acid.

Acknowledgments

The authors acknowledge financial support from the Centre for Instrumental and Developmental Chemistry of the Queensland University of Technology, the Australian Research Council and the University of Queensland. Professor Geoff Ashwell and Andrzej Kuczynski of the Centre for Molecular Electronics, Cranfield University, Bedford, UK, are thanked respectively for provision of facilities and for performing SHG measurements.

[18] Byriel, K. A., Kennard, C. H. L., Lynch, D. E., Smith, G., and Thompson, J. G., *Aust. J. Chem.*, 1992, **45**, 969.

UM00011620
NOVARTIS EXHIBIT 1517
Novartis v. Regents, IPR2023-01347
Page 366 of 4460

This Page is Inserted by IFW Indexing and Scanning Operations and is not part of the Official Record

BEST AVAILABLE IMAGES

Defective images within this document are accurate representations of the original documents submitted by the applicant.

Defects in the images include but are not limited to the items checked:

- ☐ BLACK BORDERS
- ☐ IMAGE CUT OFF AT TOP, BOTTOM OR SIDES
- ☐ FADED TEXT OR DRAWING
- ☐ BLURRED OR ILLEGIBLE TEXT OR DRAWING
- ☐ SKEWED/SLANTED IMAGES
- ☐ COLOR OR BLACK AND WHITE PHOTOGRAPHS
- ☐ GRAY SCALE DOCUMENTS
- ☐ LINES OR MARKS ON ORIGINAL DOCUMENT
- ☐ REFERENCE(S) OR EXHIBIT(S) SUBMITTED ARE POOR QUALITY
- ☐ OTHER: _____

IMAGES ARE BEST AVAILABLE COPY.
As rescanning these documents will not correct the image problems checked, please do not report these problems to the IFW Image Problem Mailbox.

Advances in Crystal Growth Research (2001) p381-400)

Crystal Morphology Control with Tailor-Made Additives; A Stereochemical Approach

Isabelle Weissbuch, Meir Lahav, Leslie Leiserowitz

Department of Materials and Interfaces,
The Weizmann Institute of Science, Rehovot 76100 Israel

Tailor-made molecules have been designed and used as additives, in crystallization processes from solution, to control the nucleation and growth of molecular crystals. These additives can be either inhibitors or promoters of crystal growth. Tailor-made inhibitors can be used for a variety of purposes that include crystal morphology engineering, kinetic resolution of racemates, reduction of crystal symmetry, assignment of absolute configuration of chiral molecules and polar crystals and control of crystal polymorphism. As for crystal growth promoters tailor-made additives, that self-assemble at the air-aqueous solution interface due to their intrinsic hydrophobic nature, have been used to induce oriented crystallization by means of a structural match.

1. INTRODUCTION

Crystals and the crystallization process from solutions play an important role in pure and applied sciences. However, the ability to design crystals with desired properties and the control over crystallization, based on structural understanding, are still limited when compared with the controlled crystal growth provided in biomineralization processes.

The ground rules for a quantitative determination of crystal morphology based on the internal crystal structure were laid by Hartman, Perdok and Bennema[1-5] in their landmark papers on the prediction of crystal morphology. Regarding the effect of additives and solvent on crystal growth and morphology, a variety of studies have been reported around the mid 20th century. The control on nucleation, growth, dissolution and morphology of molecular crystals, however, remained primarily a matter of 'mix and try'.

In the last 20 years, a stereochemical approach has been adopted involving growth and dissolution of molecular crystals in the presence of 'tailor-made' additives that interact with specific crystal faces and may be crystal growth inhibitors or nucleation promoters.[6-14] The surfaces of a growing crystal can be thought of as composed of 'active sites' that interact stereospecifically with molecules in solution, in a manner similar to enzyme-substrate or antibody-antigen interactions. The repetitive arrangement at crystal surfaces and the knowledge of their structures offer simpler means to pinpoint intermolecular interactions by using the concept of molecular recognition at interfaces. With the assistance of tailor-made additives, it is possible to examine a variety of processes concerning open questions in the field of crystal nucleation and growth, interactions with the growth environment and crystal polymorphism.

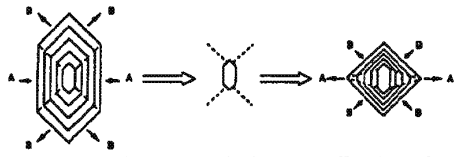
2. CRYSTAL MORPHOLOGY ENGINEERING

The habit of a crystal is defined by the relative rates of its growth in different directions; the faster the growth in a given direction the smaller the face developed perpendicular thereto. Consequently, when growth is inhibited in a direction perpendicular to a given face, the area of this face is expected to increase relative to the areas of other faces of the same crystal. Differences in the relative surface areas of the various faces can therefore be directly correlated to the inhibition in different growth directions. Such a change in crystal morphology is shown in Scheme 1.

Dramatic changes in morphology observed during growth of molecular crystals in the presence of additives revealed a high degree of specificity in the interaction of the foreign material with the different structures of the growing surfaces.

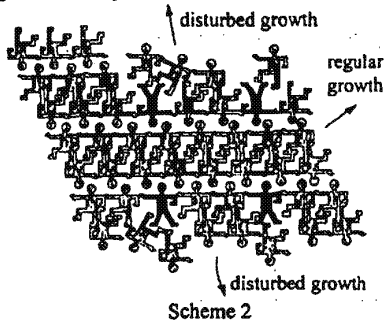
UM00011622

NOVARTIS EXHIBIT 1517
Novartis v. Regents, IPR2023-01347
Page 368 of 4460



Scheme 1

Crystal morphology engineering became possible with the use of tailor-made additives of molecular structure similar to the structure of the corresponding host molecules. From a systematic study of a variety of organic compounds crystallized in the presence of additives, it was possible to deduce a stereochemical correlation between the structures of the affected crystal surfaces and the molecular structure of the additive. We could infer that the tailor-made additive is recognized only at certain surfaces on the growing crystals, in a manner similar to the host molecules, and then adsorbed at those faces with the part of the additive that differs from that of the host emerging from the crystal. Such selective adsorption of the tailor-made additive at crystal faces and subsequent inhibition of their growth are depicted in Scheme 2.



Scheme 2

Once this mechanism was established, it became possible to exploit it to systematically modify the morphology of crystals by tailoring additives that bind at preselected faces and thus inhibit growth in a predictable manner.

An example[6] where the host-tailor-made additive interactions at the growing solid-liquid interface can be pinpointed and correlated with the change in crystal morphology is benzamide, $C_6H_5CONH_2$. This compound crystallizes from ethanol as plates, in the monoclinic space group $P2_1/c$. The packing arrangement in this crystal can be described in terms of hydrogen-bonded cyclic molecular dimers interlinked by hydrogen bonds to yield ribbons parallel to the *b* axis (Fig 1a). The ribbons are stacked along the *a* axis to form stable (001) layers.

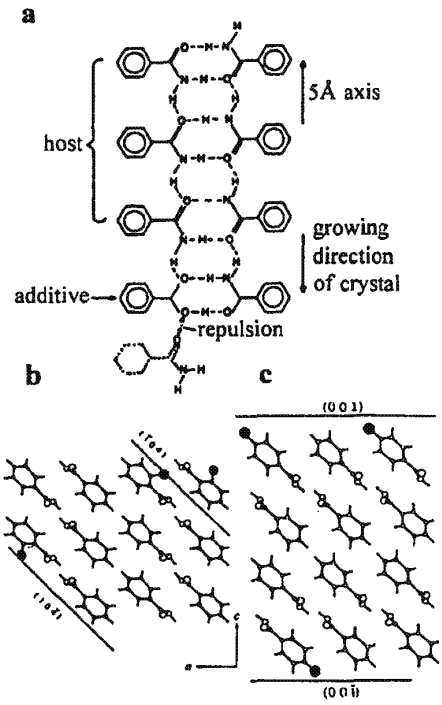


Fig. 1. (a) Schematic representation of the ribbon motif of hydrogen-bonded dimers of benzamide molecules interlinked along the 5 Å *b*-axis, showing the effect of benzoic acid additive.
(b, c) Packing arrangement of benzamide, viewed along the *b* axis, showing the effect of *o*-toluamide and *p*-toluamide, CH_3-$C_6H_4CONH_2$, respectively.

These tightly packed layers juxtapose along the *c* direction, interacting via weak van der Waals interactions between phenyl groups, thus accounting for the {001} plate-like shape of the crystals.

Benzoic acid C_6H_5COOH additive, adopting the stable O=C-OH *syn* planar conformation, can replace a molecule of benzamide at the end of a

UM00011623
NOVARTIS EXHIBIT 1517
Novartis v. Regents, IPR2023-01347
Page 369 of 4460

ribbon (Fig. 1a); however, at the site of the additive, an attractive N-H···O bond is replaced by repulsion between adjacent oxygen lone-pair electrons of the bound additive molecule and of the oncoming benzamide molecule. As predicted, benzoic acid as additive inhibits growth of the benzamide crystals along *b*, transforming the pure plates (Fig. 2a) into [100] needles (Fig. 2b). Inhibition of growth along *a* was accomplished with *o*-toluamide that yielded [010] bars (Fig. 2c). This additive can easily be adsorbed in the hydrogen-bonding chain, without disturbing growth along *b*, but with the methyl group, that emerges from the $(10\bar{4})$ side-face (Fig. 1b) interfering with growth in the *a* direction along which the dimers are stacked. Thinner plates, (Fig. 2d), are obtained by addition of increasing amounts of *p*-toluamide since its methyl group perturbs the already weak van der Waals interactions between the phenyl layers in the *c* direction (Fig. 1c).

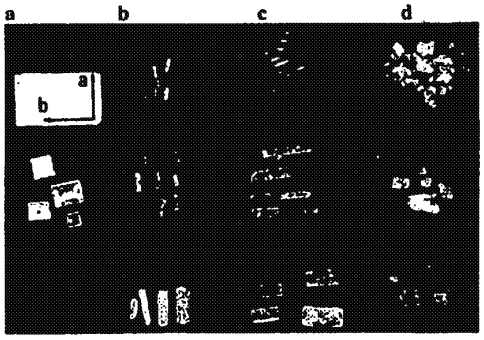
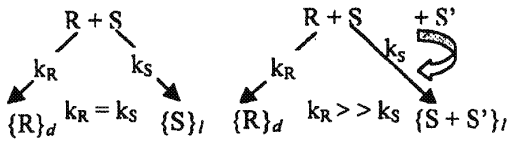


Fig. 2. Photographs of benzamide crystals: (a) pure; (b-d) grown in the presence of increasing amounts (from bottom to top) of (b) benzoic acid, (c) *o*-toluamide, (d) *p*-toluamide.

The two-step mechanism of stereospecific binding of tailor-made additives at the growing crystal surfaces followed by inhibition of growth perpendicular to these faces has been applied to a variety of molecular crystals including α-aminoacids, di-peptides, primary and secondary amides, carboxylic acids, sugars, steroids, etc., and is therefore general. It has been also successfully applied in the separation of enantiomers by kinetic resolution of conglomerates.

3. TAILOR-MADE INHIBITORS FOR RESOLUTION OF RACEMATES[7,8]

Application of the above two-step mechanism to racemic mixtures in which each enantiomer R- or S- crystallizes in enantiomorphous crystals (Scheme 3left) suggested the possibility of performing by these means a manual Pasteur-type separation, as well as a kinetic resolution. Enantiomorphous crystals behave differently when grown in the presence of enantiomeric tailor-made additives since diastereomeric interactions occur at the surfaces of the growing crystals. It follows directly from the mechanism illustrated in Scheme 3right that an enantiomeric additive S' consisting of a appropriately modified S molecule will in general be adsorbed only at the S crystal surface and not at the R crystal. As a consequence, the S crystal undergoes changes in morphology which allow easy visual identification and separation of the two enantiomorphs. This principle is illustrated with the following example.



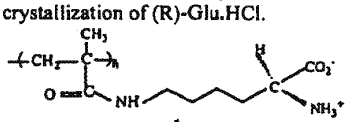
Scheme 3

Racemic (R,S)-glutamic acid.HCl (Glu.HCl), $HOOC(CH_2)_2C^*H(NH_3^+)COOH$ crystallizes as a conglomerate of (R)- and (S)- enantiomorphs. The packing arrangement and morphology of (S)-Glu.HCl crystal are shown in Fig. 3. The molecular side chains are directed along the *c* axis and form hydrogen bonds in this direction. Therefore, various other α-aminoacids can be regarded as tailor-made additives since these molecules bear the residue $^+H_3NC^*HCOOH$ of the α-aminoacid group, whereas the side chain is different. When growing (S)-Glu.HCl in the presence of such S'-α-aminoacids, the additive will enantiospecifically adsorb at the two {001} crystal faces and inhibit crystal growth perpendicular to them since the hydrogen bonding along *c* will be disrupted. In contrast, R'-α-aminoacid additives cannot be adsorbed at the same surfaces because the molecular structure of the

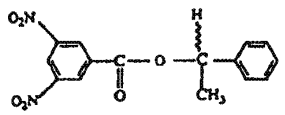
UM00011624
NOVARTIS EXHIBIT 1517
Novartis v. Regents, IPR2023-01347
Page 370 of 4460

substrate and additive are of opposite handedness. By symmetry, (R')-α-aminoacid additive can be adsorbed only at the {001} faces of (R)-Glu.HCl crystals. Indeed, crystals grown from racemic R,S-Glu.HCl in the presence of S-lysine additive (1-3% wt/wt of racemate) appear as plates of (R)-Glu.HCl covered by a crystalline powder of the (S)-Glu.HCl (Fig. 4). The pure plate-like crystals of (S)-Glu.HCl (Fig. 5a) grow thinner and become a powder with increasing S-lysine concentration (Fig. 5). Kinetic resolution of the racemic R,S-Glu·HCl can be achieved with the assistance of larger (up to 10% wt/wt) amounts of S-lysine additive that prevents the growth of (S)-Glu.HCl yielding preferred crystallization of (R)-Glu.HCl. This principle has been applied to other racemic systems, including (R,S)-asparagine monohydrate, (R,S)-threonine, (R,S)-*p*-hydoxy-phenylglycine,*p*-toluene-sulfonate.

The efficiency of the tailor-made additives could be significantly increased by anchoring the α-aminoacid moieties to a polymeric backbone. Addition of only 0.1-1% poly-(N^{ε}-metacryloyl-R-lysine), **1**, to supersaturated solutions of R,S-Glu.HCl could bring about the preferred crystallization of (R)-Glu.HCl.



1



2

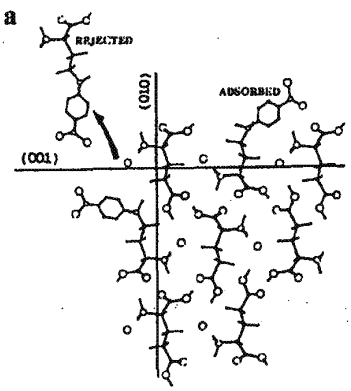


Fig. 3. (a) Packing arrangement of (S)-Glu.HCl viewed along the *a* axis and showing the effect of S-N^{γ}(*p*-nitro-phenyl)-α,γ-diamino-butyric acid, O_2N-C_6H_4-NH-$(CH_2)_2CH(NH_3^+)COO^-$, additive. (b) Morphology of pure crystals.

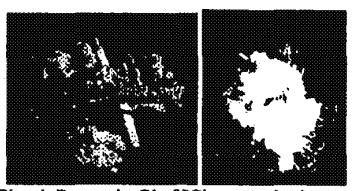


Fig. 4. Racemic Glu.HCl grown in the presence of S-lysine; the plates are the (R)-Glu.HCl, whereas the powder is the (S)-Glu.HCl.

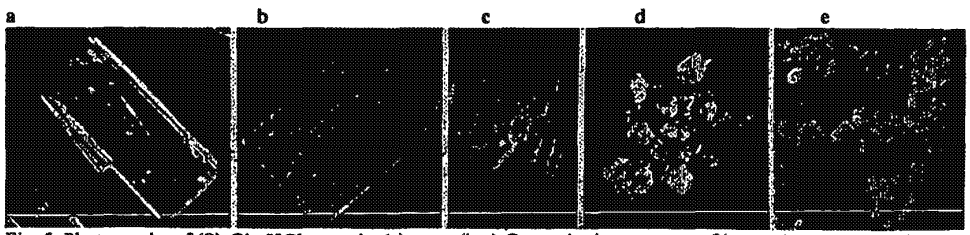
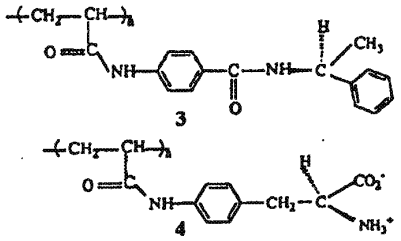


Fig. 5. Photographs of (S)-Glu.HCl crystals: (a) pure; (b-e) Grown in the presence of increasing amounts of S-lysine additive: (b) 2 mg/ml; (c) 5 mg/ml; (d) 10 mg/ml; (e) 50 mg/ml.

UM00011625
NOVARTIS EXHIBIT 1517
Novartis v. Regents, IPR2023-01347
Page 371 of 4460

An industrially feasible kinetic process for the resolution of methionine.HCl has been reported [9]. The method is also applicable to molecular crystals lacking ionic and hydrogen bonds as in the kinetic resolution of racemic (R,S)-*sec*-phenethyl-3,5-dinitro-benzoate, **2**, with poly-(N-acryloyl-(*p*-aminobenzoyl)-R-*sec*-phenethyl-amide), **3**, additive.

The kinetic resolution may encompass preferred precipitation, from a racemate solution, of one enantiomorph at the expense of the more stable racemic crystal phase. Naturally, the energy gap between the racemic crystal and the mixture of resolved enantiomorphs must be relatively small. For example, racemic R,S-histidine.HCl, $C_3H_3N_2$-CH_2-C*H(NH_3^+)COO^-, precipitates at 25°C as a stable racemic dihydrate crystal (R,S)-His.HCl.$2H_2O$. Above 45°C it precipitates as a metastable conglomerate of enantiomorphous monohydrate (R)- and (S)-His.HCl.H_2O crystals. Addition of as little as 1% of the enantiomeric poly-(*p*-acrylamido-phenylalanine), **4**, tailor-made inhibitor induced complete resolution of the desired enantiomer.[8] The polymeric inhibitor was designed by considering the packing arrangements of the two crystalline forms of histidine (Fig. 6). Following our adsorption/inhibition approach, we anticipated that an enantiomeric α-aminoacid bearing aromatic side groups grafted onto a polymeric backbone (to yield a water soluble polymer with free α-aminoacid head groups) should be enantiospecifically adsorbed onto the {011} faces of the racemic (R,S)-His.HCl.$2H_2O$ form and inhibit its growth along the *b* direction (Fig. 6a).



Analogously, the same polymer of say R-configuration should be nucleation and growth inhibitor of (R)-His.HCl.H_2O (Fig. 6b). Consequently, resolution of the racemate could be accomplished.

The need for a fine geometric match between the molecular structure of the α-aminoacid group grafted onto the polymer and that of the substrate crystal was further demonstrated by the fact that poly-(N$^\varepsilon$-methacryloyl)lysine, **1**, could not prevent crystallization of the racemate even when present in high concentrations (~10% wt/wt).

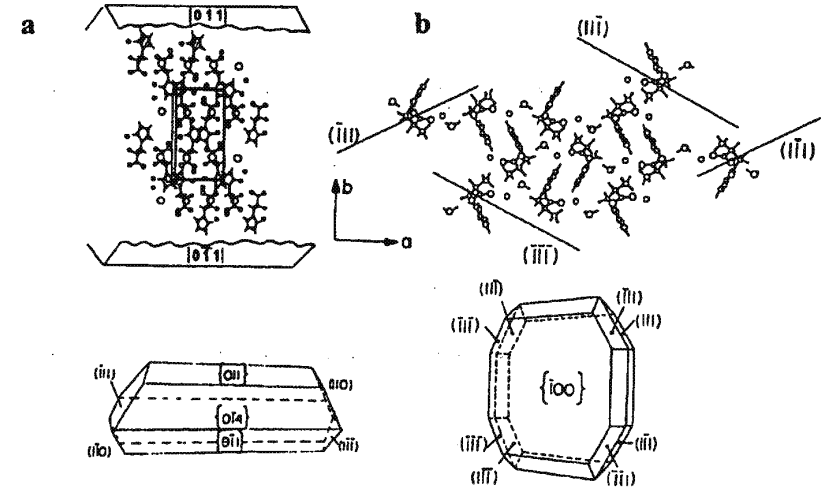


Fig. 6. Packing arrangement and computer-drawn morphology of: (a) racemic (R,S)-His.HCl.$2H_2O$; (b) (R)- or (S)-His.HCl.H_2O.

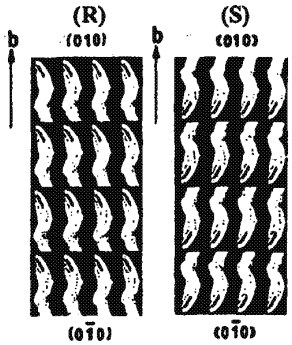
UM00011626
NOVARTIS EXHIBIT 1517
Novartis v. Regents, IPR2023-01347
Page 372 of 4460

4. EFFECT OF TAILOR-MADE ADDITIVES ON GROWTH OF POLAR CRYSTALS

The effect of tailor-made molecular additives on crystal morphology and structure could be taken advantage of to demonstrate the interplay between molecular chirality and various macroscopic phenomena. The method has been applied to assign the absolute structures of polar crystals whose constituent molecules are either chiral, racemic mixtures or nonchiral.

4.1. Polar crystals composed of enantiomerically pure molecules[10]

We first focus on polar crystals composed of enantiomerically pure molecules. The method involves the principle of fixing the orientation of the constituent molecules *vis-a-vis* the polar axis, or axes, of the crystal and subsequently determining the absolute configuration of the chiral molecules. This principle is depicted in Scheme 4 that shows two enantiomorphous sets of hands arranged in a lattice; right hands forming an (*R*)-crystal and left hands forming an (*S*)-crystal. The fingers of the hands are exposed at the (010) face of the right-handed "molecules" and, by symmetry, at the $(0\bar{1}0)$ face for the left-handed "molecules". Thus, by determining at which face of the crystal specimen the fingers or wrists are exposed, the handedness of the constituent molecules may be assigned.



Scheme 4

By applying the two-step adsorption-inhibition mechanism with appropriate tailor-made additives, such assignment can be performed. We illustrate this approach with several examples.

N-(E-cinnamoyl)-S-alanine[7,10]

The molecules of N-(*E*-cinnamoyl)-S-alanine, C_6H_5-CH=CH-CONH-C*H(CH_3)-COOH, crystallize in space group $P2_1$. The packing arrangement (Fig. 7) and the morphology of the pure crystal grown from methanol solution (Fig. 8a) show that molecules are arranged with the COOH groups emerging at the two $\{1\bar{1}1\}$ faces and with the C*(chiral)-H bonds directed along the $+b$ axis. We found, as expected, that the methyl ester, C_6H_5-CH=CH-CONH-C*H(CH_3)-$COOCH_3$, of the same absolute configuration as the host molecule induced the appearance of large $\{1\bar{1}1\}$ faces (Fig. 8b) since the O-CH_3 group replaces an O-H group emerging from such faces. Therefore the absolute direction of the O-H bond with respect to the polar *b* axis is fixed and so the absolute configuration of the substrate molecules. Tailor-made additive N-(*E*-cinnamoyl)-R-alanine of configuration opposite to that of the host induced, as expected, formation of an (010) face (Fig. 8c) because of an interchange of CH_3 and H at the guest asymmetric carbon (C*) so that the C*-CH_3 guest moiety replaces the emerging host C*-H bond.

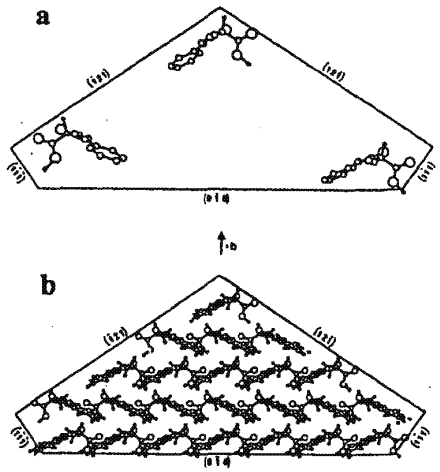


Fig. 7. Packing arrangement of N-(*E*-cinnamoyl-(S)-alanine delineated by the faces of the pure crystal.

UM00011627
NOVARTIS EXHIBIT 1517
Novartis v. Regents, IPR2023-01347
Page 373 of 4460

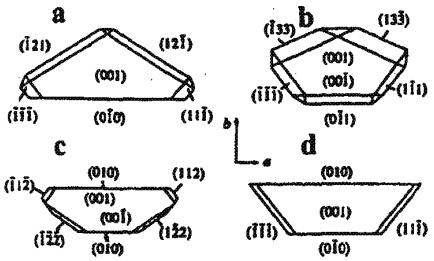
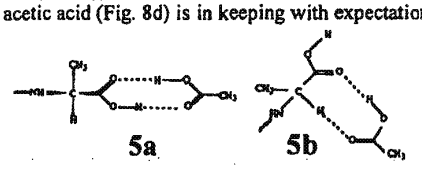


Fig. 8. Computer-drawn morphology of measured crystals of N-(*E*-cinnamoyl)-(S)-alanine.
(a-c) Grown from methanol: (a) pure, (b, c) grown in the presence of the methyl ester and N-(*E*-cinnamoyl)-(R)-alanine, respectively;
(d) Grown from glacial acetic acid.

Solvents may act in a manner similar to the tailor-made additives as illustrated by growing the crystals of N-(*E*-cinnamoyl)-S-alanine from acetic acid instead of methanol. Acetic acid is a solvent which can selectively bind at the exposed carboxylic acid groups of the two {1$\bar{1}$1} faces forming a hydrogen bonded dimer **5a**. Acetic acid can also bind to the C*HC=O moiety of N-(*E*-cinnamoyl)-S-alanine via a cyclic dimer **5b** on the (010) face. The morphology of the crystals grown from glacial acetic acid (Fig. 8d) is in keeping with expectation.



5a **5b**

(R)- or (S)-lysine.HCl.2H$_2$O[7]

The dihydrate crystals of (R)- or (S)-lysine.HCl, ^+H_3N-$(CH_2)_4$-C*H$(NH_3^+)COO^-$, crystallized from water, appear in the monoclinic space group $P2_1$. The packing arrangement is shown in Fig. 9 and the morphology of the pure form in Fig 10a. Lysine molecules are aligned parallel to the *b* axis, with the ^+H_3N-C*H-COO^- moiety emerging from the +*b* end of the crystal. The ε-NH_3^+ points toward the –*b* and is hydrogen bonded to neighboring molecules in the *ac* plane. Tailor-made α-aminoacid additives with a modified carboxyl or α-amino group, such as lysine methyl ester, inhibited growth in the +*b* direction, inducing development of the (010) face (Fig. 10b). Conversely, additives that bear a modified side group, such as norleucine or norvaline, inhibited growth along the –*b* direction with a concomitant pronounced increase in the areas of the {1$\bar{1}$0} faces (Fig. 10c).

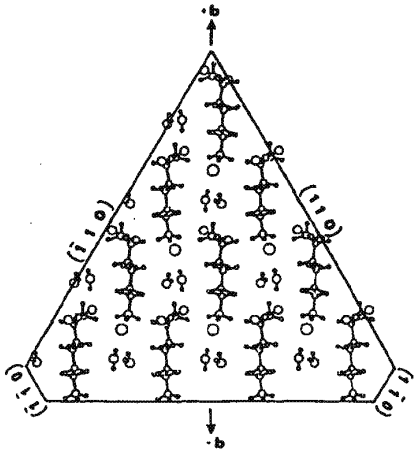


Fig. 9 Packing arrangement of (S)-lys.H_2O viewed along *c* axis.

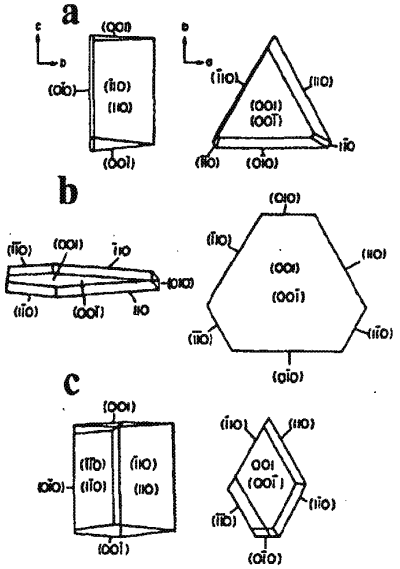


Fig. 10. (a-c) Computer-drawn morphology of measured (S)-lys.H_2O crystals: (a) pure, (b) grown with methyl ester (c) grown with S-norleucine.

UM00011628
NOVARTIS EXHIBIT 1517
Novartis v. Regents, IPR2023-01347
Page 374 of 4460

The selective adsorption of the tailor-made additive molecules at one end of the polar axis implies that the additive must be occluded only in that part of the crystal that had exposed the adsorbing face to solution during crystal growth (because the additive can be occluded only through adsorbing faces). Therefore, analysis of the occluded additive at the crystal extremities along the polar axis must reveal an anisotropic distribution, as confirmed experimentally by high performance liquid chromatography (HPLC) analysis (Fig. 11) showing the preferential occlusion of the S-norleucine additive at the $-b$ end of the crystal.

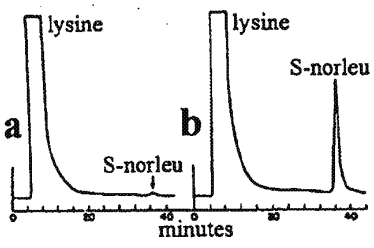


Fig. 11. HPLC analysis of the occluded S-norleucine in crystals as in Fig. 10c: (a) $+b$ side of the crystal; (b) $-b$ side of the crystal.

4.2. Polar crystals composed of racemic molecules[10]

(R,S)-alanine

The absolute orientation of the racemic (R,S)-alanine, $H_3C\text{-}C^*H(NH_3^+)COO^-$, polar crystals, of space group $Pna2_1$, could also be assigned from growth experiments in the presence of additives designed to affect either of the two polar ends of the crystal. The packing arrangement delineated by the crystal morphology is shown in Fig. 12a. In the crystal, which is needle-like along the c axis, the R- and S-molecules are oriented with respect to the polar needle c axis so that the carboxylate COO^- groups are exposed at one end of the polar axis and the amino NH_3^+ groups at the opposite end. The crystals exhibit different (hemihedral) faces at opposite ends of the c axis since they display one end face that is flat and the opposite end capped (Fig. 12b). Conventional X-ray crystallography does not allow one to assign the absolute molecular orientation with respect to the polar axis, and so at which ends are the COO^- and the NH_3^+ groups exposed.

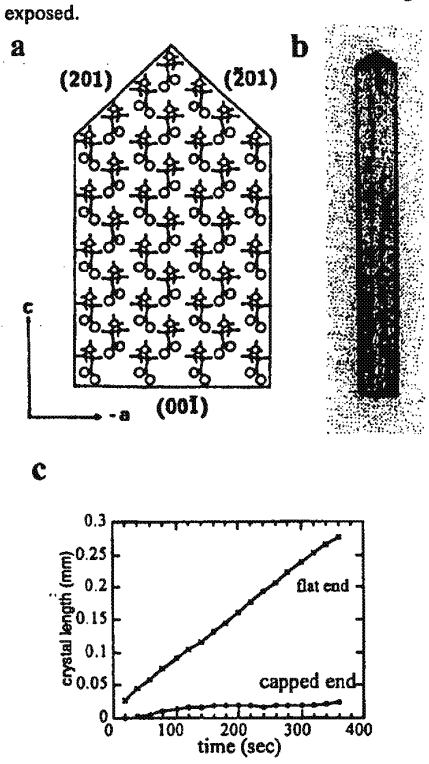


Fig. 12. (a) Packing arrangement of (R,S)-alanine delineated by crystal faces as viewed along the b axis; (b) Photograph of the pure crystal; (c) Graph of the relative growth at the opposite ends of the polar axis.

Monitoring crystal growth of (R,S)-alanine from aqueous solutions led to the conclusion that the needle-like crystals display a fast-growing flat end and a slow-growing capped end (Fig. 12c). Growth experiments in the presence of methyl-alaninate additive yielded needles much shorter than the pure crystals fixing the absolute orientation of the molecules with the COO^- groups exposed at the fast-growing flat end of the crystal. N-methyl-alanine additive, which is expected to affect the slow-growing capped end of the crystal, yielded needles as long as from the pure solution, fixing the orientation of the NH_3^+ in the crystal.

UM00011629
NOVARTIS EXHIBIT 1517
Novartis v. Regents, IPR2023-01347
Page 375 of 4460

groups

)-alanine
ıg the *b*
Graph of
he polar

-alanine
ı that the
flat end
Growth
alaninate
the pure
of the
the fast-
l-alanine
ıe slow-
l needles
cing the

4.3. Probing early stages of nucleation via twinning of (R,S)-alanine crystals[10]

The arrangements of the R- and S-molecules *vis-à-vis* the four symmetry-related {210} side faces of the (R,S)-alanine crystals are shown in Fig. 13 in the two possible orientations of the crystal structure with respect to the polar axis. Naturally, all four symmetry-related molecules are exposed at each of the four symmetry-related {210} faces, but only one of the four molecules is oriented such that its C*-CH_3 group emerges from a particular {210} crystal face. Once these orientations in a specimen crystal are determined, the absolute molecular arrangement *vis-a-vis* the polar axis is assigned.

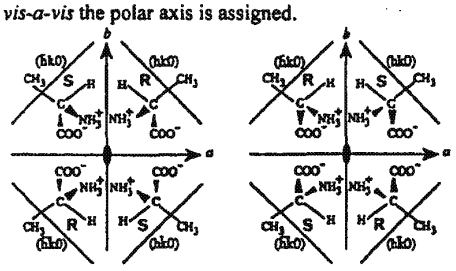


Fig. 13. Schematic (*mm*2 point group) representation of the orientation of the four molecules of (R,S)-alanine vis-à-vis the symmetry related {210} faces, when viewed along the polar *c* axis.

Crystallization in the presence of enantiomerically pure α-aminoacid additives, such as R-threonine, induced a dramatic change in the morphology of the (R,S)-alanine crystals, yielding propeller-shape crystals (Fig. 14) with $\{\bar{2}1\text{-}\Delta l\}$ (Δl = 0.05 to 0.1) affected side faces. Growth in the presence of the opposite enantiomeric S-threonine additive yielded propellers of the mirror image with $\{21\text{-}\Delta l\}$ affected side faces. The chiral nature of the propeller arises macroscopically from the fact that the affected pair of side faces, say $(21\text{-}\Delta l)$ and $(\bar{2}1\text{-}\Delta l)$, and the unaffected pair, $(2\bar{1}0)$ and $(\bar{2}10)$, have different areas and slopes. The assignment of the affected faces was explained in terms of a twinning model where each end of the crystal grows along the $-c$ end (i.e. where COO^- groups are exposed) and so the propeller is twinned about the central *ab* plane. This model is in keeping with the observation that the two crystal halves appear to be stitched across this central *ab* plane.

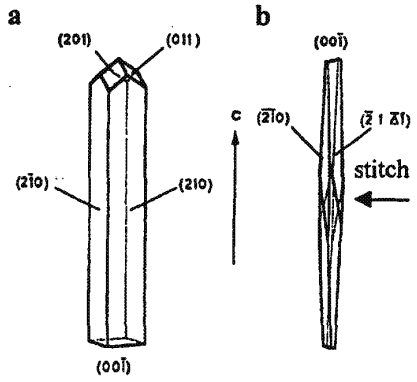


Fig. 14. Computer-drawn morphology of measured crystals of (R,S)-alanine: (a) pure; (b) twin crystal when grown in the presence of 1% R-threonine or R-phenylalanine additive.

However, the two surfaces across such a twinning plane would each expose NH_3^+ groups, which must be energetically unfavorable. One explanation of the observed effects is the inhibition of crystal nucleation of both racemic (R,S)- and chiral, say (R)-, forms of alanine with the same handedness as the additive (R') present in solution, leading to nucleation of the opposite (S)-enantiomorph through absence of steric interaction with the additive. Once formed, the chiral (S)-"nuclei" serve as templates for the epitaxial nucleation and growth of (R,S)-alanine at their two opposite {001} faces yielding the twinned crystals by virtue of the particular similarity between the racemic and chiral crystal forms.

The proposed arrangement at the epitaxial interface is shown in Fig. 15. Following this mechanism, twinning should be avoided when (R,S)-alanine is grown in the presence of racemic additives and chiral seeds should act as templates for the epitaxial growth of (R,S)-alanine, as was indeed experimentally observed. X-ray diffraction measurements of a twinned crystal revealed a misalignment between the two halves and only from the crystal center the presence of reflections that are symmetry forbidden for the space group $Pna2_1$ and so could arise from an enantiomeric alanine "nucleus" of $P2_12_12_1$ symmetry.

UM00011630
NOVARTIS EXHIBIT 1517
Novartis v. Regents, IPR2023-01347
Page 376 of 4460

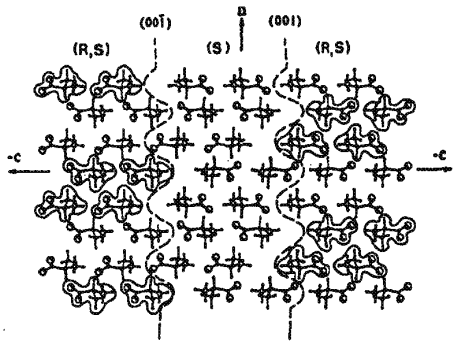
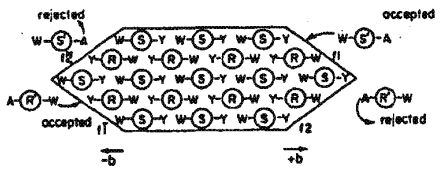


Fig. 15. Proposed molecular arrangement of the "nucleus" composed of a central (S)-"nucleus" onto whose (001) and (00$\bar{1}$) "faces" (R,S)-alanine have been epitaxially grown.

5. EFFECT OF TAILOR-MADE ADDITIVES ON GROWTH OF CENTROSYMMETRIC CRYSTALS

There is a basic difference between the effect of enantiomeric tailor-made additives on polar and centrosymmetric crystals. The morphological changes induced by enantiomeric tailor-made additives on one set of enantiotopic faces of centrosymmetric crystals with appropriate packing features can also be used for the direct assignment of the absolute configuration of the additives. A prerequisite for application of this method is that within the centrosymmetric racemic crystal a specific functional group attached to an R-molecule points toward the face f1 but not toward the opposite face f$\bar{1}$ (Scheme 5).



Scheme 5

By symmetry, the same functional group attached to an S molecule emerges at the enantiotopic face f$\bar{1}$, but not f1.

Crystallization of a centrosymmetric crystal in the presence of a R'-additive, designed so that it will fit in the site of a R-molecule on the growing crystal faces f$\bar{1}$ or f$\bar{2}$ but not on the enantiotopic faces f1 or f2, will hinder growth only in the $-b$ direction (Scheme 5). By virtue of symmetry, the enantiomeric S'-additive will inhibit growth perpendicular to faces f1 and f2 only in the $+b$ direction, while racemic R',S'-additives will inhibit growth in both directions, $+b$ and $-b$. This approach is not limited to racemic crystals, but the constituent molecules should at least be prochiral for ease of interpretation.

The interaction of tailor-made additives with the different crystal faces has also bearing on the general question regarding the distribution and arrangement of such molecules within the affected crystals and on the symmetry and structure of the formed crystalline solid solutions. We illustrate these aspects by examining the effect of a tailor-made additive on various centrosymmetric crystals.

5.1. Assignment of the tailor-made additive molecular chirality[10]

Threonine / (R,S)-serine[7,10]

Racemic (R,S)-serine, HO-CH_2-C*H(NH_3^+)COO^-, crystallizes in space group $P2_1/a$. From the packing arrangement (Fig. 16) one can see that the Cβ-H_{Si} bond vector of the rigid methylene group of R-serine molecule has a major component along $+b$ and, by symmetry, the Cβ-H_{Re} bond vector of the S-serine has a major component along $-b$. Thus, H_{Re} and H_{Si} replacement by a methyl group, as in threonine molecule, will inhibit growth in the b direction. That is, an R-threonine HO-C*H(CH_3)-C*H(NH_3^+)COO^-, molecule, with a side-chain β-carbon of chirality S, will inhibit growth along $+b$ and S-threonine will inhibit growth along $-b$.

As expected, whereas (R,S)-serine forms tabular crystals with point symmetry $2/m$ (Fig. 17a), the crystals affected by either R- or S-threonine exhibit reduced morphological point symmetry 2 (the mirror plane is lost) and are enantiomorphous (Fig. 17b,c).

When R,S-threonine is used as additive, the morphological point symmetry $2/m$ is left unchanged because the effects induced by each additive separately combine.

UM00011631
NOVARTIS EXHIBIT 1517
Novartis v. Regents, IPR2023-01347
Page 377 of 4460

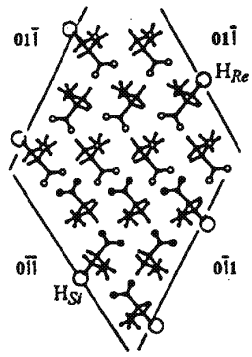


Fig. 16. Packing arrangement of (R,S)-serine viewed along the *a* axis.

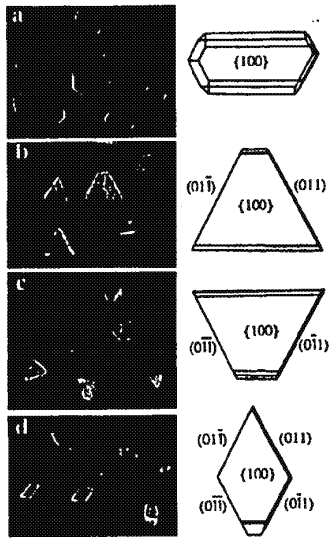


Fig. 17. Photographs and computer-drawn morphology of (R,S)-serine crystals: (a) pure. (b-d) grown in the presence of R-, S- and R,S-threonine.

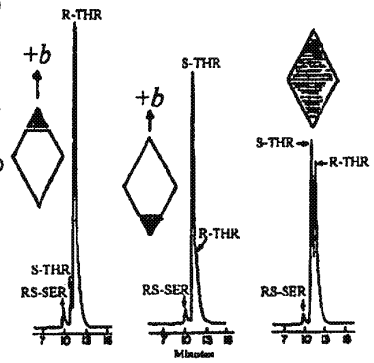


Fig. 18. Enantiomeric analysis of threonine occluded in the (R,S)-serine crystals. Material taken from: tips of the crystal at $+b$ and $-b$ end and the whole crystal, respectively.

Such crystals appear as rhombs (Fig. 17d) with a clear increase in the area of the {011} side faces relative to those of the pure form. The observed changes in crystal morphology, complemented by surface binding energy computations[11], can be interpreted only in terms of enantioselective adsorption of the R-enantiomer at faces (011) and (01$\bar{1}$), and of S-enantiomer at (0$\bar{1}$1) and (0$\bar{1}\bar{1}$). These results fix the absolute chirality of the chiral resolved threonine additive molecules.

The observed changes in crystal morphology and their interpretation in terms of an adsorption-inhibition-occlusion mechanism, imply that during crystal growth of (R,S)-serine in the presence of R,S-threonine, the occluded additive must be distributed anisotropically along the *b* axis. R-threonine, being occluded through the (011) and (01$\bar{1}$) faces, will predominate at the $+b$ half of the crystal, whereas S-threonine will predominate at the $-b$ half, being occluded through the (0$\bar{1}$1) and (0$\bar{1}\bar{1}$) faces. Thus the threonine molecules, racemic in solution, must, on occlusion into (R,S)-serine crystal, be enantiomerically segregated into domains of opposite chirality along the *b* axis, as was indeed experimentally shown by HPLC enantiomeric analysis (Fig. 18).

5.2. Enantiomeric distribution of selectively occluded tailor-made additives[10]

The interaction of tailor-made additives with the different crystal faces has bearing on the general question regarding the distribution and arrangement of such molecules within the affected crystals and on the symmetry and structure of the formed crystalline solid solutions. We illustrate this aspect by examining the effect of a tailor-made additive on a schematic arrangement, of space symmetry $P2_1/c$, delineated by four symmetry-related, diagonal faces, labeled {011}, similar to (R,S)-serine (Fig. 19a). One can easily see that an additive molecule, bearing an appropriately modified moiety, can be recognized and substitute a substrate molecule at any diagonal face, say (011), but only at one of the four different surface sites where the modified group

UM00011632
NOVARTIS EXHIBIT 1517
Novartis v. Regents, IPR2023-01347
Page 378 of 4460

does not disturb the regular pattern of interactions at the crystal surface.

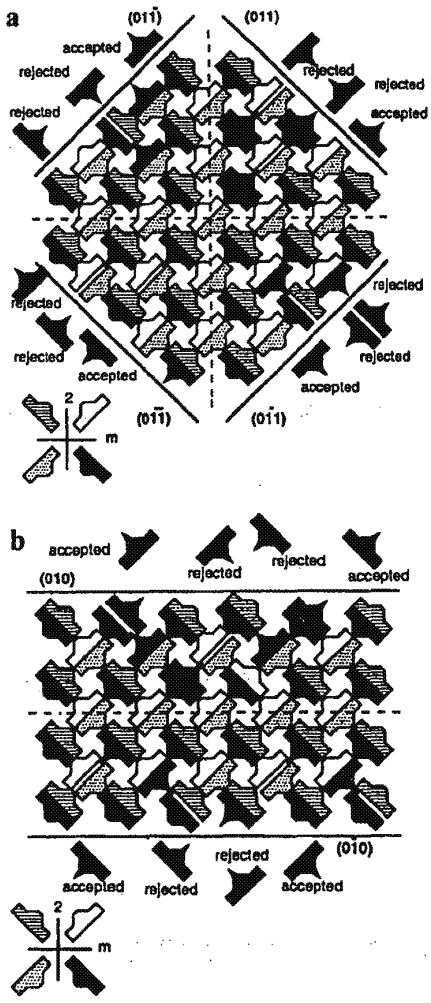


Fig. 19. Schematic representations of adsorption and occlusion of tailor-made additive molecules (in black) through: (a) the slanted {011} faces and (b) the top and bottom {010} faces in a centrosymmetric crystal of space group $P2_1/c$, containing four symmetry-related molecules (point symmetry $2/m$).

Occlusion of such a molecule through the (011) face will lead to a crystal sector in which the occluded molecules therein are related by translation symmetry only. Occlusion of additive through all four diagonal faces {011} (Fig. 19a) will lead to a crystal composed of four sectors. Consequently, in general, an additive molecule will be anisotropically distributed within the grown crystal, preferentially occluded through different surface sites on the various faces, leading to a mixed crystal composed of sectors coherently intertwined, although the occluded additive may occupy only a small fraction of the bulk sites. The reduced symmetry of each sector was predicted in several host-additive systems and experimentally demonstrated directly, by X-ray and neutron diffraction, and by a variety of methods including changes in crystal morphology, HPLC, nonlinear optical properties and solid state asymmetric photodimerization.

Symmetry lowering of somewhat similar nature has been observed in a centrosymmetric crystal when the additive molecules are occluded through the {010} crystal faces leading to a reduction in symmetry from $P2_1/c$ to $P2_1$ (Fig. 19b).

Some examples are given to illustrate these arguments and principles.

α-Aminoacids / α-form of glycine[7,10]

Glycine, $^+H_3NCH_2COO^-$, is a prochiral molecule containing two enantiotopic hydrogen atoms at the central carbon atom; namely, replacing one of these hydrogens by a different group yields a chiral molecule. Glycine crystals display polymorphism. The α-form of glycine, that appears when grown from aqueous solutions, has space group $P2_1/n$ and contains four symmetry related molecules, labeled *1*, *2*, *3*, and *4* in Fig. 20. Molecules *1* and *2*, related by twofold screw symmetry, have their C-H_{re} bonds pointing in the $+b$ direction and emerging from the (010) face. By symmetry, molecules *3* and *4*, related to *1* and *2* by a center of inversion, have their C-H_{si} bonds pointing toward $-b$ and emerging from the (0$\bar{1}$0) face.

Only the R-α-aminoacid additives can substitute a glycine molecule at the *1* and *2* sites, and then only on face (010), while only S-α-aminoacids can be adsorbed at sites *3* and *4* on face (0$\bar{1}$0). This constraint arises from the steric requirement that the additive molecule be recognized on the {010} surfaces as a "host" molecule so that the

UM00011633
NOVARTIS EXHIBIT 1517
Novartis v. Regents, IPR2023-01347
Page 379 of 4460

α–aminoacid side chain can replace the H atom of glycine only at the C-H bond emerging from the crystal surface. Otherwise, repulsion would occur between the additive and the surrounding molecules on the crystal surface.

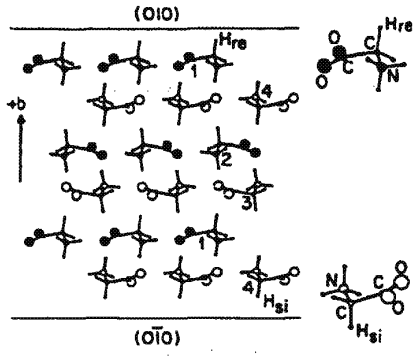


Fig. 20. Packing arrangement of the α–form of glycine viewed along the *a* axis.

α-Glycine crystallizes from water as bipyramids (Fig. 21a). Crystallization experiments in the presence of R-α-aminoacid additives leads to the formation of pyramids with a (010) basal plane, because growth in the $+b$ direction is inhibited (Fig. 21b). S-α-aminoacid additives induce the enantiomorphous morphology (Fig. 21c). Racemic α-aminoacid additives cause the formation of {010} plates (Fig. 21d) because growth at both the $+b$ and $-b$ sides of the crystal is inhibited. As expected, the *R*-enantiomers populate exclusively the $+b$, and the *S*-enantiomers the $-b$ half of the crystal, according to HPLC enantiomeric analysis (Fig. 21).

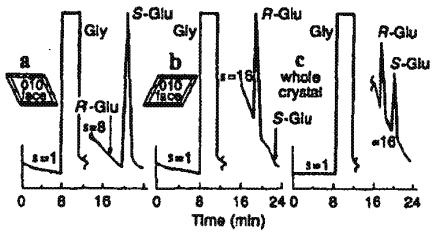


Fig. 22. HPLC enantiomeric distribution of R,S-glutamic acid occluded in {010} platelike crystals of α-glycine: (a, b) material shaved from the (0$\bar{1}$0) and (010) faces; (c) whole crystal.

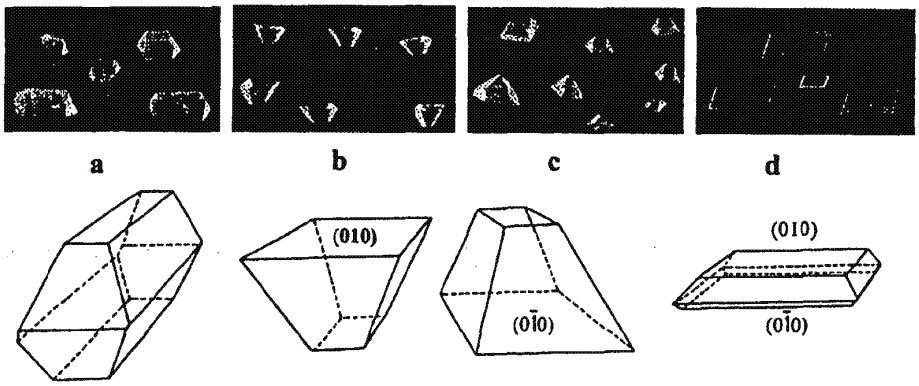


Fig. 21. Photographs and computer-drawn morphology of the α-glycine crystals: (a) pure, (b-d) grown in the presence of R-, S-, R,S-additives.

UM00011634
NOVARTIS EXHIBIT 1517
Novartis v. Regents, IPR2023-01347
Page 380 of 4460

Glycyl-leucine / glycyl-glycine[7]

The centrosymmetric single crystal of glycyl-glycine $+H_3NCH_2$-CONH-CH_2COO^- (gly-gly) was found suitable for probing the conformation and mode of occlusion of several chiral dipeptides by changes in crystal morphology, distribution of occluded additive and conformational analysis. Crystals of pure gly-gly, of space group $P2_1/c$, (Fig. 23) are diamond-shaped {100} plates (Fig. 24a). The enantioselective changes in the morphology of the gly-gly crystals grown in the presence of tailor-made additives proved that gly-R-leu induces the development of the $(12\bar{1})$ and $(\bar{1}21)$ faces whereas the gly-S-leu enantiomer adsorbs and consequently occluds through the enantiotopic $(1\bar{2}\bar{1})$ and $(\bar{1}\bar{2}1)$ faces (Fig. 24b, c).

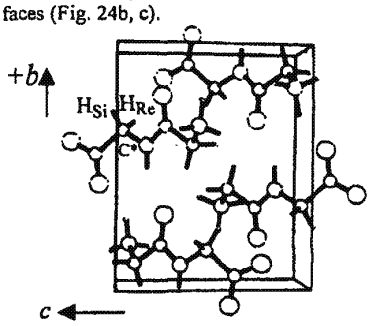


Fig. 23. Packing arrangement of the gly-gly centrosymmetric crystal viewed along the *a* axis.

When the racemic additive was used, all four faces were expressed (Fig. 24d). As expected, the occluded additive is segregated into enantiomers along the *b* axis of the host crystal, as determined by the HPLC enantiomeric analysis (Fig. 25).

Different morphologies were obtained when gly-gly crystals were grown in the presence of gly-R,S-ala and ala-R,S-gly additives, (Fig. 26), proving the effect of preferred conformation of the additive molecule during crystal growth. Atom-atom potential energy calculations[11] involving the preferred conformations of the guest molecules and their enantiospecific binding at the affected crystalline faces were in agreement with the experiments.

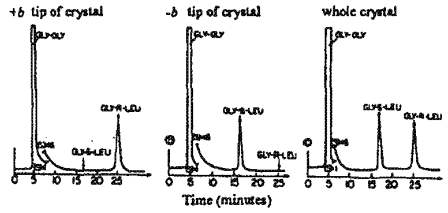


Fig. 25. HPLC enantiomeric distribution of R,S-gly-leu inside the crystals of gly-gly.

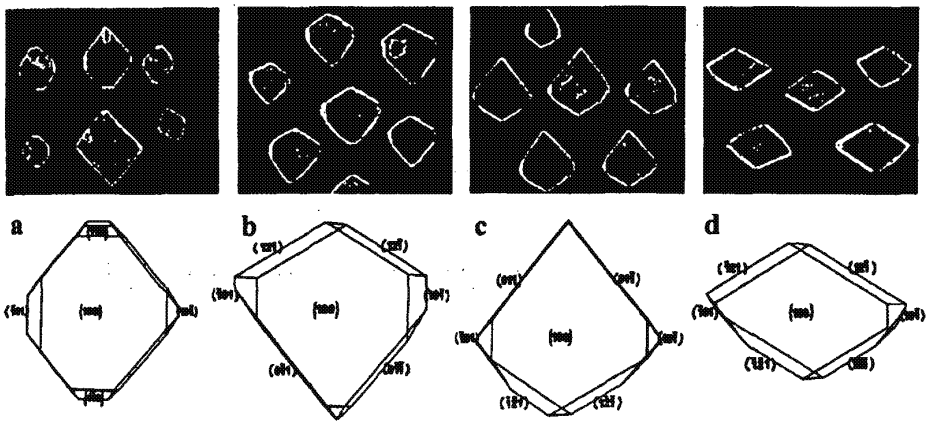


Fig. 24. Photographs and computer-drawn morphologies of the gly-gly crystals: (a) pure (b-d) grown in the presence of R-, S- and R,S- glycyl-leucine, $^+H_3NCH_2$-CONH-C*H(C_4H_9)COO^-, tailor-made additive.

UM00011635
NOVARTIS EXHIBIT 1517
Novartis v. Regents, IPR2023-01347
Page 381 of 4460

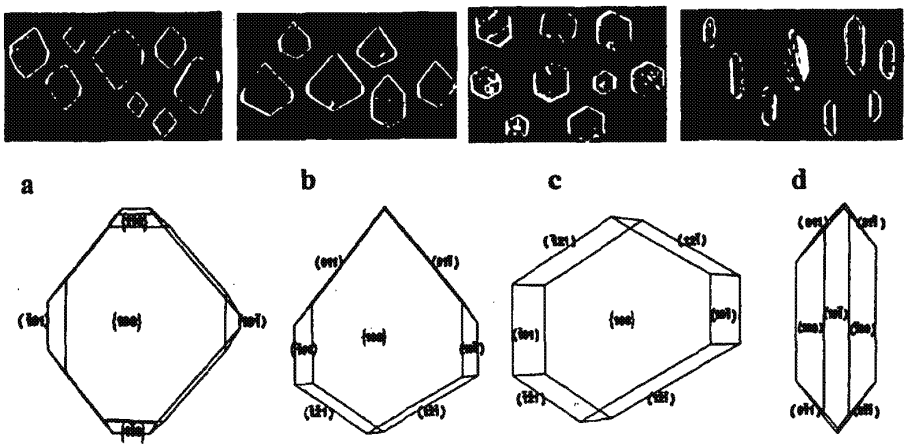


Fig. 26. Photographs and computer-drawn morphologies of the gly-gly crystals: (a) pure (b-d) grown in the presence of S-, R,S-glycyl-alanine, $^{+}H_3NCH_2$-CONH-C*H(CH_3)COO^-, and R,S-alanyl-glycine, $^{+}H_3NC$*H(CH_3)-CONH-CH_2COO^-, tailor made additives.

5.3. Probing intermolecular forces through reduced crystal symmetry[10]

We focus now on the minimal modification of a tailor-made additive with respect to the host molecule that would still be recognized and discriminated by the growing crystal surface and lead to reduction in symmetry. Indeed, solid solutions composed of host and additive molecules of similar structure and shape have been generally believed to exhibit the same symmetries as those of the host crystals. We consider solid solutions of carboxylic acids (X-COOH) in primary amides (X-$CONH_2$), where a NH_2 group of the host is substituted by an OH moiety of the guest (Fig. 1a). A strong inhibition of growth develops along the direction of the O=C-N-H···O=C hydrogen bond. Inhibition arises when an adsorbed carboxylic acid additive molecule causes repulsion between its oxygen lone-pair electrons and those of the oncoming host-amide molecule. The carboxylic acid additive molecule will thus avoid surface sites that require its OH groups to be oriented toward the surface and be preferentially adsorbed at sites where the OH group emerges from the surface. This principle is illustrated here with several examples.

Aspartic acid / (S)-Asparagine

Asparagine H_2NOCCH_2C*H(NH_3^+)COO^- crystallizes from water as a monohydrate with a tight three-dimensional net of hydrogen bonds in the $P2_12_12_1$ space group (Fig. 27a). The morphology is prismatic, with 18 developed faces (Fig. 27b). Crystallization of (S)-asparagine.H_2O in the presence of S-aspartic acid $HOOCCH_2$-$CH(NH_3^+)COO^-$ yields {010} plates (Fig. 27c). In terms of the arguments already given for amide-acid systems, the additive aspartic acid molecule should be more easily adsorbed at sites 1 and 3, on the growing (010) surface, than at sites 2 and 4 (Fig. 27d); the reverse situation holds for the opposite $(0\bar{1}0)$ face. If, on growth of the mixed crystal, the $(0\bar{1}0)$ face is blocked so that the amide and acid molecules would be occluded only through the (010) face, the symmetry of the mixed crystal should be reduced to $P12_11$. This effect was demonstrated by a low temperature (18 K) neutron diffraction study of a protonated asparagine crystal grown with deuterated S-aspartic acid additive.

UM00011636
NOVARTIS EXHIBIT 1517
Novartis v. Regents, IPR2023-01347
Page 382 of 4460

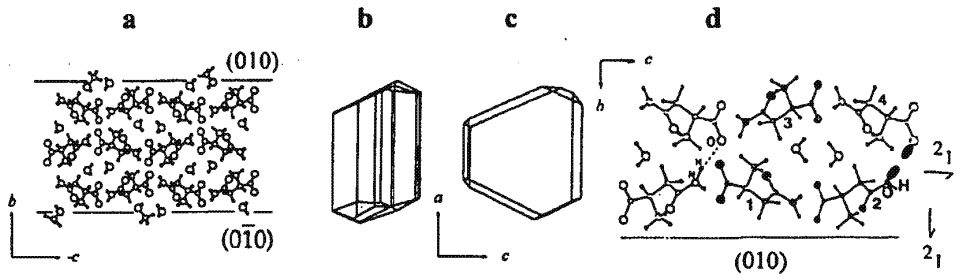


Fig. 27. (a) Packing arrangement of (S)-asparagine.H_2O viewed along the *a* axis. (b, c) Computer-drawn morphology of measured crystals: (b) pure (c) grown in the presence of S-aspartic acid. (d) Preferential adsorption of aspartic acid on the (010) surface of the crystal.

E-cinnamic acid / E-cinnamamide; asymmetric synthesis in centrosymmetric host crystals[10,12]

The site selective adsorption and occlusion of *E*-cinnamic acid, C_6H_5-CH=CH-COOH, additive into the crystal of *E*-cinnamamide C_6H_5-CH=CH-$CONH_2$ is based on the same principle of repulsion between the lone-pair electrons as discussed above. The pure crystal (Fig. 28b) of *E*-cinnamamide appears in a centrosymmetric monoclinic arrangement, space group $P2_1/c$. The crystal structure (Fig. 28a) is composed of hydrogen-bonded dimers interlinked by N-H···O bonds to form a ribbon-like motif that runs parallel to the *b* axis. During crystallization in the presence of *E*-cinnamic acid, the additive is preferentially occluded through half of the {011} surface sites of the crystal at the opposite ends of the ribbons (Fig. 28a). This effect leads to a modified mixed crystal (Fig. 28c) with two enantiomorphous halves of at most $P2_1$ symmetry. This reduced symmetry was proven photochemically. Ultraviolet irradiation of *E*-cinnamamide yields centrosymmetric photodimers, by virtue of a cyclobutane ring formation involving pairs of close packed >C=C< bonds across centers of inversion (Fig. 29). Replacement of one of such a pair by *E*-cinnamic acid results in the formation of asymmetric cinnamamide-cinnamic acid photodimers of opposite chirality at the two enantiomorphous halves of the mixed crystal, with an enantiomeric ratio of 60:40 at each opposite half (Fig. 30).

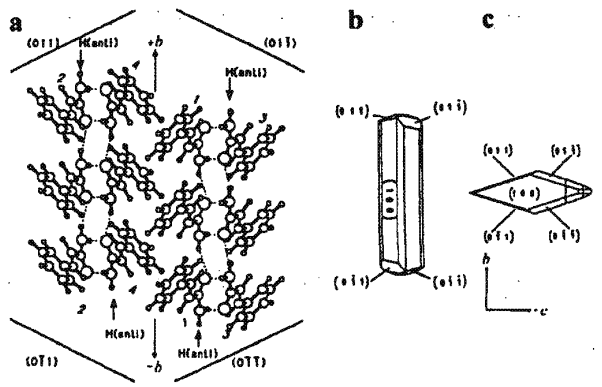


Fig. 28. (a) Packing arrangement of *E*-cinnamamide viewed along the *a* axis. (b, c) Crystal morphology: (b) pure; (c) grown in the presence of *E*-cinnamic acid.

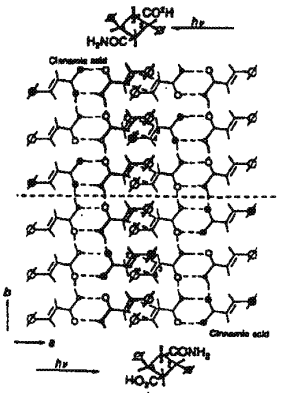


Fig. 29. Packing arrangement of *E*-cinnamamide viewed along the *c* axis showing the photodimerization reaction.

UM00011637
NOVARTIS EXHIBIT 1517
Novartis v. Regents, IPR2023-01347
Page 383 of 4460

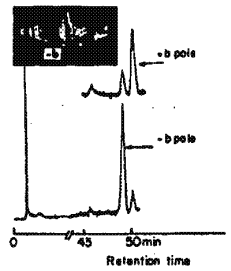


Fig. 30. GC enantiomeric analysis of photodimers isolated from the $+b$ and $-b$ poles of a crystal of *E*-cinnamamide:*E*-cinnamic acid.

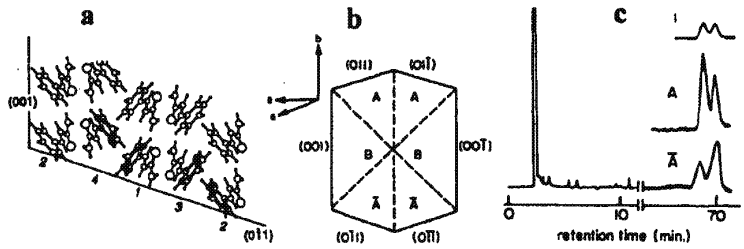


Fig. 31. (a) Packing arrangement of *E*-cinnamamide showing the β-thienyl rings of the additive that replace the phenyl rings of the host molecules. (b) morphology of the mixed crystal. (c) GC enantiomeric analysis of the photodimers generated in the A, $\bar{A}$ and B sectors of an *E*-cinnamamide: *E*-2-(β-thienyl)acrylamide mixed crystal.

2-E-thienylacrylamide / E-cinnamamide[12,13]

When crystals of *E*-cinnamamide were grown in the presence of *E*-2-(β-thienyl)acrylamide additive, the four {011} faces were more developed implying that the thienyl moieties were occluded primarily through these faces at which the host molecules display herring-bone contacts between aromatic C-H groups and π electron clouds of neighboring phenyl rings related by two-fold screw symmetry. These contacts were replaced in the host-additive mixed crystal by unfavorable contacts between sulfur lone-pair electrons and the π electron system. The additive can easily be adsorbed through each of the four {011} faces at only one of the four sites (Fig. 31a) at which the sulfur emerges from the face, e.g. at site **1** on the $(0\bar{1}1)$ face, reducing crystal symmetry to *P*1. In addition, *E*-2-(β-thienyl)acrylamide is occluded also through the {001} faces which exhibit *pm* plane symmetry and such occlusion should reduce the crystal symmetry to *Pc*. This mixed crystal should be thus divided into six sectors of reduced symmetry (Fig. 31b). The sectors A and $\bar{A}$ are related to one another by the 2/*m* point symmetry of the host crystal. Low temperature X-ray and neutron diffraction studies on A, $\bar{A}$ and B type sectors, cut from a crystal specimen proved the reduction in crystal symmetry. The chiral photodimers generated from sectors A and $\bar{A}$ are of opposite handedness, as determined by gas chromatography enantiomeric analysis (Fig. 31c), circular dichroism and NMR measurements.

6. TAILOR MADE ADDITIVES AS ENANTIOSELECTIVE NUCLEATION PROMOTERS[13]

Tailor-made additives may act as inhibitors of crystal nucleration and growth as well as promoters of crystal nucleation. The latter effect is illustrated here for the system of α-glycine / α-aminoacid additives. As described above, α–glycine pure bipyramids become pyramids with either a (010) or $(0\bar{1}0)$ basal plane when grown in the presence of R- or S-α-aminoacid additives, respectively (Fig. 21). Racemic additives cause the formation of {010} plates that contain 0.02-0.2% racemic additive molecules occluded into the crystal bulk, with the two enantiomers segregated in the two sectors at the $+b$ and $-b$ crystal halves (Fig. 22).

Systematic studies demonstrated that the presence of the hydrophobic α-aminoacids, such as valine, leucine, norleucine, phenylalanine, as co-solutes to aqueous solutions of glycine, induce crystallization of the glycine crystals floating at the air-solution interface and oriented with one of the {010} faces exposed towards the air. In the presence of hydrophobic R- or S-additives (1%wt/wt of

UM00011638
NOVARTIS EXHIBIT 1517
Novartis v. Regents, IPR2023-01347
Page 384 of 4460

glycine) all the pyramidal crystals float with their either (010) or ($0\bar{1}0$) basal plane oriented towards the air, respectively. Crystallization in the presence of hydrophobic R,S-additives induces the formation of an equal number of plate-like crystals oriented with either (010) or ($0\bar{1}0$) exposed to air (Fig. 32a). HPLC analysis of the additives occluded into such floating single crystals demonstrated that the (010)-oriented plates contain only S-additives whereas the ($0\bar{1}0$)-oriented plates contain only the R-additives (Fig. 32b), in agreement with the occlusion mechanism through the enantiotopic face exposed to the solution. These results were explained in terms of the formation, at the air-solution interface, of ordered two-dimensional clusters of the hydrophobic, say, R-α-aminoacid additive molecules oriented with their side chains exposed to air and their α-aminoacid moiety exposed to solution. Glycine solute molecules can form hydrogen-bonded centrosymmetric dimers with such exposed moieties and mimic the 010 layer of the glycine crystal that thus can serve as a template for the nucleation of (010)-oriented glycine crystals. By symmetry, hydrophobic S-additives should mimic the $0\bar{1}0$ layer of glycine crystals and induce nucleation of floating ($0\bar{1}0$)-oriented glycine crystals, in keeping with the experimental results.

Based on the above mechanism, the induced resolution of α–aminoacids via occlusion inside glycine crystals was performed by oriented crystallization of glycine in the presence of, say, S-leucine and mixtures of hydrophilic R,S-α-aminoacids such as *p*-hydroxy-phenylglycine, glutamic acid and methionine. All the floating glycine plates were formed with their ($0\bar{1}0$) faces oriented towards the air (Fig. 32c) and occluded exclusively the R-additives through the (010) face exposed towards solution, according to HPLC enantiomeric analysis (Fig. 32d). When polycrystalline crusts of glycine were formed, the enantiomeric excess of the occluded additives was higher than 70%.

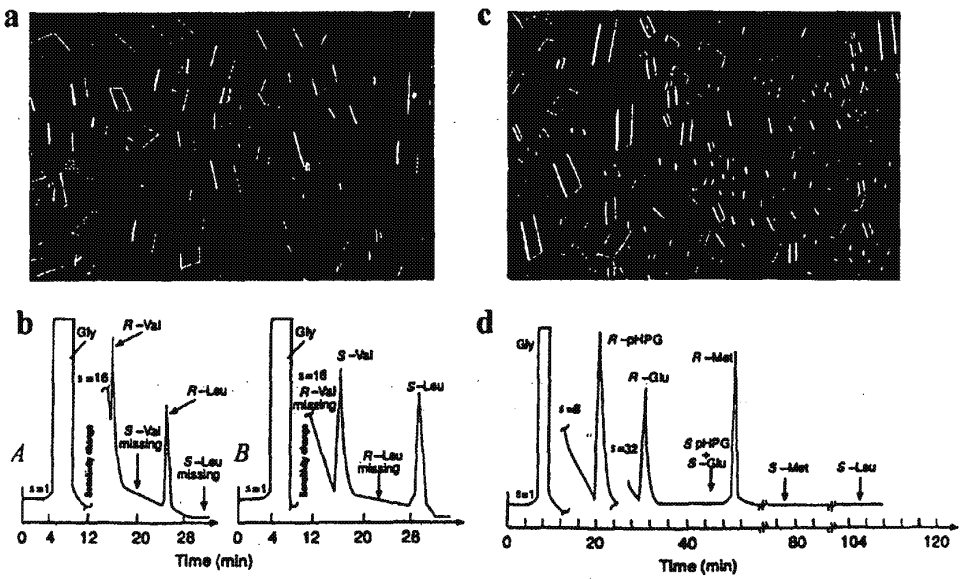
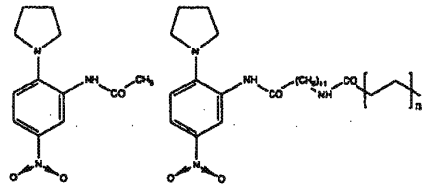


Fig. 32. (a, b) Plate-like crystals of α-glycine floating at the solution surface as grown in the presence of R,S-leucine and R,S-valine and the corresponding HPLC enantiomeric analysis of occluded additives in single crystals of type *A* and *B*; (c, d) Plate-like crystals of α-glycine floating at the solution surface as grown in the presence of S-leucine and racemic *p*-hydroxyphenylglycine, glutamic acid and methionine and the corresponding HPLC enantiomeric analysis of occluded additives inside the crystals.

UM00011639
NOVARTIS EXHIBIT 1517
Novartis v. Regents, IPR2023-01347
Page 385 of 4460

1. CONTROL OF CRYSTALLINE PHASE FORMATION[14]

We now consider preferred precipitation of a crystal containing a polar axis at the expense of the dimorph which is centrosymmetric and so nonpolar. As described above, in crystals with a polar axis, all molecules are parallel vis-a-vis the polar axis (Scheme 4) whereas in centrosymmetric crystals neighboring molecules are arranged in antiparallel manner (Scheme 5). An appropriate tailor-made additive will inhibit growth of the centrosymmetric form at the opposite ends of the crystal and so prevent its appearance, but will inhibit growth of the polar form only at one end of the crystal. This concept has been demonstrated for the system of N-(2-acetamido-4-nitrophenyl)-pyrrolidine (PAN) **6a**, whose metastable polar form is important for its nonlinear optical properties. As little as 0.03% of the polymer **6b** inhibited precipitation of the pseudo-centrosymmetric stable form of PAN allowing crystallization of the metastable form only.



6a **6b**

γ-glycine polymorph

As already mentioned, glycine usually crystallizes from aqueous solutions in the centrosymmetric α-form (Fig. 33a) but, when grown from acetic acid or ammonia solutions, glycine can precipitate as a mixture with the polar γ-form (Fig. 33d). Preferential crystallization from aqueous solution of the γ–form of glycine was achieved in the presence of racemic hexafluorovaline $(CF_3)_2CHC^*H(NH_3^+)COO^-$ and chloranil as tailor-made additive (Fig. 33e, f).

The crystal of γ-glycine appears in space group $P3_1$ (or $P3_2$), arranged in a way similar to (R,S)-alanine crystal, so that the molecules expose COO^- groups at one end of the polar trigonal axis and NH_3^+ groups at the opposite end (Fig. 34a).

As previously described, common α-aminoacid additives bind only at the {010} faces of α-glycine crystal and so inhibit its growth only along b, inducing formation of the {010} plates (Fig. 33b). In contrast, racemic hexafluorovaline is a more effective inhibitor of growth of α-glycine since it binds at the four {011} faces (Fig. 34b) and so blocks growth along both b and the fast-growing c directions (Fig. 33c). The abnormal behaviour of hexaflurovaline can be understood in terms of its molecular structure and conformation, as found in its native crystal. Steric repulsion imposed by the hexafluro-isopropyl moiety prevents adsorption onto the {010} face, but not at the {011} faces to which it is strongly bound through charge-transfer (CT) interactions. Furthermore, hexafluorovaline does not inhibit nucleation and growth of the γ-glycine form because the additive is bound thereto primarily at the NH_3+ end of its polar axis and the crystal is growing unidirectionally along its polar c axis at the COO^- end.

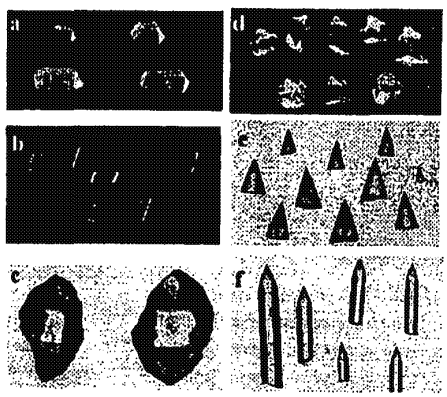


Fig. 33. (a-c) Crystals of α-glycine grown from water: (a) pure, (b) in the presence of common R,S-α-aminoacids and (c) R,S hexaflurovaline. (d) Crystals of γ-glycine grown from aqueous acetic acid solutions. (e, f) Crystals of γ-glycine grown from water in the presence of: (e) R,S-hexafluorovaline, (f) chloranil (tetrachlorobenzo-quinone).

However, the hexafluorovaline molecules can be also adsorbed on the newly developed {¡51} side faces of the trigonal pyramidal crystals (Fig. 33e). The strong inhibition of α-glycine via charge-transfer interactions was proved by using as additive

UM00011640
NOVARTIS EXHIBIT 1517
Novartis v. Regents, IPR2023-01347
Page 386 of 4460

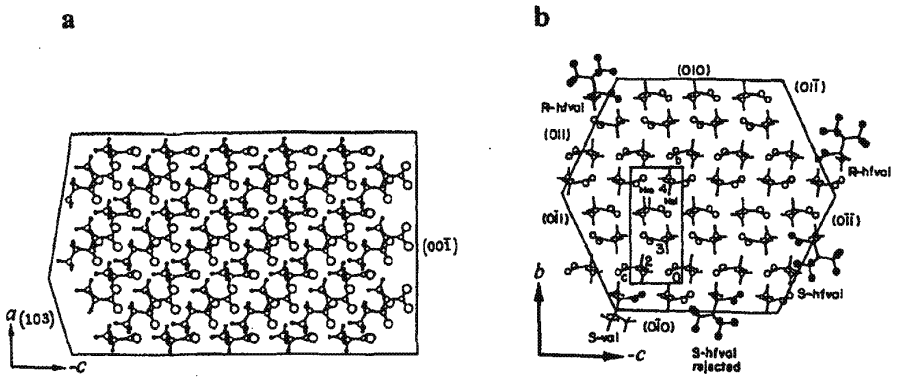


Fig. 34. (a) Packing arrangement of the γ-form of glycine viewed along the *b* axis; (b) Packing arrangement of the α-form of glycine viewed along the *a* axis and showing the effect of R,S-hexafluorovaline additive.

chloranil, a molecule known to form a CT complex with glycine as an electron donor. This CT complex was anticipated to bind at the various faces of α-glycine clusters that expose NH_3^+ groups such as {011}, {110} and {010}, and so inhibit nucleation of this phase. The CT complex can also bind at the slow-growing capped end of γ-glycine but not at the fast-growing end (fig. 33f). The conclusion of these experiments is that the inhibitor, to be effective, should bind at the fast-growing directions.

8. CONCLUSIONS

A variety of crystal properties can be controlled and modified with the use of tailor-made additives, including growth and dissolution, morphology, crystal texture and polymorphism. Such studies allows one to help understand basic scientific questions such as pinpointing fine molecular interactions at interfaces and the correlation between molecular chirality and macroscopic phenomena in crystals. Kinetic resolution of racemates and the control in the very early stages of crystal formation to yield the polymorph with desired properties have large applications in the pharmaceutical industry in particular and in applied sciences in general.

REFERENCES

1. P. Hartman, W.G. Perdok, Acta Crystallogr. 8, (1955), 49; Ibid, (1955), 525.
2. P. Hartman, in: P. Hartman (ed.), Crystal Growth An Introduction, North-Holland, Amsterdam, p. 367, 1973.
3. P. Bennema, G. Gilmer, in: P. Hartman (ed.), Crystal Growth, An Introduction, North-Holland, Amsterdam, p. 272, 1973.
4. P. Hartman, P. Benema, J. Crystal Growth 49, (1980), 145.
5. P. Bennema, J. Crystal Growth 122, (1992), 110.
6. L. Addadi, Z. Berkovitch-Yellin, I. Weissbuch, M. Lahav, L. Leiserowitz, in: E.L. Eliel, S.H. Willen and N.L. Allinger (eds.), Topics in Stereochemistry; Wiley& Sons Ltd., New York, 16, 1-85, 1986.
7. L. Addadi, Z. Berkovitch-Yellin, I. Weissbuch, J. van Mil, L.J.W. Shimon, M. Lahav, L. Leiserowitz, Angew. Chem., Int. Ed. Engl., 24, (1985), 466.
8. I. Weissbuch, L. Leiserowitz, M. Lahav, in: A. Mersmann (ed.), Handbook of Crystallization, M. Decker, New York, p. 401, 199
9. D. Zbaida, M. Lahav, K. Drauz, G. Knaup, M. Kottenhahn, Tetrahedron, 56, (2000), 6645.
10. I. Weissbuch, R. Popovitz-Biro, M. Lahav, L. Leiserowitz, Acta Crystallogr. A, LEAD ARTICLE B51, (1995), 115.
11. Z. Berkovitch-Yellin, J. Am. Chem. Soc., 107, (1985), 3375.
12. M. Vaida, L.J.W Shimon, Y. Weisinger-Lewin, F. Frolow, M. Lahav, L. Leiserowitz, R.K. McMullan, Science, 241, (1988), 1475.
13. I. Weissbuch, R. Popovitz-Biro, L. Leiserowitz, M. Lahav, in: J.P.Behr (ed.), 100 Years of the The-Lock-and-Key Priciple, Wiley&Sons Ltd., New York, Ch. 6, p. 173, 1994.
14. I. Weissbuch, L. Leiserowitz, M. Lahav, Advanced Materials, 6, (1994), 952.

UM00011641
NOVARTIS EXHIBIT 1517
Novartis v. Regents, IPR2023-01347
Page 387 of 4460

This Page is Inserted by IFW Indexing and Scanning Operations and is not part of the Official Record

BEST AVAILABLE IMAGES

Defective images within this document are accurate representations of the original documents submitted by the applicant.

Defects in the images include but are not limited to the items checked:

- ☐ BLACK BORDERS
- ☐ IMAGE CUT OFF AT TOP, BOTTOM OR SIDES
- ☐ FADED TEXT OR DRAWING
- ☐ BLURRED OR ILLEGIBLE TEXT OR DRAWING
- ☐ SKEWED/SLANTED IMAGES
- ☐ COLOR OR BLACK AND WHITE PHOTOGRAPHS
- ☐ GRAY SCALE DOCUMENTS
- ☐ LINES OR MARKS ON ORIGINAL DOCUMENT
- ☐ REFERENCE(S) OR EXHIBIT(S) SUBMITTED ARE POOR QUALITY
- ☐ OTHER: _____

IMAGES ARE BEST AVAILABLE COPY.
As rescanning these documents will not correct the image problems checked, please do not report these problems to the IFW Image Problem Mailbox.

Z. Kristallogr. 220 (2005) 340–350

© by Oldenbourg Wissenschaftsverlag, München

Crystal engineering of the composition of pharmaceutical phases. 3[1]. Primary amide supramolecular heterosynthons and their role in the design of pharmaceutical co-crystals

Jennifer A. McMahon, Joanna A. Bis, Peddy Vishweshwar, Tanise R. Shattock, Olga L. McLaughlin and Michael J. Zaworotko*

Department of Chemistry, University of South Florida, SCA400, 4202 E. Fowler Avenue, Tampa, Florida, 33620, USA

Received June 14, 2004; accepted September 22, 2004

Crystal engineering / Co-crystal / Pharmaceutical co-crystal / Pharmaceutical phases / Hydrogen bond / Supramolecular synthesis

Abstract. A Cambridge Structural Database study of supramolecular synthons involving primary amides reveals that 84% form amide-amide dimers, whereas 14% form catemers in the absence of other competing hydrogen bond donors and/or acceptors. However in the presence of chemically different but complementary functional groups, *e.g.*, carboxylic acids or aromatic nitrogen moieties, primary amides tend to form supramolecular heterosynthons. Supramolecular heterosynthons represent an opportunity for design of multi-component crystals (co-crystals) in which one molecule contains a primary amide and a second molecule (the co-crystal former) contains the functional group that is complementary to the primary amide. The results of the CSD analysis facilitated the selection of components for seven new primary amide co-crystals: **A.** Isonicotinamide/2-hydroxybenzoic acid (1 : 1); **B.** Nicotinamide/3-hydroxybenzoic acid (1 : 1); **C.** Pyrazinamide/2,5-dihydroxybenzoic acid (1 : 1); **D.** Carbamazepine (CBZ)/4,4′-bipyridine (2 : 1); **E.** CBZ/4-aminobenzoic acid (2 : 1); **F.** CBZ/4-aminobenzoic acid/H_2O (2 : 1 : 1); **G.** CBZ/2,6-pyridinedicarboxylic acid (1 : 1). The molecular recognition events involving the amide moieties are discussed in the context of our experimental results and their implications for crystal engineering of pharmaceutical co-crystals.

Introduction

Supramolecular chemistry has evolved as two distinct branches: the study of supramolecules in solution with particular emphasis upon host-guest and biomimetic chemistry; the study of solid state structures with emphasis upon crystal engineering and structure property relationships [2]. However, the concepts and principles of molecular recognition and the nature of the interactions that mediate self-assembled supramolecular structures are independent of the phase and there is therefore a synergistic relationship between solid-state and solution supramolecular chemistry. In terms of the solid-state, the term crystal engineering was introduced by Pepinsky [3] in 1955 but further conceptualized and elaborated by Schmidt in the context of organic solid-state photochemical reactions of cinnamic acids and amides [4]. Crystal engineering has subsequently attracted general interest from a wide range of molecular scientists, in particular organic, inorganic and physical chemists, crystallographers and materials scientists. A major reason for this interest is the evolution of crystal engineering into a form of supramolecular synthesis, *i.e.*, crystal engineering not only addresses a fundamental understanding of crystal packing, it also offers an opportunity for the design of new solids with desired structure and properties. Furthermore, supramolecular approaches to synthesis [5] can offer considerable advantages over traditional covalent synthesis in which compounds are generated by stepwise breaking and making of covalent bonds. In particular, supramolecular synthesis facilitates self-assembly of molecules with high molecular weight and without changing the covalent structure of the molecular components. The latter is particularly relevant in the context of materials science and, as will become evident herein, pharmaceutical formulations.

The Cambridge Structural Database (CSD) [6] allows statistical analysis not only of molecular structure but also of packing motifs. Functional groups that are common or of special interest can therefore be studied in terms of how they associate with themselves or other functional groups. These sub-structural units have been variously termed as motifs, patterns, building blocks or supramolecular synthons. The term supramolecular synthon was defined by Desiraju as "*a structural units within supermolecules, which can be formed and/or assembled by known or conceivable synthetic operations involving intermolecular interactions*" [7]. More recently we have coined the terms supramolecular homosynthon and supramolecular heterosynthon in order to differentiate between supramolecular synthons that are formed from identical and different complementary functional groups, respectively [8]. We

[1] For part 2 of this series see ref. [1].

* Correspondence author (e-mail: xtal@usf.edu)

UM00011643
NOVARTIS EXHIBIT 1517
Novartis v. Regents, IPR2023-01347
Page 389 of 4460

have made this distinction because the latter are more common and they are the key to the design of multiple component crystals, co-crystals [9]. Co-crystals represent a long known but relatively unexplored class of compound that can offer considerable advantages over single component systems in that one can modify the chemical and/or physical property of a given molecule in a systematic manner by co-crystallizing a series of compounds, i.e. supramolecular synthesis represent a type of "noncovalent derivatization" [10]. Among organic crystal structures deposited in the CSD, nearly 5% are molecular co-crystals if one includes hydrates and solvates. Most of the reported co-crystals were isolated serendipitously; however, several groups have successfully exploited crystal engineering principles for design and synthesis of molecular co-crystals [11]. The potential impact of co-crystals is broad-ranging as suggested by recent studies which indicate that co-crystals can play a role in solvent-free organic synthesis (photodimerization of olefins using linear templates) [12], for design of host-guest systems [13], in modification of photographic films [14], for reformulation of active pharmaceutical ingredients (APIs) [1, 8, 15] and for generation new classes of NLO materials [16].

The process of designing and obtaining co-crystals from solution may be thought of as counterintuitive in the sense that chemists and engineers generally consider crystallization of a mixture of soluble compounds to be an efficient method of purification of only one of the components, not for obtaining co-crystals with a desired stoichiometry between components. However, the presence of two molecules with complementary functional groups can in appropriate circumstances afford hydrogen bonds that are more favorable than those between like molecules of either component. Some common complementary supramolecular heterosynthons that, based upon CSD statistics, would appear to fit this category are acid-pyridine [11, 17], acid-amide [18], phenol-pyridine [19]. Ironically, much of this statistical information comes from analysis of single component crystals in which multiple functional groups are present, thereby allowing us to determine the statistical reliability of competitive molecular recognition processes. Co-crystals can be synthesized via a variety of methods: evaporation from a solution that contains both components; sublimation; growth from the melt; grinding the two solid components together in a ballmill with or without a small amount of solvent [20]; single crystals of gases, liquids and their co-crystals can be obtained by an *in situ* crystallization technique, called oligo diffractometry [21]. Nevertheless, this does not mean that synthesis of co-crystals is routine. A detailed understanding of the supramolecular chemistry of the functional groups present in a given molecule is the first step in designing a co-crystal since it facilitates selection of appropriate co-crystal formers. In this contribution, we address these two steps in the context of preparation of co-crystals involving primary amides with particular emphasis upon how this information can be used to generate pharmaceutical co-crystals. Pharmaceutical co-crystals are a subset of multiple component crystals that also include hydrates, solvates, clathrates, inclusion compounds and salts. Pharmaceutical co-crystals are related to solvates in that two or more components in the crystal interact by hydrogen bonding or other noncovalent interactions rather than by dipole interactions. The main difference between the two types of co-crystal lies in the physical state of the parent compounds. Solvates have at least one component that is a liquid at room temperature, while pharmaceutical co-crystals contain two components that are crystalline solids at room temperature, at least one of which must be an active pharmaceutical ingredient. This distinction is important since it has a profound impact on the stability and processing of the product. Also, while solvates have become commonplace, pharmaceutical co-crystals have yet to be fully explored.

Experimental

Preparation of co-crystals

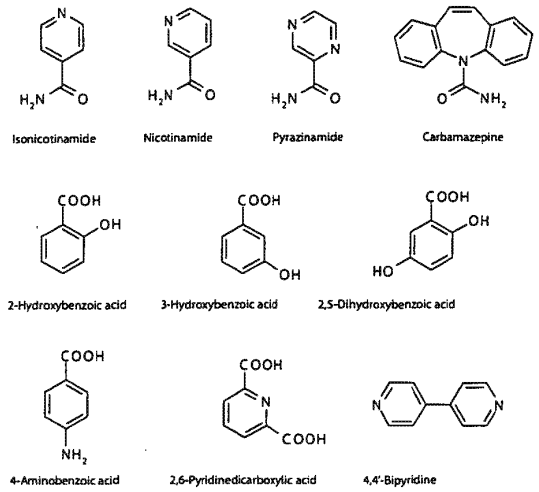
All reagents were purchased from Aldrich (Scheme 1). Co-crystals **A–G** were prepared by dissolving appropriate amounts of starting materials and slow evaporation of the solvent at room temperature. Methanol, ethanol and acetone were distilled and stored over molecular sieves prior to utilization. Acetonitrile, tetrahydrofuran and carbon disulfide were used as received. Vials containing dissolved mixtures were covered with parafilm, punctured with 2–3 holes and allowed to slowly evaporate under ambient conditions in a fume hood. Initial crystallization products were characterized by infrared spectroscopy using a Nicolet Avatar 320 FTIR instrument. Melting points for co-crystals were determined on a Mel-temp® apparatus and are presented in Table 1 along with the melting points for the parent compounds.

A. Isonicotinamide/2-hydroxybenzoic acid (1:1)
Aspirin (0.030 g, 0.166 mmol) and isonicotinamide (0.020 g, 0.166 mmol) were dissolved in 1 ml of acetone. Colorless crystals were obtained within few days and it

Table 1. Melting points of starting materials and co-crystals, **A–G**.

Co-crystals	Starting materials [°C]		Co-crystal [°C]
A. Isonicotinamide/2-hydroxybenzoic acid (1:1)	155–157	159	119–121
B. Nicotinamide/3-hydroxybenzoic acid (1:1)	130–133	203	123–125
C. Pyrazinamide/2,5-dihydroxybenzoic acid (1:1)	189–191	205	164–166
D. Carbamazepine (CBZ)/4,4′-bipyridine (2:1)	190–192	111–114	158–160
E. CBZ/4-aminobenzoic acid (2:1)	190–192	189	185–187
F. CBZ/4-aminobenzoic acid/H_2O (2:1:1)	190–192	189	143
G. CBZ/2,6-pyridinedicarboxylic acid (1:1)	190–192	248–250	214–216

UM00011644
NOVARTIS EXHIBIT 1517
Novartis v. Regents, IPR2023-01347
Page 390 of 4460



Scheme 1. Schematic diagram of molecular structures studied in this paper.

was subsequently determined that aspirin had been hydrolyzed to 2-hydroxybenzoic acid and co-crystallized with isonicotinamide in 1:1 stoichiometry.

B. Nicotinamide/3-hydroxybenzoic acid (1:1)
Colorless crystals were obtained within three days via slow evaporation of a solution containing nicotinamide (0.015 g, 0.123 mmol) and 3-hydroxybenzoic acid (0.017 g, 0.123 mmol) dissolved in 1 ml of acetonitrile.

C. Pyrazinamide/2,5-dihydroxybenzoic acid (1:1)
Colorless crystals were obtained within two days via slow evaporation of a solution containing pyrazinamide (0.020 g, 0.162 mmol) and 2,5-dihydroxybenzoic acid (0.025 g, 0.162 mmol) dissolved in 1 ml of acetonitrile.

D. Carbamazepine (CBZ)/4,4′-bipyridine (2:1)
Colorless crystals were obtained within three days via slow evaporation of a solution containing CBZ (0.015 g, 0.064 mmol) and 4,4′-bipyridine (0.020 g, 0.128 mmol) dissolved in 1 ml of a mixture of tetrahydrofuran (THF) and carbon disulfide in 1:1 volume ratio.

E. CBZ/4-aminobenzoic acid (2:1)
Yellow crystals were obtained within two days via slow evaporation of a solution containing CBZ (0.016 g, 0.068 mmol) and 4-aminobenzoic acid (0.009 g, 0.068 mmol) dissolved in 1 ml of ethanol.

F. CBZ/4-aminobenzoic acid/H_2O (2:1:1)
Yellow crystals were obtained within three days via slow evaporation of a solution containing CBZ (0.015 g, 0.063 mmol) and 4-aminobenzoic acid (0.0087 g, 0.063 mmol) dissolved in 1 ml of methanol.

G. CBZ/2,6-pyridinedicarboxylic acid (1:1)
Colorless crystals were obtained within a day via slow evaporation of a solution containing CBZ (0.034 g, 0.144 mmol) and 2,6-pyridinedicarboxylic acid 0.012 g, 0.072 mmol) dissolved in 1 ml of ethanol.

Table 2. Crystal data, experimental conditions and refinements.

	A	B	C	D	E	F	G
M	$(C_6H_6N_2O)$ $\cdot (C_7H_6O_3)$	$(C_6H_6N_2O)$ $\cdot (C_7H_6O_3)$	$(C_5H_5N_3O)$ $\cdot (C_7H_6O_4)$	$(C_{15}H_{12}N_2O)_2$ $\cdot (C_{10}H_8N_2)$	$(C_{15}H_{12}N_2O)_2$ $\cdot (C_7H_7NO_2)$	$(C_{15}H_{12}N_2O)_2$ $\cdot (C_7H_7NO_2) \cdot (H_2O)$	$(C_{15}H_{12}N_2O)$ $\cdot (C_7H_5NO_4)$
Crystallization solvent	acetone	acetonitrile	acetonitrile	THF/CS_2	ethanol	methanol	ethanol
Mol. wt.	260.25	260.25	277.24	628.72	609.67	627.68	403.39
Crystal system	monoclinic	monoclinic	monoclinic	triclinic	monoclinic	monoclinic	orthorhombic
Space group	$P2_1/c$	$P2_1/c$	$P2_1/n$	$P\bar{1}$	$C2/c$	$P2_1/n$	$P2_12_12_1$
a/Å	8.283(2)	7.370(1)	6.535(1)	7.1053(8)	31.013(3)	13.760(1)	7.208(1)
b/Å	5.105(1)	7.198(1)	17.696(3)	11.801(1)	12.1319(9)	17.457(1)	14.644(3)
c/Å	28.101(6)	22.69(4)	10.254(2)	19.648(2)	13.599(1)	14.624(1)	17.577(4)
α/°	90	90	90	93.657(2)	90	90	90
β°	90.597(5)	91.809(3)	94.645(3)	92.800(2)	99.173(1)	115.876(1)	90
γ°	90	90	90	91.061(2)	90	90	90
V/Å^3	1188.2(5)	1202.9(4)	1182.0(3)	1641.8	6028.4(8)	3160.8(4)	1855.4(6)
D_c/g cm^{-3}	1.455	1.437	1.558	1.272	1.343	1.319	1.444
Z	4	4	4	2	8	4	4
2θ range	2.90–54.00	3.60–54.00	4.60–52.74	2.08–52.74	3.54–52.74	3.88–52.74	3.62–52.74
$N_{ref}/N_{para.}$	2603/172	2620/172	2415/181	6541/433	6162/415	6429/424	3777/272
T/K	100	100	100	100	100	100	153
R_1 [$I > 2$ sigma (I)]	0.0513	0.048	0.0424	0.0487	0.0416	0.0431	0.034
wR_2	0.1509	0.1442	0.1296	0.1231	0.106	0.1112	0.0835
GOF	1.008	1.139	1.115	1.037	1.037	1.029	1.034
Abs coef.	0.11	0.108	0.124	0.081	0.089	0.089	0.105
CCDC depostion No.	240488	240489	240490	240491	240492	240493	240494

UM00011645
NOVARTIS EXHIBIT 1517
Novartis v. Regents, IPR2023-01347
Page 391 of 4460

Crystal structure determination

Crystals **A**–**G** was examined under a microscope and suitable single crystals were selected for X-ray analysis. Data were collected on a Bruker–AXS SMART APEX CCD diffractometer with monochromatized MoK_α radiation ($\lambda = 0.71073$ Å) connected to KRYO-FLEX low temperature device. Data for **A**–**F** were collected at 100 K and compound **G** was analyzed at 153 K. Lattice parameters were determined from least squares analysis, and reflection data were integrated using the program SAINT. Lorentz and polarization corrections were applied for diffracted reflections. In addition, the data was corrected for absorption using SADABS [22]. Structures were solved by direct methods and refined by full matrix least squares based on F^2 using SHELXTL [23]. All non-hydrogen atoms were refined with anisotropic displacement parameters. All H-atoms bonded to carbon atoms, except methyl groups, were placed geometrically and refined with an isotropic displacement parameter fixed at 1.2 times U_q for the atoms to which they were attached. H-atoms of methyl groups as well as N or O bonded protons were located from Fourier difference map and refined with isotropic thermal parameters based upon the corresponding N or O-atom [$U(H) = 1.2U_q(N, O)$]. Crystallographic data for **A**–**G** are presented in Table 2 and selected hydrogen bond distances are listed in Table 3.

Table 3. Geometrical parameters of intermolecular interactions.

Co-crystal	Interaction	d (H···A) /Å	D (D···A) /Å	θ/°
A	$O-H_{(alc)}\cdots O{=}C_{(acid)}$	1.84	2.631(2)	138.4
	$O-H_{(acid)}\cdots N_{(arom)}$	1.71	2.634(2)	169.1
	$N-H_s\cdots O_{(amide)}$	1.99	2.942(2)	167.3
	$N-H_a\cdots O_{(amide)}$	2.08	2.897(3)	148.2
B	$O-H_{(acid)}\cdots O_{(amide)}$	1.76	2.593(2)	172.9
	$O-H_{(alc)}\cdots N_{(arom)}$	1.83	2.693(2)	152.2
	$N-H_s\cdots O{=}C_{(acid)}$	2.10	2.943(2)	170.5
	$N-H_a\cdots O{=}C_{(acid)}$	2.06	2.934(2)	172.4
C	$O-H_{(acid)}\cdots O_{(amide)}$	1.71	2.597(2)	168.8
	$O-H_{(alc)}\cdots N_{(arom)}$	1.92	2.769(2)	167.8
	$N-H_a\cdots O_{(alc)}$	2.28	3.044(2)	142.5
	$N-H_s\cdots O{=}C_{(acid)}$	2.11	2.935(2)	161.3
D	$N-H_s\cdots O$	1.95	2.914(2)	174.4
	$N-H_s\cdots O$	2.00	2.887(2)	179.0
	$N-H_a\cdots N_{(arom1)}$	2.07	2.967(2)	159.1
	$N-H_a\cdots N_{(arom2)}$	2.08	2.992(2)	162.1
E	$O-H\cdots O_{(amide)}$	1.58	2.540(1)	169.0
	$N-H_{(amine)}\cdots O_{(amide)}$	2.12	3.014(2)	162.3
	$N-H_{s(amide)}\cdots O{=}C_{(acid)}$	2.11	2.982(2)	163.00
	$N-H_{a(amide)}\cdots O{=}C_{(acid)}$	2.00	2.907(2)	169.5
	$N-H_{a(amide)}\cdots O{=}C_{(acid)}$	2.37	3.178(2)	160.0
F	$O-H_{(acid)}\cdots O_{(water)}$	1.69	2.593(1)	170.0
	$O-H_{(water)}\cdots O_{(amide1)}$	1.80	2.672(1)	172.0
	$O-H_{(water)}\cdots O_{(amide2)}$	1.93	2.793(1)	171.1
	$N-H_{(amine)}\cdots O_{(amide2)}$	2.14	3.047(2)	170.0
	$N-H_{s(amide1)}\cdots O{=}C_{(acid)}$	2.01	2.878(2)	163.9
	$N-H_{s(amide2)}\cdots O_{(amide1)}$	2.00	2.908(2)	175.8
G	$O-H_{(acid1)}\cdots O_{(amide)}$	1.89	2.769(2)	157.7
	$O-H_{(acid2)}\cdots O_{(amide)}$	1.87	2.689(2)	154.0
	$N-H\cdots O_{(acid1)}$	2.18	2.983(2)	148.6
	$N-H\cdots O_{(acid2)}$	2.05	2.949(2)	172.0

Discussion

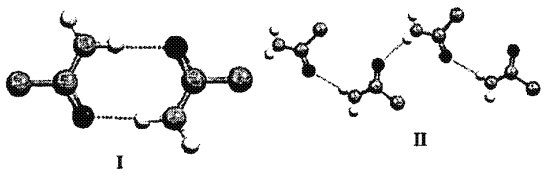
CSD analysis of primary amides

Started in 1965, the CSD has become a powerful tool for the solid-state chemist [6]. It now contains over three hundred thousand structures and the database records include bibliographic, 2D chemical and 3D structural information for carbon containing compounds characterized by X-ray and neutron diffraction. Given the large amount of data available, there are many research applications including conformational analysis, structural correlation, statistical analysis, studies of crystal packing and intermolecular interactions, crystal engineering, polymorphism and crystal structure prediction. In order to design a co-crystal, one must understand what intermolecular operations are possible and the degree of reliability.

In the context of primary amides, early research on hydrogen bonding is exemplified by Schmidt's seminal work in the 1960's [24]. Primary amides illustrate remarkable diversity in their ability to form hydrogen bonds due to the fact that they contain two hydrogen bond donors (NH_2) and an acceptor (CO) [25]. They exhibit two basic modes of self-organization to form supramolecular homosynthons: the dimer **I** and the catemer **II** (Scheme 2). A CSD survey of compounds in which a primary amide is the only functional group capable of forming strong hydrogen bonds was conducted in order to understand the statistics of supramolecular homosynthon formation of primary amides. This survey revealed the percentage of occurrence and the structural parameters of supramolecular homosynthons involving a primary amide. Contact limits for each interaction were determined from histograms obtained by applying contact distances well beyond the sum of the Van der Waals radii of the acceptor and the donor atoms. A representative histogram for N—H···O hydrogen bonds in primary amide dimers is shown in Fig. 1.

Subsequent searches focused on supramolecular heterosynthons involving the primary amide moiety. Groups that were observed to interact with primary amides and are therefore precursors to supramolecular heterosynthons (pro-synthons) include the following: carboxylic acid, secondary amide, amino-pyridine, pyridine moiety, water, alcohol, primary amine, secondary amine, carbonyl, ether, ester, cyano, nitro, chloride ion and bromide ion. The following information was obtained for each pro-synthon: (i) the number of total structures containing both the primary amide and the pro-synthon regardless of whether or not they interact with each other, (ii) the number of structures with a supramolecular heterosynthon between the primary amide and the pro-synthon, (iii) the number of structures containing an amide supramolecular homosynthon from group i, (iv) the number of structures containing the pro-synthon supramolecular homosynthon from group i, (v)

UM00011646
NOVARTIS EXHIBIT 1517
Novartis v. Regents, IPR2023-01347
Page 392 of 4460



Scheme 2. Primary amide dimer I and catemer II.

the number of structures containing a supramolecular heterosynthon exclusive of any supramolecular homosynthons and (vi) the distance range and (vii) mean length (Å) of the interaction. (Table 4). The parameters used to define the searches were as follows: 3D-coordinates present, only organics and $R < 7.5\%$. The survey revealed that there are 1231 crystal structures in which at least one primary amide functional group is present. 428 of these structures (35%) exhibit the dimer motif whereas 227 structures (18%) were found to exhibit the catemer. The average N···O distance of N–H···O hydrogen bond for the dimer and catemer are 2.95(5) and 2.96(8) Å, respectively. There are only 80 primary amide structures in which competing hydrogen bond donor and/or acceptor groups are absent. The percentage of occurrence of the dimer and catemer increases to 84% (67) and 14% (11) respectively in these structures. Two structures contain both the dimer and catemer synthons **I** and **II**.

The primary amide dimer has the potential to form larger assemblies because it has both donors and acceptors at its periphery. Three distinct patterns are possible: discrete, catenated and shallow glide motif (Fig. 2). In the discrete dimer, the anti-oriented NH does not engage in further hydrogen bonding, most frequently because of steric hindrance. The catenated dimer, sometimes referred to as an amide tape or ribbon, is a chain of translational related dimers linked along a 5.1 Å short axis by N–H···O bonds. The third pattern is the shallow glide motif in which the amide dimers are hydrogen bonded to four other dimers through exterior hydrogen bonding. The dihedral angle between the central dimer and the adjacent dimers in these structures is highly variable. Of the 67 structures found with primary amide dimer **I** in the absence of other competing donors and/or acceptors, the percentage of occurrence for each type of pattern is almost random; discrete (18%), catenated (25%) and shallow glide (54%).

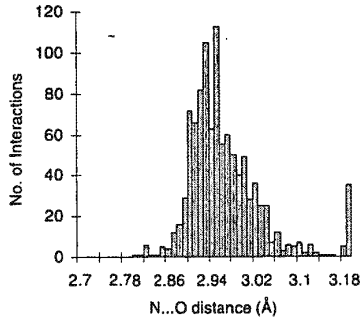


Fig. 1. Histogram of N–H···O hydrogen bond lengths in primary amide dimers, retrieved from the CSD.

The remainig three percent structures contain both catenated and glide motifs.

Primary amides can also form a diverse range of supramolecular heterosynthons with a number of other complementary functional groups such as chloride, cyano, carboxylic acid and alcohols. The primary amide-chloride ion heterosynthon (N–H···Cl^-) represents an example of a charge-assisted hydrogen bond and was found to occur in the highest percentage for heterosynthon formation. The 56 structures containing both groups reveal 41 crystal structures (73%) that exhibit the primary amide-chloride ion supramolecular heterosynthon as compared to only 8 structures (14%) that form the primary amide supramolecular homosynthon. Furthermore, of the 41 structures exhibiting the supramolecular heterosynthon, 7 contain both the amide homosynthon and amide-chloride heterosynthon whereas 34 entries occur exclusive of the amide homosynthon. The heterosynthon was found to occur within the range 3.10–3.60 Å (N···Cl^-) with an average hydrogen bond distance of 3.34(8) Å.

The primary amide-cyano supramolecular heterosynthon **III** is another example of 1-point recognition. There is a subset of 62 crystal structures in which both primary amide and cyano groups are present. Thirty three of these structures (53%) exhibit the primary amide-cyano supramolecular heterosynthon as compared to 42 structures (68%) that form the primary amide supramolecular homosynthon. However, of the 33 entries that exhibit synthon **III**, 21 structures also contain the amide homosynthon whereas only 12 occur exclusive of the amide homosyn-

Table 4. Primary amide general acceptor-donor table.

Pro-Synthon	Total Groups (i)	Total Hetero (%) (ii)	Total Amide Homo (%) (iii)	Total Pro-syn Homo (%) (iv)	Hetero exclusive of Homos(%) (v)	Range (Å) (vi)	Mean (Å) σ (vii)
Dimer	1231	–	428(34.8)	–	–	2.75–3.15	2.95(5)
Catemer	1231	–	227(18.4)	–	–	2.75–3.20	2.96(8)
Acid CO 2pt	148	69(46.6)	65(43.9)	9(6.1)	40(27.0)	2.80–3.25	2.96(8)
Acid OH 2pt	148	69(46.6)	65(43.9)	9(6.1)	40(27.0)	2.40–2.80	2.56(6)
Alcohol CO	255	110(43.1)	78(30.6)	60(23.5)	41(16.1)	2.60–3.00	2.75(8)
Alcohol NH2	255	112(43.9)	78(30.6)	60(23.5)	43(16.9)	2.73–3.20	3.00(9)
Cyano	62	33(53.2)	42(67.7)	–	12(19.4)	3.00–3.30	3.15(9)
Cl^-	56	41(73.2)	8(14.3)	–	34(60.7)	3.10–3.60	3.34(8)

UM00011647
NOVARTIS EXHIBIT 1517
Novartis v. Regents, IPR2023-01347
Page 393 of 4460

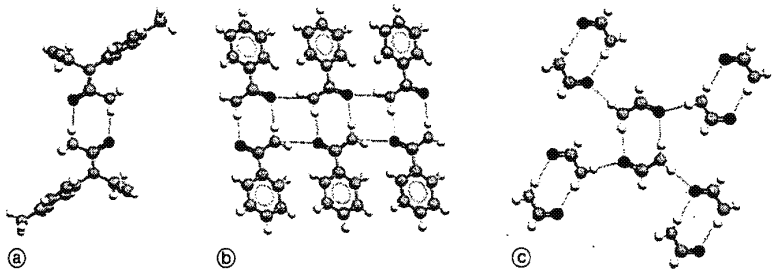
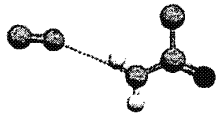


Fig. 2. (a) Discrete dimer: N-(p-methyl phenyl)-N-prop-2-ynylurea; (b) Catenated dimer: benzamide; (c) Shallow glide motif: formamide.

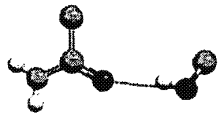
thon. In approximately 39% of supramolecular heterosynthons, the cyano group hydrogen bonds to the anti-oriented NH of the amide dimer. The supramolecular heterosynthon was found to occur within the range of 3.00–3.30 Å, with a mean hydrogen bond distance of 3.15(9) Å.



III

The primary amide-carboxylic acid heterosynthon has been previously utilized [18] in forming co-crystals and appears to be a robust and reliable supramolecular heterosynthon. There are 148 crystal structures in which both an acid and a primary amide moiety are present, 69 of these structures (47%) exhibit the amide-carboxylic acid supramolecular heterosynthon whereas only 9 structures (6%) exhibit the acid homosynthon and 65 structures (44%) form the amide homosynthon. Forty of the 69 supramolecular heterosynthons are exclusive of any acid or amide homosynthon (dimer or catemer). Since this supramolecular heterosynthon is a two-point recognition event, there are two ranges corresponding to O–H···O and N–H···O interactions. The O···O range for O–H···O hydrogen bond is 2.40–2.80 Å and the mean hydrogen bond distance is 2.56(6) Å. This distance is shorter than that of the carboxylic acid homosynthon (dimer or catemer), for which the O–H···O range is 2.40–3.00 Å with a mean of 2.65(3) Å. The N···O range for (amide)N–H···O(acid) hydrogen bonds was found to be 2.80–3.25 Å with a mean of 2.96(8) Å, which is longer than that observed for the amide dimer 2.75–3.15 Å [mean 2.95(5) Å] or catemer 2.75–3.20 Å [mean 2.96(8) Å]. These data suggest that the amide carbonyl could be a stronger H-bond acceptor than the acid carbonyl moiety.

The ability of alcohols to act as either hydrogen bond donors and/or acceptors [26], leads to two very different heterosynthons with primary amides, **IV** and **V**. The alcohol-primary amide carbonyl supramolecular heterosynthon occurs in 110 (43%) of the 255 crystal structures in which both a primary amide and an alcohol moiety is present, whereas 78 crystal structures (31%) exhibit the amide homosynthon and 60 structures (24%) form the alcohol homosynthon. Forty one (37%) of the 110 structures containing heterosynthon **IV** are exclusive of primary amide or alcohol supramolecular homosynthons. The O–H···O heterosynthon exhibits a range 2.60–3.00 Å with a mean of 2.75(8) Å. A similar trend is observed in the case of synthon **V**. One hundred twelve out of the 255 total structures (44%) were found to contain an amide NH-alcohol (N–H···O) supramolecular heterosynthon, 43 (38%) of which occur exclusive of amide or alcohol supramolecular homosynthons. The (amide)N–H···O(alcohol) distance was found to occur within the range 2.73–3.20 Å, with a mean of 3.00(9) Å.



IV



V

Model compounds

The CSD surveys described above reveal that primary amides seem to favor heterosynthon formation over that of the homosynthon motifs when certain complementary groups are also present. This understanding of self-assembly involving primary amides facilitates a rational approach to the design of co-crystals that are sustained by hydrogen bonding. In particular, co-crystal formers can be selected based upon our knowledge of the statistical probability of the occurrence of a particular supramolecular heterosynthon. If the groups that sustain this supramolecular heterosynthon are in different molecules then co-crystals are likely to be formed. However, the situation in real molecules, especially pharmaceuticals, is often more complicated since there might be several potential supramolecular heterosynthons. Compounds **A–C** represent model compounds in this context since they are examples of co-crystals in which there is a competition between multiple supramolecular homosynthons and supramolecular heterosynthons.

A. Isonicotinamide/2-hydroxybenzoic acid (1 : 1)

The presence of three competitive and complementary functionalities: carboxylic acid, primary amide and pyri-

UM00011648
NOVARTIS EXHIBIT 1517
Novartis v. Regents, IPR2023-01347
Page 394 of 4460

dine moiety would be expected to generate at least two types of supramolecular interactions. The possibilities include acid or amide supramolecular homosynthons and/or acid-amide, acid-pyridine or amide-pyridine supramolecular heterosynthons. Co-crystal **A** exhibits two supramolecular synthons; the carboxylic group of the 2-hydroxybenzoic acid and the aromatic nitrogen of isonicotinamide form an acid-pyridine supramolecular heterosynthon and the primary amide functionalities of two isonicotinamide molecules form an amide-amide supramolecular homosynthon. The result of these interactions is a four-component aggregate that consists of two isonicotinamide and two 2-hydroxybenzoic acid molecules. It is worth mentioning that the alcoholic OH present in 2-hydroxybenzoic acid does not affect this set of interactions as it is involved in an intramolecular 6-membered hydrogen bonded ring with the carbonyl group of the carboxylic acid [O···O: 2.631(2) Å] [27]. Translationally related four-component units are further extended into 2D sheets via amide-amide N–H···O [N···O: 2.897(3) Å] hydrogen bonds that generate tapes with the typical 5.1 Å short axis (Fig. 3) [24].

This set of interactions, the carboxylic acid-pyridine supramolecular heterosynthon and the amide-amide supramolecular homosynthon, has been observed in all eight previously reported co-crystals [18, 28] which contain these three functional groups and no other strong hydrogen bonding moieties. A CSD survey reveals that it is also the dominant combination even when other groups are present (22/32 compounds). The $O_{(acid)}\cdots N_{(arom)}$ hydrogen bond of 2.634(2) Å in **A** corresponds closely to the values observed in other pyridine-carboxylic acid structures [mean 2.60(4) Å]. Similarly, the amide-amide supramolecular homosynthon in **A** exhibits a typical N···O distance of 2.942(2) Å vs. a mean value of 2.91(4) Å. The previously reported co-crystals [18] containing isonicotinamide and carboxylic acids also exhibit the tetrameric adduct but **A** is the first compound in which the amide tape motif is present. The packing motifs of other co-crystals are sustained via the anti- oriented NH interacting with adjacent tetrameric adducts via N–H···O=C hydrogen bonds to the carboxylic acid group. The presence of the amide tape in co-crystal **A** might be explained by the reduced availability of the C=O of the carboxylic acid because of the presence of the strong intramolecular H-bond with the alcoholic OH group.

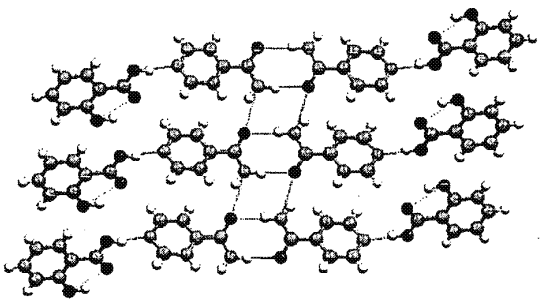
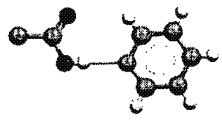


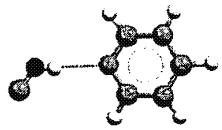
Fig. 3. Crystal structure of isonicotinamide/2-hydroxybenzoic acid co-crystal.

B. Nicotinamide/3-hydroxybenzoic acid (1 : 1)

B contains an alcohol moiety which is capable of competing with the acid moiety for the pyridine group because it is unable to form an intramolecular hydrogen bond. The CSD reveals that supramolecular heterosynthon occurrence for an acid to pyridine, **VI**, is 63% whereas alcohol to pyridine, **VII**, occurs in 50% of the structures in which both groups are present. The presence of an alcohol-nitrogen hydrogen bond would presumably free the carboxylic acid moiety to form an acid-amide heterosynthon.



VI



VII

The crystal structure of **B** reveals that the alcohol does indeed hydrogen bond to the pyridine moiety and the acid-amide supramolecular heterosynthon is formed. Each acid-amide dimer is hydrogen bonded to four other acid-amide dimers through (alc)O–H···N(amine) [O···N: 2.693(2) Å] and amide N–H···O [N···O: 2.943(2) Å] hydrogen bonds (Fig. 4). The four exterior-bonding pairs are situated at approximately a 90° angle, thereby generating a 2D network. The O–H···O [O···O: 2.593(2) Å] and (amide)N–H···O(acid) [N···O: 2.934(2) Å] hydrogen bond lengths for the acid-amide supramolecular heterosynthon are in the expected range and compare closely to mean values of 2.56(6) Å and 2.96(8) Å, respectively.

C. Pyrazinamide/2,5-dihydroxybenzoic acid (1 : 1)

C contains the same four functional groups as **B** and is therefore a second example of a co-crystal that could exhibit a combination of acid-amide and alcohol-pyridine supramolecular heterosynthons. The molecules in **C** form a tetrameric unit that consists of two molecules of each component that form two acid-amide heterosynthons connected by alcohol O–H···N interactions at the periphery of the supermolecule. Each tetramer is bridged to four others via hydrogen bonds between alcohols moieties and anti-oriented amide NH's that are not involved in the acid-amide supramolecular heterosynthon (Fig. 5). The O–H···O [O···O: 2.597(2) Å] and N–H···O [N···O: 2.935(2) Å] hydrogen bond lengths for the acid-amide heterosynthon are within the expected ranges.

The database suggest that the acid-pyridine supramolecular heterosynthon is the most robust amongst the following supramolecular homosynthons and heterosynthons: acid-acid, amide-amide, acid-amide, amide-pyridine. However, the presence of an alcohol moiety changes the hierarchy and facilitates the formation of alcohol-pyridine and acid-amide supramolecular heterosynthons.

UM00011649
NOVARTIS EXHIBIT 1517
Novartis v. Regents, IPR2023-01347
Page 395 of 4460

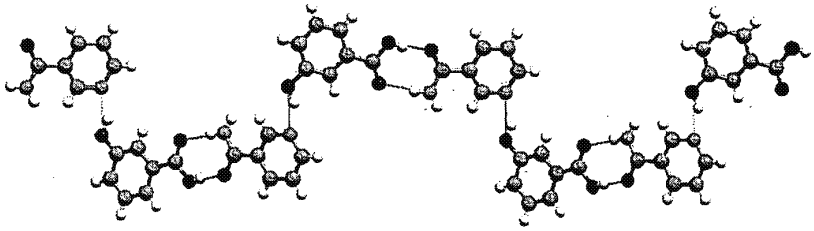


Fig. 4. Crystal structure of nicotinamide/3-hydroxybenzoic acid co-crystal.

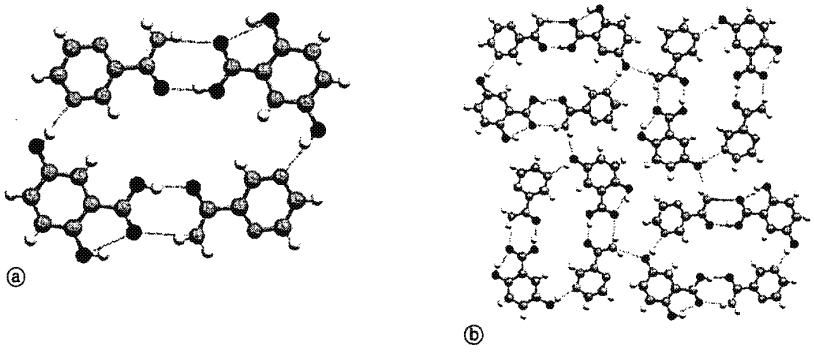


Fig. 5. (a) Two molecules of pyrazinamide and two molecules of 2,5-dihydroxybenzoic acid forming a hydrogen bonded tetramer; (b) Crystal structure of co-crystal **C**. Notice that tetramers are arranged in a herringbone fashion.

Study of an API that contains primary amide: carbamazepine (CBZ)

The nature of APIs, most of which are small to medium organics with peripheral hydrogen bonding groups, makes them amenable to the formation of pharmaceutical co-crystals. We have previously reported how CBZ, an API that contains a primary amide, can form a range of co-crystals with and without the primary amide dimer [1]. CBZ is an anti-convulsant and an analgesic with known solubility and polymorphism problems [29]. Our approach to the design of co-crystals containing CBZ exploits supramolecular synthesis, in particular, the rational generation of supramolecular heterosynthons. CBZ has four reported polymorphs that each exhibits the discrete primary amide dimer, **I** [30]. It is interesting to note that in all polymorphs that have been structurally characterized, the anti-oriented NH is left unsatisfied as it does not engage in any hydrogen bonding. Other previously reported structures of CBZ include a dihydrate [31], an acetone solvate

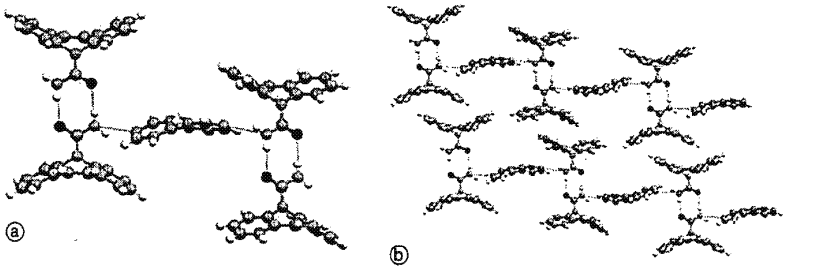


Fig. 6. (a) Building block of CBZ/4,4′-bipyridine 2:1 co-crystal; (b) Crystal packing of co-crystal **D**.

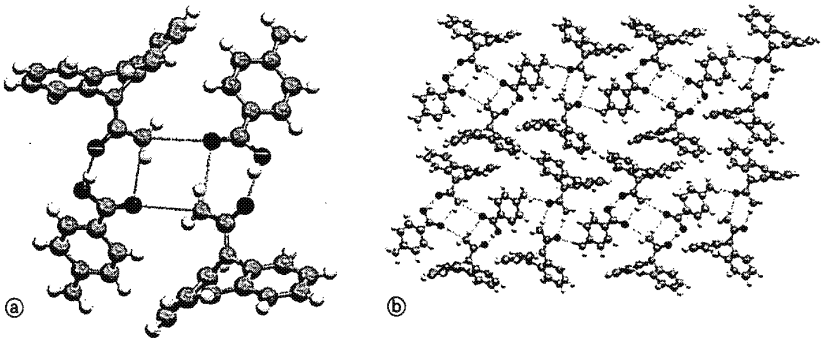


Fig. 7. (a) CBZ/4-aminobenzoic acid 2-component heterosynthon (tetramer) motif; (b) Crystal packing of **E** showing the alternating amide-amide supramolecular homosynthon and the tetrameric amide-acid supramolecular heterosynthon.

UM00011650
NOVARTIS EXHIBIT 1517
Novartis v. Regents, IPR2023-01347
Page 396 of 4460

[32], and two ammonium salts [33], all of which also contain the primary amide dimer. In these latter four structures, the anti-oriented NH is satisfied by an incorporated hydrogen bond acceptor. Suitable co-crystal formers for CBZ should therefore be capable of one of two things: act as an acceptor to the unsatisfied anti-oriented NH; form a supramolecular heterosynthon with the primary amide group. The first strategy is exemplified by the CBZ/acetone and CBZ dihydrate structures and is further demonstrated herein.

D. CBZ/4,4′-bipyridine (2:1)

Co-crystal **D** is crystallized in 2:1 stoichiometry by heat and slow evaporation from THF/CS_2. In the crystal structure of **D**, the CBZ dimer remains intact and the pyridine moieties act as acceptors to the anti-oriented NH's of the CBZ dimer (Fig. 6). There are 10 CSD structures that exhibit the same type of motif with a pyridine moiety [34] and the mean bond length for the (amide) N–H···N (pyridine) interaction is 3.06(7) Å. **D** exhibits almost two unique bond lengths, 2.967(2) and 2.992(2) Å.

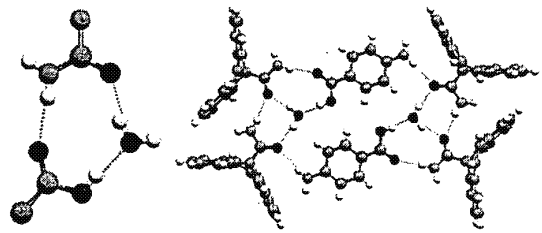
E. CBZ/4-aminobenzoic acid (2:1)

Co-crystal **E** also exhibits 2:1 stoichiometry and contains both the expected acid-amide 2-point supramolecular heterosynthon and a primary amide dimer. Two acid-amide supramolecular heterosynthons form a tetrameric motif, which is bonded to the primary amide dimers on each side through the amino N–H···O hydrogen bonds (Fig. 7). This tetrameric motif is found in 9 of the 69 (13%) structures in the CSD that contain acid-amide supramolecular heterosynthons including CBZ co-crystals with acetic acid, formic acid and butyric acid [35]. The O–H···O and N–H···O hydrogen bond lengths for the acid-amide supramolecular heterosynthon are 2.540(1) Å and 2.982(2) Å, which compare to the mean values of 2.56(6) and 2.96(8) Å, respectively.

F. CBZ/4-aminobenzoic acid/H_2O (2:1:1)

Co-crystallizing the same components as **E** but from ethanol produced a 2:1:1 co-crystal of CBZ with 4-aminobenzoic acid and adventitious H_2O. The crystal packing is markedly different from the crystal structure of **E**. It forms an eight molecule discrete unit through O–H···O and N–H···O hydrogen bonds that contains four CBZ molecules, two 4-aminobenzoic acid molecules and two water molecules (Fig. 8). The insertion of the water molecule into the amide-acid supramolecular heterosynthon to form a different supramolecular heterosynthon, **VIII**, is unusual but not unprecedented. Hydration or solvation of carboxylic acids by water or alcohol molecules as open or cyclic hydrogen bond motifs is a common phenomenon during crystallization [36] and the role of water has been aptly described as a "gluing factor" in organic crystals [37]. A CSD survey reveals that there are 116 structures in which carboxylic acids are hydrogen bond bridged to another carboxylic acid moiety through cyclic one or two water and/or alcohol molecules [38]. There are three crystal structures that exhibit supramolecular heterosynthon **VIII** [39].

The water molecules insert between the primary amide carbonyl and the acid OH, thereby sustaining 1-point



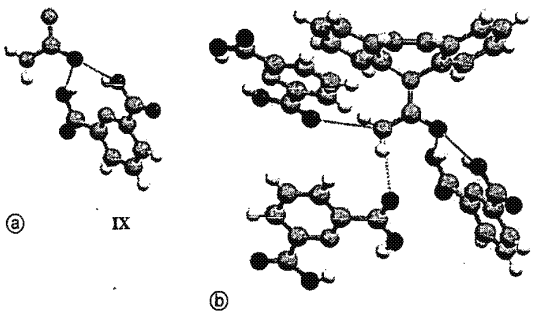
ⓐ VIII ⓑ

Fig. 8. (a) The acid-amide-H_2O supramolecular heterosynthon **VIII**; (b) Crystal structure of the 3-component discrete unit in the CBZ/4-aminobenzoic acid/H_2O (2:1:1) co-crystal containing 8 molecules.

N–H···O acid-amide supramolecular heterosynthons. The (amide) N–H···O (acid) bond length is 2.878(2) Å vs. a mean of 2.96(8) Å. Notably, the amide anti-oriented NH's are not involved in hydrogen bonding.

G. CBZ/2,6-pyridinedicarboxylic acid (1:1)

CBZ was co-crystallized with 2,6-pyridinedicarboxylic acid (2,6-PDC) from ethanol. The expected acid-amide heterosynthon is not seen in this structure. Rather, the co-crystal exhibits an unusual hydrogen bonding motif. Only 1-point interactions are present, with each CBZ molecule bonding to three different acid molecules. It is interesting to note that two carboxylic acid O–H donors are hydrogen bonding with one amide carbonyl resulting in synthon **IX**. The two (acid)O–H···O(amide) hydrogen bonds are in the normal distance and angle range [2.949(2) Å, 172°; 2.983(2) Å, 148.6°]. There is no disorder in the crystal structure and the protons are located in the difference Fourier map. The two acid O–H donors are also involved in an intramolecular O–H···N [O···N: 2.654, 2.681 Å] hydrogen bond with the pyridine moiety. Synthon **IX** is a novel hydrogen bonded motif, stabilized through both intra- and intermolecular interactions thus forming a complex hydrogen bonded network. While it is fairly common to have an acid OH hydrogen bonding to a carbonyl, bifurcation [40] of a carbonyl (amide or simple ketone) to two acid OHs without a 2-point supramolecular heterosynthon present is only seen in one structure from the CSD [41].



ⓐ IX ⓑ

Fig. 9. (a) The amide carbonyl/pyridine dicarboxylic acid supramolecular heterosynthon **IX**; (b) Crystal structure of CBZ/2,6-pyridinedicarboxylic acid co-crystal, notice the synthon **IX**.

UM00011651
NOVARTIS EXHIBIT 1517
Novartis v. Regents, IPR2023-01347
Page 397 of 4460

Planarity of amide groups

A database search was conducted in order to address the planarity of primary amide groups in general and compare values to those of the CBZ and model compound co-crystals studied herein. The range of torsion angles in 347 CSD structures containing a primary amide group attached to an aromatic core was found to be 0–84° whereas the CBZ structures exhibit amide torsion angles of 0–14°. For the model compounds, the amide torsion angles range from 0–31°. Closer examination of this data suggests that the primary amide groups in these structures do not distort to any distinguishable degree in order to form supramolecular heterosynthons. For example the amide group in isonicotinamide in co-crystal A is 31° from planarity, which compares closely with pure isonicotinamide.

Conclusions

The primary focus of our research program concerns the study of functional groups that are capable of forming hydrogen bonded supramolecular synthons and how to exploit statistical data from the Cambridge Structural Database in order to select co-crystal formers for generation of co-crystals. In this contribution, we have demonstrated that, whereas the primary amide functional group can exhibit varied hydrogen bonding motifs, there is some degree of predictability in the formation of supramolecular heterosynthons that involve primary amides. The supramolecular synthesis of seven new co-crystals, including four pharmaceutical co-crystals, was thereby achieved and all are sustained by primary amide supramolecular heterosynthons. Future work will focus on other functional groups capable of hydrogen bonding, including carboxylic acids, secondary amides, and alcohols and how to generate an even greater range of pharmaceutical co-crystals.

We do not address the issue of physical properties herein. However, it is well known that APIs can exhibit problems ranging from poor solubility, polymorphism and inadequate dissolution properties to lack of crystallinity and instability. Pharmaceutical co-crystals offer an opportunity to increase the number of forms of an API and to address some these problems. It should be stressed that such an approach to improving the physico-chemical properties of APIs remains in its infancy but there is already at least one case in which solubility enhancements have been afforded in a co-crystal form of an API [42]. The physicochemical properties of pharmaceutical co-crystals will be addressed in future papers.

Acknowledgments. We are grateful for financial support from Transform Pharmaceuticals, 29 Hartwell Avenue, Lexington, MA, 02421.

References

[1] Fleischman, S. G.; Kuduva, S. S.; McMahon, J. A.; Moulton, B.; Walsh, R. D. B.; Rodriguez-Hornedo, N.; Zaworotko, M. J.: Crystal engineering of the composition of pharmaceutical phases: Multiple-component crystalline solids involving carbamazepine. Cryst. Growth Des. **3** (2003) 909–919 (Part 2).

[2] Lehn, M. J.: Supramolecular Chemistry. Concepts and Perspectives. VCH, Weinheim, Germany, 1995; Desiraju, G. R.: Crystal Engineering. The design of Organic Solids, Elsevier, Amsterdam, 1989; Desiraju, G. R.; Sharma, C. V. K.: Crystal Engineering and Molecular Recognition. Twin facets of Supramolecular Chemistry. In: Perspectives in Supramolecular Chemistry, The Crystal as a Supramolecular Entity (Ed. G. R. Desiraju), p. 31. Wiley, Chichester Vol. 2, 1995.

[3] Pepinsky, R.: Crystal Engineering: New concepts in Crystallography. Phys. Rev. **100** (1955) 971.

[4] Schmidt, G. M. J.: Photodimerization in the solid state. Pure Appl. Chem. **27** (1971) 647–678.

[5] Whitesides, G. M.; Simanek, E. E.; Mathias, J. P.; Seto, C. T.; Chin, D. N.; Mammen, M.; Gordon, D. M.: Non-covalent synthesis: Using physical-organic chemistry to make aggregates. Acc. Chem. Res. **28** (1995) 3744; Fyfe, M. C. T.; Stoddart, J. F.: Synthetic Supramolecular Chemistry. Acc. Chem. Res. **30** (1997) 393–401.

[6] Allen F. H.; Kennard, O.: 3D Search and research using the Cambridge Structural Database. Chem. Des. Automat. News **8** (1993) 31–37; Allen, F. H.: The Cambridge Structural Database: a quarter of a million crystal structures and rising. Acta Crystallogr. **B58** (2002) 380–388; Nangia, A.: Database research in Crystal engineering. Cryst. Eng. Comm. **4** (2002) 93–101.

[7] Desiraju, G. R.: Supramolecular synthons in crystal engineering: A new organic synthesis. Angew Chem. Int. Ed. Engl. **34** (1995) 2311–2327.

[8] Walsh, R. D. B.; Bradner, M. W.; Fleischman, S. G.; Morales, L. A.; Moulton, B.; Rodriguez-Hornedo, N.; Zaworotko, M. J.: Crystal engineering of the composition of pharmaceutical phases. Chem. Commun. (2003) 186–187.

[9] Kitaigorodskii, A. I.: Mixed Crystals, Springer-Verlag, New York, 1984.

[10] Cannon, A. S.; Warner, J. C.: Noncovalent derivatization: green chemistry applications of crystal engineering. Cryst. Growth Des. **2** (2002) 255–257.

[11] Aakeröy, C. B.; Beatty, A. M.; Helfrich, B. A.: A high-yielding supramolecular reaction. J. Am. Chem. Soc. **124** (2002) 14425–14432; Aakeröy, C. B.; Beatty, A. M.; Helfrich, B. A.: "Total synthesis" supramolecular style: Design and hydrogen-bond-directed assembly of ternary supermolecules. Angew. Chem. Int. Ed. **40** (2001) 3240–3242; Etter, M. C.: Hydrogen bonds as design elements in organic chemistry. J. Phys. Chem. **95** (1991) 4601–4610; Videnova-Adrabinska, V.; Etter, M. C.: Urea-glutaric acid (2:1) structural aggregates as building blocks for crystal engineering. J. Chem. Cryst. **25** (1995) 823–829; Huang, C. M.; Leiserowitz, L.; Schmidt, G. M. J.; Molecular packing modes. XI. Crystal structures of the 2:1 complexes of benzamide-succinic acid and furamide-oxalic acid. J. Chem. Soc., Perkins Trans. 2. **5** (1973) 503–508; Zerkowski, J. A.; MacDonald, J. C.; Seto, C. T.; Wierda, D. A.; Whitesides, G. M.: Design of organic structures in the solid state: Molecular tapes based on the network of hydrogen bonds present in the cyanuric acid·melamine complex. J. Am. Chem. Soc. **116** (1994) 2382–2391; Mathias, J. P.; Simanek, E.E.; Zerkowski, J. A.; Seto, C. T.; Whitesides, G. M.: Structural preferences of hydrogen-bonded networks in organic solution- the cyclic CA3·M3 "Rosette". J. Am. Chem. Soc. **116** (1994) 4316–4325.

[12] Gao, X.; Friščić, T.; MacGillivray, L. R.: Supramolecular construction of molecular ladders in the solid state. Angew. Chem. Int. Ed. **43** (2004) 232–236; Gao, X.; Friščić, T.; MacGillivray, L. R.: "Template-switching": a supramolecular strategy for the quantitative, gram-scale construction of a molecular target in the solid state. Chem. Commun. (2003) 1306–1307; MacGillivray, L. R.: From engineering crystals to engineering molecules: emergent consequences of controlling reactivity in the solid state using linear templates. Cryst. Eng. Comm. **4** (2002) 3741.

[13] Ma, B.-Q.; Zhang, Y.; Coppens, P.: Structural variation and supramolecular isomerism in the C-Methylcalix[4]resorcinarene/bipyridine system. Cryst. Growth Des. **2** (2002) 713; Ma, B.-Q.; Zhang, Y.; Coppens, P.: Multiple structures in supramolecular solids: Benzophenone embedded in three different C-Methylcalix[4]resorcinarene/bipyridine frameworks. Cryst. Growth Des. **1** (2001) 271–275; MacGillivray, L. R.; Reid, J. L.; Ripmeester, J. A.: Conformational isomerism leads to supramolecular isomerism and nanoscale inclusion in 2D extended framework solids based on *C*-methylcalix[4]resorcinarene. Chem. Commun.

UM00011652
NOVARTIS EXHIBIT 1517
Novartis v. Regents, IPR2023-01347
Page 398 of 4460

(2001) 1034–1035; MacGillivray, L. R.; Diamente, P. R.; Reid, J. L.; Ripmeester, J. A.: Encapsulation of two aromatics by a carcerand-like capsule of nanometer-scale dimension. Chem. Commun. (2000) 359–360.

[14] Taylor, L. D.; Warner, J. C.: Process and composition for use in photographic materials containing hydroquinones. US 5338644 A 19940816 (1994) Cont. of U.S. 5,177,262.

[15] Almarsson, Ö.; Zaworotko, M. J.: Crystal Engineering of the Composition of Pharmaceutical Phases. Do Cocrystals Represent a New Path to Improved Medicines? Chem. Commun. (2004) 1889–1896.

[16] Huang, K.; Britton, D.; Etter, M. C.; Byrn, S. R.: A novel class of phenol-pyridine co-crystals for second harmonic generation. J. Mater. Chem. **7** (1997) 713–720.

[17] Bhogala, B. R.; Vishweshwar, P.; Nangia, A.: Four-fold inclined interpenetrated and three-fold parallel interpenetrated hydrogen bonds networks in 1,3,5-cyclohexane tricarboxylic acid hydrate and its molecular complex with 4,4′-bipyridine. Cryst. Growth Des. **2** (2002) 325–328; Bhogala, B. R.; Nangia, A.: Co-crystals of 1,3,5-cyclohexanetricarboxylic acid with 4,4′-bipyridine Homologues: Acid...Pyridine Hydrogen Bonding in Neutral and Ionic Complexes. Cryst. Growth Des. **3** (2003) 547–554; Bond, A. D.: *In situ* co-crystallization as a tool for low-temperature crystal engineering. Chem. Commun. (2003) 250–251.

[18] Vishweshwar, P.; Nangia, A.; Lynch, V. M.: Molecular complexes of homologous alkanedicarboxylic acids with isonicotinamide: X-ray crystal structures, hydrogen bond synthons, and melting point alternation. Cryst. Growth. Des. **3** (2003) 783–790; Reddy, L. S.; Nangia, A.; Lynch, V. M.: Phenyl-perfluorophenyl synthon mediated cocrystallization of carboxylic acids and amides. Cryst. Growth Des. **4** (2004) 8994; Aakeröy, C. B.; Beatty, A. M.; Helfrich, B. A.; Nieuwenhuyzen, M.: Do polymorphic compounds make good co-crystallizing agents? A structural case study that demonstrates the importance of synthon flexibility. Cryst. Growth Des. **3** (2003) 159–165.

[19] Vishweshwar, P.; Nangia, A.; Lynch, V. M.: Supramolecular synthons in phenol-isonicotinamide adducts. Cryst. Eng. Comm. **5** (2003) 164–168; Papaefstathiou, G. S.; MacGillivray, L. R.: Discrete versus infinite molecular self-assembly: Control in crystalline hydrogen-bonded assemblies based on resorcinol. Org. Lett. **3** (2001) 3835–3838; MacGillivray, L. R.; Atwood, J. L.: Unique guest inclusion within multi-component, extended-cavity resorcin[4]arenes. Chem. Commun. (1999) 181–182.

[20] Trask, A. V.; Motherwell, W. D. S.; Jones, W.: Solvent-drop grinding: green polymorph control of cocrystallization. Chem. Commun. (2004) 890–891; Shan, N.; Toda, F.; Jones, W.: Mechanochemistry and co-crystal formation: effect of solvent on reaction kinetics. Chem. Commun. (2002) 2372–2373.

[21] Boese, R.; Kirchner, M. T.; Billups, W. E.; Norman, L. R.: Co-crystallization with acetylene: Molecular complexes with acetone and dimethyl sulfoxide. Angew. Chem. Int. Ed. **42** (2003) 1961–1963.

[22] SADABS [Area-Detector Absorption Correction]. Siemens industrial Automation, Inc.: Madison, WI 1996.

[23] Sheldrick, G.M.: SHELXTL, Release 5.03; Siemens Analytical X-ray Instruments, Inc.: Madison, WI, 1994.

[24] Leiserowitz, L.; Schmidt, G. M. J.: Molecular packing modes. III. Primary amides. J. Chem. Soc. A**16** (1969) 2372–2382.

[25] MacDonald, J. C.; Palmore, G. T. R.: The Role of Amides in the Non-covalent Synthesis of Supramolecular Structures in Solution, at Interfaces and in Solids in The Amide Linkage: Selected Structural Aspects in Chemistry, Biochemistry, and Materials Science (Eds. A.Greenberg, C. M. Breneman, J. F. Liebman), p. 291–336. John Wiley & Sons, Inc.: New York, 2000; Meléndez, R E.; Hamilton, A. D.: Hydrogen-Bonded Ribbons, Tapes and Sheets as Motifs for Crystal Engineering in Design of Organic Solids (Eds. E. Weber) pp. 97–130. Springer, Berlin, 1998; Bernstein, J.; Etter, M. C.; Leiserowitz, L.: Structure Correlation (Eds. H.-B. Bürgi, J. D. Dunitz) Vol. 2, pp. 431–507. VCH, Weinheim, 1994; MacDonald, J. C.; Whitesides, G. M.; Solid-State Structures of Hydrogen-Bonded Tapes Based on Cyclic Secondary Diamides. Chem. Rev. **94** (1994) 2383–2420; Kuduva, S. S.; Bläser, D.; Boese, R.: Crystal Engineering of Primary Cubanecarboxamides. Repetitive Formation of an Unexpected N–H···O Hydrogen-Bonded Network. J. Org. Chem. **66** (2001) 1621–1626.

[26] Chandra, A. K.; Basu, S.: Hydrogen Bonds. 1. Trans. Faraday Soc. **56** (1960) 632–637; Chandra, A. K.; Sannigrahi, A. B.: Hydrogen-bonding properties of alcohols. J. Phys. Chem. **69** (1965) 2494–2499.

[27] Etter, M. C.: Encoding and decoding hydrogen-bond patterns in organic compounds. Acc. Chem. Res. **23** (1990) 120–126.

[28] Amai, M.; Endo, T.; Nagale, M.; Ueda, M.; Nakagali, M.: 1:1 complexes of octadecanoic acid and 3-pyridinecarboxamide. Acta Crystallogr. C**54** (1998) 1367–1369.

[29] Kobayashi, Y.; Ito, S.; Itai, S.; Yamamoto, K.: Physicochemical properties and bioavailability of carbamazepine polymorphs and dihydrate. Int. J. Pharm. **193** (2000) 137–146.

[30] Himes, V. L.; Mighell, A. D.; De Camp, W. H.: Structure of carbamazepine: 5H-dibenz[b,f]azepine-5-carboxamide. Acta Crystallogr. B**37** (1981) 2242–2245; Reboul, J. P.; Cristau, B.; Soyfer, J. C.; Astier, J. C.: 5 H-dibenz[b,f]axepine-5-carboxamide (carbamazepine). Acta Crystallogr. B**37** (1981) 844–1848; Lowes, M. M. J.; Caira, M. R.; Lotter, A. P.; Van der Watt, J. G.: Physicochemical properties and X-ray structural studies of the trigonal polymorph of carbamazepine. J. Pharm. Sci. **76** (1987) 744–752; Lisgarten, J. N.; Palmer, R. A.; Saldanha, J. W.: Crystal and molecular structure of 5-carbamyl-5H-dibenz[b,f]azepine. J. Crystallogr. Spectrosc. Res. **19** (1989) 641–649; Rustichelli, C.; Gamberini, G.; Ferioli, V.; Gamberini, M. C.; Ficarra, R.; Tommasini, S.: Solid-state study of polymorphic drugs: Carbamazepine. J. Pharm. Biomed. Anal. **23** (2000) 41–54; Ceolin, R.; Toscani, S.; Gardette, M. F.; Dzyabchenko, V. N.; Bachet, B.: X-ray characterization of the triclinic polymorph of carbamazepine. J. Pharm. Sci. **86** (1997) 1062–1065; Lang, M.; Kampf, J.; Matzger, A. J.: Form IV of carbamazepine. J. Pharm. Sci. **91** (2002) 1186–1190; Grzesiak, A. L.; Lang, M.; Kin, K.; Matzger, A. J.: Comparison of the four anhydrous polymorphs of carbamazepine and crystal structure of form 1. J. Pharm. Sci. **92** (2003) 2260–2271.

[31] Reck, G.; Dietz, G.: The order-disorder structure of carbamazepine dihydrate: 5 H-dibenz[b,f]azepine-5-carboxamide dihydrate, $C_{15}H_{12}N_2O \cdot 2\ H_2O$. Cryst. Res. Technol. **21** (1986) 1463–1468.

[32] Lowes, M. M. J.; Caira, M. R.; Lotter, A. P.; Van der Watt, J. G.: Physicochemical properties and X-ray structural studies of the trigonal polymorph of carbamazepine. J. Pharm. Sci. **76** (1987) 744–752.

[33] Reck, G.; Thiel, W.: Crystal structures of the adducts carbamazepine-ammonium chloride and carbamazepine-ammonium bromide and their transformation to carbamazepine dihydrate. Pharmazie. **46** (1991) 509–512.

[34] CSD Refcodes: AMILEN, AMILUD, BATHOU, BOHJIR, JUYGUF, MFCBXB, PYRZIN, WUPZUC, WUQMIE and ZAQTUG.

[35] CSD Refcodes: AJALAY, FURAOX, RAHGEM, UNEZIW, UNEZOC, UNEZUI, UROXAM, UROXAM01 and XEWTIC.

[36] Gillon, A. L.; Feeder, N.; Davey, R. J.; Storey, R.: Hydration in Molecular Crystals-A Cambridge Structural Database Analysis. Cryst. Growth Des. **3** (2003) 663–673.

[37] Krygowski, T. M.; Grabowski, S. J.; Konarski, J.: Water Molecules as a Gluing Factor in Organic Crystals and Biological Systems. Tetrahedron **54** (1998) 11311–11316.

[38] Herbstein, F. H.; Kapon, M.; Shteiman, V.: Determination of the structure of 2(benzene-1,3,5-tricarboxylic acid)1.5(pyrene) × 2(methanol) and comparison with that of 2(benxene-1,3,5-tricarboxylic acid)pyrene2(ethanol). Acta Crystallogr. B**57** (2001) 692–696; Kolotuchin, S. V.; Fenlon, E. E.; Wilson, S. R.; Loweth, C. J.; Zimmerman, S. C.: Self-Assembly of 1,3,5-Benzenetricarboxylic acids (Trimesic Acids) and Several Analogues in the Solid State. Angew Chem. Int. Ed. Engl. **34** (1995) 2654–2657.

[39] CSD Refcodes: GASTRN10, IHANIO and OBIZII.

[40] Saied, O.; Simard, M.; Wuest, J. D.: A complex in which the carbonyl oxygen atom of a simple ketone accepts two intermolecular hydrogen bonds. J. Org. Chem. **63** (1998) 3756–3757.

[41] Ranjbar, M.; Aghabozorg, H.; Moghimi, A.; Yanovsky, A.: Crystal structure of 2,6-diaminopyridinium bis(2,6-pyridinedicarboxylato)chromium(III) 2,6-pyridinedicarboxylic acid hemihydrate, $C_{26}H_{18}CrN_6O_{12} \cdot 0.5\ H_2O$. Z. Kristallogr. NCS **216** (2001) 626–628.

[42] Remenar, J. F.; Morissette, S. L.; Peterson, M. L.; Moulton, B.; MacPhee, J. M.; Guzmán, H. R.; Almarsson, Ö.: Crystal Engineering of Novel Cocrystals of a Triazole Drug with 1,4-Dicarboxylic Acids. J. Am. Chem. Soc. **125** (2003) 8456–8457.

UM00011653
NOVARTIS EXHIBIT 1517
Novartis v. Regents, IPR2023-01347
Page 399 of 4460

[1] a) P. J. Dyson, J. S. McIndoe, *Transition Metal Carbonyl Cluster Chemistry*, Gordon and Breach Science Publishers, Australia, **2000**, p. 1; b) A. J. Lupinetti, S. H. Strauss, G. Frenking, *Prog. Inorg. Chem.* **2001**, *49*, 1. This reference cites 50 previous review articles; c) H. Willner, F. Aubke, *Angew. Chem.* **1997**, *109*, 2506; *Angew. Chem. Int. Ed. Engl.* **1997**, *36*, 2402; d) M. F. Zhou, L. Andrews, C. W. Bauschlicher, Jr., *Chem. Rev.* **2001**, *101*, 1931.
[2] A. B. Burg, H. I. Schlesinger, *J. Am. Chem. Soc.* **1937**, *59*, 780.
[3] *Gmelins Handbuch der Anorganischen Chemie, Borverbindungen*, Teil 10, Vol. 37, Springer, Berlin, **1976** (1–4. Suppl. (1980–1996)).
[4] A. Terheiden, E. Bernhardt, H. Willner, F. Aubke, *Angew. Chem.* **2002**, *114*, 823; *Angew. Chem. Int. Ed.* **2002**, *41*, 799.
[5] M. Finze, E. Bernhardt, A. Terheiden, M. Berkei, H. Willner, D. Christen, H. Oberhammer, F. Aubke, *J. Am. Chem. Soc.* **2002**, *124*, 15385.
[6] M. F. Zhou, N. Tsumori, Z. H. Li, K. N. Fan, L. Andrews, Q. Xu, *J. Am. Chem. Soc.* **2002**, *124*, 12936.
[7] M. F. Zhou, Q. Xu, Z. X. Wang, P. v. R. Schleyer, *J. Am. Chem. Soc.* **2002**, *124*, 14854.
[8] a) G. H. Robinson, *Acc. Chem. Res.* **1999**, *32*, 773; b) P. P. Power, *Chem. Rev.* **1999**, *99*, 3463; c) J. R. Su, X.-W. Li, R. C. Crittendon, G. H. Robinson, *J. Am. Chem. Soc.* **1997**, *119*, 5471; d) Y. Xie, R. S. Grev, J. D. Gu, H. F. Schaefer, P. v. R. Schleyer, J. R. Su, X. W. Li, G. H. Robinson, *J. Am. Chem. Soc.* **1998**, *120*, 3773; e) F. A. Cotton, A. H. Cowley, X. J. Feng, *J. Am. Chem. Soc.* **1998**, *120*, 1795; f) Y. Xie, H. F. Schaefer, G. H. Robinson, *Chem. Phys. Lett.* **2000**, *317*, 174; g) K. W. Klinkhammer, *Angew. Chem. Int.* **1997**, *109*, 2414; *Angew. Chem. Int. Ed. Engl.* **1997**, *36*, 2320; h) I. Bytheway, Z. Lin, *J. Am. Chem. Soc.* **1998**, *120*, 12133.
[9] a) T. R. Burkholder, L. Andrews, *J. Chem. Phys.* **1991**, *95*, 8697; b) M. H. Chen, X. F. Wang, L. N. Zhang, M.Yu, Q. Z. Qin, *Chem. Phys.* **1999**, *242*, 81.
[10] a) T. R. Burkholder, L. Andrews, *J. Phys. Chem.* **1992**, *96*, 10195; b) Y. M. Hamrick, R. J. Van Zee, J. T. Godbout, W. Weltner, W. J. Lauerdale, J. F. Stanton, R. J. Bartlett, *J. Phys. Chem.* **1991**, *95*, 2840.
[11] DFT and CCSD(T) calculations were performed using Gaussian 98. M. J. Frisch, G. W. Trucks, H. B. Schlegel, G. E. Scuseria, M. A. Robb, J. R. Cheeseman, V. G. Zakrzewski, J. A. Montgomery, Jr., R. E. Stratmann, J. C. Burant, S. Dapprich, J. M. Millam, A. D. Daniels, K. N. Kudin, M. C. Strain, O. Farkas, J. Tomasi, V. Barone, M. Cossi, R. Cammi, B. Mennucci, C. Pomelli, C. Adamo, S. Clifford, J. Ochterski, G. A. Petersson, P. Y. Ayala, Q. Cui, K. Morokuma, D. K. Malick, A. D. Rabuck, K. Raghavachari, J. B. Foresman, J. Cioslowski, J. V. Ortiz, A. G. Baboul, B. B. Stefanov, G. Liu, A. Liashenko, P. Piskorz, I. Komaromi, R. Gomperts, R. L. Martin, D. J. Fox, T. Keith, M. A. Al-Laham, C. Y. Peng, A. Nanayakkara, C. Gonzalez, M. Challacombe, P. M. W. Gill, B. Johnson, W. Chen, M. W. Wong, J. L. Andres, C. Gonzalez, M. Head-Gordon, E. S. Replogle, J. A. Pople, Gaussian, Inc.: Pittsburgh PA, **1998**.
[12] a) S. R. Langhoff, C. W. Bauschlicher, *J. Chem. Phys.* **1991**, *95*, 5882; b) P. J. Bruna, J. S. Wright, *J. Phys. Chem.* **1990**, *94*, 1774.
[13] D. F. Shriver, P. W. Atkins, *Inorganic Chemistry*, 3rd ed., W. H. Freeman and Company, New York, **1999**, p. 165.
[14] R. Hoffmann, *Angew. Chem.* **1982**; *94*, 725; *Angew. Chem. Int. Ed. Engl.* **1982**, *21*, 711.

Received: March 1, 2003 [Z736]

The Interplay of Aryl–Perfluoroaryl Stacking Interactions and Interstack Hydrogen Bonding in Controlling the Structure of a Molecular Cocrystal

Siwaporn Meejoo, Benson M. Kariuki, and Kenneth D. M. Harris*[a]

KEYWORDS:
aryl-perfluoroaryl interactions · hydrogen bonding · powder neutron diffraction · stacking interactions

One of the most intriguing molecular materials that has been studied in recent years is the 1:1 cocrystal formed between benzene and hexafluorobenzene,[1] the structure of which comprises stacks of alternating benzene and hexafluorobenzene molecules. Neither benzene nor hexafluorobenzene has a dipole moment, and in each case the lowest order multipole moment with nonzero value is the quadrupole. The quadrupoles of benzene and hexafluorobenzene are similar in magnitude but opposite in sign, and the fact that the benzene/hexafluorobenzene cocrystal forms an alternating stack structure can be rationalised on the basis of the favourable electrostatic (quadrupole–quadrupole) interaction between adjacent molecules along the stack. In contrast, the crystal structures of pure benzene[2] and pure hexafluorobenzene[3] both exhibit herringbone rather than stacked arrangements. Clearly the formation of homomolecular stacks of these molecules would correspond to unfavourable (repulsive) quadrupole–quadrupole interactions. The benzene/hexafluorobenzene cocrystal exhibits a range of interesting structural[4, 5] and dynamic[6, 7] properties, including reorientational motions of the benzene and hexafluorobenzene molecules, which are related to a series of low-temperature phase transitions. More recently, the alternating stack motif observed in this structure has been recognized[8–10] and exploited[11–19] as the basis for "crystal engineering" strategies involving molecules containing phenyl rings and heavily fluorinated phenyl rings (e.g., pentafluorophenyl). The expectation of such design strategies is that the phenyl and fluorinated phenyl rings should stack on top of each other, such that this structural motif has a controlling influence on the crystal packing.

Recently, we have extended this theme by exploring the formation and structural properties of cocrystals containing molecules of the types C_6H_5X and C_6F_5Y, in which X and Y are hydrogen bond donor and/or acceptor groups (and may be the same group). These studies have been motivated by a number of factors, including the aim of investigating the extent to which the preference to form alternating stacks of phenyl and

[a] *Prof. K. D. M. Harris, Dr. S. Meejoo, Dr. B. M. Kariuki*
School of Chemical Sciences, University of Birmingham
Edgbaston, Birmingham B15 2TT (United Kingdom)
Fax: (+44) 121-414-7473
E-mail: K.D.M.Harris@bham.ac.uk

 © 2003 Wiley-VCH Verlag GmbH & Co. KGaA, Weinheim DOI: 10.1002/cphc.200300762

UM00011654
NOVARTIS EXHIBIT 1517
Novartis v. Regents, IPR2023-01347
Page 400 of 4460

pentafluorophenyl rings remains a significant determinant of the crystal structure when significant hydrogen bonding functionality is also present. Thus, such systems provide a clear opportunity to assess the interplay between the formation of alternating stacks of the phenyl and pentafluorophenyl components and/or the formation of hydrogen bonding between these components, in controlling the crystal structure. Herein, we focus on a 1:1 cocrystal formed between phenol (C_6H_5OH; denoted P) and pentafluorophenol (C_6F_5OH; denoted PFP).

As described in the Experimental Section, a 1:1 cocrystal of P and PFP has been prepared successfully. Although powder neutron diffraction (discussed below) proved to be the essential technique allowing details of the structure of this cocrystal to be elucidated, our initial structural characterization involved single crystal X-ray diffraction (at 178 K). The structure determined from the single-crystal X-ray data confirmed that the cocrystal contains stacks of alternating P and PFP molecules; thus, as anticipated, heteromolecular π-stacking, with its favourable electrostatic implications, is adopted. For the PFP molecules, however, assignment of the six substituents on the ring as F and/or OH could not be established unambiguously from the single-crystal X-ray data. At this stage, it was uncertain whether this is a manifestation of the very similar X-ray scattering properties of OH and F (OH and F have the same total number of electrons), or whether it arises from orientational disorder of the PFP molecules, such that there is partial occupancy of both OH and F on each substituent position in the average crystal structure. Thus, the existence and nature of hydrogen bonding between stacks could not be established from the single-crystal X-ray diffraction data. To resolve these issues, powder neutron diffraction was carried out, recalling that OH and F are readily distinguished on the basis of their neutron scattering properties. The structure of the P/PFP cocrystal was refined from the powder neutron diffraction data using the Rietveld method (Figure 1). As discussed in the Experimental Section, various disorder models for the PFP molecules were considered, with refinement of the OH and F occupancies at each substituent position. The results lead to an ordered model in which the OH group of each PFP molecule occupies one specific substituent position.

In the crystal structure (Figure 2), there are three independent P molecules and three independent PFP molecules in the asymmetric unit, which corresponds to three crystallographically independent types of stack. A given stack contains only one type of P molecule and one type of PFP molecule. The periodic repeat along each stack is 7.21 Å at 4 K; this indicates a strong interaction along the stacking direction (the corresponding distance in benzene/hexafluorobenzene is 7.43 Å at 4 K). As shown in Figure 2, the relative orientations of the P and PFP molecules in the three types of stack are different. In one case (stack A), the relative orientations of adjacent molecules in the stack are close to eclipsed, whereas the other two cases (stacks B

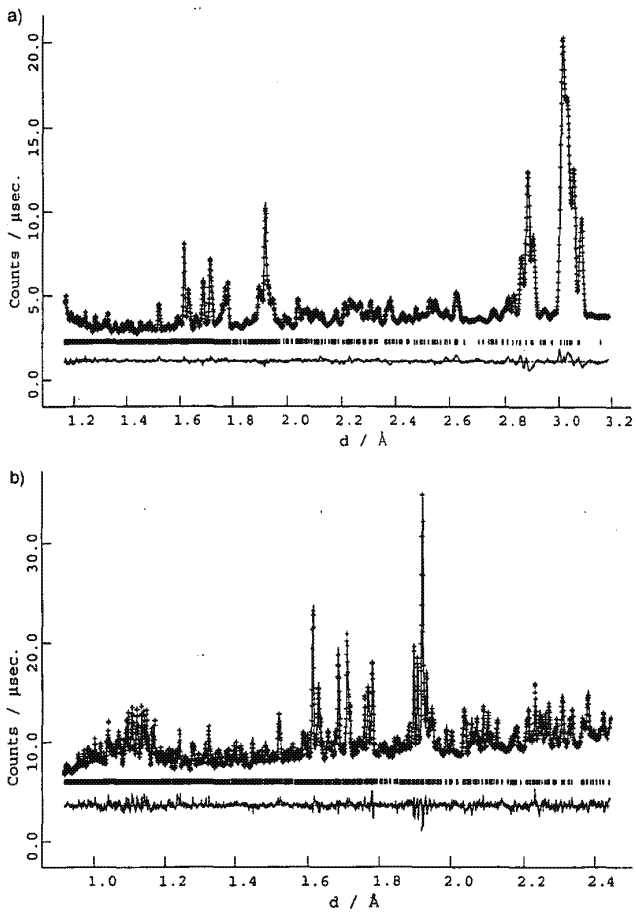


Figure 1. Powder neutron diffraction profiles for the Rietveld refinement of the P/PFP cocrystal at 4 K: a) data recorded at Bragg angle 89.58°, b) data recorded at Bragg angle 168.33°. The calculated powder diffraction profile is for the final refined crystal structure.

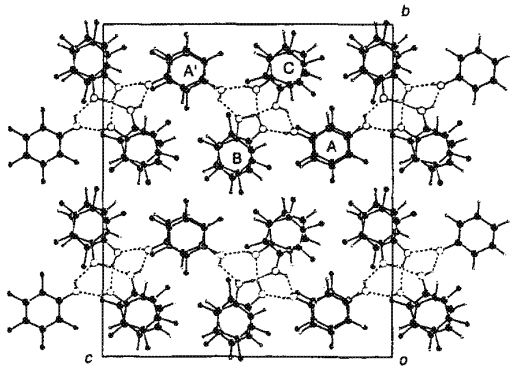


Figure 2. Crystal structure of the P/PFP cocrystal, determined from powder neutron diffraction data at 4 K, viewed along the stacking axis (a axis). Hydrogen atoms of the OH groups are shown only for the hydrogen-bonding arrangement of higher population.

 © 2003 Wiley-VCH Verlag GmbH & Co. KGaA, Weinheim

UM00011655
NOVARTIS EXHIBIT 1517
Novartis v. Regents, IPR2023-01347
Page 401 of 4460

and C) are more staggered.[20] The formation of different relative orientations of the molecules within the different stacks suggests that the relative orientations are governed by the formation of interstack interactions (hydrogen bonding; see below), rather than the formation of an optimal relative orientation with respect to intrastack interactions.

As shown in Figure 2, O–H···O hydrogen bonds are formed between stacks and are exclusively heteromolecular in nature (i.e., involving a P molecule and a PFP molecule). The hydrogen-bonding motif (Figure 3) comprises a closed loop involving six

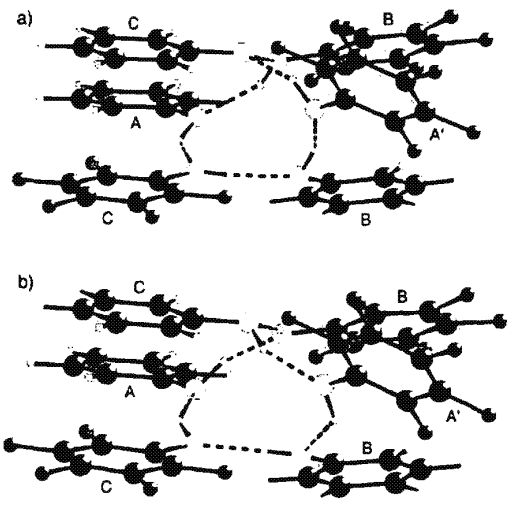


Figure 3. The six molecules involved in a hydrogen-bonded loop in the P/PFP cocrystal at 4 K, showing the two different hydrogen-bonding arrangements: a) lower population, and b) higher population.

different OH groups from alternating P and PFP molecules (the loop appears as a figure-of-eight in the projection in Figure 2); thus, each P molecule and each PFP molecule acts as both a donor and an acceptor for an O–H···O hydrogen bond. The hydrogen-bonded loop involves the six independent molecules in the asymmetric unit, and the loop itself therefore has no symmetry. The hydrogen-bonded loop involves only interstack hydrogen bonds, and comprises molecules from four stacks: two stacks of type A (denoted A and A' in Figure 2), one stack of type B and one stack of type C, with connectivity P(A)···PFP(B)···P(C)···PFP(A')···P(B)···PFP(C)···P(A). The group of four stacks involved in forming each hydrogen-bonded loop is evident in Figure 2. The stacks of type A effectively bridge two adjacent loops. From the powder neutron diffraction refinement, the H atom of each OH group is disordered between two positions, corresponding to two different hydrogen-bonding arrangements ("clockwise" and "anticlockwise") within the loop (Figure 3). These two hydrogen-bonding arrangements are not related by symmetry, and may therefore have different energies and hence different populations. The occupancies of the H atoms in each hydrogen bonding arrangement were refined (subject to the constraint that all H-atom positions in one arrangement have the same occupancy x_H and all H-atom positions in the other arrangement have occupancy $1-x_H$). As shown in Table 1, there is a significant population of both hydrogen-bonding arrangements at all temperatures studied. While the results suggest that there is a small systematic shift in the population ratio as a function of temperature, the changes in the relative populations as a function of temperature are not significantly larger than the estimated experimental errors in the refined values of the occupancy variable x_H, and independent experimental evidence (for example from solid state NMR studies) would be necessary before assigning a physical interpretation to the temperature dependence of x_H. Within the hydrogen-bonded loops, the H···O distances range from 1.75 to 1.99 Å and the O–H···O angles range from 128 to 171°, and thus some of the hydrogen bonds are comparatively long and nonlinear. The fact that the phenyl–pentafluorophenyl stacking is close to optimal geometry, but the interstack O–H···O hydrogen bonding deviates significantly from optimal geometry, may suggest that the former is the primary determinant of the structure of the P/PFP cocrystal.

From the powder neutron diffraction refinements, there are no significant structural changes in the temperature range 4 K to 200 K (apart from lattice contraction upon cooling). The lattice contraction upon cooling is not significantly anisotropic, with comparable coefficients of thermal expansion parallel and perpendicular to the direction of the stacks (Table 1).

In summary, the structure of the P/PFP cocrystal demonstrates the preferential formation of alternating stacks of P and PFP molecules together with an intricate interstack hydrogen-bonding arrangement comprising a closed loop of the OH groups of six molecules (from four different stacks), with OH groups from P and PFP molecules alternating within the loop. The H atom of each OH group is disordered between two sites, representing two different hydrogen-bonding arrangements within the loop. Although the interstack hydrogen-bonding arrangement allows each OH group to serve both as a hydrogen-bond acceptor and as a hydrogen-bond donor, the O–H···O hydrogen bonds tend to deviate from optimal geometry. We emphasise that the use of neutron diffraction was essential in order to characterise the

Table 1. Relevant crystallographic data for the P/PFP cocrystal, established from the powder neutron diffraction refinements at different temperatures.

T [K]	a [Å^{-1}]	b [Å^{-1}]	c [Å^{-1}]	β [°]	V [Å^{-3}]	R_p [%]	R_{wp} [%]	x_H
4	7.2114(1)	22.8633(3)	19.9985(2)	91.140(1)	3296.62(6)	2.11	2.36	0.60(2)
50	7.2225(1)	22.8789(3)	20.0146(2)	91.092(1)	3306.66(6)	2.05	2.35	0.56(2)
100	7.2531(1)	22.9178(3)	20.0554(2)	90.974(1)	3333.21(6)	1.77	2.02	0.50(2)
150	7.2960(1)	22.9745(4)	20.1161(3)	90.827(2)	3371.58(9)	2.17	2.52	0.40(3)
200	7.3226(1)	22.9984(3)	20.1344(2)	90.717(1)	3390.53(6)	1.93	2.10	0.38(2)

 © 2003 Wiley-VCH Verlag GmbH & Co. KGaA, Weinheim

UM00011656
NOVARTIS EXHIBIT 1517
Novartis v. Regents, IPR2023-01347
Page 402 of 4460

structural properties of this material. We are currently employing solid-state NMR techniques to assess whether the disorder in the hydrogen-bonding arrangement is static or dynamic in character.

Experimental Section

In general, the P/PFP cocrystal (melting point determined here by DSC to be 316 K) was prepared by cooling a liquid mixture comprising a 1:1 molar ratio of P and PFP. A single crystal suitable for single-crystal X-ray diffraction studies was obtained by chance during a low-temperature powder X-ray diffraction study (involving cooling the liquid mixture to 60 K at low pressure over a period of 24 h). The crystal was mounted at 278 K in a cold room to avoid melting. Single-crystal X-ray diffraction data were recorded on a Rigaku R-Axis IIc diffractometer with a Mo rotating anode source and image plate detector. Crystal size $1.2 \times 0.6 \times 0.8$ mm^3; $T = 178$ K; $\lambda = 0.71069$ Å; monoclinic, Cc; $a = 7.3153(3)$, $b = 23.0138(1)$, $c = 20.1347(1)$ Å, $\beta = 90.628(4)°$; $V = 3389.5(3)$ Å^3; $Z = 12$. The structure was solved using SHELXS86[21] and refined using SHELXL93[22] ($R_1 = 5.21$; $R_w = 23.17$ %). For all P molecules, the position of the OH group was clearly established. The substituent positions of the PFP molecules were also readily established, but the assignment of each substituent as F or OH could not be made.

Time-of-flight powder neutron diffraction data were recorded for a deuterated sample (C_6D_5OD/C_6F_5OH) of the P/PFP cocrystal at 4, 50, 100, 150 and 200 K using the high-resolution powder neutron diffractometer HRPD[23] at the ISIS neutron spallation source (Rutherford Appleton Laboratory). To prepare the sample, an equimolar mixture of C_6D_5OD and C_6F_5OH was cooled from 323 to 293 K over 10 h under a dry nitrogen atmosphere (note that H/D exchange between the OD group of C_6D_5OD and the OH group of C_6F_5OH may occur during this process). After collection of the sample, the material was stored below 277 K and transferred (in a cold room at ca. 273 K) to the cylindrical vanadium sample holder for the neutron diffraction experiments. The powder neutron diffraction data were recorded in the range 30–130 ms (0.83–3.19 Å) over 10 h and binned in time channels of $\Delta t/t = 10^{-4}$. Data were recorded simultaneously on two detector banks focused at Bragg angles of 89.58 and 168.33°. Rietveld refinement (space group Cc) was carried out simultaneously on both data sets using the GSAS program,[24] starting from the structural model determined from the single-crystal X-ray diffraction data. Bond length, bond angle and planar restraints were applied. To elucidate the positions of OH and F substituents for each PFP molecule in the asymmetric unit, both O and F were introduced at each substituent position j on the molecule ($j = 1, \ldots, 6$), with fractional occupancies x_j and $1\text{-}x_j$, respectively, and with the constraints $\Sigma x_j = 1$ and $\Sigma (1\text{-}x_j) = 5$ (note: $0 \le x_j \le 1$). The x_j were refined independently for each PFP molecule, with the O occupancy x_j found to be substantially higher for one substituent position in each molecule, which suggests that the OH group may be located with full occupancy in this position. Subsequent refinement confirmed this ordered model. The possibility that H/D exchange occurs between the C_6D_5OD and C_6F_5OH molecules during cocrystal formation was incorporated into the refinement by representing each hydroxy group as OH_yD_{1-y} ($0 \le y \le 1$). In all cases, the refined value of y was very close to 0.5, and was fixed at 0.5 for all hydroxy groups in the final refinements. Finally, each hydroxy H/D atom was allowed to be disordered between two sites, corresponding to the two different hydrogen bonding arrangements within the loop (Figure 3). For each hydrogen-bonding arrangement, the H/D occupancies were refined subject to the constraint that all H/D positions in one arrangement have the same occupancy x_H and all H/D positions in the other arrangement have occupancy $1\text{-}x_H$. All H/D sites were given a common isotropic displacement parameter (which was refined). The refined values of x_H are shown in Table 1.

We are grateful to the EPSRC and CLRC for the award of beam-time at the ISIS Neutron Spallation Source (Rutherford Appleton Laboratory), and to the Development and Promotion of Science and Technology Talents Project (DPST), Thailand, for financial support (studentship to S.M.).

[1] J. H. Williams, *Acc. Chem. Res.* **1993**, *26*, 593.
[2] G. E. Bacon, N. A. Curry, S. A. Wilson, *Proc. R. Soc. London Ser. A.* **1964**, *279*, 98.
[3] N. Boden, P. P. Davis, C. H. Stam, G. A. Wesselink, *Mol. Phys.* **1973**, *25*, 81.
[4] J. H. Williams, J. K. Cockcroft, A. N. Fitch, *Angew. Chemie* **1992**, *104*, 1666; *Angew. Chemie Int. Ed. Engl.* **1992**, *31*, 1655.
[5] S. T. Bramwell, J. H. Williams, *J. Chem. Soc. Faraday Trans.* **1992**, *88*, 2721.
[6] J. H. Williams, *Mol. Phys.* **1991**, *73*, 113.
[7] M. J. Duer, *J. Chem. Soc. Faraday Trans.* **1993**, *89*, 823.
[8] G. W. Coates, A. R. Dunn, L. M. Henling, D. A. Dougherty, R. H. Grubbs, *Angew. Chemie* **1997**, *109*, 290; *Angew. Chemie Int. Ed. Engl.* **1997**, *36*, 248.
[9] G. W. Coates, A. R. Dunn, L. M. Henling, J. W. Ziller, E. B. Lobkovsky, R. H. Grubbs, *J. Am. Chem. Soc.* **1998**, *120*, 3641.
[10] M. Weck, A. R. Dunn, K. Matsumoto, G. W. Coates, E. B. Lobkovsky, R. H. Grubbs, , *Angew. Chemie* **1999**, *111*, 2909; *Angew. Chemie Int. Ed.* **1999**, *38*, 2741.
[11] C. Y. Dai, P. Nguyen, T. B. Marder, A. J. Scott, W. Clegg, C. Viney, *Chem. Commun.* **1999**, 2493.
[12] C. J. Aspley, C. Boxwell, M. L. Buil, C. L. Higgitt, C. Long, R. N. Perutz, *Chem. Commun.* **1999**, 1027.
[13] F. Ponzini, R. Zagha, K. Hardcastle, J. S. Siegel, *Angew. Chemie* **2000**, *112*, 2413; *Angew. Chemie Int. Ed.* **2000**, *39*, 2323.
[14] M. D. Blanchard, R. P. Hughes, T. E. Concolino, A. L. Rheingold, *Chem. Mater.* **2000**, *12*, 1604.
[15] H. Adams, J. L. J. Blanco, G. Chessari, C. A. Hunter, C. M. R. Low, J. M. Sanderson, J. G. Vinter, *Chem. Eur. J.* **2001**, *7*, 3494.
[16] W. J. Feast, P. W. Lovenich, H. Puschmann, C. Taliani, *Chem. Commun.* **2001**, 505.
[17] J. C. Collings, K. P. Roscoe, R. L. Thomas, A. S. Batsanov, L. M. Stimson, J. A. K. Howard, T. B. Marder, *New J. Chem.* **2001**, *25*, 1410.
[18] A. S. Batsanov, J. A. K. Howard, T. B. Marder, E. G. Robins, *Acta Crystallogr. Sect. C* **57**, **2001**, 1303.
[19] A. S. Batsanov, J. C. Collings, J. A. K. Howard, T. B. Marder, D. F. Perepichka, *Acta Crystallogr. Sect. C* **2001**, *57*, 1306.
[20] The angles between the C–O bonds of adjacent molecules, when viewed in projection along the stack axis (see Figure 2), are approximately 120° for stack A and 38 and 42° for stacks B and C respectively (for comparison, in the benzene/hexafluorobenzene cocrystal, the angle between CH and CF bonds of adjacent molecules along the stack is 19.1°). CCDC 197491 contains the supplementary crystallographic material for this paper. These data can be obtained free of charge via http://www.ccdc.cam.ac.uk/conts/retrieving.html (or from the Cambridge Crystallographic Data Centre, 12 Union Road, Cambridge CB2 1EZ, UK; fax (+44)1223-336-033; or deposit@ccdc.cam.ac.uk).
[21] G. M. Sheldrick, SHELXS86, Program for the Solution of Crystal Structures, University of Göttingen, Germany, **1986**.
[22] G. M. Sheldrick, SHELXL93, Program for the Refinement of Crystal Structures, University of Göttingen, Germany, **1993**.
[23] R. M. Ibberson, W. I. F. David, K. S. Knight, *Rutherford Appleton Laboratory RAL-92-031*, **1992**.
[24] A. C. Larson, R. B. Von Dreele, *Los Alamos Laboratory Report No. LA-UR-86-748*, **1987**.

Received: March 25, 2003 [Z 762]

 © 2003 Wiley-VCH Verlag GmbH & Co. KGaA, Weinheim

UM00011657
NOVARTIS EXHIBIT 1517
Novartis v. Regents, IPR2023-01347
Page 403 of 4460

Improving the Filterability and Solid Density of Ranitidine Hydrochloride Form 1

MAHMOUD MIRMEHRABI,[1] SOHRAB ROHANI,[1] K.S. KESHAVA MURTHY,[2] BRUNO RADATUS[2]

[1]Department of Chemical and Biochemical Engineering, The University of Western Ontario, London, Ontario, N6A 5B9, Canada

[2]Brantford Chemicals Inc., 34 Spalding Drive, Brantford, Ontario, N3T 6B8, Canada

Received 30 September 2003; revised 23 December 2003; accepted 2 February 2004

Published online 22 April 2004 in Wiley InterScience (www.interscience.wiley.com). DOI 10.1002/jps.20074

ABSTRACT: Ranitidine hydrochloride Form 1 produced by the original method (Price et al., 1978 US patent) has poor filtration and drying characteristics, which make it less desirable commercially in comparison with Form 2. This article shows that the operating parameters have significant influence on the final properties of Form 1. In terms of filterability and solid bulk density, it was found that at a higher temperature (~48°C), the viscosity of the slurry decreased and improved product quality as compared with operating at room temperature (~25°C). It was found that the rapid addition of acid to the ranitidine base increased product density but led to higher residual solvent inclusion. The presence of excess ranitidine base in the solution and also the manner of reactant addition had a significant influence on the onset of nucleation and the rate of crystallization. The best results in terms of filterability and bulk solid density were obtained using an initial pH of 5.3 and then increasing it to 6.3–6.4 after the onset of nucleation.
© 2004 Wiley-Liss, Inc. and the American Pharmacists Association J Pharm Sci 93:1692–1700, 2004
Keywords: ranitidine hydrochloride; Form 1; solid bulk density; quality improvement; filterability

INTRODUCTION

Ranitidine hydrochloride (RAN-HCl) is one of the most frequently prescribed drugs in North America. This drug is used to block acid production in the stomach, which is implicated in indigestion, acid reflux, heartburn, ulcers, and Zollinger-Ellison syndrome. RAN-HCl works by blocking histamine H_2 receptor in the gut.[1] The chemical formula of RAN-HCl is $C_{13}H_{22}N_4O_3S \cdot HCl$ and the structure of one of the possible tautomers is shown in Scheme 1.[2]

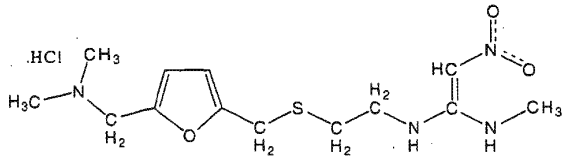
RAN-HCl is the product of reaction between HCl and RAN base (RAN-B). RAN-B, a pale-yellow to off-white powder, has two pK_a values[3] of 8.20 and 2.30, which means that it can react with more than one proton. During HCl addition, the first HCl molecule reacts with the nitrogen of the dimethylamino group, and as the pH decreases, the second HCl reacts with the ethenediamine where C-protonation rather than N-protonation occurs.[4] The use of excess hydrogen chloride in the reaction may result in the production of RAN-2HCl. Because of the very poor solubility of RAN-2HCl in organic solvents, it is very difficult to separate it from the desired RAN monohydrochloride. If the RAN monohydrochloride is contaminated with RAN-2HCl, this contaminant will rapidly absorb moisture from the atmosphere and cause the acidity of the mixture to increase. The stability will also suffer because of the existence of RAN-2HCl.[5]

RAN-HCl has two polymorphic forms and also several pseudopolymorphic forms, which contain

Correspondence to: Sohrab Rohani (Telephone: +519-661-4116; Fax: +519-661-3498; E-mail: rohani@eng.uwo.ca) or K. S. Keshava Murthy (Telephone: +519-756-8942; Fax: +519-753-3051; E-mail: kmurthy@brantfordchemicals.com)

Journal of Pharmaceutical Sciences, Vol. 93, 1692–1700 (2004)
© 2004 Wiley-Liss, Inc. and the American Pharmacists Association

UM00011658
NOVARTIS EXHIBIT 1517
Novartis v. Regents, IPR2023-01347
Page 404 of 4460



Scheme 1.

solvent.[6] In 1978, Allen and Handbury Ltd. of the Glaxo group[7] disclosed a RAN-HCl production method (Example 32 of US patent 4,128,658), which led to the formation of Form 1 RAN-HCl.

In 1985, the Glaxo group was issued a patent[8] for the production of a new polymorphic form of RAN-HCl which was designated as Form 2. They claimed that the new form did not have the disadvantages of original Form 1, namely, poor filtration and drying characteristics. Many pharmaceutical companies filed patents[9–13] in the 1990s to produce Form 1 after the expiration of the 1978 patent.

A reading of the Glaxo patent and the work of Murthy et al.,[10] suggest that an important requirement for obtaining Form 2 is the presence of water and for Form 1 is the absence of water. Mirmehrabi et al.[14] also showed that significant amounts of strongly polar solvents such as methanol would favor the production of Form 2. They also showed the importance of hydrogen bonding on the crystal growth of Form 2 and its inhibition on Form 1.

Figure 1 shows the crystal shapes of the two RAN-HCl polymorphs that are obtained by following the above two Glaxo procedures. Form 1 consists of very tiny crystals with a size in the range of 1–5 μm, which agglomerate and form bigger particles. This polymorph is fluffy, has a poor filtration characteristic, and relatively low solid bulk density ranging from 0.1 to 0.15 g/mL. Form 2, however, has big individual crystals with size of 10–100 μm, good filtration properties, and relatively high solid bulk density of >0.3 g/mL. More recently, Brantford Chemicals Inc.[10] has produced Form 1 RAN-HCl with a minimum bulk density of 0.23 g/mL and improved filtration and drying characteristics. Building on the results of the researchers at Brantford Chemicals Inc., this article presents further improvement in the quality of RAN-HCl Form 1 in terms of filterability and bulk solid density. It has been found, in this study, that the quality of RAN-HCl Form 1 is a strong function of the operating conditions such as temperature, pH, and pattern of reactants addition.

MATERIALS AND METHODS

Materials

RAN free-base and anhydrous hydrogen chloride–isopropanol (HCl/IPA) solution were produced in Brantford Chemicals Inc. facilities (Brantford, Ontario) and other chemicals were purchased from Sigma-Aldrich (Milwaukee, WI).

Experimental Setup

The experimental setup is shown in Figure 2. Crystallization was performed in a 250-mL Bellco jacketed flask (Vinelan, NJ) in which a Neslab RTE digital plus 740 bath circulator (Portmouth,

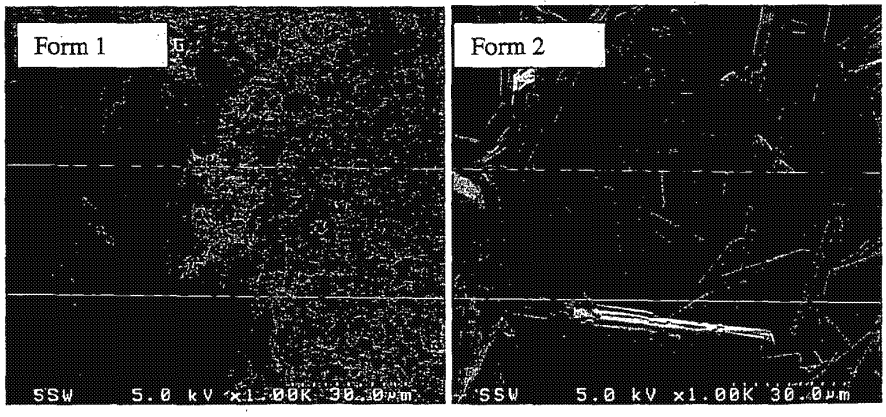


Figure 1. SEM image of RAN-HCl Forms 1 and 2.

UM00011659
NOVARTIS EXHIBIT 1517
Novartis v. Regents, IPR2023-01347
Page 405 of 4460

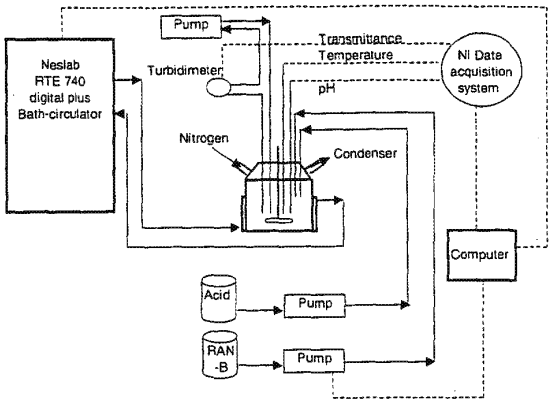


Figure 2. Diagram of the experimental setup.

NH) with corresponding remote control software provided heating and cooling. A Teflon-coated thermocouple was used for reading the temperature (Labcore, Concord, Ontario), an epoxy-coated pH meter (Oakton, Vernon Hills, IL) with temperature compensator was used for reading the pH, and a turbidimeter (Hammond Manufacturing, Guelph, Ontario) was used for monitoring the nucleation onset and, qualitatively, the rate of crystallization. Masterflex pumps (Labcore) were used for chemical injection and circulating the crystallization media through turbidimeter photocell. For mixing, a top-mounted two-bladed flat electromagnetically driven stirrer was employed. The stirrer blades were Teflon-coated in order to reduce the corrosion and particle breakage. For monitoring and controlling, a National Instrument data acquisition system (Austin, TX) as an interface between the system and computer and version 6*i* Labview™ software (Austin, TX) were employed. RAN-B is a base and HCl is an acid so that the controller adjusted the flow of RAN-B dissolved in IPA to control the solution pH using a proportional-integral-derivative controller. The logic control program for these experiments was written in Labview™ using the wire program language. For filtration, a vacuum pump (Barnant, Barrington, IL) was used to be consistent for all experiments. The vacuum gauge pressure was at −67 kPa during filtration. Grade GF/D glass microfiber filters (VWR, Mississauga, ON) with 2.7-μm pore size and 7-cm diameter were used. The mass of dry substance of RAN-HCl for all experiments was about 22 g. The filtration time was also considered to be 15 min to be able to compare the filterability of different products.

Analytical

A field emission scanning electron microscope (Hitachi S-4500) was used for morphological studies. A Bruker solid-state Fourier transformation infrared (Milton, Ontario) spectrometer was used to determine the identity of each polymorph. The samples were analyzed by Fourier transform infrared in transmission mode through a diamond window. The peak at 1045 cm^{-1}, which is a characteristic peak of Form 2, was considered for identity analysis of each polymorphic form using the standard spectra. A Mettler Toledo Karl-Fischer DL38 (London, Ontario) was used to measure the water content of the solution. A Logan Instrument TAP-2 density meter (Edmonton, Alberta) was used to measure bulk and tap densities of the product. Headspace gas chromatography (Varian CP-3800, Mississauga Ontario) was used to determine the residual solvent content of the product. An HPLC 330 (Varian) was used for purity analysis of the product.

Cake dry substance was calculated from the following equation:

$$DS\% = (W_{\text{drycake}}/W_{\text{wetcake}}) \times 100$$

where W_{drycake} is the weight of the oven-dried product and W_{wetcake} is the weight of the cake after filtration.

Experimental Procedure

In all experiments, 20 g of RAN-B was used. The total amount of IPA used including HCl/IPA was 200 mL (IPA/RAN-B = 10 mL/g). The amount of HCl/IPA (18.6 wt % acid) was one equivalent to RAN-B. The RAN-B/IPA solution was filtered using celite before each experiment. After filtrating the crystallized mixture, the cake was washed twice with 20 mL of IPA, the crystals were vacuum dried at 45°C, and then analyzed. In all steps, care was taken to prevent entering any kind of impurities into the system. For production of Form 1, the procedure of US patent 4,128,658 was adopted.[7]

To determine the effects of temperature, solvent, manner and the rate of acid and RAN-B addition, and pH, the following series of experiments were performed. All the experiments were conducted unseeded. After the completion of each experiment, the slurry was cooled down from the experimental operating temperature to 25°C in 1/2 h using a natural cooling policy:

1. Rapid addition of HCl/IPA to RAN-B/IPA solution at 25° and 42°C, maintaining at 25° and 48°C for 2 h.

UM00011660
NOVARTIS EXHIBIT 1517
Novartis v. Regents, IPR2023-01347
Page 406 of 4460

2. Gradual addition (2–6 h) of HCl/IPA to RAN-B/IPA solution at 48°C.
3. Gradual addition (2–6 h) of HCl/IPA and RAN-B/IPA concurrently to IPA at 48°C and maintaining pH. The selected pH values were 5.0, 5.5, 6.0, 6.3, and 6.5.
4. Gradual addition (2–6 h) of HCl/IPA and RAN-B/IPA concurrently to IPA at 48°C and pH of 5.30, and increasing the pH to 6.30–6.40 after nucleation.
5. Gradual addition (2.5 h) of HCl/IPA and RAN-B/*n*-propanol concurrently to *n*-propanol at 48°C keeping pH at 6.0.
6. Rapid addition similar to case #1 and also gradual addition of HCl/IPA and RAN-B/methyl isobutyl ketone (MIBK) concurrently to MIBK at 48°C keeping the pH at 6.0.
7. Gradual addition (2.7 h) of HCl/IPA and RAN-B/IPA concurrently to 50:50 IPA/ethanol at 48°C keeping the pH at 6.0.

RESULTS AND DISCUSSION

Case #1, Rapid Addition of HCl/IPA to RAN-B in IPA

Two sets of experiments were conducted in this case with the initial temperatures at 25° and 42°C, respectively. The reaction between HCl and RAN-B is exothermic. Therefore, after the rapid addition of acid to the RAN-B/IPA solution, the temperatures increased from the initial temperatures of 25° to 35°C and from 42° to 50°C in two experiments. Using these temperature changes and the heat capacity of the solutions, the heat of reaction was calculated to be equal to 193 J/g RAN-B. As soon as the HCl was added, both pH and transmittance decreased from 8.0–9.0 and 100% to <5.0 and 10%, respectively, and the system became cloudy because of the nucleation. Crystallization of Form 1 at 25°C gave a slurry that was more viscous and sticky compared with cases at higher temperatures and led to a product that had poor filtration and drying characteristics as indicated by a long filtration time of 5 h and 22% dry substance. The product had a solid bulk density of 0.20 g/mL. The product at higher temperature had a higher bulk density (0.24 g/mL) and a cake dry substance of >40% after 15 min of filtration. Based on these two experiments, it was concluded that the higher temperature results in better quality product. For further experiments, a temperature of 48°C was selected. Crystallization at higher temperatures such as at 75°C leads to degradation of the product (Murthy and Radatus. 2003. Unpublished work, Brantford Chemicals Inc.).

In general, in the case of rapid HCl/IPA addition to the RAN-B/IPA solution, pH of the solution decreased to about 3.90–4.50 and many tiny crystals formed. Rapid addition of one reactant increases the supersaturation and leads to excessive nucleation and inclusion of solvent and impurities. There is also a danger of local pH decrease, which enhances the production of RAN-2HCl. Thus, although the solid bulk density of Form 1 produced at the higher temperature was usually >0.23 g/mL, the risk of impurities and solvent inclusion was high and therefore the rapid addition of acid to the RAN-B/IPA solution should be avoided. At both temperatures, small particles agglomerated to form bigger particles but the lower temperature resulted in a spongier product. Figure 3a,b illustrate the scanning electron microscopy (SEM) images of the product of this experiment at 25° and 48°C, respectively. The SEM image of Form 1 produced by the original method[7] is shown in Figure 3c for comparison. The latter is very spongy and hygroscopic.

Case #2, Gradual Addition of HCl/IPA to RAN-B in IPA

In this case, nucleation began after the addition of about 30% of the stoichiometric amount (12.5 g) of HCl/IPA solution at a pH of about 6.3–6.4, irrespective of the rate of addition. No nucleation was observed at pH values higher than 6.4. Therefore, to initiate crystallization, pH had to be brought to <6.4.

In general, the bulk density of the particles produced by this method was in the range of 0.14–0.20 g/mL. Figure 3d illustrates leaf-like crystals obtained in this case.

Case #3, Gradual Addition of HCl/IPA and RAN-B/IPA with pH Control

In this case, all of RAN-B was dissolved in 65 mL of IPA and stored in a sealed graduated cylinder, which was connected to a pump. A controller was used to change the addition rate of RAN-B/IPA in order to maintain the pH of the solution at a constant value while HCl/IPA was added to the solution at a constant flow rate.

Nucleation started after the addition of about 9%, 10%, 15%, and 20% of the stoichiometric amount (12.5 g) of HCl/IPA solution at pH values

UM00011661
NOVARTIS EXHIBIT 1517
Novartis v. Regents, IPR2023-01347
Page 407 of 4460

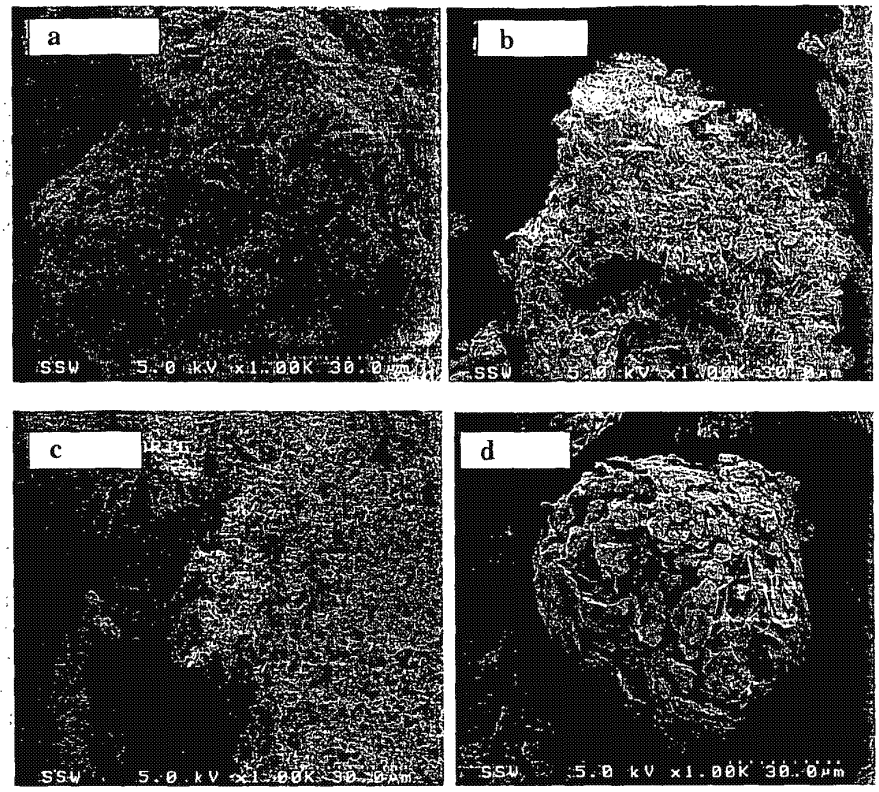


Figure 3. SEM images of the different experiments. Parts (a) and (b) are products of case 1, (c) shows the product of the original method,[7] and (d) is the product of case 2.

equal to 5.0, 5.5, 6.0, and 6.3, respectively. At these nucleation points, the consumed RAN-B amounts were 12%, 17%, 65%, and 88% of the total RAN-B to be charged to the reactor, respectively. The stoichiometric amount of HCl/IPA and RAN-B, which lead to the production of RAN-HCl in IPA, has a pH of about 4.0. Therefore, in all of the above cases, there was excess RAN-B in the solution.

Mirmehrabi et al.[15] reported that the solubility of RAN-HCl Forms 1 and 2 in IPA at 48°C are equal to 0.23 and 0.27 g solute/100 g solvent, respectively. Form 2 has higher solubility than Form 1. The solubility of RAN-HCl was found to be independent of pH.

Table 1 shows the conditions at the nucleation point at different pH values. Note that the amounts of acid and RAN-B have an important role on the onset of crystallization. We speculate that excess RAN-B, which leads to higher pH values, has an inhibitory effect on the formation of RAN-HCl clusters and consequently nucleation. Indeed, the big RAN-B molecules surround the individual RAN-HCl molecules by hydrogen bondings and prevent cluster formation that is the prerequisite for the formation of lasting nuclei. These hydrogen bonds occur between nitrogen and oxygen atoms of nitroethenediamine moiety and also polar hydrogen chloride molecule (in nonaqueous medium for the formation of Form 1).[14] At lower pH values, the amount of excess free RAN-B is less so that the nucleation starts sooner.

At the start of the experiment, the solution was clear and had maximum transmittance but as soon as crystallization started the turbidity of solution increased and consequently the transmittance decreased. Figure 4 shows the time and temporal profile of transmittance reduction in the system as a function of pH. Note that the pH is a result of the amount of acid and RAN-B in the solution. The figure shows that increasing the pH increases the induction time nonlinearly. At the same time, up to pH of 6.3, the rate of crystallization becomes slower and crystal quality (filtration and solid bulk density) improves. In the case of running the experiment at pH 6.5, all RAN-B was consumed before any nucleation occurred. At this time, just

UM00011662
NOVARTIS EXHIBIT 1517
Novartis v. Regents, IPR2023-01347
Page 408 of 4460

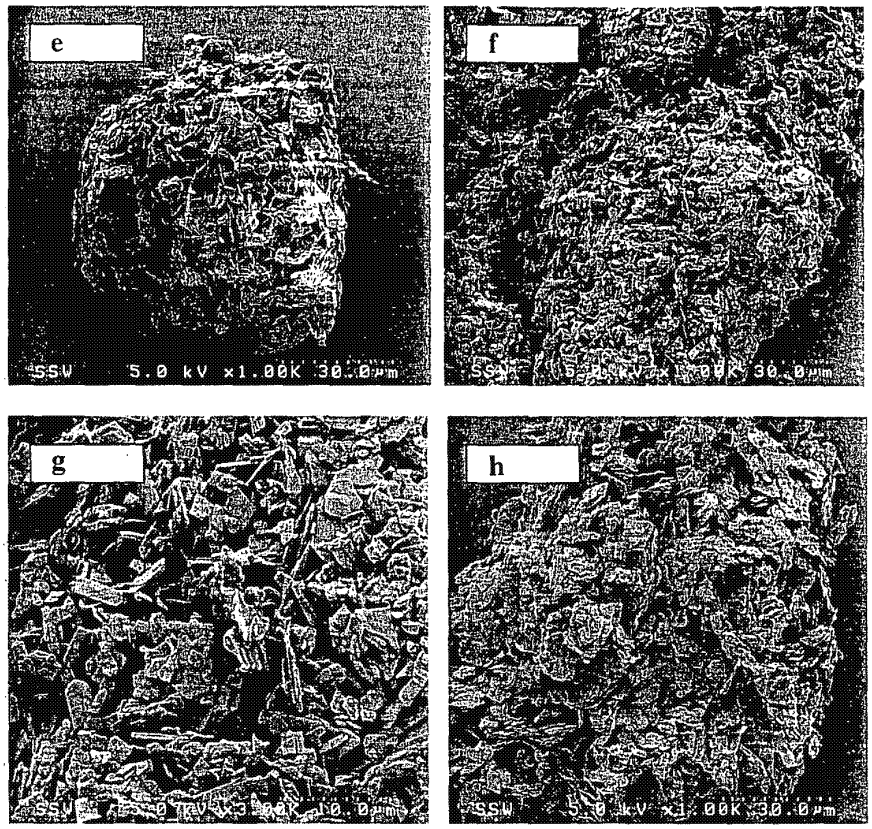


Figure 3. (*Continued*) Part (e) shows the product of case 3, (f) and (g) are two magnifications of the product of case 4, and (h) is the result of case 5.

30% of the acid had been used. Further addition of HCl/IPA decreased the pH of the solution and crystallization started at a pH of about 6.3. In general, no crystallization was observed at pH values higher than 6.4.

The rate of crystallization was the lowest at pH 6.30. In this experiment, as the process time increased, the solid bulk density also increased. Figure 3e illustrates the SEM image of the product of this experiment. The aspect ratio is lower than for the case of gradual HCl/IPA addition without pH control. The product slurry was not sticky and could be easily removed from the crystallization vessel.

Case #4, Gradual Addition of HCl/IPA and RAN-B with Optimal pH Control

The rationale was to begin the process at low pH of 5.3 (to initiate nucleation) and then increase the pH setpoint to a value between 6.3–6.4 to favor crystal growth. Figure 5 illustrates the profile of the first 100 min of this experiment recorded by the control system. As pH increased,

Table 1. Conditions at the Nucleation for Different pH Values

pH	IPA (g)	HCl (g)	RAN-B (g)	RAN-HCl Concentration, g/g Solvent (C)	Solubility, g/g Solvent (C^*)	$\frac{C - C^*}{C^*}$
5.0	113	0.21	2.4	0.0177	0.0023	6.7
5.5	115	0.23	3.4	0.0191	0.0023	7.3
6.0	135	0.35	13	0.0244	0.0023	9.6
6.3	145	0.46	17.6	0.0310	0.0023	12.5

UM00011663
NOVARTIS EXHIBIT 1517
Novartis v. Regents, IPR2023-01347
Page 409 of 4460

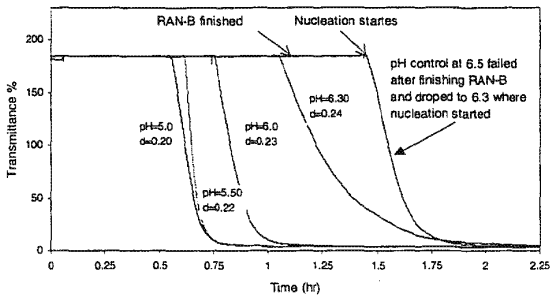


Figure 4. The effect of pH on nucleation time, rate of crystallization, and solid bulk density (d, g/mL).

the transmittance increased slightly because of the dissolution of some crystals due to the dilution.

In this method, nucleation began after the addition of about 10% of the stoichiometric amount (12.5 g) of HCl/IPA solution and the product had the highest solid bulk density with a maximum of 0.32 g/mL. The slurry was also not sticky and was easily removed from the crystallization vessel. The cake dry substance after 15 min of filtration was consistently >42%.

Figure 3f and g show two different magnifications of the SEM image of this product. Individual crystals were rectangular and more uniform compared with all other cases. They also did not agglomerate.

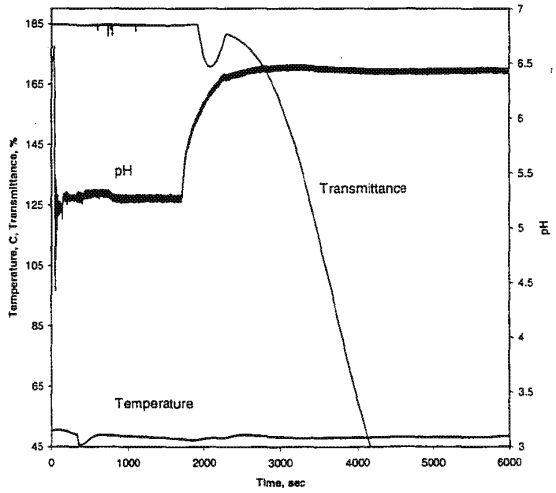


Figure 5. Gradual addition of HCl and RAN-B solutions to IPA at 48°C, nucleation at pH = 5.30, and process at pH 6.38.

Case #5, Gradual Addition of HCl/IPA and RAN-B to *n*-Propanol at pH 6.0

Nucleation began after the addition of about 62% of the HCl/IPA solution, which is four times more than the amount of HCl/IPA required when IPA was used as the solvent. The bulk density of this product was 0.14 g/mL, which is lower than the density of solids produced in case #3 using IPA (density = 0.23 g/mL). The slurry of this process was sticky. Figure 3h illustrates the SEM image of the agglomerated product of this experiment. The individual particles were very thin and flat.

Case #6, Rapid Addition with No pH Control and Gradual HCl/IPA and RAN-B/MIBK Addition in MIBK at pH 6.0

In these experiments, as soon as the crystallization began, the slurry became very sticky and gum-like, which attached to the probes, and the experiments had to be stopped.

Case #7, Gradual Addition of HCl/IPA and RAN-B/EtOH to Ethanol at pH 6.0

Nucleation began after about 30% of HCl/IPA was added. After the addition of 38% of HCl/IPA, the slurry became very viscous in such a way that the electromagnetic stirrer stopped. The product bulk solid density in this case was as low as 0.15 g/mL.

GENERAL CONSIDERATIONS

For constant pressure filtration, the following equations are applicable[16]:

$$t = \frac{\mu}{g_c(-\Delta P)}\left[\frac{c\alpha}{A}\left(\frac{V}{A}\right)^2 + R_m\frac{V}{A}\right] \qquad (1)$$

and

$$\alpha = \frac{k(1-\varepsilon)}{\varepsilon^3 \rho_p \phi^2} \qquad (2)$$

where t is the total filtration time, μ is the filtrate viscosity, ΔP is the overall pressure difference across the filter, c is a constant, α is the specific cake resistance, A is the cake area, V is the total volume of filtrate collected from the start of the filtration to time t, and R_m is the filter-medium resistance that is the same for all the performed experiments. k is a constant, ε is the cake porosity, ρ_p is the particle density, and ϕ is the particle sphericity.

UM00011664
NOVARTIS EXHIBIT 1517
Novartis v. Regents, IPR2023-01347
Page 410 of 4460

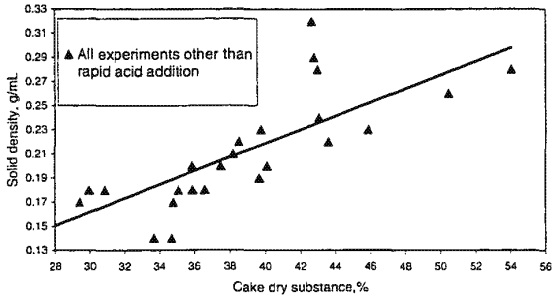


Figure 6. The general functionality of dry solid bulk density versus the cake dry substance.

In general, for the same filtration time at constant ΔP, the higher V results in more solvent removal and consequently higher dry substance. In all the performed experiments, the filtration time of 15 min, vacuum pressure of −67 kPa, filtration temperature of 25°C (to have the same filtrate viscosity), and the same type and size of filter paper were used to ensure reasonable comparison. The higher dry substance is interpreted as better filterability. Equation (1) also shows that the lower specific cake resistance, α, will result in better filterability. However, α is proportional to the inverse of particle density. Figure 6 shows the general relationship between the dry solid bulk density and the cake dry substance after filtration. From this graph, we speculate that for the same filtration conditions, the product with higher bulk solid density has a higher dry substance and also better filterability.

Table 2 presents the average bulk solid density and the ratio of tap to bulk density of the product in various cases studied in this work. The bulk density of the optimal process is more and the ratio of tap to bulk densities is closer to unity.

Figure 7 illustrates the dependence of solid bulk density on acid addition time for different cases. In general, the solid bulk density is proportional to the acid addition time. The experiments with an initial pH of 5.30 followed by an increase in pH to between 6.30 and 6.40 after nucleation, led to the highest bulk density. Some of the lowest bulk density results belong to the case with gradual addition of HCl/IPA to the RAN-B/IPA solution without pH control (case #2). However, the product belonging to the case of rapid acid addition at higher temperatures had good bulk density but the residual solvent was close to the maximum allowable limit of 5000 ppm (International Conference on Harmonization).[17] In contrast, gradual acid addition resulted in significantly lower residual solvent contents. The best results were obtained in case #4, in which the residual IPA solvent was <400 ppm.

It was found in this study that an operating pH of >4.0 is safe for preventing the production of RAN-2HCl. The high-performance liquid chromatography analysis of the product showed 98.8% purity for RAN-HCl in the final product. The remainder can be solvent inclusion, unreacted RAN-B, and undetected impurities.

CONCLUSIONS

Form 1 RAN-HCl that has been produced by the original method[7] is fluffy and spongy with poor filtration and drying characteristics. This study showed that the morphology, bulk and tap densities, and filtration characteristics are functions of process operating conditions. Higher temperatures resulted in better filterability, solid bulk density, and easier operation. Among the studied solvents, IPA led to the least slurry viscosity. Rapid acid addition led to spontaneous nucleation, agglomeration, and formation of bigger porous particles. The presence of excess RAN-B in the solution and also the manner of reactant

Table 2. Average Bulk Solid Density, the Ratio of Tap/Bulk Density, and Other Process Conditions

Regime and Solvent	Case No.	Average Bulk Density (g/mL)	Average Tap/Bulk Density Ratio	Slurry	DS%
Rapid acid addition, IPA	1	0.24 (±0.02)	1.22 (±0.16)	Sticky	40
Gradual acid addition, IPA	2	0.19 (±0.01)	1.34 (±0.08)	Not sticky	39
Constant pH, IPA	3	0.23 (±0.01)	1.31 (±0.09)	Not sticky	>40
Optimal process, IPA	4	0.30 (±0.02)	1.21 (±0.04)	Not sticky	>42
Constant pH, *n*-propanol	5	0.14 (±0.01)	1.97 (±0.11)	Sticky	33
Constant pH, MIBK	6	—	—	Gum-like	—
Constant pH, ethanol	7	0.15 (±0.01)	1.40 (±0.03)	Sticky and very viscous	28

UM00011665
NOVARTIS EXHIBIT 1517
Novartis v. Regents, IPR2023-01347
Page 411 of 4460

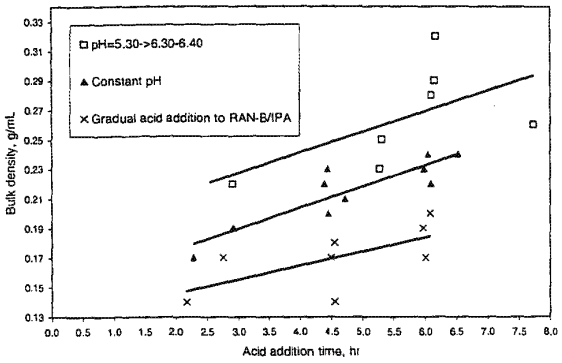


Figure 7. Effect of acid addition time on the bulk density of the product.

addition had significant influence on the onset of nucleation, rate of crystallization, and also quality of the product in terms of filterability and solid density. It was shown that starting with an initial pH of 5.30 followed by increasing the pH to 6.30–6.40 after the nucleation, resulted in the best filtration and solid density among the performed experiments. The rate of acid addition was also important. Slower rate of addition improved the product quality.

ACKNOWLEDGMENTS

The authors thank Ms. Luisa Grappolini for help in the analytical works.

REFERENCES

1. Canadian pharmacists association. 2000. Ranitidine HCl. In: Compendium of pharmaceuticals and specialties, 35th ed. Toronto: Webcom Limited, pp 1772–1774.
2. Hohnjec M, Kuftinec J, Malnar M. 1986. Ranitidine. In: Flory K, editor. Analytical profiles of drug substances. New York: Academic Press, pp 533–561.
3. Dumanovic D, Juranic I, Dzeletovic D, Vasic VM, Jovanovic J. 1997. Protolytic constants of nizatidine, ranitidine and *N,N'*-dimethyl-2-nitro-1,1-ethenediamine, spectrophotometric and theoretical investigation. J Pharm Biomed Anal 15:1667–1678.
4. Cholerton TJ, Hunt JH, Klinkert G, Smith MM. 1984. Spectroscopic studies on ranitidine: Its structure and the influence of temperature and pH. J Chem Soc Perkin Trans 2:1761–1766.
5. Yoo SH. 1997. Amine acid salt compounds and process for the production thereof. US patent 5,686,588.
6. Madan T. 1994. Preparation and characterization of ranitidine-HCl crystals. Drug Dev Ind Pharm 20:1571–1588.
7. Price BJ, Clitherow JW, Bradshaw J. 1978. Aminoalkyl furan derivatives. US patent 4,128,658.
8. Crookes DJ. 1985. Aminoalkyl furan derivatives. US patent 4,521,431.
9. Khanna JM, Kumar N, Khera B, Khanna M. 1997. Process for the manufacture of form 1 ranitidine hydrochloride. US patent 5,621,120.
10. Murthy K, Radatus BK, Sidhu KPS. 1995. reissued 2002. Process for production of an improved form of form 1 ranitidine hydrochloride having improved filtration and drying characteristics. Canadian patent 2120874.
11. Ngooi TK, McGolrick JD, Antczak C, Tindall JLA. 1994. Preparation of form 1 ranitidine hydrochloride. US patent 5,338,871.
12. Ngooi TK, Antczak C, Tindall JLA, McGolrick JD. 1998. Preparation of form 1 ranitidine hydrochloride. Canadian patent 2099530.
13. Schickaneder H, Nikolopoulos A. 1997. Process for preparing form 1 ranitidine hydrochloride. US patent 5,663,381.
14. Mirmehrabi M, Rohani S, Murthy KSK, Radatus B. 2004. Characterization of tautomeric forms of ranitidine hydrochloride: Thermal analysis, solid-state NMR, X-ray. J Cryst Growth 260:517–526.
15. Mirmehrabi M, Rohani S, Murthy KSK, Radatus B. 2003. Solubility, dissolution rate and phase transition studies of ranitidine hydrochloride tautomeric forms. Int J Pharm, submitted.
16. McCabe WL, Smith JC. 1976. Unit operations of chemical engineering, 3rd ed. New York: McGraw Hill, pp 932–938.
17. ICH topic Q3C. 1997. Residual solvent. http://www.emea.eu.int/pdfs/human/ich/028395en.pdf.

UM00011666
NOVARTIS EXHIBIT 1517
Novartis v. Regents, IPR2023-01347
Page 412 of 4460

This Page is Inserted by IFW Indexing and Scanning Operations and is not part of the Official Record

BEST AVAILABLE IMAGES

Defective images within this document are accurate representations of the original documents submitted by the applicant.

Defects in the images include but are not limited to the items checked:

- ☐ BLACK BORDERS
- ☐ IMAGE CUT OFF AT TOP, BOTTOM OR SIDES
- ☐ FADED TEXT OR DRAWING
- ☐ BLURRED OR ILLEGIBLE TEXT OR DRAWING
- ☐ SKEWED/SLANTED IMAGES
- ☐ COLOR OR BLACK AND WHITE PHOTOGRAPHS
- ☐ GRAY SCALE DOCUMENTS
- ☐ LINES OR MARKS ON ORIGINAL DOCUMENT
- ☐ REFERENCE(S) OR EXHIBIT(S) SUBMITTED ARE POOR QUALITY
- ☐ OTHER: _____

IMAGES ARE BEST AVAILABLE COPY.
As rescanning these documents will not correct the image problems checked, please do not report these problems to the IFW Image Problem Mailbox.

ELSEVIER

Advanced Drug Delivery Reviews 48 (2001) 91–114

Advanced DRUG DELIVERY Reviews

www.elsevier.com/locate/drugdeliv

Theoretical approaches to physical transformations of active pharmaceutical ingredients during manufacturing processes

Kenneth R. Morris[a,*], Ulrich J. Griesser[b], Craig J. Eckhardt[c], Joseph G. Stowell[a]

[a]*Department of Industrial and Physical Pharmacy, Purdue University, West Lafayette, IN 47907-1336, USA*
[b]*Institute of Pharmacognosy, University of Innsbruck, Innrain 52, A-6020 Innsbruck, Austria*
[c]*Department of Chemistry, University of Nebraska, Lincoln, NE 68588-0304, USA*

Received 18 October 2000; accepted 21 December 2000

Abstract

Processing-induced transformations (PITs) during pharmaceutical manufacturing are well known but difficult to predict and often difficult to control. This review of the concepts of transformations is couched in terms of the issues associated with identifying rate-controlling events from the materials side and the processing side. Specifically, the approach is reconciling the characteristic time scale of the structural change(s) in the material with the time scale of the processing-induced stress. This is definitely a model (or rather a melding of a group of existing theories) in development. This overview is a 'snapshot' of the authors' attempts to identify the categories of existing theories needed to encompass all of the relevant events for each possible PIT. The ultimate goal is to establish a framework of concepts and theories for consideration, discussion, and modeling of PITs as well as to locate much of the relevant literature in the framework. © 2001 Elsevier Science B.V. All rights reserved.

Keywords: Process-induced transformation; Wet Granulation; Drying; Lyophilization; Tabletting; Active Pharmaceutical Ingredient; Crystallization; Amorphous; Polymorph; Hydrate; Solvate; Phonon

Contents

1. Introduction 92
2. Background 92
  2.1. Time-base reconciliation 92
  2.2. Selecting appropriate phase variables for analysis 92
    2.2.1. Possible phase changes of a solid during processing 93
    2.2.2. Brief overview of phase transitions 93
    2.2.3. Possible transitions 96
  2.3. Identification of the rate-determining events 101
3. Modeling processing induced transformations 104
  3.1. Dehydration of a hydrated crystal 104
  3.2. Polymorphic transformation during wet granulation 105
    3.2.1. Conversion of a metastable form to the stable form 105

*Corresponding author. Tel.: +1-765-496-6387; fax: +1-765-494-6545.
E-mail address: morris@pharmacy.purdue.edu (K.R. Morris).

0169-409X/01/$ – see front matter © 2001 Elsevier Science B.V. All rights reserved.
PII: S0169-409X(01)00100-4

UM00011668
NOVARTIS EXHIBIT 1517
Novartis v. Regents, IPR2023-01347
Page 414 of 4460

3.2.2. Conversion of the stable form to a metastable form 106
3.2.3. Conversion of an ansolvate form to a solvate form 107
3.3. Tableting induced transitions 109
3.4. Phase changes during freeze drying 110
4. Summary 111
Acknowledgements 111
References 111

1. Introduction

In the last two decades, there has been significant emphasis on the characterization and control of the crystal form of the active pharmaceutical ingredient (API) or bulk drug [1,2]. The logical evolution of this trend is to characterize and control the crystal form of the API throughout processing and in the final dosage form. This is reflected in the new attitude within the regulatory agencies (e.g., ICH Q6A) [3] recognizing that changes in crystal form may ultimately affect dosage form performance. Although there are many interesting reports in the literature of transformations during processing, they are primarily anecdotal or very specific in nature (with the exception of the body of work from Otsuka and Matsuda [4–15]). Some of the work is elegant but there has been little attempt in pharmaceutical sciences to form a general framework within which to couch such processing induced changes. The exception to this may be found in the area of crystallization (here, the form resulting from the final crystallization is the starting material and much modeling is present in the literature) [16]. In this paper, attempts are made to combine the thermodynamics and kinetics of the relevant processes to formulate a general approach in treating these transformations. A bibliography of much of the relevant literature is included at the end of this paper; however, the focus is not on re-describing observed transformations except as it serves to elucidate the developing framework.

2. Background

2.1. Time-base reconciliation

Subjecting a given crystal form of a bulk drug in a formulation to a processing unit-operation induces some stress into the system. Stress in this sense is any physical change that *moves* the system from or towards equilibrium. This stress may be thermal, mechanical, or result from interaction with a second factor (e.g., solubilization or moisture). That is, the system may be trapped in another equilibrium under these stress conditions. When the stress is dissipated, the system may relax back to the original equilibrium position. This *trapping* and *relaxation* constitute the mechanisms for transformations. There are essentially two subdivisions of trapping in generating new phases. First, the stress may move the system to a point in phase space where the new form is the most stable, and which becomes metastable (i.e., trapped) only when the stress is removed (e.g., in tabletting). Second, the stress may serve to kinetically produce a metastable phase that is *nowhere* the most thermodynamically stable form (e.g., the formation of a metastable polymorph in a monotropic system via the melt or a hydrate that occurs during a wet granulation–drying process). All persistent metastable forms are *kinetically trapped*; however, the term *kinetically formed* will refer to the process of forming an *everywhere* metastable phase.

The nature of the transformation in question (the possible paths) and the processing stress will determine the most appropriate choice of the phase space for analysis. The often more difficult task is to identify the two or more characteristic times associated with the process and transformation/relaxation (i.e., the time of the applied stress, the stress dissipation rate, and the characteristic structural-relaxation time controlling the rearrangement to the new form and back). Each of these points will be discussed in light of applicable theory.

2.2. Selecting appropriate phase variables for analysis

To adequately describe a phase and the transitions

UM00011669
NOVARTIS EXHIBIT 1517
Novartis v. Regents, IPR2023-01347
Page 415 of 4460

with which it may be associated, it is necessary that the underlying behavior of the solid-state system being investigated be understood. This will permit selection of the thermodynamic variables that will best represent the phase behavior. For the phases these may include: (a) the number of phases and states of aggregation, (b) the thermodynamic stability of each phase under specific thermodynamic conditions (i.e., temperature, pressure, and composition), and for phase transitions: (c) the latent heat of the phase transition and thermodynamic conditions under which it occurs, and, if available from some type of structural analysis, (d) the structures of the two phases.

2.2.1. Possible phase changes of a solid during processing

First, the basic processes that can occur during formulation of a pharmaceutical material need to be considered. Because most of these materials are solids, the solid-state is taken as our reference state with the state of aggregation being the general descriptor of any general state. The transformations of the materials can be classified simply as solid–solid (phase transition, deformation), solid–liquid (melting, crystallization), or solid–gas (sublimation, condensation). Note, save for deformation, all of these transformations are just types of phase transitions. In the case of deformation, defects are introduced into a basic lattice structure that is essentially unchanged. Of course, severe deformation can also induce a global change of the lattice such that a new crystal is generated. It is clear that to deal with the transformations associated with processing, it is necessary to examine the pathology of phase transitions (see Tables 1 and 2).

2.2.2. Brief overview of phase transitions

The first useful classification of phase transitions (PT), still much in use, was that of Ehrenfest [17]

Table 1
Types of the most important phase transitions during processing of pharmaceuticals[a]

Basic process	State of aggregation	Specific process
Transformations (one component)	Solid–solid	Polymorphic transformations
		Crystallization of the amorphous form and vice versa
	Solid–liquid–solid	Incongruent melting (melting followed by crystallization of a more stable form)
		Solution mediated polymorphic transformations
Physical interactions (multicomponent)	Solid–solid	Eutectic reaction
	Solid–liquid–solid	Formation of a molecular compound or a solid solution (including solvate formation)
	Solid–solid or Solid–liquid–solid	Hydrate formation in humid air
Physical decompositions (multicomponent)	Solid–solid or Solid–liquid–solid	Desolvation

[a] Does not consider chemical changes.

Table 2
Comparison of properties between first- and second-order transitions[a]

First-order transition	Second-order transition
Highly cooperative process	Weakly cooperative process
Absorbs energy over a narrow temperature range	Gradual energy absorption over wider temperature range
Large, discreet changes in volume and entropy (1st derivatives of G)	Small changes in volume and entropy over transition
Discreet changes in 2nd derivatives of G (e.g., C_p) sensitive to translational freedom	Discreet changes in 2nd derivatives of G (e.g., C_p) sensitive to translational freedom

[a] Excluding polymers.

UM00011670
NOVARTIS EXHIBIT 1517
Novartis v. Regents, IPR2023-01347
Page 416 of 4460

who focused on the smoothness of the behavior of the chemical potential (Gibbs free energy per mole), μ, during a phase change. Of course, μ itself is continuous since, by definition, the phase transition is an equilibrium process. However, with all solid–liquid, solid–gas transitions, and liquid–gas transitions below the critical temperature as well as most solid–solid transitions, there is an associated latent heat, $T\partial S$. Since the molar entropy, S, is $-\partial\mu/\partial T$, the first derivative of the chemical potential, and thus the free energy, must be discontinuous with a finite latent heat. Thus Ehrenfest proposed that phase transitions be classified according to the order of the lowest-order derivative function of μ with respect to temperature that was found to be discontinuous. Thus, a pure second-order transition will involve a discontinuity in the specific heat $C = T(\partial^2\mu/\partial T^2)$.

Over time, other thermodynamic potentials' derivatives have been so used. It is instructive to examine another potential, the Helmholtz free energy, and apply it to a fluid. But we examine its behavior with respect to the volume. The first derivative yields the pressure and the second the bulk modulus. Clearly vaporization of a liquid would be first order. But what is of interest is that for any formulation of the free energy, the second derivative term is a kind of susceptibility, in this case a mechanical one, and thus for continuous PT the behavior of the relevant susceptibility (i.e., the electric susceptibility in a ferroelectric transition) is crucial.

This classification scheme, which relies on singularities in the thermodynamic potentials, is falling into disuse because derivatives of μ can be continuous at a transition but show extreme divergence. The currently favored nomenclature is to only term those PT as first order that have a finite latent heat and label all others as 'continuous.' Symmetry has been shown to play an important role in understanding the solid–solid PT. For example, the structure of a high temperature phase is less anisotropic than the lower temperature phase from which it was generated. The X-ray structure of the two phases can be used to demonstrate this and to determine what particular set of structural parameters changed. Although the higher temperature phase may possess higher symmetry in the sense that it becomes more isotropic, its actual order is often decreased due to disorder or thermal averaging. Location of that variable that has a finite value below the critical temperature of the transition but is zero above it may often serve as the *order parameter* that was introduced by Landau into his theory of PT. An example would be the density difference $|\rho - \rho_c|$ for a liquid where ρ is the density at any temperature T and ρ_c is the density above T_c. At temperatures below T_c the difference would be finite, but above T_c it is zero. The free energy may be expanded as a polynomial function of the order parameter and the symmetry of this function can be exploited to understand the continuous structural change.

But what is happening physically to a crystal that is undergoing a PT? Consider a molecular crystal that is being heated. The thermal energy applied to the crystal has to be absorbed. Since in nearly all molecular crystals the molecules cannot rotate freely, all they can do is vibrate against each other in small translational displacements or they can perform small rotational displacements around their centers-of-mass. The intermolecular forces that define the lattice potential determine these vibrational frequencies and displacements.

The intermolecular vibrations are of quite low frequency and act as a sink for the absorption of the thermal energy that is being pumped into the crystal. Now these lattice vibrations must conform to the translational symmetry of the crystal, which means that they must be cooperative motions of all the molecules comprising the solid. These collective vibrations of the crystal are called *phonons* and propagate through the lattice as waves. Just as with molecular vibrations, the number and symmetry of these phonon modes can be precisely determined. They form bands of very closely spaced energy levels that come as two sets: (1) the acoustic phonons that are of lowest energy and of which there are only three branches and (2) the optical phonons that are of higher energy and which make up the rest of the possible vibrational degrees of freedom available to the lattice.

The phonons provide the means for accommodating the thermal energy that is being introduced into the crystal. Since the phonons are bosons the Pauli Exclusion Principle does not apply, and the thermal energy assumes a Boltzmann distribution among the phonon energy levels. This means that the vibra-

UM00011671
NOVARTIS EXHIBIT 1517
Novartis v. Regents, IPR2023-01347
Page 417 of 4460

tional displacements of the molecules, which we regard for simplicity as rigid, will become increasingly larger. Because of the geometry of local forces and their magnitudes, one of these phonon modes will have increasingly larger displacements compared to the other modes. The thermal energy is affecting this mode more than the others and because of this violent motion the force constant for this lattice mode weakens. This results in a decrease of the frequency, the so-called *phonon mode softening*. The mode is said to be overdamped (i.e., the displacements are enormous and no longer behave linearly). Eventually the mode disappears and the molecules have vibrated themselves into a new equilibrium geometry consistent with the lattice potential of the higher temperature phase. This new phase, of course, has its own set of phonons but there will be many that are essentially unchanged.

This transformation has obviously been a continuous change with no catastrophic destruction of the lattice. The increased thermal energy has driven the molecules into a potential energy arrangement that is compatible with the additional energy of the lattice. This usually means that a lattice of higher symmetry has been formed, but possessed of higher symmetry than the low temperature phase because of the disorder due to the thermal motion. It is not, however, necessary that the PT be driven by temperature. Any mechanism capable of introducing energy into the lattice (e.g., mechanical, electrical, electromagnetic) may drive the PT. And this suggests a more mesoscopic view of the PT. Any of these perturbations introduce stress into the lattice. At low levels, the stresses are accommodated by the lattice and local strains develop. However, as the local strain fields increase and also get larger they can couple and create ever-larger domains of strain until the lattice undergoes a global transformation to the new phase. However, often the differences between the new and old phases are so great, structurally and energetically, that the change is catastrophic and the crystal shatters into smaller crystals of the new phase. Since this is invariably accompanied by the release of heat, a first order transition results although it is possible such destruction could be associated with a continuous transition.

Because of the catastrophic changes associated with first-order transitions, a general theory has not been formulated. The modern theory of critical phenomena deals almost exclusively with continuous transitions and it is with such transitions and associated concepts that our greatest understanding has been achieved. Luckily, they also represent a large number of PT behaviors such as the transformations between conformational polymorphs.

The picture presented thus far for continuous PT has focused on very local actions between essentially pairs of molecules. But a PT is obviously a global transformation, so how can such local events effect such global changes? We recognize that the energy injected into the lattice is not instantaneously and homogeneously distributed through the lattice. There will be very local fluctuations of strain throughout the lattice and these will modify the pairwise molecular interaction energy. At temperatures significantly above T_c, entropy effects will dominate the intermolecular interaction energy and disorder will be common. With decreasing temperature the intermolecular forces will become more dominant and clusters of molecules will adopt specific relative orientations: nearest neighbors will fix their local geometries to form clusters of aligned or correlated orientations. These orientations arise from the increasingly important interactions due to dipoles, polarizability, and the distribution of the free volume in the crystal. The characteristic size of the largest of the oriented clusters is associated with a quantity called the correlation length, ζ. At this point the system exhibits short-range order.

The correlation length will increase with decreasing temperature. However, the smaller scale fluctuations will still be present and are of importance. In fact, there are correlated regions of oriented molecules that exist on *all* lengths up to that of the correlation length itself. Each of the fluctuations is, therefore, not itself of homogenous orientation, but rather is composed of smaller fluctuations of oriented molecules which themselves are made of even smaller fluctuations of oriented molecules and so on to the scale of the unit cell lengths. When the correlation length becomes infinite (i.e., macroscopic) at T_c, then ordered structures exist on every length scale of the system.

The external stress causes some overdamped molecules to exert forces upon their neighbors. This chemical pressure causes local deformations of the

UM00011672
NOVARTIS EXHIBIT 1517
Novartis v. Regents, IPR2023-01347
Page 418 of 4460

lattice and the stronger the interaction between the perturbed molecule and its neighbors, the more the stress will be effectively transferred and a subsequent local strain field developed [18,19]. The intensity of the strain fields will be a function of the intermolecular potentials and will clearly influence how well the crystal can store the external energy (e.g., heat capacity) and affect the binding energy (e.g., heat of fusion). Thus, for less-stable polymorphs the strain fields can increase the heat capacity by creating more local vibrational modes. However, large strains will also decrease the intermolecular interaction and thus effectively decrease the lattice binding energy.

Below T_c, all of the molecules on all length scales are ordered and the new phase is found. This is long-range order. At $T=0$, the only forces at play are those between the molecules and complete ordering is achieved — a result consistent with the Third Law of Thermodynamics. Clearly, the configuration obtained results from the lowest energy potential available to the system. This usually results in close-packed structures but in some cases significant free volume is created because the intermolecular interactions are sufficiently energetic to overcome the increase of free volume required to optimize them. While ice is the most common example of this, resorcinol [20] and acetazolamide [21] are good examples of more complex systems adopting such behavior.

It can be shown that the change of the length correlation function $\Gamma(\ell)$ decays according to a power law:

$$\Gamma(\ell) \sim \ell^{-\lambda} e^{-\ell\zeta}$$

where Γ is the correlation length, ℓ is the length of any cluster, and ζ is some number. At T_c, $\zeta=\infty$ and we are left with the power law where ζ is a critical exponent that is dependent on the specific *type* of system. Although T_c is very dependent upon the specifics of a given system, the critical exponents are essentially universal for systems belonging to a given class (e.g., fluids, surfactants, magnets). This is a stunning result and indicates the commonalities in interactions that are involved with cooperative systems.

These fluctuations must be related to the propagation of the phonons. In most crystals, especially for those that are organic, the intermolecular interactions are highly directionally dependent. The acoustic phonons are particularly related to the elasticity of the crystal and thus the strain. Recall that the acoustic phonon is a vibrational mode of the crystal and, as such, it has a specific pattern of displacement of the molecules. If we imagine an acoustic phonon of a wavelength the size of the crystal, we can see that this displacement pattern, or a combination of them, can be used to describe the strain of a crystal. They are a measure of the lattice potential itself since it is clear that the defining characteristic of a condensed phase is its elasticity. In other words, the elasticity is a measure of the intermolecular bonding that holds the crystal together. Thus, the strain influences this 'bonding.'

Processing creates defects in lattices and therefore destroys the periodicity. This prevents propagation of the phonons and they scatter from defects creating many local, non-cooperative, vibrational modes. Applied external energy, either thermal or mechanical, will clearly concentrate at defects. Soft crystals, those with great elasticity, will be more compliant and deform more readily since the intermolecular interactions are weaker than will stiffer crystals with large intermolecular potentials. However, the soft crystals will have a more homogenous distribution of the strain and will accommodate it more easily than the stiffer crystals can. Thus, the applied stress may be expected to generate more defects in the stiffer lattice than in the softer that, although more greatly deformed, may have fewer defects.

Use of these concepts will be made when identifying the rate-determining steps for the PT (see Section 2.3).

2.2.3. Possible transitions

The appropriate phase diagram should incorporate the possible phases of the compound and be limited to only the variables affected by the processing step of interest. It is often sufficient to use the appropriate one- or two-component phase diagram to simplify circumstances even though formulations will typically consist of multiple components.

The phase relationship of polymorphic systems is frequently illustrated simply by considering the P–T section of a three-dimensional P–V–T diagram (according to the state variables: pressure, volume,

UM00011673
NOVARTIS EXHIBIT 1517
Novartis v. Regents, IPR2023-01347
Page 419 of 4460

and temperature). The experimental determination of such state diagrams is laborious and often not possible particularly for solid organic compounds, and even calculation of only the relative equilibria require a very reliable set of thermodynamic data. Fortunately, semi-schematic diagrams, based on few experimental data (e.g., melting points, transition temperature, and relative stability or solubility) are readily obtainable. Fig. 1 shows the $P–T$ phase diagram for a simple one-component system. A system described by such diagrams is clearly not able to form solid phases other than the one shown. Examination of the phase diagrams for polymorphs is more complex. The $P–T$ and $P–V–T$ diagrams for an enantiotropic system show the range of conditions under which each form is the more stable (see Fig. 2). By starting with Solid I and increasing the temperature past the co-existence curve, Solid II becomes more stable. Decreasing the temperature, Solid I reversibly becomes the thermodynamically favored form. Whether or not this form occurs readily is another question, nevertheless it is the more stable form under those conditions. In a monotropic system, the $P–T$ diagram illustrates that any stress should yield the stable form and no conditions should produce a metastable form. It may be more instructive to consider a $G–T$ (Gibbs free energy versus temperature) diagram as shown in Figs. 3 and 4. Fig. 3 shows the basic $G–T$ phase diagram for two polymorphs. Fig. 4b includes the

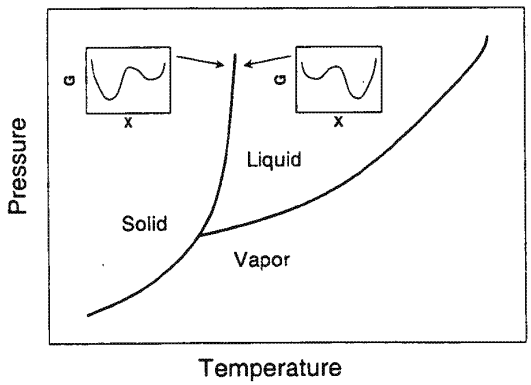


Fig. 1. $P–T$ phase diagram for a one-component system showing the relative free energies G of the phases on each side of the solid–liquid coexistence curve.

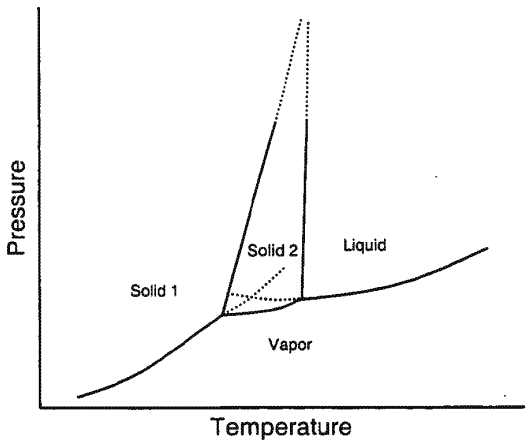


Fig. 2. A pressure versus temperature ($P–T$) phase diagram for a simple one-component system.

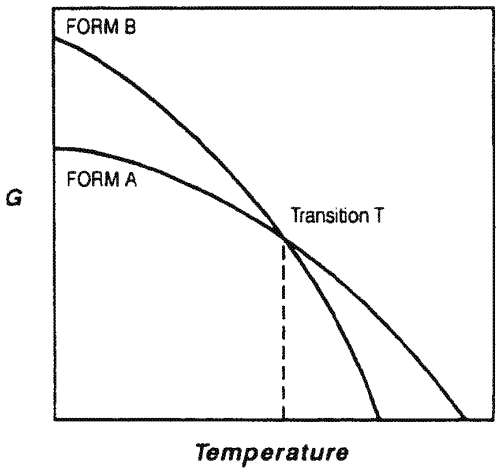


Fig. 3. A Gibbs free energy versus temperature ($G–T$) phase diagram illustrating the transition temperature for two enantiotropically related polymorphs.

liquidus curve intersecting the curves above the transition temperature for enantiotropic behavior. The occurrence of melting before the transition in monotropic behavior provides the information needed at this stage of the analysis (Fig. 4a). This is because it is known that starting with the stable form in a monotropic system, the only way to get the metastable form is through *kinetic formation*, which

UM00011674
NOVARTIS EXHIBIT 1517
Novartis v. Regents, IPR2023-01347
Page 420 of 4460

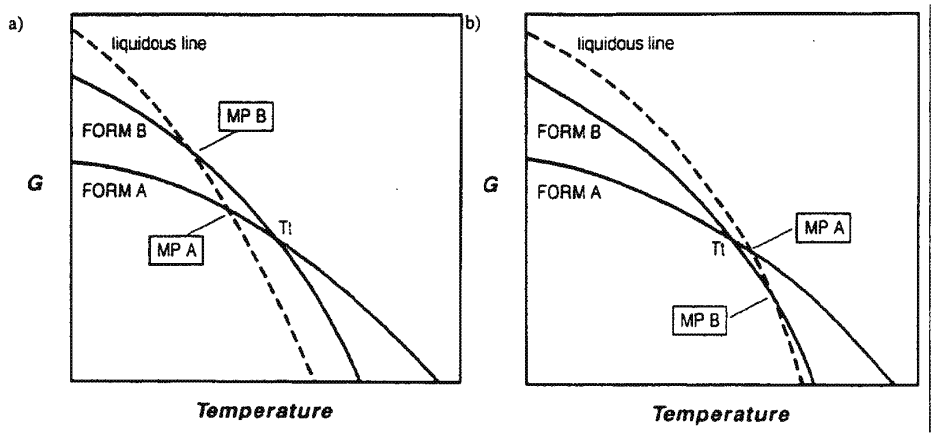


Fig. 4. (a) A Gibbs free energy versus temperature (G–T) phase diagram for two monotropically related polymorphs illustrating the liquidus line intersecting the curves at a temperature greater than the transition temperature. (b) A Gibbs free energy versus temperature (G–T) phase diagram for two enantiotropically related polymorphs illustrating the liquidus line intersecting the curves at a temperature greater than the transition temperature.

dictates that we must pass through the liquid or vapor state to access this phase. Therefore, an important objective is to determine whether the two forms are monotropically or enantiotropically related. A third option that illustrates the phase relationship of two forms is a solubility versus temperature diagram (van't Hoff plot).

For some systems, such as hydrates, solvates, or eutectic formers, a two-component diagram is required. This will often be an x–T (composition–temperature) diagram (see Fig. 5) or a hydrate sorption isotherm of the equilibrium-moisture content versus vapor pressure (*EMC* versus *VP*) of water (solvent) or relative humidity (see Fig. 6 *arginine*). Each diagram shows the region in phase space for which a given form is stable. Fig. 5 shows that the hydrate is the only crystalline form stable at compositions between the eutectic point and the peritectic point below the curve. Similar information is obtainable for a single temperature from the sorption

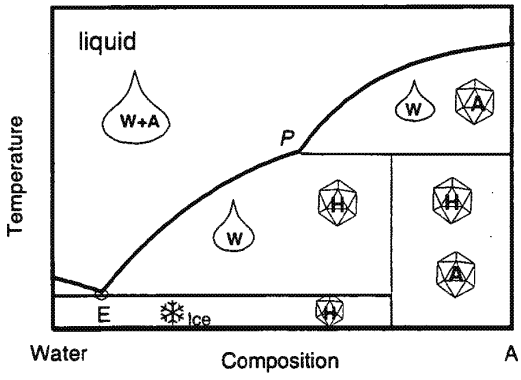


Fig. 5. A composition versus temperature (x–T) phase diagram of water and compound (A) showing an incongruently melting hydrate (H) form. The hydrate form is stable between the eutectic (E) and the peritectic (P) points below the liquidus curve.

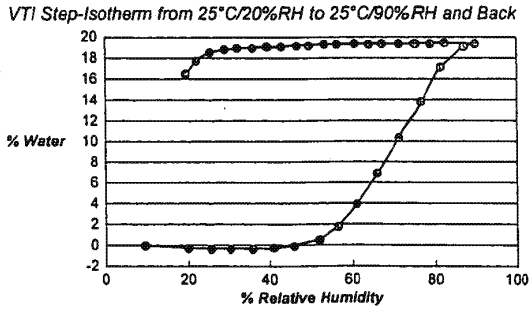


Fig. 6. A moisture-sorption isotherm showing an absorption isotherm (lower curve) and a desorption isotherm (upper curve). These data indicate that the initial phase begins to absorb moisture at humidities greater than 45% RH and subsequent hydrated form begins to loose moisture at humidities less than 30% RH.

UM00011675
NOVARTIS EXHIBIT 1517
Novartis v. Regents, IPR2023-01347
Page 421 of 4460

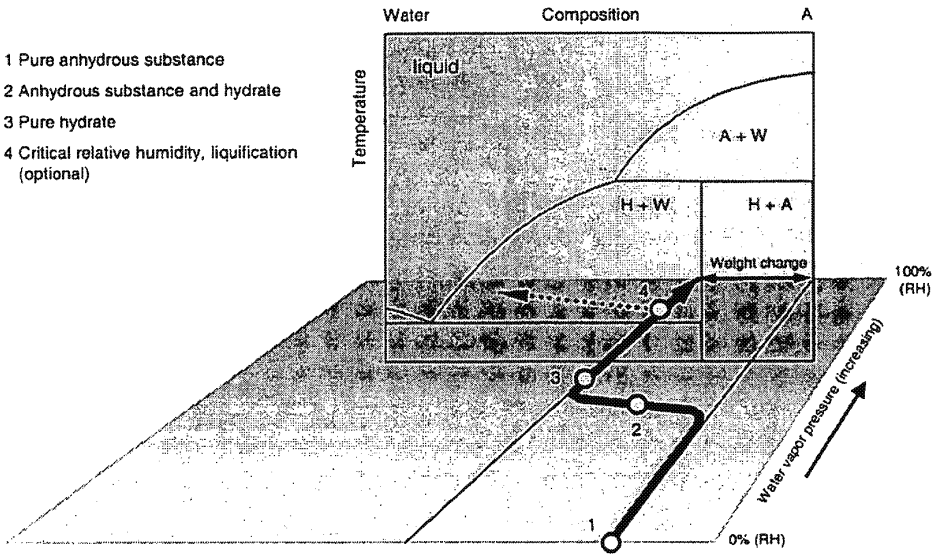


Fig. 7. Schematic phase diagram of an incongruently melting hydrate and a moisture-sorption diagram.

and desorption isotherms. This information can be very useful in determining the tendency of the hydrate to loose water as it enters what should be a region of metastability (Fig. 7). The use of one, or sometimes both diagrams, should yield the identity of the stable phase.

Amorphous–crystalline transitions are in some ways more complicated and in other ways simpler than purely crystalline systems. They are more complicated because the amorphous state is not as well characterized structurally as the crystalline state, yet the type of motion that results in recrystallization is often easier to detect than for crystal–crystal transformations. There is also a more general mechanism of formation of the amorphous phase. That is, most stresses can result in formation of the amor-

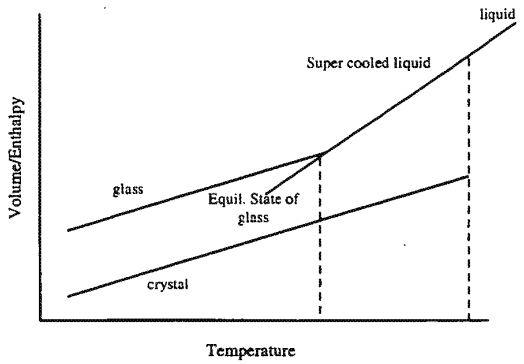


Fig. 8. Enthalpy or volume versus temperature for a system forming either a glass or a crystalline phase upon cooling.

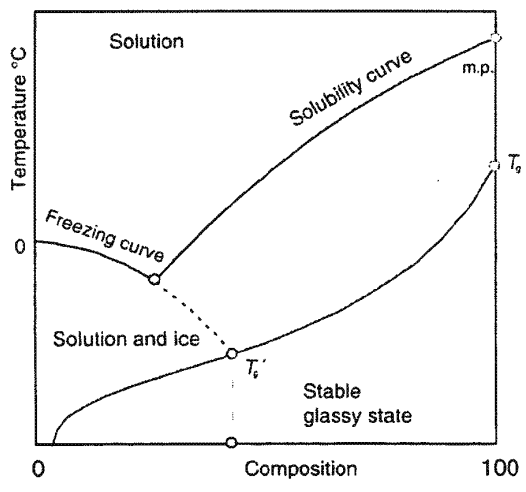


Fig. 9. Composition versus temperature diagram for a glassy system.

UM00011676
NOVARTIS EXHIBIT 1517
Novartis v. Regents, IPR2023-01347
Page 422 of 4460

phous phase (e.g., milling, drying, grinding, compression, granulation, heating, cooling, etc.). The $V-T$ or $H-T$ phase diagram (volume or enthalpy versus temperature) is generally instructive for amorphous systems (Fig. 8). Yet, $x-T$ diagrams may be more useful in mixed glassy systems (e.g., many lyophiles) if there is sufficient data to construct them (see Fig. 9). The $H-T$ diagram does provide a space in which to elucidate enthalpy relaxation. The concept is simply that as a glass sits at some temperature below its glass-transition temperature (T_g), it *relaxes* to a more favorable molecular arrangement. The energy released (as heat), as the molecules 'find' new ways of packing that may facilitate close enough approach for interaction, is absorbed as the material is heated back through the transition (to overcome the interaction) [22]. This quantity is important because the rate at which the relaxation enthalpy increases with heat storage gives some indication about the molecular mobility of the material and, therefore, its potential to recrystallize. The T_g and thus some idea of the stability of the phase might be acquired from these phase diagrams.

All of these diagrams present a 'picture' of the number of existing phases, their existence range, and their thermodynamic stability. Moreover, we can derive 'which phase transformations are principally possible' within such a system. However, the kinetic stability of any condensed state (crystal forms, amorphous form, melt, etc.) on either side of the equilibrium curves under specified conditions (temperature, pressure) is not displayed at all. Of course,

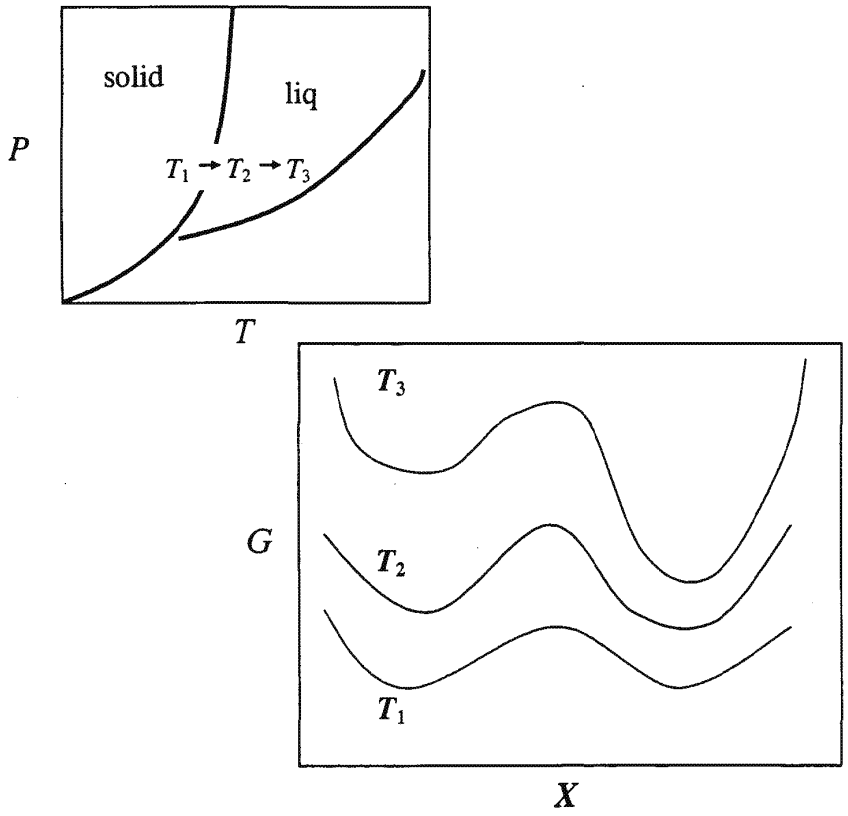


Fig. 10. $P-T$ and $G-X$ diagrams showing the change in free energy with an extensive variable as the temperature moves from the coexistence curve into the liquid region (after Callen [23]).

UM00011677
NOVARTIS EXHIBIT 1517
Novartis v. Regents, IPR2023-01347
Page 423 of 4460

it is known that thermal motions decrease at lower temperatures and makes phase changes less favored. Thus, it is possible to kinetically trap the disordered state by supercooling the melt, or to maintain the amorphous solid or any metastable crystal form at sufficiently low temperatures. On the other hand, it is known that crystallization of the amorphous form (more likely above T_g) or the transformation from a metastable to the stable form can be induced by increasing the temperature. However, for a monotropic system, the solid–solid transformation of the metastable to the stable form can (theoretically) occur throughout the entire temperature range. The actual temperature of crystallization depends on the amount of crystal defects and any agent that can serve as a catalyst for the nucleation of the more stable form (e.g., impurities, moisture).

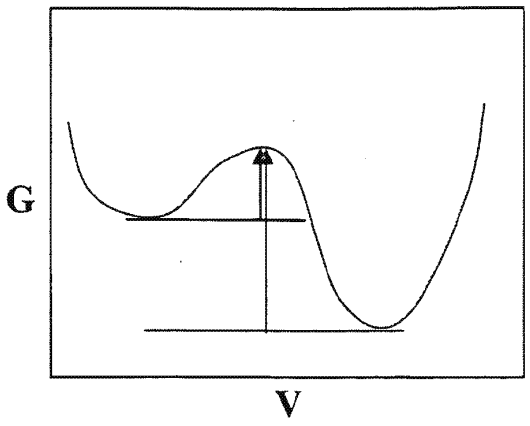


Fig. 11. A Gibbs free-energy versus volume (G–V) diagram illustrating the principle that the energy barrier is dependent on which direction the system is going.

2.3. Identification of the rate-determining events

The time-base reconciliation concept depends, as stated earlier, upon identifying directly or indirectly the time scale of the structural change responsible for the transformation. Then it must be determined if the stress is applied or removed at a rate sufficient to cause or inhibit the transformation of interest. This exercise requires combining thermodynamic and kinetic concepts. This may be attempted in the formalism of traditional chemical kinetics using a two-state model after Callen [23]. Potential diagrams lay the basis for the analysis (see Fig. 10). On either side of a coexistence curve (such as the solid–liquid one shown), the stable phase will have lower Gibbs free energy and, therefore, will be the favored state. The two minima may be thought of as representing the different conformations and/or orientations of a molecule in each of the states. Closer examination of a G–X diagram (where X is any extensive thermodynamic variable, in this case volume V) yields other implicit information (see Fig. 10). Examination of the G–V diagram (Fig. 11) shows that the energy barrier (G_a for our purposes) depends on which direction the system is going. There is a significantly larger barrier to go from the stable to the metastable state than the reverse. This may be interpreted as a decreasing probability of a molecule changing from the conformation and/or orientation in one state to another as the barrier increases. In fact, the probability of overcoming the barrier is often logarithmically related to the energy barrier [23]. At the coexistence curve, the probabilities and energy barriers are equal in each direction, but the energy barrier persists until the critical point. The slope of the G–V curve in each direction is, therefore, a measure of the *restoring force* for the system (i.e., the steeper the slope, the lower the probability of a successful jump). The relative depth of the energy wells for the two states is determined by where the processing induced stress has taken the system.

We can describe the rate of nucleation in solids in terms of the molecular level mobility and this is a conceptually (and perhaps computationally) useful approach for describing the factors controlling the kinetics of getting over the energy barrier. Turnbull [24] has derived the following relationship to describe the frequency of a molecule overcoming intermolecular forces and crossing an interface to another phase.

$$\nu' = \nu_o \exp\left(\frac{-\Delta G'_o}{kT}\right) \quad (1)$$

where ν_o is the *fundamental jump frequency* (kT/h in rate theory) and $\Delta G'_o$ is the free energy of activation

UM00011678
NOVARTIS EXHIBIT 1517
Novartis v. Regents, IPR2023-01347
Page 424 of 4460

to cross the interface between the new and the existing phase. The fundamental jump frequency ν_o (kT/h in rate theory) is related to the librational motion of the molecule(s) about the equilibrium position of the molecule or how often the molecule 'tries' to *jump* the barrier to the other phase. The exponential term represents the fraction of the molecules (or the probability of a molecule) having enough energy to overcome the barrier. (Of course, there is a competing process in the other direction.) The product of these, therefore, gives the number of molecules per unit time able to cross the barrier.

Using this equation, Turnbull and Fisher derived an expression for the absolute frequency I of homogeneous nucleation (i.e., number of nuclei forming per unit time) in condensed systems (the expression for heterogeneous nucleation differs in K, which includes a function of the contact angle):

$$I = K_V \exp\left[\frac{-(\Delta G^* + \Delta G_o')}{kT}\right] \tag{2}$$

$$K_V = n^* n \nu_o \left(\frac{\sum a\sigma}{9\pi kT}\right)^{1/2} \tag{3}$$

where ΔG^* is the free energy at the critical nucleus size, n^* is the number of molecules in the surface of the nucleus, n is the number of molecules per volume in the transforming phase, a is $(36\pi\nu^2)^{1/2}$, and σ is the interfacial tension summed over all facets of the cluster.

Turnbull describes transient homogeneous nucleation as:

$$I_t = I \exp\left(\frac{-\tau}{t}\right) \tag{4}$$

$$\tau = \frac{i^{*2}}{n^* \nu'} \tag{5}$$

So, the ν_o term is at work in both the transient and steady-state phenomena and is a fundamental quantity in our rate-determining event for the nucleation controlled conversion process. The value τ is proportional to the critical free energy of nucleation squared (ΔG^{*2}) and combines the tendency to jump with the barrier to nucleation. Although this is couched in terms of traditional thermodynamics and kinetics, the role of ν_o is related to the role of phonons as discussed earlier. The frequency of the relevant lattice vibrational modes may correlate with the relative persistence of a metastable.

If we assume that the x-coordinate in our G–X diagram (Fig. 12) is amplitude and that at the

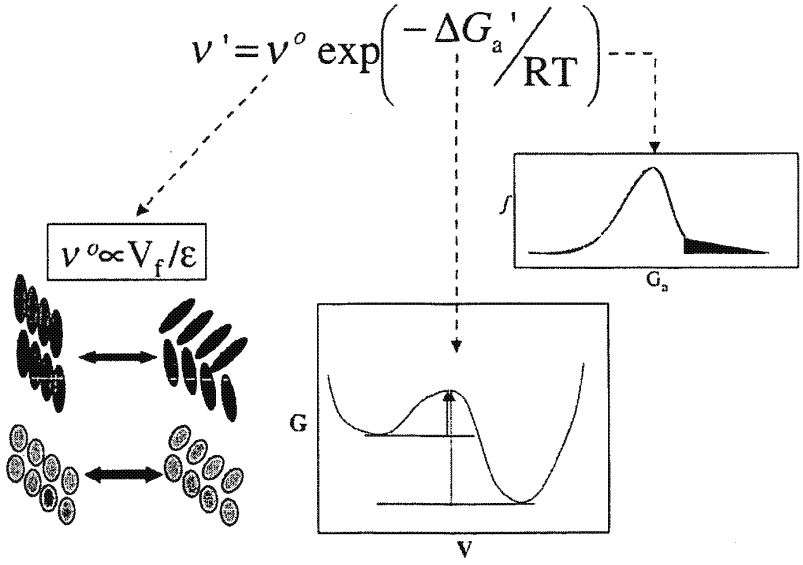


Fig. 12. Qualitative decomposition of the molecular level transition velocity equation consistent with Turnbull [24].

UM00011679
NOVARTIS EXHIBIT 1517
Novartis v. Regents, IPR2023-01347
Page 425 of 4460

maximum free energy occurs along with disorder, $\Delta G'_o$ represents the free energy needed to go from the ordered phase to the disordered phase before proceeding to its final destination. There is a related expression going in the other direction and the probability is determined by the ΔG in each direction. Rewriting the expression for ν' in terms of enthalpy and entropy gives:

$$\nu' = \nu_o \exp\left(\frac{-\Delta H'_a + T\,\Delta S'_a}{kT}\right) - \nu_o \exp\left(\frac{-\Delta H'_a + S' a_o}{kT}\right) \quad (6)$$

Assuming that for a given system at temperature that $\Delta H'_a$ is constant between the crystalline and disordered states (i.e., that the enthalpy change of the disordered portion is small compared to the crystalline), then differences in $\Delta S'_a$ within the disordered phase would control the energy barrier. Alternately, if the crystalline phase were disordered (or contained defects), the energy barrier would be lower, since $\Delta H'_a$ (which is endothermic) would be smaller, and the rate would increase. This suggests that the fundamental jump frequency is invariant in an intact system, but additional energy that induces 'interference' with the vibration (anharmonicity in the phonon mode) affects the energy barrier or molecular energy local to the disruption.

Looking at the macroscopic nucleation rate I again, an additional variable is found that may play a significant role in modifying the overall rate. That variable is the elastic strain ε. It occurs in the term for the critical free energy (ΔG^*) and represents the mechanical strain induced by the growing nucleus of the new phase in the old. At defects or process-induced amorphous regions, the system would be able to accommodate the change in volume more easily. This could also change what appears to be the characteristic time for the rate-determining event.

This rounds out the conceptual description of the possible processes that may interfere with the normal lattice vibrational modes for these types of transitions. It is, therefore, left to be determined if the processing stress 'places' the system in the 'activated' (or anharmonic) state long enough for the fundamental structural changes to occur. The rate-determining event described here is the transition to a second phase through the disordered state (or interface). It may be very difficult to identify, much less quantify, this rate as compared to the rate of process-induced stress. However, it is useful even to have a general range of time scales for comparison. This may be particularly true when trying to explain the relaxation of a kinetically-trapped metastable polymorph back to the stable form. Here, Eq. (1) (or Eq. (6)) is describing the rate-determining event and analytical strategies to quantify the events are manifold [19].

Consider two polymorphic systems that undergo transformation by a cooperative re-arrangement to a new packing motif (Fig. 12). Referring to our phonon discussion, this should be a measure of how well the lattice is able to orient to distribute the energy. Examining the two virtual polymorphic systems (Fig. 12), it can be assumed that they have the same free volume but different molecular volume and geometries. Ignoring intermolecular forces (already accounted for in $\Delta G'_a$), the more spherical molecule should have less resistance to reorienting than the more elongated molecule per free volume and therefore a higher fundamental jump frequency, υ_o. This relationship may be captured conceptually in a term combining the free volume V_f and the eccentricity ϵ of the molecule, assuming for the moment that the free-volume geometry mirrors the molecular geometry (which is often the case) in a V_f/ε term. This of course says nothing about the relative contribution of the term $\Delta G'_a$ to the rate but does hint at why some metastable forms are more persistent than others.

In identification of the rate-determining events in the induced transition, a cursory survey of rate-determining events for given types of transitions may be assembled.

There are several comments to be made about this summary. First, although the controlling events no doubt represent a fair appraisal of the possibilities, determining the specifics of an event (or sometimes which event is controlling in a specific system) can be very difficult. A polymorphic form that transforms in the solid state to another form will do so cooperatively and the pathway will be determined by comparison of the two crystal structures [25]. It may proceed through nucleation at a defect and subsequent growth, which, in turn, may or may not be topotactically related to the original structure [26]. The

UM00011680
NOVARTIS EXHIBIT 1517
Novartis v. Regents, IPR2023-01347
Page 426 of 4460

transformation may result in polycrystalline material or take place within the existing geometry of the single crystal. Second, while processing events may be controlling, they obviously are only important *relative* to the underlying molecular motion in the system (i.e., the rate-limiting event controls). The intent is to marry the basic structural change with the general environmental changes (stresses) that most directly impact upon them. Last, the time scales are intended to give a general idea of the scale of reconciliation that must occur to control the transformation.

Clearly, the rate-limiting event must be identified under any set of processing conditions. Identifying which variable is independent or dependent may be difficult. The applied stress may be controlled and considered the independent variable. Yet, the time dependence of the structural change may be relatively independent of the applied stress. It is, therefore, easier to parameterize the relationships with respect to a characteristic time necessary under a given set of conditions to induce (or observe) the phase transformation of interest (e.g., an amorphous system must be cooled to well below the T_g in a short time relative to its relaxation time at the higher temperature).

3. Modeling processing induced transformations

The primary goal of modeling of processing-induced transformations (PITs) is to determine the parameter of the time t_{PIT} it takes for a phase transformation to occur under a given processing induced stress (application and/or removal). Most of the tools and some of the relationships to accomplish such modeling are already at hand. What remains is to identify the time bases discussed above and find the appropriate interdependencies to yield the common time base. This approach may be illustrated using some common processes and transformations.

3.1. Dehydration of a hydrated crystal

Consider first the case of dehydration of a crystalline hydrate upon, for example, post-granulation drying in a fluid-bed dryer. Here the structural change is the dehydration of the hydrate and the processing stress is high temperature and relatively low humidity. The phase diagram of choice would be a sorption isotherm. This gives the critical relative humidity while the critical time is how long the material is in the dryer. Alternatively, the parameters used to establish the equilibrium conditions with which the data for the phase diagram were obtained give the dehydration rate under a given set of conditions (which must be adjusted to concentration of active and is, of course, partially dictated by the specification). The t_{PIT} is then determined by trapping the desired hydration or dehydrated state through reconciliation of the dehydration rate with the time exposed to the dehydration stress.

Drying kinetics in fluid bed dryers has been well modeled [27]. There are basically two stages during the fluid-bed drying process for typical pharmaceutical granulations. These are defined by the rate-limiting process involved with the loss of water. The *first stage* is heat-transfer limited, which occurs throughout the period where surface or loosely associated water is evaporating from the surface of particles. The *second stage* is diffusion limited, which occurs, as the water internal to the granules must diffuse to the surface of the granule before it can be lost. Each of these processes is characterized by different time dependencies.

The dependence of moisture content (M) with time during the first stage is linear.

$$M = M_o - Kt \tag{7}$$

where K is a constant at a given temperature, gas density, bed height, and heat of vaporization. The dependence during the second stage is exponential (for spherical particles).

$$M = M'_o k \exp(-k't) \tag{8}$$

where k and k' are geometric constants summed over n terms in an infinite series and M'_o is the moisture content at the beginning of the diffusion-limited phase. The first stage may be estimated from knowledge of the initial moisture content, the load, some

UM00011681
NOVARTIS EXHIBIT 1517
Novartis v. Regents, IPR2023-01347
Page 427 of 4460

physical constants, dryer properties (from the manufacturers specifications), and the above relationship. The onset of the second stage is more formulation specific, however, preliminary studies can yield good estimates of initial moisture content.

A superposition of the sorption isotherm with the drying curve matching the moisture content of interest yields the time it takes the system to dry to the critical moisture content (Fig. 13). A conservative mathematical estimate may be made by combining the above drying relationships with the critical moisture content and solving for t_{PIT}.

$$t_{PIT} = \frac{1}{k'} \ln\left(\frac{M'_o}{M}\right) \quad (9)$$

This simple example demonstrates the utility of the approach of reconciling data before committing significant resources at large scale (or small scale if your drug is expensive or limiting).

3.2. Polymorphic transformation during wet granulation

A more involved situation is that of the interconversion of polymorphs during wet granulation. Wet granulation provides an ideal medium for the crystallization of new phases of the drug. Because wet granulation involves a variety of different steps (wetting, mechanical stress, drying, sieving), several phase changes may be involved. The more crucial processes that can occur are solution-mediated transformations to a more stable polymorphic form or the formation of a solvated form (typically a hydrate). In the case of solvate formation, but also when an ingredient dissolves completely in the granulation liquid (i.e., in low-dosage formulations), a metastable or even the amorphous form may result after drying. However, the kinetics of the possible phase changes (solution-mediated transformation, solvate formation) determines whether or not the change will be complete during the time scale of the process. Logically, slow phase changes are more critical concerning the amount of secondary phase in the product and particularly require a consistent time scale of the granulation process. The starting point may be either the stable or metastable form or it may be a mixture of forms. The extent of conversion will depend upon the amount dissolved with time, which depends on the solubilities of the forms, volume of solvent, and the dissolution rate.

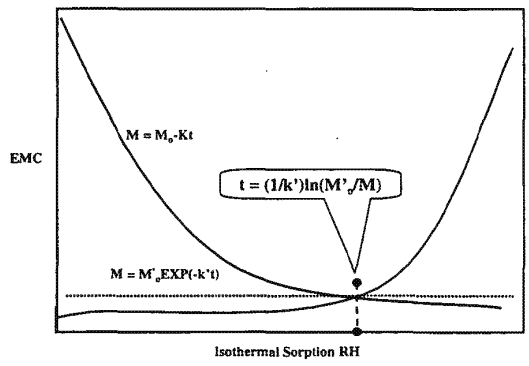


Fig. 13. Reconciliation of moisture-sorption isotherm and drying rate to control moisture content in a hydrated system.

3.2.1. Conversion of a metastable form to the stable form

Starting with a metastable form (no solvate formation) and assuming that nucleation begins when the concentration exceeds the solubility of the stable form S_I, the Noyes–Whitney relationship yields:

$$\frac{dm_{II}}{dt} = \frac{dm_I}{dt} = -kAS_{II} \text{ (or } NkaV^{2/3}S \text{ for powders)} \quad (10)$$

where dm/dt is the change in mass of the given form (Form I or II), S_{II} is the saturation solubility of the metastable form, and the other terms assume the usual meaning.

The time to reach the saturation solubility t_{SS} is then given by:

$$t_{SS} = \frac{V}{kA} \ln\left(\frac{S_I}{S_{II} - 1}\right) \quad (11)$$

Under sink conditions, the time is proportional to the following equation.

UM00011682
NOVARTIS EXHIBIT 1517
Novartis v. Regents, IPR2023-01347
Page 428 of 4460

$$t_{SS} = \frac{S_I V}{S_{II} k A} \tag{12}$$

The assumption of the metastable form crystallizing quickly is very tenuous in the short run. However, given the number of nucleation sites provided by the excipients, it may not be an issue over the extended time of granulation (of course, this assumption must be verified). Systems in solution exhibit lag times that are often short compared to the overall dissolution profiles and this is without *volunteer* nucleation sites [16]. Davey [16] used a similar approach to model polymorphic transformation in solution and the discussion in the present paper follows this logic.

The granulation time (above the saturation solubility of the stable form) is the key to the extent of conversion. Assuming that the dissolution is rate limiting and a linear growth rate G expression such as:

$$G = \frac{M_i^{1/3} - M_f^{1/3}}{(\alpha \rho N)^{1/3} t} \tag{13}$$

where M_i and M_f are initial- and final-crystal masses, N is the number of crystals, α is the volume shape factor and ρ is the density [28]. Note: Although all of the quantities in Eq. (13) will not be known, it is the time dependence that is important. It follows then that the growth rate (the mass increase of the stable form) will reflect the degree to which the assumption of immediate nucleation is obeyed.

This behavior should yield a growth curve of the form shown in Fig. 14 showing a lag time persisting until the concentration of the drug exceeds the solubility of the stable form (this may stay in the sink condition region for the metastable form depending upon the relative solubilities). Given a sufficient amount of time and no loss of solvent, all of the material in excess of the stable form's solubility (saturated solution concentration) will convert to the stable form. The amount remaining in solution at the onset of drying will be governed by both the drying kinetics and the relaxation time from the metastable to the stable form (see the next example). However, in addition to the excipients, an abundance of stable form nuclei should be present. This should favor the formation of the stable form if the drying rate is not too severe.

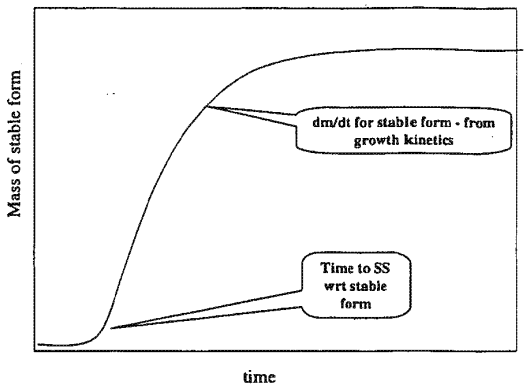


Fig. 14. Schematic growth curve for crystallization during granulation of a metastable form with conversion to the stable form.

3.2.2. Conversion of the stable form to a metastable form

Starting with the stable form (no solvate formation) and maintaining conditions under which it remains the stable form (i.e., staying in the stable region of the P–T phase space) transformation to the metastable state would not be expected to occur during granulation. During drying however, the amount of compound dissolved (assuming saturation) could be trapped as the metastable form. In terms of the time-base reconciliation language, if the metastable form nucleates, the drying rate must be *slower* than the solution mediated conversion rate to the stable form (with seeding of the stable form) to avoid trapping the metastable form. A conservative approach would be to estimate the conversion time from independent crystallization experiments and use Eq. (7) to estimate the drying conditions by solving for the t_{PIT}.

An example of this class of transitions was observed on the published system of fosinopril sodium, which exists in at least two enantiotropic polymorphs [29]. The stable Form A was found to transform under simulated granulation conditions.

UM00011683
NOVARTIS EXHIBIT 1517
Novartis v. Regents, IPR2023-01347
Page 429 of 4460

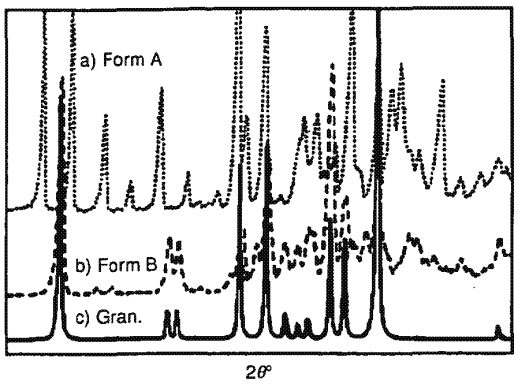


Fig. 15. Powder X-ray diffraction pattern of fosinopril sodium pure Forms A (a) and B (b) and after granulation (c) showing conversion to Form B as predicted.

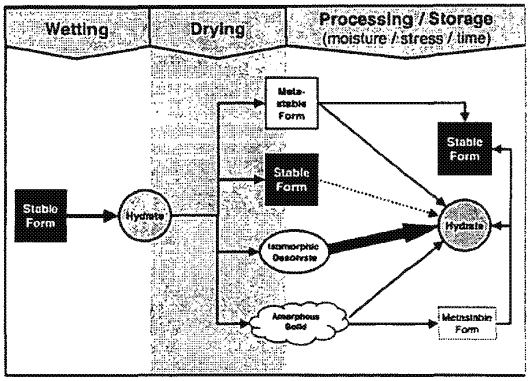


Fig. 16. Possible transformations during wet granulation when hydrate formation is involved.

Upon rapid drying from an alcoholic granulation fluid, the PXRD patterns show conversion to the metastable Form B (Fig. 15). The system was found to convert by varying amounts depending on the drying conditions and modeling. Testing of a related system is ongoing (K. Morris, S. Byrn, T. Davis, unpublished observations).

3.2.3. Conversion of an ansolvate form to a solvate form

If a solid can exist in one or more anhydrous forms as well as a hydrate, the fact that the hydrate is the most stable state in the wet material and is most likely formed must be considered. Thus, for such purposes, the hydrate is often used as the starting material to prevent considerable changes or an increase in the particle size. However, the crucial question for the subsequent drying process concerns the stability of the hydrate and the possibility to obtain a variety of solid phases, such as, the amorphous form, an isomorphic desolvate [30], a metastable anhydrate, or the thermodynamically stable anhydrous form at room temperature. This is schematically demonstrated by Fig. 16, which includes additional phase changes that are possible during processing and storage. It is clear that the path of any transformation is kinetically controlled and what actually happens depends strongly on the conditions during the wetting and drying steps as well as the duration of these processes. Well-known examples for the impact of such drying conditions on the formation of different crystal forms are phenobarbitone [31] and chlorpromazine hydrochloride [32] and microcrystalline cellulose [33].

Another example is theophylline [34], which is a frequently used model compound in pharmaceutical processing studies. Theophylline forms a monohydrate that readily dehydrates in a dry atmosphere or elevated temperatures to 'anhydrous theophylline.' However, less attention is commonly paid to the existence of polymorphic forms of theophylline. The existence of a high temperature form (Mod. I) and a low temperature form (Mod. II) has been reported as early as 1943 [35]) and investigated by several other authors [36–38]. Recently, Phandis and Suryanarayanan [33] reported that the dehydration of theophylline monohydrate can also yield a third polymorph (which is consistent with the results obtained elsewhere [38]). This form also appears upon wet granulation and fluid-bed drying of a theophylline formulation. The corresponding drying curve is shown in Fig. 17. The powder X-ray diffraction pattern of the granules after drying (see Fig. 18) clearly shows that this 'new form' was obtained mainly after fluid-bed drying (50 °C). This form is metastable and slowly transforms to the stable form (Mod. II) at room temperature; but above 60 °C, a fast transition to Mod. II takes place. It is obvious from this investigation and previous results [33] that the ideal drying conditions for the pro-

UM00011684
NOVARTIS EXHIBIT 1517
Novartis v. Regents, IPR2023-01347
Page 430 of 4460

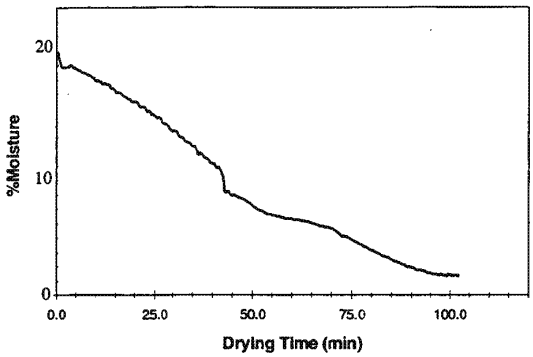


Fig. 17. Fluid-bed drying curve of theophylline after wet granulation in a Uni-Glatt fluid-bed dryer.

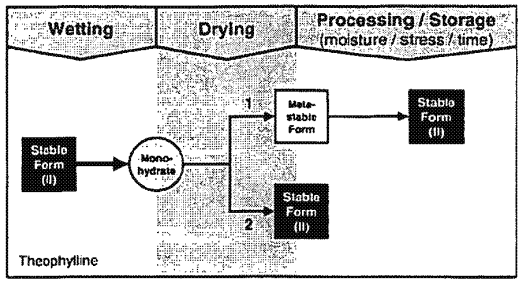


Fig. 19. Scheme for the possible transformations of theophylline crystal forms during a wet-granulation process. Condition 1: temperature <60 °C, low humidity (fast drying); Condition 2: temperature >60 °C or interaction with moisture during drying (slow drying).

duction of the metastable form from the hydrate are low temperatures (<60 °C) with a high water vapor-pressure gradient between the hydrate and the atmosphere (conditions present during fluid-bed drying and vacuum drying). Fig. 19 illustrates the possible transformations of theophylline crystal phases during wet granulation following the general scheme in Fig. 16.

It can be expected that, after such a series of phase transitions, the physical properties of the product more or less differ from those of the educt phase even though the powder X-ray diffraction patterns may match very well. The problematic nature of the processing conditions on drug release in theophylline formulations has been shown in several papers [39–41]. However, the most interesting result is that the

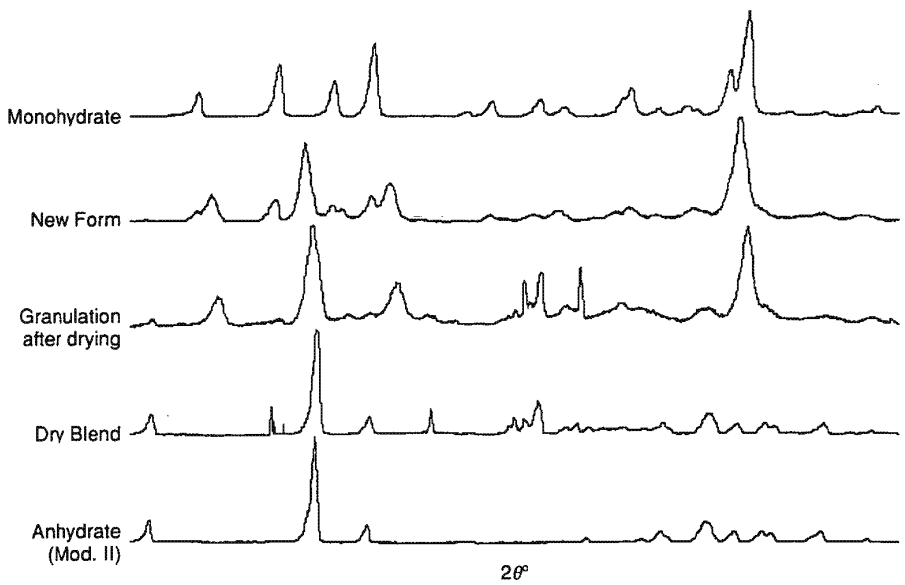


Fig. 18. Powder X-ray diffraction patterns of pure crystal forms (monohydrate, new form, anhydrate) and a formulation of theophylline before (dry blend) and after (granulation after drying) fluid-bed drying.

UM00011685
NOVARTIS EXHIBIT 1517
Novartis v. Regents, IPR2023-01347
Page 431 of 4460

dissolution of tablets containing the metastable form [33] is slower than tablets containing the stable form. This demonstrates impressively the competition between the kinetics of hydrate formation and the dissolution rate of the anhydrous form in an aqueous medium. The transition of the metastable form to theophylline monohydrate is the fastest process and consequently the actual dissolution rate is determined by the less soluble hydrate.

3.3. Tableting induced transitions

Tableting induced transitions present a special set of problems for modeling. Now pressure, temperature, and mechanical stress may all play a role. In addition, knowing the contribution of each may be difficult. Grinding studies may be useful in determining the ease of formation of the amorphous form and the stability of the resulting phase. Most data support the idea that transformations proceed through the amorphous or disordered state [42].

Examination of the $P-T$ diagrams for enantiotropic and monotropic polymorphs illustrates some basic constraints on direct crystal-to-crystal transformations (Fig. 20). In an enantiotropic system, it is clear that the only possible strictly pressure-induced transformation can occur only from Solid 2 to Solid 1 (Fig. 20, arrow b). Starting at a temperature and pressure where Solid 1 is the most stable phase requires a change in temperature to induce the transformation (Fig. 20, arrow a).

In studies where compression has formed Solid 2 from Solid 1 at constant temperature, considerable mechanical formation of amorphous phase was observed. Otsuka and co-workers [43] observed for chlorpropamide that the compression of the stable Form A in the enantiotropic system transformed to Form C and amorphous material to the extent of approximately 30% total (evenly divided between Form C and the amorphous phase). Compression of Form C resulted in conversion to Form A and approximately half the amount of amorphous material as produced by compressing Form A [43]. Further, they observed that a lower temperature (0 °C versus 45 °C) resulted in half as much conversion of Form A to Form C and amorphous material. They attribute this to a difference in the response to the mechanical stress at various temperatures, but it is not clear if

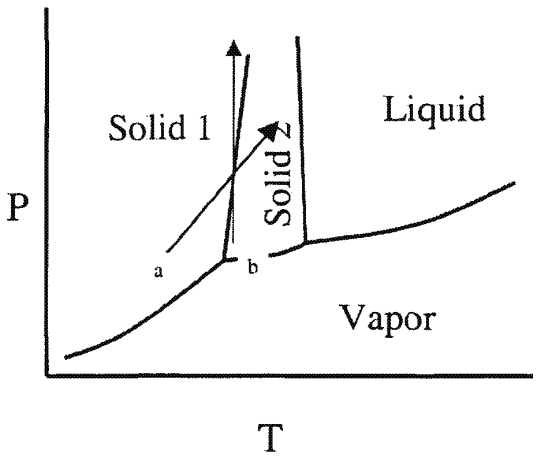


Fig. 20. $P-T$ phase diagram of an enantiotropic polymorphic system depicting possible tableting induced solid–solid transition pathways. Arrow (a) shows a path including both temperature and pressure changes, while arrow (b) shows the only possible transformation due to an increase in pressure.

there was a difference in the transformation (recrystallization) of the amorphous phase at the two temperatures. That is, the diminished conversion to Form C at the lower temperature may arise from a facile recrystallization of the amorphous phase to Form A. The apparent lack of difference in the temperature dependence of Form C under compression supports this possibility if we assume Form C is kinetically trapped and converts to Form A only in the presence of seeds of Form A. Irrespective of this interesting subtlety, the main conclusion of the studies was that the transformation proceeded through the amorphous phase. This is an extremely useful result for further analysis.

In studies where Solid 1 was maintained on compression, the system did not produce much amorphous phase nor increase temperature [44]. Therefore, it would appear that the ease of formation of the amorphous phase and the stability of the amorphous phase are key in understanding the potential for conversion. For a form that resists mechanical stress, the crystal would be expected to behave as predicted by the $P-T$ phase diagram.

Given these data, the conditions that result in conversion upon grinding and compression appear very similar. Once the tendency to undergo amor-

UM00011686
NOVARTIS EXHIBIT 1517
Novartis v. Regents, IPR2023-01347
Page 432 of 4460

phous phase formation is determined, we are essentially dealing with the rate of recrystallization (but to what form?).

3.4. Phase changes during freeze drying

The time for nucleation growth of a crystalline form is a crucial step upon freeze drying. The resulting product phase depends on the concentration and the nucleation and growth rate of the crystalline phase. Freeze drying often leads to the amorphous form (e.g., sugars, cephalosporins, peptides) [45–47]. The amorphous form often crystallizes during secondary drying [43].

The lyophilization process is of particular interest for considerations of phase-change kinetics. Lyophilization, in general, has a high potential for the production of metastable crystal forms. The product phase resulting from a freeze-drying process is mainly determined by the nucleation and growth kinetics of any crystalline form from an aqueous solution (upon freezing) or formation of the amorphous solid (during secondary drying). This crystallization behavior depends on the nature of the solute, but may be significantly affected by variables like the concentration of the solution, the pH of the solution, the freezing rate, additives (e.g., sugars, buffering substances), and more.

An example that demonstrates the complexity of a freeze-drying process when several crystal forms are involved is pentamidine isethionate [48]. This substance forms a trihydrate and a number of anhydrous forms. Freeze-dried products either result in the thermodynamically-stable form (Form A) or the metastable form (Form B) which are monotropically related. Form C is the high-temperature form and is enantiotropically related to Forms A and B. It has been shown that the nucleation of the trihydrate is the key process that determines whether Form A or Form B results from freeze drying pentamidine isethionate solutions (see Fig. 21). Thus, conditions which favor the nucleation of the trihydrate (higher concentrations) and provide sufficient time for the growth of this phase (a slow freezing rate) give Form B, which is strictly speaking the dehydration product of the trihydrate formed, during secondary drying. Lower concentrations and fast freezing rates yield Form A, which crystallizes from the amorphous form with a low degree of order. The phase diagrams that schematically represent both situations are given in Fig. 22.

Another intriguing observation of this system was that the thermodynamically stable Form A could be obtained at 20°C by fast evaporation of a pentamidine isethionate solution in pure water in which the nucleation of the hydrate did not occur. In this

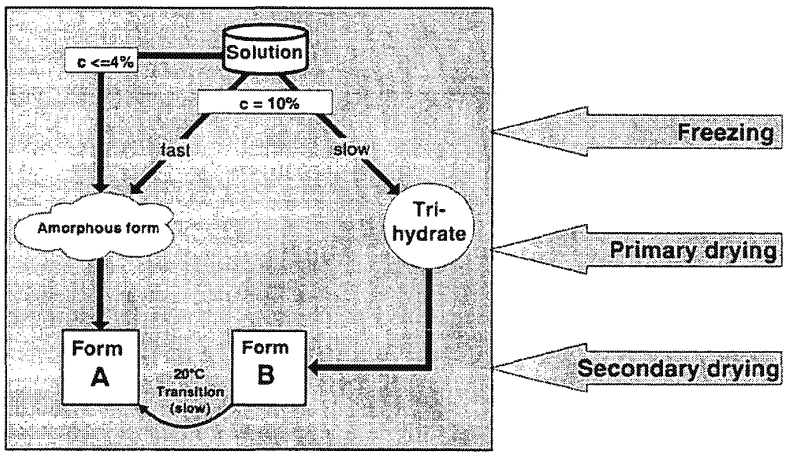


Fig. 21. Solid–liquid equilibria during freeze drying (schematic). The arrow marks the composition of the solution and the black circles indicate the point at which the crystallization and the glass transition starts, respectively.

UM00011687
NOVARTIS EXHIBIT 1517
Novartis v. Regents, IPR2023-01347
Page 433 of 4460

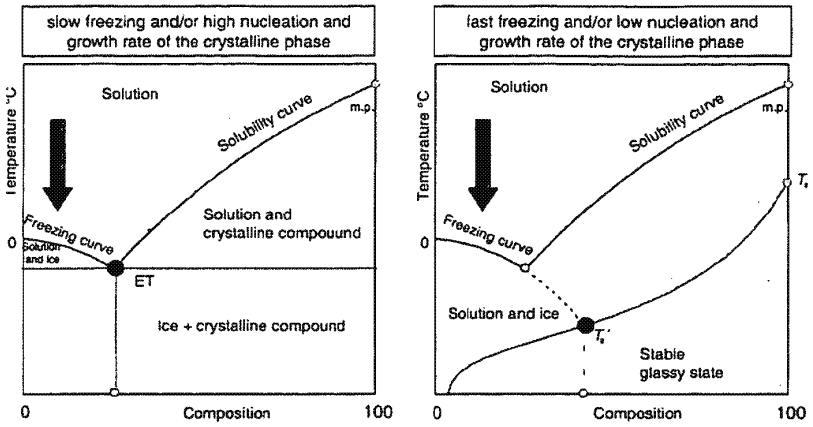


Fig. 22. Phase transitions during freeze drying, pentamidine isethionate [48].

case, Form A crystallizes from an amorphous intermediate state. Any other effort to crystallize Form A from solvents, or to transform Forms B or C to Form A by solution-mediated transformation, yielded either the trihydrate (because of traces of water in the solvent) or other solvated crystals. Thus, the production of larger amounts of pure, stable Form A is only possible via Form B, which slowly converts to Form A (within several weeks) during storage (see Fig. 16).

4. Summary

This 'review' is intended to help conceptualize PIT phenomena in a microscopic framework, molecular mobility, molecular interactions, and process-induced stress(es). While any given part of the suggested approach may be well known and in common use, it is the connection of the molecular to macroscopic phenomena that provides the opportunity to address these very complex issues in a systematic way. Research on specific applications of this approach is ongoing in our laboratories (as well as in other labs) as the need to understand PIT becomes more important to the industry and regulatory agencies. The framework proposed here is intended primarily to stimulate thought and discussion on the subject.

The (sometimes uneasy) marriage of physics and chemistry of basic pharmaceutical materials with mechanical and chemical engineering is needed to execute the approach endorsed here. Phenomenological modeling without understanding the basic phenomena is as risky as growing perfect crystals without considering what is going to happen to them during processing.

Acknowledgements

The authors wish to gratefully acknowledge the support of the Consortium for the Advanced Manufacturing of Pharmaceuticals (CAMP) and the National Science Foundation Industrial-University Processing Research Center (NSF-IUPRC) at Purdue University

References

[1] S.R. Byrn, R.R. Pfeiffer, J.G. Stowell, Solid-State Chemistry of Drugs, SSCI, Inc, West Lafayette, 1999.
[2] S. Byrn, R. Pfeiffer, M. Ganey, C. Hoiberg, G. Poochikian, Pharmaceutical solids: a strategic approach to regulatory considerations, Pharm. Res. 12 (1995) 945–954.
[3] Q6A Specifications, Test procedures and acceptance criteria for new drub substances and new drug products: chemical substances, Fed. Reg. 62 (1997) 62889–62910.
[4] M. Otsuka, N. Kaneniwa, Effect of grinding on the degree of

UM00011688
NOVARTIS EXHIBIT 1517
Novartis v. Regents, IPR2023-01347
Page 434 of 4460

crystallinity of cephalexin powder, Chem. Pharm. Bull. 31 (1983) 4489–4495.
[5] M. Otsuka, N. Kaneniwa, Effects of grinding on the physicochemical properties of cephalexin powder, Chem. Pharm. Bull. 32 (1984) 1071–1079.
[6] M. Otsuka, N. Kaneniwa, Effect of seed crystals on solid-state transformation of polymorphs of chloramphenicol palmitate during grinding, J. Pharm. Sci. 75 (1986) 506–511.
[7] M. Otsuka, N. Kaneniwa, Effect of grinding on the crystallinity and chemical stability in the solid state of cephalothin sodium, Int. J. Pharm. 62 (1990) 65–73.
[8] M. Otsuka, Y. Matsuda, Effects of environmental temperature and compression energy on polymorphic transformation during tabletting, Drug Dev. Ind. Pharm. 19 (1993) 2241–2269.
[9] M. Otsuka, H. Hasegawa, Y. Matsuda, Effect of polymorphic transformation during the extrusion-granulation process on the pharmaceutical properties of carbamazepine granules, Chem. Pharm. Bull. 45 (1997) 894–898.
[10] M. Otsuka, T. Matsumoto, N. Kaneniwa, Effect of environmental temperature on polymorphic solid-state transformation of indomethacin during grinding, Chem. Pharm. Bull. 34 (1986) 1784–1793.
[11] M. Otsuka, T. Matsumoto, N. Kaneniwa, Effects of the mechanical energy of multi-tableting compression on the polymorphic transformations of chlorpropamide, J. Pharm. Pharmacol. 41 (1989) 665–669.
[12] M. Otsuka, M. Nakanishi, Y. Matsuda, Effects of crystalline form on the tableting compression mechanism of phenobarbital polymorphs, Drug Dev. Ind. Pharm. 25 (1999) 205–215.
[13] M. Otsuka, H. Ohtani, N. Kaneniwa, Effect of humidity on solid-state isomerization of various kinds of lactose during grinding, J. Pharm. Pharmacol. 45 (1992) 2–5.
[14] M. Otsuka, M. Onoe, Y. Matsuda, Physicochemical stability of phenobarbital polymorphs at various levels of humidity and temperature, Pharm. Res. 10 (1993) 577–582.
[15] M. Otsuka, K. Otsuka, N. Kaneniwa, Relation between polymorphic transformation pathway during grinding and the physicochemical properties of bulk powders for pharmaceutical preparations, Drug Dev. Ind. Pharm. 20 (1994) 1649–1660.
[16] P.T. Cardew, R.J. Davey, The kinetics of solvent-mediated phase transformations, Proc. R. Soc. Lond. 398 (1985) 415–428.
[17] P. Ehrenfest, Phase changes classified according to the singularities of the thermodynamic potential, Proc. Acad. Sci. Amsterdam 36 (1933) 153–157, Chap. 2.
[18] C.J. Eckhardt, T. Luty, N.M. Peachey, Collective interactions and solid state reactivity, Mol. Cryst. Liq. Cryst. 313 (1998) 25–38.
[19] T. Luty, C.J. Eckhardt, General theoretical concepts for solid-state reactions: quantitative formulation of the reaction cavity, steric compression, and reaction-induced stress using an elastic multipole representation of chemical pressure, J. Am. Chem. Soc. 117 (1995) 2441–2452.
[20] S.M. Sharma, V. Vijayakumar, S.K. Sikka, R. Chidambaram, High-pressure phase-transitions in organic-solids alpha-beta transition in resorcinol, Pramana 25 (1985) 75–79.
[21] U.J. Griesser, A. Burger, K. Mereiter, The polymorphic drug substances of the European pharmacopoeia. IX Physicochemical properties and crystal structure of acetazolamide crystal forms, J. Pharm. Sci. 86 (1997) 352–358.
[22] B.C. Hancock, G. Zografi, Characteristics and significance of the amorphous state in pharmaceutical systems, J. Pharm. Sci. 86 (1997) 1–12.
[23] H.B. Callen, Thermodynamics and an Introduction to Thermostatistics, 2nd Edition, John Wiley and Sons, New York, 1985.
[24] D. Turnbull, Phase changes, in: F. Seitz, D. Turnbull (Eds.), Solid-State Physics: Advances in Research and Applications, Vol. 3, Academic Press, New York, 1956, pp. 225–306.
[25] S. Petit, G. Coquerel, Mechanism of several solid–solid transformations between dihydrated and anhydrous copper(II) 8-hydroxyquinolinates. Proposition for a unified model for the dehydration of molecular crystals, Chem. Mater. 8 (1996) 2247–2258.
[26] J.Z. Gougoutas, Senior Research Fellow, Bristol-Myers Squibb Research Institute, Princeton, NJ, (personal communication).
[27] D. Kunii, O. Levenspiel, Fluidization Engineering, 2nd Edition, Butterworth–Heinemann, Oxford, 1991, Chap. 13.
[28] J.W. Mullin, in: Crystallization, 3rd Edition, Butterworth–Heinemann, Oxford, 1997, pp. 227–228.
[29] H.G. Brittain, K.R. Morris, D.E. Bugay, A.B. Thakur, A.T.M. Serajuddin, Solid-state NMR and IR for the analysis of pharmaceutical solids: polymorphs of fosinopril sodium, J. Pharm. Biomed. Anal. 11 (1993) 1063–1069.
[30] G.A. Stephenson, J.G. Stowell, P.H. Toma, D.E. Dorman, J.R. Greene, S.R. Byrn, Solid-state analysis of polymorphic, isomorphic, and solvated forms of dirithromycin, J. Am. Chem. Soc. 116 (1994) 5766–5773.
[31] M. Otsuka, M. Onoe, Y. Matsuda, Physicochemical stability of phenobarbital polymorphs at various levels of humidity end temperature, Pharm. Res. 10 (1993) 577–582.
[32] M.W.Y. Wong, A.G. Mitchell, Physicochemical characterization of a phase-change produced during the wet granulation of chlorpromazine hydrochloride and its effects on tabletting, Int. J. Pharm. 88 (1992) 261–273.
[33] M.D. Parker, P. York, R.C. Rowe, Binder-substrate interactions in wet granulation. III. The effect of excipient source variation, Int. J. Pharm. 80 (1992) 179–190.
[34] N.V. Phadnis, R. Suryanarayanan, Polymorphism in anhydrous theophylline: implications on the dissolution rate of theophylline tablets, J. Pharm. Sci. 86 (1997) 1256–1263.
[35] H. Doser, The melting points of pantocaines, bromurals, and theophyllines, Arch. Pharm. 53 (1943) 251–256.
[36] A. Burger, R. Ramberger, On the polymorphism of pharmaceuticals and other molecular crystals. II. Applicability of thermodynamic rules, Mikrochim. Acta 2 (1979) 273–316.
[37] E. Suzuki, K. Shimomura, K. Sekiguchi, Thermochemical study of theophylline and its hydrate, Chem. Pharm. Bull. 37 (1989) 493–497.
[38] U.J. Griesser, A. Burger, Effect of different moisture con-

UM00011689
NOVARTIS EXHIBIT 1517
Novartis v. Regents, IPR2023-01347
Page 435 of 4460

ditions on phase changes of theophylline crystal forms, in: 41st Annual Congress of the Study Group for Pharmaceutical Technical Procedures e. v. (A.P.V.) Budapest, May 8–11, 1995.
[39] J. Herman, J.P. Remon, N. Visavarungroj, J.B. Schwartz, G. Klinger, Formation of theophylline monohydrate during the pelletisation of microcrystalline cellulose-anhydrous theophylline blends, Int. J. Pharm. 42 (1988) 15–18.
[40] M. Niskanen, Explaining the dissolution properties of theophylline pellets by their microstructure, Pharm. Technol. Int. Ed. 4 (1992) 20–28.
[41] C.M. Adeyeye, J. Rowley, D. Madu, M. Javadi, S.S. Sabnis, Evaluation of crystallinity and drug release stability of directly compressed theophylline hydrophilic matrix tablets stored under varied moisture conditions, Int. J. Pharm. 116 (1995) 65–75.
[42] A. Miyamae, H. Kema, T. Kawabata, T. Yasuda, M. Otsuka, Y. Matsuda, X-ray-powder diffraction study on the grinding effect of the polymorphs of a novel and orally effective uricosuric agent FR76505, Drug Dev. Ind. Pharm. 20 (1994) 2881–2897.
[43] M. Otsuka, T. Matsumoto, S. Higuchi, K. Otsuka, N. Kaneniwa, Effect of compression temperature on the consolidation mechanism of chlorpropamide polymorphs, J. Pharm. Sci. 84 (1995) 614–618.
[44] Y. Takahashi, K. Nakashima, T. Ishihara, H. Nakagawa, I. Sugimoto, Polymorphism of fostedil: characterization and polymorphic change by mechanical treatments, Drug Dev. Ind. Pharm. 11 (1985) 1543–1563.
[45] S.D. Clas, R. Faizer, R.E. O'Connor, E.B. Vadas, Quantification of crystallinity in blends of lyophilized and crystalline MK-0591 using X-ray-powder diffraction, Int. J. Pharm. 121 (1995) 73–79.
[46] S.D. Clas, M. Cotton, E. Moran, S. Spagnoli, G. Zografi, E.B. Vadas, Assessment of the physical stability of lyophilized MK-0591 by differential scanning calorimetry, Thermochim. Acta 288 (1996) 83–96.
[47] M.J. Pikal, Impact of polymorphism on the quality of lyophilized products, in: H.G. Brittain (Ed.), Polymorphism in Pharmaceutical Solids, Marcel Dekker, New York, 1999, pp. 395–419.
[48] S. Chongprasert, U.J. Griesser, A.T. Bottorff, N.A. Williams, S.R. Byrn, S.L. Nail, Effects of freeze dry processing conditions on the crystallization of pentamidine isethionate, J. Pharm. Sci. 87 (1998) 1155–1160.

For further reading

V. Andronis, G. Zografi, The molecular mobility of supercooled amorphous indomethacin as a function of temperature and relative humidity, Pharm. Res. 15 (1998) 835–842.
H.G. Brittain, Perspective on polymorphism, Pharm, Tech. 8 (1994) 50–52.
H.G. Brittain, S.J. Bogdanowich, D.E. Bugay, J. DeVincentis, G. Lewen, A.W. Newman, Physical characterization of pharmaceutical solids, Pharm. Res. 8 (1991) 963–973.
H.G. Brittain, E.F. Fiese, Effects of pharmaceutical processing on drug polymorphs and solvates, in: Polymorphism in Pharmaceutical Solids, Marcel Dekker, New York, 1999, pp. 331–361.
H.K. Chan, E. Doelker, Polymorphic transformation of some drugs under compression, Drug Dev. Ind. Pharm. 11 (1985) 315–332.
Y. Chikaraishi, A. Sano, T. Tsujiyama, M. Otsuka, Y. Matsuda, Preparation of piretanide polymorphs and their physicochemical properties and dissolution behaviors, Chem. Pharm. Bull. 42 (1994) 1123–1128.
Y. Chikaraishi, M. Otsuka, Y. Matsuda, Dissolution behavior of piretanide polymorphs at various temperatures and pHs, Chem. Pharm. Bull. 43 (1995) 1966–1969.
Y. Chikaraishi, M. Otsuka, Y. Matsuda, Preparation of amorphous and polymorph piretanide and their physicochemical properties and solubilities, Chem. Pharm. Bull. 44 (1996) 1614–1617.
O.I. Corrigan, K. Sabra, E.M. Holohan, Physicochemical properties of spray dried drugs: phenobarbitone and hydroflumethiazide, Drug Dev. Ind. Pharm. 9 (1983) 1–20.
J.L. Ford, M.H. Rubinstein, T.D. Duffy, D.S. Ireland, A comparison of the properties of some chloramphenicol and neomycin eye ointments, commercially available in the UK, Drug Dev. Ind. Pharm. 9 (1983) 21–33.
J.K. Haleblian, Characterization of habits and crystalline modification of solids and their pharmaceutical applications, J. Pharm. Sci. 64 (1975) 1269–1288.
R. Jain, A.S. Railkar, A.W. Malick, C.T. Rhodes, N.H. Shah, Stability of a hydrophobic drug in presence of hydrous and anhydrous lactose, Eur. J. Pharm. Biopharm. 46 (1998) 177–182.
J. Joachim, D.O. Opota, G. Joachim, J.P. Reynier, P. Monges, L. Maury, Effect of solvate formation on lyoavailability of lorazepam during wet granulation, Stp Pharma Sci. 5 (1995) 486–488.
L. Juslin, J. Yliruusi, The effect of fluidized bed granulation on the crystal properties of lactose, glucose and mannitol, Stp Pharma Sci. 6 (1996) 173–178.
N. Kaneniwa, K. Imagawa, M. Otsuka, Effect of tabletting on the degree of crystallinity and on the dehydration and decomposition points of cephalexin crystalline powder, Chem. Pharm. Bull. 33 (1985) 802–809.
N. Kaneniwa, M. Otuska, Effect of grinding on the transformations of polymorphs of chloramphenicol palmitate, Chem. Pharm. Bull. 33 (1985) 1660–1668.
A. Katrusiak, M. Szafranski, Structural phase transitions in guanidinium nitrate, J. Mol. Struct. 378 (1996) 205–223.
Y. Kawashima, S.Y. Lin, H. Takenaka, Polymorphism and drug release behavior of spray-dried microcapsules of sulfamethoxazole with polysaccharide gum and colloidal silica, Drug Dev. Ind. Pharm. 9 (1983) 1445–1463.
T. Matsumoto, J. Ichikawa, N. Kaneniwa, M. Otsuka, Effect of environmental temperature on the polymorphic transformation of phenylbutazone during grinding, Chem. Pharm. Bull. 36 (1988) 1074–1085.
T. Matsumoto, K. Nobuyoshi, S. Higuchi, M. Otsuka, Effects of

UM00011690
NOVARTIS EXHIBIT 1517
Novartis v. Regents, IPR2023-01347
Page 436 of 4460

temperature and pressure during compression on polymorphic transformation and crushing strength of chlorpropamide tablets, J. Pharm. Pharmacol. 43 (1990) 74–78.

S. McGuigan, J.H. Strange, J.M. Chezeau, The temperature and pressure dependence of molecular motion in solid naphthalene studied by NMR, Mol. Phys. 49 (1983) 275–282.

K.R. Morris, A.W. Newman, D.E. Bugay, S.A. Ranadive, A.K. Singh, M. Szyper, S.A. Varia, H.G. Brittain, A.T.M. Serajuddin, Characterization of humidity-dependent changes in crystal properties of a new HMG-CoA reductase inhibitor in support of its dosage form development, Int. J. Pharm. 108 (1994) 195–206.

C. Moynihan, A.J. Easteal, J. Wilder, Dependence of the glass transition temperature on heating and cooling rate, J. Phys. Chem. 78 (1974) 2673–2677.

M. Otsuka, N. Kaneniwa, Effect of environment of crystallinity and chemical stability in solid-state of ground cephalotin sodium during storage, Drug Dev. Ind. Pharm. 17 (1991) 909–918.

M. Otsuka, M. Onoe, Y. Matsuda, Physicochemical characterization of phenobarbital polymorphs and their pharmaceutical properties, Drug Dev. Ind. Pharm. 20 (1994) 1453–1470.

C.N.R. Rao, Phase transitions and the chemistry of solids, Acc. Chem. Res. 17 (1984) 83–89.

P.J. Saidon, N.S. Cauchon, P.A. Sutton, C.J. Chang, G. E Peck, S.R. Byrn, Solid-state nuclear magnetic resonance (NMR) spectra of pharmaceutical dosage forms, Pharm. Res. 10 (1993) 197–203.

K. Sato, Polymorphic transformations in crystal-growth, J. Phys. D, App. Phys. 26 (1993) 77–84.

S.L. Shamblin, X. Tang, L. Chang, B. C Hancock, M.J. Pikal, Characterization of the time scales of molecular motion in pharmaceutically important glasses, J. Phys. Chem. B 103 (1999) 4113–4121.

G.A. Stephenson, T.B. Borchardt, S.R. Byrn, J. Bowyer, C.A. Bunnell, S.V. Snorek, L. Yu, Conformational and color polymorphism of 5-methyl-2[(2-nitrophenyl)amino]-3-thiophenecarbonitrile, J. Pharm. Sci. 84 (1995) 1385–1386.

S. Sudo, K. Sato, Y. Harano, Growth and solvent-mediated phase-transition of cimetidine polymorphic form-A and form-B, J. Chem. Eng. Jpn. 24 (1991) 628–632.

M.P. Summers, R.P. Enever, J.E. Carless, The influence of crystal form on the radial stress transmission characteristics of pharmaceutical materials, J. Pharm. Pharmac. 28 (1976) 89–99.

H. Takenaka, Y. Kawashima, S.Y. Lin, Polymorphism of spray-dried microencapsulated sulfamethoxazole with cellulose acetate phthalate and colloidal silica, montmorillonite, or talc, J. Pharm. Sci. 70 (1981) 1256–1260.

UM00011691
NOVARTIS EXHIBIT 1517
Novartis v. Regents, IPR2023-01347
Page 437 of 4460

A Model for Resonance-Assisted Hydrogen Bonding in Crystals and Its Graph Set Analysis

Robert W. Munn*,† and Craig J. Eckhardt*,‡

Department of Chemistry, UMIST, Manchester M60 1QD, U.K., and Department of Chemistry, University of Nebraska—Lincoln, Lincoln, Nebraska 68588-0304

Received March 20, 2001

Resonance-assisted hydrogen bonding is treated by the simple quantum-mechanical model of a particle on a ring with different effective masses in the hydrogen bond and in the conjugated segment attached to its ends. The model is applied to an intramolecular hydrogen bond and extended to a hydrogen-bonded dimer and rings of arbitrary size up to an infinite chain of molecules, thus covering the main patterns of bonding identified by graph-set analysis. Analysis of intramolecular hydrogen bonding yields an electron effective mass in the hydrogen bond segment of about 34 electron masses. Conjugation always lowers the energy, but the lowering per molecule decreases with increasing ring size, that for the chain being one-third of that for the intramolecular hydrogen bond. This result rationalizes a predominance of intramolecular hydrogen bonds and dimer rings, given that geometrical factors also affect bonding.

Introduction

The role of hydrogen bonds as a structural organizing feature in chemistry and biology is well-known. In particular, there has been extensive work to classify and interpret the structural motifs associated with hydrogen bonds within and between molecules in crystals. For example, graph-set analysis[1,2] has been used to identify four basic patterns of hydrogen bonding: an intramolecular or self-bond ring (S), a dimer ring (R), an infinite chain (C), and other finite or discrete patterns (D). Such classification is extremely useful in providing a soundly based taxonomy for describing the diversity of hydrogen bonding patterns in crystals. It would be even more useful if in addition to this codification there were a physical picture of similar scope and generality that would help to interpret and rationalize the observed diversity. The present paper seeks to provide such a model.

The Ferrara group[3−8] has surveyed experimental results which show that noticeably short hydrogen bonds with the hydrogen atom nearly at the center occur in systems of the general structure −X−H···X=, where the two identical X atoms (homonuclear hydrogen bonding) are connected by a conjugated π-electron system. This in turn requires an odd number of atoms in the π system. It is plausible that in such systems the two resonance hybrids of the π system, which require the transfer of the H atom from one X atom to the other, as illustrated in Figure 1, should lead to an equalization of bond lengths not only in the π system, as usual, but also in the hydrogen bond system. More recently, the Ferrara group has also provided evidence that such *resonance-assisted hydrogen bonding* may also occur when the two electronegative atoms X are not the same (heteronuclear hydrogen bonding).[9−13] Because hydrogen bond strength is exponentially dependent on length,[14,15] mechanisms for shortening hydrogen bonds are of particular significance.

The substantial theoretical literature on hydrogen bonding has employed both the valence-bond and molecular-orbital models.[16]

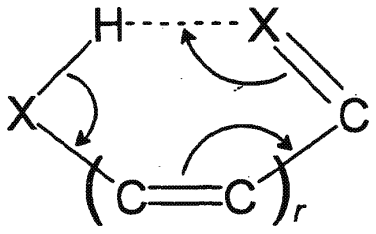


Figure 1. Structural pattern for resonance-assisted hydrogen bonding.

The resonance-assisted mechanism for strong hydrogen bonding starts from the valence-bond model, which has the advantage of permitting the use of curly arrows to show how the resonance hybrids are related. This, of course, is a familiar and productive approach in chemistry. On the other hand, valuable insights into conjugated systems are also obtained from the molecular-orbital model, where delocalization is built in at the start. Some of these insights are available even in highly simplified quantum mechanical models such as the particle in a box or on a ring. The particle in a box model is invoked in elementary chemistry to rationalize such matters as the red shift in optical spectra of conjugated polyenes with increasing chain length. The particle on a ring model is perhaps less familiar but is used in understanding NMR shielding and deshielding at different positions near a benzene ring in terms of a ring current[17] and as the perimeter free electron orbital model in classifying the excited states of aromatic hydrocarbons.[18] Here we explore a highly simplified but useful conceptual model for resonance-assisted hydrogen bonding in terms of a particle on a ring. We consider first the intramolecular hydrogen bond (type S) and then extend the treatment to the dimer (type R) and hence to larger rings, culminating in the infinite ring, which corresponds to the infinite chain (type C) with cyclic boundary conditions. Thus, we treat the three main graph set patterns.

Model for the Intramolecular Hydrogen Bond. For the intramolecular hydrogen bond (type S), the basic model consists of a ring of radius R divided into two segments. One segment that we label b represents the hydrogen bond −X−H···X= and

* To whom correspondence should be addressed.
† UMIST.
‡ University of Nebraska—Lincoln.

10.1021/jp011038g CCC: $20.00 © 2001 American Chemical Society
Published on Web 06/22/2001

UM00011692
NOVARTIS EXHIBIT 1517
Novartis v. Regents, IPR2023-01347
Page 438 of 4460

the other segment that we label c represents the conjugated system that connects the two X atoms. An electron moves in segment c with an effective mass m_c and in segment b with an effective mass m_b, where the concept of *effective mass* is borrowed from solid-state physics. As explained in standard solid-state physics texts, a particle at the bottom of an energy band moves as though it has a mass determined by the inverse of the curvature of the band, a quantity that may differ markedly from the normal inertial mass of the free particle. Here it allows for the fact that the mobile particle is not an isolated electron but an electron that is interacting with other electrons and with nuclei. In particular, it enables us to use electron transfer in the hydrogen bond as a surrogate or alias for proton transfer from one side to the other of the hydrogen bond, because the two transfers are strongly correlated.[19] We expect $m_b > m_c$, because the transfer of an electron through the hydrogen bond region requires significant movement of the much heavier hydrogen nucleus. In any case, we expect m_b to change markedly if we replace hydrogen by deuterium, thus providing us with a mechanism for an isotope effect.

The position of the electron on the ring is described by an angular variable P ($0 \le P \le 2\pi$). The bond segment b corresponds to $0 \le P \le 2\pi f$ and the conjugated segment c to $2\pi f \le P \le 2\pi$. Here f is the fraction of the ring that is occupied by the hydrogen bond. This changes with the length of the conjugated system, which is known to modify the hydrogen bond characteristics.[3-8] The parameters f and R are directly related to the chemical system being considered. The hydrogen-bond segment b comprises three atoms and the conjugated segment c comprises an odd number of atoms, as Figure 1 indicates. The whole chemical ring therefore comprises an even number of atoms n and, hence, the same number of bonds. Two of these bonds comprise segment b, and hence, $f = 2/n$. If we suppose that each bond contributes the same length d to the model ring, then the circumference is nd and $R = nd/2\pi$. One could alternatively treat the chemical ring as a regular polygon with n sides of length d and take the model ring as the circumscribed circle, in which case $R = d/(2 \sin \pi/n)$. For large n, these treatments become equivalent.

The wave function of the system is ψ_b in segment b and ψ_c in segment c. For energy E, the time-independent Schrödinger equation in the two segments is

$$-\frac{\hbar^2}{2m_bR^2}\frac{\partial^2\psi_b}{\partial\phi^2} = E\psi_b \tag{1}$$

$$-\frac{\hbar^2}{2m_cR^2}\frac{\partial^2\psi_c}{\partial\phi^2} = E\psi_c \tag{2}$$

Here m_bR^2 corresponds to the moment of inertia of the electron in segment b and m_cR^2 to that in segment c. Set

$$E = L_b^2/2m_bR^2 = L_c^2/2m_cR^2 \tag{3}$$

so that L_b and L_c (which may be positive or negative corresponding to opposite senses of circulation) are the classical angular momenta in segments b and c, where we shall set $L_b = \rho L_c$ so that $\rho^2 = m_b/m_c$. Then eqs 1 and 2 have solutions

$$\psi_b = \psi_b^0 \exp(iL_b\varphi/\hbar) \tag{4}$$

$$\psi_c = \psi_c^0 \exp(iL_c\varphi/\hbar) \tag{5}$$

The solutions are subject to the boundary conditions that the wave functions must be equal at the ends where the segments join. The first boundary condition is $\psi_b(0) = \psi_c(2\pi)$, i.e.

$$\psi_b^0 = \psi_c^0 \exp(2\pi iL_c/\hbar) \tag{6}$$

and the second is $\psi_b(2\pi f) = \psi_c(2\pi f)$, i.e.

$$\psi_b^0 \exp(2\pi ifL_b/\hbar) = \psi_c^0 \exp(2\pi ifL_c/\hbar) \tag{7}$$

Substitution from (6) into (7) and expressing L_b in terms of L_c yields

$$\exp[(1 - f + \rho f)(2\pi iL_c/\hbar)] \tag{8}$$

By comparison with the result $\exp(2\pi ik) = 1$ for integer k, we find that the angular momentum in segment c must be quantized in the form

$$L_c = \hbar k/(1 - f + \rho f) \tag{9}$$

where k is a nonzero integer. Hence the energy in state k is

$$E_k = \frac{\hbar^2k^2}{2m_cR^2(1 - f - \rho f)^2} \tag{10}$$

It follows that a single electron in the lowest level has energy

$$E_1 = \frac{\hbar^2}{2m_cR^2(1 - f - \rho f)^2} \tag{11}$$

Given the quantized value of the angular momentum L_c, one obtains L_b at once as $\rho > L_c$. From eqs 4–6, the wave function in the two segments is given in terms of L_c by

$$\Psi_c = \Psi_c^0 \exp(iL_c\varphi/\hbar) \tag{12}$$

$$\Psi_b = \Psi_c^0 \exp(2\pi iL_c/\hbar) \exp(iL_c\rho\varphi/\hbar) \tag{13}$$

The real part of the total wave function for $k = 1$ is plotted in Figure 2 for parameter values $f = 1/3$ (corresponding to one hydrogen bond in a six-membered ring) and $\rho = 5$. In the hydrogen-bonded segment, which lies at the bottom right-hand corner, the wave function ψ_b varies only slowly, but in the conjugated segment, ψ_c varies much more rapidly, owing to the additional factor ρ that multiplies P in eq 13 compared with eq 12.

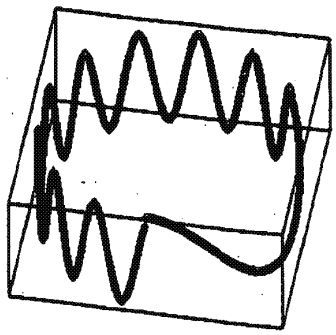


Figure 2. Real part of the wave function for $f = 1/3$ and $\rho = 5$.

Usually energy changes are more significant than energies themselves. Here the question is what effect the resonance assistance has on the hydrogen bonding, and therefore, we must

UM00011693
NOVARTIS EXHIBIT 1517
Novartis v. Regents, IPR2023-01347
Page 439 of 4460

consider the isolated hydrogen bond. In the absence of the conjugated segment of the ring c, the hydrogen bond comprises just segment b, for which we shall use the label B instead of b. The wave function in this segment is still given by eq 4, but the boundary conditions become $\psi_B(0) = 0 = \psi_B(2\pi f)$. The solutions in this instance are not traveling waves as those in eqs 4 and 5, but standing waves obtained by combining degenerate solutions (4) with equal and opposite L_B. As for an electron in a box, the solution that satisfies the boundary condition at the origin $\psi_B(0) = 0$ follows if the combination leading to a sine function is taken, i.e.

$$\psi_B = \psi_B^0 \sin(L_B\varphi/\hbar) \tag{14}$$

The other boundary condition $\psi_B(2\pi f) = 0$ yields

$$\sin(2\pi f L_B/\hbar) = 0 \tag{15}$$

and hence L_B must be of the form

$$L_B = \hbar K/f \tag{16}$$

where K is a nonzero integer. The energy is then

$$E_K^0 = \frac{\hbar^2 K^2}{2m_b R^2 f^2} \tag{17}$$

(where the superscript zero denotes the unconjugated hydrogen bond), so that an electron in the lowest level has energy

$$E_1^0 = \frac{\hbar^2}{2m_b R^2 f^2} = \frac{\hbar^2}{2m_c R^2 \rho^2 f^2} \tag{18}$$

We can now compare E_1^0 (without conjugation) with E_1 (with conjugation). Because $f < 1$, E_1 has a larger denominator than E_1^0 and, hence, is smaller. The energy lowering per electron is

$$\Delta E_1 = \frac{\hbar^2}{2m_c R^2}\left[\frac{1}{\rho^2 f^2} - \frac{1}{(\rho f + 1 - f)^2}\right] \tag{19}$$

$$= \frac{\hbar^2}{2m_b R^2}\left[\frac{1}{f^2} - \frac{\rho^2}{(\rho f + 1 - f)^2}\right] \tag{20}$$

This is zero when $f = 1$, because then there is no conjugated segment in either case. It also tends to zero as $\rho f/(1 - f) \to \infty$ for $f \neq 1$, when the two terms in the square bracket in eq 19 become equal. Increasing ρ, as happens on deuteration, thus reduces the energy lowering produced by the conjugated pathway. Increasing the radius R of the ring can also be seen to reduce the energy lowering.

With f and R expressed in terms of the number of bonds n and the bond length d, the energy lowering per electron becomes

$$\Delta E_1 = \frac{h_2}{8m_b d^2}\left[1 - \frac{4\rho^2}{(n - 2 + 2\rho)^2}\right] \tag{21}$$

For $n \gg \rho$, ΔE_1 reaches its maximum value $h^2/8m_b d^2$, which is just the lowest energy of a particle of mass m_b in a box of length d. Increasing the length of the conjugated chain thus increases the stabilization of the hydrogen bond toward this value.

The Ferrara group characterizes resonance-assisted hydrogen bonds by a parameter λ derived from the bond lengths in the hydrogen-bonded system.[3-8] This parameter ranges from 0 to 1 as the hydrogen bonding varies from complete localization of the proton on one side to complete localization on the other, so that a value of $^1/_2$ corresponds to complete delocalization. The present model envisages complete delocalization as one limit, with complete localization on either side as the other. Intermediate situations are represented by a mixture in which the fractional contribution of the delocalized model depends on an auxiliary parameter ξ that we define to equal $4\lambda(1 - \lambda)$, which takes the value unity for $\lambda = {}^1/_2$ and zero for $\lambda = 0$ or 1. The energy lowering relative to completely localized hydrogen bonding is then consistent with Figure 2 in ref 3. This shows that for S-type intramolecular hydrogen bonds the oxygen−oxygen distance (which serves as a surrogate for the hydrogen bond energy) has a dependence on λ that is symmetric about $\lambda = {}^1/_2$ and is roughly parabolic.

We have explored this idea using our model to analyze the data for oxygen−oxygen distances, taking values of the parameter λ from ref 3 and converting the oxygen−oxygen distances to hydrogen bond energies using a procedure described in the literature.[7] We then examined the hydrogen bond energies as a function of ξ by linear regression against ξ, ξ^2, and $\sqrt{\xi}$. In practice, owing to the large scatter in the data, all of these simple fits give values of the squared correlation coefficient r^2 of 0.6−0.7, so that none can be preferred on the grounds of a statistically superior fit. However, only the regression on ξ^2 gives a reasonable unconstrained value of the hydrogen bond energy in the absence of resonance assistance (the intercept at $\xi = 0$), namely, 17 kJ mol^{-1}. This is consistent with a model in which ξ determines the contribution from the conjugated structure to the wave function, because then ξ^2 determines the contribution to the energy. For this plot, the slope is 52 kJ mol^{-1}, which we equate to $2\Delta E_1$ for two electrons in the bond. We have ΔE_1 given by eq 21, in which $n = 6$ ($f = {}^1/_3$) for the structures under investigation, for which we take $d = 1.344$ Å as the average bond length in the unperturbed geometry.[3]

Taking m_c as the usual electron inertial mass m_e leads finally to a value of $\rho = 5.85$, so that the effective mass of the electron in the hydrogen bond segment is $m_b = 34.2m_e$. Clearly, this is much higher than the electron inertial mass but much lower than the inertial mass of the proton, $m_p = 1836m_e$. This is consistent with the use of the electron motion as a surrogate for the proton motion, where the effective mass represents the curvature of the potential energy in which the electron moves and hence differs from the inertial mass. In our model, the electron that represents the proton certainly moves more slowly than a normal electron, but the reduction is less than the ratio of the proton and electron inertial masses would suggest, implying that the electron movement takes place in a rather flat effective potential.

We can also compare our results for the ring with the two segments with those for a simple conjugated ring of the same size in which two more conjugated bonds replace the hydrogen-bonded segment. In such systems, the ring current model[17] affords insights into the NMR spectrum. Applying a magnetic field perpendicular to the ring induces a circulation of current around the ring equivalent to an induced magnetic dipole moment. This induced moment produces an additional magnetic field that deshields nuclei outside the ring (and shields nuclei inside it, such as the protons held over the ring in *para*-cyclophanes) to an extent that depends inversely on the effective mass of the circulating electrons. For the simple conjugated ring, with no hydrogen bond, the energy in the lowest level is obtained from eq 10 with $f = 0$. Comparison with eq 10 itself, describing the ring with the hydrogen bond, shows that the effective mass has been increased by the factor $(1 - f + >f)^2$.

UM00011694
NOVARTIS EXHIBIT 1517
Novartis v. Regents, IPR2023-01347
Page 440 of 4460

It follows as a prediction from our model that the deshielding of nuclei outside the ring with the hydrogen bond should be reduced by this factor relative to a simple conjugated ring of the same size. As noted earlier, deuteration increases ρ, which reduces deshielding still further. On the other hand, stronger hydrogen bonds have lower energies that correspond to reduced values of ρ and, hence, lead to less reduction in the deshielding. The Ferrara group has reported a strong correlation between proton NMR shifts and hydrogen bond strength,[8] but this concerns the hydrogen atom that forms part of the hydrogen-bonded system. In our model, this atom is considered as lying on the ring rather than outside it, and the ring-current model is then uninformative.

Extension to Hydrogen-Bonded Dimers and Beyond. We now consider the extension of our treatment to a hydrogen-bonded dimer (type R) comprising two conjugated segments, labeled c1 and c2, and two hydrogen-bonded segments, labeled b1 and b2. To make comparisons with the intramolecular hydrogen bond for the monomer, we take a total of n atoms for each molecule, of which three form each hydrogen bond. Hence, there are $2n$ atoms and $2n$ bonds in total, with two hydrogen-bonded segments of two bonds each. As a result, each segment b1 and b2 occupies a fraction $1/n$ of the whole ring, whereas together they occupy the fraction $f = 2/n$, the same as that for the intramolecular hydrogen bond. Corresponding segments are equivalent, so the effective masses are the same as before: m_c in the conjugated segments and m_b in the hydrogen bond segments.

In the different segments, the wave functions are ψ_{bi} and ψ_{ci}, where $i = 1$ or 2. They obey Schrödinger equations such as (1) and (2) which we solve as before by expressing the energy E in terms of classical angular momenta to obtain solutions of the forms (4) and (5) and applying suitable boundary conditions. The boundary conditions at the hydrogen bonds between different molecules are $\psi_{b1}(0) = \psi_{c2}(2\pi)$ and $\psi_{c1}(\pi) = \psi_{b2}(\pi)$, whereas those within the individual molecules are $\psi_{b1}(\pi f) = \psi_{c1}(\pi f)$ and $\psi_{b2}(\pi + \pi f) = \psi_{c2}(\pi + \pi f)$. Note that, for ease of comparison, the fraction f is defined to be the same as that for the monomer: each hydrogen bond subtends half the angle it did in the monomer, but this is the same fraction f of π, which is half the total angle 2π. The procedures applied for the monomer then lead to exactly the same quantization condition as before, eq 9. The primary difference from the monomer case is that the size of the ring is doubled for the dimer, and as a result, the energy eigenvalues are all a factor of 4 smaller than those in the monomer.

From this derivation, it follows that extension to a ring of N monomers would simply result in reducing all of the energy eigenvalues by a factor of N^2. In the limit $N \rightarrow \infty$, we obtain the result for an infinite chain (with the common device of cyclic boundary conditions), which is type C.

To compare the results for the dimer and larger rings with those for the monomer, we have to consider how to populate the energy levels. For the monomer, a valence-bond description of switching the hydrogen bond from one side to the other of segment b requires the movement of a pair of electrons. These can be accommodated in the degenerate states of lowest energy, which have quantum numbers ± 1 corresponding to opposite senses of movement. Together these yield a standing wave rather than a traveling wave with one nodal line across the ring. Movement of just one pair of electrons can also switch all of the hydrogen bonds simultaneously for any number of molecules conjugated in a ring. On the other hand, it seems that the relevant comparison must consider the energy lowering per molecule produced by the conjugated pathway in rings of different size, and this requires movement of one pair of electrons per molecule. This can be regarded as representing a process of switching one hydrogen bond per molecule. Then for N molecules there are two electrons in each of the lowest energy levels up to and including those with quantum numbers $\pm N$. This yields standing waves with 1 to N nodal lines across the ring.

The total energy lowering for a ring of N molecules populated by $2N$ electrons is then found by adapting eq 21 to be

$$\frac{\Delta E}{N} = \frac{2}{N}\frac{h^2}{8m_b(Nd)^2}\left[1 - \frac{4\rho^2}{(n-2+2\rho)^2}\right](1^2 + 2^2 + \ldots N^2) \quad (22)$$

$$= \frac{h^2}{4m_b d^2}\left[1 - \frac{4\rho^2}{(n-2+2\rho)^2}\right]\frac{(N+1)(2N+1)}{6N^2} \quad (23)$$

The function of N on the right-hand side of eq 23 is equal to 1 for $N = 1$ and tends to $^1/_3$ as $N \rightarrow \infty$. Hence, there is a significant energy lowering caused by conjugation for rings of all sizes, but the intramolecular hydrogen-bonded monomer and smaller rings are favored, all things being equal. This conclusion is broadly consistent with the hydrogen bond lengths tabulated by the Ferrara group, which tend to be larger in chains[7] than in intramolecular rings,[8] hence, implying greater stability of the latter.

Discussion

We have treated a very simple model of a particle on a ring that comprises two different kinds of segments corresponding to conjugated paths and hydrogen bonds with different effective masses in the different kinds of segments. Although the model is simple, solving it and deducing its consequences for different graph set patterns requires detailed analysis. We have shown that the conjugation lowers the energy, consistent with the Ferrara group's concept of resonance-assisted hydrogen bonding,[3-8] and that the model can fit data for intramolecular bonds of type S with an electron effective mass in the hydrogen bond segment of some 34 electron inertial masses. Using effective mass in the context of hydrogen bonding is unusual but is helpful conceptually. For example, it serves to give the proton an implicit role in resonance-assisted hydrogen bonding by its effect on the electron dynamics. The effective mass also indicates the relative flatness of the hydrogen bond potential, and presumably takes some account of proton tunneling. The present model for a hydrogen-bonded ring of molecules is conceptually similar to the coordinated proton tunneling observed by NMR relaxometry in a calixarene,[20] although in that case no conjugated segments intervened between the four hydrogen bonds.

The energy lowering applies not only to a simple intramolecular hydrogen bond but also to a hydrogen-bonded dimer and larger rings that in the limit become an infinite chain. In practice, geometrical constraints on bonding will govern which structure may reasonably occur, but our results indicate that an intramolecular ring or a dimer will tend to be favored, consistent with the graph-set classification that identifies such types of hydrogen bonding (S and R) separately from chains (C) and others (D). In our analysis, the chain is least favored, but this structural feature may benefit from other favorable factors such as the cooperative effect in α helices, whereby it becomes easier to form second and subsequent hydrogen bonds.[21] For example, a molecular orbital comparison between hydrogen-bonded chains of urea molecules and chains of 1,3-propanedione molecules[22]

UM00011695
NOVARTIS EXHIBIT 1517
Novartis v. Regents, IPR2023-01347
Page 441 of 4460

indicates that the resonance-assisted mechanism is more important where covalent rather than electrostatic interactions prevail.

Our treatment is most likely to be relevant to homonuclear hydrogen bonds with the same electronegative atom at either end, as originally discussed by the Ferrara group.[3-8] However, the qualitative effects are likely to be the same for heteronuclear hydrogen bonds with different atoms at either end.[9-13] This would imply less delocalization, i.e., a value of the parameter λ introduced earlier that departs from $^1/_2$, and presumably a modified value of the effective mass m_b. It would also imply a correspondingly more ionic rather than covalent structure[22] that would rather stretch the validity of the model. Nevertheless, such an extension should be valuable in providing extended interpretation.

Acknowledgment. This work was stimulated by the NATO Advanced Research Workshop "Crystals: Supra-molecular Materials". We are grateful to the Organizing Committee for invitations and support to attend this meeting.

References and Notes

(1) Etter, M. C.; MacDonald, J. C.; Bernstein, J. *Acta Crystallogr. B* **1990**, *46*, 256−262.

(2) Bernstein, J.; Davis, R. E.; Shimoni, L.; Chang, N.-L. *Angew. Chem., Int. Ed. Engl.* **1995**, *34*, 1555−1573.

(3) Gilli, G.; Bellucci, F.; Ferretti, V.; Bertolasi, V. *J. Am. Chem. Soc.* **1989**, *111*, 1023−1028.

(4) Bertolasi, V.; Gilli, P.; Ferretti, V.; Gilli, G *J. Am. Chem. Soc.* **1991**, *113*, 4917−4925.

(5) Gilli, G.; Bertolasi, V.; Ferretti, V.; Gilli, P. *Acta Crystallogr. B* **1993**, *49*, 564−576.

(6) Gilli, P.; Bertolasi, V.; Ferretti, V.; Gilli, G. *J. Am. Chem. Soc.* **1994**, *116*, 909−915.

(7) Bertolasi, V.; Gilli, P.; Ferretti, V.; Gilli, G. *Chem.−Eur. J.* **1996**, *2*, 925−934.

(8) Bertolasi, V.; Gilli, P.; Ferretti, V.; Gilli, G. *J. Chem. Soc., Perkin Trans. 2* **1997**, 945−952.

(9) Bertolasi, V.; Ferretti, V.; Gilli, P.; Gilli, G.; Issa, Y. M.; Sherif, O. E. *J. Chem. Soc., Perkin Trans. 2* **1993**, 2223−2228.

(10) Bertolasi, V.; Nanni, L.; Gilli, P.; Ferretti, V.; Gilli, G.; Issa, Y. M.; Sherif, O. E. *New J. Chem.* **1994**, *18*, 251−261.

(11) Bertolasi, V.; Gilli, P.; Ferretti, V.; Gilli, G. *Acta Crystallogr. B* **1994**, *50*, 617−625.

(12) Bertolasi, V.; Gilli, P.; Ferretti, V.; Gilli, G. *Acta Crystallogr. B* **1995**, *51*, 1004−1015.

(13) Bertolasi, V.; Gilli, P.; Ferretti, V.; Gilli, G. *Acta Crystallogr. B* **1998**, *54*, 50−655.

(14) Espinosa, E.; Molins, E.; Lecomte, C *Chem. Phys. Lett.* **1998**, *285*, 170−173.

(15) Spackman, M. A. *Chem. Phys. Lett.* **1999**, *301*, 425−429

(16) Smith, D. A., Ed.; Modeling the Hydrogen Bond. *ACS Symposium Series, Vol 569*; American Chemical Society: Washington, DC, 1994. Scheiner, S. *Hydrogen Bonding*; Oxford University Press: New York, 1997.

(17) Pople, J. A. *J. Chem. Phys.* **1956**, *24*, 1111.

(18) Platt, J. R. *J. Chem. Phys.* **1949**, *17*, 484−495.

(19) This situation resembles the old token system used on single-track sections of a railroad to ensure that only one train can enter the section at a time. At the beginning of the section, the locomotive engineer receives a token that permits the train to travel to the other end, where the token is left for the next train in the opposite direction. Although the significant movement is that of the train, it can be monitored (aliased) by the corresponding movement of the token.

(20) Brougham, D. F.; Caciuffo, R.; Horsewill, A. J. *Nature* **1999**, *397*, 241−243.

(21) Milner-White, E. J. *Protein Sci.* **1997**, *6*, 2477−2481.

(22) Dannenberg, J. J.; Haskamp, L.; Masunov, Artëm *J. Phys. Chem A* **1999**, *103*, 7083−7086.

UM00011696
NOVARTIS EXHIBIT 1517
Novartis v. Regents, IPR2023-01347
Page 442 of 4460

This Page is Inserted by IFW Indexing and Scanning Operations and is not part of the Official Record

BEST AVAILABLE IMAGES

Defective images within this document are accurate representations of the original documents submitted by the applicant.

Defects in the images include but are not limited to the items checked:

- ☐ BLACK BORDERS
- ☐ IMAGE CUT OFF AT TOP, BOTTOM OR SIDES
- ☐ FADED TEXT OR DRAWING
- ☐ BLURRED OR ILLEGIBLE TEXT OR DRAWING
- ☐ SKEWED/SLANTED IMAGES
- ☐ COLOR OR BLACK AND WHITE PHOTOGRAPHS
- ☐ GRAY SCALE DOCUMENTS
- ☐ LINES OR MARKS ON ORIGINAL DOCUMENT
- ☐ REFERENCE(S) OR EXHIBIT(S) SUBMITTED ARE POOR QUALITY
- ☐ OTHER: _____

IMAGES ARE BEST AVAILABLE COPY.
As rescanning these documents will not correct the image problems checked, please do not report these problems to the IFW Image Problem Mailbox.

X-ray Structural Studies on Two Forms of β-Cyclodextrin·barbital Complexes

Isao NAKANISHI, Masako ARAI, Takaji FUJIWARA, and Ken-ichi TOMITA

Faculty of Pharmaceutical Sciences of Osaka University,
1-6, Yamada-oka, Suita, Osaka 565 JAPAN

Abstract

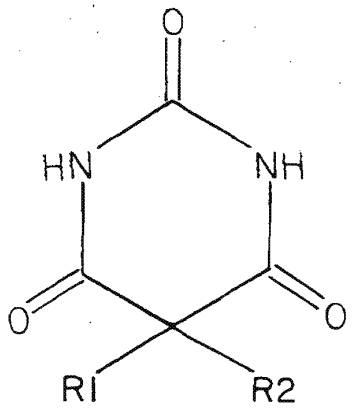
The crystal structures of two forms of β-cyclodextrin·barbital complexes (Form I and Form II) were investigated by X-ray analysis. In Form I crystal, two β-cyclodextrin(β-CyD) molecules including two barbital molecules form a dimeric structure by the hydrogen bonds among their secondary hydroxyl groups. The unit cell volume of Form II is about twice as large as that of Form I and there exist two β-CyD dimers in Form II. Although the (Host)/(Guest) ratio is 1/1, only one barbital molecule can be found in Form II at the present stage. The similarities and differences between the two crystal structures are mainly discussed here.

1. Introduction

CyDs can be obtained by acting the cyclodextrin glucosyl transferases on starch and are the cyclic oligomers of α-1,4 linked D-glucopyranose residues. Well known α-, β-, and γ-CyD are constructed by six, seven, or eight D-glucopyranose units. β-CyD as well as the other CyDs has a conical cavity which can include various compounds and can change some properties such as the solubility and the stability of the included compounds. As β-CyD is also harmless and less expensive than the other CyDs, it has been used in the field of medicinal chemistry. As the barbituric acid derivatives(TABLE I) which have hypnotic and sedative properties are sparingly soluble in water, some work to improve the poor solubility by the aid of β-CyD had been done and it has been reported that the apparent solubility of them increased[1,2]. The stability constants and the thermodynamic parameters of the β-CyD inclusion complexes with barbital derivatives in aqueous medium have also been studied[3]. It is very interesting that these values are very different among the derivatives.

Journal of Inclusion Phenomena 2, 689–699. 0167-7861/84.15.
© 1984 *by D. Reidel Publishing Company.*

TABLE I. The barbituric acid derivatives.



R1	R2	
$-C_2H_5$	$-C_2H_5$	: Barbital
$-C_2H_5$		: Phenobarbital
$-C_2H_5$		: Cyclobarbital
$-C_2H_5$	$-CH_2CH_2CH(CH_3)_2$	: Amobarbital
$-CH_2CH=CH_2$	$-CH_2CH=CH_2$	: Allobarbital

It is our intention to do X-ray structure analyses of these inclusion complexes in order to elucidate how these derivatives having various substituents at C5 position are included in the β-CyD cavity and why some physicochemical constants and parameters are different among the derivatives. Firstly we chose barbital(5,5-diethylbarbituric acid) as a guest molecule and found two different crystals(Form I and II).

2. Experimental

2.1. Form I complex

The colorless plate crystals were obtained by gradually cooling 1.5 ml of the hot aqueous solutions containing about $2X10^{-4}$ mol of β-CyD and barbital, respectively. The specific gravity of the crystals was measured by the floatation method using carbon tetrachloride and o-dichlorobenzene. After a crystal was enclosed in the 0.5 mmϕ glass capillary with a little amount of mother liquid, the lattice constants and the intensity data were measured with nickel-filtered CuKα radiation using the Rigaku Rotor AFC-5FOS automated four-circle diffractometer (40kV, 200mA). A total of 8356 independent reflections with $F_o > 3\sigma F_o$ were collected by using ω-2θ scan mode up to 125° in 2θ. The crystal data are listed in TABLE II. As the cell dimensions and the location of the big peaks on the Patterson map were very similar to those of the β-CyD·aspirin complex[4], we regarded Form I as isomorphous with β-CyD·aspirin. Therefore as the β-CyD model we used the coordinates of dimeric β-CyDs from β-CyD·aspirin and then the guest and water molecules could be found by the successive Fourier syntheses. The refinement of the atomic coordinates are in progress by the full-matrix least-squares method[5] with restraints applied to the bond lengths and angles of β-CyD and barbital molecules and at the present stage, R factor is 25.4 % for the 4363 strong reflections using isotropic thermal parameters for all the non-hydrogen atoms.

UM00011699
NOVARTIS EXHIBIT 1517
Novartis v. Regents, IPR2023-01347
Page 445 of 4460

X-ray Structural Studies on Two Forms of β-Cyclodextrin·barbital Complexes

Isao NAKANISHI, Masako ARAI, Takaji FUJIWARA, and Ken-ichi TOMITA

Faculty of Pharmaceutical Sciences of Osaka University,
1-6, Yamada-oka, Suita, Osaka 565 JAPAN

Abstract

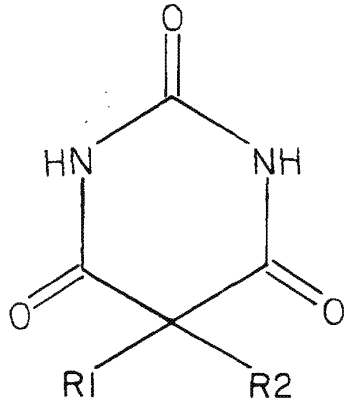
The crystal structures of two forms of β-cyclodextrin·barbital complexes (Form I and Form II) were investigated by X-ray analysis. In Form I crystal, two β-cyclodextrin(β-CyD) molecules including two barbital molecules form a dimeric structure by the hydrogen bonds among their secondary hydroxyl groups. The unit cell volume of Form II is about twice as large as that of Form I and there exist two β-CyD dimers in Form II. Although the (Host)/(Guest) ratio is 1/1, only one barbital molecule can be found in Form II at the present stage. The similarities and differences between the two crystal structures are mainly discussed here.

1. Introduction

CyDs can be obtained by acting the cyclodextrin glucosyl transferases on starch and are the cyclic oligomers of α-1,4 linked D-glucopyranose residues. Well known α-, β-, and γ-CyD are constructed by six, seven, or eight D-glucopyranose units. β-CyD as well as the other CyDs has a conical cavity which can include various compounds and can change some properties such as the solubility and the stability of the included compounds. As β-CyD is also harmless and less expensive than the other CyDs, it has been used in the field of medicinal chemistry. As the barbituric acid derivatives(TABLE I) which have hypnotic and sedative properties are sparingly soluble in water, some work to improve the poor solubility by the aid of β-CyD had been done and it has been reported that the apparent solubility of them increased[1,2]. The stability constants and the thermodynamic parameters of the β-CyD inclusion complexes with barbital derivatives in aqueous medium have also been studied[3]. It is very interesting that these values are very different among the derivatives.

Journal of Inclusion Phenomena 2, 689–699. 0167-7861/84.15.
© 1984 *by D. Reidel Publishing Company.*

TABLE I. The barbituric acid derivatives.



R1	R2	
$-C_2H_5$	$-C_2H_5$	: Barbital
$-C_2H_5$		: Phenobarbital
$-C_2H_5$		: Cyclobarbital
$-C_2H_5$	$-CH_2CH_2CH(CH_3)_2$	: Amobarbital
$-CH_2CH=CH_2$	$-CH_2CH=CH_2$	: Allobarbital

It is our intention to do X-ray structure analyses of these inclusion complexes in order to elucidate how these derivatives having various substituents at C5 position are included in the β-CyD cavity and why some physicochemical constants and parameters are different among the derivatives. Firstly we chose barbital(5,5-diethylbarbituric acid) as a guest molecule and found two different crystals(Form I and II).

2. Experimental

2.1. Form I complex

The colorless plate crystals were obtained by gradually cooling 1.5 ml of the hot aqueous solutions containing about $2X10^{-4}$ mol of β-CyD and barbital, respectively. The specific gravity of the crystals was measured by the floatation method using carbon tetrachloride and o-dichlorobenzene. After a crystal was enclosed in the 0.5 mmϕ glass capillary with a little amount of mother liquid, the lattice constants and the intensity data were measured with nickel-filtered CuKα radiation using the Rigaku Rotor AFC-5FOS automated four-circle diffractometer (40kV, 200mA). A total of 8356 independent reflections with $F_o > 3\sigma F_o$ were collected by using ω-2θ scan mode up to 125° in 2θ. The crystal data are listed in TABLE II. As the cell dimensions and the location of the big peaks on the Patterson map were very similar to those of the β-CyD·aspirin complex[4], we regarded Form I as isomorphous with β-CyD·aspirin. Therefore as the β-CyD model we used the coordinates of dimeric β-CyDs from β-CyD·aspirin and then the guest and water molecules could be found by the successive Fourier syntheses. The refinement of the atomic coordinates are in progress by the full-matrix least-squares method[5] with restraints applied to the bond lengths and angles of β-CyD and barbital molecules and at the present stage, R factor is 25.4 % for the 4363 strong reflections using isotropic thermal parameters for all the non-hydrogen atoms.

UM00011701
NOVARTIS EXHIBIT 1517
Novartis v. Regents, IPR2023-01347
Page 447 of 4460

TABLE II. Crystal Data

	Form I	Form II
Chemical Formula*	$(\beta\text{-CyD})_2\cdot(\text{Barbital})_2\cdot 31H_2O$	$(\beta\text{-CyD})_4\cdot(\text{Barbital})_4\cdot 50H_2O$
Molecular Weight	3197.0	6177.7
Crystal System	Triclinic	Triclinic
Space Group	P1	P1
Z	1	1
Cell Dimensions;		
a (Å)	19.716(3)	34.341(5)
b (Å)	15.497(1)	15.529(2)
c (Å)	15.549(2)	15.568(2)
α (°)	103.63(1)	103.82(1)
β (°)	116.65(1)	100.58(2)
γ (°)	104.56(1)	106.67(1)
V ($Å^3$)	3762(1)	7434(1)
Dm (g/cm^3)	1.41(1)	1.38(2)
Dx (g/cm^3)	1.41	1.38

* β-CyD : $C_{42}H_{70}O_{35}$, Barbital : $C_8H_{12}N_2O_3$

2.2. Form II complex

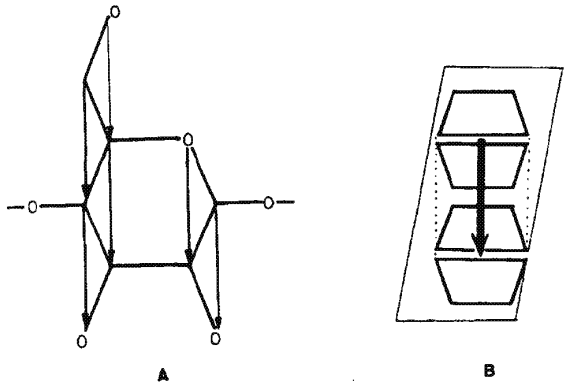
Form II was crystallized using similar conditions to that for Form I except for reducing the amount of water to 0.8 ml. Although both Form II and Form I crystals came out from the same batch, we could find the Form II crystals with higher certainty because the Form II crystals were much thinner than Form I crystals. The crystals were also enclosed in the glass capillary. The lattice constants and the intensity data were measured with graphite monochromatized CuKα radiation using the Rigaku AFC-5 automated four-circle diffractometer (40kV, 30mA). A total of 2827 independent reflections with $F_o > 3\sigma F_o$ were measured by using ω-2θ scan mode up to 70° in 2θ. The crystal data are also listed in TABLE II. We expected that four β-CyD molecules existed in an unit cell since the volume of the unit cell was about two times as large as those of the normal β-CyD dimers. Moreover as listed in TABLE III, there were two large peaks on the Patterson map in addition to the origin. A peak(b) 2.5 Å from the origin is characteristic of the interatomic vectors of the glucopyranose moiety and shows the orientation of CyD molecules. On the other hand, a peak(c) was found at 16.3 Å from the origin. Considering the existence of four β-CyD molecules in an unit cell, we judged that there existed two dimeric β-CyDs and peak(c) indicated inter-dimer vectors. Then a dimeric β-CyD model was constructed using the structure of the β-CyD·3,4-xylidine complex[6]. Based on a Patterson map, the orientations and the shifts were given to two dimer models, then the minimum R factor was searched by rotating the models around the molecular axes of dimeric β-CyDs. Thus we decided the position of the host molecules and then could find one guest molecule and fourteen water molecules by the successive Fourier method.

UM00011702
NOVARTIS EXHIBIT 1517
Novartis v. Regents, IPR2023-01347
Page 448 of 4460

As the elemental analysis of Form II crystals indicated 1/1 (Host)-/(guest) ratio, we have to look for three more barbital and 36 more water molecules. However, at the present stage, we can not assign these molecules because the separation of the peaks on Fourier maps are not good owing to the use of low resolution reflection data and/or the existence of the notable disorder at these areas. The R factor is 21.9 % for all available reflections using isotropic thermal parameters.

TABLE III. The large peaks in addition to the origin on Patterson maps.

	U	V	W	L^* (Å)
peak(a)	9.0/60	4.8/50	6.1/50	2.4
peak(b)	7.5/100	1.4/50	0.6/50	2.5
peak(c)	49.0/100	6.1/50	1.2/50	16.3



A B

The peak(a) and peak(b) indicate the interatomic vectors of glucopyranose moiety illustrated in **A** for Form I and Form II, respectively. The peak(c) indicates the inter-dimer vectors illustrated in **B** for Form II.
* : Length from the origin to the peak.

2.3. Computations

All the crystallographic computations were carried out on an NEAC ACOS 850S computer at The Crystallographic Research Center, Institute for Protein Research, Osaka University.

UM00011703
NOVARTIS EXHIBIT 1517
Novartis v. Regents, IPR2023-01347
Page 449 of 4460

3. Results and Discussion

3.1. Form I complex

The numbering scheme of the β-CyD and barbital molecules is shown in Fig. 1, and the inclusion status of Form I is shown in Fig. 2. Two β-CyDs form a dimeric structure by the intermolecular hydrogen bonds among their secondary hydroxyl groups. Such a structure has been frequently seen when β-CyDs are used for the host molecules. This fact is explained by the existence of the tight inter-molecular hydrogen bonds between two β-CyDs[6]. While one guest molecule could be assigned in the round shaped hydrophobic sphere, another one was included shallowly thrusting its one ethyl group from the primary hydroxyl side of β-CyD.

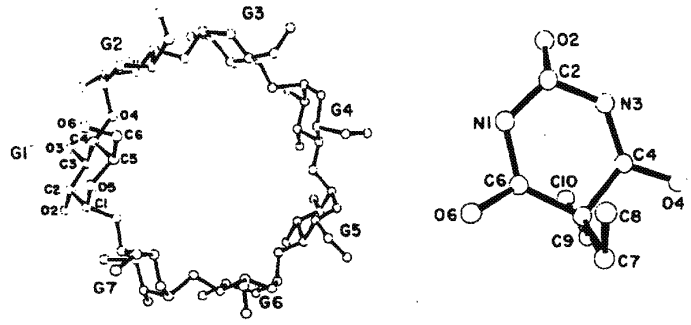


Fig. 1. The numbering schemes of each β-CyD and barbital molecules. G1,G2...G7 means the number of the glucosyl residues.

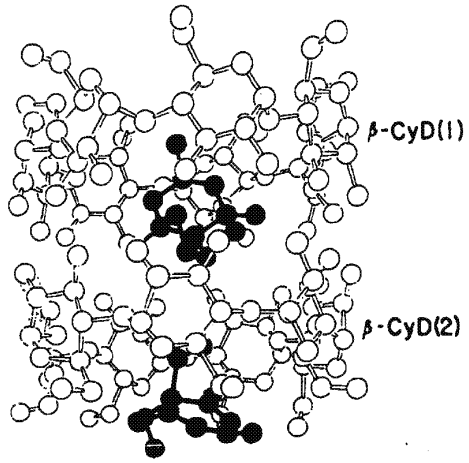


Fig. 2. The ORTEP drawing of the inclusion state of Form I. Barbital molecules are in the full lines and circles.

UM00011704
NOVARTIS EXHIBIT 1517
Novartis v. Regents, IPR2023-01347
Page 450 of 4460

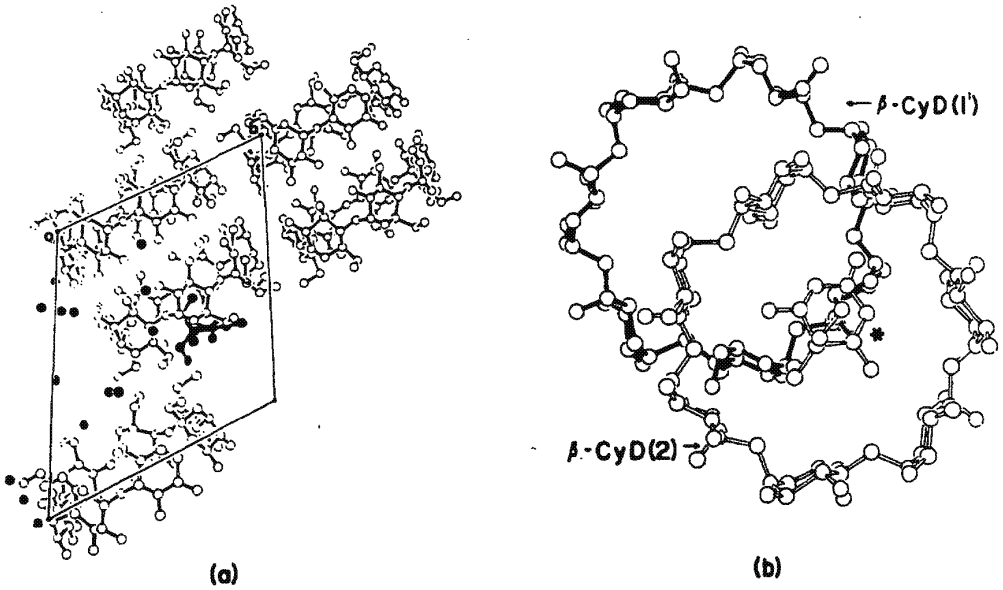


Fig. 3. The packing status of Form I complex; (a) The cage type packing system with the brickwork pattern. Only one barbital molecule which is in full lines and circles is drawn in the packing mode. Water molecules are also drawn in full circles. (b) The stacking of β-CyD(2), barbital and shifted β-CyD(1') molecules. Barbital molecule denoted by the asterisk is included in β-CyD(2).

Such an inclusion state was also observed in the structure of β-CyD• phenobarbital complex[7] which was determined as one of our serial structural studies of β-CyD•guest complexes, but in this case it was not the ethyl group but the more bulky phenyl group of phenobarbital which was included. These facts indicate that the β-CyD cavity has the selectivity to include the moiety which fits better into its own space when there are many guest molecules with different hydrophobic groups.

The packing of each molecule in the crystal is shown in Fig. 3. The β-CyD dimers are packed in the manner of the brickwork pattern which is one of the cage type packing structures and has been frequently seen in the β-CyD inclusion complex structure of the triclinic space group P1. It is obvious that the barbital molecule included shallowly in the β-CyD(2) can not escape easily because of the existence of the shifted β-CyD(1') as depicted in Fig. 3-(b). As the maximum molecular diameter of barbital molecule is larger than the minimum cavity diameter of β-CyD, a barbital molecule buried in the dimeric β-CyD also can not escape from the crystalline state. So barbital molecules are bound very tightly by β-CyDs. However, when the crystals are dissolved in aqueous medium and the matrix structure of β-CyD is broken, the barbital molecules included only at their ethyl groups are easily released.

UM00011705
NOVARTIS EXHIBIT 1517
Novartis v. Regents, IPR2023-01347
Page 451 of 4460

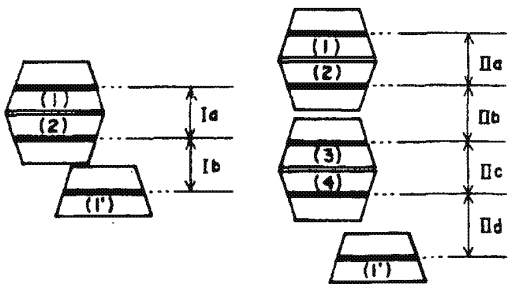
On the contrary, phenobarbital, which is stabilized by van der Waals forces between the hydrophobic β-CyD cavity and the phenyl ring in the β-CyD·phenobarbital crystal, is much more difficult to release and accounts for the eleven times larger stability constant for β-CyD·phenobarbital than β-CyD·barbital complex[3].

As shown in TABLE IV, the planes through seven glucosyl O4 atoms of β-CyD are layered one another with a 7 Å interval. There exist many water molecules in the space among these packed dimeric β-CyD units. Although in these spheres there are still many peaks at a low level on the difference Fourier map, these could be assigned as disordered water molecules. But what is important to remark here is the locations of ordered water molecules. At the present stage, we could find 19 water molecules, in which 13 waters occupied the same positions as those in β-CyD·aspirin complex used as the starting model. This fact implies that these waters are necessary to form the cage type matrix structure. Whereas disordered waters locating like clusters of grapes[6] except those relating to the host or guest molecules through hydrogen bonding are regarded as spacers to fill the vacant sphere.

3.2. Form II complex

As with the Form I complex, four β-CyDs in an unit cell form two dimeric structures by the hydrogen bond among the secondary hydroxyl groups. As described above, we could assign no more than one guest molecule. As shown in Fig. 4, the inclusion status is very similar to Form I, that is, the hydrophobic ethyl group is inserted in the β-CyD cavity from the primary hydroxyl group side leaving also the base skeletone of barbital i.e. pyrimidine-tri-one ring near the primary hydroxyl side of β-CyD.

TABLE IV. The distances between O4-planes.



	distances (Å)
Ia	6.8
Ib	7.0
IIa	7.1
IIb	8.9
IIc	7.0
IId	10.6

The number in the parentheses is β-CyD unit number.

UM00011706
NOVARTIS EXHIBIT 1517
Novartis v. Regents, IPR2023-01347
Page 452 of 4460

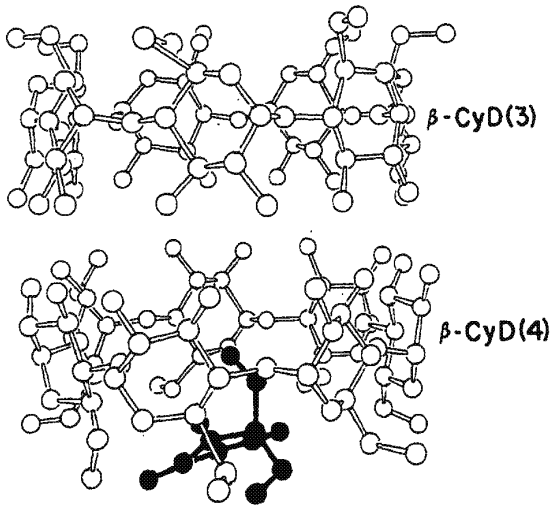


Fig. 4. The ORTEP drawing of the inclusion state of Form II. β-CyD(1) and β-CyD(2) are not drawn. Barbital molecule is in full lines and circles.

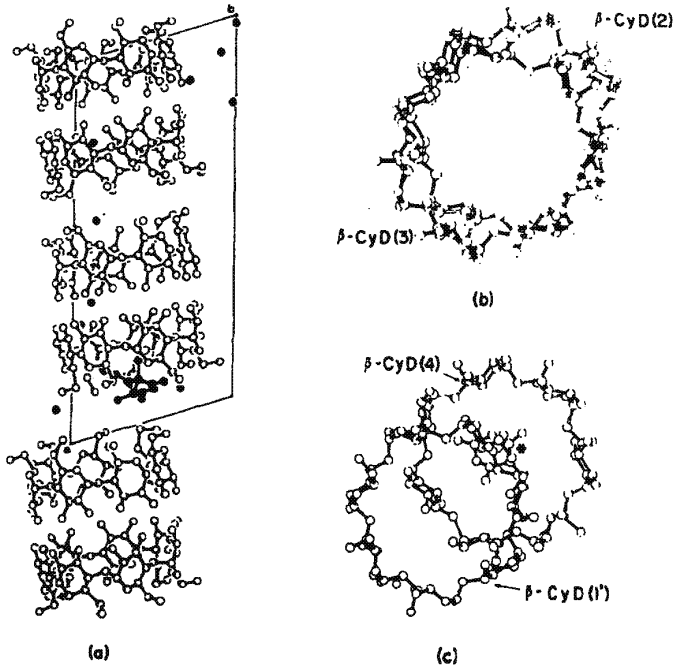


Fig. 5. The packing status of Form II complex; (a) Both channel and cage type packing systems of β-CyD molecules. Barbital and water molecules are drawn by full lines and circles. (b) The stacking of β-CyD(2) and β-CyD(3) molecules in the channel type packing area. (c) The stacking of β-CyD(4) and shifted β-CyD(1') molecules in the cage type packing area. Barbital molecule included in β-CyD(4) is denoted by an asterisk.

UM00011707
NOVARTIS EXHIBIT 1517
Novartis v. Regents, IPR2023-01347
Page 453 of 4460

Fig. 5 shows the packing in the crystal. Two β-CyD dimers stack like a tube in an unit cell(Fig. 5-(a) and (b)) forming a channel type packing system. At the present stage, there is only one direct hydrogen bond among the primary hydroxyl groups of β-CyDs, so the interactions here are weaker than those of the secondary hydroxyl side which play an important role to form a dimer. However, comparing the distances between O4-planes(TABLE III), the distance of IIb is shorter than that of IId but is longer than that of Ib. So there must be some important interactions in this area. On the contrary, at the unit cell edge along the a-axis, the next unit β-CyD(1') is arranged so as to close the barbital molecule in β-CyD(4) as well as in Form I complex(Fig. 5-(a) and (c)). As the distances between the barbital and β-CyD(1') are longer than that of the Form I complex, the host-guest interactions may be weak in this crystal. If we regard two dimers in the channel type packing as a β-CyD tetramer, this tetramer packs also in the way of the brickwork pattern, that is the cage type mode. This is the first time that both channel and cage type packing systems appear in a crystal at the same time. But we can not explain why Form II crystals with such a packing system results in the smaller amount of crystalline water.

4. Conclusion

Comparing Form I with the Form II complex, we can pick out the following points;

Similarities:

1) Both crystals are colorless and plates.
2) The (Host)/(Guest) ratio is 1/1.
3) Two β-CyDs form a dimer by hydrogen bonds between the secondary hydroxyl sides.
4) Both crystals are formed on the basis of the cage type packing mode with the brickwork pattern so as to fix the guest molecules at the primary hydroxyl side.
5) One barbital molecule is shallowly included inserting an ethyl group into the β-CyD cavity.

Differences:

1) The specific gravity of Form I crystals is larger than that of Form II.
2) The unit cell volume of Form II is about two times as large as that of Form I, whereas the volume per one dimeric β-CyD of Form I is a little larger than that of Form II.
3) The packing along the molecular axis of β-CyD of Form I is closer than that of Form II.
4) Although the distance between two O4-planes of each β-CyD in Form I is about 7 Å, the intervals of those in Form II range from 7 to 11 Å.
5) Form II constructs a β-CyD tetramer-like structure, which form the channel type packing.

UM00011708
NOVARTIS EXHIBIT 1517
Novartis v. Regents, IPR2023-01347
Page 454 of 4460

The important points to be considered about the formation of the two different crystals of β-CyD·barbital complex are in Differences 1) and 3). As the (Host)/(Guest) ratio is equal in both form, Form II, having a smaller crystal volume per one β-CyD dimer, is considered to have a lighter density, but not actually. We can not make a sweeping statement about this fact because the positions of the whole water molecules are not clear, but if the environment of water molecules around the β-CyD dimer for both complexes is the same, we may say that the β-CyD dimer units pack more closely along the molecular axis in Form I. By detailed observation of the water molecules existing in the loose packing area of Form II, we will explain the problems more clearly. J.STEZOWSKI et al. have obtained the stable and metastable crystals of the β-CyD·n-propanol complex[8]. M.YAMAZAKI et al. also have obtained the stable and metastable crystals of the β-CyD·water complex[9]. In the latter case, both crystals had the cage type packing by monomeric β-CyD and their cell dimensions are almost the same. The main difference is the number of water molecules. On the contrary in the former complex, β-CyD forms a typical dimeric structure and the cell dimensions are considerably different. And that in the stable crystal dimeric β-CyD packs in the cage type system with a brickwork pattern, however, dimeric β-CyD showed a channel type packing system in the metastable crystal. In view of these facts, our crystals are similar to the β-CyD·n-propanol crystals. But as we could not observe the transition from the metastable to the stable crystals in aqueous solution as seen in the β-CyD·n-propanol crystals, we can not conclude which form is in the stable state at the present stage. Considering the more loose packing status of Form II than that of Form I, we can expect that Form I complex may be in a more stable crystalline state.

Now we proceed with the refinement of Form I structure and collect the high resolution reflection data of Form II crystals using a Rotor-diffractometer. In the near future we hope to solve the above problems more clearly.

5. Acknowledgements

We thank the staff of The Crystallographic Research Center, Institute for Protein Research, Osaka University for our use of the computing facilities and the Rotor-diffractometer for Form I complex.

6. References

1) K.Koizumi and K.Fujimura, Yakugaku Zasshi, **92**, 32-36 (1972).
2) K.Koizumi, K.Mitsui and K.Higuchi, Yakugaku Zasshi, **94**, 1515-1519 (1974).
3) M.Otagiri, T.Miyaji, K.Uekama and K.Ikeda, Chem. Pharm. Bull., **24**, 1146-1154 (1976).
4) F.Nishioka, I.Nakanishi, T.Fujiwara and K.Tomita, Journal of Inclusion Phenomena, in preparation.

UM00011709
NOVARTIS EXHIBIT 1517
Novartis v. Regents, IPR2023-01347
Page 455 of 4460

5) W.R.Busing, K.O.Martin, H.A.Levy, ORXFLS4, Oak Ridge National Laboratory, Tennessee, (1978).
6) T.Fujiwara, R.Tokuoka, Y.Tanaka, K.Komazawa, K.Tomita, and W.Saenger, Journal of Inclusion Phenomena, in preparation.
7) I.Nakanishi, T.Fujiwara, and K.Tomita, Acta Cryst(A), in press.
8) K.H.Jogun and J.J.Stezowski, Nature, **278**, 667-668 (1979).
9) T.Fujiwara, M.Yamazaki, Y.Tomizu, R.Tokuoka, K.Tomita, T.Matsuo, H.Suga, and W.Saenger, Nippon Kagaku Kaishi, **1983**, 181-187 (1983).

UM00011710
NOVARTIS EXHIBIT 1517
Novartis v. Regents, IPR2023-01347
Page 456 of 4460

FORSYTH, J. B. & WELLS, M. (1959). *Acta Cryst.* **12**, 412–415.
GERMAIN, G., MAIN, P. & WOOLFSON, M. M. (1971). *Acta Cryst.* A**27**, 368–376.
HOWELLS, E. R., PHILLIPS, D. C. & ROGERS, D. (1950). *Acta Cryst.* **3**, 210–214.
MIGCHELSEN, T., OLTHOF, R. & VOS, A. (1965). *Acta Cryst.* **19**, 603–610.
SCHOMAKER, V. & TRUEBLOOD, K. N. (1968). *Acta Cryst.* B**24**, 63–76.
SUTOR, D. J. (1963). *J. Chem. Soc.* pp. 1105–1110.

Acta Cryst. (1977). B**33**, 1373–1378

The Crystal and Molecular Structure of the 2:1 Molecular Complex of Theophylline with Phenobarbital

BY SAKIKO NAKAO, SATOSHI FUJII, TOSHIMASA SAKAKI AND KEN-ICHI TOMITA

Faculty of Pharmaceutical Sciences, Osaka University, Yamadakami, Suita, Osaka, Japan 565

(*Received* 23 *August* 1976; *accepted* 15 *October* 1976)

The 2:1 molecular complex of theophylline with phenobarbital crystallizes in the orthorhombic space group *Pnma*, with the unit-cell dimensions $a = 6{\cdot}991\ (5)$, $b = 25{\cdot}554\ (17)$, $c = 15{\cdot}129\ (7)$ Å. The approximate structure in the space group $Pn2_1a$ was initially solved by the application of *MULTAN*. The correct structure was then refined in *Pnma* to give a final R index of 0·095. The phenobarbital molecule has mirror symmetry and participates in weak N—H···N hydrogen bonds to two symmetrically related theophylline molecules. The N(7) atom of theophylline forms a hydrogen bond with the O(2) atom of the adjacent theophylline molecule, and the C(8) atom of theophylline may form a weak C—H···O hydrogen bond with the O(4) atom of the adjacent phenobarbital.

Introduction

Xanthines and barbiturates form crystalline complexes with a variety of other molecular series as well as with each other. In fact, theophylline and phenobarbital form a molecular complex (Higgins & Dunker, 1944; Bender & Nelson, 1973) with a 2:1 molar ratio, similar to the complex of phenobarbital with 8-bromo-9-ethyladenine (Kim & Rich, 1968). However, the modes of hydrogen bonding in these two complexes seem to be distinct: the ring N(1) atom of theophylline is unable to participate in a hydrogen bond, while the N(1) atom of adenine may take part in the hydrogen-bond formation (see Fig. 1). Phenobarbital (a derivative of uracil) is physiologically used as a sedative hypnotic agent, while theophylline (a derivative of xanthine) is effective as a diuretic and cardiac stimulant; these two drugs are frequently used at the same time. To explore the possibility that the specific interaction between phenobarbital and theophylline may play a significant role in the multiple pharmacological effect of these drugs, the crystal structure analysis of the 2:1 molecular complex of theophylline with phenobarbital was carried out, and the mode of the specific hydrogen bonding was elucidated.

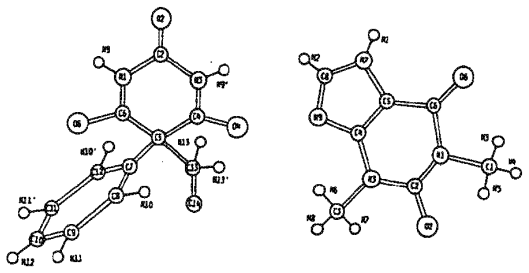


Fig. 1. Theophylline and phenobarbital (atomic numbering).

Experimental

Colourless needles were obtained by distillation of a 50% aqueous ethanol solution of theophylline and phenobarbital in a 2:1 molar ratio under reduced pressure. The unit-cell dimensions were initially obtained from precession photographs and refined by a diffractometer: $a = 6{\cdot}991\ (5)$, $b = 25{\cdot}554\ (17)$, $c = 15{\cdot}129\ (7)$ Å. The density (measured by the flotation method) is 1·459 g cm^{-3}, which is in good agreement with that calculated for four units of two theophylline and one phenobarbital in a unit cell. The observed ex-

UM00011711
NOVARTIS EXHIBIT 1517
Novartis v. Regents, IPR2023-01347
Page 457 of 4460

tinctions, $0kl$ when $k + l$ is odd and $hk0$ when h is odd, indicate the space group to be either $Pn2_1a$ or $Pnma$; the latter, containing one-half of the 2:1 complex in an asymmetric unit, was confirmed to be correct. Some crystal data are listed in Table 1.

Table 1. *Crystal data for the theophylline–phenobarbital complex*

Chemical formula $C_7H_8N_4O_2 \cdot \frac{1}{2} C_{12}H_{12}N_2O_3$
FW 296·3
Orthorhombic, space group *Pnma*

$a = 6{\cdot}991 \pm 0{\cdot}005$ Å	$Z = 8$
$b = 25{\cdot}554 + 0{\cdot}017$	$D_m = 1{\cdot}459$ g cm^{-3}
$c = 15{\cdot}129 \pm 0{\cdot}007$	$D_x = 1{\cdot}459$
$V = 2702{\cdot}8$ Å^3	

The intensity data were collected on an automatic four-circle Rigaku Denki diffractometer with Cu $K\alpha$ radiation and the ω–2θ scan technique. Three standard reflexions were measured every 40 reflexions and their intensities showed no unusual fluctuation or decay during the run. 1830 independent reflexions were measured and consequently corrected for Lorentz and polarization factors, but no correction for absorption was made. The structure factors were normalized to an absolute scale by the usual Wilson method.

Table 2. *Final atomic parameters with estimated standard deviations in parentheses.*

All quantities for non-hydrogen atoms are $\times 10^4$. All coordinates for hydrogen atoms are $\times 10^3$.
The form of the anisotropic ellipsoid is $\exp[-(B_{11}h^2 + B_{22}k^2 + B_{33}l^2 + B_{12}hk + B_{13}hl + B_{23}kl)]$.

Theophylline

	x	y	z	B_{11}	B_{22}	B_{33}	B_{12}	B_{13}	B_{23}
N(1)	1917 (8)	5457 (2)	3440 (3)	161 (14)	11 (1)	31 (3)	1 (7)	8 (11)	−1 (3)
C(2)	2246 (10)	5142 (3)	4164 (4)	164 (17)	10 (1)	35 (3)	−1 (8)	−2 (13)	−5 (3)
N(3)	2766 (8)	4631 (2)	4000 (3)	168 (14)	12 (1)	22 (3)	7 (6)	−2 (10)	2 (3)
C(4)	2969 (10)	4463 (3)	3152 (4)	125 (16)	12 (1)	24 (3)	−4 (8)	−7 (12)	5 (3)
C(5)	2619 (9)	4784 (2)	2450 (5)	123 (15)	9 (1)	33 (3)	4 (7)	7 (13)	−2 (4)
C(6)	2065 (10)	5309 (2)	2544 (5)	139 (16)	12 (1)	35 (3)	−14 (7)	18 (13)	−1 (4)
N(7)	2976 (8)	4487 (2)	1698 (3)	124 (13)	12 (1)	31 (3)	−4 (6)	−3 (10)	−3 (3)
C(8)	3497 (10)	4007 (3)	2000 (4)	134 (17)	14 (1)	32 (3)	1 (8)	−21 (13)	−4 (4)
N(9)	3527 (8)	3974 (2)	2882 (3)	148 (14)	12 (1)	29 (3)	13 (6)	−13 (10)	−4 (3)
C(1)	1370 (13)	6010 (3)	3640 (5)	341 (26)	10 (1)	44 (3)	24 (10)	−10 (17)	−8 (4)
O(2)	2084 (8)	5311 (2)	4909 (3)	320 (16)	16 (1)	32 (2)	5 (7)	−2 (11)	−17 (3)
C(3)	3081 (13)	4272 (3)	4746 (4)	333 (26)	16 (1)	26 (3)	46 (11)	22 (16)	12 (4)
O(6)	1711 (8)	5626 (2)	1949 (3)	277 (15)	14 (1)	34 (2)	6 (6)	−14 (10)	8 (3)

Phenobarbital

	x	y	z	B_{11}	B_{22}	B_{33}	B_{12}	B_{13}	B_{23}
N(1)	4707 (8)	2040 (2)	3658 (3)	117 (12)	10 (1)	31 (3)	2 (6)	−12 (10)	−1 (3)
C(2)*	4059 (13)	2500	3280 (6)	88 (21)	15 (2)	28 (5)	0	−6 (17)	0
O(2)*	2982 (10)	2500	2656 (5)	170 (18)	20 (1)	45 (4)	0	−75 (15)	0
C(4)	5984 (9)	2989 (3)	4335 (4)	90 (14)	12 (1)	29 (3)	2 (7)	31 (12)	−2 (3)
O(4)	6747 (7)	3400 (2)	4523 (3)	199 (13)	11 (1)	35 (2)	−43 (6)	−8 (9)	5 (2)
C(5)*	6283 (13)	2500	4884 (6)	83 (20)	12 (2)	23 (4)	0	−27 (16)	0
C(7)*	4825 (13)	2500	5637 (6)	78 (20)	10 (2)	23 (4)	0	−9 (16)	0
C(8)	4160 (10)	2966 (3)	5992 (4)	154 (17)	12 (1)	30 (3)	8 (8)	−15 (13)	−4 (3)
C(9)	2838 (11)	2971 (3)	6684 (5)	143 (17)	17 (1)	47 (4)	25 (9)	6 (15)	2 (4)
C(10)*	2175 (15)	2500	7019 (6)	132 (25)	28 (3)	20 (5)	0	22 (18)	0
C(13)*	8373 (14)	2500	5274 (6)	99 (22)	21 (2)	27 (5)	0	−49 (17)	0
C(14)*	9936 (16)	2500	4561 (8)	86 (24)	31 (3)	55 (7)	0	35 (22)	0

Theophylline

	x	y	z	B_0 (Å^2)
H(1)[N(7)]	267 (13)	461 (3)	102 (5)	5 (2)
H(2)[C(8)]	388 (11)	367 (3)	153 (5)	3 (2)
H(3)[C(1)]	201 (13)	625 (3)	324 (5)	5 (2)
H(4)[C(1)]	188 (14)	615 (3)	422 (6)	5 (2)
H(5)[C(1)]	26 (13)	608 (3)	317 (5)	5 (2)
H(6)[C(3)]	452 (13)	407 (3)	467 (5)	5 (2)
H(7)[C(3)]	296 (14)	386 (3)	464 (6)	6 (2)
H(8)[C(3)]	191 (14)	435 (3)	524 (6)	6 (2)

Phenobarbital

	x	y	z	B_0 (Å^2)
H(9)[N(1)]	425 (13)	172 (3)	334 (6)	6 (2)
H(10)[C(8)]	466 (13)	335 (3)	575 (5)	3 (2)
H(11)[C(9)]	250 (12)	333 (3)	699 (5)	2 (2)
H(12)[C(10)]	138 (16)	250	753 (8)	3 (2)
H(13)[C(13)]	866 (12)	279 (3)	569 (5)	4 (3)

* The parameters B_{12}, B_{23}, of the atoms with $y = 0{\cdot}25$ are equal to zero by symmetry.

UM00011712
NOVARTIS EXHIBIT 1517
Novartis v. Regents, IPR2023-01347
Page 458 of 4460

Structure determination and refinement

The first approximate structure in the space group $Pn2_1a$ was solved with the multisolution tangent-formula procedure *MULTAN* (Germain, Main & Woolfson, 1971). In the first E map all the non-hydrogen atoms, except two atoms of the ethyl group in phenobarbital, were located. After refinement it was suggested that the phenobarbital molecule itself may possess a mirror plane through seven atoms [C(2), O(2) and C(5) of the oxopyrimidine moiety, C(7) and C(10) of the benzene ring and the ethyl C atoms, C(13) and C(14)]. Therefore, the correct space group should be *Pnma*. In fact, the following Fourier calculation in the space group *Pnma* revealed the positions of the remaining two ethyl C atoms on the mirror plane. Four cycles of the full-matrix least-squares refinement with isotropic temperature factors reduced the R index to 0·137. Further refinement with block-diagonal least squares with anisotropic temperature factors for all the non-hydrogen atoms gave an R index of 0·115. At this point a difference Fourier map was calculated, and all the H atoms, excluding the three of the terminal methyl group in the phenobarbital molecule, were found. Three more cycles of the final refinement including H atoms with isotropic temperature factors were carried out and the R index was reduced finally to 0·095. Final atomic parameters with their estimated standard deviations are listed in Table 2.*

Table 3. *Bond lengths* (Å) *and bond angles* (°) *with standard deviations in parentheses*

Theophylline

N(1)–C(2)	1·379 (9)	N(7)–C(8)	1·360 (9)
C(2)–N(3)	1·377 (9)	C(8)–N(9)	1·337 (9)
N(3)–C(4)	1·361 (9)	C(4)–N(9)	1·371 (9)
C(4)–C(5)	1·365 (10)	N(7)–H(1)	1·09 (9)
C(5)–C(6)	1·402 (10)	C(8)–H(2)	1·15 (8)
N(1)–C(6)	1·413 (9)	C(1)–H(3)	0·97 (9)
N(1)–C(1)	1·495 (11)	C(1)–H(4)	1·01 (9)
C(2)–O(2)	1·211 (9)	C(1)–H(5)	1·07 (9)
N(3)–C(3)	1·473 (11)	C(3)–H(6)	1·14 (9)
C(6)–O(6)	1·236 (9)	C(3)–H(7)	1·07 (9)
C(5)–N(7)	1·390 (9)	C(3)–H(8)	1·12 (10)
C(6)–N(1)–C(2)	126·5 (6)	N(7)–C(5)–C(6)	130·9 (7)
C(1)–N(1)–C(2)	115·7 (6)	N(7)–C(5)–C(4)	106·0 (6)
C(1)–N(1)–C(6)	117·8 (6)	C(5)–C(6)–N(1)	112·0 (6)
N(1)–C(2)–N(3)	117·0 (6)	O(6)–C(6)–N(1)	120·6 (7)
O(2)–C(2)–N(3)	122·1 (7)	O(6)–C(6)–C(5)	127·5 (7)
O(2)–C(2)–N(1)	120·9 (7)	C(5)–N(7)–C(8)	105·4 (6)
C(2)–N(3)–C(4)	119·9 (6)	H(1)–N(7)–C(8)	129 (5)
C(3)–N(3)–C(4)	120·6 (6)	H(1)–N(7)–C(5)	125 (5)
C(3)–N(3)–C(2)	119·5 (6)	N(7)–C(8)–N(9)	113·4 (6)
N(3)–C(4)–C(5)	121·6 (6)	H(2)–C(8)–N(9)	125 (4)
N(9)–C(4)–C(5)	111·6 (6)	H(2)–C(8)–N(7)	122 (4)
N(9)–C(4)–N(3)	126·8 (6)	C(8)–N(9)–C(4)	103·6 (6)
C(4)–C(5)–C(6)	123·1 (7)		

Phenobarbital

N(1)–C(2)	1·384 (11)	C(9)–C(10)	1·385 (13)
N(1)–C(6)	1·361 (8)	C(5)–C(13)	1·576 (13)
C(5)–C(6)	1·516 (11)	C(13)–C(14)	1·536 (15)
C(2)–O(2)	1·207 (12)	N(1)–H(9)	1·00 (9)
C(4)–O(4)	1·212 (8)	C(8)–H(10)	1·10 (8)
C(5)–C(7)	1·528 (12)	C(9)–H(11)	1·05 (8)
C(7)–C(8)	1·386 (11)	C(10)–H(12)	0·96 (12)
C(8)–C(9)	1·397 (10)	C(13)–H(13)	1·00 (8)
C(6)–N(1)–C(2)	124·9 (6)	C(5)–C(7)–C(8)	120·8 (7)
H(9)–N(1)–C(2)	112 (5)	C(12)–C(7)–C(8)	118·4 (7)
H(9)–N(1)–C(6)	122 (5)	C(7)–C(8)–C(9)	121·3 (7)
N(1)–C(2)–N(3)	116·4 (7)	H(10)–C(8)–C(9)	117 (4)
O(2)–C(2)–N(1)	121·8 (8)	H(10)–C(8)–C(7)	121 (4)
C(5)–C(6)–N(1)	117·3 (6)	C(8)–C(9)–C(10)	119·2 (8)
O(6)–C(6)–N(1)	120·9 (6)	H(11)–C(9)–C(10)	121 (5)
O(6)–C(6)–C(5)	121·7 (6)	H(11)–C(9)–C(8)	119 (4)
C(4)–C(5)–C(6)	111·2 (7)	C(9)–C(10)–C(11)	120·5 (9)
C(6)–C(5)–C(7)	108·4 (7)	H(12)–C(10)–C(11)	120 (7)
C(6)–C(5)–C(13)	109·5 (7)	H(13)–C(13)–C(14)	108 (5)
C(7)–C(5)–C(13)	109·9 (7)	H(13)–C(13)–C(5)	115 (5)
C(5)–C(13)–C(14)	113·4 (8)		

* A list of structure factors has been deposited with the British Library Lending Division as Supplementary Publication No. SUP 32241 (8 pp.). Copies may be obtained through The Executive Secretary, International Union of Crystallography, 13 White Friars, Chester CH1 1NZ, England.

Table 4. *Deviations* (Å) *of the atoms from some least-squares planes, and the dihedral angles between the planes*

An asterisk denotes the atoms used in the plane calculation.

(*a*) Theophylline

Plane 1: $-0·9607x - 0·2777y - 0·0067z + 5·1926 = 0·0$
Plane 2: $-0·9611x - 0·2763y - 0·0012z + 5·1436 = 0·0$
Plane 3: $-0·9560x - 0·2932y - 0·0086z + 5·3693 = 0·0$

	Plane 1	Plane 2	Plane 3
N(1)	−0·002*	−0·003*	−0·045
C(2)	−0·006*	−0·003*	−0·039
N(3)	0·009*	0·009*	−0·001
C(4)	0·000*	−0·008*	0·000*
C(5)	0·014*	0·002*	0·002*
C(6)	0·013*	0·004*	−0·021
N(7)	−0·007*	−0·027	−0·004*
C(8)	−0·019*	−0·038	0·004*
N(9)	−0·025*	−0·036	−0·003*
C(1)	−0·029*	−0·026	−0·097
O(2)	−0·025*	−0·015	−0·067
C(3)	0·045*	0·049	0·048
O(6)	0·032*	0·019	−0·015

∠ (plane 2)–(plane 3) 1·1°.

(*b*) Phenobarbital

Plane 4: $0·7606x - 0·0000y - 0·6492z + 1·0822 = 0·0$

N(1)	−0·011*	C(4)	0·003*	C(7)	−1·892
C(2)	0·016*	C(5)	−0·377	C(13)	0·351
N(3)	−0·011*	C(6)	0·003*		

Plane 5: $-0·7489x - 0·0000y - 0·6627z + 8·1827 = 0·0$

C(7)	0·005*	C(10)	0·007*	C(12)	−0·002*
C(8)	−0·002*	C(11)	−0·004*	C(5)	−0·004
C(9)	−0·004*				

∠ (plane 4)–(plane 5) 98·0°.

UM00011713
NOVARTIS EXHIBIT 1517
Novartis v. Regents, IPR2023-01347
Page 459 of 4460

The *UNICS* (1973) system was used in the refinement of the structure. Atomic scattering factors for all atoms were taken from *International Tables for X-ray Crystallography* (1962), and all the computations were carried out on the NEAC 2200-700 computer at this University.

Results and discussion

The final bond lengths and bond angles, and the atomic numbering are shown in Table 3 and Fig. 1 respectively.

Phenobarbital

C(5) of phenobarbital is 0·38 Å out of the oxopyrimidine least-squares plane towards the phenyl group; similar puckering conformations in barbiturates were also observed in the crystalline complexes phenobarbital – 8-bromo-9-ethyladenine (Kim & Rich, 1968) and alloxan – 9-ethyladenine (Shieh & Voet, 1975). This phenomenon has not been detected for several other barbiturates involved in molecular complexes, *e.g.* 5-isopropyl-5-bromoallylbarbituric acid – 9-ethyladenine (Voet & Rich, 1972), barbituric acid – 9-ethyladenine (Voet, 1971, 1972) and barbital – caffeine (Craven & Gartland, 1974). Three independent barbiturate anions, each having different ring conformations, were observed in the crystal of potassium 5-ethylbarbiturate (Gartland, Gatehouse & Craven, 1975). Such puckerings may be due to the nature of the substituents at the 5 and 5′ positions and/or the variety of packing forces in the crystal. It is hard to explain why the C(13)–C(14) bond of the ethyl group (1·64 Å) is significantly longer than the normal C–C single bond. The peak corresponding to C(14), broadened on either side of the mirror plane, was found in the Fourier map, but the three H atoms attached to C(14) could not be detected in this map.

Theophylline

The crystal structures of the following theophylline-related compounds have so far been reported: theophylline (Sutor, 1958), *cis* and *trans*-theo-

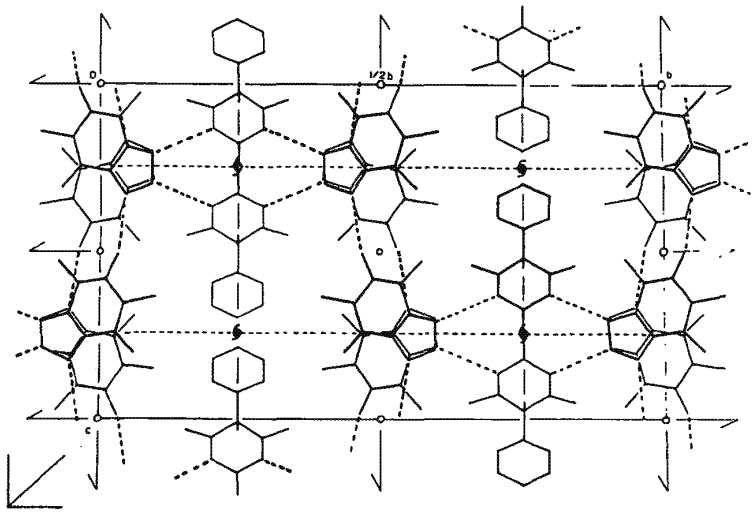


Fig. 2. The crystal packing of the theophylline–phenobarbital complex viewed along a.

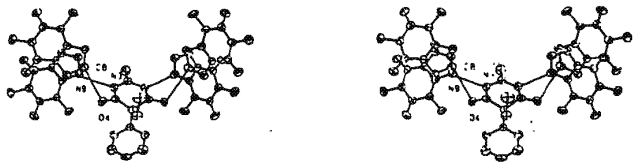


Fig. 3. Stereo projection of the molecular complex of theophylline with phenobarbital. Open bonds represent the hydrogen-bonding contacts.

UM00011714
NOVARTIS EXHIBIT 1517
Novartis v. Regents, IPR2023-01347
Page 460 of 4460

Table 5. *Hydrogen bonds and short van der Waals contacts, with standard deviations in parentheses*

(*a*) Hydrogen bonds (X–H $\cdots$ Y)

				Distance (Å)		Angle (°)
X	H	Y	X–H	$X\cdots Y$	H$\cdots Y$	X–H$\cdots Y$
$N(7)^T_a$	$H(1)^T_a$	$O(2)^T_b$	1·09 (9)	2·756 (8)	1·70 (9)	160 (8)
$N(1)^P_c$	$H(9)^P_c$	$N(9)^T_a$	1·00 (8)	2·961 (8)	1·98 (9)	170 (8)
$C(8)^T_a$	$H(2)^T_a$	$O(4)^P_a$	1·15 (8)	3·034 (9)	2·29 (8)	120 (5)

(*b*) Short contacts ($X\cdots Y$)

		Distance (Å)			Distance (Å)			Distance (Å)
X	Y	$X\cdots Y$	X	Y	$X\cdots Y$	X	Y	$X\cdots Y$
$O(4)^P_a$	$C(3)^T_a$	3·412 (11)	$C(8)^T_a$	$C(5)^T_g$	3·599 (10)	$C(4)^T_a$	$N(7)^T_g$	3·508 (9)
$N(7)^T_a$	$O(4)^P_d$	3·445 (8)	$N(9)^T_a$	$N(7)^T_g$	3·436 (8)	$C(5)^T_a$	$C(6)^T_g$	3·385 (10)
$C(14)^P_a$	$O(2)^P_e$	3·583 (14)	$O(6)^T_a$	$C(1)^T_g$	3·517 (11)	$C(6)^T_a$	$O(6)^T_g$	3·435 (9)
$O(2)^T_a$	$O(4)^P_f$	3·500 (8)	$C(2)^P_a$	$O(2)^P_g$	3·087 (12)	$N(7)^T_a$	$C(4)^T_g$	3·499 (9)
$C(4)^T_a$	$C(5)^T_g$	3·474 (10)	$O(2)^P_a$	$O(2)^P_g$	3·527 (15)	$C(8)^T_a$	$C(4)^T_g$	3·345 (10)
$C(5)^T_a$	$C(5)^T_g$	3·499 (14)	$O(6)^T_a$	$C(3)^T_b$	3·346 (11)	$N(9)^T_a$	$C(5)^T_g$	3·568 (9)
$C(6)^T_a$	$C(6)^T_g$	3·498 (15)	$C(14)^P_a$	$C(2)^P_e$	3·373 (15)	$N(9)^T_a$	$C(8)^T_g$	3·480 (9)
$N(7)^T_a$	$N(3)^T_g$	3·530 (8)	$C(1)^T_a$	$O(4)^P_f$	3·425 (11)	$N(1)^P_a$	$O(2)^P_g$	3·253 (9)
$N(7)^T_a$	$C(5)^T_g$	3·574 (9)	$N(1)^T_a$	$O(6)^T_g$	3·430 (8)	$C(4)^P_a$	$O(2)^P_g$	3·548 (10)

The superscripts T, P refer to the molecules theophylline and phenobarbital. The symmetry operations implied by the subscripts are the following:

(*a*) x,y,z
(*b*) $0{\cdot}5-x, 1{\cdot}0-y, -0{\cdot}5+z$
(*c*) $x, 0{\cdot}5-y, z$
(*d*) $-0{\cdot}5+x, y, 0{\cdot}5-z$
(*e*) $1{\cdot}0+x, y, z$
(*f*) $1{\cdot}0-x, 1{\cdot}0-y, 1{\cdot}0-z$
(*g*) $0{\cdot}5+x, y, 0{\cdot}5-z$

phyllinatochlorobis(ethylenediamine)cobalt(III) perchlorate (Kistenmacher & Szalda, 1975; Kistenmacher, 1975), and theophylline – 5-chlorosalicylic acid (Shefter, 1969). The C(2)–N(3) and C(4)–N(9) bond lengths (1·38 and 1·37 Å) seem to be slightly longer than the average values of 1·35 and 1·34 Å found for the comparable bonds in other related compounds. The maximum deviation of an atom from the best plane of the purine ring is 0·049 Å for the methyl C(3), as shown in Table 4.

A similar atomic displacement is reported for the theophylline molecule in the cobalt(III) complex with ethylenediamine. The deviation of C(3) may be due to the repulsion between this atom and O(4) of the phenobarbital molecule connected to theophylline by a N–H $\cdots$ N hydrogen bond.

Molecular packing and the intermolecular hydrogen bond

The molecular packing and hydrogen bonding of this complex viewed along **a** is shown in Fig. 2, in which the dashed lines indicate hydrogen bonds.

The phenobarbital molecule itself possesses exact mirror symmetry. A phenobarbital molecule has two symmetrically related N–H $\cdots$ N bonds with two adjacent theophylline molecules. Such a mode of hydrogen bonding is quite distinct from the cyclic hydrogen-bonded base pairing found in many complexes of barbiturate with adenine or xanthine derivatives. Theophylline molecules associate *via* N(7)–H $\cdots$ O(2) hydrogen bonds nearly parallel to **c**. It is known that the C(8)–H group is more acidic than the C(2)–H group in the purine derivatives, and the observed short contact between the H atom attached to the C(8) of theophylline and the O(4) of phenobarbital (2·29 Å) may support the additional weak C–H $\cdots$ O hydrogen-bond formation, similar to that found in the complex of barbital with caffeine (Craven & Gartland, 1974) (Fig. 3).

The imidazole moieties of the theophylline molecules are stacked in the **a** direction with a stacking distance of 3·48–3·50 Å. The distance between the carbonyl groups of adjacent phenobarbital molecules related by the *a*-glide symmetry operation is short, as shown in Table 5; this contact might be attributed to a

UM00011715
NOVARTIS EXHIBIT 1517
Novartis v. Regents, IPR2023-01347
Page 461 of 4460

dipole–dipole interaction (Bolton, 1964). It might be important in the multiple pharmacological effect that each phenobarbital molecule is surrounded by four theophylline molecules with N–H···N and C–H···O hydrogen bonds.

References

BENDER, M. & NELSON, J. A. (1973). *J. Chem. Soc. Faraday I*, **69**, 2074–2079.

BOLTON, W. (1964). *Nature, Lond.* **201**, 987–989.

CRAVEN, B. M. & GARTLAND, G. L. (1974). *Acta Cryst.* B**30**, 1191–1195.

GARTLAND, G. L., GATEHOUSE, B. M. & CRAVEN, B. M. (1975). *Acta Cryst.* B**31**, 203–211.

GERMAIN, G., MAIN, P. & WOOLFSON, M. M. (1971). *Acta Cryst.* A**27**, 368–376.

HIGGINS, W. M. & DUNKER, M. F. W. (1944). *J. Amer. Pharm. Assoc. Sci. Ed.* **33**, 310–314.

International Tables for X-ray Crystallography (1962). Vol. III, pp. 202–203. Birmingham: Kynoch Press.

KIM, S. H. & RICH, A. (1968). *Proc. Natl. Acad. Sci. US.* **60**, 402–408.

KISTENMACHER, T. J. (1975). *Acta Cryst.* B**31**, 85–89.

KISTENMACHER, T. J. & SZALDA, D. J. (1975). *Acta Cryst.* B**31**, 90–96.

SHEFTER, E. (1969). *J. Pharm. Sci.* **58**, 710–714.

SHIEH, H. S. & VOET, D. (1975). *Acta Cryst.* B**31**, 2192–2201.

SUTOR, D. J. (1958). *Acta Cryst.* **11**, 83–87.

UNICS (1973). *The Universal Crystallographic Computing System*. Library programs in the Computation Center of Osaka Univ.

VOET, D. (1971). *Amer. Cryst. Assoc. Abs. Pap.* p. 74.

VOET, D. (1972). *J. Amer. Chem. Soc.* **94**, 8213–8222.

VOET, D. & RICH, A. (1972). *J. Amer. Chem. Soc.* **94**, 5888–5891.

Acta Cryst. (1977). B**33**, 1378–1384

The Crystal Structure of $(-)_{589}$-Oxalatobis(ethylenediamine)cobalt(III) $(+)_{589}$-Dicyanomalonatodiamminecobaltate(III) Trihydrate

BY K. TORIUMI, S. SATO AND Y. SAITO

The Institute for Solid State Physics, The University of Tokyo, Roppongi-7, Minato-ku, Tokyo 106, *Japan*

(*Received* 21 *September* 1976; *accepted* 13 *October* 1976)

$(-)_{589}$-$[Co(ox)(en)_2]$ $(+)_{589}$-$[Co(CN)_2(mal)(NH_3)_2].3H_2O$ crystallizes in the orthorhombic space group $P2_12_12_1$, with $a = 16{\cdot}709\ (1)$, $b = 18{\cdot}139\ (1)$, $c = 7{\cdot}569\ (1)$ Å and $Z = 4$. The structure was refined by least-squares calculations to give an R value of 0·034 for 3304 observed amplitudes. The complex anion is a *cis–cis* isomer: a Co atom is surrounded nearly octahedrally by two C atoms of cyano groups, two N atoms of ammonia molecules, both in *cis* positions, and two O atoms of a malonato group. The absolute configuration of the complex anion, $(+)_{589}$-$[Co(CN)_2(mal)(NH_3)_2]^-$, can be designated as Δ, provided that the chirality is defined by the line joining the two C atoms of the cyano groups and that joining the two N atoms of the ammonia molecules. During the data collection, some strong reflexions with low diffraction angles strikingly increased their intensities. The increase in intensity may be ascribed to a change in the extinction effect under X-irradiation.

Introduction

Seven optically active complexes of Co^{III} were isolated whose optical activity arises from the chiral configuration of monodentates coordinated to the central Co atom (Ito & Shibata, 1976). The absolute configuration of the complex ion is of particular importance since no empirical relation between the circular dichroism spectra and the absolute configuration of such complexes has been established. The absolute configuration of one of these complexes, $(-)_{589}$-$[Co(NO_2)_2(ox)(NH_3)_2]^-$, was determined by X-ray methods (Shintani, Sato & Saito, 1976). In this paper, the absolute configuration of the title compound will be described.

Experimental

Crystals of $(-)_{589}$-$[Co(ox)(en)_2]$ $(+)_{589}$-$[Co(CN)_2(mal)(NH_3)_2].3H_2O$ were kindly supplied by Professor M. Shibata of Kanazawa University. They are orange-red square prisms. Unit-cell dimensions were determined from Weissenberg photographs and refined on a diffractometer. The intensities of the reflexions were

UM00011716

NOVARTIS EXHIBIT 1517
Novartis v. Regents, IPR2023-01347
Page 462 of 4460

Zeitschrift für Kristallographie 198, 265–270 (1992)
© by R. Oldenbourg Verlag, München 1992 – 0044-2968/92 S 3.00 + 0.00

Reinvestigation of the crystal structure of diglycine hydrochloride

S. Natarajan, C. Muthukrishnan, S. Asath Bahadur, R. K. Rajaram

School of Physics, Madurai Kamaraj University, Madurai 625 021, India

and S. S. Rajan

Department of Biophysics and Crystallography, University of Madras, Madras 600 025, India

Received: December 10, 1990

Crystal structure / Glycine complexes

Abstract. A reinvestigation of the crystal structure of diglycine hydrochloride, $(NH_2CH_2COOH)_2HCl$, was carried out. The structure is orthorhombic, space group $P2_12_12_1$, with $a = 5.2992(6)$, $b = 8.083(2)$, $c = 17.973(2)$ Å and $Z = 4$. Three-dimensional intensity data collected on a CAD 4 diffractometer using Cu$K\alpha$ radiation was used for the structure elucidation and refinement. The final R value is 0.055 for 779 reflections. All the hydrogen atoms have been located in the present study. The glycine molecules are held together by a network of N–H...Cl, N–H...O and O–H...O hydrogen bonds. One of the glycine molecules exists as a zwitterion whereas the other one in the cationic form.

Introduction

Since amino acids and their complexes are of considerable chemical and biological interest, we have taken up a systematic investigation of several complexes of glycine, the simplest amino acid with inorganic acids and salts and elucidated their crystal structures (Natarajan et al., 1984). The crystal structure of the complex of glycine with hydrochloric acid was reinvestigated and is reported here. The structure of this complex is already known (Hahn and Buerger, 1957; Hahn, 1960). The final value of the

Address for correspondence: Dr. S. Natarajan, School of Physics, Madurai Kamaraj University, Madurai 625 021, India.

UM00011717
NOVARTIS EXHIBIT 1517
Novartis v. Regents, IPR2023-01347
Page 463 of 4460

Table 1. Crystal data for diglycine hydrochloride.

	Present work	Earlier work*
Molecular formula	$(NH_2CH_2COOH)_2 \cdot HCl$	
Molecular weight	186.6 g mol^{-1}	
a	5.2992(6) Å	5.34 Å
b	8.083(2)	8.15
c	17.973 (2)	18.03
Volume of the unit cell	769.8 $Å^3$	784 $Å^3$
Number of the molecules in the unit cell	4	4
Density (expt.)	1.60 gm · cm^{-3}	1.581 gm · cm^{-3}
Density (calc.)	1.61	1.579
Linear absorption coefficient (for Cu$K\alpha$)	46.0 cm^{-1}	
Space group	$P2_12_12_1$	

* Hahn and Buerger (1957).

reliability index was only of the order of 0.10 for 937 reflections, collected on one of the first few Geiger counter diffractometers. The present study was undertaken with the idea of providing more accurate structural parameters for this substance, which is reported to have some therapeutic value (Frost, 1942).

Crystal growth and X-ray data collection

Single crystals of the above complex were grown at room temperature (28°C) by slow evaporation of an aqueous solution containing glycine and monochloroacetic acid. The solution was actually prepared with the aim of preparing a complex of glycine with monochloroacetic acid. But, the crystals obtained turned out to be the complex reported here. The crystals were transparent colourless needles with a maximum size of $5 \times 0.5 \times 0.25$ mm. The density was determined by the flotation method using a liquid-mixture of bromoform and xylene. The crystal data are furnished in Table 1. The cell parameters reported by the earlier workers (Hahn and Buerger, 1957) are also given for comparison.

Three-dimensional intensity data were collected using an Enraf Nonius CAD 4 diffractometer, with graphite-monochromated CuKα radiation at the I.I.T., Madras. Cell parameters were refined with 22 strong reflections. Lorentz and polarisation corrections were applied on the 884 unique reflections for which intensity data were collected. No absorption correction was applied.

UM00011718
NOVARTIS EXHIBIT 1517
Novartis v. Regents, IPR2023-01347
Page 464 of 4460

Earlier work*

5.34 Å
8.15
18.03
784 Å^3

4
1.581 gm · cm^{-3}
1.579

:ctions, collected
he present study
te structural pa-
ome therapeutic

om temperature
ning glycine and
d with the aim of
id. But, the crys-
The crystals were
× 0.5 × 0.25 mm.
a liquid-mixture
in Table 1. The
d Buerger, 1957)

an Enraf Nonius
ıKα radiation at
rong reflections.
84 unique reflec-
n correction was

Table 2. Fractional atomic coordinates and equivalent isotropic thermal parameters for the nonhydrogen atoms.

Atom	x	y	z	$^*U_{eq}$ (Å^2)
Cl	−0.6639(2)	0.9249(2)	0.5335(1)	0.0248(2)
O11	0.3819(7)	0.7800(5)	0.2101(2)	0.0262(7)
O21	0.6972(7)	0.8380(5)	0.2883(2)	0.0239(7)
C11	0.4887(10)	0.7737(7)	0.2730(3)	0.0202(10)
C21	0.3612(10)	0.6764(6)	0.3339(3)	0.0214(10)
N1	0.1201(8)	0.6019(5)	0.3083(2)	0.0214(8)
O12	1.1738(8)	1.0388(5)	0.3349(2)	0.0317(8)
O22	0.2724(8)	0.2801(5)	0.3888(2)	0.0255(8)
C12	1.1370(11)	1.1467(6)	0.3811(2)	0.0187(10)
C22	0.9166(10)	1.1368(7)	0.4335(3)	0.0203(10)
N2	0.8160(9)	0.9681(6)	0.4344(2)	0.0274(9)

$^* U_{eq} = \frac{1}{3}(U_{11} + U_{22} + U_{33})$.

Structure solution and refinement

From a three-dimensional Patterson synthesis, the position of the chlorine atom was determined. Thereafter, successive Fourier and difference Fourier syntheses revealed all the other nonhydrogen atoms in the structure. A few cycles of refinement calculations using isotropic thermal parameters for all the nonhydrogen atoms were carried out. After this, a few more cycles of refinement calculations using anisotropic thermal parameters for all the nonhydrogen atoms brought the R factor down to 0.073. All the hydrogen atoms were located from a difference Fourier map computed at this stage. A few cycles of refinement calculations using anisotropic thermal parameters for all the nonhydrogen atoms and isotropic thermal parameters for the hydrogen atoms were carried out till convergence. In the final cycle of refinement calculations, all the parameters (positional as well as thermal) of the hydrogen atoms were fixed and only the parameters of the nonhydrogen atoms were allowed to refine. The final R value was 0.055 for 779 reflections [1]. The crystallographic computer programs SHELX 76 and SHELX 400 (Sheldrick, 1976) were used for all the computations on the CYBER 180/830 A computer at the Department of Computer Science of Madurai Kamaraj University.

[1] Additional material to this paper can be ordered from the Fachinformationszentrum Energie-Physik-Mathematik, D-7514 Eggenstein-Leopoldshafen 2, FRG. Please quote reference no. CSD 53547, the names of the authors and the title of the paper.

UM00011719
NOVARTIS EXHIBIT 1517
Novartis v. Regents, IPR2023-01347
Page 465 of 4460

Table 3. * Fractional atomic coordinates and isotropic thermal parameters of the hydrogen atoms.

Atom	x	y	z	U_{eq} (Å)^2
H	0.3873	0.3015	0.3469	0.091
H11	0.4878	0.5910	0.3547	0.050
H21	0.3404	0.7463	0.3799	0.034
H31	0.1721	0.5067	0.2779	0.061
H41	0.0609	0.5476	0.3321	0.033
H51	0.0492	0.7031	0.2935	0.054
H12	0.9957	1.1858	0.4900	0.044
H22	1.7915	0.2163	0.4207	0.049
H32	1.9546	1.8940	0.4616	0.045
H42	1.6746	1.9664	0.4568	0.052
H52	1.7973	1.9144	0.3912	0.059

* These parameters were not refined in the final cycle of least-squares refinement.

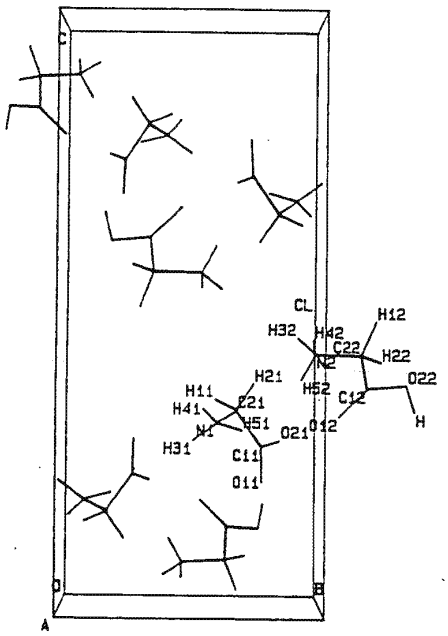


Fig. 1. A view of the crystal structure of diglycine hydrochloride down the a-axis.

UM00011720
NOVARTIS EXHIBIT 1517
Novartis v. Regents, IPR2023-01347
Page 466 of 4460

s of the hydrogen

U_{eq} (Å)²
0.091
0.050
0.034
0.061
0.033
0.054
0.044
0.049
0.045
0.052
0.059

res refinement.

Table 4. Bond lengths (Å) and angles (°). The e.s.d.s are given in parentheses.

C11 – O11	1.265(6)	O11 – C11 – O21	125.0(5)
C11 – O21	1.252(6)	O11 – C11 – C21	118.0(5)
C11 – C21	1.508(7)	O21 – C11 – C21	116.9(4)
C21 – N1	1.486(7)	C11 – C21 – N1	111.8(4)
C21 – H11	1.033(5)	H11 – C21 – H21	98.5(4)
C21 – H21	1.007(5)	H31 – N1 – H41	88.5(4)
N1 – H31	0.983(4)	H31 – N1 – H51	129.6(4)
N1 – H41	0.688(4)	H41 – N1 – H51	123.3(5)
N1 – H51	0.939(4)		
C12 – O12	1.220(6)	O12 – C12 – O22	125.2(5)
C12 – O22	1.303(6)	O12 – C12 – C22	120.9(5)
C12 – C22	1.502(7)	O22 – C12 – C22	114.0(4)
C22 – N2	1.464(7)	C12 – C22 – N2	109.9(4)
O22 – H	0.983(4)	H – O22 – C12	113.9(4)
C22 – H12	1.168(5)	H12 – C22 – H22	103.3(4)
C22 – H22	0.952(5)	H32 – N2 – H42	112.4(4)
N2 – H32	1.066(5)	H32 – N2 – H52	101.6(4)
N2 – H42	0.850(5)	H42 – N2 – H52	107.7(5)
N2 – H52	0.895(4)		

Table 5. Hydrogen bond parameters.

Hydrogen bond	Distance between donor and acceptor atoms (Å)	Hydrogen bond angle (°)
N1 – H31...O21^{I}	2.915	172.2
N1 – H41...Cl^{II}	3.225	134.8
N1 – H51...O21^{III}	2.965	142.8
O11 – H...O22^{IV}	2.552	160.3
N2 – H32...Cl^{II}	3.231	113.5
N2 – H42...Cl^{V}	3.124	168.3
N2 – H52...O21	2.900	166.6

Symmetry code:
I: $-x+1, 1/2+y-1, 1/2-z$
II: $1/2+x, 1/2-y+1, -z+1$
III: $x-1, y, z$
IV: $-x+1, y, z$
V: $1+x, y, z$

Table 6. Conformational angles (°)

O11 – C11 – C21 – N1	−0.3
O21 – C11 – C21 – N1	−178.1
O12 – C12 – C22 – N2	16.5
O22 – C12 – C22 – N2	−165.6

e *a*-axis.

UM00011721
NOVARTIS EXHIBIT 1517
Novartis v. Regents, IPR2023-01347
Page 467 of 4460

Description and discussion

The fractional atomic coordinates and equivalent isotropic thermal parameters of the nonhydrogen atoms are given in Table 2. The fractional atomic coordinates and isotropic thermal parameters of the hydrogen atoms are given in Table 3. A view of the crystal structure down the *a*-axis is shown in Fig. 1.

The main new features of the present reinvestigation are the precision of the structural parameters and the accurate determination of the positions of the hydrogen atoms in the structure. The bond lengths and bond angles of the glycine molecules are given in Table 4. The e.s.d.s are much smaller in the present work in comparison with the earlier study by Hahn and Buerger (1957). The glycine molecule 1 exists as a zwitter ion, i.e. $NH_3^+CH_2COO^-$, whereas glycine molecule 2 exists in the cationic form, i.e. $NH_3^+CH_2COOH$, in this structure. This is evident from the fact that the C–O distances and the bond angles around the carbon atom of the carboxlic group have values expected for such configurations. The molecular parameters of the glycine molecules are normal as found in other similar structures (Natarajan, 1979).

The glycine molecules are held together by a network of N–H...Cl, N–H...O and O–H...O hydrogen bonds. The geometry of the hydrogen bonds are given in Table 5. The conformational angles for the two glycine molecules are given in Table 6. It is seen that glycine 1 is very nearly planar whereas glycine 2 is deviating considerably from planarity.

References

Frost, W. S.: Bis(Amino acid) derivatives. I. Diglycine halogen acid addition products. J. Am. Chem. Soc. **64** (1942) 1286–1287.

Hahn, T.: Systematische Einflüsse bei Verfeinerung der Kristallstruktur von Diglycinhydrochlorid. Z. Kristallogr. **113** (1960) 403–429.

Hahn, T., Buerger, M. J.: The crystal structure of diglycine hydrochloride, $2(C_2H_5O_2N) \cdot HCl$. Z. Kristallogr. **108** (1957) 419–453.

Natarajan, S.: Studies in crystal structure analysis (Ph. D. Thesis), Madurai Kamaraj University, pp. 96–142 (1979).

Natarajan, S., Ravikumar, K., Rajan, S. S.: Crystal structure of diaqua nitrato glycine calcium(II) nitrate. Z. Kristallogr. **168** (1984) 75–82.

Sheldrick, G. M.: A program for crystal structure determination, University of Cambridge, England (1976).

UM00011722
NOVARTIS EXHIBIT 1517
Novartis v. Regents, IPR2023-01347
Page 468 of 4460

This Page is Inserted by IFW Indexing and Scanning Operations and is not part of the Official Record

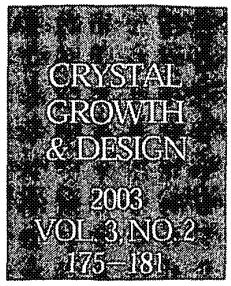
BEST AVAILABLE IMAGES

Defective images within this document are accurate representations of the original documents submitted by the applicant.

Defects in the images include but are not limited to the items checked:

- ☐ BLACK BORDERS
- ☐ IMAGE CUT OFF AT TOP, BOTTOM OR SIDES
- ☐ FADED TEXT OR DRAWING
- ☐ BLURRED OR ILLEGIBLE TEXT OR DRAWING
- ☐ SKEWED/SLANTED IMAGES
- ☐ COLOR OR BLACK AND WHITE PHOTOGRAPHS
- ☐ GRAY SCALE DOCUMENTS
- ☐ LINES OR MARKS ON ORIGINAL DOCUMENT
- ☐ REFERENCE(S) OR EXHIBIT(S) SUBMITTED ARE POOR QUALITY
- ☐ OTHER: _____

IMAGES ARE BEST AVAILABLE COPY.
As rescanning these documents will not correct the image problems checked, please do not report these problems to the IFW Image Problem Mailbox.



Cooperative and Anticooperative Effects in the Cocrystals of Mono- and Diazanaphthalenes with *meso*-1,2-Diphenyl-1,2-ethanediol

Britta Olenik,[†] Roland Boese,*[,‡] and Reiner Sustmann*[,†]

Institut für Organische Chemie and Institut für Anorganische Chemie, Universität Essen, 45117 Essen, Germany

Received January 6, 2003

ABSTRACT: *meso*-1,2-Diphenyl-1,2-ethanediol (**1**) as a hydrogen-bond donor and azanaphthalenes as hydrogen-bond acceptors form cocrystals, mostly in the ratio of 1:2. The X-ray structures provide detailed information on the binding motifs that consist of strong O−H···N hydrogen bonds and C−H···π interactions between C−H bonds of the heterocycles and the phenyl rings of *meso*-1,2-diphenyl-1,2-ethanediol. These motifs are found whenever a nitrogen atom is in the 2-position of the naphthalene skeleton (isoquinoline (**3**), quinazoline (**2**), and phthalazine (**4**)). Nitrogen atoms in the 1,3- and 2,3-positions, 1,3-diazanaphthalene (quinazoline) (**2**) and 2,3-diazanaphthalene (phthalazine) (**4**), alter the crystal lattice only in the case of phthalazine, due to additional hydrogen-bond- and π-stacking interactions. If a nitrogen atom is present in 1-position of naphthalene, 1,5-diazanaphthalene (naphthyridine) (**5**), the bonding motif consists of O−H···N hydrogen bridges between the nitrogen atoms in the 1- and 5-positions and the O−H groups of **1** leading to infinite strings of alternating naphthyridine and diol molecules. C−H···π interactions are found in this case between C−H groups of the adjacent six-membered "pyridyl" ring and the phenyl group attached to the carbon atom which is not involved in the formation of O−H···N hydrogen bonds as in the other three cases. This motif enables the incorporation of a second naphthyridine molecule without leading to additional hydrogen bonds, but with two C−H···π interactions. Attempts to generate cocrystals between **1** and 1-azanaphthalene (quinoline) as well as a tri-cocrystal between **1**, **5**, and naphthalene which should be of interest in this context have failed so far. Further attempts at cocrystallization of diazanaphthalenes with **1** also failed, which demonstrates the fine-tuned balance of cooperative and anticooperative effects for secondary intermolecular interactions.

Introduction

The rational design of solid-state structures is the essence of crystal engineering.[1−3] Cocrystallization of two different molecules is a possible way of intentionally influencing the position of molecules in a crystal lattice and allows for the investigation of newly generated macroscopic properties. In recent years, we have been involved in the construction of cocrystals of phenyl substituted diols as hydrogen bond donors and phenyl substituted bisimines or related heterocyclic compounds as hydrogen bond acceptors.[4−9] Due to the relative position of the aromatic units in the cocrystals, solid-state photochromism was observed when an electron donor substituent was introduced in one component and an electron acceptor substituent in the other. The phenomenon was explained by a correlated electron−proton transfer. In continuation of this work, we describe here cocrystals of *meso*-1,2-diphenyl-1,2-ethanediol (**1**) and mono- and diazanaphthalene molecules. Quinazoline (**2**), isoquinoline (**3**), phthalazine (**4**), and naphthyridine (**5**) were successfully cocrystallized with **1**. The crystal structures are determined and the forces governing the packing pattern are analyzed.

Results and Discussion[15]

meso-1,2-Diphenyl-1,2-ethanediol (**1**) and 1,3-diazanaphthalene (quinazoline) (**2**) form a 1:2 cocrystal (**2·1**) when crystallized from a 1:1 ethanol solution of the components. Single-crystal X-ray analysis shows that the asymmetric unit of the cell (space group $P2_1/n$) contains a molecular complex, consisting of two molecules of quinazoline **2** and one molecule of **1** (Table 1). Consequently, the complex is centrosymmetric and the 1:2 ratio results from hydrogen bonding of the 1,2-*meso*-diol and only one of the nitrogen atoms of each quinazoline (**2**). The interaction motif is shown in Figure 1a, and is characterized by a OH···N hydrogen bridge,[10] which is almost linear and in which the nitrogen atom in the 3-position of the heterocycle (N2 in Figure 1a) is involved. The plane of the phenyl group assumes an angle of 71° relative to the plane of the heterocycle. The almost orthogonal positioning of the rings allows for a favorable C_{sp^2}−H···π interaction[11] between the hydrogen atom H3 of the heterocycle and the π electrons of the adjacent phenyl group of the diol. Due to the crystallographic centrosymmetry of the complex, the second hydroxy group of the diol binds in an identical manner to a second molecule of quinazoline. This leads to the subunits of two molecules of **2** with one molecule of **1** which are packed in stacks (Figure 1b). Because of the spacial requirements of the phenyl groups of the diol these stacks are shifted relative to each other. This face-to-face offset induces stabilizing interactions of the π-systems (edge to face).[12] Viewing along [$\bar{1}$ 0 2] (Figure 1c) an additional C_{sp^2-H}···π interaction[11] is recognized between a hydrogen atom at the benzene site of quinazoline and the π-electrons of a phenyl group of a diol molecule. The packing of the 2:1 subunits is thus

[†] Institut für Organische Chemie.
[‡] Institut für Anorganische Chemie.
* To whom correspondence should be addressed. (R.B.) E-mail: roland.boese@uni-essen.de; fax: +49 201/183 2535 and (R.S.) E-mail: reiner.sustmann@uni-essen.de Fax: +49 201/183 4259.

10.1021/cg034002h CCC: $25.00 © 2003 American Chemical Society
Published on Web 03/05/2003

UM00011724
NOVARTIS EXHIBIT 1517
Novartis v. Regents, IPR2023-01347
Page 470 of 4460

Table 1. Data Collection and Refinement for Cocrystals of *meso*-1,2-Diphenyl-1,2-ethanediol 1 with 2–5

	2(quinazoline)·*meso*-1,2-diphenyl-1,2-ethanediol (**22·1**)	2(isoquinoline)·*meso*-1,2-diphenyl-1,2-ethanediol (**23·1**)	2(phthalazine)·*meso*-1,2-diphenyl-1,2-ethanediol (**24·1**)	2(naphthyridine)·*meso*-1,2-diphenyl-1,2-ethanediol (**25·1**)
formula	$2(C_8H_6N_2)\cdot C_{14}H_{14}O_2$	$2(C_9H_7N)\cdot C_{14}H_{14}O_2$	$2(C_8H_6N_2)\cdot C_{14}H_{14}O_2$	$2(C_8H_6N_2)\cdot C_{14}H_{14}O_2$
form wt (Da)	474.55	472.56	474.55	474.55
density ($g\cdot cm^{-3}$)	1.303	1.245	1.242	1.327
T (K)	293(2)	293(2)	293(2)	203(2)
cryst size (mm)	0.48·0.38·0.32	0.47·0.36·0.32	0.53·0.47·0.41	0.38·0.14·0.05
cryst color	colorless	colorless	pale yellow	colorless
crystal system	monoclinic	triclinic	monoclinic	triclinic
space group	$P2_1/n$	$P\bar{1}$	$P2_1/n$	$P\bar{1}$
a (pm)	559.48(6)	566.96(11)	1006.9(3)	560.9(2)
b (pm)	1197.83(16)	979.3(12)	963.1(2)	951.3(3)
c (pm)	1822.15(14)	1168.5(13)	1387.1(3)	1170.1(4)
α (°)	90	84.196(8)	90	107.940(6)
β (°)	97.783(7)	80.850(12)	109.331(13)	90.901(7)
γ (°)	90	80.781(13)	90	90.027(7)
V ($10^6\cdot pm^3$)	1209.9(2)	630.18(16)	1269.3(5)	593.9(4)
Z	2	1	2	1
$2\theta_{max}$ (°)	50	56	56	56.8
refln collected	2361	3321	3132	7047
refln indepen	2130	3020	2967	3768
R_{int}	0.0603	0.0391	0.0247	0.0300
refln obs ($>4\sigma F$)	1718	2519	1783	2227
param refin	164	164	172	173
R_1 (F)	0.0494	0.0581	0.0670	0.0576
wR_2 (F^2, all data)	0.1391	0.1693	0.1951	0.1593
residual electron density ($10^6\cdot e\cdot pm^{-3}$)	0.183	0.223	0.159	0.407
disorder		O of hydroxy		O of hydroxy

supported by offset face to face interactions of the heterocycles in the stacks and CH···π stabilizations between subunits.

As the nitrogen atom in position 1 of quinazoline does not seem to be essential for the crystal packing it was attempted to obtain a cocrystal of 2-azanaphthalene (isoquinoline) (**3**) and **1** in a ratio of 2:1. If an isomorphous replacement of **1** is possible, the cocrystal (**3·1**) should show a packing comparable to the cocrystal of **2** (**2·1**). A 2:1 solution of the components in ethyl acetate provided a cocrystal when the solvent was slowly evaporated. X-ray analysis of a single crystal of **3·1** (space group $P\bar{1}$) confirmed the presumption of a 1:2 composition (Figure 2a), although both structures are not isomorphous. The angle between the planes of the heterocycle and the phenyl group is 72°, also leading to a $C_{sp^2}H\cdots\pi$ interaction. Again, the dominating packing criterion is a strong O–H···N hydrogen bridge, almost identical to that in the cocrystal of quinazoline. Figure 2b shows the stacking where the distance of the centroids of the pyridine is similar to the **3·1** molecular complex. However, the difference of the packing, reflected in the different crystal symmetries, becomes apparent when viewing down [$\bar{4}$ 1 1] (Figure 2c). The heterocycles are much more shifted with respect to each other than in the previous case so that no additional C–H···π interaction can be identified. Nevertheless, the experiment proves that the analysis of a crystal packing of one cocrystal may lead to the planned construction of a second cocrystal with similar bonding motifs.

Can this type of approach, i.e., the rational design of the solid-state structure of a cocrystal of **1** with mono- or diazanaphthalenes, be generalized? 2,3-Diazanaphthalene (phthalazine) (**4**) was, therefore, studied next as a partner for **1**. As anticipated a 2:1 cocrystal (**24·1**) resulted from the crystallization of a 1:1 mixture of the components in ethyl acetate. X-ray analysis revealed a packing with similarities but also essential differences to the two other examples. The main binding motif is given in Figure 3a with only one active nitrogen atom in each heterocycle involved in a O–H···N bridge. Here, orientational disorder of the oxygen atoms of **1** occurs, which is not presented in the figure. The oxygen atom adopts different positions, while the bridging H-atom remains essentially in the same location. Like in the previous case, there is an additional $C_{sp^2}H\cdots\pi$ interaction between the hydrogen atom at the carbon atom next to the nitrogen (H4) and the π electrons of a phenyl group. The planes of the phenyl groups of the diol and phthalazine are orthogonal to each other (Figure 3b).

The crystal packing of the cocrystal **24·1** is primarily determined by the 2:1 subunits. The overall packing follows from the arrangement of these units relative to each other. The subunits of the cocrystals **22·1** and **23·1** are positioned in such a way that no π stacking is realized. The heterocycles are shifted relative to each other so that only edge-to-face interactions exist. In contrast to these arrangements (Figures 1a,b and 2a,b), two phthalazine molecules of two subunits in **24·1** are placed on top of each other. Figure 3c demonstrates that the phthalazine molecules attached to different but identically oriented diol molecules are almost perfectly π-stacked displaced only slightly along the short and long axis of the molecules. The separation of the centroids of juxtaposed six-membered rings is 365 pm. The heterocycles are positioned in such a way that the nitrogen atoms are at opposite ends of the dimer, i.e., the dipole moments of the two molecules point in opposite directions providing a stabilizing dipole–dipole interaction. This type of π-stacking is also typical for the phthalazine crystal structure.[13]

Why does the same phenomenon not happen in **2·1** and **3·1**? The reason is likely that the polarization of phthalazine is stronger than that of **2** and **3**, the dipole

UM00011725
NOVARTIS EXHIBIT 1517
Novartis v. Regents, IPR2023-01347
Page 471 of 4460

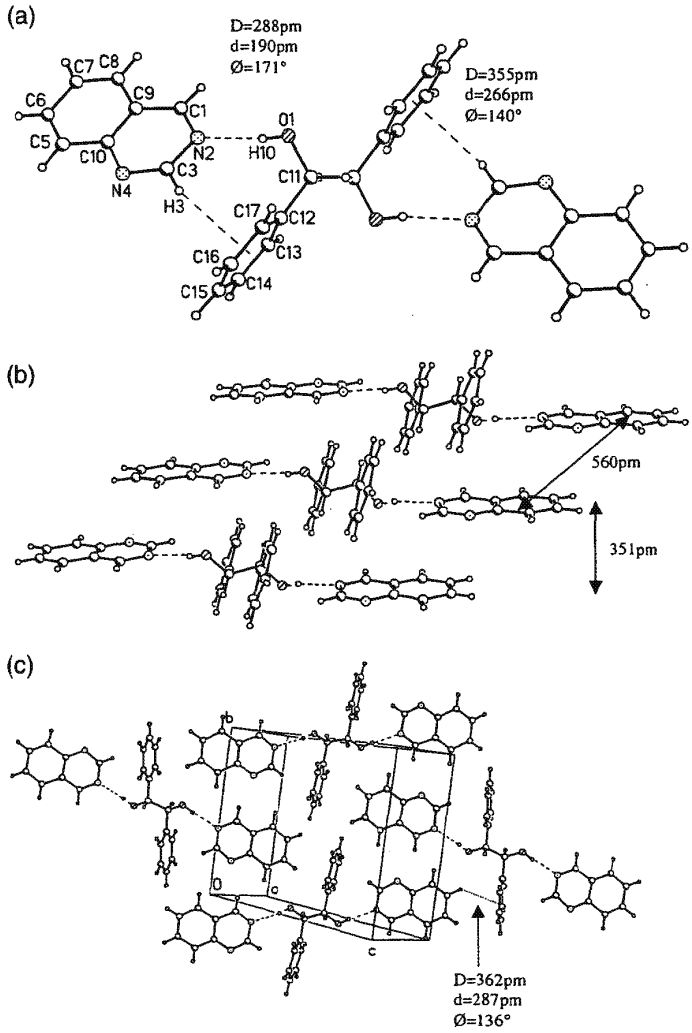


Figure 1. Cocrystal of *meso*-1,2-diphenyl-1,2-ethanediol and 1,3-diazanaphthalene (quinazoline), (a) interaction motif of **1** and two molecules of **2**, (b) arrangement of individual **1** and **2·2** units, (c) unit cell of **1** and **2·2**. According to the convention, D corresponds to the distance of the non-hydrogen atoms in a hydrogen bridge or the distance of a non-hydrogen atom and the geometric center of an aromatic ring; d corresponds to the distance of the normalized hydrogen atom to the hydrogen bridged non-hydrogen atom or the geometric center of an aromatic ring, and Ø is the angle between the non-hydrogen atom, the attached normalized hydrogen atom and the bridged non-hydrogen atom or the geometric center of an aromatic ring. This applies to all the Figures 1–4.

moment pointing from the benzene to the pyridazine part of the molecule. The way the molecules are stacked provides the best possible dipole–dipole interaction. Assuming that this stabilization is primarily responsible for generating pairs of subunits, which form infinite chains in the crystal, then the spacial situation leads to the incorporation of subunits almost orthogonal filling the space between the phenyl groups of **1**. Due to the symmetry, the π stacking continues along both axes (Figure 3c), where the angle between the central CC bond of two diol molecules is 68°. Within the crystal, therefore all phthalazine molecules occur in pairs.

The nitrogen atom of phthalazine which is not involved in the OH···N hydrogen bridge forms a C_{sp^2}–H··· N hydrogen bridge to a hydrogen atom of a phthalazine molecule of the other type of subunit (Figure 3c). The same phthalazine molecule establishes also a C–H···O hydrogen bond to a diol, the bond lengths are 341 pm (C···O) and 236 pm (CH···O).

These findings prompted a search for further examples of cocrystals between *meso*-1,2-diphenyl-1,2-ethanediol and diazanaphthalenes. Quinoxaline (1,4-diazanaphthalene) and naphthyridine (1,5-diazanaphthalene) were subjected to cocrystallization with *meso*-1,2-diphenyl-1,2-ethanediol. Unfortunately all attempts to obtain a cocrystal with quinoxaline failed, whereas naphthyridine formed a cocrystal (**25·1**).

Part of the primary-bonding motif of the other cocrystals is retained (Figure 4a) in **25·1**. There is a subunit of *meso*-1,2-diphenyl-1,2-ethanediol and two molecules

UM00011726
NOVARTIS EXHIBIT 1517
Novartis v. Regents, IPR2023-01347
Page 472 of 4460

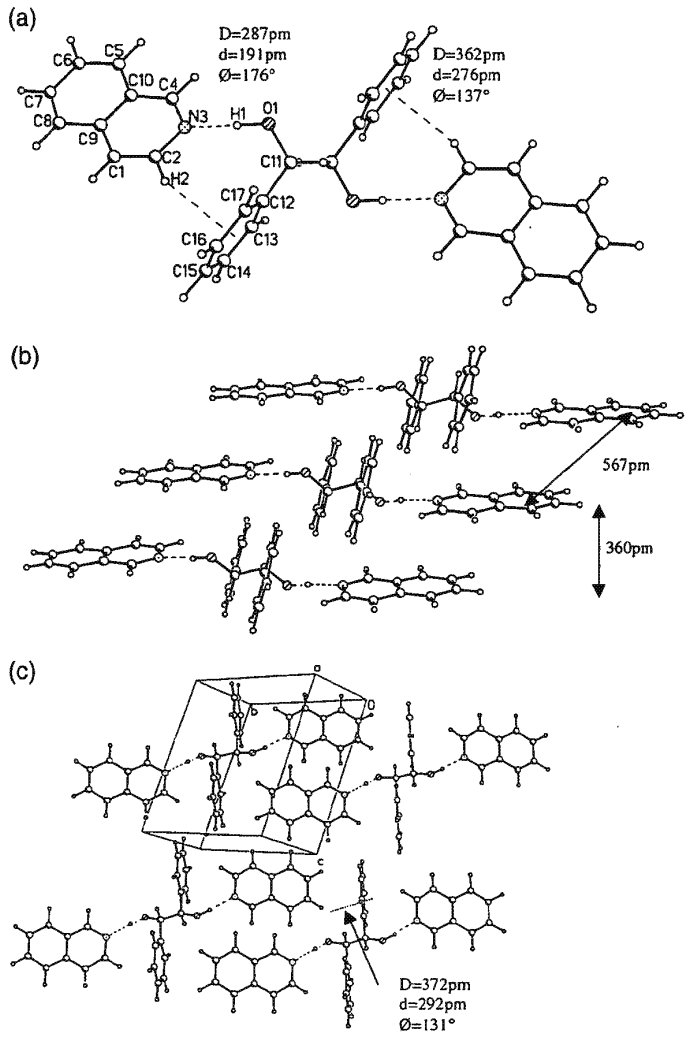


Figure 2. Cocrystal of *meso*-1,2-diphenyl-1,2-ethanediol and 2-azanaphthalene (isoquinoline), (a) interaction motif of **1** and two molecules of **3**, (b) arrangement of individual **1** and **2**·**3** units, (c) unit cell of **1** and **2**·**3**.

of naphthyridine which is held together by O−H···N hydrogen bonds and C_{sp^2}−H···π hydrogen bonds. Again, disorder of the OH groups produce different geometries of the hydrogen bridges. Contrary to the former cases the C_{sp^2}−H···π interaction does not derive from the CH bond adjacent to the heteroatom involved in the O−H··· N bridge (H25′) but stems from a CH bond of the second ring (H23). The phenyl ring of the diol participating in this interaction is not as in the other examples the one adjacent to the OH group which binds to the nitrogen atom (Figure 4a). This pattern generates an open space at the site of one phenyl group which is filled by a second molecule of naphthyridine. This is placed in such a way that two C_{sp^2}−H···π interactions are possible, one with the phenyl group of a diol and one with a CH group of the hydrogen-bonded naphthyridine (Figure 4b).

As the central unit has an inversion center, the geometrical arrangement at both sides of *meso*-1,2-diphenyl-1,2-ethanediol are identical. Naphthyridine has two nitrogen atoms in the 1- and 5-positions of the naphthalene skeleton, and therefore the crystal packing is determined by a second hydrogen bonded molecule of *meso*-1,2-diphenyl-1,2-ethanediol molecule. This leads to an infinite chain of alternating diol and naphthyridine molecules. Figure 4c shows that a second naphthyridine molecule is filled in the structure which is not involved in strong hydrogen bonds. What is the reason for the different alignment of the heterocycle naphthyridine relative to the diol compared to the other cocrystals? The structural difference in the heterocycle consists of the position of the nitrogen atoms. Instead of forming a C−H···π interaction with the C−H group adjacent to the nitrogen atom forming the hydrogen bond, naphthyridine prefers a C−H bond of the adjacent ring. Among the cases considered it is the first example in which a heteroatom is found in this second ring. Is it possible that the electronegativity of this nitrogen atoms renders the C−H bond in *para* position more strongly

UM00011727
NOVARTIS EXHIBIT 1517
Novartis v. Regents, IPR2023-01347
Page 473 of 4460

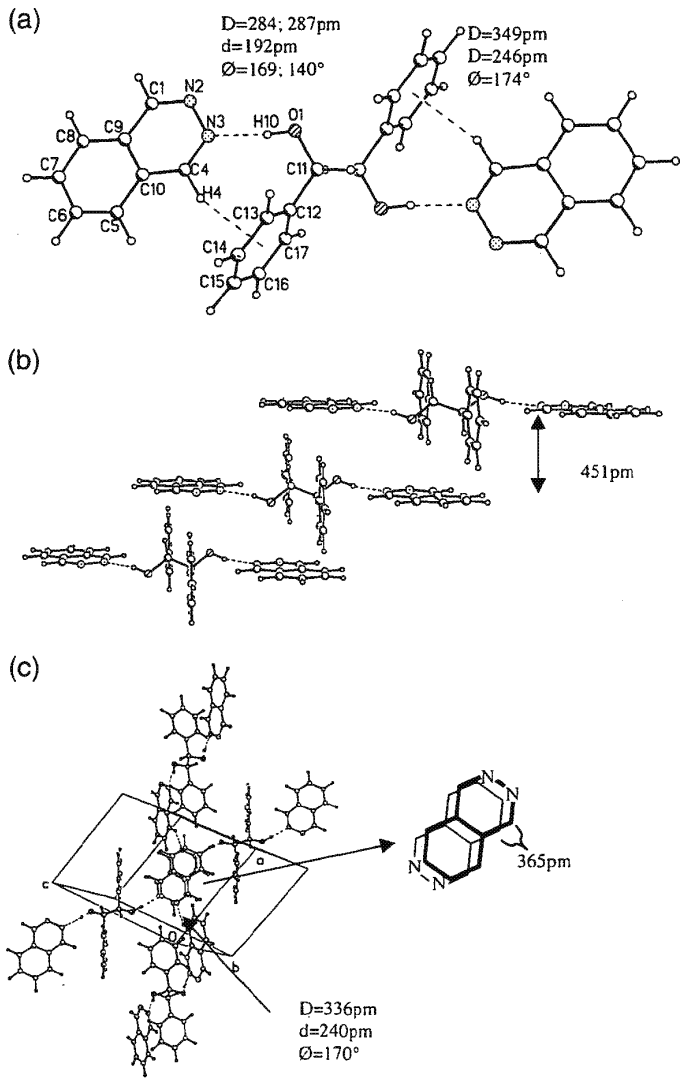


Figure 3. Cocrystal of *meso*-1,2-diphenyl-1,2-ethanediol and 2,3-diazanaphthalene (phthalazine), (a) interaction motif of **1** and two molecules of **4**, (b) arrangement of individual **1** and **2·4** units, (c) unit cell of **1** and **2·4** with the stacking of the heterocycles emphasized.

polarized, thus making stronger electrostatic interactions with the π electrons possible? If this is the determining interaction a cocrystal of *meso*-1,2-diphenyl-1,2-ethanediol with quinoline should revert the arrangement of the heterocycle to that of the previous cases. Unfortunately, no cocrystal was obtained from **1** and quinoline. Also, replacement of one of the two heterocycles in the complex **5·21** which is only C−H···π bonded by naphthalene did not succeed so far, as well as further experiments to cocrystallize **1** with further diazanaphthalenes.

Conclusion

X-ray structures of cocrystals between *meso*-1,2-diphenyl-1,2-ethanediol and mono- and diazanaphthalenes provide valuable information on synthons for crystal engineering. The primary interaction motif in the *meso*-1,2-diols cocrystallized with the azanaphthalenes is always governed by O−H···N hydrogen bonds. The resulting 1:2 complexes are stabilized by additional C−H···π interactions of the 1,2-diphenyl groups at the diols with the hydrogen atoms at the azanaphthalenes. If a second nitrogen atom exists in the azanaphthalene, it does not contribute essentially to the stabilization of the structure as long as it is too close to the first N-atom as it was found in 1,4-diazanaphthalene, but it polarizes the heterocycles to stabilize an *anti*-parallel stacking in 2,3-diazanphathalene, still working cooperatively with the crystal packing. In 1,5-diazanaphthalene, the second nitrogen atom takes the same function as the first to form chains, but now a second heterocycle needs to be filled in to maintain the C−H···π interactions,

UM00011728
NOVARTIS EXHIBIT 1517
Novartis v. Regents, IPR2023-01347
Page 474 of 4460

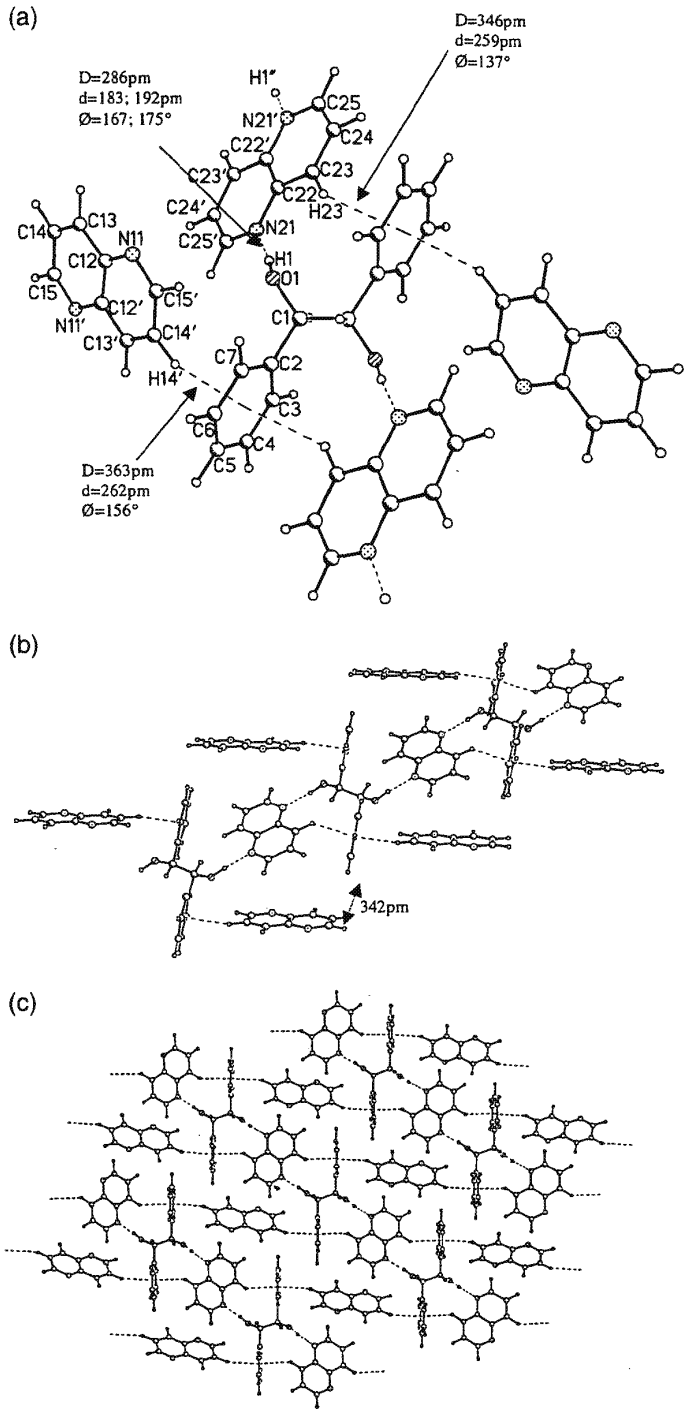


Figure 4. Cocrystal of *meso*-1,2-diphenyl-1,2-ethanediol and 1,5-diazanaphthalene (naphthyridine), (a) interaction motif of **1** and two molecules of **5**, (b) chains of **1** and **5** together with non-O–H···N bonded naphthyridine molecules, (c) planes of networked molecules of **1** and **5** in the cocrystal.

none of its nitrogen atoms is active. It is quite likely that this molecule can be replaced by 1-azanaphthalene or even naphthalene. There exists a general problem in cocrystallization experiments, since it is the fine-tuned balance of packing energies of the cocrystal versus that of the neat components.

In the case of the diazanaphthalenes the O–H···N hydrogen bonded nitrogen can sit in the 1- and the

UM00011729
NOVARTIS EXHIBIT 1517
Novartis v. Regents, IPR2023-01347
Page 475 of 4460

2-positions, but it is the second nitrogen that defines the packing as a cooperative or anticooperative one, which then prevails cocystallization.

Experimental Section

The compounds were either commercially available or, as in the case of naphthyridine (**5**), were synthesized according to a literature procedure.[14] Cocrystals were obtained by dissolving the components in a 1:1 ratio in the reported solvent, if not otherwise indicated, and letting the solvent slowly evaporate at ambient temperature. Cocrystal **1·22**: ethyl acetate, mp: 86 °C. Cocrystal **1·23**: ethyl acetate (ratio **1**:**3** = 1:2), mp: 104 °C. Cocrystal **1·24**: acetone, mp: 120 °C. Cocrystal **1·25**: acetone, mp: 120 °C. The ratio of the components in the cocrystal was also checked by solution ^{1}H NMR spectra.

Crystallographic data (excluding structure factors) for the structures reported in this paper have been deposited with the Cambridge Crystallographic Data Centre as supplementary publication no. CCDC-190520 for **1·22**, 190521 for **1·23**, 190522 for **1·24** and 190523 for **1·25**. Copies of the data can be obtained free of charge on application to CCDC, 12 Union Road, Cambridge CB2 1EZ, UK [Fax: int. code +44(1223)336-033; E-mail: deposit@ccdc.com.ac.uk].

Acknowledgment. This work has been supported by the Deutsche Forschungsgemeinschaft and Sonderforschungsbereich SFB 452. We thank Prof. Dr. M. Mazik for the preparation of one of the cocrystals (**1·23**).

References

(1) Desiraju, G. R. *Crystal Engineering. The Design of Organic Solids*; Elsevier: Amsterdam, 1989.
(2) Desiraju, G. R. *Angew. Chem.* **1995**, *107*, 2541−2558.
(3) Desiraju, G. R. In *Comprehensive Supramolecular Chemistry*, Vol. 6; MacNicol, D. D., Toda, F., Bishop, R., Eds.; Pergamon: Oxford, 1996; Chapter 1, pp 1−22.
(4) Reyes-Arellano, A.; Boese, R.; Steller, I.; Sustmann, R. *Struct. Chem.* **1995**, *6*, 391−396.
(5) Felderhoff, M.; Steller, I.; Reyes-Arellano, A.; Boese, R.; Sustmann, R. *Adv. Mater.* **1996**, *8*, 402−405.
(6) Felderhoff, M.; Smolka, T.; Sustmann, R.; Steller, I.; Weiss, H.-C.; Boese, R. *J. Prakt. Chem.* **1999**, *341*, 639−648.
(7) Smolka, T.; Sustmann, R.; Boese, R. *J. Prakt. Chem.* **1999**, *341*, 378−383.
(8) Smolka, T.; Boese, R.; Sustmann, R. *Struct. Chem.* **1999**, *10*, 429−431.
(9) Smolka, T.; Schaller, T.; Sustmann, R.; Bläser, D.; Boese, R. *J. Prakt. Chem.* **2000**, *342*, 465−471.
(10) The C−H and O−H distances in the crystal structures have been normalized to 108 and 98.3 pm, their respective distances found by neutron diffraction methods.
(11) (a) Desiraju, G. R.; Steiner, T. *The Weak Hydrogen Bond in Structural Chemistry and Biology*; Oxford University Press: Oxford, 1999. (b) Nishio, M.; Hirota, M.; Umezawa, Y. *The CH/π Interaction: Evidence, Nature and Consequences*; Wiley-VCH: New York, 1998.
(12) Dance, I.; Scudder, M. *Chem. Eur. J.* **1996**, *2*, 481−484.
(13) Huiszoon, C.; van de Woal, B. W.; van Egmond, A. B.; Harkema, S. *Acta Crystallogr.* **1972**, *B28*, 3415−3419.
(14) Rapoport, H.; Batcho, A. D. *J. Org. Chem.* **1963**, *28*, 1753−1759.
(15) For all discussions, C−H and O−H distances have been normalized to their distances from neutron diffraction with 108 and 98.3 pm, respectively.

CG034002H

UM00011730
NOVARTIS EXHIBIT 1517
Novartis v. Regents, IPR2023-01347
Page 476 of 4460

CRYSTAL GROWTH & DESIGN
2003
VOL. 3, NO. 2
183–188

Supramolecular Synthesis by Cocrystallization of Oxalic and Fumaric Acid with Diazanaphthalenes

Britta Olenik,[†] Tanja Smolka,[†] Roland Boese,*[,‡] and Reiner Sustmann*[,†]

Institut für Organische Chemie and Institut für Anorganische Chemie, Universität Essen, 45117 Essen, Germany

Received January 6, 2003

ABSTRACT: 1:1 cocrystals of oxalic and fumaric acid with 1,4-diazanaphthalene (quinoxaline) and 2,3-diazanaphthalene (phthalazine) were prepared. 1,5-Diazanaphthalene (naphthyridine) formed a 1:1 cocrystal only with oxalic acid. X-ray structural analyses are reported. The influence of the position of the two nitrogen atoms in these diazanaphthalenes on the crystal packing is analyzed. The gross crystal structure is governed by strong OH···N hydrogen bonds. The fine-tuning of the packing of the cocrystals of quinoxaline with oxalic and fumaric acid occurs via CH···O hydrogen bonds. The stabilization by the CH···O hydrogen bonds leads to a planar sheetlike structure in the cocrystal with fumaric acid, in contrast to the cocrystal with oxalic acid where the optimization of the CH···O hydrogen bonds results in a nonplanar bent structure. The geometrical arrangement of the nitrogen atoms in 1- and 5-positions in naphthyridine allows a planar sheetlike structure in the cocrystal with oxalic acid. In the case of phthalazine complete proton transfer from one carboxy group of oxalic and fumaric acid to a nitrogen atom of the heterocycle, generating ionic interactions is observed. The hydrogen atom of the second carboxy group of the acids is involved in a OH···O=C hydrogen bond.

Introduction

The design of organic solids by crystal engineering is presently of high interest.[1,2] Attempts are made to understand the rules that govern the construction of particular solid-state structures. Concepts that have been developed for covalent synthesis are extended to the area of noncovalent synthesis.[3] Synthons can be defined that can be used as a guideline in the preparation of particular solid-state structures. The strength of noncovalent interactions ranges from weak, like van der Waals forces, CH···X hydrogen bonds (X = O, N, π),[4,5] π···π stacking, or CH···π interactions,[6] to strong forces such as O−H···X hydrogen bonds (X = O, N).[7] Apart from the strong interactions that are often structure determining, it is the sum of a number of different weak forces which leads to the observed solid-state structure.[8] This was demonstrated by Jones et al. with the molecular complexes of phenazine with various dicarboxylic acids.[9] Other systems that utilize O−H···O and C−H···O interactions with carboxylic acids[10] or O−H···N and C−H···O in heterodimers[11] face the same problem of the dependence on many cooperative factors which is the main problem in predicting crystal structures.

In recent years, we have been interested in the formation of cocrystals of functional diols as hydrogen-bond donors and imino nitrogen atom carrying molecules as hydrogen-bond acceptors, either in aliphatic bismines or in heterocyclic structures.[12,13] In some cases, the construction of hydrogen bonded networks of such components has led to interesting macroscopic properties, like a thermally reversible photochromism.[14−16]

In this contribution, we use quinoxaline, phthalazine, and naphthyridine as diazanaphthalenes in the cocrystallization with fumaric and oxalic acid. The systematic study is directed toward the understanding of the influence of nitrogen atoms in different positions of the naphthalene skeleton on the observed crystal packing. Cocrystals could be obtained for all combinations of the synthons except for naphthyridine where only a cocrystal with oxalic and not with fumaric acid could be prepared. Cocrystals of these heterocycles with dicarboxylic acids were reported so far only for phthalazine, where Rogers et al. described cocrystals of phthalazine and phthalic acid in the ratio 2:1 and 2:3.[17] Recently, we described cocrystals of azanaphthalenes and *meso*-1,2-diphenyl-1,2-ethanediol.[18]

Results and Discussion[24]

Quinoxaline and Oxalic Acid. 1,4-Diazanaphthalene (quinoxaline) and oxalic acid were cocrystallized in a 1:1 ratio from an acetone solution. X-ray structural analysis (Table 1) reveals two molecules of quinoxaline and two molecules of oxalic acid in the asymmetric unit (space group $P\bar{1}$) (Figure 1a). A first inspection shows that the four molecules are held together by OH···N hydrogen bonds with alternating molecules of oxalic acid and quinoxaline, forming four different hydrogen bonds to build infinite chains. The oxalic acid molecules are almost planar, but it is remarkable to see that the molecules in the chain are not arranged in a single plane. The mean planes of the oxalic acid molecules and quinoxalines are almost coplanar, but the mean planes of the heterocycle (I) and oxalic acid (II) as well as the mean plane of heterocycle (III) and oxalic acid (IV) are considerably tilted. This torsion brings O6 in a position to build a CH···O=C bridge to the hydrogen atom at C6. This geometry allows further the formation of weak C−H···O=C hydrogen bonds (hydrogen atom at C2 and

[†] Institut für Organische Chemie.
[‡] Institut für Anorganische Chemie.
* To whom correspondence should be addressed. (R.B.) Fax: +49 201/183. E-mail: roland.boese@uni-essen.de and (R.S.) Fax: +49 201/1834259. E-mail: reiner.sustmann@uni-essen.de.

10.1021/cg034003+ CCC: $25.00 © 2003 American Chemical Society
Published on Web 03/05/2003

UM00011731
NOVARTIS EXHIBIT 1517
Novartis v. Regents, IPR2023-01347
Page 477 of 4460

Table 1. Data Collection and Refinement for Cocrystals of Diazanaphthalenes with Oxalic and Fumaric Acid

formula	$C_8H_6N_2 \cdot C_2H_2O_4$	$C_8H_6N_2 \cdot C_4H_4O_4$	$C_8H_6N_2 \cdot C_2H_2O_4$	$C_8H_7N_2 \cdot C_2HO_4$	$C_8H_6N_2 \cdot C_4H_4O_4$
form wt (Da)	220.18	246.22	220.18	220.18	246.22
density (g cm^{-3})	1.536	1.450	1.544	1.491	1.448
T (K)	299(2)	293(2)	203(2)	203(2)	203(2)
cryst size (mm)	0.18·0.02·0.01	0.53·0.46·0.32	0.21·0.18·0.07	0.12·0.03·0.02	0.18·0.08·0.06
cryst color	blue	colorless	pale yellow	pale yellow	colorless
crystal system	triclinic	triclinic	triclinic	monoclinic	monoclinic
space group	$P\bar{1}$	$P\bar{1}$	$P\bar{1}$	$P2_1/c$	$P2_1/m$
a (pm)	373.3(6)	575.4(3)	371.0(6)	561.26(6)	378.44(13)
b (pm)	1226.6(14)	884.2(3)	668.0(11)	1812.74(17)	4260.2(14)
c (pm)	2109(3)	1193.1(5)	974.0(16)	991.98(10)	1057.5(4)
α (°)	87.59(3)	72.43(3)	86.48(4)	90	90
β (°)	85.43(4)	82.26(4)	79.37(6)	103.594(2)	96.547(7)
γ (°)	81.90(5)	77.80(4)	88.19(4)	90	90
V (10^6 pm^3)	952(2)	564.1(4)	236.7(7)	980.98(17)	1693.9(10)
Z	4	2	1	4	6
$2\theta_{max}$ (°)	50	59.90	56.48	56.18	56.64
refln collected	8724	4175	1441	8384	14587
refln indepen	2867	3142	885	2211	4247
R_{int}	0.0844	0.1416	0.0225	0.0515	0.0300
refln obs ($>4\sigma F$)	1431	1759	676	1571	1516
param refin	289	163	73	145	244
R_1 (F)	0.0769	0.0736	0.0763	0.0601	0.0846
wR_2 (F^2, all data)	0.2189	0.2298	0.1996	0.1656	0.2094
residual electron density (10^6 e pm^{-3})	0.298	0.292	0.780	0.515	0.290

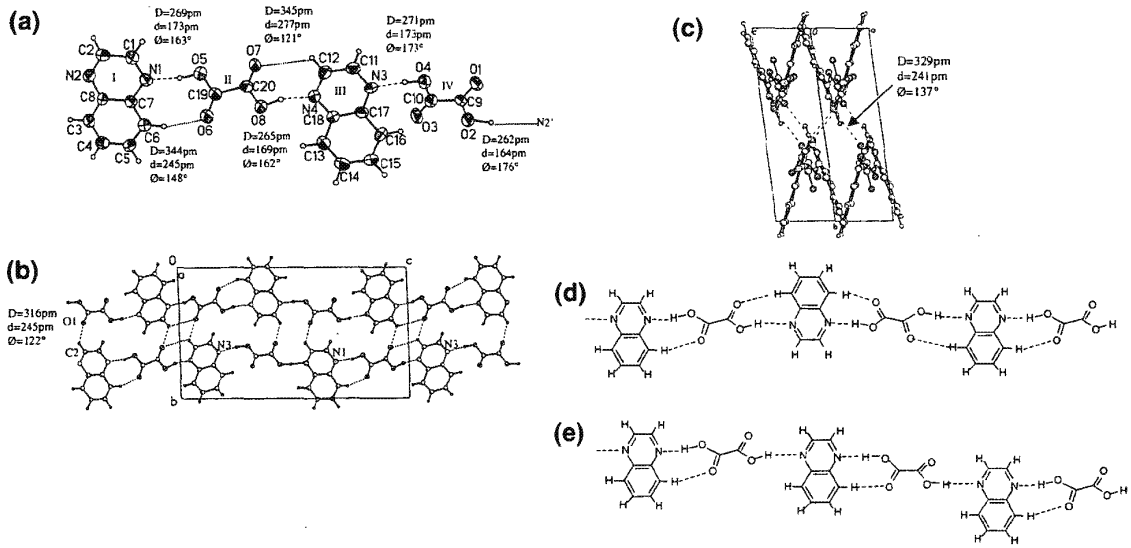


Figure 1. Cocrystal of 1,4-diazanaphthalene (quinoxaline) and oxalic acid, (a) thermal ellipsoid plot (50%) of the molecules in the asymmetric unit with numbering scheme, (b) molecular packing viewing down [100], (c) molecular packing viewing down [101], (d) schematic representation of a planarized chain, (e) schematic representation of a hypothetical linear and planar chain with synperiplanar oxalic acid and quinoxaline as in the cocrystal.

C15 of quinoxaline molecules), which interconnect the chains formed by the O–H···N hydrogen bonds. Figure 1b displays two such chains viewing down the [100] vector. It is noteworthy that the chains are arranged antiparallel so that the nitrogen atoms of quinaxoline are on the inner side of the dimeric chain. This means that such dimer chains are positioned next to each other when constructing the cocrystal. The next dimer would appear above or below the chain shown in Figure 1b. The quinoxaline molecules in this new dimer fill the free space above or below the oxalic acid molecules of the original dimer leading to a close packing, which however is not as dense as within the dimers. The interplanar angle of the molecules in a single chain is especially visible in Figure 1c viewing down the [101] vector. Neighboring V-shaped chains are alternately interlocked and linked by weak hydrogen bonds to the chains displayed below in Figure 1c.

To gain more insight in the reason for the observed packing the question may be asked whether a fully planar arrangement as observed in other cases (see below) might be an option? Planarization in the actual disposition of oxalic acid and quinoxaline (Figure 1) does not seem to be feasible. If oxalic acid (II) is rotated about the central bond into the plane of quinoxaline (I), severe steric interaction between the hydrogen atom at C6 and O6 would be the consequence. The O···H distance would be smaller than the van der Waals radii, unless oxalic acid (II) would be rotated about an axis perpendicular to the molecular plane which passes through the

UM00011732
NOVARTIS EXHIBIT 1517
Novartis v. Regents, IPR2023-01347
Page 478 of 4460

midpoint of the central bond C19−C20. This rotation could lead to C···O distances expected for a CH···O hydrogen bridge. It would however disturb the linearity of the individual chains (Figure 1d). On the other hand, a linear arrangement could be imagined as oxalic acid (II) and quinoxaline (III) demonstrate where besides the strong OH···N hydrogen bond a CH···O bridge exists between O7 and the hydrogen atom at C12. Distances and angles are such that no steric hindrance is established due to the planar disposition. This observation allows the construction of two planar and linear arrangements of the two molecules which are shown in Figure 1d,e. In both strimgs oxalic acid assumes an *antiperiplanar* conformation with respect to the carbonyl groups. In Figure 1d, the quinoxaline molecules are rotated alternatively by 180° about the axis connecting the two nitrogen atoms, similar to the cocrystal, in Figure 1e the nitrogen atoms of the quinoxaline molecules remain on the same same side of a string. Both arrangements have the disadvantage with respect to the cocrystal that there is no three-dimensional hydrogen bond network and that they are less compact, i.e., they constitute structures with less van der Waals contacts. The real arrangement has the advantage in having two hydrogen bridges within the chain and an additional one between different chains. The structure could be said to be optimized with respect to compactness and the maximum number of C−H···O bridges.

Quinoxaline and Fumaric Acid. The two carboxy groups in fumaric acid are separated by a CC double bond which can be considered a spacer between two carboxy groups that are directly linked in oxalic acid. The influence of this structural change on the crystal packing of a cocrystal with quinoxaline should produce insight in the factors which govern the placement of the molecules in the crystal lattice. The 1:1 triclinic cocrystal (space group $P\bar{1}$) was produced from an acetone solution. The asymmetric unit consists of one molecule of quinoxaline and one molecule of fumaric acid (Figure 2a). One carbonyl group of fumaric acid is positioned anti- and the other synperiplanar to the double bond. Fumaric acid is almost planar and is coplanar to quinoxaline. Due to the OH···N hydrogen bridges, chains are formed that are different from the previous case. The quinoxaline molecules in the chain are identically oriented (Figure 2b) in contrast to the former cocrystal (Figure 1). An additional weak hydrogen bond is established between O2 and the hydrogen atom at C2, the geometrical conditions allowing planarity of the two molecules. Remember, that the nonplanar arrangement of oxalic acid and quinoxaline in the former case was due to the formation of a hydrogen bridge between the hydrogen atom at C8 (*peri* hydrogen) and O=C of the acid. This is avoided here allowing the complete planarity of the array. Again, C−H···O interactions couple the chains. As in the case of oxalic acid, it is possible to identify dimeric chains in which the nitrogen atoms of quinoxaline point to the inside (the two chains in the middle of Figure 2b). Each pair of quinoxaline and fumaric acid in this dimeric arangement is held together by four CH···O hydrogen bonds. The interaction to the next chain, above or below in the figure, is characterized by only two CH···O interactions per dimer of quinoxaline and fumaric acid. In the case of the longer

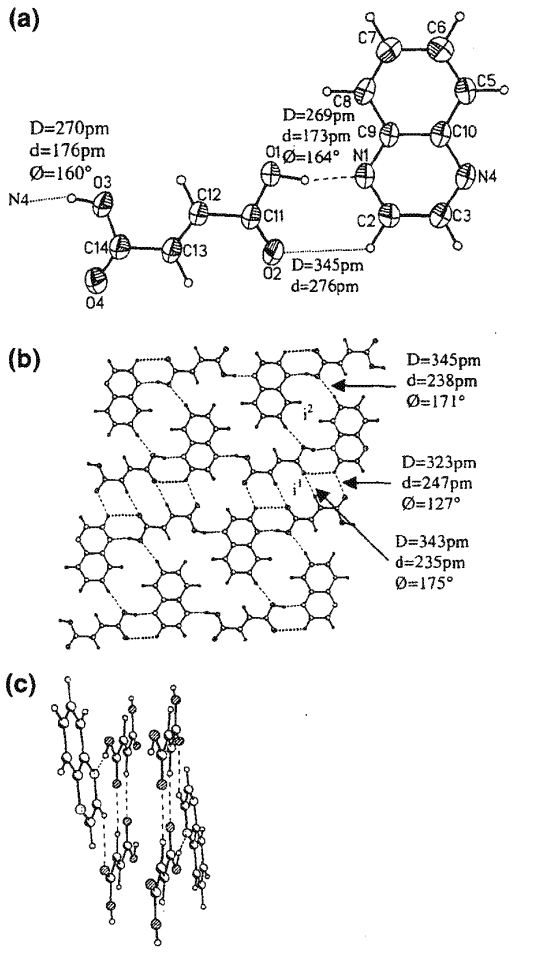


Figure 2. Cocrystal of 1,4-diazanaphthalene (quinoxaline) and fumaric acid, (a) thermal ellipsoid plot (50%) of the molecules in the asymmetric unit with numbering scheme; (b) molecular packing viewing onto the molecular planes. (c) molecular packing viewing along the OH···N connected chains.

fumaric acid molecules, the benzene part of a quinoxaline molecule in a second chain fits perfectly between a unit of fumaric acid and two molecules of quinoxaline in the chain, producing a planar sheet. The arrangement of the planar chains is displayed in a view almost along the chains (Figure 2c). Two different C−H···O interactions, arranged around an inversion center i^1 couple the chains in one direction and one C−H···O interaction exists at the other inversion center i^2 at (benzene part of quinoxaline).

Clearly, the CC double bond spacer of fumaric acid leads to separations of quinoxaline molecules in a single chain which produces an optimal space for the positioning of a quinoxaline molecule of another dimeric chain in between. This pattern also provides an explanation of the different asymmetric unit in the cocrystal of quinoxaline and oxalic acid. There nonplanar chains of alternating molecules of the components are formed. The nonplanar arrangement allows optimal CH···O interactions between different chains which would not have been possible if the carbonyl groups were arranged as in the case of fumaric acid to form hydrogen bridges

UM00011733
NOVARTIS EXHIBIT 1517
Novartis v. Regents, IPR2023-01347
Page 479 of 4460

to the hydrogen atom at C2. The nonplanar arrangement leads to chains with smaller lateral extension allowing better interchain CH···O bridges. A planar situation as in the case of fumaric acid would generate a less tight packing with a reduced number of CH···O hydrogen bridges. Thus, the difference in crystal packing results from the fact to build as many CH···O hydrogen bridges as possible. In the case of the cocrystal of quinoxaline and fumaric acid, planar sheets of molecules are superimposed and form a three-dimensional crystal lattice. The quinoxaline molecules of different layers are shifted offset face to face, probably generating additional stabilizing interactions between the sheets in view of the small separation of the different planes. There are no evident additional interactions between aromatic rings in different planes.

Naphthyridine and Oxalic Acid. The two nitrogen atoms of naphthyridine are in 1- and 5-positions of the naphthalene skeleton, i.e., each six-membered ring of the bicycle is of pyridine type. The relative position of the nitrogen atoms leads to a hydrogen bonding motif which resembles the chains in the cocrystal of quinoxaline and fumaric acid and not the chains in the cocrystal with oxalic acid, with the essential difference that the position of the OH···N bond connecting naphthyridine and fumaric acid alternates between the 1- and the 5-position and not between the 1- and the 4-position in quinoxaline. This disposition provides free space between two naphthyridine molecules in a chain to place a second chain so that oxalic acid can establish the maximum number of C−H···O bridges to the neighboring naphthyridine molecule. Figure 3a represents the symmetry completed molecules, both being planar due to their respective centrosymmetry, both are almost coplanar to each other. The chains with the strong OH···N hydrogen bridges are interconnected by CH···O interactions in which all oxygen atoms of oxalic acid are involved shown in Figure 3b. The layers of the molecules, which are separated by 312 pm are shifted with respect to each other, so the carbonyl oxygens are situated almost above the C-atoms of the oxalic acid molecules, the equivalent atoms have distances according to the *a*-axis (371 pm) of the unit cell (Figure 3c).

Phthalazine and Oxalic Acid. A 1:1 cocrystal was isolated from an acetone solution and characterized by X-ray analysis (Table 1). The asymmetric unit (space group of the monoclinic crystal $P2_1/c$) consists of one molecule of each component (Figure 4a). The major difference of this cocrystal to those of the previous diazanaphthalene molecules is a complete proton transfer from one carboxy group of oxalic acid to one of the nitrogen atoms of phthalazine. No significant electron density is found in the surrounding of O2. The hydrogen atom located at N2 could be clearly located and refined without constraints at a distance of 93 pm. Such a proton transfer is also observed in a 2:1 and a 2:3 cocrystal of phthalazine with phthalic acid and indicates a higher basicity of the nitrogen atoms of phthalazine as compared to those of the other heterocycles.[17] It leads to salt formation, thus additional electrostatic interactions are generated. The N^+−H···O^- hydrogen bridge is characterized by a relatively short O2···N2 distance. A further but weaker and bifurcated interaction can be identified between H2 and O4. Oxalic acid is planar as

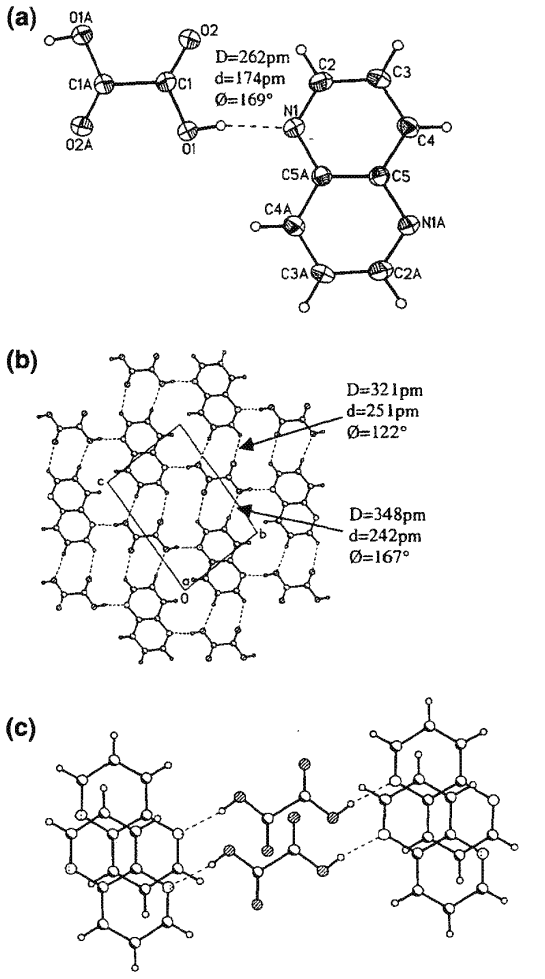


Figure 3. Cocrystal of 1,5-diazanaphthalene (naphthyridine) and oxalic acid, (a) thermal ellipsoid plot (50%) of the molecules in the asymmetric unit with numbering scheme, (b) molecular packing viewing down [100], (c) molecular packing viewing perpendicular to the molecular plane, showing the stacking of the molecules.

well as the heterocycle (max devation from mean plane 3.0 pm), but the two molecules of the asymmetric unit are not arranged in the same plane. The dihedral angle between the CC bond connecting the two carboxy groups of oxalic acid and the C1−N2 bond of phthalazine (C12−C11···N2−C1) is −36.8°. Intermolecular interactions can further be identified between C1−H1 and the oxygen atom O1 of oxalic acid as well as between a hydrogen atom (H8) in the benzene part of the heterocycle and a carboxy oxygen (O3) (Figure 4b). The geometric parameters, however, are such that only a weak stabilization should result.

An analysis of the packing (Figure 4b) reveals that the oxalic acid molecules form linear chains (catamer motif) which are held together by strong O−H···O hydrogen bridges. It is interesting to note that this hydrogen bond is established between a protonated and deprotonated carboxy group. The carboxylate group displays two almost identical C−O bond distances of 124 and 126 pm, respectively, in the carboxy group they are

UM00011734
NOVARTIS EXHIBIT 1517
Novartis v. Regents, IPR2023-01347
Page 480 of 4460

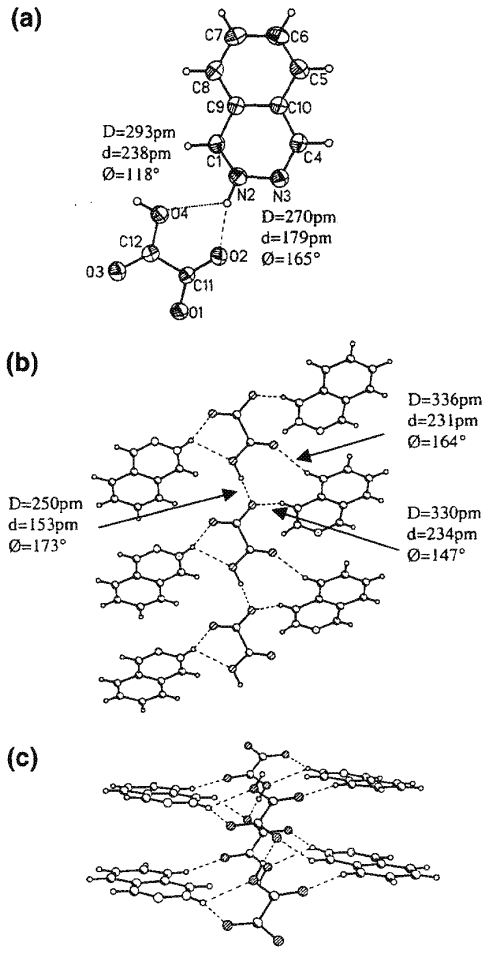


Figure 4. Cocrystal of 2,3-diazanaphthalene (phthalazine) and oxalic acid, (a) thermal ellipsoid plot (50%) of the molecules in the asymmetric unit with numbering scheme, (b) molecular packing viewing down [001], (c) molecular packing viewing along the molecular plane, showing the tilt and offset face-to-face arrangement of the molecules.

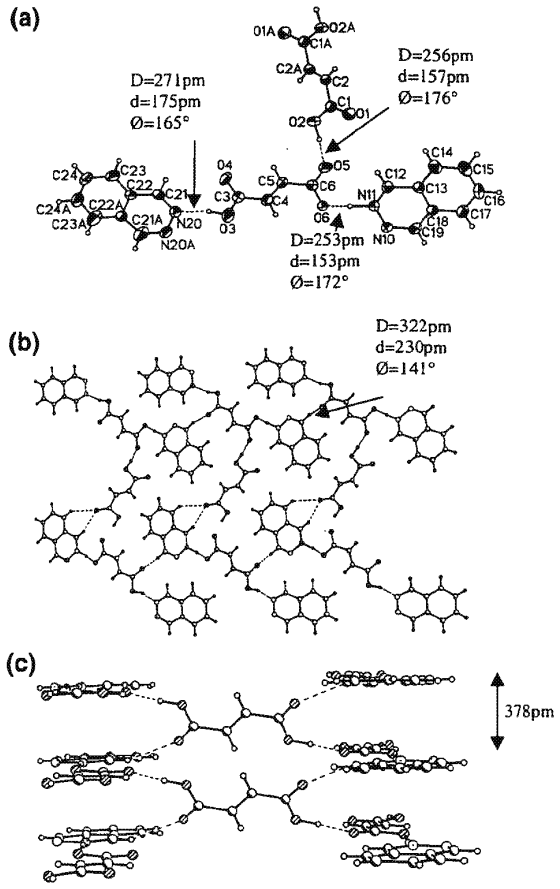


Figure 5. Cocrystal of 2,3-diazanaphthalene (phthalazine) and fumaric acid, (a) thermal ellipsoid plot of the molecules in the asymmetric unit completed by crystallographic mirror symmetry for one 2,3-diazanaphthalene and centrosymmetry for fumaric acid, with numbering scheme, (b) molecular packing viewing down [100], (c) molecular packing viewing along the chains, linked by OH···N bridges and networked by CH···O bridges.

120 for C=O and 130 pm for the C−O bond. The latter situation is very similar in the crystal structure of pure oxalic acid (C=O 121 pm, C−O 131 pm).[19−22] whereas the egalization of the CO bonds in the former case is typical for carboxylate groups.

The arrangement of the phthalazine molecules along the chain of oxalic acid shows that at one side the molecules are bonded by the NH···O hydrogen bridges and at the other side by CH···O interactions. The phthalazine molecules on each side form stacks with centroid−centroid distances of 561 pm, corresponding to the *a*-axis of the unit cell, and indicating the offset face to face arrangement which contributes to favorable interactions between the π systems of the heterocyclic ring systems (Figure 4c). The interactions take place between the heterocyclic and the benzene part of phthalazine molecules. In one stack, bonded by CH···O, phthalazine is positioned to the oxalic acid parallel to the long axis, wheres in the other one, due to the NH···O bridge this is parallel to the short axis. Although phthalazine is a diazanaphthalene, an important distinction to the above-discussed cases is that the two nitrogen atoms of phthalazine are too close to be both hydrogen bonded to an acid molecule. This leads to the completely different pattern of the crystal packing.

Phthalazine and Fumaric Acid. An acetone solution in the ratio 1:1 of the components led to the formation of 1:1 cocrystals which were analyzed by X-ray crystallography (Table 1). The asymmetric unit consists of one and a half molecule of each component (monoclinic space group $P2_1/m$). One phthalazine molecule (N20, C21−C24) is intercepted by the crystallographic mirror plane and one fumaric acid (O1, O2, C1, C2) has crystallographically centrosymmetry, thus both are completed by the respective symmetry operations (Figure 5a). Three crystallograpic independent strong hydrogen bonds can be identified, one between a protonated nitrogen atom of phthalazine and a deprotonated oxygen atom of fumaric acid, the second one between the same fumaric acid OH group and the C_s symmetric phthalazine and the third between the OH

UM00011735
NOVARTIS EXHIBIT 1517
Novartis v. Regents, IPR2023-01347
Page 481 of 4460

group of the C_i symmetric fumaric acid molecule and an oxygen atom of the deprotonated carboxy group of the acid molecule. Thus, the two molecules of each kind are diffferent in the unit cell. the phthalazine molecules are protonated and one of the fumaric acid molecules is deprotonated.

The deprotonated acid is almost planar, and is coplanar with the protonated, again planar heterocycle (max deviation from mean plane 2.3 pm) and on the other side it is almost coplanar with the C_s symmetric heterocycle. These 1:2 complexes (one acid and two bases) are linked among each other via weak C−H···O hydrogen bonds, with all these molecules lying almost in one plane. These units are further connected by the centrosymmetric acid molecules via the strong O−H···O and weaker C−H···O bridges (Figure 5b), forming an interplanar angle of 50° with the planar units. The planar units form stacks along the *a*-axis corresponding to a separation of 378 pm (Figure 5c).

Conclusion

OH···N and CH···O hydrogen bonds determine the crystal packing in the 1:1 cocrystals of quinoxaline with oxalic acid and fumaric acid. The double bond in fumaric acid as spacer between two carboxy groups leads to a planar arrangement of quinoxaline and fumaric acid molecules. In contrast, the cocrystal of quinoxaline and oxalic acid is characterized by a nonlinear placement of the constituents. The position of the nitrogen atoms in naphthyridine as component of the cocrystal with oxalic acid permits a planar sheetlike structure as in the case of the cocrystal of quinoxaline and fumaric acid. The structures of the cocrystals of phthalazine with oxalic- and fumaric acid exhibit a proton transfer from one carboxy group to a nitrogen atom and a OH···O hydrogen bond between two acid molecules leading to a backbone to which the nitrogen heterocycles are attached. The discussion has shown that the position of the two nitrogen atoms in these diazanaphthalenes influence strongly the crystal packing.

Experimental Section

The compounds were either commercially available or, as in the case of naphthyridine (**5**), were synthesized according to a literature procedure.[23] Cocrystals were obtained by dissolving the components in a 1:1 ratio in the reported solvent, if not otherwise indicated, and letting the solvent slowly evaporate at ambient temperature. Cocrystal quinoxaline/oxalic acid: acetone, mp: 175 °C. Cocrystal quinoxaline/fumaric acid: acetone, mp: 230 °C. naphthyridine/oxalic acid: acetone, mp: 155 °C. Cocrystal phthalazine/oxalic acid: acetone, mp: 155 °C. Cocrystal phthalazine/fumaric acid: acetone, mp: 160 °C. The 1:1 composition of the cocrystal was also checked by solution ^{1}H NMR spectra.

Crystallographic data (excluding structure factors) for the structures reported in this paper have been deposited with the Cambridge Crystallographic Data Centre as supplementary publication no. CCDC-190623 for **1·3**, 190624 for **2·3**, 190625 for **1·4**, 190626 for **1·5**, and 190627 for **2·5**. Copies of the data can be obtained free of charge on application to CCDC, 12 Union Road, Cambridge CB2 1EZ, UK [Fax: int. code + 44-(1223)336-033; e-mail: deposit@ccdc.cam.ac.uk].

Acknowledgment. This work has been supported by the Deutsche Forschungsgemeinschaaft and Sonderforschungs-bereich SFB 452.

References

(1) Desiraju, G. R. *Crystal Engineering. The Design of Organic Solids*; Elsevier: Amsterdam, 1989.
(2) Desiraju, G. R. *Comprehensive Supramolecular Chemistry*; Vol. 6; MacNicol, D. D., Toda, F., Bishop, R., Eds.; Pergamon: Oxford, Chapter 1, pp 1−22, 1996.
(3) Desiraju, G. R. *Angew. Chem.* **1995**, *107*, 2541−2558.
(4) Calhorda, M. J. *Chem. Commun.* **2000**, 801−809.
(5) Braga, D.; Grepioni, F. *New J. Chem.* **1998**, 1159−1161.
(6) Nishio, M. *The CH/π Interaction*, 1st ed.; Wiley-VCH: New York, 1998.
(7) Jeffrey, G. A.; Saenger, W. *Hydrogen Bonding in Biological Structures*, 2nd ed.; Springer: Berlin, 1994.
(8) Desiraju, G. R.; Steiner, T. *The Weak Hydrogen Bond in Structural Chemistry and Biology*; Oxford University Press: Oxford, 1999.
(9) Batchelor, E.; Klinowski, J.; Jones, W. *J. Mater. Chem.* **2000**, *10*, 839−848.
(10) Senthil, V. S.; Nangia, A.; Katz, A. K.; Carrell, H. L. *Cryst. Growth Des.* **2002**, *2*, 313−318.
(11) Vishweshwar, P.; Nangia, A.; Lynch, V. M. *J. Org. Chem.* **2002**, *67*, 556−565.
(12) Reyes-Arellano, A.; Boese, R.; Steller, I.; Sustmann, R. *Struct. Chem.* **1995**, *6*, 391−396.
(13) Smolka, T.; Schaller, T.; Sustmann, R.; Bläser, D.; Boese, R. *J. Prakt. Chem.* **2000**, *342*, 465−471.
(14) Felderhoff, M.; Steller, I.; Reyes-Arellano, A.; Boese, R.; Sustmann, R. *Adv. Mater.* **1996**, *8*, 402−405.
(15) Felderhoff, M.; Smolka, T.; Sustmann, R.; Steller, I.; Weiss, H.-C.; Boese, R. *J. Prakt. Chem.* **1999**, *341*, 639−648.
(16) Smolka, T.; Sustmann, R.; Boese, R. *J. Prakt. Chem.* **1999**, *341*, 378−383.
(17) Rogers, R. D.; Sharma, C. V. K.; Whitcomb, D. R. *Cryst. Eng.* **1998**, *1*, 255−262.
(18) Olenik, B.; Boese, R.; Sustmann, R. *Cryst. Growth Eng.* **2003**, *2*, 175−182.
(19) Derissen, J. L.; Smit, P. H. *Acta Crystallogr.* **1974**, *B30*, 2240−2242.
(20) Delaplane, R. G.; Ibers, J. A. *Acta Crystallogr.* **1969**, *B25*, 2413−2437.
(21) Sabine, T. M.; Cox, G. W.; Craven, B. M. *Acta Crystallogr.* **1969**, *B25*, 2437−2441.
(22) Coppens, P.; Sabine, T. M. *Acta Crystallogr.* **1969**, *B25*, 2451−2460.
(23) Rapoport, H.; Batcho, A. D. *J. Org. Chem.* **1963**, *28*, 1753−1759.
(24) For all discussions, C−H and O−H distances have been normalized to their distances from neutron diffraction with 108 and 98.3 pm, respectively.

CG034003+

UM00011736
NOVARTIS EXHIBIT 1517
Novartis v. Regents, IPR2023-01347
Page 482 of 4460

Crystallography Reviews, 2004, Vol. 10, No. 1, pp. 57–66

Taylor & Francis
Taylor & Francis Group

RATIONALISATION OF CO-CRYSTAL FORMATION THROUGH KNOWLEDGE-MINING

IAIN D.H. OSWALD[a,*], W.D. SAMUEL MOTHERWELL[b], SIMON PARSONS[a], ELNA PIDCOCK[b] and COLIN R. PULHAM[a]

[a]*Department of Chemistry, School of Chemistry, The University of Edinburgh, King's Buildings, West Mains Road, Edinburgh, EH9 3JJ, UK;* [b]*Cambridge Crystallographic Data Centre, 12 Union Road, Cambridge CB2 1EZ, UK*

The crystal structures of five hemiadducts of paracetamol and a related 1 : 1 adduct of paracetamol are described. All structures are characterised by the formation of chains of paracetamol molecules, linked either via OH···O=C interactions [C(9) chains in graph set notation] or NH···O=C interactions [C(4) chains], depending on the presence or absence of substituent groups on the guest molecule. Throughout the series the structural rearrangement due to each guest molecule can be followed by comparison of H-bond strengths with those in the Cambridge Structural Database. In addition, the role of both molecular and space group symmetry in crystal formation can now be investigated with the help of a new relational database from the CCDC, CSD symmetry.

Keywords: Rationalisation; Co-crystal formation; Knowledge-mining

Contents

1. INTRODUCTION 57
2. CO-CRYSTALS CONTAINING PARACETAMOL 58
3. SYMMETRY AND CO-CRYSTAL FORMATION 64
4. CONCLUDING REMARKS 66
References 66

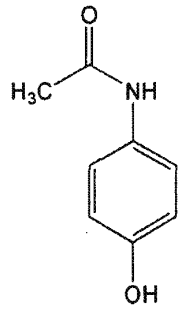
1. INTRODUCTION

The design of co-crystals or molecular adducts to promote specific properties in a material is an important application of crystal engineering. Traditional approaches to the optimisation of properties such as solubility, colour, hardness etc. have focussed

*Corresponding author. Tel.: 0131 650 4806. E-mail: I.D.H.Oswald@ed.ac.uk

ISSN 0889-311X print: ISSN 1476-3508 online © 2004 Taylor & Francis Ltd
DOI: 10.1080/08893110410001664855

UM00011737
NOVARTIS EXHIBIT 1517
Novartis v. Regents, IPR2023-01347
Page 483 of 4460



SCHEME 1 Molecular structure of paracetamol.

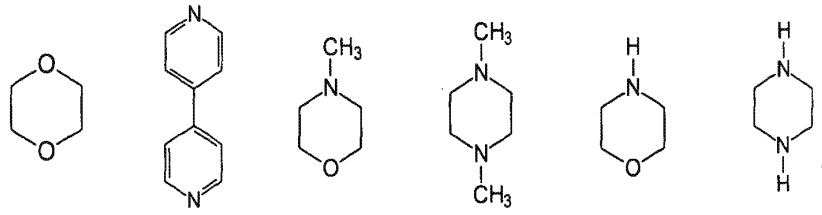
on the synthesis of covalent derivatives containing functional groups that enhance or inhibit a particular property. Synthetic routes frequently employ solvents or toxic reagents, and often yield by-products. The alternative means of controlling material properties by co-crystal formation has therefore received a great deal of interest in the context of 'green' chemical applications, where it has become regarded as 'non-covalent derivatisation' (Anastas and Warner, 2002). Pharmaceutical compounds are ideal candidates for co-crystallisation studies because they contain functional groups of the type that are involved in molecular recognition of biomolecules (Bailey Walsh *et al.*, 2003). Such studies also hold great potential as a means to control important pharmaceutical properties such as bioavailability and processing characteristics.

We recently reported a systematic study of the co-crystallisation of the analgesic drug paracetamol (acetaminophen, *p*-hydroxylacetanilide or Tylenol, see Scheme 1) with a series of H-bond acceptors (Oswald *et al.*, 2002). Hydrogen bonding patterns in crystals were studied extensively by Etter (1990) and co-workers, who recognised that (1) all good proton donors and acceptors tend to be used in hydrogen bonding interactions, and (2) that the strongest donors tend to pair with the strongest acceptors. On the assumption that the length of a hydrogen bond can be taken as a reflection of its strength, the average lengths of hydrogen bonds drawn from the Cambridge Structural Database (CSD, Allen, 2002) can be used to rationalise hydrogen bond formation in crystal structures. Here we describe the application of this approach to adducts of paracetamol. We also briefly explore the role that the interaction between molecular and space group symmetry might have to play in co-crystal formation.

2. CO-CRYSTALS CONTAINING PARACETAMOL

In this article we use data on typical hydrogen bond geometry extracted from the CSD to help rationalise the intermolecular interactions observed in adducts of paracetamol with 1,4-dioxane, 4,4′-bipyridine, *N*-methylmorpholine, *N*,*N*-dimethylpiperazine, morpholine and piperazine (Scheme 2). Hydrogen bonding dominates the intermolecular interactions in all the adducts. The hydrogen bond donor groups which appear in this series are amidic NH, phenol OH and secondary amine NH; the acceptors are amidic O, phenolic O, secondary or tertiary amine N, ether O and pyridine N. The results of CONQUEST (Bruno *et al.*, 2002) searches of the CSD for typical H-bond

UM00011738
NOVARTIS EXHIBIT 1517
Novartis v. Regents, IPR2023-01347
Page 484 of 4460



SCHEME 2 Guest molecules used to form adducts with paracetamol. From left to right the structures show dioxane, bipyridine, *N*-methylmorpholine, *N,N*-dimethylpiperazine, morpholine and piperazine.

geometries involving these functionalities are listed in Table I, searching criteria are given in the legend to that table.

Crystal structures of the monoclinic and orthorhombic polymorphs of paracetamol have been reported several times, and we have used the structures reported by Nichols and Frampton (1998) [CSD reference codes HXACAN07 and HXACAN08]. In paracetamol the donor set is comprised by an amidic NH and a phenolic OH; the acceptor functions are an amide carbonyl and a phenolic oxygen. Reference to Table I shows that the strongest interaction that can be formed in this set is between the phenolic OH donor and the amide carbonyl acceptor. Striking out the row and column in the table containing this entry leaves the NH (donor) to OH (acceptor). The stronger of these two interactions leads to the formation of C(9) chains (Bernstein *et al.*, 1995). The weaker (NH donor to OH acceptor) connects the chains via a C(7) motif.[1] Packing in both polymorphs is dominated by the formation of NH···OH and OH···O=C hydrogen bonds (Fig. 1) giving rise to layered two-dimensional networks.

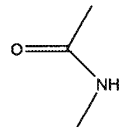
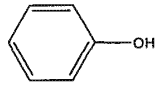
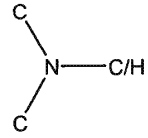
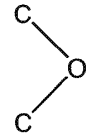
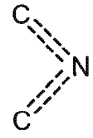
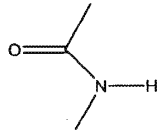
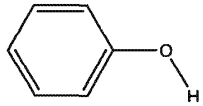
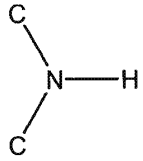
The asymmetric unit of the dioxane adduct of paracetamol consists of two paracetamol molecules and two half molecules of dioxane on crystallographic inversion centres. In addition to the functionality described above for paracetamol the dioxane adduct contains an ether acceptor moiety. Nevertheless the strongest H-bond available in the system is still the OH···O=C interaction observed in paracetamol itself, and as in paracetamol this leads to C(9) chain formation. This leaves the amide NH to form a hydrogen bond with the dioxane, an interaction which replaces the weaker NH···OH interactions observed in the paracetamol structure. The strengths of the competing NH···O(phenol) and NH···O(ether) interactions are comparable, but the adduct was formed from a solution of paracetamol in dioxane. The excess solvent that was used to form the adduct may favour the formation of amide–ether H-bonds rather than the amide–phenol H-bonds. Overall the structure consists of two-dimensional sheets in which chains of paracetamol are linked by dioxane bridges (Fig. 2).

The crystal structure of paracetamol : bipyridine contains two independent molecules each of paracetamol and bipyridine. As in the dioxane adduct the paracetamol molecules retain the strong C(9) chains through OH···O=C hydrogen bonds (Fig. 3). The weaker NH···OH interaction in paracetamol is replaced by a stronger NH···N interaction in this adduct (Table I). Since this crystal is a 1 : 1 adduct there are insuffi-

[1]Note that where no-sub- and superscripts appear in the graph set descriptor, one donor and one acceptor are implied.

UM00011739
NOVARTIS EXHIBIT 1517
Novartis v. Regents, IPR2023-01347
Page 485 of 4460

TABLE I Summary of the results of searches of the CSD (version 5.23, April 2002) for typical distances in hydrogen bonded systems containing identical functional groups to the paracetamol adducts studied. The distances to hydrogen atoms were normalised to typical neutron distances (C–H 1.083, N–H 1.009 and O–H 0.983 Å). Only 'organic' structures where the *R*-factor is less than 0.05, with no errors or disorder were included, and ionic or polymeric structures were excluded. The C-atoms attached to the amine moieties were specified to be sp^3 hybridised. The donor-H to acceptor distance was specified to be 1.50–2.20 Å

Donor (NH or OH)		*Acceptor (O or N in each case)*				
						
	Sample size	1250	14	11	31	40
	Max NH···A/Å	(2.2)	2.14	2.17	2.19	2.19
	Min NH···A/Å	1.73	1.79	1.80	1.83	1.81
	Mean NH···A/Å	**1.92**	**2.01**	**1.96**	**2.03**	**1.96**
	Sample size	49	256	49	53	76
	Max OH···A/Å	2.19	2.20	2.19	2.20	2.18
	Min OH···A/Å	1.60	1.67	1.66	1.62	1.53
	Mean OH···A/Å	**1.78**	**1.87**	**1.82**	**1.90**	**1.81**
	Sample size	5	1 (HOLZOD)	12	4	Not applicable
	Max NH···A/Å	2.17	–	2.20	2.18	
	Min NH···A/Å	2.08	–	2.00	2.11	
	Mean NH···A/Å	**2.13**	**2.03**	**2.14**	**2.13**	

UM00011740

NOVARTIS EXHIBIT 1517
Novartis v. Regents, IPR2023-01347
Page 486 of 4460

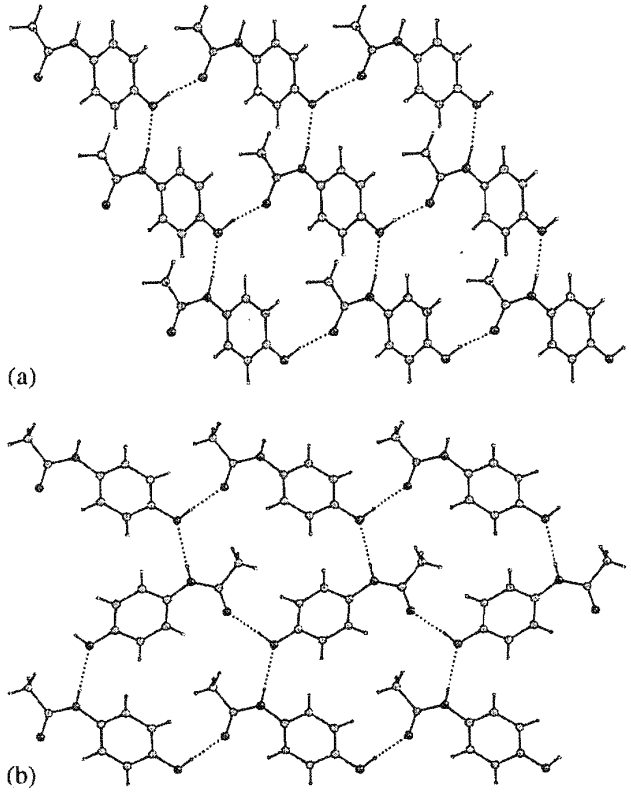


FIGURE 1 Top: (a) Monoclinic paracetamol (Form I) viewed along the *b*-axis; the *c*-axis runs diagonally from top left to bottom right, so that the C(9) chains are established by the *n*-glide. Bottom: (b) orthorhombic paracetamol (Form II) viewed along the *c*-axis; the *a*-axis runs horizontally, the *b*-axis runs from top to bottom. The C(9) chains referred to in the text run from left to right, and the C(7) chains run approximately vertically. Figures were produced using CAMERON (Watkin *et al.*, 1993).

cient H-bond donors for the number of acceptors present, and only one of the two N-atoms in each bipyridine acts as an acceptor. The structure consists of a paracetamol backbone with attached bipyridine molecules. These motifs are interconnected by π-stacking between the bipyridine molecules, again building-up a layered structure.

Straightforward application of the results presented in Table I enables the hydrogen bonds formed in paracetamol and its adducts with dioxane and bipyridine to be rationalised. The phenolic OH $\cdots$ O=C(amide) interaction is the strongest listed in Table I, and a similar approach to the one described above would predict, incorrectly, that all the adducts in our series would be based on C(9) chains of paracetamol linked by hydrogen bonds in which amidic NH acts as a donor to the N or O acceptor functions of the guest molecules. While neither dioxane nor bipyridine has any group attached to the donor oxygen or nitrogen atoms, all of the other molecules studied carry either hydrogen or methyl groups in these positions, and reference to Figs. 2

UM00011741
NOVARTIS EXHIBIT 1517
Novartis v. Regents, IPR2023-01347
Page 487 of 4460

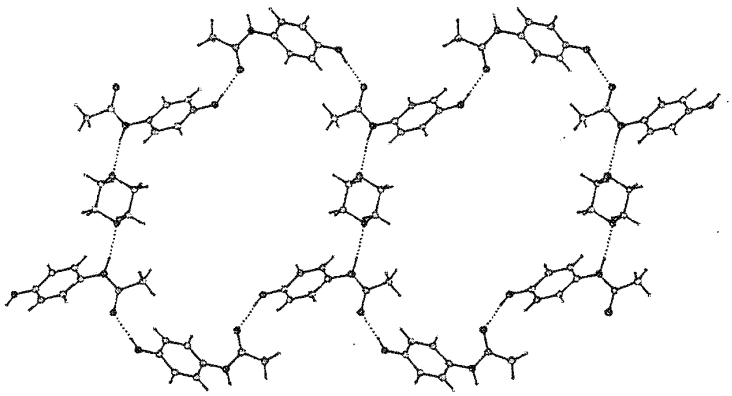


FIGURE 2 Paracetamol:1,4-dioxane adduct viewed perpendicular to (2 1 0), the *c*-axis runs horizontally. The C(9) chains referred to in the text run from left to right and are linked together by dioxane molecules.

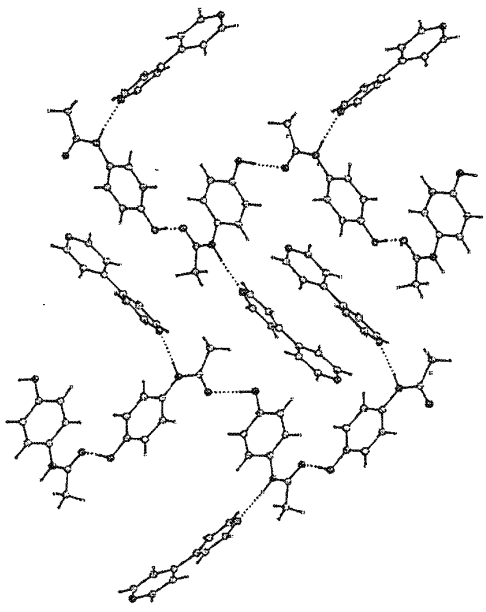


FIGURE 3 Paracetamol:4,4-bipyridine viewed perpendicular to (1 0 -1), the *b*-axis runs from top to bottom. The C(9) chains referred to in the text run from left to right and are linked together by a pair of π-stacked bipyridine molecules.

or 3 show that a structure based on C(9) paracetamol chains would suffer some steric crowding between these groups and either the phenyl or methyl group attached to the amide moiety.

In the presence of a secondary amine acceptor the strongest interaction that can be formed, if the phenolic OH···O=C(amide) interaction is excluded, is phenolic OH···N(amine). This leaves the phenolic OH and the amide carbonyl to act as

UM00011742
NOVARTIS EXHIBIT 1517
Novartis v. Regents, IPR2023-01347
Page 488 of 4460

acceptors for the amidic NH. Of these the NH···O=C H-bond is stronger, and in the *N,N*-dimethylpiperazine adduct C(4) chains are formed through NH···O=C bonds between paracetamol molecules. These chains are linked together by phenolic OH···N(amine) hydrogen bonds (Fig. 4) with the *N,N*-dimethylpiperazine molecules, which reside on inversion centres. The *N*-methylmorpholine adduct is isostructural with the *N,N*-dimethylpiperazine adduct, with the guest molecule disordered about an inversion centre.

The pattern of H-bonding in the *N,N'*-dimethylpiperazine adduct leaves an acceptor function (the phenolic O-atom) unsatisfied. Piperazine is related to *N,N*-dimethylpiperazine by replacement of the two methyl groups by hydrogen. In the piperazine the C(4) chains, consisting of NH···O=C H-bonds linked by OH···N bonds to the amine which characterised the structure of the *N,N'*-dimethylpiperazine, are again observed. The addition of an extra donor function in the form of the amide NH enables the acceptor capacity of the phenolic oxygen to be satisfied, leading to the formation of a ribbon-like structure (Fig. 5).

Morpholine is related to *N*-methylmorpholine by the replacement of the methyl group by hydrogen, and it is unique in this series because the H-bonding characteristics of the two hetero-centres are not the same: the NH group is a donor and acceptor, the ether O-atom potentially a double, but more usually a single, acceptor. The asymmetric unit of the morpholine hemi-adduct consists of two crystallographically independent paracetamol molecules (labelled A and B in Fig. 6) and one molecule of morpholine. The crystallographically independent paracetamol molecules alternate in the pattern ···ABABAB··· along a C(4) chain formed by NH···O=C hydrogen bonds between

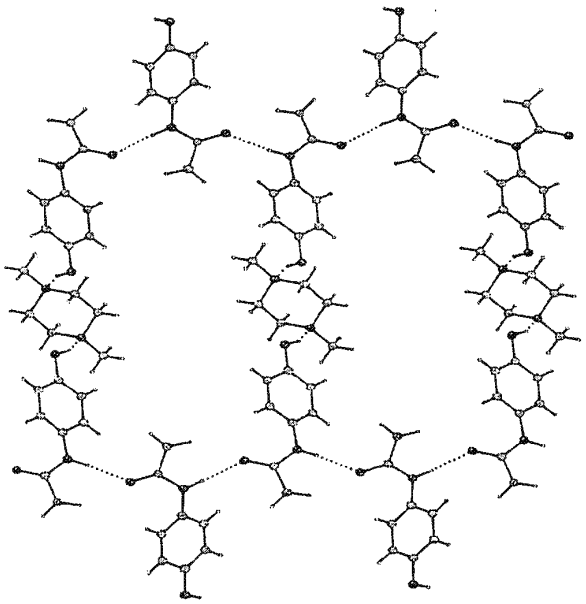


FIGURE 4 Paracetamol: *N,N*-dimethylpiperazine adduct (isostructural to *N*-methylmorpholine adduct) viewed along the *a*-axis, the *c*-axis runs from left to right and the *b*-axis from top to bottom. The C(4) chains referred to in the text run from left to right and are linked together by *N,N*-dimethylpiperazine molecules.

UM00011743
NOVARTIS EXHIBIT 1517
Novartis v. Regents, IPR2023-01347
Page 489 of 4460

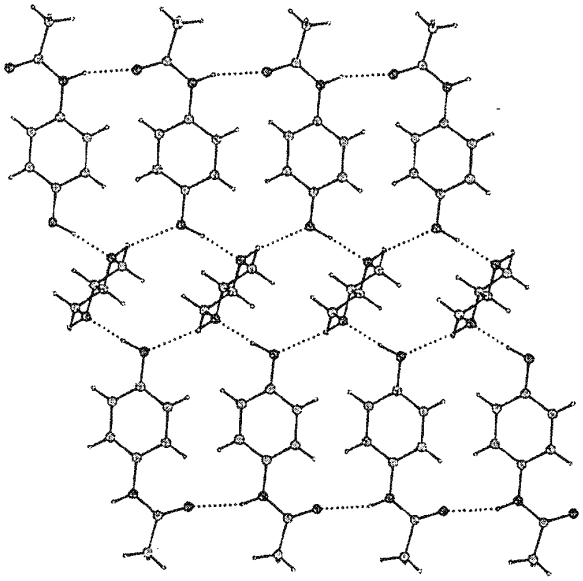


FIGURE 5 Paracetamol : piperazine adduct viewed perpendicular to (3 0 2), the *b*-axis runs from left to right. The C(4) chains referred to in the text run from left to right and are linked together by piperazine molecules. The latter also act as weak hydrogen bond donors. The dihedral angles between the amide and phenyl mean planes in the paracetamol molecule is 33.21(14)°.

amide linkages. Of the remaining amine NH and phenolic OH moieties the latter is a better hydrogen donor. The best acceptors for this group are phenolic O and amine N, and each of the two crystallographically unique paracetamol molecules hydrogen bonds to one of these. This scheme satisfies all the H-bonding potential of the two paracetamol molecules, with the exception of the hydroxyl acceptor of molecule A. The weakest acceptor in the system (the ether function of the morpholine) does not participate in H-bonding at all. A rather surprising feature of this structure given the excess of acceptors present, is that the NH donor functionality of the morpholine amine moiety is also unsatisfied. However, this is consistent with Table I, which shows that secondary aliphatic amines are particularly poor hydrogen bond donors.

3. SYMMETRY AND CO-CRYSTAL FORMATION

With the exception of morpholine, all the guest molecules studied are at least pseudo-centrosymmetric with respect to their H-bonding properties, and in the dioxane, *N*-methylmorpholine, *N*,*N*-dimethylpiperazine and piperazine adducts the guest molecule occupied a crystallographic inversion centre. Centrosymmetric molecules often occupy inversion centres in crystal structures, but we have been able to quantify this observation in the case of dioxane using the new CSD symmetry database.

CSDSymmetry is a new relational database that has been developed at the Cambridge Crystallographic Data Centre using Microsoft *Access* software (Yao *et al.*, 2002). The database holds information on *ca.* 200 000 entries from the CSD (April 2000,

UM00011744
NOVARTIS EXHIBIT 1517
Novartis v. Regents, IPR2023-01347
Page 490 of 4460

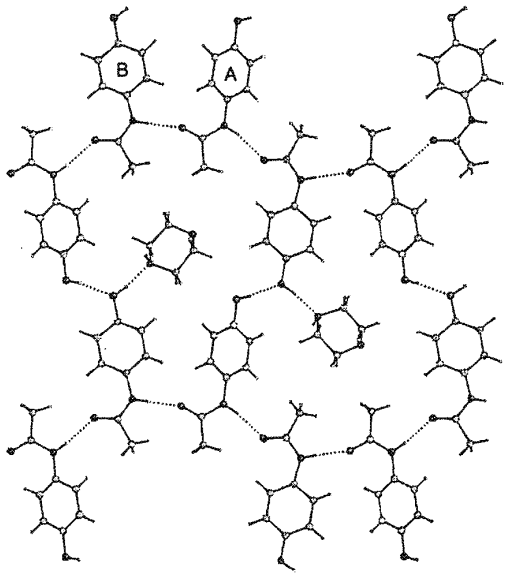


FIGURE 6 Paracetamol: morpholine adduct viewed along the *a*-axis. The *c*-direction runs from left to right, the *b* direction up and down. The labels A and B refer to the crystallographically independent paracetamol molecules referred to in the text. The C(4) chains referred to in the text run from left to right and are linked together by hydrogen bonds between opposed OH groups. This forms a grid-like array with the morpholine molecules residing in the grid cavities.

version 5.19). Information pertaining to single residues such as number of atoms and point groups is deposited in the database along with crystallographic properties such as occupied Wyckoff positions and space group information. These properties can be combined in a search of the database to give statistical information on symmetry and the role that it plays in crystal formation.

A search of the CSD (version 5.24) for dioxane was performed with the only restriction being that the structure must have 3D co-ordinates available. Similar searches for the other guest molecules studied here were also carried out, but it was only possible to obtain a statistically meaningful sample for dioxane adducts. The search yielded 350 structures that contained dioxane as one of the residues, and these structures were imported into the CSDsymmetry database. CSDsymmetry was built using version 5.19 of the CSD and structures added to the CSD after the release of that version will not have their symmetry characteristics coded; these structures were therefore removed from the data set.

Each residue in a crystal structure has a separate entry in CSDsymmetry. The entries corresponding to dioxane molecules were identified by searching for entries with 6 or 14 atoms (depending on whether the hydrogen atoms were present). Those remaining entries not corresponding to dioxane were removed by hand. The data set, which contained 226 separate entries, was analysed according to the symmetry of the Wyckoff positions occupied. The results were 1 : 100, -1 : 110, 2 : 6, m : 4 and $2/m$: 6.

All the crystal structures obtained for paracetamol adducts belonged to centrosymmetric space groups. Kitaigorodskii (1961) recognised that the presence of an inversion

UM00011745
NOVARTIS EXHIBIT 1517
Novartis v. Regents, IPR2023-01347
Page 491 of 4460

centre in a crystal structure makes for efficient molecular packing, and this may promote formation of adducts with centrosymmetric guest molecules. It is, perhaps, noteworthy in this regard that we have been unable to prepare a co-crystal of paracetamol with trioxane, which contains the same ether functionality as dioxane, but lacks its inversion symmetry.

4. CONCLUDING REMARKS

In this review, we have shown that given a set of cocrystals we can rationalise their formation by way of knowledge mining the Cambridge Structural Database. Information gained from this investigation can allow us to rank different hydrogen bonds in order of importance and with a little chemical intuition we can explain the formation of a particular cocrystal. CSDsymmetry has given the structural chemist a tool for searching the CSD on symmetry alone, which may provide an insight into the role symmetry plays in crystal formation.

Acknowledgements

We thank Mrs. A. Dawson and Dr. A. Parkin for assistance with data collections, and the EPSRC, the Cambridge Crystallographic Data Centre and the University of Edinburgh for funding.

References

Allen, F.H. (2002). *Acta Crystallogr.*, **B58**, 380–388.
Anastas, P.T. and Warner, J.C. (2002). *Green Chemistry*. Oxford, UK: Oxford University Press.
Bailey Walsh, R.D., Bradner, M.W., Fleischman, S., Morales, L.A., Moulton, B. Rodriguez-Hornedo, N. and Zaworotko, M.J. (2003). *Chem Commun.*, 186–187.
Bernstein, J., Davis, R.E., Shimoni, L. and Chang, N.-L. (1995). *Angew. Chem. Int. Ed. Engl.*, **34**, 1555–1573.
Bruno, I.J., Cole, J.C., Edgington, P.R., Kessler, M., Macrae, C.F., McCabe, P., Pearson, J. and Taylor, R. (2002). *Acta Crystallogr.*, **B58**, 389–397.
Etter, M.C. (1990). *Acc. Chem. Res.*, **23**, 120–126.
Fachaux, J.-M., Guyot-Hermann, A.-M., Guyot, J.-C., Conflant, P., Drache, M., Veesler, S. and Boistelle, R. (1995) *Powder Technol.*, **82**, 123–128.
Haisa, M., Kashino, S., Kawaii, R. and Maeda, H. (1976). *Acta Crystallogr.*, **B32**, 1283–1285.
Haisa, M., Kashino, S. and Maeda, H. (1974). *Acta Crystallogr.*, **B30**, 2510–2512.
Kitaigorodski, A.I. (1961). *Organic Chemical Crystallography*. Consultants Bureau, New York.
Nichols, G. and Frampton, C.S. (1998). *J. Pharm. Sci.*, **87**, 684–693.
Oswald, I.D.H., Allan, D.R., McGregor, P.A., Motherwell, W.D.S., Parsons, S. and Pulham, C.R. (2002). *Acta Crystallogr.*, **B58**, 1057–1066.
Watkin, D.J., Pearce, L. and Prout, C.K. (1993). *CAMERON – A Molecular Graphics Package*. Chemical Crystallography Laboratory, University of Oxford, England.
Yao, J.W., Cole, J.C., Pidcock, E., Allen, F.H., Howard, J.A.K. and Motherwell, W.D.S. (2002). *Acta Crystallogr.*, **B58**, 640–646.

UM00011746
NOVARTIS EXHIBIT 1517
Novartis v. Regents, IPR2023-01347
Page 492 of 4460

J|A|C|S
COMMUNICATIONS

Published on Web 09/20/2003

Single-Crystal-to-Single-Crystal Topochemical Polymerizations of a Terminal Diacetylene: Two Remarkable Transformations Give the Same Conjugated Polymer

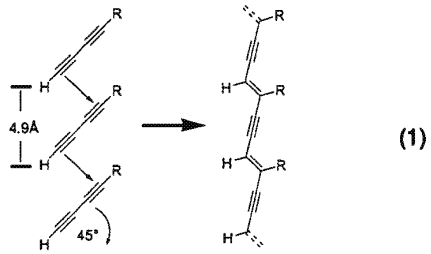
Xi Ouyang, Frank W. Fowler,* and Joseph W. Lauher*

Department of Chemistry, State University of New York, Stony Brook, New York 11794-3400

Received July 26, 2003; E-mail: ffowler@notes.cc.sunysb.edu; jlauher@notes.cc.sunysb.edu

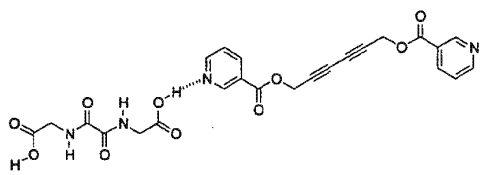
The organization of reactants with the objective of selecting one reaction pathway among many is an important goal of chemistry. This process controls the structure of the product including absolute stereochemistry. Nature achieves this high level of specificity using enzymes. However, this goal is usually beyond our reach. The regularity and order of a crystalline lattice rival an enzyme with respect to molecular organization. Unfortunately, the application of a crystal lattice to organize molecules for a chemical reaction is a formidable problem. It requires a careful choice of the chemical reaction and a successful strategy for supramolecular assembly of the reactants. We have recently developed host–guest chemistry as a strategy for assembling monomers for topochemical polymerization. This approach has led to the first successful triacetylene and triene 1,6-polymerizations.[1,2] We now report the application of this strategy to the first terminal diyne polymerization.

Polydiacetylenes have been known for about 35 years,[3] resulting in the publication of over 2000 papers. Nearly all of this work has been carried out on fully substituted diacetylenes; indeed symmetrical diacetylenes are the most popular. Much rarer are studies of terminal diacetylenes. Little structural work has been carried out; the Cambridge Structural Database[4] contains only four entries for terminal diacetylenes,[5] none with the necessary structural parameters (eq 1) for a topochemical polymerization.[6]



(1)

How could one prepare such an array by design? In earlier work,[7] we demonstrated that one could use a host–guest cocrystal to produce a network of hydrogen bonded oxalamide host molecules (2) that controlled the spacing and alignment of a diacetylene guest.



(2)

This host–guest approach works very well when both the host and the guest have matching end functionalities, that is, a *di*carboxylic acid and a *di*pyridine. We envisioned that an analogous motif could be achieved using a mono-substituted diacetylene with a *di*functional headgroup such as resorcinol[8] **1** and oxalamide **2**.[9]

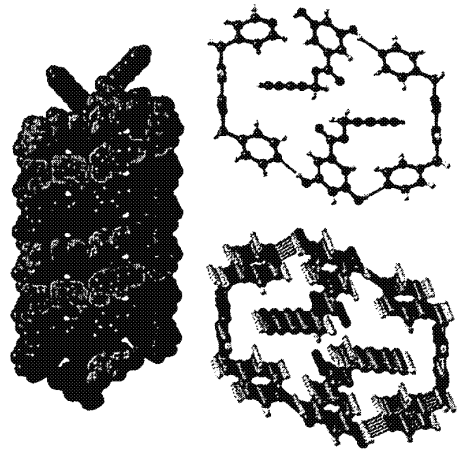
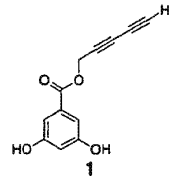
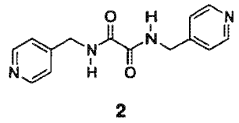


Figure 1. Three views of the crystal structure of the **1**·**2** cocrystal. If one focuses on the stronger phenol–pyridine hydrogen bond, the molecules form a hydrogen bonded chain in the form of a triple-helix of alternating molecules of **1** and **2**. The resorcinol headgroups are on the outer surface of the helix with the diacetylene tails in the center. The top drawing shows the four molecules of one turn of the helix. The left view shows that the helix is of order three. The lower right view shows the same structure from the top with the diacetylenes poised for topochemical polymerization.



1



2

Resorcinol **1** was prepared and formed cocrystals with **2** from a methanol water solution. Figure 1 shows the structure, a beautiful triple-helical array. As designed, the diacetylene functionalities are arranged in a manner suitable for a topochemical reaction. The repeat distance is 5.090(4) Å, with an angle of 45.1°. The C1–C4′ intermolecular distance is 3.638(4) Å. Heating the same single crystal to a temperature of 150 °C for 24 h gave the polymer structure shown in Figure 2. The polymerization motion is similar to the motion found in the various symmetrically substituted diacetylene polymerizations,[10] a rotation about the diacetylene center with the C1 and C4 carbons each moving a similar distance with a pivot of the attached methylene group. The repeat distance shortens to 4.925(5) Å upon polymerization, Table 1.

10.1021/ja037557+ CCC: $25.00 © 2003 American Chemical Society

UM00011747
NOVARTIS EXHIBIT 1517
Novartis v. Regents, IPR2023-01347
Page 493 of 4460

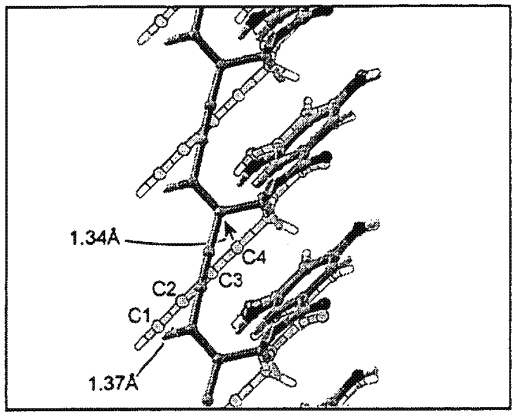


Figure 2. The pale background drawing shows the structure of the **1·2** cocrystal diacetylene monomers. The bold foreground drawing shows the structure of the resulting polydiacetylene. The main motion is a rotation of the diacetylene accompanied by a pivot of the methylene group. The C1 and C4 atom movements are similar, 1.37 and 1.34 Å.

Table 1. Crystallographic Data

	1·H_2O monomer	**1·H_2O** polymer	**1·2** monomer	**1·2** polymer
a (Å)	4.725(1)	4.876(2)	14.345(1)	14.607(1)
b (Å)	7.878(2)	7.814(3)	5.090(4)	4.925(5)
c (Å)	30.482(8)	27.407(9)	33.38(3)	33.14(3)
α (deg)	90	90	90	90
β (deg)	90.502(5)	87.203(7)	94.83(1)	91.92(1)
γ (deg)	90	90	90	90
vol ($Å^3$)	1134.5(5)	1043.0(6)	2450(4)	2382(4)
den. g/cm^3	1.371	1.491	1.318	1.356
space grp.	$P2_1/c$	$P2_1/c$	$P2_1/n$	$P2_1/n$

We were pleased with our designed structure, but in carrying out the synthesis we found an unexpected bonus. When pure resorcinol **1** is recrystallized from a methanol water mixture, large single crystals formed that showed an unexpected reddish brown color. These crystals turned black at 85 °C and showed no melting point up to 300°. A well-formed crystal was selected, and a structure determination revealed that the molecule had crystallized as a monohydrate with alignment of the diacetylene functionalities in reasonable agreement with the requirements for a topochemical polymerization, Figure 3.

The all important repeat distance is a bit short at 4.725(1) Å with a declination angle of 54.3°; the C1−C4′ intermolecular contact is 3.95 Å. These parameters are at the fringe of the range normally associated with crystal-to-crystal polymerizations, but upon heating the same single crystal at a relatively low temperature of 50 °C for 20 h a smooth single-crystal-to-single-crystal polymerization took place.

The polymerization of **1·H_2O** is accompanied by a significant change in both unit cell constants and crystal density. The polymerization occurs along the short *a* axis. This axis lengthens from 4.725(1) Å in the monomer crystal to 4.876(1) Å in the polymer crystal. At the same time, the long *c* axis of 30.482(8) Å dramatically contracts to a value of 27.407(8) Å in the polymer crystal. The density increases by 8.8%. The extreme motion of the terminal diacetylene groups causes this 3 Å shrinkage of the *c* axis. There is a bend at C4 with C1 moving inward by an unprecedented 2.45 Å to approach the C4′ atom of the molecule below.

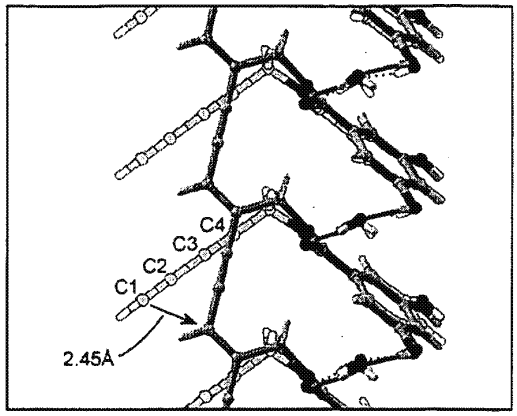


Figure 3. The pale background drawing shows the structure of the **1·H_2O** terminal diacetylene monomer structure. The bold foreground drawing shows the structure of the resulting polydiacetylene. The main motion is an inward swing of the diacetylene unit with a bend at C4. Atom C1 moves inward 2.45 Å. This inward motion of the diacetylene causes a shrinkage of the unit cell *c* axis and a 9% increase in crystal density.

It is interesting to note that the repeat distance in the **1:2** structure decreases from 5.090(4) Å for the monomer to 4.925(5) Å for the polymer. The **1·H_2O** structure starts short at 4.725(1) Å and lengthens to 4.876(1) Å. The polymer repeat distances approach the ideal 4.9 Å from opposite directions.

In conclusion, molecule **1** has turned out to be an interesting molecule. It undergoes the first structurally characterized polymerization of terminal diacetylene, and it does it twice. In the hydrate, the diacetylene functionality is "free", and there is a dramatic 2.45 Å swinging movement of C1. In the designed structure, the diacetylene polymerization takes place in a triple-helix "cage", and the diacetylene movement is much more constrained. A detailed comparison of these two sets of structural changes offers an interesting insight into the precise trajectories of polymerization reactions.

Acknowledgment. We wish to thank the National Science Foundation (CHE9980350) for support of this work.

Supporting Information Available: Details of the synthetic procedures and tables of X-ray diffraction data (PDF and CIF). This material is available free of charge via the Internet at http://pubs.acs.org.

References

(1) (a) Xiao, J.; Meng, M.; Lauher, J. W.; Fowler, F. W. *Angew. Chem., Int. Ed.* **2001**, *39*, 2132−2134. (b) Hong, T.; Lauher, J. W.; Fowler, F. W. *J. Am. Chem. Soc.* **2002**, *124*, 10656−10657.
(2) For similar work on diene polymerizations, see: Matsumoto, A. *Polym. J.* **2003**, *35*, 93−121.
(3) Wegner, G. *Z. Naturforsch* **1969**, *24b*, 824−832.
(4) Allen, F. H.; Motherwell, W. D. S. *Acta Crystallogr.* **2002**, *B58*, 407−422.
(5) There have been attempts to polymerize terminal diacetylenes. For example: Inoue, K.; Koga, N.; Iwamua, H. *J. Am. Chem. Soc.* **1991**, *113*, 9803−9810.
(6) Monomers need to be spaced at 4.9 Å with a 45°-declination angle. Enkelmann, V. *Chem. Mater.* **1994**, *6*, 1337−1340.
(7) (a) Kane, J. J.; Liao, R. F.; Lauher, J. W.; Fowler, F. W. *J. Am. Chem. Soc.* **1995**, *117*, 12003−12004. (b) Fowler, F. W.; Lauher, J. W. *J. Phys. Org. Chem.* **2000**, *13*, 850−857.
(8) Resorcinols have been used as supramolecular hosts. Papaefstathiou, G. S.; MacGillivray, L. R. *Org. Lett.* **2001**, *3*, 3835−3838.
(9) Schauer, C. L.; Matwey, E.; Fowler, F. W.; Lauher, J. W. *J. Am. Chem. Soc.* **1997**, *119*, 10245−10246.
(10) Baughman, R. H. *J. Polym. Sci., Polym. Phys. Ed.* **1974**, *12*, 1511−1535.

JA037557+

UM00011748
NOVARTIS EXHIBIT 1517
Novartis v. Regents, IPR2023-01347
Page 494 of 4460

Table 2. *Selected bond lengths* (Å) *and angles* (°) *in* (−)-(6′R)-3′,6′-*epoxyaurapten*

C5—O1	1·347 (4)	C9—O1	1·440 (4)
C8—O2	1·447 (4)	C17—O2	1·438 (5)
C2—O3	1·378 (4)	C4—O3	1·390 (5)
C4—O4	1·210 (5)	C8—C1	1·549 (5)
C9—C1	1·501 (5)	C18—C1	1·567 (5)
C6—C2	1·380 (5)	C10—C2	1·385 (5)
C10—C3	1·427 (6)	C12—C3	1·334 (6)
C12—C4	1·438 (6)	C6—C5	1·387 (5)
C14—C5	1·399 (5)	C18—C7	1·521 (6)
C13—C8	1·531 (5)	C15—C8	1·519 (5)
C16—C10	1·403 (5)	C18—C11	1·531 (6)
C19—C13	1·538 (6)	C16—C14	1·364 (6)
C18—C17	1·530 (5)	C19—C17	1·534 (6)

C9—O1—C5	117·8 (3)	C17—O2—C8	96·6 (3)
C4—O3—C2	121·8 (3)	C9—C1—C8	114·9 (3)
C18—C1—C8	101·9 (3)	C18—C1—C9	116·4 (3)
C6—C2—O3	116·1 (4)	C10—C2—O3	120·8 (4)
C10—C2—C6	123·2 (4)	C12—C3—C10	120·9 (5)
O4—C4—O3	116·1 (4)	C12—C4—O3	116·7 (4)
C12—C4—O4	127·2 (5)	C6—C5—O1	125·4 (4)
C14—C5—O1	115·7 (4)	C14—C5—C6	118·9 (4)
C5—C6—C2	118·9 (4)	C1—C8—O2	102·0 (3)
C13—C8—O2	101·8 (3)	C13—C8—C1	108·1 (3)
C15—C8—O2	109·9 (3)	C15—C8—C1	118·1 (3)
C15—C8—C13	114·9 (4)	C1—C9—O1	106·7 (3)
C3—C10—C2	118·1 (4)	C16—C10—C2	116·9 (4)
C16—C10—C3	124·9 (4)	C4—C12—C3	121·5 (5)
C19—C13—C8	102·2 (4)	C16—C14—C5	121·3 (4)
C14—C16—C10	120·8 (4)	C18—C17—O2	102·3 (3)
C19—C17—O2	101·7 (4)	C19—C17—C18	113·7 (4)
C7—C18—C1	112·8 (4)	C11—C18—C1	113·2 (4)
C11—C18—C7	109·1 (4)	C17—C18—C1	99·9 (3)
C17—C18—C7	114·7 (4)	C17—C18—C11	106·9 (4)
C17—C19—C13	101·0 (4)		

rather than of an aryl ring. It can be seen also that the positive charge may migrate to C5 which explains the shortened length (π character) of the O1—C5 bond *versus* the O1—C9 bond.

Finally, there is evidence of the *syn* relationship between the O2 bridge and the coumarin chain bonded to C1, a problem incompletely resolved until now by the nuclear Overhauser effect difference in NMR analysis. This verifies that anterior assignments based upon biogenetic pathways by Van Tamelen & Coates (1982) were correct.

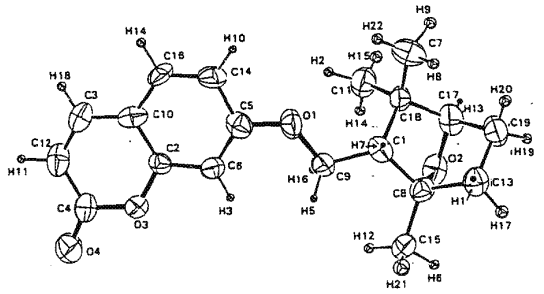


Fig. 1. *ORTEP* plot of the molecule of (−)-(6′R)-3′,6′-epoxyaurapten. For the sake of clarity, the isotropic thermal parameters of the H atoms were divided by ten.

References

BOHLMANN, F., ZDERO, C. & KAPTEYN, H. (1968). *Justus Liebigs Ann. Chem.* **717**, 186–192.

BONDI, A. (1964). *J. Phys. Chem.* **68**, 441–451.

CLEGG, W. (1981). *Acta Cryst.* A**37**, 22–28.

COATES, R. M. & MELVIN, L. S. JR (1970. *Tetrahedron*, **26**, 5699–5706.

HAMILTON, W. C. (1959). *Acta Cryst.* **12**, 609–610.

International Tables for X-ray Crystallography (1974). Vol. IV. Birmingham: Kynoch Press. (Present distributor Kluwer Academic Publishers, Dordrecht.)

JOHNSON, C. K. (1965). Report ORNL-3794. Oak Ridge National Laboratory, Tennessee, USA.

KATSUKI, T. & SHARPLESS, K. B. (1980). *J. Am. Chem. Soc.* **102**, 5974–5976.

SHELDRICK, G. M. (1976). *SHELX*76. Program for crystal structure determination. Univ. of Cambridge, England.

VAN TAMELEN, E. & COATES, R. M. (1982). *Bioorg. Chem.* T**11**, 171–196.

Acta Cryst. (1988). C**44**, 1264–1267

Structure of the 1:1 Complex between 4-Amino-*N*-(4,6-dimethyl-2-pyrimidinyl)-benzenesulfonamide (Sulfadimidine) and 2-Hydroxybenzoic Acid (Salicylic Acid)

BY U. PATEL,* M. HARIDAS AND T. P. SINGH†

Department of Biophysics, All India Institute of Medical Sciences, New Delhi-110029, *India*

(*Received* 4 *February* 1988; *accepted* 24 *March* 1988)

Abstract. $C_{12}H_{14}N_4O_2S.C_7H_6O_3$, $M_r = 416{\cdot}46$, orthorhombic, *Pbca*, $a = 15{\cdot}7783\ (8)$, $b = 25{\cdot}3419\ (12)$, $c = 10{\cdot}2212\ (5)$ Å, $V = 4087{\cdot}0\ (4)$ Å^3, $Z = 8$, $D_m = 1{\cdot}360\ (5)$, $D_x = 1{\cdot}3535\ (2)$ Mg m^{-3}, $\lambda(\text{Cu } K\alpha) = 1{\cdot}5418$ Å, $\mu = 1{\cdot}69$ mm^{-1}, $F(000) = 1744$, $T = 293$ K, final $R = 0{\cdot}053$ for 2733 observed reflections. The molecular complex between sulfadimidine and salicylic acid is obtained as a result of two hydrogen bonds

* Present address: Narmada College of Science, Technology and Commerce, Narmadanagar, Bharuch, Gujarat, India.

† Author to whom correspondence is to be addressed.

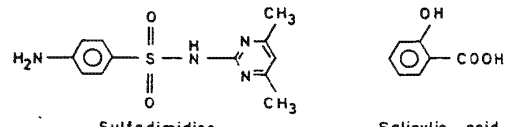
0108-2701/88/071264-04$03.00

© 1988 International Union of Crystallography

UM00011749
NOVARTIS EXHIBIT 1517
Novartis v. Regents, IPR2023-01347
Page 495 of 4460

involving both the carboxyl group O atoms of salicylic acid and the imino and pyrimidine N atoms of sulfadimidine. The torsion angle C1—S8—N11—C12 of sulfadimidine is −66·4 (3)°. The two planar six-membered rings in sulfadimidine are rotated with respect to each other by 109·0 (4)°. The structure contains an extensive scheme of hydrogen bonding and a distinct environment of van der Waals interactions involving six-membered rings of sulfadimidine and salicylic acid.

Introduction. Sulfonamides are well known antibacterial agents. They produce antimicrobial effects by competitively inhibiting the enzyme dihydropteroate synthase (DHPS) to its substrate *p*-aminobenzoic acid (PABA) (Bock, Miller, Schaper & Seydel, 1974). As part of our programme of systematic studies on sulfonamides, their complexes with other biologically interesting molecules and the enzyme DHPS (Haridas & Singh, 1987), we report here the crystal structure of a 1:1 complex between sulfadimidine and salicylic acid (I). We have reported earlier the crystal structure of sulfadimidine (Tiwari, Haridas & Singh, 1984).



(I)

Experimental. Samples of sulfadimidine and salicylic acid obtained commercially, crystallized from solution in acetonitrile of sulfadimidine and salicylic acid in equimolar ratio at 293 K. Thin, transparent, platy hexagonal crystals; one 0·50 × 0·30 × 0·20 mm used for data collection. Unit-cell dimensions and space group from oscillation and Weissenberg photographs. Cell dimensions refined on an automatic computer-controlled diffractometer using 20 independent reflections (θ range: 4·0 to 25·0°). Density by flotation in benzene and carbon tetrachloride. Intensity data collected on Enraf–Nonius CAD-4 automatic four-circle diffractometer in ω–2θ scan mode using graphite-monochromated Cu $K\alpha$ radiation. Total number of reflections measured 3458, total number of independent reflections 27 $[I \geq 2{\cdot}5\sigma(I)]$ for $(\sin\theta)/\lambda \leq 0{\cdot}47$ Å^{-1} with $h = 0$ to 18, $k = 0$ to 30, $l = 0$ to 11. Corrections for Lorentz and polarization effects but not for absorption ($\mu R = 0{\cdot}51$). Intensity measurements of two standard reflections (240 and 042) repeated after every 50 reflections. Variations in intensity throughout the experiment $\leq 4{\cdot}5\%$, R_{int} (for merged data) = 4·1%. Structure solved by *MULTAN*71 (Germain, Main & Woolfson, 1971) and refined by block-diagonal structure-factor least-squares procedure. Positions of H atoms from difference Fourier map. Non-H atoms refined anisotropically and H atoms isotropically. For 2733 observed reflections, final $R = 0{\cdot}053$, $wR = 0{\cdot}072$, $S = 4{\cdot}64$. Final $\Delta\rho$ fluctuations −0·15 to 0·14 e Å^{-3} and $(\Delta/\sigma)_{max} = 0{\cdot}18$. Weighting function $w = 1/(7{\cdot}62\,|F_{obs}| + 0{\cdot}0047\,|F_{obs}|^2)$ (Cruickshank, 1961) adjusted to make the average independent of F_{obs}. $\sum w(\Delta F)^2$ used in block-diagonal least-squares refinement. *SFLS* programs originally written by Shiono (1968/1971) and extensively modified by the authors. Atomic scattering factors for S atom from *International Tables for X-ray Crystallography* (1962), for C,N,O atoms from Cromer & Mann (1968) and for H atoms from Stewart, Davidson & Simpson (1965). All calculations on the HP computers at the All India Institute of Medical Sciences, New Delhi.

Table 1. *Fractional coordinates* (×10^4) *of the non*-H *atoms and equivalent isotropic thermal parameters* (Å^2×10^3)

$U_{eq} = \frac{1}{3}(U_{11} + U_{22} + U_{33})$.

	x	y	z	U_{eq}
C1	−805 (2)	3213 (1)	1202 (3)	47 (2)
C2	−1410 (2)	3429 (1)	2044 (3)	58 (2)
C3	−2251 (2)	3293 (1)	1892 (4)	66 (2)
C4	−2502 (2)	2941 (1)	907 (4)	61 (2)
C5	−1881 (2)	2725 (1)	94 (3)	57 (2)
C6	−1041 (2)	2863 (1)	232 (3)	53 (2)
N7	−3333 (2)	2812 (1)	760 (4)	98 (3)
S8	255 (1)	3385 (1)	1435 (1)	48 (1)
O9	384 (1)	3525 (1)	2780 (2)	63 (1)
O10	778 (1)	2983 (1)	868 (3)	68 (1)
N11	427 (2)	3951 (1)	681 (2)	52 (1)
C12	402 (2)	4035 (1)	−651 (3)	48 (2)
N13	132 (2)	3651 (1)	−1419 (2)	52 (1)
C14	114 (2)	3754 (1)	−2701 (3)	57 (2)
C15	374 (2)	4241 (1)	−3200 (3)	82 (2)
C16	649 (2)	4621 (1)	−2313 (3)	54 (2)
N17	658 (2)	4515 (1)	−1037 (2)	36 (1)
C18	−194 (3)	3318 (2)	−3579 (4)	80 (3)
C19	944 (3)	5155 (1)	−2741 (4)	75 (2)
C20	1884 (2)	5571 (1)	2413 (3)	55 (2)
C21	2158 (2)	6043 (1)	1844 (4)	68 (2)
C22	2529 (3)	6425 (1)	2627 (5)	82 (3)
C23	2614 (2)	6348 (2)	3938 (4)	79 (2)
C24	2345 (2)	5888 (2)	4520 (4)	75 (2)
C25	1989 (2)	5489 (1)	3753 (3)	65 (2)
C26	1478 (2)	5162 (1)	1602 (3)	56 (2)
O27	1321 (2)	5277 (1)	394 (2)	64 (1)
O28	1286 (2)	4727 (1)	2081 (2)	75 (2)
O29	1755 (2)	5040 (1)	4353 (3)	91 (2)

Discussion. There are two molecules in the asymmetric unit, one each of sulfadimidine and salicylic acid. The final positional and equivalent isotropic temperature factors of non-H atoms are given in Table 1.* The bond lengths and valence angles involving non-H atoms are listed in Table 2. A perspective view with the numbering scheme is illustrated in Fig. 1. The crystal

* Lists of structure factors, anisotropic thermal parameters, H-atom parameters, torsion angles, hydrogen-bond parameters, least-squares-planes data and intermolecular contact distances have been deposited with the British Library Document Supply Centre as Supplementary Publication No. SUP 44895 (27 pp.). Copies may be obtained through The Executive Secretary, International Union of Crystallography, 5 Abbey Square, Chester CH1 2HU, England.

UM00011750
NOVARTIS EXHIBIT 1517
Novartis v. Regents, IPR2023-01347
Page 496 of 4460

Table 2. *Bond lengths* (Å) *and bond angles* (°) *involving non-*H *atoms*

C1–C2	1·397 (4)	C14–C18	1·504 (5)
C1–C6	1·381 (4)	C15–C16	1·392 (4)
C1–S8	1·744 (3)	C16–N17	1·332 (4)
C2–C3	1·380 (4)	C16–C19	1·496 (4)
C3–C4	1·402 (5)	C20–C21	1·399 (4)
C4–C5	1·397 (4)	C20–C25	1·400 (4)
C4–N7	1·359 (4)	C20–C26	1·474 (4)
C5–C6	1·378 (4)	C21–C22	1·386 (5)
S8–O9	1·435 (2)	C22–C23	1·361 (8)
S8–O10	1·433 (2)	C23–C24	1·376 (7)
S8–N11	1·651 (2)	C24–C25	1·397 (5)
N11–C12	1·379 (4)	C25–O29	1·344 (4)
C12–N13	1·322 (3)	C26–O27	1·293 (4)
C12–N17	1·341 (3)	C26–O28	1·245 (4)
N13–C14	1·336 (3)		
C14–C15	1·397 (4)		

C2–C1–C6	120·6 (3)	N13–C14–C15	121·7 (3)
C2–C1–S8	118·3 (2)	N13–C14–C18	116·6 (3)
C6–C1–S8	121·1 (2)	C15–C14–C18	121·7 (3)
C1–C2–C3	119·3 (3)	C14–C15–C16	117·7 (3)
C2–C3–C4	120·8 (3)	C15–C16–N17	120·1 (3)
C3–C4–C5	118·6 (3)	C15–C16–C19	122·2 (3)
C3–C4–N7	120·3 (3)	N17–C16–C19	117·8 (3)
C5–C4–N7	121·1 (3)	C12–N17–C16	117·9 (3)
C4–C5–C6	121·0 (3)	C21–C20–C25	119·9 (3)
C1–C6–C5	119·7 (3)	C21–C20–C26	120·1 (3)
C1–S8–O9	109·2 (1)	C25–C20–C26	120·0 (3)
C1–S8–O10	108·7 (1)	C20–C21–C22	119·2 (3)
C1–S8–N11	108·1 (1)	C21–C22–C23	120·7 (3)
O9–S8–O10	118·8 (1)	C22–C23–C24	121·1 (4)
O9–S8–N11	102·0 (1)	C23–C24–C25	119·8 (4)
O18–S8–N11	109·6 (1)	C20–C25–C24	119·2 (3)
S8–N11–C12	126·2 (2)	C20–C25–O29	122·8 (3)
N11–C12–N13	118·8 (2)	C24–C25–O29	117·8 (3)
N11–C12–N17	115·0 (2)	C20–C26–O27	117·5 (2)
N13–C12–N17	126·2 (2)	C20–C26–O28	120·5 (3)
C12–N13–C14	116·4 (2)	O27–C26–O28	122·0 (3)

structure and the hydrogen-bonding scheme are shown in Fig. 2. The average C–H and N–H distances are 0·96 (3) and 1·03 (4) Å, respectively. The bond lengths and angles of sulfadimidine in the complex with salicylic acid are very similar to those observed in the free molecule of sulfadimidine (Basak, Mazumdar & Chaudhuri, 1983; Tiwari, Haridas & Singh, 1984; Rambaud, Maury, Pauvert, Audran, Lasserre & Berge, 1985). This is in agreement with the molecular dimensions in sulfonamides found by Haridas & Singh (1987).

The two planar rings of sulfadimidine in the structure of the complex are inclined with respect to each other at 109·0 (4)°, whereas the corresponding value in free sulfadimidine is 102 (1)°. The plane of the benzene ring of salicylic acid is rotated with respect to the planes of the benzene and pyrimidine rings of sulfadimidine by 5·7 (3) and 108·7 (4)° respectively. The torsion angle about the S8–N11 bond is −66·4 (3)°, while in free sulfadimidine it is −84·9 (9)°. The other torsion angles (with the values for the free molecule in square brackets) are O9–S8–N11–C12 = 178·6 (3) [160·4 (9)], O10–S8–N11–C12 = 51·8 (3) [33·5 (10)], N11–S8–C1–C6 = 97·6 (3) [130·6 (9)], N11–S8–C1–C2 = −84·0 (3) [−55·0 (10)], O10–S8–C1–C6 = −21·2 (3) [−11·0 (9)] and O10–S8–C1–C2 = 157·2 (2)° [174·7 (9)°]. These values of torsion angles show that the conformation of sulfadimidine is different in its free state and in the complexed state with salicylic acid. The above observations on sulfadimidine suggest that the conformation of sulfonamides changes upon interaction with other molecules but its molecular dimensions remain constant. These results are in good agreement with the conclusions drawn on sulfonamides by Haridas & Singh (1987).

The molecular dimensions of salicylic acid in the complex are similar to those observed in free salicylic acid (Cochran, 1953; Sundaralingam & Jensen, 1965), many of its derivatives (Bertinotti, Giacomello & Liquori, 1954; Sasada, Takano & Kakudo, 1964; Wheatley, 1964; Mootz & Fayos, 1970) and its hydrogen-bonded complexes with caffeine (Shefter, 1968), with theophylline (Shefter, 1969) and with antipyrine (Singh & Vijayan, 1974). The hydroxyl group (O29) in salicylic acid is internally hydrogen-bonded to one of the O atoms (O28) of the carboxyl group; the length of this hydrogen bond is 2·537 (4) Å. The plane of the carboxyl group is inclined to the plane of the benzene ring by 6·5 (4)°, which is only slightly different from those observed in free salicylic acid, its derivatives and other hydrogen-bonded complexes.

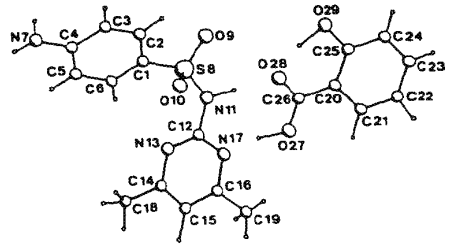


Fig. 1. A perspective view of the molecules with the numbering scheme.

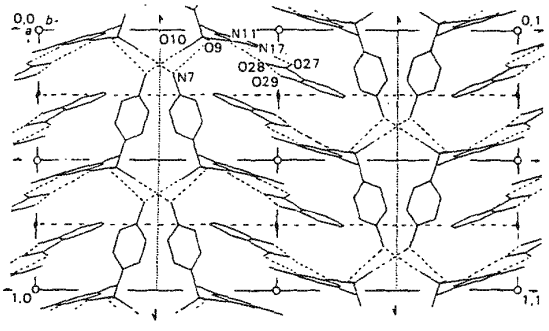


Fig. 2. The crystal structure as viewed along the *c* axis. The dashed lines indicate hydrogen bonds.

UM00011751
NOVARTIS EXHIBIT 1517
Novartis v. Regents, IPR2023-01347
Page 497 of 4460

Molecular packing. The molecular association between sulfadimidine and salicylic acid is achieved through two intermolecular hydrogen bonds: (1) the imino N11 atom and the carboxyl O28 atom of length 2·719 (4) Å; and (2) the carboxyl O27 atom and the pyrimidine N17 atom of length 2·603 (3) Å. In addition to these, the amino N7 atom forms two hydrogen bonds with atoms O9 ($x-\frac{1}{2}$, y, $\frac{1}{2}-z$) and O10 ($x-\frac{1}{2}$, $\frac{1}{2}-y$, $-z$) of the symmetry-related molecules which are of lengths 2·945 (4) and 2·899 (4) Å, respectively. The structure contains a pattern of strong hydrogen bonds interlinking groups of four molecules of sulfadimidine and pairs of sulfadimidine and salicylic acid. It also contains distinct environments of van der Waals interactions involving six-membered rings of sulfadimidine and salicylic acid.

The authors thank Professor H. Schenk for his kind help in data collection and the financial support from the Indian Council for Medical Research is gratefully acknowledged.

References

BASAK, A. K., MAZUMDAR, S. K. & CHAUDHURI, S. (1983). *Acta Cryst.* C**39**, 492–494.

BERTINOTTI, F., GIACOMELLO, G. & LIQUORI, A. M. (1954). *Acta Cryst.* **7**, 808–812.

BOCK, L., MILLER, G. H., SCHAPER, K. J. & SEYDEL, J. K. (1974). *J. Med. Chem.* **17**, 2–28.

COCHRAN, W. (1953). *Acta Cryst.* **6**, 260–268.

CROMER, D. T. & MANN, J. B. (1968). *Acta Cryst.* A**24**, 321–324.

CRUICKSHANK, D. W. J. (1961). In *Computing Methods and the Phase Problem in X-ray Crystal Structure Analysis*, edited by R. PEPINSKY, pp. 32–62. Oxford: Pergamon Press.

GERMAIN, G., MAIN, P. & WOOLFSON, M. M. (1971). *Acta Cryst.* A**27**, 368–376.

HARIDAS, M. & SINGH, T. P. (1987). Proceedings of the II Int. Symposium held in conjunction with the XIII IBS Meeting, Punjab Univ., Chandigarh, 31 January–2 February, 1986. In the press.

International Tables for X-ray Crystallography (1962). Vol. II, pp. 202–203. Birmingham: Kynoch Press. (Present distributor Kluwer Academic Publishers, Dordrecht.)

MOOTZ, D. & FAYOS, J. (1970). *Acta Cryst.* B**26**, 2046–2054.

RAMBAUD, J., MAURY, L., PAUVERT, B., AUDRAN, M., LASSERRE, Y. & BERGE, G. (1985). *Acta Cryst.* C**41**, 133–134.

SASADA, Y., TAKANO, T. & KAKUDO, M. (1964). *Bull. Chem. Soc. Jpn.* **37**, 940–947.

SHEFTER, E. (1968). *J. Pharm. Sci.* **57**, 1163–1168.

SHEFTER, E. (1969). *J. Pharm. Sci.* **58**, 710–714.

SHIONO, R. (1968/1971). *SFLS*. Tech. Reps. 48 and 49. Crystallography Laboratory, Univ. of Pittsburgh, USA.

SINGH, T. P. & VIJAYAN, M. (1974). *Acta Cryst.* B**30**, 557–562.

STEWART, R. F., DAVIDSON, E. R. & SIMPSON, W. T. (1965). *J. Chem. Phys.* **42**, 3175–3187.

SUNDARALINGHAM, M. & JENSEN, L. H. (1965). *Acta Cryst.* **18**, 1053–1058.

TIWARI, R. K., HARIDAS, M. & SINGH, T. P. (1984). *Acta Cryst.* C**40**, 655–657.

WHEATLEY, P. J. (1964). *J. Chem. Soc.* pp. 6036–6048.

Acta Cryst. (1988). C**44**, 1267–1269

Structure Cristalline de la Dihydroxyméthyl-3,6 Pyridazine

PAR F. ABRAHAM, B. MERNARI, M. LAGRENEE ET S. SUEUR

Laboratoire de Cristallochimie et Physicochimie du Solide, UA CNRS 452, Ecole Nationale Supérieure de Chimie de Lille, BP 108, 59652 Villeneuve d'Ascq CEDEX, France

(*Reçu le 29 octobre 1987, accepté le 24 mars 1988*)

Abstract. $C_6H_8N_2O_2$, 3,6-pyridazinedimethanol, $M_r = 140{\cdot}1$, orthorhombic, $Pca2_1$, $a = 13{\cdot}059$ (6), $b = 4{\cdot}224$ (1), $c = 12{\cdot}046$ (4) Å, $V = 664$ (1) Å^3, $Z = 4$, $D_m = 1{\cdot}37$ (3), $D_x = 1{\cdot}40$ g cm^{-3}, λ(Mo $K\bar{\alpha}$) = 0·7107 Å, $\mu = 1{\cdot}16$ cm^{-1}, $F(000) = 296$, $T = 298$ K, $R = 0{\cdot}030$, $wR = 0{\cdot}029$ ($w = 1$) for 536 independent reflexions. The most characteristic feature of the molecular structure is the absence of symmetry, essentially at the hydroxyl group level; the distances of these groups to the ring plane are significantly different. This molecular distortion is at least partially due to the hydrogen-bond scheme.

Introduction. La préparation et l'étude structurale de la dihydroxyméthyl-3,6 pyridazine s'inscrit dans le cadre général de la synthèse et de la caractérisation de ligands polydentates azotés pouvant conduire à des complexes polymétalliques (Sueur, Lagrenee, Abraham & Brémard, 1987; Mernari, 1987). La rigidité de la liaison N–N nécessaire au positionnement futur des atomes métalliques est assurée par la structure du cycle pyridazine. La substitution de cet hétérocycle en position 3,6 par le groupement hydroxyméthyle permet sa transformation en dérivés carbonyles, précurseurs de nombreux dérivés azotés tétrachélatants tels que les oximes et les hydrazones. Nous avons modifié la synthèse de ce diol réalisée précédemment par Novitskii, Sadovaya & Baskina (1970) de façon à obtenir des quantités plus importantes de produit.

Partie expérimentale. Le diacétoxyméthyl-2,5 furanne, obtenu par acétylation du dihydroxyméthyl-2,5 furanne

0108-2701/88/071267-03$03.00

© 1988 International Union of Crystallography

UM00011752

NOVARTIS EXHIBIT 1517
Novartis v. Regents, IPR2023-01347
Page 498 of 4460

This Page is Inserted by IFW Indexing and Scanning Operations and is not part of the Official Record

BEST AVAILABLE IMAGES

Defective images within this document are accurate representations of the original documents submitted by the applicant.

Defects in the images include but are not limited to the items checked:

- ❑ BLACK BORDERS
- ❑ IMAGE CUT OFF AT TOP, BOTTOM OR SIDES
- ❑ FADED TEXT OR DRAWING
- ❑ BLURRED OR ILLEGIBLE TEXT OR DRAWING
- ❑ SKEWED/SLANTED IMAGES
- ❑ COLOR OR BLACK AND WHITE PHOTOGRAPHS
- ❑ GRAY SCALE DOCUMENTS
- ❑ LINES OR MARKS ON ORIGINAL DOCUMENT
- ❑ REFERENCE(S) OR EXHIBIT(S) SUBMITTED ARE POOR QUALITY
- ❑ OTHER: _____

IMAGES ARE BEST AVAILABLE COPY.
As rescanning these documents will not correct the image problems checked, please do not report these problems to the IFW Image Problem Mailbox.

CRYSTAL GROWTH & DESIGN
2004
VOL. 4, NO. 1
89–94

Phenyl-Perfluorophenyl Synthon Mediated Cocrystallization of Carboxylic Acids and Amides

L. Sreenivas Reddy,[†] Ashwini Nangia,*,[†] and Vincent M. Lynch[‡]

School of Chemistry, University of Hyderabad, Hyderabad 500 046, India, and Department of Chemistry and Biochemistry, University of Texas, Austin, Texas 78712

Received June 24, 2003; Revised Manuscript Received August 6, 2003

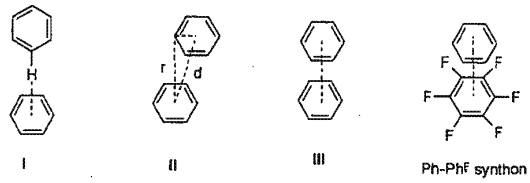
ABSTRACT: The significance of face-to-face $\pi-\pi$ stacking of phenyl and perfluorophenyl rings (Ph-Ph^F), a robust supramolecular synthon in aromatic and perfluoroaromatic crystal structures, is studied in the cocrystallization of simple aromatic carboxylic acids and amides. X-ray crystal structures of $C_6H_5COOH{\cdot}C_6F_5COOH$ **1**, $C_6H_5CONH_2{\cdot}C_6F_5CONH_2$ **2**, and $C_6H_5CONH_2{\cdot}C_6F_5COOH$ **3** are analyzed to understand the role of Ph-Ph^F synthon in directing self-assembly and hydrogen bonding in these cocrystals. The strong hydrogen bond donor acidity of C_6F_5COOH and $C_6F_5CONH_2$ together with mixed stacks of phenyl and perfluorophenyl rings steer acid···acid and amide···amide hydrogen bonding in cocrystals **1** and **2**. Acid···amide hydrogen bonding is sufficiently strengthened by donor acidity and acceptor basicity in **3** that the role of the Ph-Ph^F synthon is weaker because the aromatic rings stack with lateral offset. The complex $C_6H_5COOH{\cdot}C_6F_5CONH_2$ **4** could not be obtained under similar crystallization conditions. The crystal structure of $C_6F_5CONH_2$ is determined to compare molecular conformation and hydrogen bonding with motifs in the cocrystals. This study shows the viability of the Ph-Ph^F synthon in the presence of strong hydrogen bonding COOH and $CONH_2$ groups for crystal engineering.

Introduction

Aromatic–aromatic interactions are important in crystal engineering, supramolecular chemistry, biological recognition, and most recently highlighted for their significance in drug design.[1] Recognition between phenyl rings adopts low energy dimers of the edge-to-face geometry or herringbone T-motif **I**, parallel-displaced geometry with lateral offset **II**, and face-to-face or π-stacked sandwich geometry **III** (Scheme 1).[2] Unperturbed phenyl rings generally adopt the herringbone motif **I** with major stabilization to the T-geometry arising from dipole–quadrupole interaction between the positively polarized hydrogen and the negatively charged π-cloud of the benzene ring. Electron-deficient and electron-rich aromatic rings (e.g., C_6F_5 and C_6H_5) have an overwhelming preference for the stacked geometry **III** because favorable quadrupole–quadrupole interaction between aromatic rings with − and + quadrupole moment is maximized and unfavorable electrostatic repulsion in the T-geometry is minimized. The most remarkable example of phenyl–perfluorophenyl stacking (hereafter Ph-Ph^F synthon) is the crystal structure of the 1:1 complex of benzene–hexafluorobenzene[3] with an interplanar distance (r) of 3.4 Å and an intercentroid distance (d) of 3.7 Å. Noncovalent interactions in the molecular complex are so strong that melting point of the cocrystal (23.7 °C) is about 19 °C higher than the individual components. Several research groups have used the Ph-Ph^F synthon to steer supramolecular organization in the crystal[4] and to prealign molecules for solid-state photopolymerization.[5]

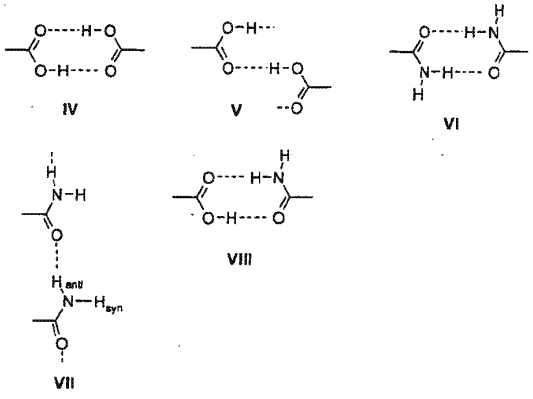
Cocrystallization is a current theme in several research groups to study hydrogen bonding by X-ray diffraction, for the synthesis of supramolecular architectures and interpenetrated networks, and in pharmaceutical development.[6] Carboxylic acids and carboxamides are reliable functional groups in crystal engineering[7] because they form robust aggregates as dimers and catemers (synthons **IV**–**VII**) via strong O–H···O and N–H···O hydrogen bonds (8–10 kcal mol^{-1}). The energy

Scheme 1. Edge-to-Face and Face-to-Face Interactions between Phenyl Rings[a]



[a] Center-to-center distance (d) and interplanar distance (r) are defined in synthon II.

Scheme 2. Hydrogen Bond Synthons of COOH and $CONH_2$ Groups



* E-mail: ansc@uohyd.ernet in.
† University of Hyderabad.
‡ University of Texas.

10.1021/cg034106s CCC: $27.50 © 2004 American Chemical Society
Published on Web 09/11/2003

UM00011754
NOVARTIS EXHIBIT 1517
Novartis v. Regents, IPR2023-01347
Page 500 of 4460

Table 1. Crystallographic Data and Structure Refinement Parameters[a]

	1	2	3	$C_6F_5CONH_2$
chemical formula	$(C_7H_6O_2)\cdot(C_7HF_5O_2)$	$(C_7H_7NO)\cdot(C_7H_2F_5NO)$	$(C_7H_7NO)\cdot(C_7HF_5O_2)$	$C_7H_2F_5NO$
formula weight	334.20	332.23	333.21	211.10
crystal system	monoclinic	monoclinic	monoclinic	monoclinic
space group	*Cc*	$P2_1$	$P2_1/n$	$P2_1/c$
a/Å	24.7320(4)	7.3546(3)	11.290(2)	12.749(3)
b/Å	7.7420(1)	6.0207(2)	6.7326(13)	6.1977(12)
c/Å	14.3430(3)	14.7507(5)	18.085(4)	9.5974(19)
α/°	90.00	90.00	90.00	90.00
β/°	108.4210(10)	90.568(2)	105.04(3)	99.94(3)
γ/°	90.00	90.00	90.00	90.00
Z	8	2	4	4
V/Å^3	2605.61(8)	653.13(4)	1327.5(5)	747.0(3)
T/K	153(2)	153(2)	293(2)	293(2)
D_{calc}/g cm^{-3}	1.704	1.689	1.667	1.877
μ/mm^{-1}	0.170	0.162	0.163	0.210
reflns collected	6107	4261	5535	2784
unique reflns	6103	2706	3018	1672
obsd reflns	4307	2243	1966	718
R_1 [$I > 2\sigma(I)$]	0.0474	0.0412	0.0421	0.0678
wR_2 [all]	0.1221	0.0987	0.1165	0.1764
goodness-of-fit	1.047	1.099	1.032	0.982

[a] CCDC deposit nos. 216156–216159.

of the C_6H_6–C_6F_6 dimer in the eclipsed face-to-face arrangement is 4–5 kcal mol^{-1} (r = 3.6–3.7 Å) by ab initio, semiempirical, and DFT calculations.[8] Furthermore, the heterodimer is calculated to be more stable than the homodimer in all cases. Given that the energy of Ph-Ph^F synthon is about half that of a strong O–H···O or N–H···O hydrogen bond we examined cocrystallization of aryl and perfluoroaryl carboxylic acids and amides. There are other favorable considerations in exploiting the Ph-Ph^F synthon to mediate cocrystallization. The pentafluorophenyl group activates the COOH and $CONH_2$ donor groups for hydrogen bonding because of the high electronegativity of fluorine (F 4.0, H 2.1, C 2.5; Pauling scale), while the similar van der Waals radius of H and F (1.20 Å, 1.47 Å; Bondi radius) means that the aryl/perfluoroaryl rings are nearly isosteric. Furthermore, organic fluorine has little hydrogen-bond acceptor ability,[9] and hence phenyl–perfluorophenyl stacking was expected to prevail in the presence of other strong hydrogen bonding groups, e.g., COOH, $CONH_2$. X-ray crystal structures of benzoic acid·pentafluorobenzoic acid **1**, benzamide·pentafluorobenzamide **2**, and benzamide·pentafluorobenzoic acid **3** are reported and discussed in this paper to highlight the role of the Ph-Ph^F synthon in cocrystallization. While the crystal structure of C_6F_5COOH is known,[10] the structure of $C_6F_5CONH_2$ was determined as part of this study to compare the conformation and hydrogen bonding of the fluorinated molecule with that in the molecular complex.

Experimental Section

In all cocrystallization experiments, the components were finely ground using mortar-and-pestle and dissolved in EtOAc/hexane (1:1). The molecular complex was characterized by its difference in melting point from the pure components and the structure confirmed by X-ray diffraction. Melting point of benzoic acid is 122 °C, benzamide is 129 °C, pentafluorobenzoic acid is 101 °C, and pentafluorobenzamide is 145 °C. Melting point is determined on Fisher-Johns apparatus (visual inspection) and confirmed by the onset temperature of endotherm measured on Perkin-Elmer DSC4 instrument (scan rate 10° min^{-1}). Crystals of pentafluorobenzamide were obtained from CH_2Cl_2 at ambient temperature. Although single crystals of $C_6F_5CONH_2$ are of good quality they are soft and do not cut easily. The mosaicity factor is about 2 compared to typical values of 0.5–1.0.

Cocrystallization

(Benzoic Acid)·(Pentafluorobenzoic Acid) 1. A 1:1 mixture of benzoic acid (0.030 g, 0.25 mmol) and pentafluorobenzoic acid (0.053 g, 0.25 mmol) was dissolved in hot EtOAc/hexane (1:1). Plate-shaped colorless crystals were obtained after few days at room temperature. m.p. 85–87 °C.

(Benzamide)·(Pentafluorobenzamide) 2. A 1:1 mixture of benzamide (0.030 g, 0.25 mmol) and pentafluorobenzamide (0.052 g, 0.25 mmol) was dissolved in hot EtOAc/hexane (1:1). Needle-shaped colorless crystals were obtained after few days at room temperature. m.p. 103–105 °C.

(Benzamide)·(Pentafluorobenzoic Acid) 3. A 1:1 mixture of benzamide (0.030 g, 0.25 mmol) and pentafluorobenzoic acid (0.053 g, 0.25 mmol) was dissolved in hot EtOAc/hexane (1:1). Needle-shaped colorless crystals were obtained after few days at room temperature. m.p. 85 °C.

Cocrystallization of benzoic acid and pentafluorobenzamide using the above conditions did not afford the expected molecular complex **4**. Crystals of benzoic acid precipitated after a few days.

X-ray Diffraction. Reflections were collected on Nonius Kappa CCD diffractometer using incident X-ray radiation Mo–Kα (λ = 0.71073 Å). Crystals were cooled with an Oxford Cryosystem device attached to a CCD machine. Data reductions were performed using DENZO–SMN.[11] Structures were solved by direct methods using SHELXS-97 and refined by full-matrix least-squares refinement on F^2 with anisotropic displacement parameters for non-H atoms using SHELXL-97.[12] In complex **1** H1A, H6A, and H3A atoms are fixed. Geometrical analysis was carried out in PLATON.[13] Details of cell parameters, data collection, and structure refinement are summarized in Table 1, hydrogen bond metrics are given in Table 2, and selected torsion angles are listed in Table 3.

CCDC reference numbers are 216156–216159.

Results and Discussion

$PhCO_2H\cdot C_6F_5CO_2H$ **1** crystallizes in the monoclinic space group *Cc* with two residues of each component in the asymmetric unit. The molecules adopt different conformations about the C_{aryl}–C_{COOH} bond (Table 3): twisted conformation (designated A) and near-planar conformation B.[14] $C_6H_5CO_2H$ and $C_6F_5CO_2H$ of both A

UM00011755
NOVARTIS EXHIBIT 1517
Novartis v. Regents, IPR2023-01347
Page 501 of 4460

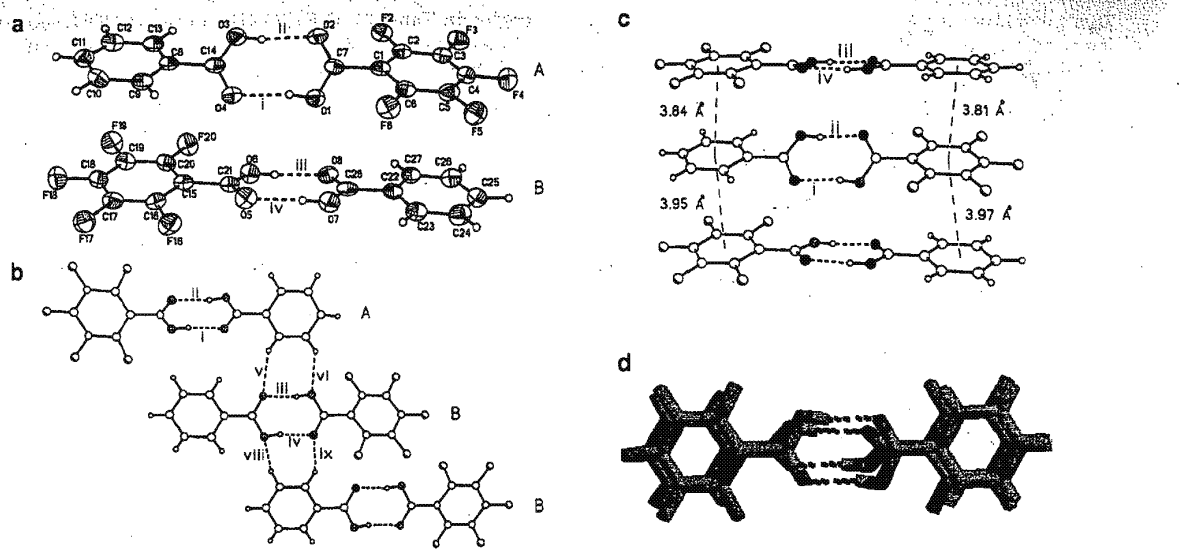


Figure 1. (a) ORTEP plot of $C_6H_5COOH{\cdot}C_6F_5COOH$ **1** drawn at 50% probability level for non-H atoms. Symmetry-independent carboxylic acid dimers are labeled A and B. Hydrogen bonds are shown as dotted lines and listed in Table 2. (b) C−H···O interactions between acid dimers. (c) Phenyl−perfluorophenyl stacking along the *b*-axis. (d) View down [010] to show the excellent $\pi-\pi$ stacking in Ph-Ph^F synthon with no offset. H atoms are shown as small circles (or blue) and F atoms are shown as large circles (or green).

Table 2. Geometrical Parameters of Hydrogen Bonds

crystal		H-bond[a]	*d*/Å	*D*/Å	*θ*/°
1	i	O−H···O	1.67	2.647(3)	169.4
	ii	O−H···O	1.68	2.653(3)	168.7
	iii	O−H···O	1.63	2.605(3)	171.2
	iv	O−H···O	1.65	2.624(3)	170.2
	v	C−H···O	2.50	3.478(4)	149.1
	vi	C−H···O	2.50	3.437(4)	143.7
	vii	C−H···O	2.68	3.479(4)	130.6
	viii	C−H···O	2.56	3.503(4)	144.7
	ix	C−H···O	2.46	3.318(4)	135.2
	x	C−H···F	2.49	3.220(5)	123.7
2	i	N−H···O	2.16	3.118(3)	159.0
	ii	N−H···O	2.15	3.088(3)	152.9
	iii	N−H···O	2.03	2.997(3)	159.5
	iv	N−H···O	1.94	2.936(3)	169.7
	v	C−H···O	2.35	3.415(3)	167.7
3	i	N−H···O	2.02	3.003(2)	164.4
	ii	N−H···O	2.02	2.983(2)	157.3
	iii	O−H···O	1.51 (1.39)[b]	2.4873(18)	170.8
	iv	C−H···O	2.37	3.429(2)	164.1
	v	N−H···F	2.53	3.1589(19)	120.0
$C_6F_5CONH_2$	i	N−H···O	1.90	2.902(5)	168.6
	ii	N−H···O	1.96	2.906(5)	154.2

[a] O−H, N−H, C−H bonds are neutron-normalized. [b] Experimental X-ray distance in very short hydrogen bond.

Table 3. Selected Torsion Angles

crystal	atoms	*θ*/°
1	C2−C1−C7−O2	32.6
	C9−C8−C14−O4	27.2
	C16−C15−C21−O5	11.3
	C27−C22−C28−O8	5.0
2	C2−C1−C7−O8	42.9
	C6A−C1A−C7A−O8A	21.6
	N9A−C7A−O8A−N9	47.9
	N9−C7−O8−N9A	44.9
3	C2−C1−C7−O1	22.8
	C9−C8−C14−O3	22.5
$C_6F_5CONH_2$	C6−C1−C7−O1	41.0

and B type molecules engage in symmetry-independent dimer **IV** (Figure 1a). The O−H···O hydrogen bond[15] from $C_6F_5CO_2H$ to $C_6H_5CO_2H$ is shorter (iii, O···O 2.605(3) Å, electron-deficient donor to electron-rich acceptor) than the other hydrogen bond in **IV** from $C_6H_5CO_2H$ to $C_6F_5CO_2H$ (iv, O···O 2.624(3) Å, electron-rich donor to electron-deficient acceptor, difference > 3σ) for B molecule, but the difference is not significant for A molecule. The hydrogen bonds in synthon **IV** of twisted A molecules are longer (i, ii, O···O 2.647(3) Å, 2.653(3) Å) than iii, iv because conjugation between phenyl ring and carboxylic acid group in planar B molecules strengthens hydrogen bonding (O−H···O: i 1.67 Å, 169.4°; ii 1.68 Å, 168.7°; iii 1.63 Å, 171.2°; iv 1.65 Å, 170.2°; neutron-normalized geometry is reported). Such dimers are connected via C−H···O interactions listed in Table 2 and shown in Figure 1b. The structure has an overall van der Waals close packing such that the phenyl and perfluorophenyl groups are in proximity. The phenyl and perfluorophenyl rings of dimer aggregates A and B have excellent π-stacking with little offset (Ph-Ph^F synthon, Scheme 1) at an intercentroid distance (*d*) of 3.81, 3.84, 3.95, 3.97 Å (Figure 1c,d) and an interplanar distance (*r*) of ca. 3.5 Å. (3.53, 3.49, 3.47, 3.55 Å).

The crystal structure of binary component **1** may be compared with the structure of 1-pentafluorophenyl-4-phenylbutadiyne **5**.[4a] Molecules of **5** are stacked in a head-to-tail fashion at interlayer distance (*r*) of ca. 3.7 Å. The diyne covalent spacer in **5** and hydrogen bond synthon **IV** in **1** are interchangeable, and, moreover, the $C_{aryl}-C_{aryl}$ distance between Ph and Ph^F rings is very similar in the two structures (6.64 Å in **5**, 6.80 and 6.78 Å for A and B molecules of **1**). The identical packing in **1** and **5** strengthens the idea stated in the introduction that the hydrogen bonding and aromatic stacking domains in these structures are insulated from one another. We have noted the equivalence between molecular and supramolecular connectors in a family of wheel-and-axle host−guest structures.[16]

UM00011756
NOVARTIS EXHIBIT 1517
Novartis v. Regents, IPR2023-01347
Page 502 of 4460

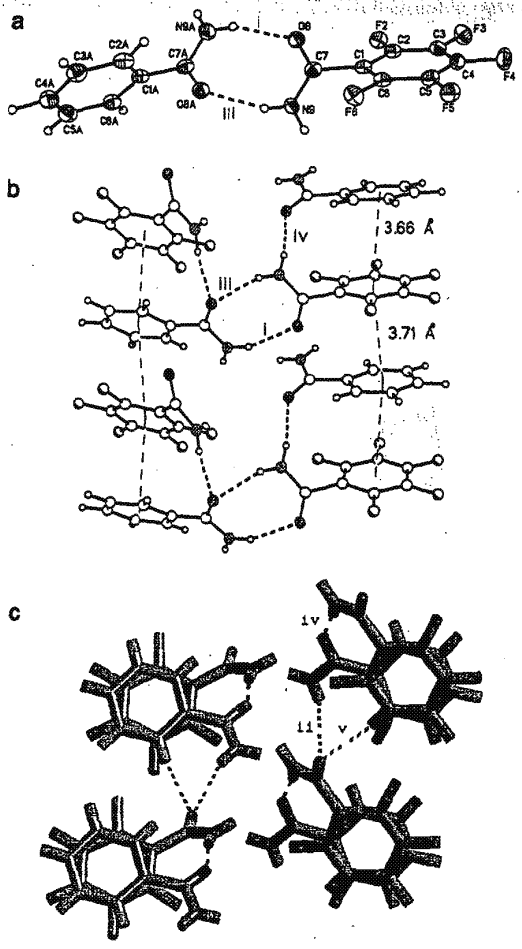


Figure 2. (a) ORTEP plot of $C_6H_5CONH_2 \cdot C_6F_5CONH_2$ **2**. (b) Ph-Ph^F stacking and $N_{anti}-H\cdots O$ bond iv along the *a*-axis. (c) View down [100] to show the excellent overlap of phenyl and perfluorophenyl rings. The $N_{syn}-H\cdots O$ hydrogen bond is not shown for clarity.

The assignment of *Cc* space group is fraught with the possibility that there might be true higher symmetry that is overlooked,[17] and this error is even more likely when there are two symmetry-independent molecules ($Z' = 2$) as in **1**. We have verified that the assignment of *Cc* space group is correct in this case. There is an approximate, noncrystallographic inversion center at 0.4, 0.25, 0.2, which explains the centrosymmetric intensity statistics observed in data collection. However, from examination of the molecular conformations of $PhCO_2H$ and $C_6F_5CO_2H$ and the two hydrogen-bonded dimers **IV** it is obvious that they are different. A check of the cif file in Platon for MISSYM also agrees with our assignment and the higher symmetry *C2/c* space group is ruled out for **1**.

$C_6H_5CONH_2 \cdot C_6F_5CONH_2$ **2** crystallizes in the polar space group $P2_1$ with one molecule of each residue in the asymmetric unit. The $CONH_2$ group in $C_6F_5CONH_2$ is twisted with respect to the aromatic ring when compared with $C_6H_5CONH_2$ (Figure 2a, see torsion angles in Table 3). $C_6F_5CONH_2$ and $C_6H_5CONH_2$ are connected via $N-H_{anti}\cdots O$ hydrogen bonds as catemer **VII** that run parallel to [1 1 0] and [1−1 0] directions. The $N_{anti}-H\cdots O$ hydrogen bond iv from $C_6F_5CONH_2$ to $C_6H_5CONH_2$ is significantly shorter than the bond from $C_6H_5CONH_2$ to $C_6F_5CONH_2$ (Figure 2b, iv 1.94 Å, 169.7°; ii 2.15 Å, 152.9°, interaction ii to *b*-translated mixed stack is not shown). The syn NH groups form a twisted noncentrosymmetric dimer **VI** (iii 2.03 Å, 159.5°; i 2.16 Å, 159.0°) with N−C−O−N torsion angles of 47.9° and 44.9° (Table 3). Hydrogen bond iv is shorter than the other three $N-H\cdots O$ bonds in the same structure because the donor and acceptor groups are activated and it is simultaneously stabilized by the attractive Ph-Ph^F synthon (Figure 2b, $d = 3.66$ Å). The π-cloud of phenyl and pentafluorophenyl rings have excellent quadrupole−quadrupole interactions because they stack with little offset (Figure 2c). The shortness of $N_{anti}-H\cdots O$ compared to $N_{syn}-H\cdots O$ is significant because syn NH is generally assumed to be the stronger hydrogen bond donor than anti NH in primary amide.[18] Weak $C-H\cdots O$, $C-H\cdots F$, and $F\cdots F$ interactions are present in the crystal. Thus, cocrystals of simple aromatic carboxylic acids and amides may be synthesized with perfluoroaromatic acids/amides keeping aryl group size considerations in mind. Crystallization of **1** and **2** in noncentrosymmetric space groups is an interesting observation but generally difficult to rationalize. That the carboxylic acid and amide dimers in structures with isomorphous substitution are devoid of center of symmetry could be a contributing factor insofar as the crystallographic inversion center is coincident with the centrosymmetric dimer.

$C_6F_5CONH_2$ crystallizes in the monoclinic space group $P2_1/c$. The amide group is highly twisted with respect to the C_6F_5 ring (Table 3). Molecules are hydrogen bonded via the centrosymmetric amide dimer **VI** (i 1.90 Å, 168.6°) and such dimers are connected to the glide-related O atom via $N_{anti}-H\cdots O$ bond (ii 1.96 Å, 154.2°, Figure 3). The shallow glide motif is adopted by some primary amides with *c*-axis of 9.8 ± 0.3 Å.[19]

Both dimer and catemer synthons **VI** and **VII** are present in $C_6F_5CONH_2$ and its cocrystal **2**. The question arises: which is the primary motif and which is the secondary one? We believe that the 0D dimer **VI** is the primary synthon in the structure of $C_6F_5CONH_2$ because the space group is centrosymmetric. On the other hand, the $N_{anti}-H\cdots O$ bond from $C_6F_5CONH_2$ donor to $C_6H_5CONH_2$ acceptor, strengthened by the Ph-Ph^F synthon, is the primary structural motif in cocrystal **2**. The weak amide dimer synthon and noncentrosymmetric packing of **2** argue in favor of a catemer as the main recognition motif. This hints toward the structure-directing role of the Ph-Ph^F synthon in cocrystallization of **1** and **2**.

Crystallization of benzamide and pentafluorobenzoic acid was attempted next. Crystals of 1:1 complex **3** were obtained from EtOAc/hexane at ambient temperature that solved in the $P2_1/n$ space group. The twist in molecular conformation of acid and amide molecules is listed in Table 3. The crystal structure is stabilized by acid···amide heterodimer **VIII** (Figure 4a, $O-H\cdots O$ iii 1.51 Å, 170.8°; $N-H\cdots O$ i 2.02 Å, 164.4°). $O-H\cdots O$ bond iii is in the range of a very short (strong) hydrogen

UM00011757
NOVARTIS EXHIBIT 1517
Novartis v. Regents, IPR2023-01347
Page 503 of 4460

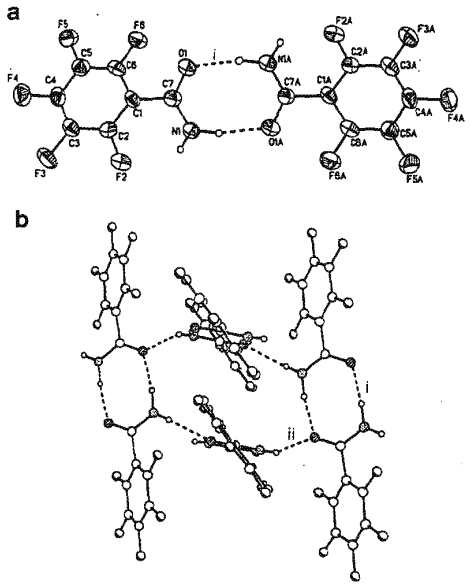


Figure 3. (a) ORTEP plot of $C_6F_5CONH_2$ to show the amide dimer synthon. (b) N_{anti}–H···O bond to glide-related molecule.

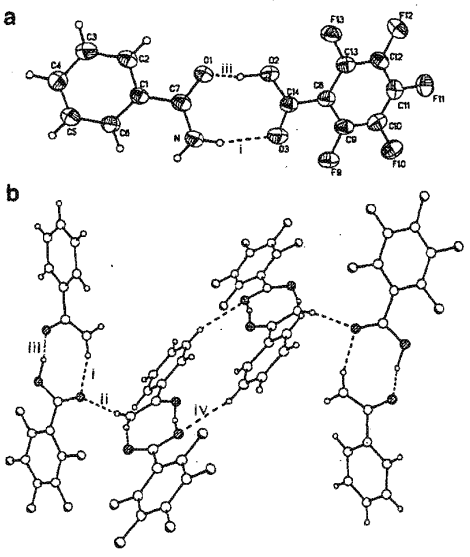


Figure 4. (a) ORTEP plot of $C_6H_5CONH_2 \cdot C_6F_5COOH$ **3** to show acid···amide heterodimer **VIII**. (b) N_{anti}–H···O bond and C–H···O interaction with C_6F_5COOH of glide- and inversion-related aggregate.

bond[20] (O···O 2.4873(18) Å) with an H···O distance of 1.39 Å (X-ray). The shortness of O–H···O is due to the very strong donor ($C_6F_5CO_2H$) and highly basic acceptor group ($PhCONH_2$). Short O–H···O hydrogen bonds have been noted in acid–amide cocrystals, e.g., oxalic acid·*trans*-cinamamide (O···O 2.489 Å, O–H···O 174.3°).[21] The heterodimers are connected to the COOH group of a glide-related aggregate by N–H···O bond (ii 2.02 Å, 157.3°), and such inversion-related dimers are connected by C–H···O interaction (iv 2.37 Å, 164.1°; Figure 4b).

The hydrogen bond acceptor in ii is the carbonyl group of C_6F_5COOH because of auxiliary contribution from bifurcated N–H···F interaction v (Table 2). Weak C–H···F and F···F interactions (distance ≥ Σr_{vdW}) can be identified in the structure. While the sandwich stack Ph-Ph^F geometry **III** stabilizes structures **1** and **2**, the interaction is weaker in **3** via lateral offset motif **II** (d = 3.93 Å, r = 3.47 Å). Phenyl–perfluorophenyl mediation during cocrystallization of **3** is weaker because acid···amide heterodimer **VIII** is stronger that homodimers **IV** and **VI**. It appears that the role of the Ph-Ph^F synthon toward cocrystallization is based on need, akin to anchimeric assistance in S_N2 displacement reaction.[22]

The higher strength of acid···amide heterodimer **VIII** compared to acid···acid and amide···amide homodimer **IV** and **VI** is explained by the best hydrogen bond donor (COOH) approaching the best acceptor (amide C=O) and the second-best donor (CONH) bonding with the next acceptor (acid C=O) in $CO_2H\cdots CONH_2$.[23] Another reason for the formation of heterodimer is to avoid lone-pair repulsion between hydroxyl and carbonyl O atoms that occurs in hydrogen-bonded chains built from homodimers and connected via N–H···O hydrogen bonds. In the heterodimer arrangement, the distance between neighboring N–H groups hydrogen bonded to the same O atom increases and so the lone-pair repulsion is minimized.[19] Database survey shows that heterodimer **VIII** is formed in 4:1 preference compared to dimer **IV** and catemer **V** motifs between CO_2H groups.[24] Despite these factors, several attempts to cocrystallize pentafluorobenzamide and benzoic acid did not yield any adduct crystal $C_6F_5CONH_2 \cdot C_6H_5CO_2H$ **4** presumably because both the CO_2H donor and the amide C=O acceptor are weaker hydrogen bonding groups compared to **3**.

Last we note that while the melting point of phenyl–perfluorophenyl adduct crystals is generally higher than the pure components,[4] both **1** and **2** melt at a temperature significantly lower than the pure acids and amides. Thus, despite the attractive Ph-Ph^F synthon and the stronger hydrogen bonding in these cocrystals there are possibly other factors contributing to crystal lattice forces that are not additive. Apart from enthalpy, entropy is equally important in explaining melting point lowering, though much more difficult to quantify. Factors such as the different number of residues, symmetry-independent molecules, and their conformation in the component and adduct crystals are likely to complicate a lattice energy-based approach to calculate enthalpy. This interesting observation prompts further thinking about correlation between melting point, crystal packing, and lattice energies.

There are several advantages in studying X-ray crystal structures of closely related molecules. (1) Correlation between molecular structure and crystal packing may be established because changes occur in a graded manner and these may be attributed to steric and/or electronic effects. (2) The criticism that carefully selected crystal structures from a large diverse pool of unpublished structures are presented to give the impression of "high fidelity crystal engineering"[25] is rebutted. (3) A strategy developed with model compounds

UM00011758
NOVARTIS EXHIBIT 1517
Novartis v. Regents, IPR2023-01347
Page 504 of 4460

guides the study of complex systems to test hydrogen bond hierarchy and interplay during crystallization.

Conclusions

Although carboxylic acids and carboxamides are the two most popular functional groups in crystal engineering, very few general methods are available to synthesize their cocrystals. Molecular complexes have been prepared from electron-deficient and electron-rich aromatic carboxylic acids[26] (e.g., 3,5-dinitrobenzoic acid, 3,5-dinitrocinnamic acid, 4-dimethylaminobenzoic acid, 4-dimethylaminocinnamic acid, etc.). Earlier studies on the Ph-Ph^F synthon have dealt with molecules in which strong hydrogen bonding groups were generally absent.[4,5] We demonstrate that the phenyl−perfluorophenyl stacking synthon is a viable recognition motif for the cocrystallization of strong hydrogen bonding carboxylic acids and carboxamides. Further scope of the Ph-Ph^F synthon as a facilitating group for the directed synthesis of acid/amide cocrystals and their topochemical reactions is an ongoing theme in our research.

Acknowledgment. A.N. thanks the CSIR (01/1738/02/EMR-II) for research funding. The UPE program of UGC supports UoH. L.S.R. thanks the CSIR for fellowship. V.M.L. thanks the NSF (CHE-9807702) for funding. We thank both reviewers for their useful comments and suggestions.

Supporting Information Available: X-ray crystallographic files (CIF) are available free of charge via the Internet at http://pubs.acs.org.

References

(1) Meyer, E. A.; Castellano, R. K.; Diederich, F. *Angew. Chem., Int. Ed* **2003**, *42*, 1210.
(2) (a) Hunter, C. A.; Sanders, J. K. M. *J. Am. Chem. Soc.* **1990**, *112*, 5525. (b) Janiak, C. *J. Chem. Soc., Dalton Trans.* **2000**, 3885. (c) Jennings, W. B.; Farrell, B. M.; Malone, J. F. *Acc. Chem. Res.* **2001**, *34*, 885.
(3) Patrick, C. R.; Prosser, G. S. *Nature* **1960**, *187*, 1021.
(4) (a) Coates, G. W.; Dunn, A. R.; Henling, L. M.; Dougherty, D. A.; Grubbs, R. H. *Angew. Chem., Int Ed. Engl.* **1997**, *36*, 248. (b) Ponzini, F.; Zagha, R.; Hardcastle, K.; Siegel, J. S. *Angew. Chem., Int Ed.* **2000**, *39*, 2323 (c) Collings, J. C.; Roscoe, K. P.; Thomas, R. L.; Batsanov, A. S.; Stimson, L. M.; Howard, J. A. K.; Marder, T. B. *New J. Chem.* **2001**, *25*, 1410. (d) Vangala, V. R.; Nangia, A.; Lynch, V. M. *Chem. Commun.* **2002**, 1304. (e) Collings, J. C.; Roscoe, K. P.; Robins, E. G.; Batsanov, A. S.; Stimson, L. M.; Howard, J. A. K.; Clark, S. J.; Marder, T. B. *New J. Chem* **2002**, *26*, 1740. (f) Liu, J.; Murray, E. M.; Young, Jr., V. G. *Chem. Commun* **2003**, 1904.
(5) (a) Coates, G. W.; Dunn, A. R.; Henling, L. M.; Ziller, J. W.; Lobkovsky, E. B.; Grubbs, R. H. *J. Am. Chem. Soc.* **1998**, *120*, 3641. (b) Renak, M. L.; Bartholomew, G. P.; Wang, S.; Ricatto, P. J.; Lachicotte, R. J.; Bazan, G. C. *J. Am. Chem. Soc.* **1999**, *121*, 7787. (c) Feast, W. J.; Lövenich, P. W.; Puschmann, H.; Taliani, C. *Chem. Commun.* **2001**, 505. (d) Vishnumurthy, K.; Row: T. N. G.; Venkatesan, K. *Photochem. Photobiol. Sci.* **2002**, *1*, 427.
(6) (a) Bhogala, B. R.; Vishweshwar, P.; Nangia, A. *Cryst. Growth Des.* **2002**, *2*, 325. (b) Kumar, V. S. S.; Nangia, A.; Katz, A. K.; Carrell, H. L. *Cryst. Growth Des.* **2002**, *2*, 313. (c) Kumar, V. S. S.; Nangia, A.; Kirchner, M. T.; Boese, R. *New J. Chem.* **2003**, *27*, 224. (d) Bhogala, B. R.; Nangia, A. *Cryst. Growth Des.* **2003**, *3*, 547. (e) Vishweshwar, P. Nangia, A.; Lynch, V. M. *Cryst. Growth Des.* **2003**, *3*, 783. (f) Shan, N.; Bond, A. D.; Jones, W. *Cryst. Eng.* **2002**, *5*, 9. (g) Shan, N.; Bond, A. D.; Jones, W. *New J. Chem.* **2003**, *27*, 365. (h) Olenik, B.; Smolka, T.; Boese, R.; Sustmann, R. *Cryst. Growth Des.* **2003**, *3*, 183. (i) Aakeröy, C. B.; Beatty, A. M.; Helfrich, B. A. *J. Am. Chem. Soc.* **2002**, *124*, 14425. (j) Walsh, R. D. B.; Bradner, M. W.; Fleischman, S. G.; Morales, L. A.; Moulton, B.; Rodríguez-Hornedo, N.; Zaworotko, M. J. *Chem. Commun.* **2003**, 186. (k) Fleischman, S. G.; Kuduva, S. S.; McMahon, J. A.; Moulton, B.; Walsh, R. D. B.; Rodríguez-Hornedo, N.; Zaworotko, M. J. *Cryst. Growth Des.* **2003**, ASAP, DOI: 10.1021/cg034035x.
(7) Desiraju, G. R *Crystal Engineering. The Design of Organic Solids*; Elsevier: Amsterdam, 1989.
(8) West, A. P., Jr.; Mecozzi, S.; Dougherty, D. A. *J. Phys. Org. Chem.* **1997**, *10*, 347. (b) Hernández-Trujillo, J.; Colmenares, F.; Cuevas, G.; Costas, M. *Chem. Phys. Lett.* **1997**, *265*, 503. (c) Lozman, O. R.; Bushby, R. J.; Vinter, J. G. *J. Chem. Soc., Perkin Trans. 2* **2001**, 1446.
(9) (a) Dunitz, J. D.; Taylor, R. *Chem. Eur. J.* **1997**, *3*, 89. (b) Howard, J. A. K.; Hoy, V. J.; O'Hagan, D.; Smith, G. T. *Tetrahedron* **1996**, *52*, 12613.
(10) Benghiat, V.; Leiserowitz, L. *J. Chem. Soc., Perkin Trans. 2* **1972**, 1778. (b) Bach, A.; Lentz, D.; Luger, P. *J. Phys. Chem. A* **2001**, *105*, 7405.
(11) Otwinowski, Z.; Minor, W. DENZO−SMN, in *Methods in Enzymology, Macromolecular Crystallography, Part A, Vol. 276*; Carter, C. W., Jr.; Sweets, R. M., Eds.; Academic Press: New York, 1997.
(12) Sheldrick, G. M. SHELX-97, *Program for the Solution and Refinement of Crystal Structures*, University of Göttingen, Germany, 1997.
(13) Spek, A. L. PLATON, Bijvoet Center for Biochemical Research, Vakgroep Kristal-en Structure-Chemié, University of Utrecht, The Netherlands, 2002.
(14) The C−C−C−O torsion angle in $C_6F_5CO_2H$ (ref 10) is 30° to avoid intramolecular F···O repulsion. The torsion angle in $C_6F_5CONH_2$ is 41° (this paper).
(15) Monographs on H-bonding: (a) Jeffrey, G. A. *An Introduction to Hydrogen Bonding*; OUP: Oxford, 1997. (b) Desiraju, G. R.; Steiner, T. *The Weak Hydrogen Bond in Structural Chemistry and Biology*; OUP: Oxford, 1999.
(16) Jetti, R. K. R.; Xue, F.; Mak, T. C. W.; Nangia, A. *J. Chem. Soc., Perkin Trans. 2* **2000**, 1223.
(17) Baur, W. H.; Kassner, D. *Acta Crystallogr.* **1992**, *B48*, 356.
(18) Kobayashi, K.; Sato, A.; Sakamoto, S.; Yamaguchi, K. *J. Am. Chem. Soc.* **2003**, *125*, 3035.
(19) Leiserowitz, L.; Hagler, A. T. *Proc. R. Soc. London* **1983**, *A388*, 133.
(20) ref 15a, pp 33−55.
(21) Ito, Y.; Hosomi, H.; Ohba, S. *Tetrahedron* **2000**, *56*, 6833.
(22) March, J. *Advanced Organic Chemistry. Reactions, Mechanisms, and Structure*, 3rd ed.; Wiley: New York, 1985; pp 268−286.
(23) Etter, M. C. *J. Phys. Chem.* **1991**, *95*, 4601.
(24) Steiner, T. *Acta Crystallogr.* **2001**, *B57*, 103.
(25) Sharma, C. V. K. *Cryst. Growth Des.* **2002**, *2*, 465.
(26) (a) Sarma, J. A. R. P.; Desiraju, G. R. J. Chem. Soc., *Chem. Commun.* **1983**, 45. (b) Sharma, C. V. K.; Panneerselvam, P.; Pilati, T.; Desiraju, G. R. *J. Chem. Soc., Perkin Trans. 2* **1993**, 2209. (c) Lynch, D. E.; Smith, G.; Byriel, K. A.; Kennard, C. H. L. *Aust. J. Chem.* **1998**, *51*, 1019.

CG034106S

UM00011759
NOVARTIS EXHIBIT 1517
Novartis v. Regents, IPR2023-01347
Page 505 of 4460

This Page is Inserted by IFW Indexing and Scanning Operations and is not part of the Official Record

BEST AVAILABLE IMAGES

Defective images within this document are accurate representations of the original documents submitted by the applicant.

Defects in the images include but are not limited to the items checked:

- ☐ BLACK BORDERS
- ☐ IMAGE CUT OFF AT TOP, BOTTOM OR SIDES
- ☐ FADED TEXT OR DRAWING
- ☐ BLURRED OR ILLEGIBLE TEXT OR DRAWING
- ☐ SKEWED/SLANTED IMAGES
- ☐ COLOR OR BLACK AND WHITE PHOTOGRAPHS
- ☐ GRAY SCALE DOCUMENTS
- ☐ LINES OR MARKS ON ORIGINAL DOCUMENT
- ☐ REFERENCE(S) OR EXHIBIT(S) SUBMITTED ARE POOR QUALITY
- ☐ OTHER: _____

IMAGES ARE BEST AVAILABLE COPY.
As rescanning these documents will not correct the image problems checked, please do not report these problems to the IFW Image Problem Mailbox.

J|A|C|S
COMMUNICATIONS

Published on Web 06/21/2003

Crystal Engineering of Novel Cocrystals of a Triazole Drug with 1,4-Dicarboxylic Acids

Julius F. Remenar,*,† Sherry L. Morissette,† Matthew L. Peterson,† Brian Moulton,‡ J. Michael MacPhee,† Héctor R. Guzmán,† and Örn Almarsson†

Transform Pharmaceuticals, Inc., 29 Hartwell Avenue, Lexington, Massachusetts 02421-3102, and Department of Chemistry, University of South Florida, Tampa, Florida 33620-5205

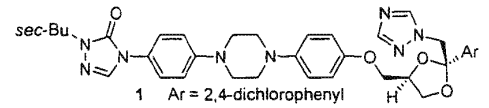
Received April 24, 2003; E-mail: jremenar@transformpharma.com

Crystal engineering of pharmaceutical solids represents a fertile, emerging area of research.[1,2] The impetus for discovery of diverse crystal forms of drugs stems from the critical need to balance stability, bioavailability, and other performance characteristics, and also to provide valuable intellectual property protection. In the case of poorly water-soluble drugs, the dissolution rate and oral absorption of the compound can be strongly influenced by the physical state of the drug.[3] Current strategies to deal with inadequate solubility, dissolution rate, and absorption of neutral crystal forms include salt formation,[4] physical stabilization of amorphous solids,[5] complexation,[6-8] or encapsulation of organic solutions.[9] The use of a crystalline solid is nearly always the best approach for limiting physical and chemical instability of a marketed drug.[5] In addition to stability and bioavailability, crystal form characteristics such as morphology and moisture sorption can impact pharmaceutical development. The challenges of pharmaceutical research and development provide a unique opportunity to showcase the power and utility of crystal engineering to solve real-world problems.[10]

Itraconazole (1) is an example of an extremely water-insoluble antifungal drug that is marketed in the amorphous form (Sporanox capsule) to achieve the required oral bioavailability (Table 1).[11] Co-administration of acidic beverages with Sporanox capsules is required to achieve maximum absorption of the weak base.[12] Although the use of an acid addition salt would seem to be a logical strategy for improving the absorption properties of **1**, a survey of the patent literature failed to reveal specific reports of crystalline salts of **1**. Solution chemistry suggests that a pK_a difference of two units between acid and base is needed to form a salt that is stable in water.[13] Given the pK_a value of 3.7 for the piperazine of **1**, conventional wisdom would limit a salt screen to those strong acids having dissociation constants below 1.7. However, recent examples[1,2] illustrate that crystalline phases can be engineered by combining molecules[14] selected to match hydrogen-bond donors with acceptors and by considering structural complementarities. In short, it is becoming clear that supramolecular synthesis[15] can be applied to active pharmaceutical ingredients in the same way that it has been applied in model compounds.[16] These systems, referred to as cocrystals, could be extended to include organic acid and base combinations with pK_a differences that are inconsistent with salt formation in water. On the basis of these premises, a high-throughput (HT) crystallization screen was conducted to search for salts and cocrystals of **1** with a large number of pharmaceutically acceptable acids, which were chosen to provide a wide range of dissociation constants, shapes, sizes, and heterosynthons.

We report here the discovery of stable cocrystals consisting of hydrogen-bonded trimers of two molecules of **1** and one molecule of a 1,4-dicarboxylic acid resulting from a HT crystallization screen

Table 1. Cocrystal Forms of *cis*-Itraconazole (**1**)



1 Ar = 2,4-dichlorophenyl

[**1**]$_2$X	X	[**1**]$_2$X	X
2a	fumaric acid	**2d**	L-tartaric acid
2b	succinic acid	**2e**	D-tartaric acid
2c	L-malic acid	**2f**	DL-tartaric acid

for **1**. The crystal structure of one congener (Figure 1) reveals an unanticipated and specific interaction between the triazole of **1** and the diacid in the solid state, which suggests a new heterosynthon for cocrystallizing triazole-containing compounds into binary (and potentially higher order) phases.[17]

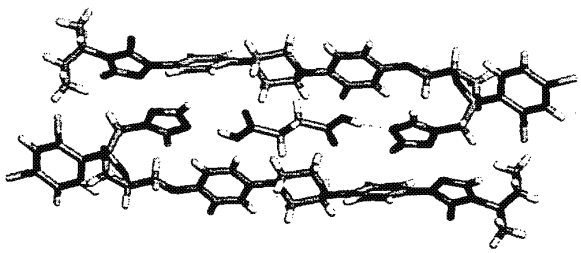


Figure 1. Trimer unit of **2b** from the single-crystal X-ray structure.

Multicomponent crystals of **1** formed from polar aprotic solvents or solvent mixtures of hydrocarbons with polar aprotic solvents and required the presence of dicarboxylic acids. Polar protic solvents, including water and C_{1-3} alcohols, yielded only crystalline free base of **1**, suggesting that H-bond donating solvents interfere with cocrystal formation. Likewise, no salts or cocrystal forms of **1** were found with monoprotic carboxylic acids, such as acetic and benzoic acid. The ratio of **1** to diacid in the binary phases of **1** with fumaric acid (**2a**) and DL-tartaric acid (**2f**) was shown to be 2:1 by solution ^{1}H NMR of dissolved crystal samples. Thus, it appeared that 1 equiv of a dicarboxylic acid was tethering two drug molecules. Additional diacid−**1** combinations, selected on the basis of their similarity to fumaric and tartaric acid, containing 0.5 equiv of diacid relative to **1** yielded crystalline compounds **2b**−**2e** from THF. Compound **2b** is perhaps the most surprising of these, because succinic acid has pK_a values of 4.2 and 5.6, both of which exceed the pK_a of the conjugate acid of **1**. Maleic acid, with *Z* regiochemistry around the C=C bond, is the only 1,4-dicarboxylic acid tested that has not produced cocrystals with **1**, despite being the strongest acid (pK_{a1} of 1.9). Cocrystals could not be made with **1** and malonic, glutaric, or adipic acid. The results indicate that

† Transform Pharmaceuticals, Inc.
‡ University of South Florida.

10.1021/ja035776p CCC: $25.00 © 2003 American Chemical Society

UM00011761
NOVARTIS EXHIBIT 1517
Novartis v. Regents, IPR2023-01347
Page 507 of 4460

geometric fit may be more important than acid−base chemistry in directing crystallization of **1** with 1,4-dicarboxylic acids.

Hexagonal platelike crystals of **2b** were grown for single-crystal X-ray structure determination from a solution in 10/2/1 1,2-dichloroethane/ethyl acetate/1,4-dioxane. Figure 1 shows the trimeric building block from the single-crystal structure. The two molecules of **1** are oriented in antiparallel fashion to form a pocket with a triazole at either end. The extended succinic acid molecule fills the pocket, bridging the triazole groups.[18] Interestingly, interaction between the 1,4-diacid and the strongest base on **1** (piperazine) is absent in the structure of **2b**, but we cannot rule out an interaction of the α hydroxyl groups on tartaric or malic acid with the piperazine nitrogens.[19] There are no current examples of a 1,2,4-triazole-1,4-dicarboxylic acid cocrystal structure in the Cambridge Structural Database (CSD).[20] It should be noted that the crystal structure contains only two of the four stereoisomers of **1**; studies probing enantiomeric enrichment are ongoing.

Identification of multiple crystal forms of the same drug with acceptable solubility, dissolution, and stability allows for selection of the optimal form for dosage form development. To demonstrate this feature, the dissolution of the cocrystals in aqueous medium was studied to assess their potential impact on bioavailability of the drug from a solid dosage form. Figure 2 compares the dissolution profiles of **2b**−**d** into 0.1 N HCl to those of crystalline **1** (95% of all crystalline particles < 10 μm) and commercial Sporanox beads (amorphous **1**). Crystal form **2c** rivals the dissolution of the commercial product containing amorphous **1**. In general, the cocrystals behave more similarly to Sporanox than to crystalline **1**. The cocrystal forms achieve and sustain from 4- to 20-fold higher concentrations than that achieved from crystalline **1**. The practical implication is significant, because the ability to form a supersaturated solution, even transiently, can have a dramatic impact on absorption and bioavailability.[21]

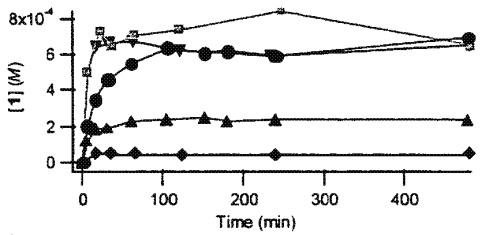


Figure 2. Dissolution profiles into 0.1 N HCl at 25 °C for Sporanox beads (■), **2c** (▼), **2d** (●), **2b** (▲), and **1** (◆).

Crystal morphology and particle size are important for handling of a drug substance and for reliable manufacture of dosage forms with uniform drug content. The morphology of the cocrystals of **1** ranges from fine needles for **2a** and **2d**−**f**, to needles or rectangular plates for **2c**, and hexagonal plates for **2b**. Form **2b** is particularly easy to filter and dry to a free-flowing powder.

In conclusion, cocrystals of **1** possessing diverse physical properties have been engineered on the basis of structures identified from HT crystallization. The solubility and dissolution properties of cocrystals can be similar to those of the amorphous compound and superior to the crystalline pure phase, thus presenting opportunities to increase bioavailability even in cases where stable, crystalline salt forms cannot be found. It is clear that satisfying the geometric constraints is a criterion of cocrystal formation and must be considered when attempting to tailor crystal forms. The observation that the acid moieties in **2b** do not associate with the strongest base in **1** is inconsistent with the principle of strongest-to-strongest interactions dominating self-assembly.[22] Differences in pK_a in water may not reliably predict interactions in the solid state or the capacity for a drug and salt-former to form cocrystals. Thus, studies limited to systems that follow the generally accepted rules of matching pK_a values to ensure a strong salt pair in water are likely to overlook real opportunities for producing optimal medicines with minimal process and formulation issues.

Acknowledgment. The authors wish to thank Profs. Joël Bernstein, Leslie Leiserowitz, and Roger Davey for helpful discussions.

Supporting Information Available: Micrographs and powder X-ray diffraction patterns for **2a**−**2f** (PDF); crystallographic data from **2b** (CIF). This material is available free of charge via the Internet at http://pubs.acs.org.

References

(1) Walsh, B. R. D.; Bradner, M. W.; Fleischman, S.; Morales, L. A.; Moulton, B.; Rodríguez-Hornedo, N.; Zaworotko, M. J. *Chem. Commun.* **2003**, 186−187.
(2) Oswald, I. D. H.; Allan, D. R.; McGregor, P. A.; Motherwell, W. D. S.; Parson, S.; Pulham, C. R. *Acta Crystallogr., Sect. B: Struct. Crystallogr. Cryst. Chem.* **2002**, *B58*, 1057−1066.
(3) Hörter, D.; Dressman, J. B. *Adv. Drug Delivery Rev.* **1997**, *25*, 3−14.
(4) *Handbook of Pharmaceutical Salts*; Stahl, P. H., Wermuth, C. G., Eds.; Verlag Helvetica Chimica Acta; Zürich and Wiley-VCH: Weinheim, 2002; Chapter 6.
(5) Byrn, S. R.; Pfeiffer, R. R.; Stowell, J. G. *Solid-State Chemistry of Drugs*; SSCI Inc.: West Lafayete, IN, 1999; p 250.
(6) Kataoka, K.; Harada, A.; Nagasaki, Y. *Adv. Drug Delivery Rev.* **2001**, *47*, 113−131.
(7) Loftsson, T.; Brewster, M. E. *J. Pharm. Sci.* **1996**, *85*, 1017−1025.
(8) Uekama, K.; Otagiri, M. *Crit. Rev. Ther. Drug Carrier Syst.* **1987**, *3*, 1−40.
(9) Walker, S. E.; Ganley, J. A.; Bedford, K.; Eaves, T. *J. Pharm. Pharmacol.* **1980**, *32*, 389−393.
(10) Seddon, K. R.; Zaworotko, M. *Crystal Engineering: The Design and Application of Functional Solids*; NATO-ASI Series; Kluwer: Norwell, MA, 1999; Vol. 539.
(11) Sporanox capules (made by Janssen Pharmaceutica) contain amorphous itraconazole coated on 0.4−0.5 mm diameter sucrose spheres. Other inactive ingredients include hydroxypropyl methylcellulose, poly(ethylene glycol) (PEG) 20 000, and starch.
(12) Only about 30% bioavailability of **1** is achieved from commercial Sporanox capsules under optimal conditions, while up to 55% can be absorbed from the marketed solution formulation in acidified HP-β-cyclodextrin (Physician's Desk Reference, Electronic Library, Thomson MicroMedex Inc., 2003).
(13) Serajuddin, A. T. M.; Pudipeddi, M. In *Handbook of Pharmaceutical Salts*; Stahl, P. H., Wermuth, C. G., Eds.; Verlag Helvetica Chimica Acta; Zürich and Wiley-VCH: Weinheim, 2002; p 138.
(14) Aakeröy, C. B.; Beatty, A. M.; Helfrich, B. A. *Angew. Chem., Int. Ed.* **2001**, *40*, 3240−3242.
(15) Desiraju, G. R. *Angew. Chem., Int. Ed. Engl.* **1995**, *34*, 2311−2327.
(16) Moulton, B.; Zaworotko, M. J. *Chem. Rev.* **2001**, *101*, 1629−1658.
(17) $2(C_{35}H_{38}Cl_2N_8O_4)\cdot C_4H_6O_4$; $P2_1/c$; a = 30.145(4) Å, b = 5.7435(7) Å, c = 21.580(3) Å, β = 105.133(2)°; Z = 4; T = 100(2) K; GOF = 1.010; R^2 = 0.0925; wR^2 = 0.2153.
(18) The bond distances (N···O = 2.755 Å and (C=O)O−H = 0.925 Å) and the N···H−O bond angle (170.4°) are consistent with a hydrogen-bonding interaction between the 4-nitrogen of each 1,2,4-triazole and a carboxylic acid moiety. The carboxylic acid bond distances (C1B···O1B = 1.205(5) Å and C1B···O2B = 1.326(4) Å) indicate that the acid proton has not been transferred to the triazole. Furthermore, a peak consistent with intensity normally observed for protons was located from the difference map at 0.961(2) Å from O2B along the O2B···N3 vector.
(19) In the crystal structure of Figure 1, the α carbon pro-S hydrogen of succinic acid that is closest to a piperazine nitrogen is 2.65 Å, and the angle is 131°.
(20) A search of the CSD using ConQuest v. 1.5 revealed one example of intermolecular hydrogen bonding between a triazole and a carboxylic acid (REFCODE KOPSOX) and seven examples where a triazole is protonated by a carboxylic acid. There are many examples of hydrogen-bonding interactions between carboxylic acids and heterocyclic nitrogen in the CSD.
(21) Kwei, G. Y.; Novak, L. B.; Hettrick, L. A.; Reiss, E. R.; Ostovic, D.; Loper, A. E.; Lui, C. Y.; Higgins, R. J.; Chen, I. W.; Lin, J. H. *Pharm. Res.* **1995**, *12*, 884−888.
(22) Etter, M. C. *Acc. Chem. Res.* **1990**, *23*, 120−126.

JA035776P

UM00011762
NOVARTIS EXHIBIT 1517
Novartis v. Regents, IPR2023-01347
Page 508 of 4460

This Page is Inserted by IFW Indexing and Scanning Operations and is not part of the Official Record

BEST AVAILABLE IMAGES

Defective images within this document are accurate representations of the original documents submitted by the applicant.

Defects in the images include but are not limited to the items checked:

- ☐ BLACK BORDERS
- ☐ IMAGE CUT OFF AT TOP, BOTTOM OR SIDES
- ☐ FADED TEXT OR DRAWING
- ☐ BLURRED OR ILLEGIBLE TEXT OR DRAWING
- ☐ SKEWED/SLANTED IMAGES
- ☐ COLOR OR BLACK AND WHITE PHOTOGRAPHS
- ☐ GRAY SCALE DOCUMENTS
- ☐ LINES OR MARKS ON ORIGINAL DOCUMENT
- ☐ REFERENCE(S) OR EXHIBIT(S) SUBMITTED ARE POOR QUALITY
- ☐ OTHER: _____

IMAGES ARE BEST AVAILABLE COPY.
As rescanning these documents will not correct the image problems checked, please do not report these problems to the IFW Image Problem Mailbox.

Proc. Natl. Acad. Sci. USA
Vol. 73, No. 11, pp. 3807–3811, November 1976
Chemistry

Crystal structure of a complex between lumiflavin and 2,6-diamino-9-ethylpurine: A flavin adenine dinucleotide model exhibiting charge-transfer interactions

(x-ray crystal structure/hydrogen bonding/ring stacking/base pairing/coenzyme)

F. E. SCARBROUGH, HUEY-SHENG SHIEH, AND DONALD VOET*

Department of Chemistry and Laboratory for Research on the Structure of Matter, University of Pennsylvania, Philadelphia, Pa. 19174

Communicated by Alexander Rich, August 13, 1976

ABSTRACT **The x-ray structure of the deep red crystalline complex lumiflavin-2,6-diamino-9-ethylpurine has been determined. The flavin and adenine derivatives form hydrogen-bonded base pairs of the Watson–Crick type. The molecules in the crystal also associate via extensively overlapped flavin/adenine and flavin/flavin stacking interactions in which there are several contacts that are closer than van der Waals distances. This, together with the red color of the crystals, is indicative of the formation of a charge-transfer complex.**

An intriguing problem of flavin biochemistry is the function of the adenine moiety of FAD. A study of the activity of the flavoenzyme D-amino acid oxidase upon binding adenosyl-modified FAD analogues has shown that this enzyme exhibits considerable specificity with regard to the adenine portion of FAD (1). Yet it is clear that the adenine residue in FAD does not directly affect the oxidation potential of the flavin moiety. It has therefore been suggested that the role of the adenine group in FAD may involve its participation in an intramolecular complex with the flavin moiety (2). This report is concerned with the elucidation of a structural model for such a complex.

The component molecules of Watson–Crick base pairs exhibit a selective affinity in hydrogen bonding that has been observed using infrared studies (3). Thus, uracil derivatives have a higher association constant for binding adenine derivatives than for derivatives of guanine or cytosine (4). The close resemblance of the pyrimidinoid ring of isoalloxazine to uracil suggests that FAD may form a strongly hydrogen-bonded intramolecular complex. This has been confirmed in nonaqueous solutions by infrared studies (5) and in aqueous solutions by nuclear magnetic resonance studies (6). In the solid state, flavin-adenine base pairing of the Hoogsteen variety has been directly observed by x-ray studies of the crystalline complexes of riboflavin with 5′-bromo-5′-deoxyadenosine (2, 7) and with adenine (8).

In aqueous solutions the majority of FAD molecules assume a folded, internally stacked conformation in much the same manner as do oligonucleotides (9). This has been shown by a variety of techniques including fluorescence measurements, both at normal (10) and elevated pressures (11), and by nuclear magnetic resonance measurements (12). The adenine and isoalloxazine derivatives in the above-mentioned structural studies associate by normal stacking interactions (2, 7, 8). There have been occasional reports of charge-transfer bands in the spectra of flavin-purine complexes in solution but it appears that donor–acceptor interactions are unimportant in the stabilization of such complexes (13). Slifkin (14) has reported that evaporating aqueous solutions of purines and riboflavin to dryness yields strongly colored residues that are apparently composed of charge-transfer complexes.

The complexing properties of reduced flavins are less familiar than those of oxidized flavins. Hence in an effort to elucidate the manner in which reduced flavins associate with adenine derivatives we attempted to cocrystallize the relatively air-stable reduced flavin derivative 5-acetyl-1,5-dihydrolumiflavin with the adenine derivative 2,6-diamino-9-ethylpurine. However, preliminary analysis of the resulting crystals indicated that the flavin derivative had lost its acetyl group during the crystallization process to form oxidized lumiflavin. Nevertheless, these crystals are of considerable interest because they are deep red rather than the yellow-brown of the previously reported crystalline riboflavin-adenine complexes. The latter color is characteristic of oxidized neutral flavins.

It will be shown below that in addition to the expected Watson–Crick type base pairs, the lumiflavin and the adenine derivative associate via extensively overlapped flavin/flavin and flavin/adenine stacking interactions. The geometry of these stacking associations is such that the red color of the crystals must be attributed to charge-transfer interactions. Such interactions may have biological significance in reactions mediated by FAD-requiring enzymes.

MATERIALS AND METHODS

The reduced flavin derivative 5-acetyl-1,5-dihydrolumiflavin was synthesized according to the method of Hemmerich and Erlenmyer (15), using lumiflavin that had been synthesized by the procedure of Hemmerich *et al.* (16). The identities of these compounds were confirmed by their infrared spectra (17).

Deep red tabular crystals of the title complex were reproducibly obtained by the evaporation, in air, of dimethylsulfoxide/ethanol solutions containing equimolar amounts of 5-acetyl-1,5-dihydrolumiflavin and 2,6-diamino-9-ethylpurine (Cyclo Chemical Co.). The UV spectrum of a dimethylsulfoxide solution of the red crystals indicated that they contained equimolar quantities of lumiflavin and 2,6-diamino-9-ethyladenine. However, attempts to cocrystallize lumiflavin with 2,6-diamino-9-ethylpurine by the above procedure invariably yielded only a yellow precipitate.

An electron paramagnetic resonance measurement of the red crystals was performed at 300°K and at the temperature of liquid helium by John Salerno and George Reed using a Varian E4 electron paramagnetic resonance spectrometer. In both cases the crystals were found to be diamagnetic.

Preliminary Weissenberg and precession x-ray photographs of the crystals established that their space group is $P2_1/c$. In addition, the intensities of the $h0l$ reflections with h odd are

* To whom correspondence should be addressed.

UM00011764
NOVARTIS EXHIBIT 1517
Novartis v. Regents, IPR2023-01347
Page 510 of 4460

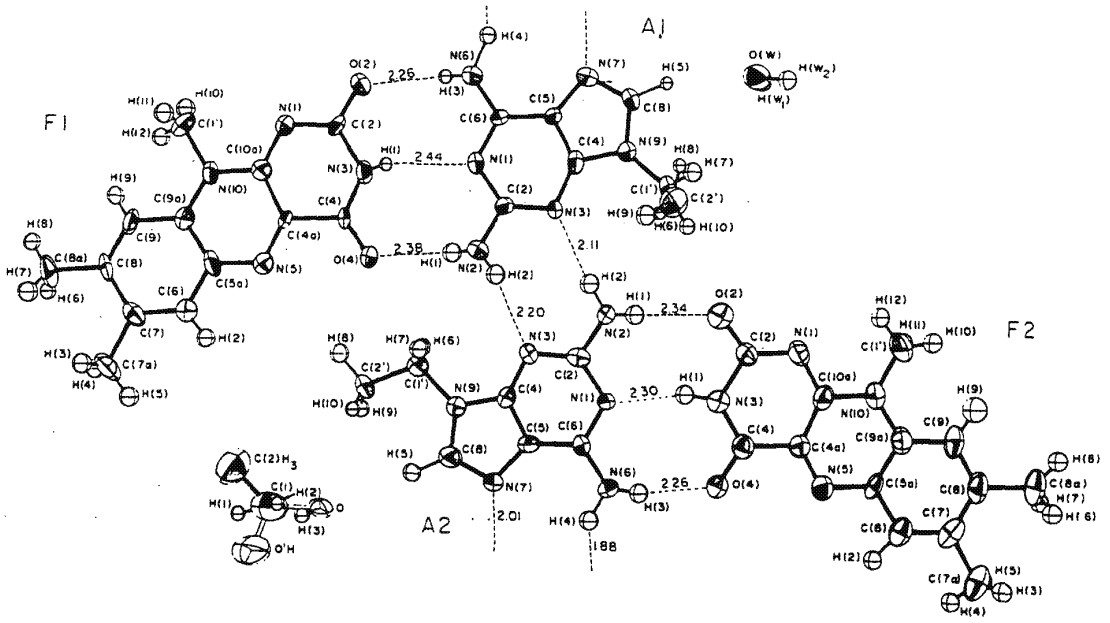


FIG. 1. A perspective drawing of the hydrogen-bonded intermolecular complex between lumiflavin and 2,6-diamino-9-ethylpurine. The atoms are shown as thermal ellipsoids. Hydrogen bonds are represented as broken lines accompanied by their corresponding hydrogen bond lengths in Å. The bonds to each of the half-weighted ethanol hydroxyl groups are unfilled.

systematically weak. This indicates that the crystal has a noncrystallographic *a* glide plane.

All further x-ray measurements were made using a Picker FACS-I diffractometer equipped with a pyrolytic graphite monochromator and employing Cu Kα radiation. The unit cell dimensions, as determined by the least-squares fit of the angular positions of 12 reflections are $a = 16.479(7)$, $b = 13.613(5)$, $c = 22.214(8)$, Å and $\beta = 115.92(3)°$. The density of the crystals, as determined by flotation in a CCl_4/*n*-hexane mixture, is 1.382 g/cm^3. This is in agreement with the contents of the asymmetric unit of the unit cell being (lumiflavin)$_2$-(2,6-diamino-9-ethylpurine)$_2$-H_2O-ethanol ($C_{42}H_{52}N_{20}O_6$). The water molecule was undoubtedly absorbed from the air by the hygroscopic solution from which the crystals were grown.

A detailed description of the techniques used in intensity measurement, data treatment, structure determination, and parameter refinement will appear elsewhere†. A total of 7137 unique reflections was measured to the limit $2\theta = 125°$ using the 2θ scan method. Of these, 2840 had $I < 2.33\sigma(I)$ and hence were considered to be unobserved. The distribution of the intensity data indicated the presence of extensive hypersymmetry. Many of the calculated normalized structure factors were unusually large, e.g., five of them had $E > 6.0$.

The structure was solved, with considerable difficulty, by direct methods. Initial isotropic refinement of the structure lead to the location of a water molecule and an ethanol molecule in which the hydroxyl group was disordered between two positions. Further refinement of the structure, in which the thermal parameters of the nonhydrogen atoms were varied anisotropically and those of the hydrogen atoms, which had been located in difference Fourier maps, were varied isotropically, reduced the discrepancy index to its final value of $R = \Sigma||F_o| - |F_c||/\Sigma|F_o| = 0.075$ based on only the 3821 observed reflections with $|F_o| > 3.5$.

† F. E. Scarbrough, H.-S. Shieh, and D. Voet, manuscript submitted.

DESCRIPTION OF THE STRUCTURE

The contents of the asymmetric unit and the atomic numbering system used in this report are shown in Fig. 1. The final atomic parameters of the structure together with its covalent distances and angles will be presented elsewhere†. The latter are in excellent agreement with published values of corresponding distances and angles in similar molecules (18, 19). For example, the bond distances of the lumiflavin molecules in the present structure show an average deviation of 0.009 Å from the corresponding average lumiflavin distances as determined by Wang and Fritchie (19). The average differences between the corresponding bond distances and angles of the two chemically equivalent halves of the asymmetric unit are 0.011 Å and 0.9°, respectively, for bonds not involving hydrogen atoms. This is consistent with the finding that the average estimated standard deviations of these bond parameters are 0.007 Å and 0.5°, respectively.

It can be seen from Fig. 1 that the flavin-adenine complex is characterized by hydrogen-bonded base-pairing interactions between its component molecules. Thus, flavin F2 forms a Watson–Crick type base pair with adenine derivative A2. The amine group substituent to atom C(2) of the adenine derivatives permits the formation of a third hydrogen bond that is not possible in the normally doubly hydrogen-bonded adenine-uracil base pairs. Flavin F1 and adenine A1 form a similar triply hydrogen-bonded base pair but one in which the orientation of A1 with respect to F1 has been reversed relative to that of the A2-F2 interaction. It is this alternation in the orientations of the adenine derivatives together with the placement of the water and ethanol molecules that constitute the greatest deviations of the structure from exact *a* gide symmetry.

The adenine derivatives also self-associate via base pairing

UM00011765
NOVARTIS EXHIBIT 1517
Novartis v. Regents, IPR2023-01347
Page 511 of 4460

to form endless ribbons of the sort···A1·A2·A1·A2···. Here the adenine derivatives hydrogen bond across pseudo centers of symmetry that are generated by a combination of the crystallographic 2-fold screw axis and the noncrystallographic *a* glide plane. The A1·A2 pairing in which adenine atoms N(6) and N(7) are hydrogen bond donors and acceptors, respectively, is a commonly observed mode of adenine self-association (18). Similarly, the A1·A2 pairing in which atoms N(2) and N(3) are hydrogen bond donors and acceptors, respectively, is often seen in crystal structures containing 2,6-diaminopurine or 2-aminopurine derivatives (18, 20). Alternate adenine molecules in the foregoing endless ribbon are related by the *b* axis translation. The parameters describing the above hydrogen bonds, which are given in part in Fig. 1, are all within the normal ranges observed for such interactions (18, 21). It can be seen from Fig. 1 that the above described interactions exhaust the capacity of the flavin and adenine rings to engage in mutual hydrogen-bonding associations.

The ring molecules of the structure are all very nearly planar. The root mean square deviations of the nonhydrogen atoms of molecules A1, A2, F1, and F2 from their respective least-squares planes [with the exception of adenine atoms C(2′)] are 0.014, 0.015, 0.034, and 0.057 Å. The major distortion of lumiflavin F1 is best described as a small twist along its longitudinal molecular axis. That of lumiflavin F2 is largely a fold about its N(5)–N(10) axis. Such distortions are commonly observed in crystal structures of flavin derivatives.

The asymmetric unit of the structure, as is shown in Fig. 1, is very nearly coplanar. These planes of molecules are essentially parallel to and halfway between the 4 0 $\bar{6}$ crystallographic planes. The dihedral angles between the least-squares planes of the component molecules of the A1·F1, the A2·F2, and the A1·A2 base pairs are 4.1°, 6.8°, and 7.7°, respectively. The 62 nonhydrogen atoms comprising the four heterocyclic molecules shown in Fig. 1, less adenine atoms C(2′), have a root mean square deviation of 0.144 Å from their collective least-square plane. The degree of coplanarity of the individual base pairs is typical for such complexes (18). However, the coplanarity of the entire asymmetric unit is remarkable, considering that it extends over rather large lateral distances.

The structure exhibits stacking interactions which are among the most extensive that have been observed in crystal structures containing molecules of the nucleic acid base type (22). Each lumiflavin molecule is bounded on one side by a symmetry nonequivalent lumiflavin molecule and on the other side by a purine ring. In this manner the order of stacking of the molecules is $A2/F2^{a}/F1^{b}/A1^{c}$, where the superscripts refer to the molecules related to those in Fig. 1 by (a) a center of symmetry, (b) a 2-fold screw axis, and (c) a *c* glide plane. The geometry of these stacking interactions, in the order described, can be seen in Fig. 2a–c.

The F2/F1 stacking interaction, which is illustrated in Fig. 2b, is perhaps the most striking intermolecular association in the structure. It can be seen that the two lumiflavin molecules, which are related by a pseudo center of symmetry, and which have a mutual dihedral angle of 4.3°, stack such that there is extensive overlap between the two molecules. The average perpendicular distance of the atoms of lumiflavin F2 from the least-squares plane of lumiflavin F1 is 3.31 Å. There are eight interatomic distances in this association that are less than 3.4 Å. Of these, the F1C(4)–F2C(9a), the F1C(6)–F2C(2), and the F1C(2)–F2C(6) contacts of 3.317, 3.335, and 3.338 Å are less than the minimum van der Waals C–C distance of 3.4 Å (23).

Fig. 2c illustrates the F1/A1 stacking interactions. The two

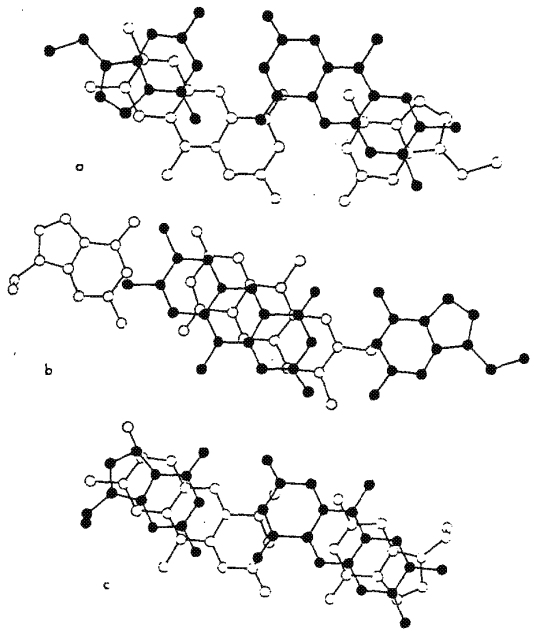


FIG. 2. Projections onto the planes of the aromatic rings of two consecutive molecular layers illustrating the stacking relationships between (a) two centrosymmetrically related F2·A2 complexes; (b) the pseudo centrosymmetrically related F2·A2 and F1·A1 complexes; and (c) two centrosymmetrically related F1·A1 complexes. The atoms are represented as spheres of arbitrary radii. Hydrogen atoms have been omitted for the sake of clarity.

F1·A1 base pairs shown in this figure are related by a crystallographic center of symmetry. The long axes of the adenine and flavin molecules are parallel. The adenine derivative exhibits extensive overlap with the benzenoid ring of the lumiflavin molecule. The interplanar separation in this interaction is 3.35 Å and it has three interatomic approaches that are less than 3.4 Å. One of them, the F1C(5a)–A1C(6) contact of 3.338 Å, is less than the minimum van der Waals C—C distance. Fig. 2c also shows a second type of lumiflavin/lumiflavin stacking interaction in which flavin atoms C(2), N(3), C(4), and O(4) overlap across a center of symmetry. The smallest interatomic distance here is the 3.264 Å N(3)–C(4) contact.

Fig. 2a shows a second lumiflavin/adenine stacking association in which two F2·A2 base pairs are related by a crystallographic center of symmetry in much the same manner as are the previously discussed F1·A1 base pairs. However, the long axes of the adenine and flavin molecules in the F2/A2 stack are not parallel as they are in the F1/A1 stack. Nevertheless, there is considerable similarity in the geometry of these two independent flavin/adenine stacking interactions. Thus, in the F2/A2 stack, the purine molecule and the benzenoid ring of the lumiflavin molecule also exhibit extensive overlap. The interplanar distance here is 3.42 Å, with three interatomic approaches and under 3.4 Å. Of these, the F2C(5a)–A2C(6) contact of 3.357 Å is less than the minimum C–C van der Waals distance. It should be noted that this same contact in the F1/A1 stack is also less than the minimum van der Waals distance.

A third lumiflavin/lumiflavin interaction is also shown in Fig. 2a. In this case atoms of the C(4)–O(4) carbonyl groups of flavin F2 interact across a center of symmetry, thereby making

UM00011766

NOVARTIS EXHIBIT 1517
Novartis v. Regents, IPR2023-01347
Page 512 of 4460

nonbonding C(4)–O(4) and C(4)–C(4) contacts of 3.118 and 3.260 Å, respectively. The latter contact is significantly less than the minimum C–C van der Waals distance. Such close carbonyl/carbonyl interactions are commonly observed in the structures of compounds, such as the barbiturates, that contain three or more conjugated carbonyl groups (24). However, in all previously observed carbonyl/carbonyl associations the oxygen atoms have not taken part in hydrogen bonding interactions with other heterocycles. In fact, the participation of a carbonyl group in a close carbonyl/carbonyl contact has been taken as an indication that the carbonyl oxygen atom is a poor hydrogen bond acceptor (25). Thus, it is of interest that atom O(4) participates in the F2·A2 base pairing interaction in addition to the carbonyl/carbonyl association.

The cocrystallized solvent molecules are located between the planes of the heterocycles. The disorder of the ethanol molecule caused difficulties in its refinement, as is evidenced by the failure to locate several of its hydrogen atoms. One of the half-weighted ethanol hydroxyl groups forms a hydrogen bond with atom O(2) of flavin F1. The other receives a hydrogen bond from a neighboring water molecule. No other hydrogen bonds appear to be made by the solvent molecules. Therefore, it seems that the solvent molecules are merely occupying cavities in the structure.

DISCUSSION

The base pairing associations of the Watson–Crick type that are illustrated in Fig. 1 were expected on the basis of the similar base pairing geometries of all previously observed crystalline complexes of 2,6-diaminopurine and uracil derivatives (18, 20). In the complexes riboflavin·5′-bromo-5′-deoxyadenosine (2, 7) and riboflavin·adenine (8) the flavin and adenine moieties associate as Hoogsteen base pairs in which flavin atom O(2) is the hydrogen bond acceptor. Model building studies using space filling models indicate that FAD could form an intramolecularly hydrogen-bonded complex with any of the foregoing base pairing configurations. The nuclear magnetic resonance studies by Raszka and Kaplan (6) indicate that FAD forms an internally hydrogen-bonded complex in aqueous solutions. These authors suggest that this complex is of the Hoogsteen variety in which flavin atom O(4) is a hydrogen bond acceptor. However, there is no strong evidence that favors any of the four possible intramolecular base pairing configurations for FAD over one another.

The fact that we were unable to crystallize the present complex from solutions containing lumiflavin but could reproducibly do so from solutions containing 5-acetyl-1,5-dihydrolumiflavin suggests the possibility that the deep red color of the crystalline complex is due to the presence of diradicals. However, this hypothesis must be rejected in light of the observed diamagnetism of the crystals at 300°K as well as at liquid helium temperatures. Therefore, the color of the crystals and the close proximity of the atoms in neighboring molecular layers together with the regular packing of these layers (see below) indicate that the molecules in the crystal associate via charge-transfer interactions.

The regularity of the base-stacking pattern observed in the present strucure is unique among the crystal structures of nucleic acid bases and their analogues (22). All of the hexagonal rings in the structure, including those that are formed by hydrogen bonds, are in almost parallel orientations so as to form noncrystallographic hexagonal nets. Such a net can be visualized in Fig. 1. Neighboring hexagonal nets remain very nearly in register, that is, the atoms of the hexagonal rings in one plane of molecules lie almost directly over the intersections of the adjacent hexagonal nets. This is seen in Fig. 2. Furthermore, the atoms comprising the imidazole rings of the purine derivatives depart only slightly from the hexagonal pattern. It is this noncrystallographic regularity of the structure that is responsible for the large values of some of the normalized structure factors and for the difficulties in solving the structure.

Stacking regularities such as the foregoing have been observed in several flavin-containing charge-transfer complexes such as 10-propylisoalloxazine bis(naphthalene-2,3-diol) (26), lumiflavin bis(naphthalene-2,3-diol) trihydrate (27), and riboflavin dihydrobromide·hydroquinone (28). Somewhat less symmetrical associations are seen in the similar charge-transfer complexes lumiflavinium bromide·hydroquinone (29) and lumiflavinium chloride·hydroquinone (30). The interplanar spacings in all of these highly colored donor–acceptor complexes are less than the 3.4 Å distance expected for normal stacking interactions.

The previously discussed riboflavin·adenine complexes (2, 7, 8), which show no sign of charge-transfer interactions, exhibit unsymmetrical stacking associations. Flavins that stack in a regular pattern have been observed in the crystal structures of several flavin derivatives. These compounds include 1,10-ethylene-7,8-dimethylisoalloxazinium iodide monohydrate (31) and 9-bromo-3, 7, 8, 10-tetramethylisoalloxazine monohydrate (32). However, there are no close intermolecular spacings in these structures nor are there any other indications that these flavins associate via charge-transfer interactions.

The net atomic charges of adenine (33) and isoalloxazine (34) have been estimated by semi-empirical molecular orbital calculations. This information, taken together with the F1/F2, the F1/A1, and the F2/A2 stacking patterns illustrated in Fig. 2, indicates that these stacking associations are characterized by lack of strong Coulomb interactions. Therefore, it appears that these stacked complexes are stabilized by donor–acceptor interactions together with the more prosaic nonbonding forces such as van der Waals interactions. It is, of course, not possible from this study alone to determine the relative contributions of these various types of interactions to the overall stabilities of the stacked complexes. However, the fact that charge-transfer interactions are not observed in other crystalline flavin-adenine complexes (2, 7, 8) suggests that such forces are not major contributors to the stability of the present complex. This is in agreement with the conclusion of Slifkin that the characteristics of charge-transfer complexes are highly dependent on the relative orientations of the donor and acceptor and on the contribution of other weak binding forces to the total potential energy of the complex (13).

The present study constitutes structural information pertaining to the nature of flavin–adenine and flavin–flavin charge-transfer interactions. It would be of interest to ascertain the biological significance of these interactions. It seem doubtful that charge-transfer forces contribute significantly to the binding of flavins to an enzyme or a substrate (35). However, even a rather minor reduction of the activation energy of a chemical reaction can significantly accelerate that reaction. Therefore, an intramolecular charge-transfer complex in FAD may have a catalytic role in certain flavoenzyme-mediated reactions (35). Similarly, a flavin–flavin charge-transfer interaction may be of importance in flavoenzymes that utilize multiple nonequivalent flavin coenzymes.

We would like to thank Drs. John Salerno and George Reed for making the electron paramagnetic resonance measurements. This research was supported, in part, by grants from the National Institutes of Health (GM 18632 and AM 05105) and the National Science Foundation (DMR72-03025).

UM00011767
NOVARTIS EXHIBIT 1517
Novartis v. Regents, IPR2023-01347
Page 513 of 4460

1. McCormick, D. B., Chassy, B. M. & Tsibris, J. C. M. (1964) *Biochim. Biophys. Acta* 89, 447–452.
2. Voet, D. & Rich, A. (1971) in *Flavins and Flavoproteins*, ed. Kamin, H. (University Park Press, Baltimore, Md.), Vol. 3., pp. 23–33.
3. Hamlin, R. M., Jr., Lord, R. C. & Rich, A. (1965) *Science* 148, 1734–1737.
4. Kyogoku, Y., Lord, R. C. & Rich, A. (1966) *Science* 154, 518–520.
5. Kyogoku, Y. & Yu, B. S. (1969) *Bull. Chem. Soc. Jpn.* 42, 1387–1393.
6. Raszka, M. & Kaplan, N. O. (1974) *Proc. Natl. Acad. Sci. USA* 71, 4546–4550.
7. Voet, D. & Rich, A. (1971) *Proc. Natl. Acad. Sci. USA* 68, 1151–1156.
8. Tomita, K., Fujii, S., Fujiki, K. & Fujiwara, T. (1975) *Acta Crystallogr. Sect. A* 31, S43–S44.
9. Davis, R. C. & Tinoco, I., Jr. (1968) *Biopolymers* 6, 223–242.
10. Weber, G. (1966) in *Flavins and Flavoproteins*, ed. Slater, E. (Elsevier, Amsterdam), Vol. 1, pp. 15–20.
11. Weber, G., Tanaka, F., Okamoto, B. Y. & Drickamer, H. G. (1974) *Proc. Natl. Acad. Sci. USA* 71, 1264–1266.
12. Sarma, R. H., Dannies, P. & Kaplan, N. O. (1968) *Biochemistry* 7, 4359–4367.
13. Slifkin, M. A. (1973) in *Physico-Chemical Properties of Nucleic Acids*, ed. Duchesne, J. (Academic Press, New York), Vol. 1., pp. 67–98.
14. Slifkin, M. A. (1971) *Chem. Phys. Lett.* 9, 416–419.
15. Hemmerich, P. & Erlenmyer, H. (1957) *Helv. Chim. Acta* 40, 180–186.
16. Hemmerich, P., Fallab, S. & Erlenmyer, H. (1956) *Helv. Chim. Acta* 39, 1242–1252.
17. Hemmerich, P., Prijs, B. & Erlenmyer, H. (1960) *Helv. Chim. Acta* 43, 372–394.
18. Voet, D. & Rich A. (1970) *Prog. Nucl. Acid Res. Mol. Biol.* 10, 183–265.
19. Wang, M. & Fritchie, C. J. (1973) *Acta Crystallogr. Sect. B* 29, 2040–2045.
20. Sobell, H. M. (1972) in *The Purines, Theory and Experiment*, eds. Bergmann, E. D. & Pullman, B. (Academic Press, New York), pp. 124–146.
21. Hsu, I.-N. & Craven, B. M. (1974) *Acta Crystallogr. Sect. B* 30, 988–993.
22. Bugg, C. E., Thomas, J. M., Rao, S. T. & Sundaralingham, M. (1971) *Biopolymers* 10, 175–219.
23. Pauling, L. (1960) *The Nature of the Chemical Bond* (Cornell Univ. Press, Ithaca, N.Y.).
24. Voet, D. (1974) in *Molecular and Quantum Pharmacology*, eds. Bergmann, E. D. & Pullman, B. (Reidel, Dordrecht, Holland), pp. 429–439.
25. Epstein, R. H., Zeiger, A. V., Crocker, C. & Voet, D. (1976) *Acta Crystallogr. Sect. B* 32, 2180–2188.
26. Kuo, M. C., Dunn, J. B. R. & Fritchie, C. J., Jr. (1974) *Acta Crystallogr. Sect. B* 30, 1766–1771.
27. Fritchie, C. J., Jr. & Johnston, R. M. (1975) *Acta Crystallogr. Sect. B* 31, 454–461.
28. Bear, C. A., Waters, J. M. & Waters, T. N. (1970) *Chem. Commun.*, 702.
29. Tillberg, O. & Norrestam, R. (1972) *Acta Crystallogr. Sect. B* 28, 890–898.
30. Karlsson, R. (1972) *Acta Crystallogr. Sect. B* 28, 2358–2364.
31. Leijonmarck, M. & Werner, P.-E. (1970) *Acta Chem. Scand.* 24, 2916–2928.
32. von Glehn, M. & Norrestam, R. (1972) *Acta Chem. Scand.* 26, 1490–1502.
33. Song, P. S. (1969) *Ann. N.Y. Acad. Sci.* 158, 410–423.
34. Geissner-Prettre, C. & Pullman, A. (1968) *Theor. Chim. Acta* 9, 279–287.
35. Massey, V. & Ghisla, S. (1973) *Ann. N.Y. Acad. Sci.* 227, 446–465.

UM00011768
NOVARTIS EXHIBIT 1517
Novartis v. Regents, IPR2023-01347
Page 514 of 4460

Pure Appl. Chem. Vol. 27 (1971)

PHOTODIMERIZATION IN THE SOLID STATE

G. M. J. SCHMIDT

Department of Chemistry, Weizmann Institute of Science, Rehovot, Israel

ABSTRACT

Following a brief historical review of solid-state photochemistry current research is discussed under four parallel headings: first, analysis of the *topochemical postulate* according to which the course of the solid-state reaction and the stereochemistry of the photodimer (if any) can be predicted from the configuration and nearest-neighbour geometry of closest monomer molecules in the crystal lattice; secondly, the study of the *locus of the reaction*, that is the dependence of the course of the reaction or (dimerization, *cis* → *trans* isomerization) on crystal texture (dislocation, grain and phase boundaries); thirdly, a better understanding of the *packing principles of organic molecules* in their crystal structure to enable us to construct photoreactive (or lightstable) crystal structures of any given monomer as well as mixed crystals of potentially co-dimerizable monomers for synthetic purposes or energy-transfer studies.

Several approaches to this problem of '*crystal engineering*' based on generalizations of packing modes of primary amides and of dichlorophenyl derivatives are outlined, and their application to a *systematic photochemistry of the solid state* discussed.

I. INTRODUCTION

Thermal reactions of organic compounds in the solid state are nearly as old as organic chemistry itself. Light-induced reactions such as the photodimerization of solid cinnamic acids, the reversible photochromy of the anils of salicylaldehyde, fulgides, tetrachloronaphthoquinone, and other solid-state reactions were already being studied towards the end of the last and the beginning of this century, by Marckwald[1], Ciamician and Silber[2], Stobbe[3], de Jong[4], Senier[5], to mention but a few. By the end of the nineteen-twenties this phase of solid-state chemistry, which I would call the heroic era, had come to an end[6], mainly because physical methods for the description of the solid state were as yet unable to provide insight into the molecular structure of organic solids. Thus, optical crystallography of organic compounds, by then a well established discipline which had passed through an intensive descriptive phase, had not progressed beyond the recognition of structural types in organic chemistry[7]. Treatment of the phenomena of polymorphism and phase transformation had not yet moved from the thermodynamic to the molecular stage. Solid-state chemists and crystallographers of the mid-twenties shared the belief that the phenomena which they were investigating, surely depended upon molecular packing arrangement; some expressed the hope that the novel technique of x-ray structure analysis would provide new impetus to their work.

UM00011769
NOVARTIS EXHIBIT 1517
Novartis v. Regents, IPR2023-01347
Page 515 of 4460

Certain general concepts had nevertheless been formulated already: thus, de Jong postulated in 1923[4] that the two known crystal modifications of *trans*-cinnamic acid comprised identical molecules arranged differently in space, and the stereo-structure of the two photoproducts, α-truxillic and β-truxinic acids, was directly related to the packing geometry of the monomer units in the two crystal structures from which the dimers were derived.

In assessing the more recent history of research on solid-state photochemistry one can, I believe, discern at least four concurrent and connected phases; the first has seen the experimental correlation of crystal structure on the one hand with photo-activity (or -stability) and product structure on the other[8,9]. We may call this *the phase of the topochemical principle.*

The second phase now actively investigated is concerned with the limits of this topochemical correlation of physical structure and chemical behaviour, particularly in the simple equation of physical structure with the crystal lattice as seen by the normal method of x-ray structure analysis. The effect of crystal texture, e.g. disclocations[10–12], is the major trend of this phase. We may call this *the phase of the locus of the solid-state reaction.* The present status of these two phases of solid-state research has provided the basis for the broad generalization that sophisticated solid-state techniques can define the initial state of the photochemical reaction, i.e. the conformation of the photoreactant in its ground state as well as the structure of the rigid matrix surrounding the reactant.

The third and fourth phases are in their infancy; in my view they must aim at the systematic development of solid-state photochemistry as a synthetic tool and as a methodology for the study of the mechanisms of photochemical reactions. To this end organic solid-state chemistry must be placed on a firmer basis. In an earlier review[8] we emphasized the point that the rule of homology which has been essential to the development of solution chemistry does not hold in solid-state chemistry: 'the reactions of homologous compounds, $R'(CH_2)_nR''$, RHal, R^-metal^+ are not necessarily identical for all values of *n*, or for Cl, Br etc., or for Na^+, K^+ etc. Since solid-state reactions are controlled by the molecular packing arrangement which is sensitive to *n*, to the size of the substituent, to the coordination requirements of the cation (to mention but a few factors affecting the structure of organic crystals), generalizations based on one or two representatives of a homologous series can be highly misleading.'

The systematic development of our subject will be difficult if not impossible until we understand the intermolecular forces responsible for the stability of the crystalline lattice of organic compounds; a theory of the organic solid state is a requirement for the eventual control of molecular packing arrangement. Once such a theory exists we shall, in the present context of synthetic and mechanistic photochemistry, be able to 'engineer' crystal structures having intermolecular contact geometry appropriate for chemical reaction, much as, in other contexts, we shall construct organic conductors, catalysts, etc. In short, any rational development of the physics and chemistry of the solid state must be based upon a theory of molecular packing; since the molecules studied are complex, the theory will most likely be empirical for some time yet. Rules are now becoming available[13–16] in what I would regard as phase three, *the phase of crystal engineering.*

UM00011770
NOVARTIS EXHIBIT 1517
Novartis v. Regents, IPR2023-01347
Page 516 of 4460

Given the observation that double bonds separated by a translation axis of 4 Å can undergo cyclodimerization one might want to construct crystal structures in which this 4 Å axis is predictably achieved for as large a class of unsaturated compounds as possible. A technique which could impose this β-type packing (or any other specified packing arrangement) by means of a simple chemical modification without affecting the photochemical process would be such a desirable goal. It would stimulate phase four, *the phase of systematic solid-state photochemistry*.

Once the solid-state chemist has the tools with which to control molecular packing arrangements he will be able to follow new lines of experimentation which so far have been largely denied to him. He will construct two-component single-phase systems of definable structure such as substitutional solid solutions; thus, experiments on energy transfer in the undisturbed crystal structure, so far confined to transfer between normal and deuterated molecules, the classical example of the use of solid solutions in photochemical work[17], will be extended, both for mechanistic and synthetic purposes, to molecules of greater variation. In this manner experiments on solid-state sensitization will become possible once a structured solid solution of monomer and sensitizer can be obtained. On the synthetic side mixed dimers of predictable stereochemistry will become accessible. Other lines of work are conceivable, and some of them will be discussed below.

Having tried to place solid-state photochemical research into a somewhat personal perspective I should now like to review very briefly phase one, discuss at some length phase two, and present current work in phases three and four.

II. THE TOPOCHEMICAL ARGUMENT

The classes of photodimerizable compounds to which the topochemical rules apply, have been summarized in a paper submitted to the Solvay meeting on the Photo-excited Organic Molecule in 1967 and published in condensed form[8]; there is no need to quote this material in detail. More recent and unpublished material will be referred to below.

The very high yield of C_4-dimer (up to 90 per cent) from α,β-unsaturated carbonyl compounds, and its equally high sterical purity, particularly as compared with solution reactions, strongly argue for effective lattice control over the dimerization reaction. Its all-or-none-nature, i.e. photoreactivity or light-stability, is further evidence. Finally, dependence of reactivity and of the stereostructure of the product on the structure of each of the polymorphic crystalline phases of a given monomer is proof positive for the inter-relationship of crystal structure and reaction course.

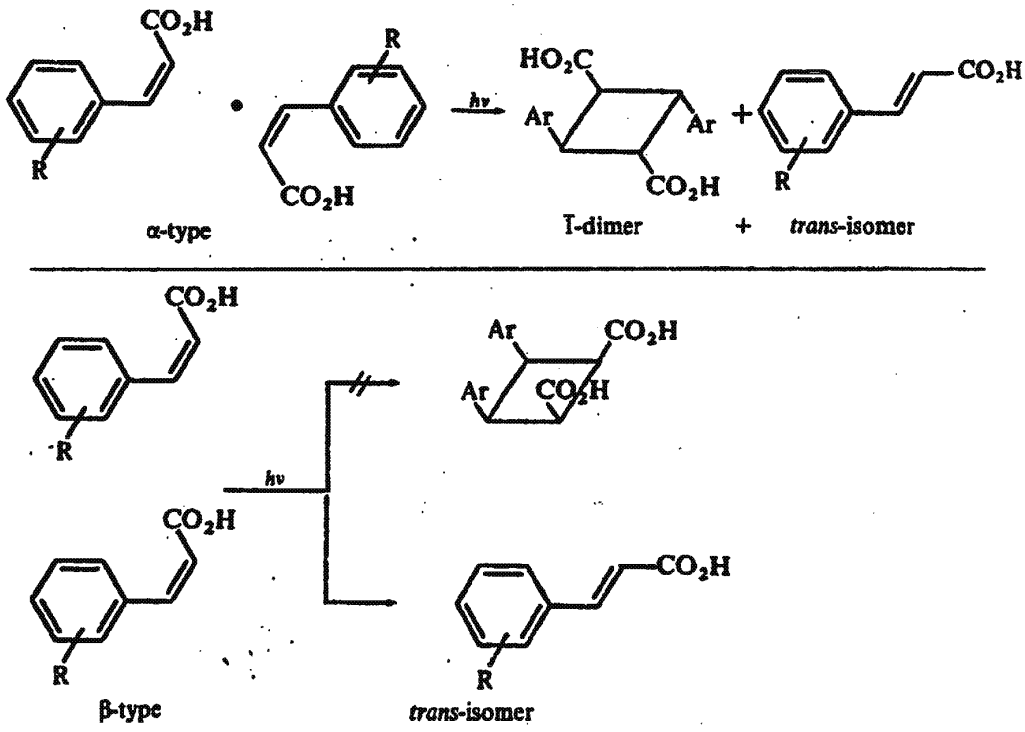
The topochemical rules state that the stereochemistry of the dimer ($\bar{1}$ or *m*) is determined by the contact geometry [antiparallel (i.e. related by a crystallographic centre of symmetry) or parallel (i.e. related by a translation axis)] of nearest-neighbour double bonds, provided that the centre-to-centre distance *d* of these double bonds is of the order of 4 Å (experimentally observed limits $4.2 > d > 3.5$ Å)†.

† The limit of 4.2 Å is set by the *absence of experimental data* in the range 4.2 to 4.7 Å, and is not to be construed necessarily as an upper limit of dimerizability. At 4.7 Å and above reaction does not take place.

UM00011771
NOVARTIS EXHIBIT 1517
Novartis v. Regents, IPR2023-01347
Page 517 of 4460

The structure of the cyclodimers correlates very well with the contact geometry of nearest-neighbour monomer molecules in the reactive crystal structures of *trans*-configurated Ar.CH:CH.COR systems where Ar = C_6H_5 and substituted phenyl, 2-furyl, 2-thienyl, pyridyl and R = OH,OMe,OAr, NH_2, NHR, Ar[18-20] and of β-unsaturated lactones (coumarins)[21], lactams (e.g. pyrimidines)[22], and *p*-quinones[23]. The photobehaviour of fumaric acid derivatives[24,25] including fumaronitrile follows the topochemical rules, as do the symmetrically and unsymmetrically substituted 1,4-butadiene derivatives *trans,trans*- and *cis,cis*-muconic acids (including derivatives of the former)[26], sorbic acid and sorbamide[27] (see below).

There is evidence from the solid-state chemistry of *p*-quinones that the formation of oxetanes follows the topochemical requirement of proper parallel alignment of >C=C< and >C=O bonds[23]. More recently, substituted *trans*-stilbenes[28] and *trans,trans*-1,4-diphenylbuta-1,3-dienes[29] have been shown to undergo topochemically controlled dimerization indicating that the carbonyl-function is not an essential feature of C_4-cyclodimerization in the solid state.



Scheme 1. The solid-state photochemistry of *cis*-cinnamic acids

There is limited evidence that close centrosymmetric contact of *cis*-cinnamic acids can give the Ī-dimer, and very much stronger evidence that close translational packing of *cis*-cinnamic acids does not yield the all-*cis*-cyclobutane of symmetry *m*; in both packing types the *cis*-acids undergo

UM00011772
NOVARTIS EXHIBIT 1517
Novartis v. Regents, IPR2023-01347
Page 518 of 4460

isomerization to the *trans*-cinnamic acid[30] (*Scheme 1*). Topochemical dimerization of *cis*-configurated double bonds is observed in non-aromatic systems such as *cis,cis*-muconic acid.

In summary, *planar* or *near-planar* monomers having appropriate packing geometry give the anticipated cyclobutane with retention of configuration of monomer geometry. *Non-planar* molecules (e.g. *cis*-cinnamic acids, β-chloro-, bromo- and methyl-*trans*-cinnamic acids) undergo in the main *trans,cis* isomerization. The photochemistry of anthracene derivatives, that is cyclization to dianthracenes, is discussed below.

We now ask how precisely the π-electron system of two double bonds must be aligned for reaction to occur. Several lines of approach to this question have been followed: In the methyl ester of *m*-bromo-cinnamic acid[31] the contact geometry of the double bonds of adjacent molecules is unusual (*Figure 1*): the centre-to-centre distance of $\rangle C{=}C\langle$ groups in glide-plane related molecules is short (3.93 Å); however, the double bonds are not parallel. After irradiation over long periods during which substituted methyl cinnamates packing in the β-type have been completely dimerized, the material is essentially unchanged[32].

Another demonstration of this point is provided by the photostability of the α,ω-diphenyl-all-*trans*-polyenes. As an example we show the packing arrangement of the octatetraene[33] in *Figure 2*. The molecules, occupying centres of symmetry and being glide-plane related in space group *Pbca*, are not parallel; distances between carbon *atoms* such as C(7)···C(7) are short (3.7 Å), but the separation of *centres* of double bonds is greater than 4.8 Å throughout the crystal structure. Photoreaction does not occur; instead the material and its homologues in closely related crystal structures fluoresce very strongly. The observation[29] that diphenylbutadienes in the 4 Å packing arrangement yield photodimers, eliminates the possible argument that these polyenes are intrinsically incapable of dimerization in the solid state.

The specificity of molecular contact geometry required for dimerization in the rigid phase is well demonstrated by the photobehaviour of *cis*-cinnamic acids. We have earlier reported[30] that the photoreaction of *cis*-cinnamic acids leads to *trans*-acids and the topochemical photoproducts of the latter, and concluded that this process takes place in the sequence of events in equation 1

$$\{cis\} \xrightarrow{h\nu} \{cis,trans\} \rightleftharpoons \{cis\} + \{trans\} \qquad (1)$$

photoproducts of the crystal forms of *trans*-acids

that is, the *trans*-isomer is formed in solid solution within the *cis*-lattice from which it separates in a thermally controlled recrystallization step into its own lattice. There was no evidence of cross-dimers from a molecule each of *cis*- and *trans*-cinnamic acid, although the latter was clearly located in the immediate neighbourhood of the former. To check this point two systems were investigated in quantitative detail[34], see *Schemes 1* and *2* overleaf. (1) is partially converted to the *cis*-isomer (2) which is light-stable in its own crystal structure, and partially dimerized to centrosymmetric cyclobutane (3).

UM00011773
NOVARTIS EXHIBIT 1517
Novartis v. Regents, IPR2023-01347
Page 519 of 4460

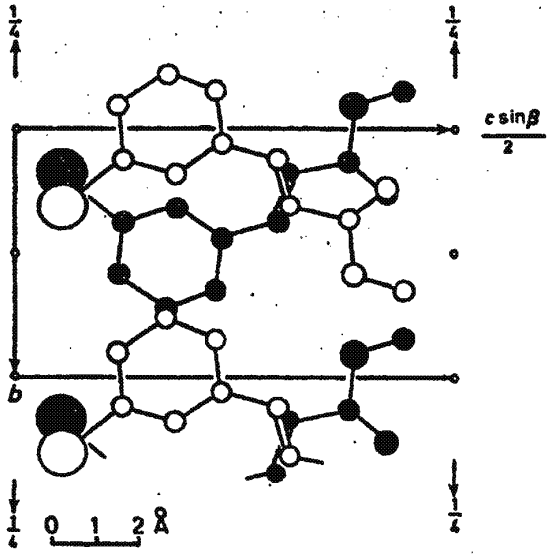


Figure 1. Methyl-*m*-bromocinnamate. Packing arrangement seen along [100]

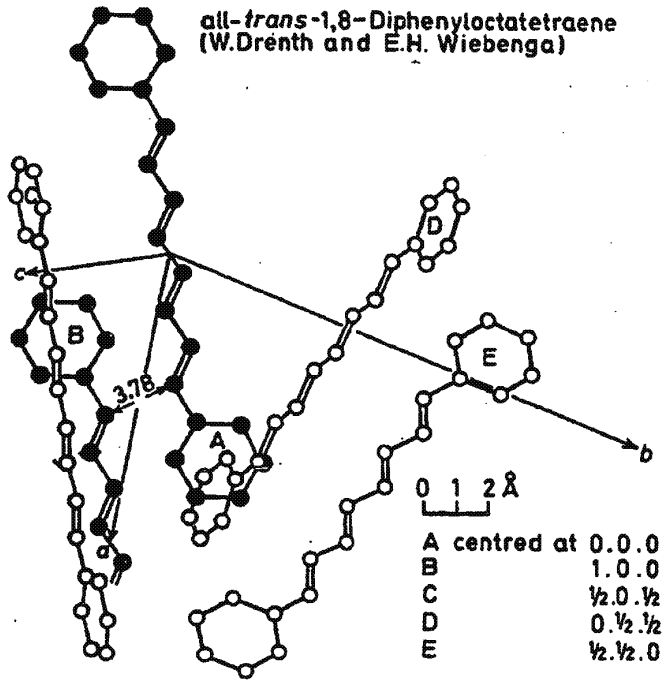
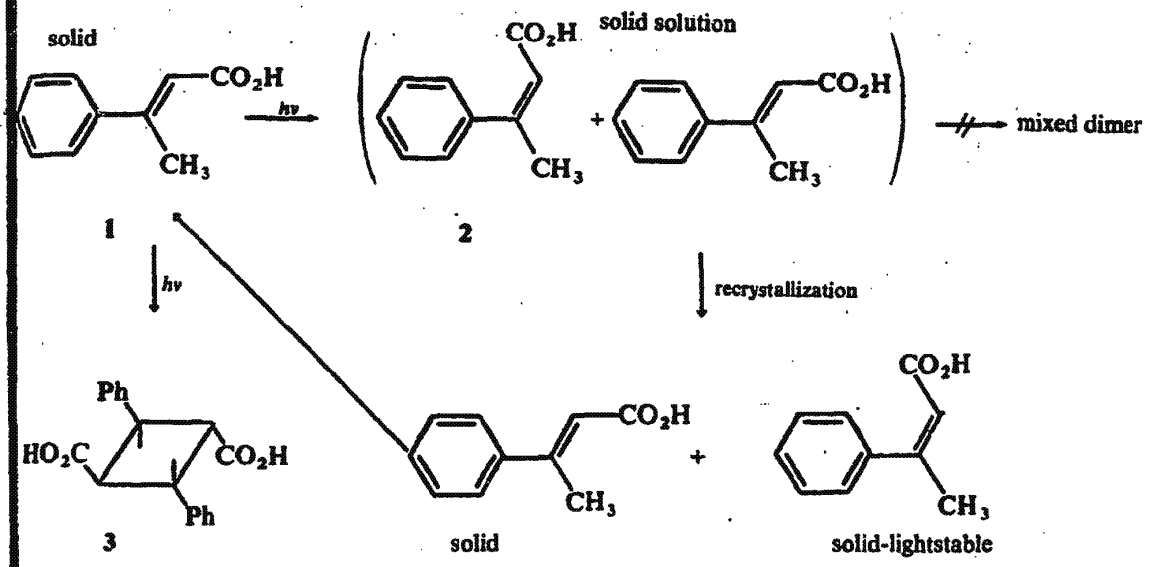
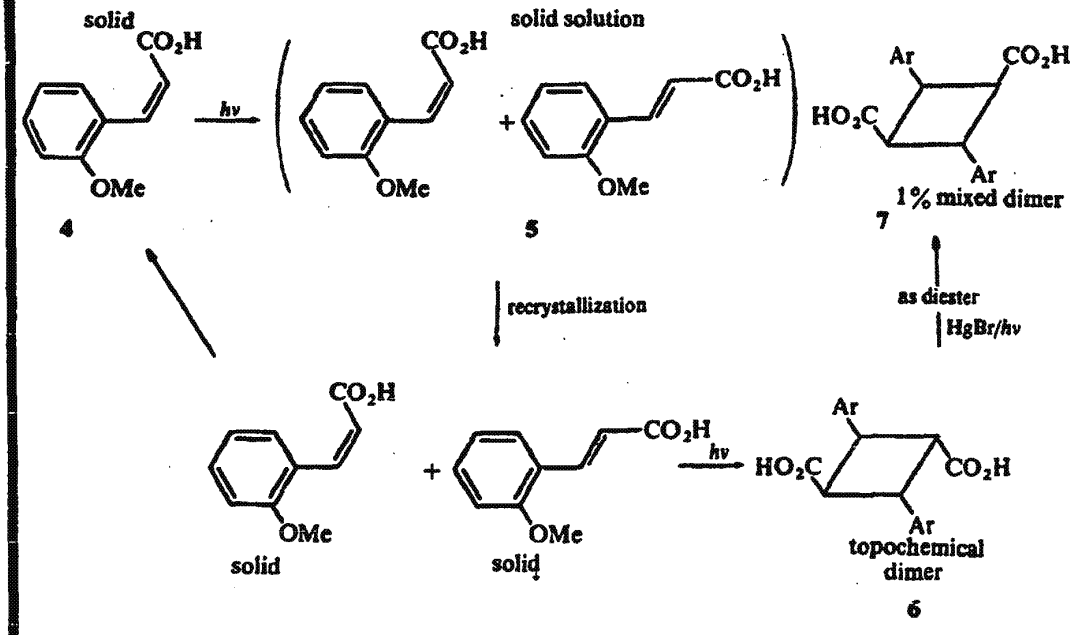


Figure 2. Packing diagram seen normal to molecular plane of molecule A at (*x*, *y*, *z*)

UM00011774
NOVARTIS EXHIBIT 1517
Novartis v. Regents, IPR2023-01347
Page 520 of 4460



Scheme 2. The solid-state photochemistry of β-methyl-*trans*-cinnamic acid



Scheme 3. The solid-state photochemistry of *o*-methoxy-*cis*-cinnamic acid

UM00011775
NOVARTIS EXHIBIT 1517
Novartis v. Regents, IPR2023-01347
Page 521 of 4460

VPC analysis of the esterified (diazomethane) reaction mixture shows the presence of the three components (1), (2) and (3) and essentially negligible amounts of another product, possibly a second dimer (*Scheme 2*). Similarly the *cis*-acid (4) is converted to the *trans*-isomer (5) which we know to be capable of dimerization to the centrosymmetric cyclobutane (6). Again, VPC analysis of the esterified reaction mixture shows the three components (4), (5) and (6), and a trace (less than one per cent) of a second dimer. The last was tentatively identified on the basis of retention time as (7) prepared independently from the α-dimer (6) by epimerization with mercuric bromide and light[35] (*Scheme 3*.)

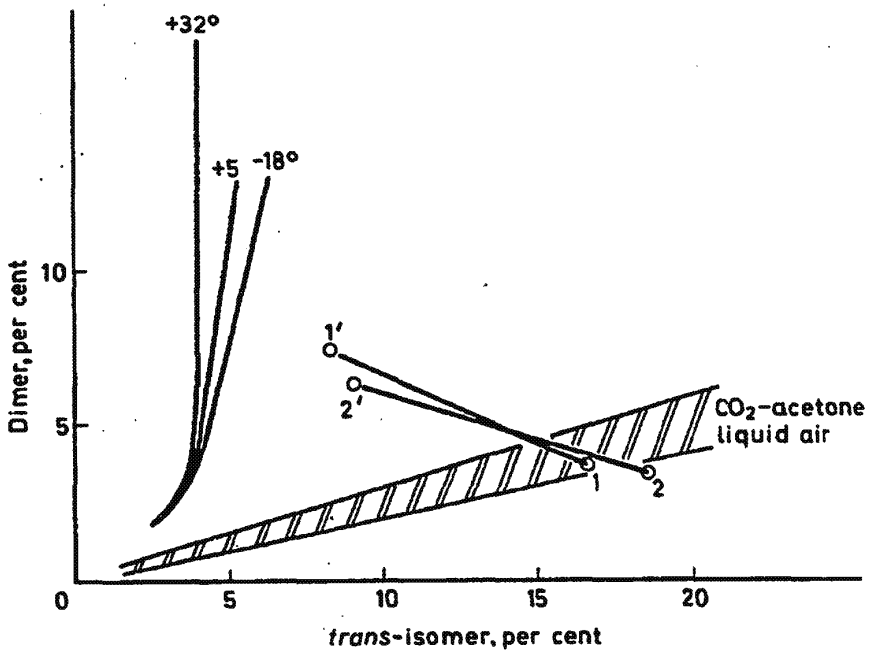


Figure 3. o-Methoxy-*cis*-cinnamic acid. Product distribution at various temperatures

Thus in both systems solid solutions are formed during the course of continuous irradiation, containing both *cis*- and *trans*-isomers in what must be obviously close juxtaposition. In spite of the presence within the solid matrix of the two isomeric species, cross-dimerization between *trans*- and *cis*-acids takes place to only negligible extent. This picture has been further clarified by Mr Ron's study of the system (4) at various temperatures (*Figure 3*). Photoreaction of the *cis*-acid (4) at *room temperature* produces mainly dimer (6) whose yield increases with exposure time while the amount of *trans*-isomer remains constant at about four or five per cent. At *low temperatures* (between −80° and −180°C) *trans*-isomer accumulates and relatively little dimer is formed. That this low-temperature effect is not due to a slow-down of the dimerization process could be established in independent experiments demonstrating negligible temperature dependence of the photoreaction of the *trans*-acid. Instead, it is caused by the absence of recrystallization of the

UM00011776
NOVARTIS EXHIBIT 1517
Novartis v. Regents, IPR2023-01347
Page 522 of 4460

solution of *trans*- in the lattice of *cis*-acid: samples such as represented by points 1 and 2 in *Figure 3* which had been irradiated at −80° and −180°C respectively, were warmed in the dark, to +60°C for a period of 20 h, then re-cooled to −80° and −180°C, re-irradiated for another short period, and analysed to the composition shown in points 1′ and 2′. This line of experimentation strongly suggests that the thermally activated step is the recrystallization of the solution of photoproduct in the lattice of the starting materials, whose activation energy must be of the order of magnitude of the heat of sublimation of the monomer crystal, i.e. in the neighbourhood of 20 to 30 kcal/mole, characteristic of organic crystals. If this interpretation is accepted then the low-temperature accumulation of *trans*-monomers strongly supports the topochemical argument that dimerization is very precisely controlled by the alignment of nearest-neighbours, even in the ground state.

There is no doubt that the example quoted here of the absence of cross-dimerization in a solid solution of product in monomers is an extreme case: in systems such as the pyrimidines 'errors' in dimerization arise after (varying) degrees of conversion to the topochemical product.

The phenomenon of photo-crosslinking of polyvinyl cinnamates, recently reviewed by Williams[36] should be mentioned at this stage; while u.v. irradiation produces diminution of the absorbance in the region characteristic of the cinnamate group there is very little evidence that the products are cyclobutanes: Sonntag and Srinivasan[37] claim to have demonstrated the presence of α-truxillic acid among the hydrolysis products of irradiated poly(vinylcinnamates). On the other hand, the e.s.r. spectrum[38] of the polymer irradiated with 240–250 nm at 77°K indicates that at least two radical species are present, one of crosslinked cinnamoyl radicals, the other belonging to radicals on the main chain; unfortunately the exciting wavelength chosen is rather short, it being known that at this wavelength diphenylcyclobutanes are split; experiments at longer wavelengths, say near 300 nm, would be desirable. Although the literature speaks of cyclobutanes formed by the crosslinking process of cinnamate-containing polymers the evidence for intra- or inter-strand cyclodimerization is of very limited value; until more reliable data for cyclobutane become available the problem of cyclodimerization of not necessarily parallel cinnamoyl residues must be left in abeyance.

Summarizing this discussion of the topochemical rules as they apply to the photodimerization of α,β-unsaturated acids we conclude that the exact parallel alignment, within a regular crystal lattice, of double bonds is an essential pre-requisite for cyclodimerization.

III. THE LOCUS OF THE REACTION

A meaningful discussion of the mechanism of reactions in the solid state requires the precise definition of the locus of the chemical event. On the one hand, x-ray structure analysis, which has provided the basis for the topochemical arguments, describes the crystalline species as an idealized time- and space-averaged three-dimensional repeat pattern: on the other hand we know that the real solid has surfaces, grain boundaries, dislocations adsorbed molecules, substitutional and other impurities (e.g. occluded

UM00011777

NOVARTIS EXHIBIT 1517
Novartis v. Regents, IPR2023-01347
Page 523 of 4460

solvent), and other defects which are not readily or not all detectable by x-ray diffraction techniques.

Since molecules sited at surfaces or dislocations are likely to have a higher chemical potential than molecules in the bulk phase the assumption is justified that thermal reactions will take place at the discontinuities; again, those photochemical reactions in which energy is transported through the bulk phase composed of suitably overlapped π-systems, are more likely to occur at these sites than in the bulk because these irregularities can serve as traps in the exciton-propagation mechanism. It is not obvious *a priori* whether reaction at these particular sites is subject to the topochemical rules though, as we have seen, the topochemical approach adequately described the photochemistry of α,β-unsaturated acids etc. On the other hand, evidence has been accumulating[8,10] that the photobehaviour of anthracene, 9-cyanoanthracene and 9-anthraldehyde could not be reconciled with the crystal structure of the monomers, and Craig and Sarti-Fantoni[10] suggested that 'reaction occurs at defects or surfaces or zones already disordered by dimerization'.

A systematic chemical and crystallographic study in our Laboratory by Drs E. Heller[39] and J. C. J. Bart has shown that the substituted anthracenes fall into at least three packing types corresponding to our α,β,γ-classification: in the γ-types [e.g. 9-methoxyanthracene[40], *Figure 4*; 1-cyanoanthracene; 1-chloroanthracene] the molecular planes are not parallel and the distances between the *meso*-atoms of neighbouring molecules greater than 5 Å. As expected these compounds are lightstable in the crystalline phase though they photodimerize in solution.

In the α-type anthracene units are packed pairwise across centres of symmetry such that the C(9)···C(10′) distances are short (3.6 Å)[40] (*Figure 5*). With the exception of 9-nitroanthracene monosubstituted anthracenes crystallizing in the α-type, whether substituted at position 9(R = Cl, Br, Me, CO_2Me) or elsewhere [1-chloroanthracene (second modification)] produce the topochemically expected 1-dimer in high yield.

The anthracene derivatives which crystallize in the β-type fall into three classes (*Scheme 4*): first, 1,5-dichloroanthracene and the 2,4-dichlorophenyl ester of 1-anthroic acid which dimerize to the (topochemical) head-to-head dimers; secondly, a lightstable group [R = Br, CO_2Me (both second modifications); CO_2H] and, third, a group yielding the T-dimer [R = Cl (second modification); CHO; CN (*Figure 6*)]. Thus, of these three groups only the one substituted elsewhere than at the *meso*-position gives the head-to-head *m*-dimer expected on geometrical grounds, whilst the 9-substituted derivatives either do not react or give the non-topochemical head-to-tail dimer.

Now it is known that all 9-substituted monomers, even on photodimerization in solution, yield only the head-to-tail dimers and do not produce the head-to-head dimers; the conclusion has been drawn that 9,9′-substituted head-to-head dimers cannot be formed, at least under photochemical conditions. If we accept this conclusion then the behaviour of the *lightstable* anthracenes in the β-type is in effect topochemically normal since the head-to-head product is presumably unstable. The formation of the centrosymmetric dimers from parallel monomer molecules in the β-packing mode

UM00011778
NOVARTIS EXHIBIT 1517
Novartis v. Regents, IPR2023-01347
Page 524 of 4460

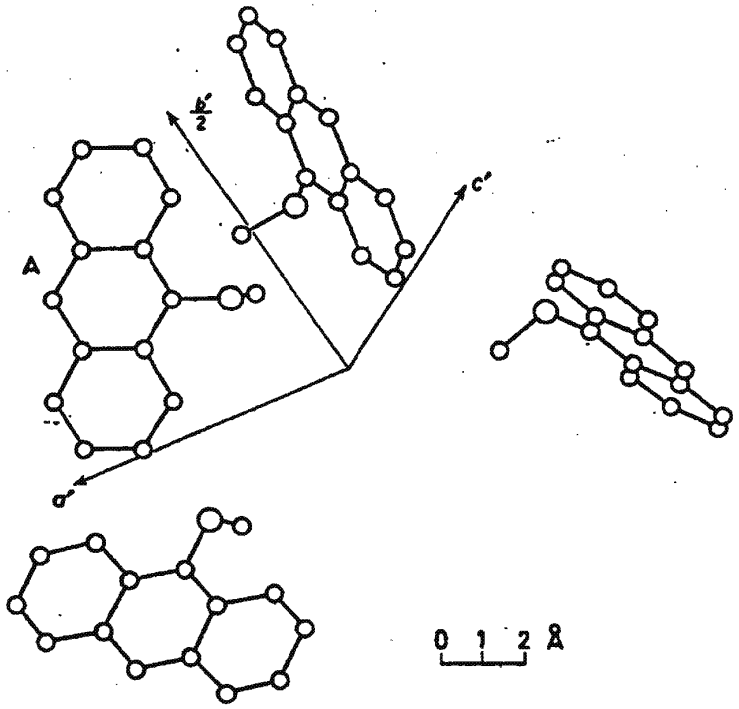


Figure 4. 9-Methoxyanthracene. Packing diagram seen normal to molecular plane of molecule A at (*x*, *y*, *z*)

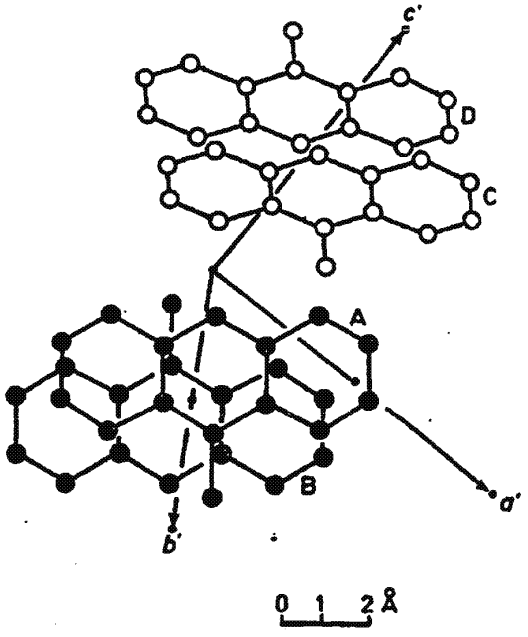
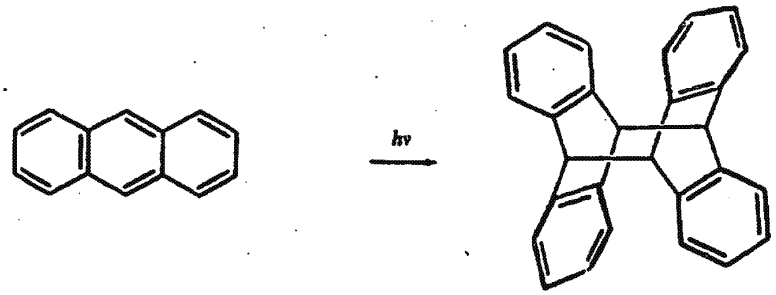


Figure 5. 9-Methylanthracene. Packing diagram seen normal to molecular plane of molecule A at (*x*, *y*, *z*)

UM00011779
NOVARTIS EXHIBIT 1517
Novartis v. Regents, IPR2023-01347
Page 525 of 4460



β-type
1-(2,4-dichlorophenoxycarbonyl) $\xrightarrow{h\nu}$ Head-to-head dimer
1,5-dichloro

space group		
$P2_12_12_1$	9-Cl	$\xrightarrow{h\nu}$ Head-to-tail dimer
$P2_12_12_1$	9-CHO	
$P2_12_12_1$	9-CN	
$P2_12_12_1$	1,10-dichloro	$\xrightarrow{h\nu}$ Lightstable
$P2_1/a$	9-Br	
$P2_1/a$	9-CO_2Me	
$P\bar{1}$	9-CO_2H	

α-type

isomorphous	1-Cl	$\xrightarrow{h\nu}$ Head-to-tail dimer
	9-Cl	
	9-Br	
	9-Me	
	9-CO_2Me	
	9-$CONH_2$	

Scheme 4. Photodimerization of anthracenes

must be due to an abnormality of their crystal structures, such as the presence of dislocations which permit dimerization; such dislocations are, by implication, absent in the lightstable subclass. These photoactive dislocations have indeed been demonstrated in anthracene crystals, which were held responsible by Thomas and Williams[11] for the 'topochemically forbidden' dimerization of solid anthracene, as well as in 9-cyanoanthracene[41].

In summary: light stability in the solid state of monomers which can photodimerize in solution; the existence of two crystal forms of the same monomer which are lightstable and dimerizable respectively; the formation of the topochemically expected dimers from centrosymmetrically close-packed anthracenes and from translationally close-packed anthracenes substituted elsewhere than in the 9-position, argue for topochemically controlled reactions between nearest neighbours. The formation of $\bar{1}$-dimers from some but not all 9-substituted monomers packing in the β-type must mean that the particular dislocations present in the photo-active forms bring about contact of monomer molecules of the correct geometry for photodimerization to be possible; equally, whatever the disclocations present

UM00011780
NOVARTIS EXHIBIT 1517
Novartis v. Regents, IPR2023-01347
Page 526 of 4460

in the photostable β-type, they are apparently not of suitable structure to cause the close antiparallel packing of monomer units which would permit formation of the head-to-tail dimer. It follows that the molecular environment at a particular dislocation may, but need not, be favourable to dimerization and, conversely, that the formation of 'topochemically forbidden' dimers is an indication of a dislocation type which brings monomers into correct geometrical juxtaposition for dimerization.

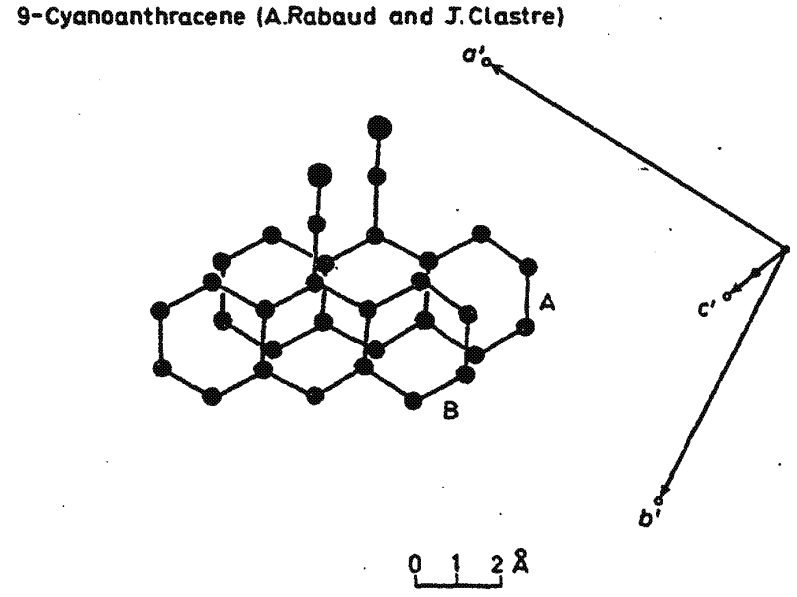


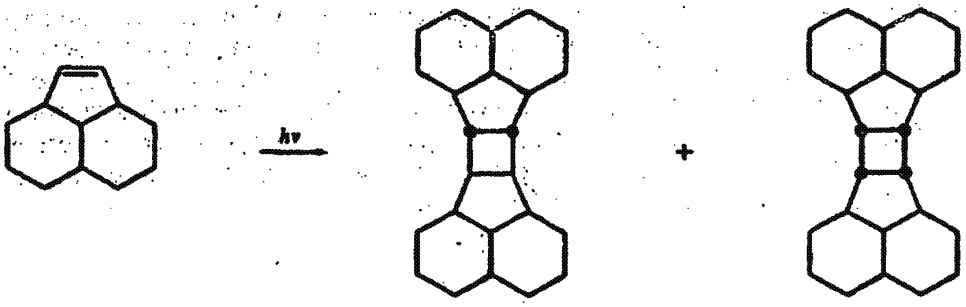
Figure 6. Packing diagram seen normal to molecular plane of molecule A at (x, y, z): Molecule B at $(x, y, 1 + z)$

An alternative explanation according to which non-topochemical dimerization occurs at sites of high molecular mobility not requiring correct molecular alignment prior to reaction is ruled out by our results on the photo-chemical behaviour of 1,5-dichloroanthracene (β-type) and 1-chloroanthracene (α- and γ-types): irradiation of *solutions* of these two monomers yielded the theoretical number of dimers (two and four, respectively); the light-active solids gave each the one topochemical dimer. Thus, while these monomer molecules can take up, in the dissolved phase, all mutual orientations, to produce all possible dimers, they are not free to move in their crystal structures: solid-state dimers are only formed from correctly pre-aligned and sufficiently close nearest neighbours.

Therefore, even in systems at first sight not obeying the topochemical rules cyclodimerization in fact takes place between correctly aligned monomer units at sufficiently short distances, such alignment being provided, if not by the bulk of the crystal lattice, then by dislocations of appropriate geometry.

UM00011781

NOVARTIS EXHIBIT 1517
Novartis v. Regents, IPR2023-01347
Page 527 of 4460



8 9 10

Scheme 5. Photoproducts of acenaphthylene

When we undertook a detailed study of the photochemistry of solid acenaphthylene (8) (*Scheme 5*) much information on the reaction to the two dimers (9) and (10) was already available. A recent study[42] had claimed the formation of the I-dimer (9) with essentially zero 'energy of activation' and of the *m*-dimer (10) with ΔE^{*} ~40 kcal/mole. The solid-state radiation chemistry of acenaphthylene had been investigated by Chapiro and Lozach[43] who observed similar kinetics of dimerization and pointed out that acenaphthylene was the first hydrocarbon to undergo radiochemically-induced cyclodimerization. The solution photochemistry had also been studied in detail by several groups[44].

The mechanism of solution dimerization is now pictured as proceeding to the *cis*-isomer from a π-complex probably via the singlet excited state; the *trans*-isomer is believed to derive from the triplet excited state sufficiently long-lived to permit a normal bimolecular reaction with a ground-state monomer molecule. The conclusion that the *m*-dimer was formed in a solid-state reaction requiring an activation energy as high as 40 kcal/mole seemed to us inherently improbable; indeed, the very complexity of the photochemical system suggested novel features worthy of further investigation. Our work can be summarized as follows: photoreaction to the I-dimer takes place not in the bulk of the crystalline material but only at disclocations; this observation, i.e. the *decoration* of the dislocation lines by dimer, was the first example of such an effect in organic crystals, for the recognition of which we are indebted to Professor Thomas[12]. Irradiation of acenaphthylene films between two quartz plates (rather than with crystals contained in vessels with free volume) has shown that formation of the *m*-dimer is inhibited, even at temperatures greater than 50°, throughout the film except at crystal discontinuities such as cracks, holes, etc. The value of the heat of sublimation ($\Delta H_{sbl.}$ = 15.4 kcal/mole, determined here from vapour pressure measurements) is low, compared with, say, acenaphthene (19.7 kcal/mole) and naphthalene (17.4 kcal/mole), and suggests that the gas phase in vessels where free volume is appreciable, should be considered as a possible locus of

UM00011782
NOVARTIS EXHIBIT 1517
Novartis v. Regents, IPR2023-01347
Page 528 of 4460

reaction. A simple calculation which assumes that *m*-dimer arises from absorption of a photon by a pre-associated pair in the vapour phase leads to a value of a minimum of the 'activation energy' of $2\Delta H_{sub.} = 31$ kcal/mole, a value which may account for the observed value of 40 kcal/mole for 'solid state' reaction.

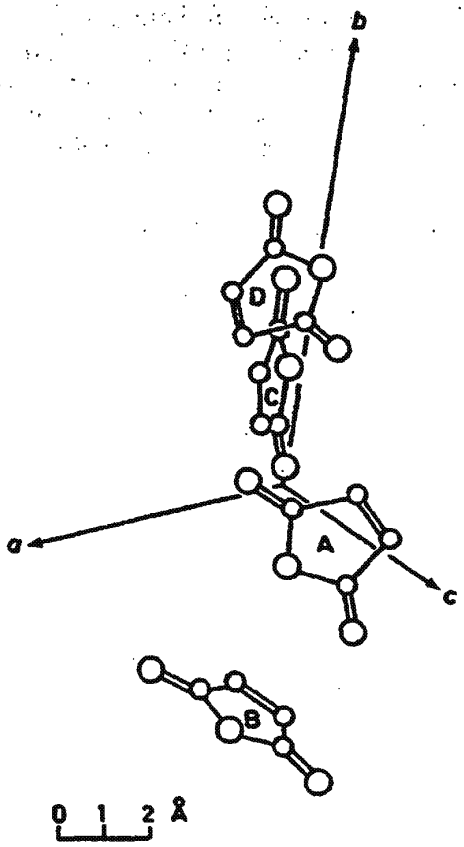


Figure 7. Packing diagram seen normal to molecular plane of molecule A at (*x*, *y*, *z*). Maleic anhydride (R. E. Marsh, E. Ubell and H. E. Wilcox)



11 12

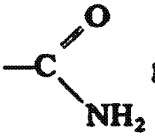
Maleic anhydride (11) has been reported[45] to photodimerize to (12), in a yield of less than nine per cent after exposure for 240 h. The crystal structure of the monomer[46] shown in *Figure 7* has neither parallel nor short contacts between —CH=CH— groups and appears unsuited to photodimerization. Experiments in this Laboratory[34] indicate essentially complete inhibition of dimer formation at 5°. In view of the high vapour pressure of maleic anhydride at room temperature we suggest that the reaction takes place in the vapour phase and not in the crystal.

P.A.C.—27/4—H

UM00011783

NOVARTIS EXHIBIT 1517
Novartis v. Regents, IPR2023-01347
Page 529 of 4460

IV. CRYSTAL ENGINEERING

Systematic work on the forces controlling molecular packing arrangement is leading to the evolution of a general theory of crystal structures. A number of attempts[13, 14] are being made to derive unit-cell dimensions of compounds from potential-energy curves accounting for molecular interaction, particularly of small and medium-sized aromatic systems. A more qualitative approach is being followed in our Laboratory by Dr Leiserowitz[15] who has considered the packing types of primary amides (including α,β-unsaturated derivatives) in terms of the geometry of the hydrogen-bonded networks generated by the  groups. From this study resulted the observation that the probability of α,β-unsaturated amides crystallizing in the (photodimerizable) α-type was very high, certainly higher than for the corresponding acids, and further that their packing arrangements, except for minor differences in molecular conformation, were sufficiently similar to suggest binary miscibility studies of primary amides. These are discussed below.

A second approach to controlled packing geometry has been found in the introduction of a dichlorophenyl group into unsaturated systems[16], which brings about crystallization in a unit cell having a shortest axis of ~4 Å. By this method a large number of compounds of the type $Ar(CH:CH)_mX$, where Ar = 2,4-, 3,4-, and 2,6-dichlorophenyl; ($m = 0, 1$); X = CHO, CO_2H, CO_2Me, CN, NO_2, Ph, $CO(CH:CH)_nPh$ ($n = 0, 1$) have been obtained in the β-packing type, and their photoproducts characterized as *m*-dimers appropriate to this packing type.

As an alternative technique of forcing, the 4 Å structure type α,β-unsaturated ketones etc. can be co-crystallized with mercuric chloride into molecular complexes. The crystal structure of the complex is evidently controlled by the packing of mercuric chloride which itself crystallizes in a cell of dimensions $a = 5.96$, $b = 12.74$, $c = 4.33$ Å[49]. Thus, coumarin[47], cinnamaldehyde, benzalacetophenone[48] and others give crystalline 1:1 complexes having 4 Å axes. The topochemically expected formation of the *cis,syn*-dimer from [coumarin.$HgCl_2$] has been described[30]; this totally stereospecific reaction is the easiest route to this isomer.

V. TOWARDS A SYSTEMATIC SOLID-STATE PHOTOCHEMISTRY

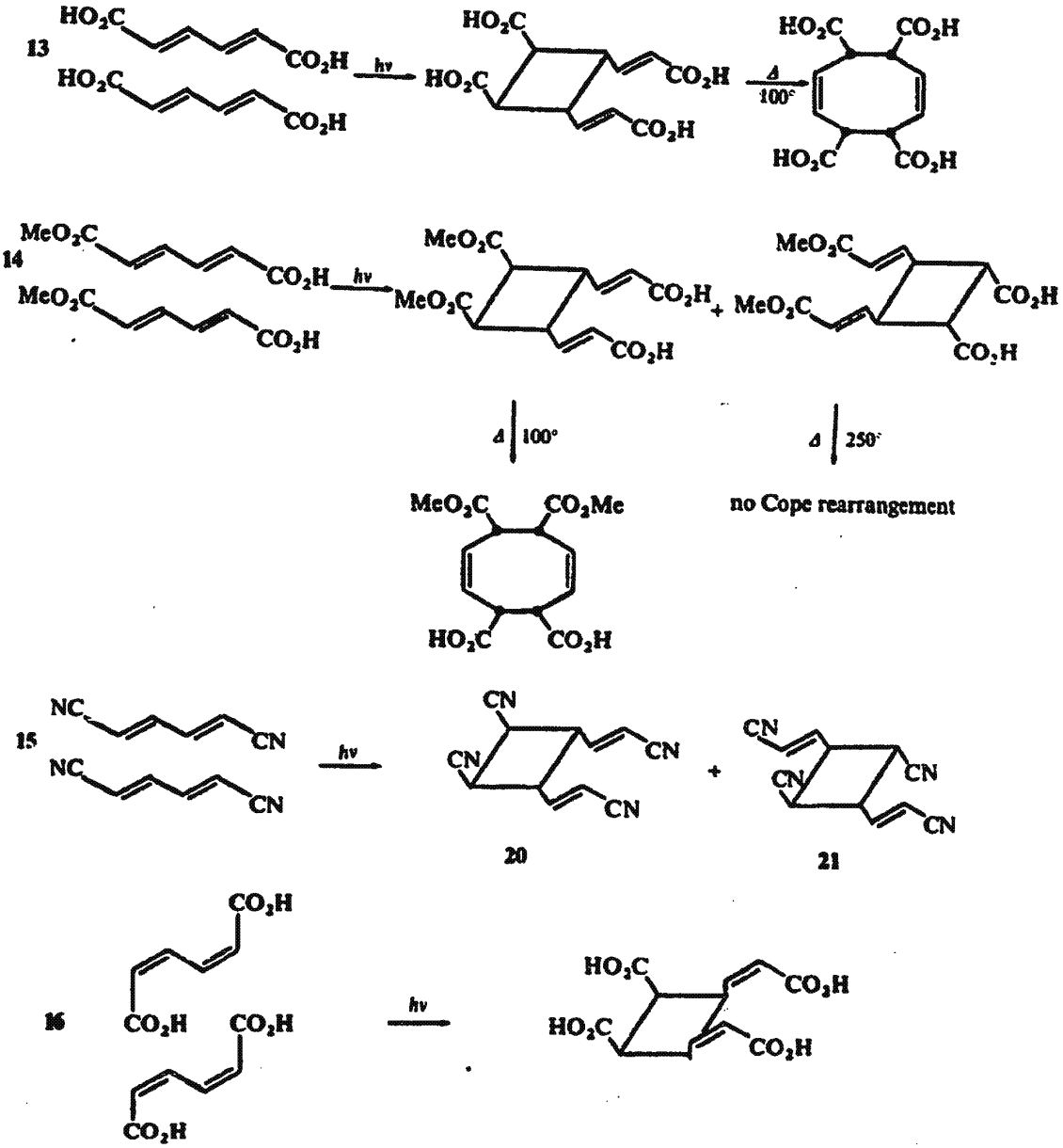
In this last section we report recent results on cyclodimerization in the solid state, some of which have become possible through the application of the packing rules sketched in the previous section, and discuss some possible future lines of research.

(A) The photochemistry of 1,3-butadienes

A survey of the crystallography of *trans,trans*-muconic acid (13) and its derivatives, of *cis,cis*-muconic acid (16)[26], of crotonic (17) and sorbic acids (18)

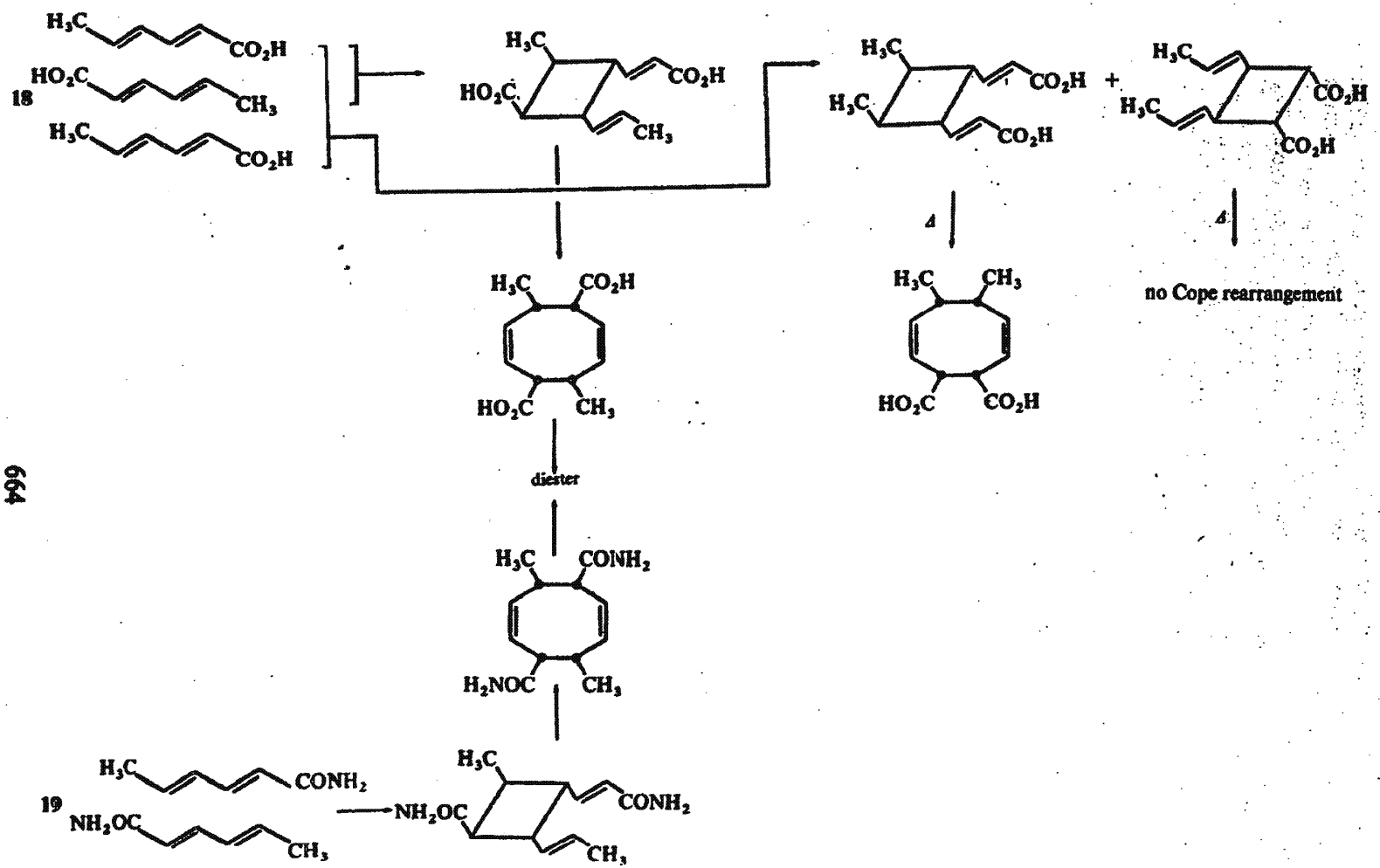
UM00011784
NOVARTIS EXHIBIT 1517
Novartis v. Regents, IPR2023-01347
Page 530 of 4460

and derivatives[27] has shown that many compounds in this series crystallize in the β-type (4 Å axis); the structure analyses carried out here and elsewhere have shown all these molecules to crystallize in the extended planar *s-trans*-conformation in packing arrangements which should be lightactive. The photochemistry of these compounds is summarized in *Schemes 6* and *7*. *trans,trans*-Sorbamide (**19**) does not crystallize in the β-type, the molecules being close-packed pairwise across centres of symmetry[50]: its photochemistry is summarized in *Scheme 7*.



Scheme 6. Solid-state photoproducts of muconic acid and some derivatives.

UM00011785
NOVARTIS EXHIBIT 1517
Novartis v. Regents, IPR2023-01347
Page 531 of 4460



Scheme 7. Solid-state photoproducts of sorbic acid and sorbamide

UM00011786

NOVARTIS EXHIBIT 1517
Novartis v. Regents, IPR2023-01347
Page 532 of 4460

The following conclusions are of interest:

(1) The yields of 1,2-divinylcyclobutanes of the configuration required by the stereochemistry of the starting material and its packing geometry are high.

(2) Cyclobutanes having the non-topochemical configuration, if formed at all, constitute a negligible fraction of the photoproducts. In particular, dimers from the β-packing types not having symmetry *m* and thereby suggesting rotation around the 1,2-bond after formation of the 1,1'-bond and prior to ring closure at bond 2,2' are present, if at all, in negligible quantities.

(3) There is no evidence that *trans,trans*-cyclo-octadienes are formed or any of its rearrangement products; conceivably, the small amount of (amorphous) oligomeric material which accompanies the crystalline photoproducts derives from *trans,trans*-cyclo-octadienes. However, these oligomers can also be rationalized as being formed via reactions not passing through the *trans,trans*-C_8-species.

(4) Some of the cyclobutanes undergo rearrangement to *cis,cis*-1,5-cyclo-octadienes in the solid state. The Cope products have been shown to be formed in secondary thermal dark reactions.

(5) Light stability of dimethyl *trans,trans*-muconate follows from the packing geometry[51] of the diester; a variety of photoproducts has been isolated from the (sensitized) solution reaction[52].

(6) Irradiation in the long wavelength end of the absorption ($300 < \lambda < 350$ nm) is very effective in bringing about reaction. By extrapolation from work on ethyl acrylate and diethylfumarate in which the $\pi^* \leftarrow n$ transition has been identified[53] in the tail-end of the absorption spectrum we may perhaps assume a similar transition in the higher homologue of fumaric acid.

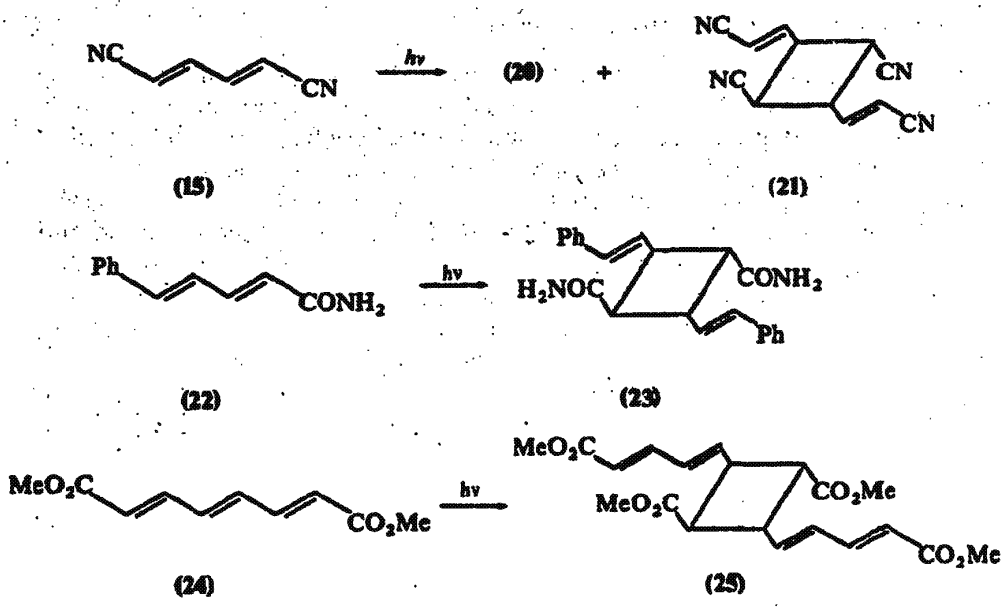
(7) The example of *trans,trans*-muconodinitrile (15) is interesting from the topochemical and mechanistic points of view: the two products (20) and (21) are formed in yields which we could not estimate accurately so far, but which are comparable. It will be noted that the monomers are geometrically related in such a way that the distances between centres of (crystallographically) non-equivalent and equivalent double bonds are 3.64 and 3.96 Å respectively[54]. Reaction across the former leads to the centrosymmetric, and across the latter distance to the *m*-cyclobutane. The question whether both dimers are formed from the same state of the excited monomer is interesting but unanswered.

(8) Cyclobutanes are formed not only by 1,1'–2,2' but also by 1,2'–1',2 interaction, as from muconodinitrile to (21), from *trans,trans*-styrylacrylamide (22) to (23), and from dimethyl hexatrienoate (24) to (25)[55] (*Scheme 8*). The latter pathway distinguishes the solid-state reaction from sensitized solution reactions; Hammond indicates[56] that direct irradiation of liquid butadienes gives this type of dimer, but full information on this point is not available.

In summary, the photochemistry of the planar (or near-planar) *cis,cis*- and *trans,trans*-butadienes substituted in positions 1 and 4 such that at least one substituent is an electron-withdrawing group (CO_2H, CO_2Me, CN) leads to 1,2-divinyl substituted cyclobutanes having the topochemically expected configuration. The reaction corresponds to [2+2] addition; [4+4] addition to *trans,trans*-cyclo-octadienes is a negligible pathway of the reaction.

SCHEME 7. Solid-state photodimerization of muconodinitrile

UM00011787
NOVARTIS EXHIBIT 1517
Novartis v. Regents, IPR2023-01347
Page 533 of 4460



Scheme 8. 1,2'–1',2-cyclodimerization

(B) Eight-centre dimerizations

No evidence has been found for 8-centre reaction of 1,3-butadienes in the solid state to the bicyclo-octane system rather than to the observed divinyl-substituted cyclobutanes. On the other hand, the cyclization of the cross-conjugated dienone (26) has been reported[57], the product being claimed to be (27) on the basis of its chemical behaviour[57, 58]. The reaction is likely to be topochemically controlled: (26) does not give the dimer in solution, and the solid diethyl ester (28) gives polymeric material rather than dimer; the dimerization of the free dicarbocyclic acid (29) to the corresponding tetra-acid has been described[59]. The cell dimensions of the dimethyl ester (26) were measured here: $a = 15.45, b = 7.92, c = 3.96$ Å, $\beta = 102.3°$; $d_x = 1.38$ g/cm^3; $Z = 2$. *Space group*: *A2*. *Molecular symmetry*: 2. The monomer must have one or other of the two symmetric conformations (26a, 26b) of which the former is more probable in view of the cell dimensions. The parallel alignment of such monomers along the short *c* axis (β-type) suggests the configuration of the dimer to be (27); this structure differs from that proposed by Corse *et al.*[60] which, for other reasons such as *trans*-fusion of the two rings at the cyclobutane, seems less plausible[61, 62].

The direct formation of the tricyclo[6,2,0,0^{3,6}]decane system in a solid-state reaction was of sufficient interest to suggest the scan for further examples; the generalization that dichloro-substituted phenyl derivatives tend to crystallize in 4 Å cells, pointed to the bis-(dichlorobenzylidene) acetones as likely to come in the β-type, and indeed several such derivatives have the desired crystal structures. Dr B. Green has investigated the derivative (30) in some detail and obtained a saturated photodimer to which we ascribe the

UM00011788
NOVARTIS EXHIBIT 1517
Novartis v. Regents, IPR2023-01347
Page 534 of 4460

Scheme 9

UM00011789
NOVARTIS EXHIBIT 1517
Novartis v. Regents, IPR2023-01347
Page 535 of 4460

Scheme 9. Eight-centre dimerization to the tricyclo-[6,2,0,0^{3,6}]-decane system

UM00011790
NOVARTIS EXHIBIT 1517
Novartis v. Regents, IPR2023-01347
Page 536 of 4460

structure (31) on the basis of n.m.r., mass-spectrometric, and u.v. spectral data[61]. Irradiation of the monomer with light of various short-wavelength cut-offs gave either the doubly ring-closed tricyclic system or no product at all. Light of > 470 nm was inactive; $\lambda > 445$ nm gave the fully saturated product but no trace of the cinnamoyl derivative (32). There can be little doubt that the reaction is monophotonic, that is, (32) in its ground state is not an intermediate in the path to the tricyclic compound (*Scheme 9*).

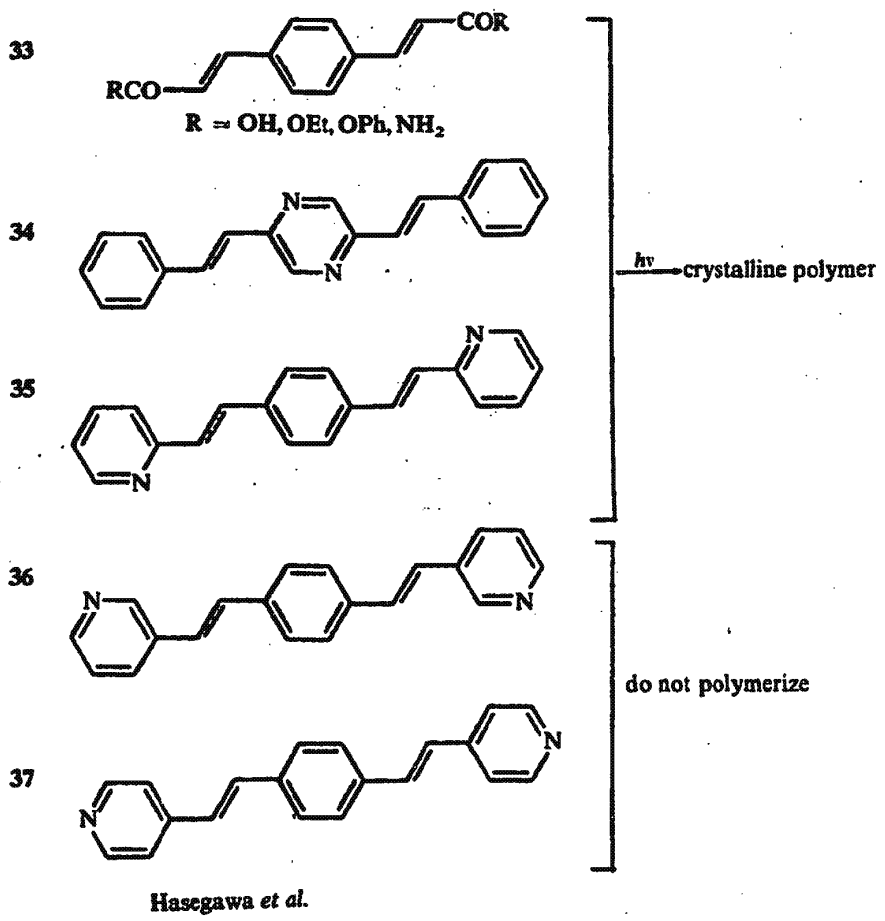
Eight-centre photopolymerization in the solid state has been noted by Japanese workers[63–65]: they polymerized crystalline *p*-phenylene diacrylic acid (33), its methyl, ethyl and phenyl esters, and amide, as well as 2,5-distyrylpyrazine (34) and its analogue (35) though they could not polymerize (36) or (37) under comparable conditions. The two dimerizable monomers (34) and (35) are isomorphous according to powder photographs and different from (36) and (37). The polymers from these dienes were highly crystalline; the degree of crystallinity of the diacrylic acid derivatives decreased with increasing temperature. Irradiation of the diethylester (33) in the melt failed to yield polymer. The spectroscopic (u.v., i.r., n.m.r.) data indicate the presence of cyclobutane rings in the polymers. These results suggest that the polymerization reaction is topochemically controlled; full crystallographic data on these compounds would be interesting for a description of the type of motion that these molecules undergo during the process of polymerization (*Scheme 10*).

(C) The photochemistry of solid solutions

The analysis of the packing arrangement of primary amides[15] suggested miscibility in the solid state of α,β-unsaturated amides; indeed, irradiation of several pairs of substituted cinnamides co-crystallized from the melt produced a number of unsymmetrical α-truxillamides (heterodimers) in excellent yield alongside the two homodimers. These chemical results can be interpreted in the reverse direction; configuration of the dimers serves as a chemical probe for the orientation of monomer units in the substitutional solid solution whose detailed structure could not so far be investigated by other methods. From solid solutions of mixed monomers crystallizing in the α-type only the symmetrical and unsymmetrical α-truxillamides were isolated; other dimers formed were present in less than five per cent yields. Similar experiments on mixed crystals from substituted cinnamic acids crystallizing in the α- and/or β-arrangements give useful information on the structure of substitutional solid solutions in these packing types[66].

The photochemistry of solid solutions has been extended in directions of both theoretical and synthetic interest. Thus, crotonamide (12) and crotonic acid, which pack in potentially reactive crystal structures (short antiparallel and parallel contacts respectively), do not dimerize; on the other hand, the former could be incorporated into the lattice of cinnamide and of thienylacrylamide; these solid solutions yielded the mixed dimers. The precise stereochemistry of the former heterodimer is still uncertain; we tentatively propose structure (38) on topochemical grounds. A similar experiment has been carried out on the mixed system (39, 40): both compounds crystallize in a 4 Å cell and yield *m*-dimers, (39) being much more reactive than (40). The mixed crystal gives both (41) and the heterodimer (42) (*Scheme 11*).

UM00011791
NOVARTIS EXHIBIT 1517
Novartis v. Regents, IPR2023-01347
Page 537 of 4460



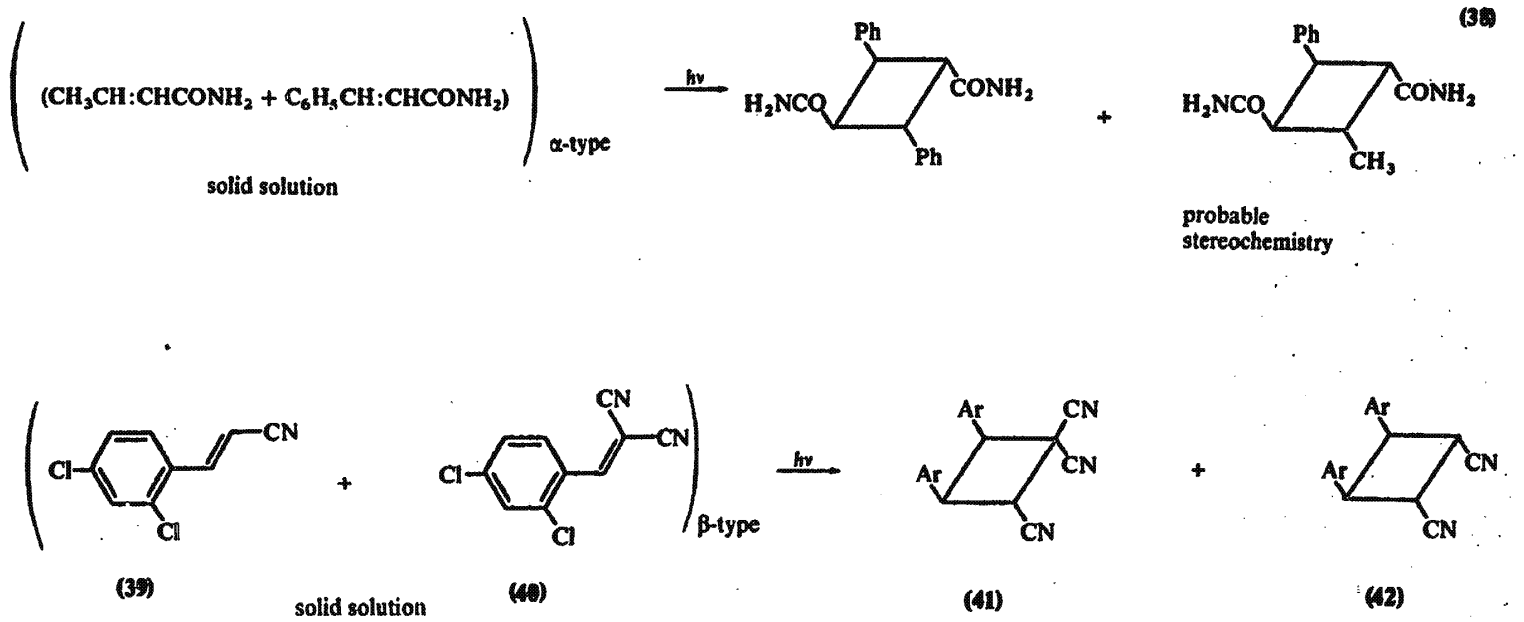
Scheme 10. Topochemical effects in eight-centre polymerization

Photoreactions of mixed crystals, consisting of compounds crystallizing in 4 Å cells, from stilbenes–benzalanilines, stilbenes–tolanes and a variety of other pairs are under active investigation[29]. We return below to the significance of the mixed-crystal experiments to considerations of energy transfer.

(D) Spectroscopic states and quantum yields

Much of our work on cyclodimerization having been concerned with α,β-unsaturated ketones, acids, etc. I shall confine myself to a discussion of these systems. There is no evidence for the dimerization of cinnamic acid in fluid solution; the only recorded reaction is the establishment of the photostationary equilibrium between the *cis*- and *trans*-isomers. Reaction in the presence of photosensitizers via the triplet state of the *trans*-acid reported to be in the neighbourhood of 50 kcal/mole[67] has not yet been studied.

UM00011792
NOVARTIS EXHIBIT 1517
Novartis v. Regents, IPR2023-01347
Page 538 of 4460



Scheme 11. **Formation of heterodimers from binary solid solutions**

UM00011793

NOVARTIS EXHIBIT 1517
Novartis v. Regents, IPR2023-01347
Page 539 of 4460

Krönert[68] has reported dimerization of *neat* ethyl cinnamate to the ethyl ester of α-truxillic acid to the extent of approximately two per cent; his data indicate a definite wavelength effect of dimerization versus polymerization. The poor yield of photodimer from unsensitized (neat) ethyl cinnamate contrasts with the formation of non-volatile, predominantly dimeric products from ethyl cinnamate in the presence of sensitizers (*p*-nitroaniline, picramide)[69]. No attempts were made to separate or characterize the 'dimers'. The authors observed an isosbestic point at 248 nm in spectra of dilute methanolic solutions of ethyl cinnamate irradiated in the 274 nm region; this they interpreted as characteristic of the *trans* ⇌ *cis* equilibrium. On the other hand, they state that very little permanent *trans* ⇌ *cis* isomerization occurred in the sensitized undiluted systems. Whilst the dimerization of cinnamic esters proceeds only to an insignificant extent by direct irradiation, bis-*trans*-cinnamimide (43) in 1,2-dimethoxyethane yielded 48 per cent of β-truxinimide (44) and a mixture of *trans*- and *cis*-cinnamides by irradiation through Pyrex[70] (*Scheme 12*).

The very limited evidence so far available suggests that in cinnamic acid itself the singlet state is too shortlived for dimerization to occur in the liquid phase though dicinnamoyl derivatives such as (43) can dimerize. In the esters sensitization probably leads to dimers.

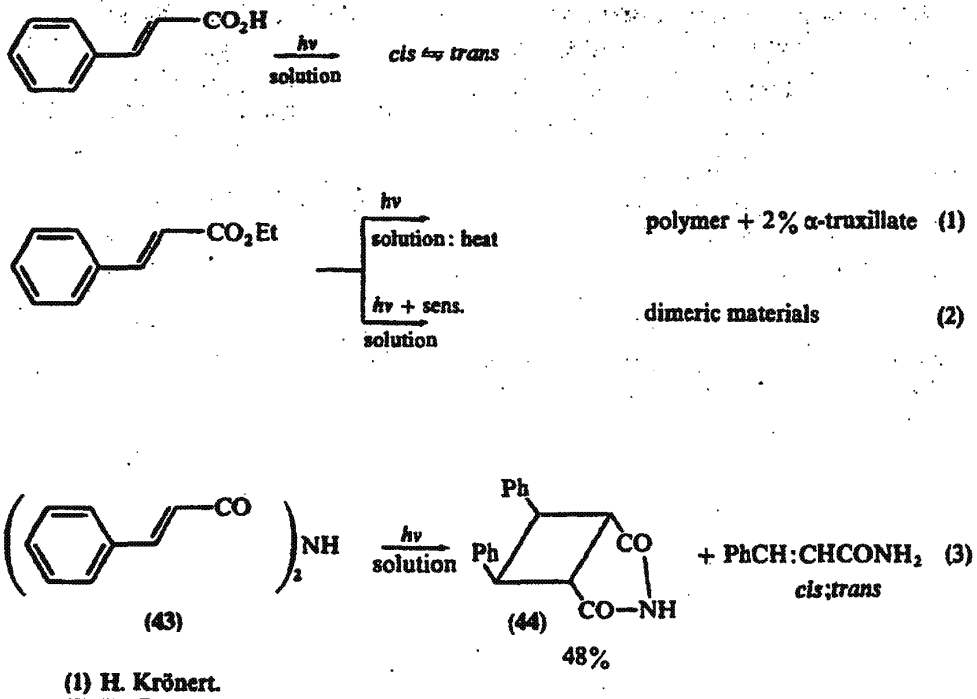
The quantum yield of the photodimerization of cinnamic acid in the solid state has been determined by Rennert *et al.*[71] to be 0.7 for light of $\lambda = 302$ nm; no difference was found in the photosensitivity of the α- and β-modifications of the monomer†. The authors concluded that the photoreaction proceeds by the attack of an excited monomer molecule on a ground state molecule, as follows:

$$M \xrightarrow{h\nu} M^*$$
$$M^* + M \rightarrow M_2$$

The electronic states involved in the photochemical process of cyclodimerization of cinnamic acid and their analogues have been investigated here by means of the mixed-crystal technique. As mentioned earlier the amides of variously substituted cinnamic acids could be pairwise cocrystallized from the melt, and the mixture irradiated to give the two homodimers and one heterodimer, all three compounds belonging to the α-truxillamide type. Pairs of amides were now chosen such that the end-absorption of one of the pair fell at longer wavelength than that of the second amide (*Figure 8*). Irradiation at wavelengths absorbed by both amides gave the two homodimers and the heterodimer; on the other hand, irradiation, at the long wavelength end, by light absorbed by one species only, totally inhibited formation of the homodimer of the non-absorbing species: now only the homodimer of the longer-wavelength absorbing amide was found together with the heterodimer.

† The authors state that Schmidt's prediction[18] that the α-material should be more photosensitive than the β was not borne out by their work. No such prediction was made; the statement[18] that 'concerning the yield of these dimerization reactions it is clear that the α- and β-types differ in the theoretical maximum possible conversion into dimer' obviously does not refer to *quantum* but rather to *chemical* yield.

UM00011794
NOVARTIS EXHIBIT 1517
Novartis v. Regents, IPR2023-01347
Page 540 of 4460



(1) H. Krönert.
(2) H. G. Crume, C. C. Natale and D. J. Kelley.
(3) R. T. LaLonde and C. B. Davies.

Scheme 12. Solution photochemistry of some cinnamic acid derivatives

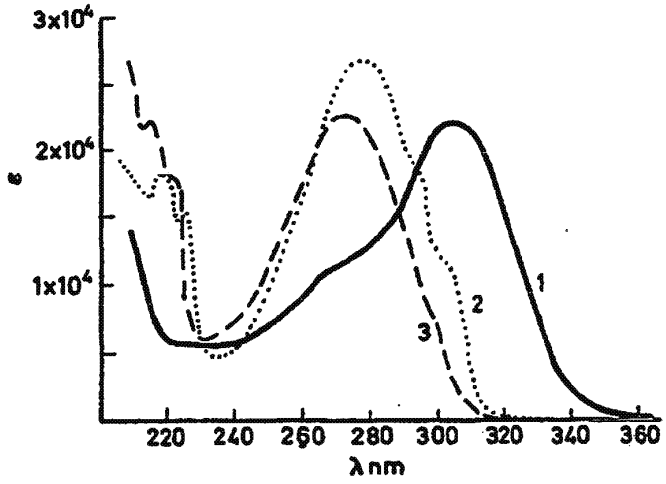


Figure 8. Absorption spectra of α, β unsaturated amides (2×10^{-5} M in ethanol): (1) thienylacrylamide, (2) *p*-chlorocinnamide, (3) cinnamide

UM00011795
NOVARTIS EXHIBIT 1517
Novartis v. Regents, IPR2023-01347
Page 541 of 4460

The reaction can to a first approximation be described as follows[72]:

	$A \xrightarrow{h\nu} A^*$	$B \xrightarrow{h\nu} B^*$
for unfiltered light	$A^* + A \rightarrow A_2$	$B^* + B \rightarrow B_2$
	$A^* + B \rightarrow AB$	$B^* + A \rightarrow AB$
		$B \xrightarrow{h\nu} B^*$
for filtered light		$B^* + A \rightarrow AB$
		$B^* + B \rightarrow B_2$

Since the ^1A level is higher than ^1B energy transfer from ^1B to ^1A is not expected. On the other hand, energy transfer $^1A + {}^0B \rightarrow {}^0A + {}^1B$ which could take place in the experiment with unfiltered light, could quench either of the two processes:

$$^1A \rightarrow \text{dimer}$$
$$^1A \rightarrow {}^3A \rightarrow \text{dimer}$$

There is no experimental evidence that incorporation of B into the lattice of A affects the formation of A_2: energy transfer in the singlet state seems improbable.

If the photoreactive state derives from the triplet ^3A or ^3B, then energy transfer in the triplet states

$$^3B + {}^0A \rightarrow {}^3A + {}^0B$$
$$^3A + {}^0B \rightarrow {}^0A + {}^3B$$

depending upon the relative triplet energy levels is ruled out by a similar argument, namely the absence of the homodimer in the filtered, and the absence of quenching in the unfiltered, experiment.

These qualitative arguments leave us with two possibilities. The reaction may proceed from the singlet excited state at a rate faster than that of energy transfer; alternatively, the reaction proceeds from the triplet state with intersystem crossing faster than singlet energy transfer and with reaction faster than triplet energy transfer. In either case the reaction would occur near the site of light absorption.

Since excitation of B leads to B_2 and AB only and energy is not transferred from B to A the only photochemical path to AB is via

$$B^* + A \rightarrow AB$$

that is, the combination of an excited with a ground-state molecule, a conclusion which bears out the result derived from the quantum yield measurements quoted above.

The solution photochemistry of the chalcones has been investigated systematically; there is evidence that these ketones can undergo dimerization, isomerization and other reactions. Dr Luwisch[20] has shown in this Laboratory that, while dimerization in the solid state follows the topochemical rules (see above), the photochemistry is not as clean as that of, say, cinnamic acid; the non-dimeric products have not, however, been investigated.

For the detailed analysis of coumarin photochemistry the original literature must be consulted. We note the general agreement that the *cis,syn* dimer,

UM00011796
NOVARTIS EXHIBIT 1517
Novartis v. Regents, IPR2023-01347
Page 542 of 4460

unlike the *trans,syn* and *trans,anti* dimers, is formed from the singlet excited state[73,74]. In this connection the observation that the [coumarin, mercuric chloride] complex yields the *cis,syn* dimer is of interest; one wonders which excited state of coumarin is involved in the solid medium mainly composed of heavy atoms likely (in solution) to promote intersystem crossing.

The photochemistry of thymine and other pyrimidines has been studied in some detail[75,76]. Triplet dimerization in the fluid state has been demonstrated by sensitization and quenching experiments on thymine and derivatives. There is highly suggestive evidence from thymine in frozen aqueous solution (i.e. under conditions where crystalline thymine hydrate is formed which is known to yield *cis,syn* dimer on irradiation with $\lambda > 290$ nm) that dimerization in the crystalline phase takes place from the singlet state; the less probable alternative, that intersystem crossing to the triplet precedes dimerization, requires the former process to be 10^4 times faster in the crystal than in isolated thymine molecules as well as totally efficient reaction to dimer of the triplet species[75].

We can only briefly mention the use of the KBr pellets containing solid monomers for the determination of quantum yields of dimerization in the pyrimidine series[76]. The quantum yields of dimer formation range from 0.1 for 3-methylthymine to 0.4 for 1-methylthymine and 0.45 for orotic acid; the authors suggest that a relationship might exist between effective rate of reaction and geometry of the crystal lattice, i.e. that with increasing separation between $\rangle C{=}C \langle$ bonds the value of the quantum yield falls off. We feel that a word of caution is needed here: the crystallography of pyrimidines (including the monohydrates of thymine and of methylthymine) is complex, and it is more than doubtful whether the crystalline species in KBr pellets are those crystal forms on which the geometrical arguments are based. It seems likely that the preparation of the pellets introduces into the crystalline material a higher than normal dislocation density, and that it is the quantum yield in such stressed materials which is reported, rather than that of the normal crystal lattice. It is also doubtful whether the monohydrate of thymine is stable under condition of pellet formation.

We summarize the information on the electronic states involved in solid-state dimerization with the generalization that in the majority of cases the reaction proceeds from the first singlet state. The benzalacetophenones (chalcones) as aromatic ketones likely to have a high probability of intersystem crossing to the triplet state, may be a genuine exception; it is tempting to speculate that the more complex photochemistry of solid chalcones is connected with longer lifetimes of the triplet as compared with the singlet states.

We may reasonably assume, in the light of all that has been said so far about solid-state cyclodimerization, that reaction between excited monomer and its ground-state neighbour takes place with the minimum of molecular motion. Consequently, it should be possible to consider the variation of energy with the reaction coordinate such as the continuously decreasing intermolecular separation of the two monomer molecules.

Lamola and Eisinger[77] have suggested that this path can be divided into three steps, apart from a fourth in which monomers are separated by more

UM00011797
NOVARTIS EXHIBIT 1517
Novartis v. Regents, IPR2023-01347
Page 543 of 4460

than 5 Å and emit absorbed energy from the singlet excited state by monomer fluorescence. The excitonic region somewhere near 3 Å can be reached in experiments in which the dimer is imbedded in a rigid glass and then photodissociated; the two monomer units formed are held in parallel or near-parallel separation estimated to be 2.8 Å (for dimethylthymine) from the exciton splitting of the absorption spectrum. These monomer pairs which show no fluorescence, are redimerized with a quantum yield of unity. The authors suggest that this state is an intermediate in the dimerization of thymine in the crystalline state and propose to connect the (lower) exciton state with the excimer state 'so that the latter is most likely an intermediate in the photodimerization'.

In my opinion there is yet inadequate evidence for the hypothesis that the excimer state is an intermediate in the sequence of non-radiative relaxation steps connecting the monomer in its excited state with the chemical product in its ground state, at least that excimer state which is currently defined as the species that emits unstructured fluorescence red-shifted with respect to monomer emission.

Pending elucidation of the energy surface over which the two molecules move, we may look for information on the changes in molecular structure during the course of the reaction. Thus, whilst there is little nuclear re-organization of cyclic monomers such as pyrimidines, coumarins, etc. during cyclodimerization, some changes in molecular conformation obviously must occur in the reaction of open-chain systems.

We know from the position of the fluorescence emission that, in the majority of organic molecules, the change in their nuclear configuration during the interval between absorption and re-emission is small; major re-organization must begin during the motion of the two molecules towards each other, that is during the rehybridization ($sp^2 \rightarrow sp^3$) of the four reacting centres at distances which permit partial bond formation but also imply repulsion between the substituent groups of the four centres. Such repulsion sets in at the latest at 2.8 Å so that at this separation of the reacting atoms the molecule is almost certainly no longer planar.

I suggest that a study of the molecular deformation which takes place as the molecules move towards each other, can throw light on the type of molecular interaction which is responsible for the passage via the first singlet-ground-state pair to the dimer. I believe further that this study is by no means as impossible as it appears at first sight. I am thinking in particular of reactions in chiral crystal structures where dimerization within the molecular stack of twisted and hence *prochiral* monomer units may proceed in a preferred direction leading to chiral product; in other words, front-side and rear-side attack of the excited molecule on the prochiral ground-state molecule (that is: attack on the upper or lower partner in the translation stack) may have sufficiently different probability to generate excess of one or the other enantiomer. Several variants of this experiment are possible and being investigated in our Laboratory. Determination of x-ray methods of the absolute configuration of one of the crystals and of the product generated in excess from this enantiomer will permit a still more detailed description of the reaction course.

UM00011798
NOVARTIS EXHIBIT 1517
Novartis v. Regents, IPR2023-01347
Page 544 of 4460

ACKNOWLEDGEMENTS

The solid-state chemistry group of the Department of Chemistry gratefully acknowledges financial support by the National Bureau of Standards, Washington, D.C. and by the Stiftung Volkswagen. The author thanks Mrs T. Schwarz for help in the preparation of the manuscript.

REFERENCES

[1] W. Marckwald, *Z. Phys. Chem.* **30**, 140 (1899).
[2] G. Ciamician and P. Silber, *Ber. Dtsch. Chem. Ges.* **34**, 2040 (1901).
[3] H. Stobbe and F. K. Steinberger, *Ber. Dtsch. Chem. Ges.* **55**, 2225 (1922).
[4] A. W. K. de Jong, *Ber. Dtsch. Chem. Ges.* **56**, 818 (1923).
[5] A. Senier and F. G. Shephard, *J. Chem. Soc.* **95**, 1943 (1909).
[6] For summary of the results of this phase see H. Bacher, in *Handbücher der biologischen Arbeitsmethoden*, Abt. I, Teil 2, II, 1, p 1829. Ed. Abderhalden, Urban and Schwarzenberg. Springer: Berlin–Vienna (1929).
[7] P. Groth, *Chemische Krystallographie*, W. Engelmann: Leipzig (1917).
[8] For summary see G. M. J. Schmidt, 'The photochemistry of the solid state'. Contribution to the 13° Conseil de Chimie de l'Institut International de Chimie (Bruxelles 1965), which appeared in condensed form in *Reactivity of the Photoexcited Organic Molecule*, Interscience: London (1967).
[9] M. D. Cohen, *Mol. Cryst. Liquid Cryst.* **9**, 287 (1969).
[10] D. P. Craig and S. Sarti-Fantoni, *Chem. Commun.* 742 (1966).
[11] J. M. Thomas and J. O. Williams, *Chem. Commun.* 432 (1967).
[12] M. D. Cohen, I. Ron, G. M. J. Schmidt and J. M. Thomas, *Nature, London*, **224**, 167 (1969).
[13] D. P. Craig, R. Mason, P. Pauling and D. P. Santry, *Proc. Roy. Soc. A*, **286**, 98 (1965).
[14] D. E. Williams, *J. Chem. Phys.* **45**, 3770 (1966);
D. E. Williams, *Acta Cryst.* **A25**, 464 (1969).
[15] L. Leiserowitz and G. M. J. Schmidt, *J. Chem. Soc. A*, 2372 (1969).
[16] B. S. Green and G. M. J. Schmidt, to be published.
[17] e.g. M. A. El Sayed, M. T. Wauk and G. W. Robinson, *Molec. Phys.* **5**, 205 (1962).
[18] G. M. J. Schmidt, *J. Chem. Soc.* 2014 (1964).
[19] M. Lahav and G. M. J. Schmidt, *J. Chem. Soc. B*, 239 (1967).
[20] M. Luwisch, *Ph.D. Thesis*, Weizmann Institute of Science: Rehovot (1968).
[21] F. I. Sonntag and G. M. J. Schmidt, unpublished results.
[22] R. Goldstein, *Ph.D. Thesis*, Weizmann Institute of Science: Rehovot (1967).
[23] D. Rabinovich and G. M. J. Schmidt, *J. Chem. Soc. B*, 144 (1967).
[24] G. W. Griffin, A. F. Vellturo and K. Furukawa, *J. Amer. Chem. Soc.* **83**, 2725 (1961).
[25] T. Sadeh and G. M. J. Schmidt, *J. Amer. Chem. Soc.* **84**, 3970 (1962).
[26] M. Lahav and G. M. J. Schmidt, *J. Chem. Soc. B*, 312 (1967).
[27] B. S. Green, M. Lahav and G. M. J. Schmidt, *J. Chem. Soc. B*, 1552 (1971).
[28] M. D. Cohen, B. S. Green, Z. Ludmer and G. M. J. Schmidt, *Chem. Phys. Letters*, **7**, 486 (1970).
[29] B. S. Green, A. Elgavi and G. M. J. Schmidt, unpublished results.
[30] J. Bregman, K. Osaki, G. M. J. Schmidt and F. I. Sonntag, *J. Chem. Soc.* 2021 (1964).
[31] L. Leiserowitz and G. M. J. Schmidt, *Acta Cryst.* **18**, 1058 (1965).
[32] B. S. Green, unpublished results.
[33] W. Drenth and E. H. Wiebenga, *Acta Cryst.* **8**, 755 (1955).
[34] I. Ron and G. M. J. Schmidt, to be published.
[35] M. Gorodetzky and Y. Mazur, *J. Amer. Chem. Soc.* **90**, 6540 (1968).
[36] J. L. R. Williams, in *Topics in Current Chemistry*, **13**, 227 (1969).
[37] F. I. Sonntag and R. Srinivasan, quoted in ref. 36.
[38] S. Kikuchi and K. Nakamura, quoted in ref. 36.
[39] E. Heller, *Ph.D. Thesis*, Weizmann Institute of Science: Rehovot (1969).
[40] J. C. J. Bart and G. M. J. Schmidt, to be published.
[41] M. D. Cohen, Z. Ludmer, J. M. Thomas and J. O. Williams, *Chem. Commun.* 1172 (1969).
[42] K. S. Wei and R. Livingston, *J. Chem. Phys.* **71**, 548 (1967).
R. Livingston and K. S. Wei, *J. Chem. Phys.* **71**, 541 (1967).
[43] A. Chapiro and G. Lozach, *C.R. Acad. Sci., Paris*, Sér. C, **267**, 37 (1968).

UM00011799

NOVARTIS EXHIBIT 1517
Novartis v. Regents, IPR2023-01347
Page 545 of 4460

[44] D. O. Cowan and R. L. Drisko, *J. Amer. Chem. Soc.* **89**, 30 (1967).
[45] G. W. Griffin, J. E. Basinski and A. F. Vellturo, *Tetrahedron Letters*, No. 3, 13 (1960); G. W. Griffin, *U.S. Pat.* No. 3 139395 to American Cynamid Co. (30 June 1964).
[46] R. E. Marsh, E. Ubell and H. E. Wilcox, *Acta Cryst.* **15**, 35 (1962).
[47] Ju. T. Struchkov, A. J. Kitaigorodskii and T. L. Khotsyanova, *Dokl. Akad. Nauk SSSR*, **93**, 675 (1953).
[48] D. Rabinovich and G. M. J. Schmidt, unpublished results.
[49] W. Nieuwenkamp and J. M. Bijvoet, *Z. Kristallogr.* **84**, 49 (1932).
[50] S. E. Filippakis, L. Leiserowitz and G. M. J. Schmidt, *J. Chem. Soc. B*, 297 (1967).
[51] S. E. Filippakis, L. Leiserowitz and G. M. J. Schmidt, *J. Chem. Soc. B*, 290 (1967).
[52] H. P. Kaufmann and A. K. Sen Gupta, *Liebigs. Ann. Chem.* **681**, 39 (1965).
[53] W. D. Closson, S. F. Brady, E. M. Kosower and P. C. Huang, *J. Org. Chem.* **28**, 1161 (1963).
[54] S. E. Filippakis, L. Leiserowitz and G. M. J. Schmidt, *J. Chem. Soc. B*, 305 (1967).
[55] M. Lahav and G. M. J. Schmidt, *Tetrahedron Letters*, 2957 (1966).
[56] W. L. Dilling, *Chem. Rev.* **69**, 845 (1969).
[57] H. Stobbe and E. Färber, *Ber. Dtsch. Chem. Ges.* **58**, 1548 (1925).
[58] R. C. Cookson, D. A. Cox and J. Hudec, *J. Chem. Soc.* 4499 (1961).
[59] H. Midorikawa, *Bull. Chem. Soc. Japan*, **26**, 302 (1953).
[60] J. Corse, B. J. Finkle and R. E. Lundin, *Tetrahedron Letters*, 1 (1961).
[61] B. S. Green and G. M. J. Schmidt, *Tetrahedron Letters*, 4249 (1970).
[62] N. E. Rowland, F. Sondheimer, G. A. Bullok, E. LeGoff and K. Grohmann, *Tetrahedron Letters* 4769 (1970).
[63] M. Hasegawa, F. Suzuki, H. Nakamishi and Y. Suzuki, *Polymer Letters*, **6**, 293 (1968).
[64] M. Hasegawa and Y. Suzuki, *Polymer Letters*, **5**, 815 (1967).
[65] M. Iguchi, H. Nakamishi and M. Hasegawa, *J. Polym. Sci. A*, **6**, 1055 (1968).
[66] D.-J. Hung, *M.Sc. Thesis*, Weizmann Institute of Science: Rehovot (1969).
[67] M. Tsudas, *J. Soc. Sci. Phot. Japan*, **28**, 7 (1965).
[68] H. Krönert, *Ph.D. Thesis*, Technische Universität: Berlin (1967).
[69] H. G. Curme, C. C. Natale and D. J. Kelley, *J. Phys. Chem.* **71**, 767 (1957).
[70] R. T. LaLonde and C. B. Davies, *Canad. J. Chem.* **47**, 3250 (1969).
[71] J. Rennert, E. M. Ruggiero and J. Raff, *Photochem. Photobiol.* **6**, 29 (1967).
[72] P. N. Nie, *M.Sc. Thesis*, Weizmann Institute of Science: Rehovot (1969).
[73] G. S. Hammond, C. A. Stout and A. A. Lamola, *J. Amer. Chem. Soc.* **86**, 3103 (1964).
[74] H. Morrison, H. Curtis and T. McDowell, *J. Amer. Chem. Soc.* **88**, 5415 (1966).
[75] A. A. Lamola, *Photochem. Photobiol.* **7**, 619 (1968).
[76] R. Lisenski and K. L. Wierzchowski, *Photochem. Photobiol.* **11**, 327 (1970).
[77] A. A. Lamola and J. Eisinger, *Proc. Nat. Acad. Sci., Wash.* **59**, 46 (1968).

OBITUARY

Professor Gerhard M. J. Schmidt died in Zurich on 12 July 1971, aged 51, where, characteristically, he was delivering a series of lectures in spite of his illness; from there he was planning to travel to the XXIII IUPAC Congress in Boston where he was to have chaired a Photochemistry section.

Professor Schmidt was at home both in pure scientific research and in the application of that research, bringing dynamic imagination and dedication to both. His unique approach to solid-state chemical reactions, reflected so well in the present contribution on Solid State Photodimerization, was based on his conviction that the results obtained from a combination of the disciplines of organic chemistry, crystallography, and spectroscopy were important for the intimate understanding of the factors governing chemical reactivity. He further believed that an understanding of the behaviour of crystalline systems would help elucidate the role of short-range and long-range order in highly organized biological systems as well.

His death, at the peak of his active investigation into problems such as organic photochemistry, high-pressure reactions, heterogeneous catalysis, gas–solid, liquid–solid, and solid–solid chemical reactions, systematics of molecular packing in crystals, spectroscopy in organic crystals, and asymmetric synthesis, is a major blow. The loss of his incisive and original contributions will be deeply felt both by his immediate co-workers in these areas and by the international scientific community.

BERNARD S. GREEN

UM00011800
NOVARTIS EXHIBIT 1517
Novartis v. Regents, IPR2023-01347
Page 546 of 4460